Compréhension des mécanismes de transferts de gaz et de composés organiques dans le Polylactide (PLA)

Cécile Courgneau

Doctorat ParisTech

T H È S E

pour obtenir le grade de docteur délivré par

L'Institut des Sciences et Industries du Vivant et de l'Environnement

(AgroParisTech)

Spécialité : Sciences et Procédés des Aliments et Bioproduits

présentée et soutenue publiquement par

Cécile COURGNEAU

le 9 Mai 2011

Compréhension des mécanismes de transferts de gaz et de composés organiques dans le Polylactide (PLA)

Directeur de thèse : **Violette DUCRUET**
Co-encadrement de la thèse : **Sandra DOMENEK**

Jury
M. Eric DARGENT, Professeur, LECAP, IMR Université de Rouen   Rapporteur
M. Frédéric DEBEAUFORT, Professeur, EMMA EA 581, Université de Bourgogne   Rapporteur
M. Luc AVÉROUS, Professeur, LIPHT-ECPM, Université de Strasbourg   Examinateur
Mme Valérie MIRI, Maître de Conférences, UMR CNRS 8207, Université de Lille   Examinateur
M. Olivier TALON, R&D Scientist, MateriaNova   Invité
Mme Violette DUCRUET, Ingénieur de Recherche, UMR1145, INRA   Directrice de thèse
Mme Sandra DOMENEK, Maître de Conférences, UMR1145, AgroParisTech   Co-encadrante

Remerciements

Ce travail représente l'aboutissement de trois années de recherche sous la direction de Violette Ducruet, Ingénieur de Recherche INRA, et de Sandra Domenek, Maître de Conférences à AgroParisTech, au sein de l'équipe Interaction Matériaux Milieux au Contact (I2MC) de l'UMR Ingénierie Procédés Aliments.

Je les remercie sincèrement pour avoir encadré ce travail et surtout pour leur apport scientifique tout au long de ces trois années. Leur enthousiasme, leur disponibilité et surtout leurs conseils m'ont permis de faire avancer ce projet.

J'exprime mes sincères remerciements à Mr Eric Dargent, Professeur à l'Université de Rouen, et Mr Frédéric Debeaufort, Professeur à l'Université de Bourgogne, pour avoir accepté de juger ce travail en tant que rapporteur.

Je tiens à exprimer mes remerciements aux autres membres du jury qui ont accepté d'évaluer mon travail de thèse en tant qu'examinateur : Olivier Talon, R&D Scientist, Valérie Miri, Maître de Conférence à l'Université de Lille 1, et Luc Avérous, Professeur à l'ECPM de Strasbourg.

Je voudrais témoigner ma sympathie et ma reconnaissance à Anne-Marie Riquet et à Olivier Vitrac pour leur aide précieuse, leurs conseils, ainsi que les longues heures passées en ma compagnie. J'exprime ma gratitude à Alain Guinault et Luc Avérous pour m'avoir accueillie au sein de leur laboratoire et surtout pour m'avoir permis de réaliser toutes ces analyses indispensables. Je remercie également Valérie Miri pour son aide précieuse dans la réalisation des échantillons biétirés.

Mes remerciements seraient incomplets si je n'y associais toutes les personnes que j'ai rencontrées pendant ces 3 années aussi bien à Massy qu'au CNAM et qu'à Strasbourg : Cédric, Flavien, Catherine, Anne, Cyrille, Chheng pour leur aide et leurs conseils mais aussi Rómulo, Alexis, Abdou, Aurélien, Mai, Jean-Michael, Nathalie, Roberto, Elodie, Marie pour leur gentillesse et leur amitié. Je n'oublierais pas Jennifer et Xiaoyi avec qui j'ai partagé de très bons moments de complicité et de fous rires (I already miss you and the food smells in

Ce travail de thèse a donné lieu à des publications et des communications :

Publications:

n°1 :   Domenek S., Courgneau C., Ducruet V., « Characteristics and Applications of PLA », (Chap. 20), dans *Biopolymers: Biomedical and Environmental Applications*, Susheel Kalia & Luc Avérous (Eds). **John Wiley & Scrivener Pub**. Date de publication: 08/**2011**. 400 p.

n°2 :   Courgneau C., Domenek S., Guinault A., Avérous L., Ducruet V., "Analysis of the structure-properties relationships of different multiphase systems based on plasticized poly(lactic acid)", Journal of polymers and the environment, **2011,** 19 (2), 362-371.

n°3   Courgneau C., Domenek S., Avérous L., Ducruet V., "Non-isothermal crystallization kinetics of poly(L,D-lactide) : effect of plasticizers and talc", Journal of Polymer Science, Part B – Polymer Physics (en projet).

n°4   Colomines G., Ducruet V., Courgneau C., Guinault A., Domenek S. "Barrier properties of poly(lactic acid) and its morphological changes induced by aroma sorption", Polymer International, **2010**, *59* (6), 818-826.

n°5   Courgneau C., Domenek S., Guinault A., Avérous L., Ducruet V., "Effect of crystallization on barrier properties of formulated polylactide", Polymer International (accepté).

n°6   Courgneau C., Vitrac O., Riquet A.-M., "Probing molecular dynamics along the thickness of neat and plasticized polylactides by ESR methods", Polymer (en projet).

Proceeding:

-    Guinault A., Menary G. H., Courgneau C., Griffith D., Ducruet V., Miri V., Sollogoub C. "The effect of the stretching of PLA extruded films on their crystallinity and gas barrier properties", ESAFORM 2011.

Communications orales :

- Courgneau C., Domenek S.*, Colomines G., Guinault A., Avérous L., Ducruet V. "Barrier properties of PLA and PHB in relation with the formulation and the crystallinity", Conference of Food Engineering CoFE, 5-8 avril 2009, Colombus, OH, Etats-Unis.
- Domenek S.*, Courgneau C., Colomines G., Guinault A., Avérous L., Ducruet V. "Barrier properties of poly(lactic acid): effects on formulation and crystallinity", European Polymer Federation EPF'09, 12-17 juillet 2009, Graz (Autriche).
- Courgneau C.*, Domenek S., Colomines G., Guinault A., Avérous L., Ducruet V. "Effects of Poly(lactic acid) formulation and crystallinity on barrier properties", 8th World Congress of Chemical Engineering, 23-27 Août 2009, Montréal (Canada).
- Courgneau C., Domenek S.*, Guinault A., Avérous L., Ducruet V. "Influence of plasticization on barrier properties of poly(lactic acid)", Biopol 2009 International conference on Biodegradable Polymers and sustainable composites, 30 septembre-2 octobre 2009, Alicante (Espagne).
- Courgneau C.*, Domenek S., Guinault A., Avérous L., Ducruet V. "Influence of plasticization and annealing on mechanical and barrier properties of poly(lactic acid)", First Meeting on Material/Bioproduct Interaction, MatBim, 3-5 mars 2010, Paris (France).
- Courgneau C.*, Domenek S., Guinault A., Avérous L., Ducruet V. "Influence de la plastification et du recuit sur les propriétés mécaniques et barrière de l'acide polylactique" Matériaux 2010, 17-22 octobre 2010, Nantes (France).

Communications par affiche:

- Courgneau C., Domenek S., Colomines G., Guinault A., Avérous L., Ducruet V. "Barrier properties of PLA and PHB in relation with their formulation and crystallinity", Journées Chimie Verte, 4-5 décembre 2008, La Baule (France).
- Courgneau C., Domenek S., Colomines G., Guinault A., Avérous L., Ducruet V. "Barrier properties of PLA in relation with the formulation and the crystallinity", Journées scientifiques ABIES, 17-18 mars 2009, Paris (France).
- Courgneau C., Domenek S., Colomines G., Guinault A., Avérous L., Ducruet V. "Barrier properties of PLA and PHB in relation with the formulation and the

crystallinity", Journées Arômes Plate-Forme Lipides-Arômes, 2-3 avril 2009, INRA, Dijon (France).

- Courgneau C., Domenek S., Colomines G., Guinault A., Avérous L., Ducruet V "Effects of PLA and PHB formulation on morphology and barrier properties", European Polymer Federation 4th Summer School "Bioplastics and Related Materials", 24-29 Mai 2009, Gargnano (Italie).

- Courgneau C., Idrac J., Lebossé R., Domenek S., Ducruet V. "Influence of annealing on the microstructure of poly(lactic acid)", First Meeting on Material/Bioproduct Interaction, MatBim, 3-5 mars 2010, Paris (France).

- Ducruet V., Domenek S., Guinault A., Courgneau C., Bernasconi M., Plessis C. "Barrier properties of PLA towards oxygen and aroma compounds", 4th Shelf Life International Meeting, SLIM 2010, 23-25 juin 2010, Zaragosse (Espagne).

- Courgneau C., Domenek S., Ducruet V. "Compréhension des mécanismes de transfert de gaz et de composés d'arôme dans des polyesters biodégradables", Agoriales, Salon International du Process Alimentaire, 17-21 octobre, Villepinte (France).

Table des matières

Chapitre 3 – Effet de la formulation sur les propriétés du P(D,L)LA ____ *117*

Liste des tableaux

Liste des figures

Abréviations

A (m²)	Aire de la surface
ABS	Acrylonitrile butadiène styrène
aPET	Poly(éthylène téréphthalate) amorphe
ATBC	Acétyl tributyl citrate
AT/AminoTEMPO	4-amino– 2,2,6,6 – tetramethylpiperidine-1-oxyl
b	Constante d'affinité pour les trous
B	Composante entropique du paramètre d'interaction
BE	Butyrate d'éthyle
BHT	hydroxytoluène butylé
CES / SEC	Chromatographie d'exclusion stérique
C (mol.g^{-1})	Concentration en pénétrant
C'$_H$	Constante de saturation des trous
C$_M$	Constante de la vitesse de cristallisation de Malkin
C$_0$	Exposant de Malkin
d/ρ	Densité
D (m².s^{-1})	Coefficient de diffusion
Đ	Dispersité
D$_0$ (m².s^{-1})	Coefficient de diffusion pour D tend vers 0
DMTA ou DMA	Analyse thermo-mécanique dynamique
DRX	Diffraction des rayons X
DSC	Calorimétrie différentielle à balayage
E (MPa)	Module d'Young ou module élastique
E' (Pa)	Module de conservation
E'' (Pa)	Module de perte
Ea (kJ.mol^{-1})	Energie d'activation
EA/AE	Acétate d'éthyle
E$_D$ (kJ.mol^{-1})	Energie d'activation de la diffusion
FDA	Food and Drug Administration
FID/DIF	Détecteur à ionisation de flamme

F(T)	Paramètre cinétique de Liu et Mo
FT-IR	Infra-Rouge à Transformée de Fourier
G	Vitesse de nucléation primaire
HDPE	Polyéthylène haute densité
HE	Hexanoate d'éthyle
HeTr $(m^3.m^{-2}.s^{-1})$	Vitesse de transmission de l'hélium
J	Flux de perméant
K	Transfert de masse totale
k_a (min^{-n})	Constante de cristallisation d'Avrami
k_D	Constante d'Henry
k_o (min^{-n})	Constante de cristallisation d'Ozawa
k_p	Affinité pour le polymère
k_s	Affinité pour le soluté
k_t (min^{-n})	Constante de cristallisation de Tobin
k_{us} (min^{-n})	Constante de cristallisation de Urbanovici et Segal
l (m)	Epaisseur
LA	Acide lactique
LDPE	Polyéthylène basse densité
MAF	Fraction amorphe mobile
MDSC	Calorimétrie différentielle à balayage à température modulée
M_n $(g.mol^{-1})$	Masse molaire moyenne en nombre
M_w $(g.mol^{-1})$	Masse molaire moyenne en poids
m	Ratio des exposants de Liu et Mo
m_t (%)	Prise de masse au temps t
m_∞ (%)	Prise de masse à l'équilibre
n_a	Exposant d'Avrami
n_o	Exposant d'Ozawa
n_t	Exposant de Tobin
n_{us}	Exposant d'Urbanovici et Segal
OTR $(m^3.m^{-2}.s^{-1})$	Vitesse de transmission de l'oxygène
p (Pa)	Pression partielle de vapeur

P (m^3.m.m^{-2}.s^{-1}.Pa^{-1})	Coefficient de perméabilité
p_0 (Pa)	Pression de vapeur saturante
PA	Polyamide
PBS	Poly(butyrate succinate)
PBSA	Poly(butyrate succinate-co-adipate)
PBSAT	Poly(butyrate succinate-co-adipate téréphthalate)
PBSL	Poly(butyrate succinate-co-lactate)
PBST	Poly(butyrate succinate téréphthalate)
PBT	Poly(butyrate téréphthalate)
PC	Polycarbonate
PCBS	Poly(l-cystine bisamide-g-sulfadiazine)
PCL	Polycaprolactone
PDLA	Poly(D-acide lactique)/ Poly(D-lactide)
P(D,L)LA	Poly(D,L-acide lactique)/ Poly(D,L-lactide)
PEG	Poly(éthylène glycol)
PEIT	Poly(éthylène-co-isosorbite téréphthalate)
PEN	Poly(éthylène naphthalate)
PET	Poly(éthylène téréphthalate)
PHA(s)	Polyhydroxyalcanoate(s)
PHB	Polyhydroxybutyrate
PHBV	Poly(hydroxybutyrate-co-hydroxyvalérate)
PLA	Poly(acide lactique) ou polylactide
PLGA	Poly(lactide-co-glycol)
PLLA	Poly(L-acide lactique)/ Poly(L-lactide)
PO3G	Poly(triméthylène éther glycol)
PP	Polypropylène
PS	Polystyrène
PTMAT	Poly(tetraméthylène adipate téréphthalate)
PTT	Poly(triméthylène téréphthalate)
PU	Polyuréthane
PVC	Poly(chlorure de vinyle)

Q	Quantité de perméant
R (J.mol^{-1}.K^{-1})	Constante des gaz parfait
RAF	Fraction amorphe rigide
RH (%)	Humidité relative
ROP	Polymérisation par ouverture de cycle
RPE	Résonance paramagnétique électronique
S (m^3.m^{-3}.Pa^{-1})	Coefficient de solubilité
S$_0$ (m^3.m^{-3}.Pa^{-1})	Coefficient de solubilité pour C tend vers 0
SBR	Styrène butadiène
t et dt (s)	Temps et sa dérivée
T et dT (°C)	Température et sa dérivée
tan δ	Tangente de l'angle de perte
T$_c$ (°C)	Température de cristallisation
t$_{corr}$ (s)	Temps de corrélation de réorientation
TEMPO	2,2,6,6-Tetramethylpiperidin-1-oxyl
TEMPOL/Tol	4-hydroxy – 2,2,6,6 – tetramethylpiperidine-1-oxyl
T$_f$ /T$_m$ (°C)	Température de fusion
T$_g$ (°C)	Température de transition vitreuse
TPS	Amidon thermoplastique
TPU	Polyuréthane thermoplastique
T$_{0,01}$ (°C)	Température à laquelle la cristallinité relative est de 1%
T$_{0,99}$ (°C)	Température à laquelle la cristallinité relative est de 99%
t$_{1/2}$ (s)	Temps de demi-cristallisation
T$_{50G}$ (°C)	Température à laquelle le couplage hyperfin est de 50 G
V*	Taille minimum de volume de trous
V$_f$	Fraction de volume libre
V$_1$ (cm^3.mol^{-1})	Volume molaire du composé 1
WAXD	Diffraction des rayons X aux grands angles
Wm	Fraction de méso-lactide
WVTR (g.m^{-2}.j^{-1})	Vitesse de transmission de la vapeur d'eau
Xam (%)	Fraction de phase amorphe mobile

X_{ar} (%)	Fraction de phase amorphe rigide
X (%)	Taux de cristallinité relatif
α (°C.min^{-1})	Vitesse de montée en température
δ_1 (J.cm^{-3})$^{1/2}$	Paramètre de solubilité du composé 1
$\Delta C_p^{\,0}$ (J.g^{-1}.K^{-1})	Saut de chaleur spécifique
ΔH_c (J.g^{-1})	Enthalpie de cristallisation
ΔH_m (J.g^{-1})	Enthalpie de fusion
ΔH_m 100% (J.g^{-1})	Enthalpie de fusion du polymère 100% cristallin
ΔH_{mix}	Enthalpie de mélange
ΔH_s	Enthalpie de la solution dans le polymère
ΔH_{vap}	Enthalpie de vaporisation
ε_b (%)	Elongation à la rupture
θ (s)	Temps de retard/Time-lag
ρ_c	Densité du cristal
σ (MPa)	Contrainte au seuil
σ_e (J.m^{-2})	Energie de surface à l'extrémité d'une lamelle
φ	Fraction de volume
χ	Paramètre d'interaction
χ_c (%)	Taux de cristallinité
ω_1	Fraction massique du composé 1
$2A_{zz}$ (G)	Couplage hyperfin/Distance séparant les deux extrémités du spectre
2θ (°)	Angle de diffraction

Introduction générale

Les matières plastiques synthétiques ont été découvertes il y a plus de 170 ans (polystyrène en 1839) et développées au début du siècle dernier (Bakélite en 1907). Depuis, de nombreux polymères synthétiques, dérivés du pétrole, ont vu le jour et ont été commercialisés, en particulier après la seconde guerre mondiale. Si bien qu'aujourd'hui, leur diversité et leurs propriétés variées permettent de les utiliser pour un grand nombre d'applications : emballage, construction/bâtiment, électronique/électrique, médical, transport, ameublement, vêtements, agriculture, loisir…

Ainsi la production mondiale de plastiques en 2008 a atteint environ 245 millions de tonnes (Plastic Europe, 2009). Cette importante production a induit des questions environnementales de plus en plus récurrentes telles que la raréfaction et l'augmentation du prix des ressources fossiles, la gestion des déchets et le recyclage. En réponse à ces préoccupations, les gouvernements, industriels et scientifiques se sont tournés vers les polymères biosourcés. Ces polymères apparaissent comme une alternative de plus en plus crédible aux polymères synthétiques avec des propriétés comparables et un impact environnemental réduit.
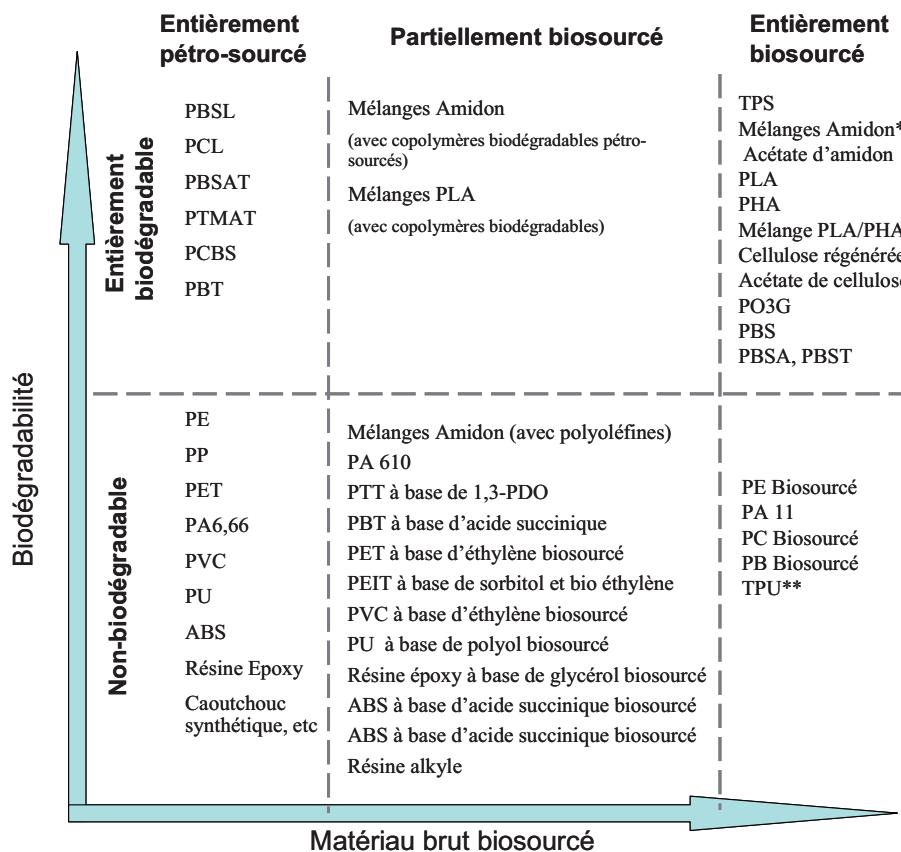
Figure i. Polymères actuels et émergeants classés selon la matière première utilisée pour leur fabrication (pétrole et/ou biomasse) et leur biodégradation. Adaptée de (Shen, 2009)

* avec copolymères biosourcés et biodégradables, ** partiellement biodégradable

Une large gamme de polymères peut être produite complètement ou partiellement à partir de la biomasse et de résidus de l'agriculture, peu coûteux, et être ainsi complètement ou partiellement biodégradables (Figure 1).

Ces matériaux biosourcés représentaient, en 2007, 260 000 tonnes dans le monde sur les 245 millions de tonnes de plastiques produits, i.e. 0,1 % de la production mondiale annuelle de plastiques. Leur intérêt majeur aussi bien pour les politiques que pour le secteur du plastique fait que la capacité de production de ces polymères devrait atteindre 1,6 millions de tonnes d'ici 2013 (Alcimed, 2011). Celle-ci pourrait même atteindre 2,3 millions de tonnes selon les annonces faites par les industriels (Shen, 2009).

Le polylactide (PLA) est un polyester entièrement produit à partir de la biomasse et biodégradable dans des environnements adaptés. Son volume de production arrive en troisième position après les matériaux à base de cellulose et d'amidon. Synthétisé et commercialisé principalement par NatureWorks (95 % de la capacité mondiale), à près de 2 €/kg, sa capacité de production de 2010 devrait être triplé d'ici 2013 pour atteindre 232,5 kt par an. Néanmoins des producteurs de quantité inférieure existent sur le marché asiatique (ex : Teijin/Musashino, Toyobo) tandis que de nouveaux acteurs commencent à investir ce marché, tels que Futerro ou Pyramid Bioplastics (Shen, 2009). Une estimation des principales applications du PLA en 2020 par Purac, un des principaux producteurs d'acide lactique, est résumée dans la figure suivante.
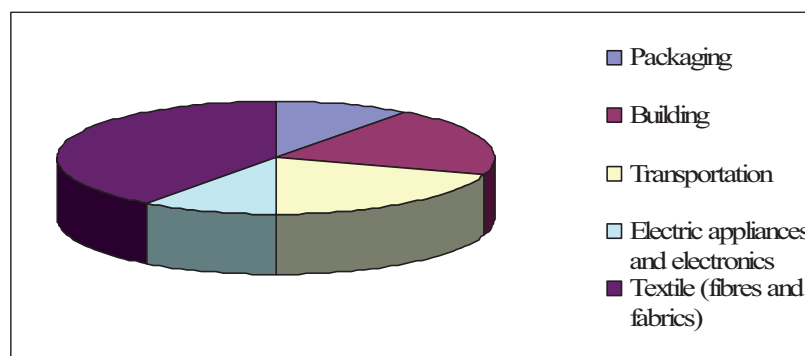
Figure ii. Répartition par secteur d'activité de la production de PLA selon PURAC à l'horizon 2020 (Shen, 2009).

Cependant le PLA présente des propriétés limitées qui réduisent son développement pour des applications industrielles viables. De nombreuses études sont actuellement réalisées aussi bien pour évaluer sa biodégradabilité que pour améliorer ses propriétés. En effet, des approches

sont testées telles que d'une part la synthèse par voie enzymatique ou la synthèse de stéréocomplexes, et d'autre part la formulation avec des additifs, la production de matériaux composites et nanocomposites, le mélange avec d'autres polymères…

Une des voies les plus communément utilisées pour l'amélioration des propriétés barrière de polymères semi-cristallins est la cristallisation. En effet Michaels et Parker (Michaels, 1959) ont montré en 1959 que la cristallisation du polyéthylène résulte en une diminution des coefficients de solubilité et de diffusion des gaz. Cette tendance a été expliquée par le concept de cristallites imperméables à travers lesquels les molécules diffusantes ne peuvent diffuser et dans lesquelles elles ne peuvent être sorbées. Cet effet de la cristallisation a été montré dans le cas du poly(éthylène téréphtalate) pour lequel le coefficient de perméabilité de l'oxygène a été divisé par deux entre 0 et 38 % de cristallinité (Hu, 2005).

Le PLA est un polymère dont la cinétique de cristallisation est lente. Ceci a pour avantage de pouvoir faire varier son taux de cristallinité. Toutefois, il est difficilement envisageable de pouvoir cristalliser le PLA au cours d'un procédé de mise en forme industriel, tout en conservant des vitesses de production élevées. Afin de remédier à cela, plusieurs stratégies existent pour promouvoir la cristallisation de polymères semi-cristallins, notamment le procédé tel que le mono-étirage, le bi-étirage ou le soufflage et la formulation. Cette dernière permet de maîtriser la morphologie du polymère en ajoutant, par exemple, des agents nucléants et des plastifiants. La plastification et la nucléation du PLA font l'objet de nombreuses publications. Peu en revanche ont porté sur l'effet synergique du plastifiant et de l'agent nucléant sur les propriétés du PLA, et encore moins ont eu pour but d'améliorer des propriétés barrière du polymère.

Ce travail de thèse s'inscrit dans le cadre de l'équipe I2MC « Interaction Matériaux /Milieu au Contact » dont l'objectif est de comprendre les mécanismes qui contrôlent les propriétés barrière ou de sélectivité des matériaux au contact notamment de produits alimentaires. Une thématique « polyesters biodégradables » a été développée au sein de cette équipe en 2007 initiant ainsi ce projet de thèse qui vise à étudier les relations structure-propriétés du PLA. L'influence de la formulation et de la cristallinité sur les propriétés barrière et mécaniques a ainsi été évaluée dans le cas d'un poly(D,L-lactide) (P(D,L)LA).

Ce mémoire est organisé en 5 chapitres s'articulant autour de 6 publications scientifiques (soumises ou acceptées) :

➤ L'étude bibliographique, présentée au chapitre 1, est consacrée dans un premier temps à une présentation générale du PLA (publication n°1). Ainsi, sa synthèse selon 4 voies principales, mais aussi ses propriétés physiques, thermiques et mécaniques sont abordées avant de s'intéresser plus particulièrement à ses applications. Cette revue de la littérature met en évidence un manque de données sur la relation de la structure du PLA avec ses propriétés et ses applications. Dans un second temps, la structure et la cinétique de cristallisation de polymère semi-cristallin sont abordées de manière théorique avant de présenter l'organisation et la cristallisation isotherme du PLA. Enfin, dans un troisième temps, après avoir rappelé les différents facteurs pouvant influer sur les propriétés barrière et avoir présenté quelques méthodes de détermination des coefficients de transport, les propriétés barrière du PLA sont présentées.

➤ Le second chapitre présente les matériels et méthodes utilisés tout au long de ce travail afin de caractériser les films de P(D,L)LA et de déterminer ses propriétés barrière à l'hélium, à l'oxygène, à la vapeur d'eau et à divers composés organiques.

Les résultats expérimentaux sont présentés en 3 chapitres successifs :
➤ Le troisième chapitre aborde l'effet de la formulation sur les propriétés thermiques, mécaniques et barrière du P(D,L)LA (publication n°2) ainsi que l'influence de l'ajout de plastifiant et d'agent nucléant sur la cinétique de cristallisation du P(D,L)LA (publication n°3).

➤ L'effet de la cristallisation sur les propriétés de transport du P(D,L)LA pur et formulé grâce à trois molécules sondes inter-agissant plus ou moins fortement avec la matrice P(D,L)LA (publications n°4 et 5) est étudié dans le chapitre 4. Il y est également question de l'effet du procédé de biétirage sur les propriétés barrière du P(D,L)LA non formulé. (proceeding).

➤ Enfin, le chapitre 5 propose plusieurs méthodes exploratoires de détermination des propriétés de transport dans le P(D,L)LA. Trois types de molécules diffusantes sont étudiés, des composés organiques volatils par un système de perméation semi-dynamique, des molécules fluorescentes par microscopie et des molécules paramagnétiques grâce à un appareil de résonance paramagnétique électronique (publication n°6).

Chapitre 1

-

Synthèse bibliographique

Ce chapitre bibliographique contient et complète le chapitre « Characteristics and Applications of PLA » à paraître dans *Biopolymers : Biomedical and Environmental Applications*, Susheel Kalia & Luc Avérous (Eds). **John Wiley & Scrivener Pub**. Date de publication: 08/**2011**. 600 p.

1.1. Characterization and Applications of PLA

Poly(lactic acid) or poly(lactide) (PLA), has been first reported in 1932 by Wallace Carothers and his co-workers, chemists at DuPont whose aim was to obtain high molecular weight polymers. Their work showed the dimerization of polycondensated lactic acid into lactide and the ring-opening polymerization of lactide (Carothers, 1932). Further work by DuPont, patented in 1954, yielded a high-molecular weight product due to improved lactide purification processes (Lowe, 1954). However, the aliphatic polyester PLA was abandoned because it was considered not sufficiently stable at this time due to its susceptibility to hydrolytic degradation. It was only in the 1960's that interest was renewed because of the advantages of hydrolysable structures perceived to be useful for biomedical applications. In 1972, high-strength, biocompatible fibres for medical resorbable sutures were introduced by Ethicon. Since the 1970's the biomedical applications of PLA are fields of active research and have brought about a number of major developments in controlled drug release or implants. However, the high cost of lactic acid, and therefore of the resulting polymers, restricted however commodity applications. In the late 1980's, advances in the fermentation technique for obtaining lactic acid enabled a substantial increase in world-wide production and a substantial decrease in cost. In 1992, Cargill Inc. patented a solvent-free process and novel distillation technique to convert lactic acid into high-molecular weight polymers based on the ring-opening polymerization (ROP) method. The first industrial production plant of PLA was finished in 2002 and has actually an estimated production potential of 140 ktonnes per year. Several other investments in industrial scale production facilities are underway, which has resulted in PLA being the third most produced bioplastic at present time after starch-based and lignocellulosic materials. PLA is already successfully applied in the biomedical field, and a recent publication has also shown its substitution potential for commodity applications, such as textiles or packaging (Shen, 2010).

1.1.1. Synthesis of PLA

1.1.1.1. Production of lactic acid

The basic constitutional unit of PLA is lactic acid. Lactic acid (2-hydroxy propionic acid) is an hydroxyl acid with an asymmetric carbon atom and exists either as L (+) or D(-) stereoisomer, as shown in Figure 1.1.
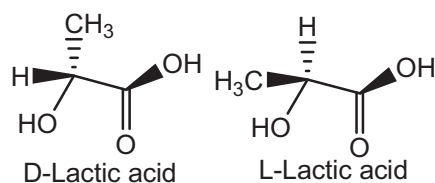
Figure 1.1. Stereoisomers of 2-hydroxypropionic acid (lactic acid).

The L-isomer is produced in humans and other mammals, whereas both the D- and L-enantiomers are produced in bacterial systems. Lactic acid can also be derived chemically from renewable resources such as ethanol or acetaldehyde or from chemicals coming from coal (e.g. acetylene) or oil (e.g. ethylene) (Holten, 1971). However, the large majority of lactic acid produced today is obtained by bacterial fermentation of simple sugars, using homofermentative strains of the genus *Lactobacilli*. The homofermentative pathway yields 1.8 moles of lactic acid per mole of hexose, and conversion rates of glucose are higher than 90 % (Auras, 2004b). Processing conditions are generally batch fermentation at pH of 5.4-6.4, temperature around 40 °C and low oxygen concentration. The lactic acid produced is neutralized with $Ca(OH)_2$ or $CaCO_3$. Strains such as *L. amylophilus*, *L. bavaricus*, *L. casei*, *L. maltromicus*, and *L. salivarius* produce L-lactic acid exclusively, while strains such as *L. delbrueckii*, *L. jensenii*, and *L. acidophilus* yield mixtures of both L- and D-lactic acid. The main carbon sources are glucose and maltose form corn, sugar beet, sugar cane or potato, supplemented with other complex nutrients, supplied by complex sources, such as corn steep liquor or yeast extract (Hartmann, 1998). Down-stream processing includes filtration of the culture broth to remove insolubles and biomass, evaporation, recrystallization, acidification of the calcium lactate by sulphuric acid to yield crude lactic acid. The insoluble calcium sulphate is discarded, which generates one metric tonne of waste ($CaSO_4$ called gypsum) per metric tonne of lactic acid. For use of lactic acid in food and pharmaceutical applications, further purification by distillation is required (Datta, 1995).

Main bottlenecks of the process are the inhibition of bacterial growth at a pH lower than 4, while the pKa of lactic acid is 3.78 causing the need for continuous neutralization of the culture medium. Also, the cost of pre-treatment of raw materials is high because of the need for saccharification to obtain simple sugars, and the cost and waste generation during downstream processing has to be considered as well. To address these points, optimization of production strains and downstream processing is required.

Recombinant strategies have been employed to generate more pH tolerant lactic acid bacteria and to enable the use of complex carbon sources, such as starch or cellulose, or to generate lactic acid producing strains of other microorganisms, such as *Escherichia coli*, *Corneybacterium glutamicum* or yeasts. Okano *et al.* (Okano, 2010) recently published a review about different strategies for strain optimization, showing for example a result from their group in which they redirected metabolic pathways in *L plantarum ΔldhL1* using arabinose coming form hemicellulose in order to obtain efficient production of lactic acid and significantly decrease the by-production of acetic acid. The use of hemicellulose for the fermentative production of chemical building blocks is one of the major challenges for the utilisation of lignocellulosic feedstocks, because pentoses are unavailable to most micro-organisms. The use of *E. coli* and *C. glutamicum* seems to be promising. *E. coli* is, for example, able to grow on simple mineral salt media without the need for expensive nutriments such as vitamin B. However pH tolerance of those bacteria is very low and lactic acid yield needs to be improved (Okano, 2010).

A complementary strategy to increase the efficiency of the lactic acid production is process intensification. Continuous removal of lactic acid or lactate is required, which can be achieved by adsorption, extraction, and membrane separation. Membrane separation has been the object of intensive research in recent years, because it cumulates the advantages of not requiring process steps for regeneration and recycling, and offers the possibility of cell recycling into the bioreactor to maintain high cell densities. Main techniques are microfiltration, ultrafiltration, nanofiltration, reverse osmosis and electrodialysis. One of the main challenges is membrane fouling by microbial cells and proteins. Furthermore, a selective separation of lactic acid is desirable, which also allows also for the recycling of unused nutrients into the bioreactor. However, the retention of neutral solutes, such as glucose, by nanofiltration or reverse osmosis in the presence of charged ones generally decreases, probably because of increased charge density in the presence of charged solutes (Pal, 2009). To overcome these drawbacks, multi-stage systems are probably required. One proposal is a two-step process with first microfiltration, which is less susceptible to fouling, and following

it with nanofiltration, which is capable of separating lactic acid in the permeate stream and while retaining useful solutes for recycling into the bioreactor (Pal, 2009).

1.1.1.2. Synthesis of PLA

Lactic acid based polymers can be synthesized by different routes, as shown in Figure 1.2. Globally, there are two routes to obtain high molecular weight polymers: direct lactic acid condensation, often including the use of coupling agents to increase molecular weight and ring-opening polymerization (ROP) of lactide (Garlotta, 2001). The nomenclature used in literature for these polymers is sometimes contradictory. Polymers derived from direct polycondensation should be referred to as poly(lactic acid) and polymers synthesized by ROP of lactide as poly(lactide). Both types are generally named PLA. In the function of stereochemistry of polymer chain, different types are obtained and summarized in Table 1.1.

Table 1.1. Stereoisomers of PLA.

PLA form	Structure
Isotactic poly(L-lactide), PLLA	LLLLLLLL
Isotactic poly(D-lactide), PDLA	DDDDDDDD
Random optical copolymers	Random level of meso or D-lactide in L-lactide or D-lactic acid in L-lactic acid
Stereocomplex PLLA/PDLA	LLLLLLLL mixed with DDDDDDDD
PLLA/PDLA stereoblock complexes	LLLLLLLLDDDDDDDD
Syndiotactic poly(meso-lactide)	DLDLDLDL
Heterotactic poly(meso-lactide)	Al-centered R-chiral catalyst LLDDLLDDLLDD
Atactic poly(meso-lactide)	No stereocontrol
Atactic poly(lactide), PDLLA	No stereocontrol

PLA polymerization by direct polycondensation (route 1 in Figure 1.2), the least expensive route, yields low molecular mass polymers (Hyon, 1997), having mechanical properties which are insufficient for most applications. To increase molecular weight, chain coupling agents, such as anhydrides, epoxides or isocyanates, are added. They react preferentially with the hydroxyl or the carboxyl group leading to different reaction rates. An answer to this problem is the polycondensation of lactic acid in the presence of diacids or diols, being difunctional monomers, which leads to the formation of telechelic prepolymers, being either all hydroxyl or all carboxyl terminated (Hiltunen, 1996). However, a purification step has to be performed to remove unreacted coupling agents and prepolymers (Garlotta, 2001). The multiplication of the steps for this polymerization induces an enhancement of the production cost.

Azeotropic dehydration and condensation polymerization (route 2 in Figure 1.2) yields directly high molar mass polymers. The procedure, patented by Mitsui Toatsu Chemicals (Enomoto, 1994; Kashima, 1995), consists in the removal of condensation water via a reduced pressure distillation of lactic acid for 2-3 h at 130 °C. The catalyst (in high amounts) and diphenyl ester are added and the mixture is heated up to reflux for 30-40 h at 103 °C. Polycondensated PLA is purified to reduce residual catalyst content in the ppm range (Auras, 2004b; Avérous, 2008; Garlotta, 2001).
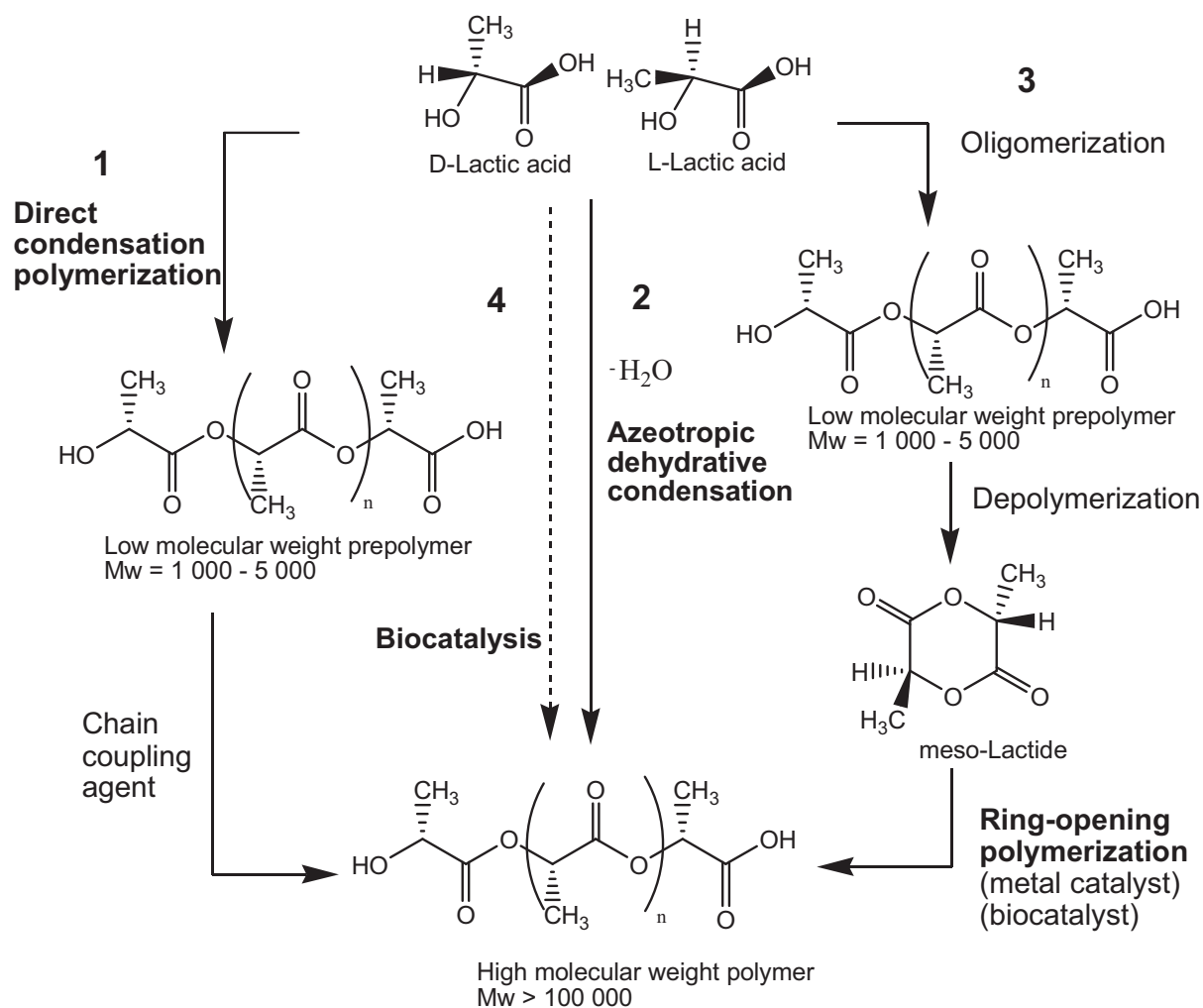
Figure 1.2. Routes for the synthesis of PLA.

Ring Opening Polymerization (ROP) of lactide (route 3 in Figure 1.2) is today by far the route that is most employed to obtain high molecular weight polymers. This route requires several steps. First, a direct polycondensation reaction is carried out to produce a low molar mass prepolymer (Hiltunen, 1997). The prepolymer is depolymerized in order to obtain lactides (3,6-dimethyl-1,4-dioxane-2,5-dione), dehydrated cyclic dimers, which are the

starting material for ROP into high molar mass polymers. Depolymerization is done under reduced pressure, high temperature and distillation of the lactide product. Three forms of lactide: L,L-lactide, D,D-lactide and D,L-lactide (meso-lactide) (Figure 1.3) are obtained as a function of the stereochemistry of the feedstock, temperature and catalyst (Garlotta, 2001). Polymerization through lactide formation is currently used by Cargill (NatureWorks[TM]), which patented a continuous process (Gruber, 1992; Gruber, 1994).

L,L-lactide   D,D-lactide   Meso- (or L,D-) lactide
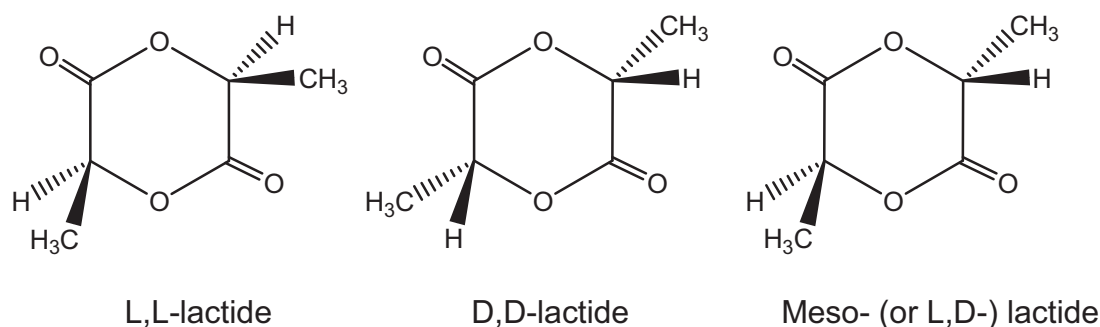
Figure 1.3. Stereoforms of lactide (3,6-dimethyl-1,4-dioxane-2,5-dione).

ROP is carried out in solution, in the melt, in the bulk or in suspension. The involved mechanism can be ionic (anionic or cationic), coordination-insertion or free-radical polymerization (Södergård, 2002). The cationic polymerization is initiated by only two catalysts, trifluoromethane-sulphonic acid and its methyl ester (Avérous, 2008; Garlotta, 2001). Initiators such as potassium methoxide, potassium benzoate, zinc stearate, *n-*, *sec-*, *ter-*butyl lithium or 18-crown-6-ether complexes are added for the anionic polymerization to induce a nucleophilic reaction on the carbonyl to lead to an acyl-oxygen link cleavage. According to Jedkinski *et al.* (Jedlinski, 1991; Kurcok, 1995) only the primary alkoxides, such as the first mentioned catalyst, can yield polymers with negligible racemization, transesterification and termination (Garlotta, 2001).

For a large scale production, the melt and bulk polymerization is preferable to the solution process. Tin (Kowalski, 2000), zinc, iron (Stolt, 1999), aluminium (Dubois, 1996) or other heavy metal catalysts with tin(II) and zinc are used to produce the high molecular mass polymers. The best results are obtained with tin oxide and octoate at 120-150 °C with conversions above 90 % (Garlotta, 2001). Stannous octoate or Stannous-2-ethyl hexanoate is an efficient catalyst for PLA, FDA approved due to its low toxicity, and capable of inducing the production of high mass polymers with low racemisation (Garlotta, 2001). However the reaction mechanism is still being debated. Two mechanisms are proposed to explain the reaction. The first one postulates that the reaction is primed by monomer or impurities and

catalysed by a Lewis acid, stannous octoate (Kricheldorf, 1995; Penczek, 2000). The second one corresponds to the mechanism of coordination-insertion which takes place in two steps: (i) covalent bonds of a complex formed from a monomer and an initiator rearrange, (ii) a second monomer reacts with this intermediate, which makes possible the ring-opening by the cleavage of the oxygen-acyl bond (Avérous, 2008; Kowalski, 2000; Stridsberg, 2000). Reaction time, temperature, ratio monomer/catalyst and catalyst type, chosen for the polymerization, are limiting parameters for yield, degradation and polymerization products.

In the case of biomedical applications, metallic impurities coming from the organo-metallic catalysts of ROP may be of concern, because they can accumulate within matrix remnants after degradation (Schwach, 1996). A recent strategy to reduce such problems and to shift polymer synthesis further towards green chemistry is the use of enzymes as catalysts. Kobayashi and Makino (Kobayashi, 2009) published a recent general review on the topic and Albertsson and Srivastava (Albertsson, 2008) focused more precisely on ROP. In most cases, as in the case of PLA, enzymes used are lipases. Lipases are the most versatile class of biocatalysts in the synthesis of organic compounds, because they can work with a wide variety of substrates and are stable in organic solvents and at elevated temperatures. Being part of the hydrolase family, lipases catalyze the hydrolysis of fatty acid esters. In organic solvent, they can be used for the catalysis of esterification and transesterification reactions. Matsumura et al. (Matsumura, 1997) reported the lipase PS catalyzed ROP of lactide in the bulk yielding molecular weights (M_w) up to 1.26×10^5 g.mol^{-1}. Meso-lactide gave higher molecular weight than L,L-lactide or D,D-lactide. Recently, Novozyme 435 was used as a catalyst in toluene solution. The enantioselectivity of the enzyme enabled the selective polymerization of D,D-lactide, but no polymerization of L,L-lactide or meso-lactide occurred. However, molecular weight was quite low ($M_n = 3\ 300$ g.mol^{-1}) (Hans, 2009). Novozyme 435 seems to catalyze the ROP of L,L-lactide in ionic liquids. In '[HMM]''[PF$_6$]' at 90 °C, yields up to 65 % could be obtained, but still molecular weight remained low (max. $M_n = 3.78 \times 10^4$ g.mol^{-1}) (Chanfreau, 2010). Generally speaking, the use of lipase in ROP still suffers from low yields and/or low molecular weights, but the problems are the subject of an actual research effort.

Whole-cell synthesis of lactate containing polyesters is a new route (route 4, Figure 1.2) of research that is still in the beginning stages. Taguchi et al. reported in 2008 (Taguchi, 2008) the discovery of a lactate-polymerizing enzyme, being a PHA synthase with acquired polymerizing activity of the lactide in lactide-CoA. PhaC1$_{PS}$STQK is an engineered class II

PHA synthase form *Pseudomonas sp* and is able to form a co-polymer P(LA-*co*-3HB) inside engineered *Escherichia coli*. Polymer cell content in *E.coli* amounted to 51 % of the dry mass and LA molar fraction in the polymer was 28 %. At this stage, yields and lactide fraction appear moderate, however, the groundwork has been laid for future mutation/selection or modified strategies of selection in similar enzyme lines for generating a lactide enriched polymer, and eventually a PLA homopolymer.

Reactive extrusion is a continuous process to polymerizing the lactic acid by ROP in the molten state in one single process step. However, this method requires a fast reaction rate which is determined by the residence time in the extruder (typically 7 min). The extruder presents a sophisticated design of screw which makes it possible to assure the blending and the shearing in the molten state. A common design is an intermeshing co-rotating twin-screw extrusion (Raquez, 2008). The short reaction times require efficient catalysts with reduced side-reactions such as inter- and intramolecular transesterification due to the high reaction temperatures. To limit these reactions a Lewis acid, triphenylphosphine, in an equimolar complex with $Sn(Oct)_2$, was used to enhance the polymerization rate and delay the occurrence of undesirable back-biting reactions for a monomer-catalyst molar ratio of at least 5000 (Degee, 1999; Jacobsen, 2000). Jacobsen *et al.* showed that the number average molecular weight, around 80 000 $g.mol^{-1}$, the dispersity and the degree of conversion vary according to the mass flow rate and the screw speed (Jacobsen, 2000).

Stereocomplexation

Recently stereocomplexes of PLA appeared on the market and lead to promising applications in durable devices (see below: PLA applications). The stereocomplexes are defined as the association of polymers with different tacticity or conformation. Three synthesis routes are used to produce a PLA stereocomplex, either in solution or in melt state during polymerization or hydrolysis. The complexe formation begins from (i) two monomers (L-lactide and D-lactide), (ii) polymer and monomer or (iii) two polymers (PLLA and PDLA). This synthesis is often performed with stannous tin and 1-dodecanol (lauryl alcohol) as initiator or co-initiator of the reaction (Tsuji, 2005; Tsuji, 1999; Tsuji, 2004). According to Tsuji *et al.* (Tsuji, 2005), some other parameters affect the formation of stereocomplexes:

- Equimolarity of the blending of D-lactide and L-lactide units.
- Low molecular weight for both the isomeric polymers.
- Sufficiently long sequences of both isotactic L-lactide and D-lactide units.

Moreover, the solvent and the blending mode are also parameters which strongly influence the stereocomplexation (Tsuji, 1999).

1.1.2. PLA physical properties

PLA properties are strongly dependent on the molecular weight (Garlotta, 2001) and stereochemistry, being L- and D-lactic acid content (Kolstad, 1996). Indeed a PLLA or PDLA homopolymer can develop a crystalline structure whereas an atactic polymer whose L-lactic acid content is below 93 % remains amorphous. Consequently, the polymer structure, crystalline or amorphous form, can be at the origin of modification in the thermal, optical, physical, mechanical and barrier properties of PLA.

1.1.2.1. Density

Few values of the density of PLA are shown in the literature. Auras *et al.* reported that the density of amorphous PLLA is 1.248 whereas it is 1.290 for the crystalline PLLA (Auras, 2004b; Avérous, 2008; Madhavan Nampoothiri, 2010). NatureWorks LLC gives, according to the polymer type and the L-lactic acid content, a density value between 1.24 and 1.25 for its amorphous PLA grades (Shen, 2009). In agreement with these values, Auras *et al.* measured 1.240 ± 0.002 for poly(98% L-lactide) and 1.243 ± 0.002 for poly(94% L-lactide)(Auras, 2004b).

1.1.2.2. Solubility

The solubility of PLA is dependent on the molar weight and the crystallinity degree of the polymer. For the enantiopure PLA, chloroform and other chlorinated organic solvent, furan, dioxane, dioxolane and pyridine are good solvents. In addition to these organic solvents, the non enantiopure PLA is soluble in ethyl acetate, dimethylsulfoxide, tetrahydrofuran, acetone, xylene, methyl ethyl ketone, ethyl lactate and dimethylformamide. However, lactic acid based polymers are non soluble in water, alcohol (e.g. ethanol, methanol), isopropyl ether and unsubstituted hydrocarbons (e.g. cyclohexane, heptane) (Södergård, 2002).

1.1.2.3. Optical properties

The optical properties of PLA have been measured. The refractive index of a polymer is characteristic of its structure and so, for PLA, is directly correlated with its isotropy. Tsuji *et al.* (Tsuji, 1994) measured this index at 25 °C, at a PLA concentration of 1 g.L^{-1} in chloroform at 589 nm to -156° and 156°.dm^{-1}.g^{-1}.cm^3 for PLLA and PDLA respectively.

In the range 190-800 nm, PLA has been compared to other standard commercial films (Figure 1.4). No UV is transmitted by PLA in 190-220 nm range (UV-C). However, from 225 nm, the amount of UV light transmitted increases significantly. So at 300nm, 95 % of UV light is transmitted. It appears that PLA transmits less UV-C than LDPE but much more UV-B and UV-A than PET and PS.
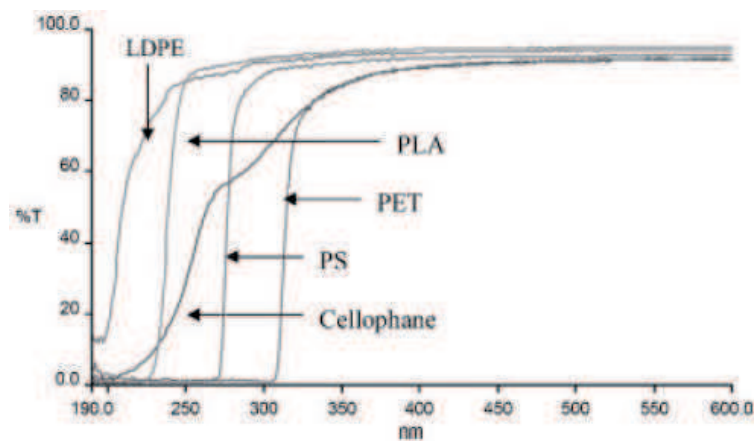
Figure 1.4. Transmission versus wavelength for LDPE, PLA(98% L-lactide), Cellophane, PS and PET (Auras, 2004b).

The infrared spectrum of commercial PLA was determined by Fourier Transform Infrared (FT-IR). Table 1.2, which contains data published in the review paper of Auras *et al.* (Auras, 2004b) and by Furukawa *et al.* (Furukawa, 2005), summarizes the main PLA absorption bands.

Two bands are related to the crystalline and amorphous phase of PLA (98% L-lactic acid): one band at 871cm^{-1} which is assigned to the amorphous phase and one band at 756 cm^{-1} which is related to the crystalline phase (Auras, 2004b). As shown in Table 1.2 Furakawa *et al.* (Furukawa, 2005) showed that some other bands are linked to the crystallinity of PLA.

Table 1.2. Infrared Spectroscopy peak band assignment for PLA.

Assignment	Peak Position (cm^{-1})	
	Furukawa *et al.* (Furukawa, 2005)	Auras *et al.* (Auras, 2004b)
-OH stretch (free)		3 571
-CH- stretch		2 997 (asym), 2 946 (sym), 2 877
-C=O carbonyl stretch	1 752 (C), 1 744 (A)	1 748
-CH3 bend	1 450 (asym), 1 380 (sym), 1 356 (sym, C)	1 456
-CH- deformation (symmetric and asymmetric bend)	1 356, 1 265 (A)	1 382, 1 365
-C=O bend		1 225
-C-O- stretch	1 265, 1 210 (C), 1 179, 1 080	1 194, 1 130, 1 093
-OH bend		1 047
-CH3 rocking modes	1 125	956, 921
-C-C- stretch	1 044	926, 868

C = Crystalline; A =Amorphous.

1.1.3. Microstructure and Thermal properties

PLA undergoes several phase transitions during a temperature ramp depending on its L-lactic acid content, its crystallinity degree and its preparation process. A typical DSC signal of the semi-crystalline polyester PLLA is shown in Figure 1.5. Upon heating from 0 °C, the polymer is in a glassy state at low temperature, becomes rubber once the glass transition (T_g) is over and then crystallizes at its cold crystallization temperature (T_{cc}) and finally melts at its melting temperature (T_m). Upon cooling, PLLA crystallizes at higher temperature than T_{cc} for a same heating and cooling rate.
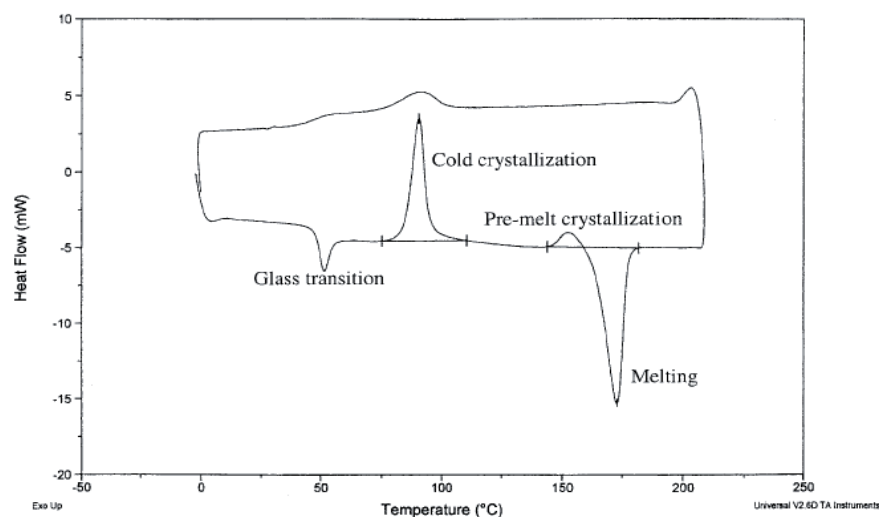
Figure 1.5. DSC trace for neat PLLA displaying the glass transition, cold crystallization, premelt crystallization and melting (Ljungberg, 2002).

The crystallinity of PLA depends largely on its architecture, i.e. the stereochemistry of the monomers which constitute the polymer. Atactic PLA containing more than 93 % of L-lactic acid is semi-crystalline in contrast to atactic PLA with L-lactic acid between 50 and 93 % which is amorphous. D-lactic acid, in high proportion, induces some imperfections which prevent polymer crystallization (Auras, 2004b). The crystalline phase proportion varies according to the L-lactic acid content. The higher the L-lactide percentage is, the more the chains can be organized and crystallize. So the PLLA crystallinity degree can reach 70 % (Di Lorenzo, 2006), whereas a PDLLA with a L-lactic acid content close to 93 % can crystallize up to 45 %.

1.1.3.1. Glass transition

The glass transition temperature (T_g) is the temperature at which the amorphous phase of the polymer changes from the glassy to the rubbery states. The glass transition temperature of amorphous PLA lies between 55 and 60 °C (Auras, 2004b; Baiardo, 2003; Coltelli, 2008; Södergård, 2002) and is function of the PLA molecular weight and stereochemistry. An endothermic peak is usually superimposed on the glass transition, whose intensity depends on the thermal history. Arnoult et al. showed that ageing PLA at 45 °C from 0 to 1000 h results in the appearance of more and more intense relaxation peak (0 to 4 $J.g^{-1}$) and a T_g shift of 10 °C (Arnoult, 2007). This enthalpic relaxation, due to cooperative rearranging movement, is

a non linear and non exponential phenomenon (Hutchinson, 2003, 2009). It disappears when the sample is heated over the glass transition temperature (Auras, 2004a; Solarski, 2005). The T_g of semi-crystalline PLA shifts to higher temperature compared to amorphous PLA, being between 60 and 80 °C.

1.1.3.2. Crystallization

The PLA crystallization has been widely investigated but most of the studies have been carried out on PLLA. The crystallization rate of PLLA is rather slow and dependent on its molecular weight (Garlotta, 2001) and its enantiomeric purity (Huang, 1998; Kolstad, 1996; Ling, 2006). This material crystallizes usually between 85 and 150 °C but its fastest rate of crystallization occurs between 95 and 115 °C (Di Lorenzo, 2005). The value of the crystallization half time ($t_{1/2}$) varies according to author. So in the temperature range 95-115 °C, the $t_{1/2}$ of PLLA for crystallization from the melt varies between 1.5 min to 5 min (Day, 2006; Di Lorenzo, 2006; Tsuji, 2006c) whereas Day *et al.* showed that the $t_{1/2}$ of PLLA for crystallization from cold state is close to 3 min. Nevertheless, despite a large range of $t_{1/2}$ values, the lowest one is obtained around 110 °C. So the crystallinity degree of PLLA is strongly dependent on the crystallization time and temperature but can reach 45-70 % in the appropriate conditions (Day, 2006; Tsuji, 1995). The crystallinity degree (χ_c) is calculated according to the Equation 1.1 in which ΔH_m is the measured enthalpy of melting, ΔH_c, the measured enthalpy of cold crystallization and $\Delta H_m^{100\%}$ the enthalpy of melting per gram of repeating unit of the perfect crystal of infinite size. This latter feature has been estimated by Fischer at 93 J.g^{-1} (Fischer, 1973) for PLLA. This value is the one most often used but other values can be found in literature (91 J.g^{-1} (Pyda, 2004), 106 J.g^{-1} (Sarasua, 1998), 146 J.g^{-1} (Loomis, 1990) and 203 J.g^{-1} (Jamshidi, 1988)).

$$\chi_c = \frac{\Delta H_m - \Delta H_{cc}}{\Delta H_m^{100\%}} \tag{1.1}$$

1.1.3.3. Melting

The melting temperature (T_m) of PLA occurs between 130 and 180 °C according to the L-lactide content and the crystals formed during crystallization. The presence of meso-lactide in

the PLA structure induces a decrease in the melting temperature according to the Equation 1.2 where W_m is the meso-lactide fraction in the matrix and 175 is the melting temperature of PLLA (Auras, 2004b).

$$T_m (°C) = 175 - 300 W_m \qquad (1.2)$$

It is therefore possible to widely reduce the melting temperature by adding D-lactide in the polymeric structure. Nevertheless the melting temperature is also dependent of the molecular weight according to Tsuji and Ikada (Tsuji, 1995). Therefore T_m increases with increasing M_w to an asymptotic value.

The melting temperature of PLLA can be increased 40-50 °C up to 200 °C by physically blending the polymer with PDLA (Tsuji, 2004).

The melting peak is simple or double according to the crystalline forms and the lamellae thickness of the spherulites by the Gibbs-Thomson relation as shown in Equation 1.3:

$$T_f = T_f^{\infty} \left[1 - \frac{2\sigma_e}{L_c \Delta H_f^{\infty} \rho_c} \right] \qquad (1.3)$$

The melting temperature for the thermodynamic equilibrium, T_f^{∞}, representing the melting point of an infinite size and molecular mass crystal, equals to 207 °C for PLLA (Garlotta, 2001). This value of T_f^{∞} is estimated at 279 °C for stereocomplexes of PLA by extrapolation of T_f^{∞} values for different optical purities (Tsuji, 1996). The melt enthalpy for an enantiopure PLA of 100 % crystalline has been estimated at 93 J.g^{-1} (Fischer, 1973). The crystal density, ρ_c, is reported to be 1.29 and the surface energy for the extremity of the lamellae, σ_e, is 53.6×10^{-11} J.m^{-2}.

1.1.4. Mechanical properties of PLA

The mechanical properties of PLA, which have been extensively studied, are dependent on the production process and the amorphous or semi-crystalline state of the sample. Amorphous PLA presents a tensile modulus between 2.05 and 3.25 GPa (Coltelli, 2008; Hu, 2003c; Jacobsen, 1999; Martin, 2001; Martino, 2009; Pillin, 2006; Sheth, 1997), except according to Murariu *et al.* who showed a PLA with 1.02 GPa tensile modulus (Murariu, 2008). This considerable range is due to the tensile test rate which varies from 1 mm.min^{-1} to 50 mm.min^{-1}. The yield stress and the strain at break lie between 32 and 68 MPa and between

3 and 20 %, respectively (Coltelli, 2008; Hu, 2003a; Kulinski, 2005; Labrecque, 1997; Martino, 2009; Murariu, 2008; Rhim, 2006; Sheth, 1997; Yu, 2008). The crystallization of neat PLA slightly modifies the mechanical properties. According to Kulinski and Piorkowska (Kulinski, 2005), the cold crystallization induces a slight decrease in the yield stress and strain at break. However Perego *et al.* (Perego, 1996) did not notice this modification in the stress and strain whereas they showed an increase in the modulus of elasticity and in the impact resistance, presumably due to the crosslinking effects of the crystalline domains. Perego *et al.* (Perego, 1996) also showed an influence of the molar mass of the amorphous polymer on the impact resistance and the flexural strength which was multiplied by 1.5 to 2 when the molecular mass was raised from 23 000 to 66 000 g.mol^{-1}. These evolutions are the same when the samples are annealed.

The comparison of two grades of PDLLA, one for general purpose and the other one for injection, showed a possible difference in the modulus which can be due to a molecular mass discrepancy. Moreover the comparison of the mechanical properties of oriented and unoriented films displayed an increase in the elongation at break with orientation.

Table 1.3. Mechanical properties of polymers.

Polymer	Modulus of elasticity (GPa)	Stress at yield (MPa)	Strain at break (%)
PET(Auras, 2003)	2,8-4,1	275	60-165
Bioriented PS(Auras, 2003)	3,2	55-82	3-40
HDPE(Petersen, 2001)	-	38 ± 11	586 ± 47
HDPE(Walker, 2007)	0,95	24,5	
LDPE (Petersen, 2001)	-	25 ± 7	706 ± 77
PP(Wang, 2003)		44,5	20
PLA (98% L-lactic acid)(Auras, 2003)	2,11	72	10,7
PHB(Baltieri, 2003)	0,911 ± 0,020	31,0 ± 0,3	7,0 ± 0,1

At room temperature, the mechanical properties of PLA are close to the one of PS but smaller than the one of PET (Table 1.3). Polyolefins present reduced stress at yield compared to PLA but the strain at break of LDPE and HDPE are much higher than the one of PLA. Compared to another biobased polymer, poly(hydroxybutyrate) (PHB), PLA shows better mechanical properties with higher modulus of elasticity and stress at yield.

The influence of plasticizers on the mechanical properties of PLA has been extensively studied. Various plasticizer have been tested with PLA such as, e.g., glycerol, PLA oligomers,

poly(ethylene glycol) monolaurate (Martin, 2001), triacetine (Ljungberg, 2003a; Murariu, 2008), diethyl bishydroxymethyl malonate (Ljungberg, 2004), poly(1,2-butanediol), dibutyl sebacate, acetyl glycerol monolaurate (Pillin, 2006), poly(propylene glycol) (Kulinski, 2006; Piorkowska, 2006) and polyadipates (Martino, 2009; Martino, 2006; Murariu, 2008). However, only a few substances brought about substantial improvements of mechanical properties. The two most used plasticizer are poly(ethylene glycol) (PEG) (Baiardo, 2003; Hu, 2003b; Jacobsen, 1999; Kulinski, 2005; Martin, 2001; Pillin, 2006; Sheth, 1997) with variable molecular masses and citrate derivatives, in particular acetyl tributyl citrate (ATBC) (Baiardo, 2003; Labrecque, 1997; Ljungberg, 2003a; Murariu, 2008; Yu, 2008). To observe significant modification of the mechanical properties, the plasticizer content in PLA should be around 20 %. After plasticization, the modulus of elasticity and the yield strength decrease whereas the stress at break increases dramatically. At 20 % ATBC content in PLA, the material presents a strength at break between 23.1 and 30 MPa, a modulus of elasticity between 0.1 and 0.27 GPa and a strain at break above 298 % (Baiardo, 2003; Labrecque, 1997; Murariu, 2008). As ATBC, PEG induces an increase in the stress at break and a decrease in the strain and in the modulus of elasticity. However, at concentration which is dependent on the molecular mass, a phase separation is observed. The higher the molecular weight, the lower the plasticizer content is at which a phase separation is observed. For this reason, the low molecular mass of poly(ethylene glycol) is preferentially used for plasticization. The addition of PEG at 20 %, whose molecular mass is 400 g.mol^{-1}, leads to a strength at break around 16 MPa, a strain at break between 21.2 and 71 % and a modulus of elasticity around 0.5-0.6 GPa.

1.1.5. Degradation behaviour of PLA

The degradation behaviour of PLA has been subject to extensive study, because it is one of the primary functions of the polymer giving rise to applications. Hence, degradation can be either desired, in the case of biomedical applications or for biodegradation, or unwanted when it takes place during processing. Degradation of PLA can be either abiotic or biotic, the latter being a process involving biocatalysts.

1.1.5.1. Thermal degradation

Thermal degradation is an abiotic process taking place mainly during processing, and is therefore highly unwanted. Generally speaking, aliphatic polyesters as PLA have no high thermo-stability. Degradation processes can already start at temperatures as low as 215 °C (Kopinke, 1996), while main degradation is observed by thermogravimetric analysis to extent between 215 and 370 °C (Carrasco, 2010; Gupta, 1982a; Kopinke, 1996). The thermal decomposition peak lies at approximately 360 °C (Carrasco, 2010; Kopinke, 1996). Carrasco *et al.* (Carrasco, 2010) observed moreover, that thermal stability increased with increasing molecular weight. In the case of the α-hydroxyester PLA, it was concluded that the carbonyl-carbon – oxygen linkage was the most likely to break upon heating (Gupta, 1982b) and the kinetics being first order (Gupta, 1982a). The mechanisms of the thermal degradation are rather complex, involving thermohydrolysis by trace amounts of water, zipper-like depolymerization, inter- and intra-molecular transesterification, and oxidative random main chain scission (Södergård, 2002). Moreover, reactive end groups, residual catalyst (Kopinke, 1996; Zhang, 1992), unreacted starting monomer and impurities have been reported to enhance the PLA thermal degradation (Hyon, 1998; Kopinke, 1996). Hydrolysis of PLA during processing is one of the main factors of decrease in molecular weight, as observed by several authors (Taubner, 2001; von Oepen, 1992; Wang, 2008). Thus, careful drying of PLA granules is of importance in the extrusion process for minimizing process temperature and residence time. Kopinke *et al.* (Kopinke, 1996) proposed that PLA also degrades through intra- and interchain transesterification, in accordance with the results of McNeill and Leiper (McNeill, 1985), through cis-elimination and through radical and non-radical reactions, which yields CO, CO_2, acetaldehyde, methylketene, acrylic acid and acyclic oligomers. McNeill and Leiper (McNeill, 1985) and Jamshidi *et al.* (Jamshidi, 1988) showed the importance of non-radical backbiting ester exchange involving terminal hydroxyl groups. Additives, such as deactivators of remaining catalysts or the derivation of hydroxyl end groups can increase PLA melt stability (Jamshidi, 1988; McNeill, 1985; Sodergard, 1994). Tsuji and Fukui (Tsuji, 2003) showed that the formation of a stereocomplex PDLA/PLLA enhances the thermal stability below 260 °C. Beyond that temperature, no advantage of the blended films was found, which the authors attributed to the breaking of the stereocomplex, and thus to returning to the properties of single PLA chains.

1.1.5.2. Hydrolysis

Hydrolysis is the main route to PLA degradation. It can be either (i) abiotic and undesired, as in the case of thermohydrolysis during processes, or (ii) abiotic and desired, as in the case of hydrolysis under physiological conditions in biomedical applications, or (iii) biotic and desired, as in the case of biodegradation by microorganisms. Hydrolysis kinetics of PLA in mild temperature conditions (T < 40 °C), as they exist in a physiological environment, are of dramatic importance for the design of products, such as surgical implants or drug delivery devices. Upon immersion in an aqueous environment, water penetrates only into the amorphous phase, because it cannot penetrate the crystallites. This yields primary degradation of amorphous domains, therefore hydrolysis is considered to be a bulk erosion process (Hakkarainen, 1996). In the presence of water and a catalyst, ester hydrolysis occurs, bringing about decrease of molecular weight. Once oligomers are small enough to dissolve, mass loss of the polymer sample is observed (Pitt, 1981). Ester hydrolysis can be either acid- or base-catalyzed. De Jong *et al.* (de Jong, 2001) recently studied the degradation of PLA oligomers as a function of pH. They proposed the following mechanism shown in Figure 1.6.

Before the polymer sample loses weight, carboxylic acid end groups accumulate in the amorphous phase, having an autocatalytic effect. Therefore, the degradation of amorphous samples proceeds more rapidly in the centre than at the surface of the specimens (Li, 1990). Degradation kinetics are furthermore dependent on initial crystallinity and, of course, temperature. Moreover, degradation induces crystallization of PLA (Li, 1990). For exemple, the complete degradation of PLLA Bioscrew can take 4 years (Barber, 2000). PLLA rod specimens were tested *in vivo* and *in vitro* under physiological conditions. No weight loss was obtained *in vivo* for 44 weeks (Weir, 2004a), while the polymer was degraded in 25 days at 70 °C and similar pH *in vitro* (Weir, 2004b). However, the use of high temperatures in order to predict the degradation kinetics needs to be carefully validated, because activation energies change significantly beyond the glass transition of the polymer (Lyu, 2007).

There has been evidence of enzymatic degradation, where the main mechanism is hydrolysis, in microbial proteinases, esterases and lipases. Different enzymes are described in a recent review (Madhavan Nampoothiri, 2010). MacDonald *et al.* (MacDonald, 1996) investigated the effects of stereochemistry and crystallinity on the degradation of PLA by proteinase K. The enzyme showed a large substrate tolerance. Amorphous films of PDLLA with L-lactide contents ranging from 80 % to 95 % exhibited film weight loss rates that were nearly

identical. Proteinase K was, however, sensible to the unit distribution of the D and L stereoisomers. Films prepared by L-lactide/meso-lactide copolymerization showed slower weight loss rates compared to L-/D-lactide copolymerizations. Moreover, proteinase K proved to be very sensitive to crystallization, which strongly decreased the degradation kinetics. Biaxial orientation has also a retarding effect on the enzymatic degradation of PLLA by proteinase K, which also seems to be more important than the effect of crystallinity (Tsuji, 2006a). Different hypotheses were formulated to explain this observation: a diminished attachment of the enzyme to strained chains, decreased cleavage of strained chains, or the observation that action was located exclusively at the surface, while in non-oriented samples degradation proceeded beneath the spherulitic crystalline residues (Tsuji, 2006a).
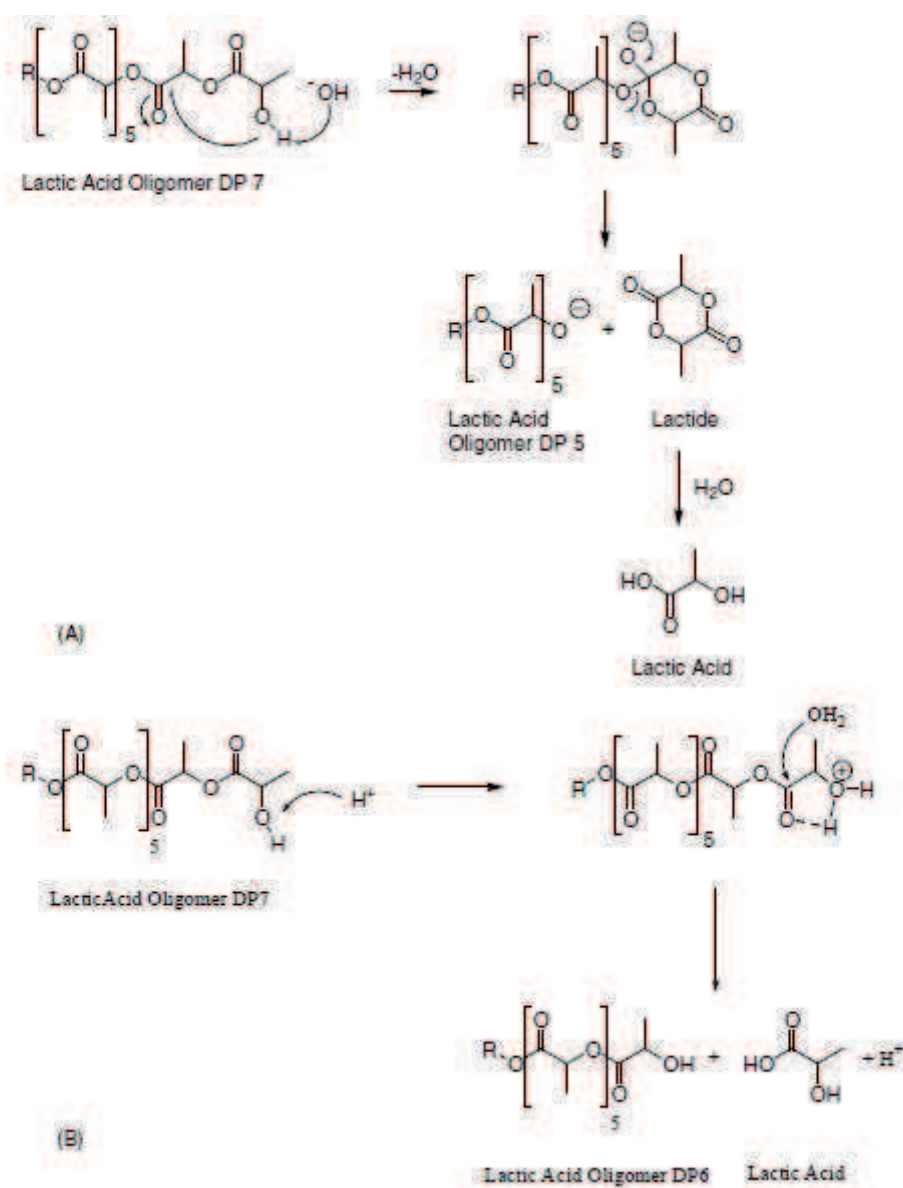
Figure 1.6. Suggestion for hydrolysis mechanisms of PLA in alkaline solution (A) and in acid solution (B). adapted from De Jong *et al.* (de Jong, 2001).

1.1.5.3. Biodegradation

Biodegradability of polymers is a multifunctional property referring to end-of-life options of materials in different biological environments (e.g. composting, anaerobic digestion). According to the ATSM standard D-5488-94-d, biodegradation is defined as being "a process capable of the decomposition of materials into carbon dioxide, methane, water, inorganic compounds, or biomass in which the predominant mechanism is the enzymatic action of microorganisms, that can be measured by standard tests, in a specified period of time, reflecting available disposal conditions." Biodegradation can therefore involve different mechanisms, such as mainly dissolution, hydrolysis and enzyme-catalyzed degradation, but also oxidation, photolysis or radiolysis. In the case of PLA, an abiotic (catalyzed) hydrolysis step leads to the decrease of the molecular weight of the polymer. Once oligomers form, they are able to dissolve and be attacked and assimilated by microorganisms, which will metabolize them into CO_2 and water under aerobic conditions (Auras, 2004b; Pitt, 1981). Biodegradation of PLA has been studied in soil, in sea water and in compost. It has been found, not surprisingly, to depend on the structure (molecular weight, stereochemistry) and the crystallinity of the polymer. Increase in molecular weight and crystallinity considerably slow down biodegradation (Tokiwa, 2006). Furthermore, environmental conditions, such as temperature and water availability have a strong influence on biodegradation time. Biodegradation of PLA has been studied in different environments. In soil activation the time can be very long. For example, in one study no degradation was observed within 6 weeks (Ohkita, 2006), in another study a weight loss between 20 and 75 % in function of PLA stereochemistry was found after 20 weeks (Urayama, 2002). Tsuji *et al.* (Tsuji, 2002a) investigated the degradation of aliphatic polyesters in seawater. In static conditions no weight loss of PLLA could be observed in 10 weeks, elsewhere the weight loss was accelerated upon immersion into the sea inside mesh grids. However, loss of particles due to mechanical shear and breakdown could not be excluded in this case (Tsuji, 2002b). Many studies of PLA biodegradation in composting environment were carried out. Ghorpade *et al.* (Ghorpade, 2001) showed full degradation of PLA in compost mixed with yard waste within 30 days at 52 °C, although high PLA concentration (30 % w/w) retarded the biodegradation because of the drop in pH in the compost. Figure 1.7 shows the biodegradation of PLA bottles in real compost conditions (Kale, 2007b). PLA bottles were shown to biodegrade to 80 % upon 58 days at 58 °C under simulated composting conditions according to ASTM and ISO standards (Kale, 2007a). Furthermore, creating of composite structures with PLA has been shown to

accelerate biodegradation. Some examples are the increase of the biodegradation kinetics for PLA/wheat straw and PLA/ soy straw composites (Pradhan, 2010) or PLA/ layered silicate nanocomposites (Ray, 2003c).
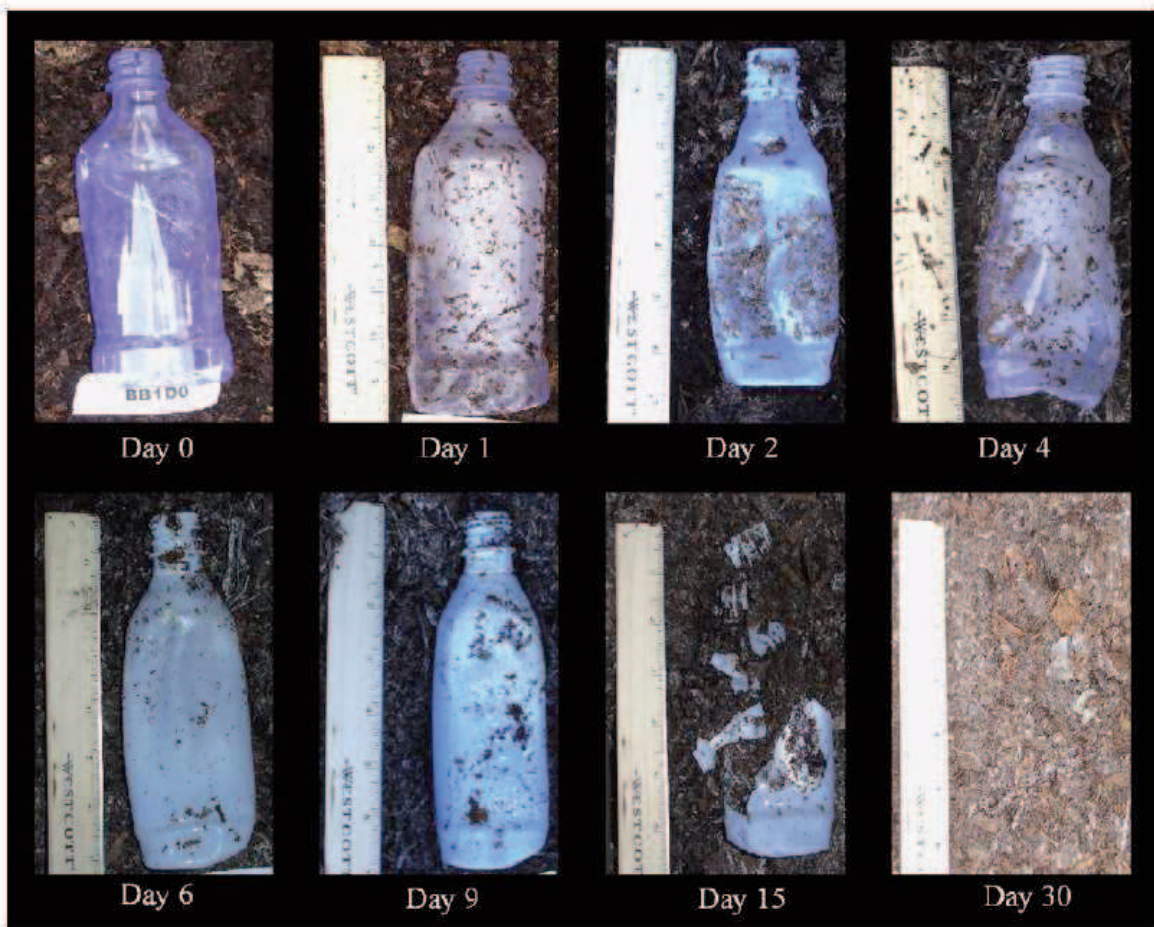
Figure 1.7. Biodegradation of PLA bottles in real composting condtions, from (Kale, 2007b).

However, although the initial chemical hydrolysis process has been extensively studied and well accepted, a clear understanding of the microbial degradation processes is still missing (Sangwan, 2008). It has been suggested that PLA degradation may even be an entirely abiotic process (Agarwal, 1998). Suyama *et al.* (Suyama, 1998) investigated microbial populations from soil capable of degrading aliphatic polyesters, such as PHB or poly(caprolactone). However, no PLA degrading strain was found. This suggests that PLA degrading microorganisms are not widely distributed in natural environments. In a mini-review Tokiwa and Calabia (Tokiwa, 2006) published a list of several PLA degrading strains, highlighting the importance of the actinomyces or thermophilic strains of the genera of *Bacillus*. Sangwan *et al.* (Sangwan, 2008) recently proposed a study identifying PLA-degrading microorganism from PLA enriched compost with the help of molecular ecological techniques, showing the

importance of fungi of the genera *Thermophylospora*, *Thermomonospora*, and *Paecilomyces*. This study also suggests that several numbers of PLA degrading strains might not be readily cultivable with laboratory techniques and are therefore difficult to identify. Further work certainly will be required using both screening isolation strategies as well as molecular ecological techniques for direct identification in order to gain understanding of PLA degradation and exploit the microbial potential for biotechnological applications.

1.1.6. Processing

PLA processing has recently been the subject of an excellent review by Lim *et al.* (Lim, 2008). PLA has been processed by a large variety of transformation methods: extrusion, extrusion film sheeting, extrusion casting, extrusion blowing, injection moulding, stretch blow moulding, thermoforming, foaming, and fibre spinning. A general point to look out for in the thermal processing of PLA is its susceptibility to thermal hydrolysis. Therefore, PLA pellets need to be carefully dried, typically to less than 100 ppm (Lim, 2008). Suppliers recommend drying to at least 250 ppm moisture content before extrusion. Commercial PLA resins can be processed on conventional extruders equipped with a general purpose screw of L/D ratio of 24-30, or on screws for PET processing. The recommended compression ratio is 2-3, and the heater setpoint usually between 200-210 °C (Lim, 2008). PLA has low melt strength, therefore horizontal roll stack configurations are preferred for film extrusion, and relatively high roller temperatures are required to prevent lactide condensation (25-50 °C). Temperatures that are too high should be avoided, however, to prevent sticking to the rollers. For the extrusion blow process, viscosity enhancers, mostly coupling agents, are used. Additives are generally proprietary and not disclosed in open literature. One commercial example is a coupling agent of styrene, copolymerized with methyl methacrylate and glycidyl methacrylate (Tweed, 2009).

The mechanical properties of PLA can be enhanced by orientation, generally in machine direction orientation with a draw ratio from 2 to 3, and in transverse direction with a draw ratio from 2 to 4 (Lim, 2008). Especially, toughness can be dramatically improved. For example, elongation at break in machine direction can be increased to 160 % upon biaxial orientation (Drumright, 2000). PLLA shows strain-induced crystallization upon drawing above glass transition temperature (Drumright, 2000; Stoclet, 2007). Furthermore, stress-strain curves show strain-hardening behaviour, which is sensitive to the draw temperature. Structure investigation of uniaxially drawn samples showed the occurrence of a mesomorphic

phase at low drawing temperature (70 °C) starting at 130 % strain. At higher draw temperatures (90 °C) a well defined crystalline phase developed at strains higher than 250 %. In the mid-temperature range (80 °C), both phases coexisted (Stoclet, 2010).

Fibre spinning of PLA has been done by melt spinning, solvent spinning, and more recently electrospinning. Lim *et al.* give a good overview of the different spinning conditions and fibre properties (Lim, 2008). In general, solution spun fibres have superior mechanical properties compared to melt spun fibres, which is attributed to the lower chain entanglement in the solution state compared to the melt state.

A strategy to improve PLA properties and/or to reduce material costs is blending with other polymers or compounding for the fabrication of composites. A number of articles have been published treating PLA blends with polymers such as starch (Averous, 2004; Martin, 2001), poly(hydroxyalkanoates) (Noda, 2004; Takagi, 2004), or poly(butylene succinate) (Wang, 2009; Yokohara, 2010). For example, PLA/ thermoplastic starch blends suffer from low adhesion between the phases, causing modest mechanical properties (Martin, 2001). PLA/poly(hydroxybutyrate) blends are immiscible within a wide range of conditions, and an improvement of mechanical properties can be observed (Zhang, 1996). Small quantities of Nodax^{TM}, being a poly(hydroxybutyrate) copolymer (Noda, 2004) or of chemically modified poly(hydroxyalkanoates) (Takagi, 2004) improved toughness of PLA. PBS was found to have a nucleating effect on PLA upon blending, yielding higher crystallinity and enhanced cold crystallization (Wang, 2009; Yokohara, 2010).

Various composite materials of PLA have been prepared in order to overcome mechanical limitations and to decrease material costs. Among different filler materials, minerals and materials derived from renewable resources have received the most interest. The reinforcing effect of a filler depends mainly on interfacial adhesion between filler and polymer and on its dispersion in the polymer matrix. In most cases the effective dispersion requires twin screw extruder mixing. For example, PLLA-cellulose composites were produced with microcrystalline cellulose, cellulose fibres and wood flour by twin screw extrusion and injection moulding. Wood flour and microcrystalline cellulose had a better nucleating effect on PLLA than cellulose fibres, resulting in very high crystallinity degrees upon slow cooling and reheating (66 %) (Mathew, 2006). Microcrystalline cellulose composites also maintained transparency of the PLA film and enhanced barrier properties (Fortunati). An increasing number of articles has been published in recent years on nanocomposites of PLA, and on nano-biocomposites which have been recently reviewed by Bordes *et al.* (Bordes, 2009). For example, PLA-nanocomposites have been extensively studied by Shina Ray and Okamoto

(Hiroi, 2004; Ray, 2003a; Ray, 2003b). They successfully prepared PLA-nanocomposites using melt-extrusion processes. Nanofillers enhanced PLA properties, such as mechanical moduli, thermal stability, crystallization, gas barrier properties and biodegradability.

1.1.7. Applications

As claimed on the website of Omnexus in 2010 (Omnexus, 2010), many corporations have adopted as part of their corporate objectives the need to develop sustainable raw materials. The use of legislative instruments is a significant driving influence for the adoption of bioplastics. In Europe and Japan, the automotive and packaging sectors are the most affected by legislation. The Packaging and Packaging Waste Directive 94/62/EC and the End of Life Vehicle Directive 2000/53/EC are two examples of such legislative drivers. Increasing oil prices, depleting oil reserves, biodegradability/total life cycle impact from sustainable resources and the use of legislative instruments are major driving forces for the use of biopolymers by corporations. Moreover the suitability of material properties for converters, the technical feasibility of processing options, the versatility of applications and ultimately, commercial viability of production and processing are the key factors which will decide actual use of biodegradable polymers (Omnexus, 2010).

In this context, PLA is the most mature and versatile polymer derived from a natural source that can be processed by the existing technologies used for petroleum–based polymers. By tuning the molecular weight and its copolymerization with other polymers, by controlling several factors affecting the lifetimes and degradation rates, including molecular mass, crystallinity and additives, the tailoring of PLA properties can be achieved leading to a large range of applications.

In 2010, the European Polysaccharide Network of Excellence (EPNOE) prepared a research road map vision to 2020 focusing on polysaccharides used in material structuring (Persin, 2011). This report was completed with a market study on biomass-based polymers and products reviewed by Shen *et al.* (Shen, 2009). Future and present applications have been reported by the two leading producers of PLA (Natureworks LLC and Purac) at the horizon 2020. It clearly appears that the most promising sectors are the textile, automotive and building sectors, which require more durable PLA products (Figure 1.8).
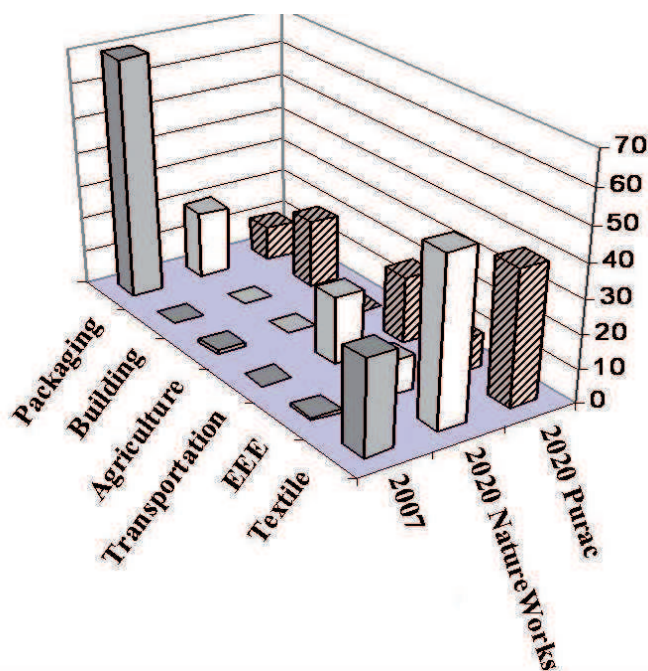
Figure 1.8. Percentage of actual and future applications of PLA from Shen *et al.* (Shen, 2009).

In the past and nowadays, biomedical and food packaging applications sectors have been sources of numerous developments:

1.1.7.1. Biomedical applications of PLA

One of the main routes to degradation of PLA is cleavage of the ester linkages by hydrolysis leading to a successive reduction in molecular weight. This degradability coupled with its biocompatibility are the reasons why PLLA has been extensively used in the past four decades for medical applications purposes including suture and scaffold for tissue engineering. High molecular weight PLLA was used for orthopedic products such as bone fixation material (Puppi, 2010; Vert, 1992). Low molecular weight with narrow molecular weight was especially desirable for rapidly degrading biomaterials such as those used for short-duration parenteral drug delivery systems (Gu, 2010).

Drug delivery microspheres, in particular smart systems with controlled release, have been developed with PLA and its copolymers with glycolide to produce poly[(D,L-lactic acid)-co-(glycolic acid)]. Since the 80's up until the present, many publications have reported on the various applications in the pharmaceutical field for using PLA copolymers and polymers for their sustained release parenteral formulations and performance in drug release in a controlled manner from microspheres (Bodmeier, 1989; Kumari).

1.1.7.2. Packaging applications commodity of PLA

1.1.7.2.1. Passive PLA packaging

While the rapid hydrolytic degradation of the PLA is an advantage for medical uses, this property becomes a main drawback for food packaging applications (Lunt, 1998). PLA meets many requirements as a packaging thermoplastic and has been suggested as a commodity resin for general packaging applications (Petersen, 1999). Since the 1990's, looking to extend PLA applications, properties such as impact strength or flexibility, stiffness, barrier properties and thermal stability, have been studied. The extensive research to improve PLA for food packaging purposes was well reviewed by different authors (Auras, 2004b; Avérous, 2008; Siracusa, 2008). Particular attention focused on the barrier properties against water vapour and oxygen by Mensitieri *et al.* (Mensitieri, 2010) who showed that PLA like others biopolymers has lower oxygen barrier performances than petrochemical polymers coupled to its moisture susceptibility. To improve the barrier properties of biopolymers, several approaches are available (Petersen, 1999): i) use of coating with materials which would add hydrophobicity to the packaging material, ii) lamination of two or more biopolymers (co-extrusion), and iii) development of blends of biopolymers with different properties. Some examples include PLA/polyethylene glycol blends, PLA/polyhydroalkanoates blends and PLA/polycaprolactone blends. Supplementary possibilities are v) chemical and/or physical modification of biopolymers, vi) development of micro- and nanocomposites based on biopolymers (Bordes, 2009; Cabedo, 2006).

Another major limitation of PLA relative to PET widely used in food packaging applications is due to its poor barrier properties mainly against oxygen and CO_2. For the food industry, the prediction and control of the ageing of packed food are a major goal in order to meet the consumer expectations. Packaging contributes to the end quality of the product by employing appropriate barrier properties. However the interaction of packed food and oxygen is very complex and depends on residual oxygen in the freshly packed food, along with the oxygen tolerance of the food.

Table 1.4 presents the oxygen tolerance of foods, meaning how much oxygen a substrate can take up until first sensory deviations can be detected. If this oxygen tolerance is known, packaging can be developed or chosen to reach optimal storage conditions to increase shelf-life.

Table 1.4. Oxygen tolerance of foods, data from (Lopez Rubio, 2005; Salame, 1986).

Oxygen tolerance of food

Food or Beverages at 25 °C	Maximum oxygen tolerance gain in ppm/year
Beer	1-2
Canned soups	1-3
Baby foods	1-3
Finewine	2-5
Fresh ground coffee	2-5
Lyophilised food	5-15
Tomato products	8-20
Fruit juices	10-40
Carbonated soft drinks	10-40
Oils and Shortening	50-200
Salad Dressings, Peanut butter	50-200

The packaging industry has been constantly looking to replace glass with polymeric materials and has recently focused on biobased polymers. However for very delicate food products such as beer or coffee, there is a challenge to keep the freshness of the food that is related to the lowest increase of oxygen into the pack. Salame *et al.* (Salame, 1986) presented the Table 1.4 and proposed a relationship that will allow a rough estimation of the shelf life t:

$$t = (p_c.l)/(P.10^{10}\,a.500) = p_c/R.\tag{1.4}$$

with p_c is the O_2 sensitivity of the food given in Table 1.4, l the container thickness, a the area to volume relationship of the package, R the O_2 transmisssion rate of the package in air as ppm.day^{-1} and P the O_2 permeation rate.

Table 1.4 shows that some food products do not require high oxygen barrier properties. Haugaard *et al.* (Haugaard, 2003) showed that cups based on PLA were found to be as effective as high-density polyethylene cups in protecting an orange juice simulant and a dressing from quality changes during storage. Moreover the properties of PLA may even be better with respect to the packaging of yoghurt due to the lower oxygen permeabilities of PLA cups compared to PS cups. The authors claimed that the use of PLA for packaging has been demonstrated by Danone in Germany and Valio Ltd, a Finnish dairy company. These studies

show that PLA has the potential to replace broadly used polymers in food applications, polyolefins and PS, in particular for small containers which are not recycled today.

One other drawback of PLA in the packaging sector is the heat deflection temperature at 50-60 ºC that will provoke poor resistance to heat and lumping of pellets during transport, storage, and processing, as well as cause deformation of trays, preforms, bottles, and cups during food conditioning. The melting temperature of PLLA can be increased by 40-50 °C up to 200 °C and its heat deflection temperature can be increased from approximately 60 °C to up to 190 °C by forming a PDLA/PLLA sterocomplex. The temperature stability is maximized when a 50:50 blend is used. New PLA stereocomplex grades with enhanced heat-stability will widen the applicability in higher value applications, where hot-filling of foodstuff is required (bottles, cups) or for microwable trays (Nampoothiri, 2010).

1.1.7.2.2. Active PLA packaging

Active packaging has been one of the major innovations in food packaging in the past years. Its aim is to respond to consumer expectations for freshness and high quality foodstuffs. Contrary to passive, inert packaging, active packaging promotes interactions with the food in order to extend shelf life, to improve sensorial properties, or to inhibit the spoilage by microorganisms (Vermeiren, 1999). Antioxidant active packaging is a promising technology for the preservation of fat-containing foods. Lipid oxidation, in dairy products, is a major cause of deterioration during processing and storage with appearance of sensorial defects. Active packaging with natural antioxidants, such as α-tocopherol, has been developed in the past based on petrochemical polymers and more recently with PLA and its copolymers. Two modes of action were tested either by limiting the penetration of oxygen into the package (Byun, 2011; Goncalves) or by a controlled release into the food in contact. Poly(lactide-co-glycolide) films loaded with natural and synthetic antioxidants, α-tocopherol, or butylated hydroxytoluene (BHT) were tested in contact with milk powders and food simulating liquids. The antioxidant release was driven by hydrolytic degradation of PLGA in the first case, or by volatilisation with solid contact. This work showed valuable result on dry milk products (van Aardt, 2007).

Antimicrobial PLA films were also developed by loading nisin onto PLA film surface (Liu, 2007), melt incorporation of lysozyme, thymol, lemon into the PLA films (Del Nobile, 2009), or solvent casting with propolis being a natural active agent having antibacterial, antifungal and antioxidant activities (Mascheroni, 2010). However, the use of melt extrusion based processing is however difficult because of the temperature sensitivity of most antimicrobial

compounds, wherefore coating techniques are often employed (Mensitieri, 2010). The correct balance has to be found between the durability of the packaging needed for the preservation of packed food during its shelf-life and the expected biodegradability at the end of the life cycle. Addition of nanocomposites in PLA can improve barrier properties for food applications and increase degradation in compost conditions (Fukushima, 2010). On the other hand, plasticizers are commonly added to promote flexibility of PLA but degradation increases, and food shelf life is often negatively affected by increasing plasticizer content (Kulinski, 2005).

1.1.7.3. Textile applications

The ease of melt processing, unique property spectrum, renewable source origin, and the possibility of composting and recycling are sources of the growing interest for PLA fibres and acceptance in a range of commercial textile sectors. In the form of fibres and non-woven textiles, PLA also has many potential uses, for example as upholstery, disposable garments, awnings, feminine hygiene products, and nappies. Textile, fibres and fabrics represent a sector that is forecast to become the first sector of use for Natureworks LLC and Purac's productions (Shen, 2009). In recent years, the polymer has been available on the market and its applicability has already been proven in a number of processes and final applications. However, to date its breakthrough is slower than expected in textile applications. The technological challenges to be solved were reviewed by Avinc and Khoddami (Avinc, 2009, 2010). PLA fibres can be dyed with disperse dyes, like PET fibres. However, a variety of wet processing applications (pretreatment, dyeing, clearing, and subsequent finishing treatments) impart chemical and physical stresses on the PLA fibres. The development of the PLA stereocomplexes with higher thermal stability has the potential to limit the shrinkage of PLA fibres and fabrics during dying or ironing.

Special attention has been focused on the flammability and fire stability of PLA needed during ironing. Solarski *et al.* (Solarski, 2008a) showed that the incorporation of 4 wt% organomodified layered silicate (Bentone 104) improves the shrinkage properties and reaction to fire of PLA filaments. They concluded that this ''nano effect'' can be considered as permanent (*i.e.* the separated nanoplatelets are imbedded within the matrix), in contrast to some classical textile finishes, which are sensitive to washing.

PLA fabrics exhibit the comfort and touch of natural fibres such as cotton, silk and wool while having the performance, cost, and easy care characteristics of synthetics. PLA fibres

demonstrate excellent resiliency, outstanding crimp retention and improved wicking compared with natural fibres. Fabrics produced from PLA are being utilized for their silky feel, drape, durability and water vapour permeability used to create breathability suitable for sport clothing applications (Omnexus, 2010).

1.1.7.4. Automotive applications of PLA

Since the 1950's, the automotive corporations have shown a great interest for the of synthetic polymers (PS, PA, Polyurethans, PP) and nowadays plastic materials represent 50 to 55 % and 25 to 30 % w/w of the total mass of a car comprising the passenger compartment and the body of the car, respectively. In the last decade, composites of synthetic polymers with glass or carbon fibres emerged from aeronautic sector and penetrated the automotive sector with the aim of reducing vehicle weight. However these composites with non-organic fillers are not easy to recycle. Driven by environmental concerns and triggered by EU legislation on the End of Life Vehicle (Directive 2000/53/EC), biocomposites have been developed that offer certain environmental advantages at the end of the use cycle when composites are landfilled or incinerated. European Union legislation implemented in 2006 states that 85 % of a vehicle must be reused or recycled by 2015. Japan requires 95 % of a vehicle to be recovered (which includes incineration of some components) by 2015 (Pandey 2010).

Car and part manufacturers manufacturers turned their attention to natural fibres to reinforce plastic polymers. The most used natural fibres are hemp, sisal, flax, wood, and kenaf used in a biodegradable or non-biodegradable matrix. However, combining the biofibres with a biodegradable and renewable resource-based polymer such as PLA enables the creation of a completely biobased solution. One impediment in creating good bio-composites is a lack of interfacial adhesion between the natural fibre fillers and polymer matrix. Many approaches geared towards enhancing interfacial adhesion have been pursued including the use of grafting agents and chemical modifications (Oksman, 2003; Pandey 2010).

Recently Purac (Purac, 2010) has developed a PLA compound with heat stability and impact strength comparable to poly(acetonitrile butadiene styrene) (ABS) in injection moulding applications based on the stereocomplex technology.

1.1.7.5. Building and E&E applications

As of now, biopolymers are very rare in the building sector, although this sector might prove promising for PLA development in the future. As shown by their use in textile applications, carpet tiles and moquettes can be made with PLA fibre and would be useful in non-perennial uses such as salons and expositions. Expandable foams are traditionally produced from fossil-based polymers (i.e. polystyrene or polypropylene) and largely used for insulation in building. In 2010, the Dutch company Synbra in collaboration with Purac and Sulzer started the production expandable PLA named BioFoam®, a biodegradable and biobased alternative to EPS-foam in a variety of application areas, in particular insulation for building. PLA has also been used in France by Buitex to serve as the binder in Isonat Nat'isol, a hemp fibre used in building insulation. Bourbigot and Fontaine (Bourbigot, 2010) reviewed the flame retardancy of PLA focusing on its use as a substitution for traditional polymers in the transportation, electric and electronic equipment sectors, where fire hazard is an issue and flame retardancy is required. The solution and approach used for flame retarding PLA such as blending, use of conventional flame retardants or nanoparticles, and ingredients of intumescence were discussed. The authors concluded that the mechanism of action remains similar to those observed in other polymers when incorporating the same kind of additives. However, more scientific research specifically exploring the flame retardancy of PLA and its mechanisms is needed. In particular, combined with nanofillers of graphite and silica, PLA could present good mechanical and thermal properties, which would improve the flame retardant properties of PLA (Fukushima, 2010).

1.1.7.6. Other applications of PLA

Polylactic acid (PLA) has been proposed for use in the production of horticultural materials in order to reduce the environmental problem caused by the large quantity of plastic used in this sector, and for use as a matrix for the controlled release of herbicides. Chang *et al.* (Chang, 1996) evaluated the impact of PLA in the growth stimulation and yield improvement of soybeans. Greenhouse studies confirmed that both lactide and PLA increased soybean leaf area, pod number, bean number, and bean and plant dry weight. Low molecular weight polylactic acid was used as a matrix to formulate biodegradable matrix granules and films with bromacil using a melt process (Zhao, 2005). Low molecular weight PLA-based

formulations were shown to be useful for the application of pesticides to sensitive systems such as seeds. PLA as an encapsulation matrix for herbicides or pesticides could help to reduce their environmental impact.

Within the field of durable applications, Japanese companies are using PLA and other biopolymers in cell phone and computer housings. Sanyo Mavic Media Co Ltd. (Japan), a subsidiary of Sanyo Electric Co, Ltd, has introduced the world's first biodegradable compact disc-based PLA, including its film packaging and case. Developed jointly by Mitsui Chemicals Inc. (Japan) and Sanyo Mavic Media, the new disks, marketed under the name MildDisc, are virtually indistinguishable from conventional discs made of polycarbonate, with no trade-off in sound or picture quality. With estimates of worldwide disc demand at more than 10 billion pieces, market opportunity is substantial. Sanyo Electric is targeting volume customers producing pre-recorded CDs, such as music CDs, video CDs, or software CD-Roms. The company is also working on recordable and rewritable versions of the MildDisc and on DVDs (Omnexus, 2010).

1.2. Structure of semi-crystalline polymers

1.2.1. Semi-crystalline structure

The polymer matrix is constituted by entangled polymer chains whose organization is dependent on the monomers. Indeed, the tacticity and the ramification of polymer and the conformation of the polymer segments (bond and rotation angles) are major elements for the local orientation. So to crystallize the polymer stereochemistry has to be highly regular and the ramification not too rigid to make it possible the orientation of the polymer.

1.2.1.1. Crystalline phase

1.2.1.1.1. Crystallization processes

The crystallization of a polymer can be classified under three groups: crystallization during polymerization, crystallization induced by orientation and crystallization under quiescent conditions. The crystallization during polymerization consists in forming the crystal due to chemical reactions at the gas/solid or liquid/solid interface. Indeed the monomers join up by solid state polymerization to form the polymer crystal. The crystallization by orientation corresponds to the formation of fibrous crystals due to the stretching of long chains. The decrease in the entropy, due to this chain orientation, induces the crystallization of the polymer. The last one, the crystallization under quiescent condition is the process observed for a large number of macromolecules, from dilute solutions or from the melt. The latter is the object of the present study.

1.2.1.1.2. Crystalline structure

The crystalline phase is a well organized fraction as well in the atomic scale as in the microscopic scale (Figure 1.9). The majority of semi-crystalline polymers crystallizes under the form of lamellar crystals which is first brought to light in 1938 by Storks (Storks, 1938).

The polymer chains are organized so as the atoms, which composed them, form crystal lattices whose dimensions are nanometric. These chains, folded up on themselves, form crystalline lamellae whose thickness is around 10 nm. Then these lamellae tend to stack, let between them a space in which polymer chains are not organized, the amorphous phase. These stacks rearrange themselves and grow radially to form a structure, from 1 to few

micrometers, whose centre is the germination point. This structure, named spherulite, is birefringent which make it possible to observe them, in polarized optical microscopy, in the form of Maltese cross.
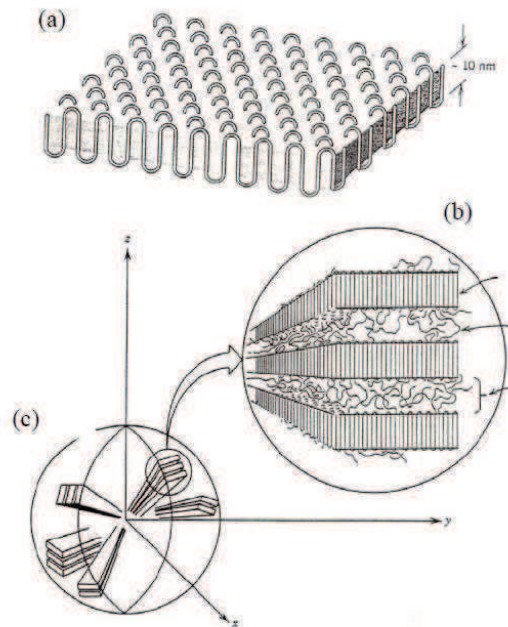
Figure 1.9. Crystalline organizations: (a) crystalline lamella, (b) lamellae stack, (c) view of a spherulite.

Several crystalline structures may be found in the polymeric matrix but there is usually a polymorph which is thermodynamically more stable. The different crystal form can be due to the packing of chains with different conformation or different packing modes of molecular chains with identical conformation in the unit cell (Pan, 2009). This polymorphism is induced by several factors but mainly by the crystallization temperature, the crystallization processes (different fusion conditions before melt or cold crystallization or solution crystallization) and the stress. The others factors are:

- the molecular weight, which induces different thermodynamic parameters and crystallization kinetics,
- the microstructure, that is to say the stereoregularity or defects in the polymeric chains,
- the blending with miscible compound which may alter the thermodynamic and kinetic parameters of the crystallization,
- the epitaxial crystallization which can regulate the crystal morphology and structure,
- the nucleating agent which can change the crystalline structure.

1.2.1.2. Amorphous phase

The semi-crystalline polymer structure has been described during a long time as a two phase model: a crystalline phase and an amorphous phase. This latter, constituted by polymer chains or parts of polymer chains which cannot be organized, is characterized by a glass transition temperature. It separates the glass state, in which the amorphous phase is rigid, from the rubber state in which the chains are mobiles.

However, 25 years ago, the three phase model was first introduced for the poly(ethylene terephthalate) (Androsch, 2005; Chen, 2008; Kattan, 2002). Numerous semi-crystalline polymers showed similar morphology, such as polyoxymethylene, poly(tetrafluoroethylene) (Dlubek, 2005), poly(3-hydroxybutyrate) (El-Taweel, 2004), isotactic polystyrene (Righetti, 2008) and poly(lactic acid) (Arnoult, 2007). The molecular dynamic analyses during the glass transition showed a third fraction which does not contribute neither to the crystallization enthalpy nor to the change in the heat capacity at T_g. This fraction, called rigid amorphous fraction (in contradiction with mobile amorphous fraction) does not stay rigid up to the melting but disappears progressively above T_g (Wunderlich, 2003). Nevertheless a T_g of this fraction is also detected at higher temperature than the one of MAF.

So three fractions coexist: a crystalline fraction, a mobile amorphous fraction (MAF) and a rigid amorphous fraction (RAF). The rigid amorphous fraction is related to the presence of crystalline lamellae. Indeed, the lamellae are separated by thin layer of amorphous fraction called interlamellar amorphous fraction, whose polymer chains segments can be schematized under different configurations (Figure 1.10).
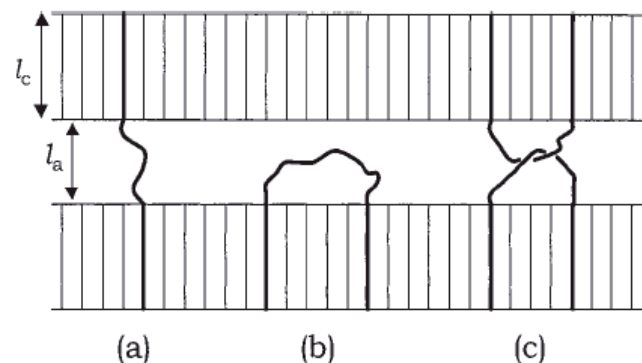
Figure 1.10. Schematic sketch of three possible configurations of the polymer chains segments in the interlamellar amorphous space: (a) tie molecules, (b) loose loops, (c) entangled loose loops.

This latter is formed by chains or parts of chain, whose portions are located in the crystalline fraction and consequently are blocked, thus forming the rigid amorphous fraction (El-Taweel, 2004). The mobile amorphous fraction is also made up of interspherulitic amorphous fraction and the amorphous fraction located between the lamellae stacks (interfibrillar phase) as shown in Figure 1.11.
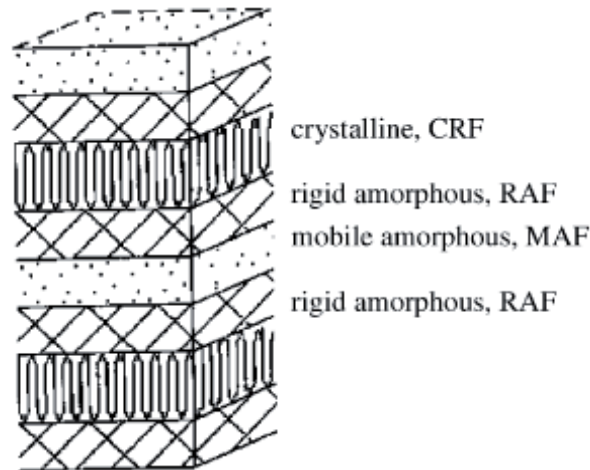
Figure 1.11. Schematic sketch of the arrangement of crystalline, rigid amorphous and mobile amorphous fractions in a lamellae stack (Schick, 2003).

The calculation of the mobile amorphous fraction is performed from ΔC_p at the glass transition:

$$X_{am} = \frac{\Delta C_p}{\Delta C_p^0} \tag{1.5}$$

where ΔC_p is the thermal heat capacity step at T_g for a semi-crystalline polymer and ΔC_p^0 is the thermal heat capacity step at T_g for the 100 % amorphous polymer (Arnoult, 2007; Kattan, 2002; Schick, 2003).

The determination of the rigid amorphous fraction is carried out from the Equation 1.6:

$$X_{am} + X_{ar} + \chi_c = 1 \tag{1.6}$$

with χ_c the calculated crystallinity degree of the polymer.

1.2.1.3. Crystallization kinetics

The polymer crystallization is a phase transition in two steps, germination and growing, which can occur between the glass transition temperature and the melting temperature.

The first step, germination or nucleation, can occur spontaneously or artificially. It can be induced by friction, stirring, under a high pressure or due to an external influence such as electrical field, UV light, sonic irradiations, and so on…Two types of nucleation have been defined: primary and secondary nucleation. The primary nucleation can be homogeneous (spontaneous) or heterogeneous (induced by external element). The primary homogeneous nucleation consists in an arrangement of polymer chains which make it possible the contact between monomers to form crystals, that is to say nucleation germs or nuclei. This germ can also grow from impurity or from a nucleating agent added to the polymer to provoke the germination, it is the primary heterogeneous crystallization. This germ is formed by the joining of chain segments on the impurity. The secondary nucleation is the one occurring from crystals already formed (Mullin, 2001).

Once the critical radius of the germ is reached, the second step, the crystal growing, starts. Some chains or chain segments join successively to the lateral surface of the germ. So the thickness of the initial germ, almost kept, defines the crystalline thickness.

The crystallization of polymers takes place from cold or melted state and can be an isothermal or non isothermal process.

1.2.1.3.1. Isothermal crystallization kinetic

The isothermal crystallization makes it possible to study the nucleation and the crystal growth without the variation of physical parameters with the temperature (Di Lorenzo, 1999). In semi-crystalline polymers, the overall process of crystallization can be shared into the primary and the secondary crystallization. The first one is the macroscopic development of the crystallization whereas the second one corresponds to the crystallization of the amorphous part trapped between the lamellae stacks, the interfibrillar amorphous phase. To describe this evolution of the polymers, a lot of models has been proposed these last 70 years, such as the most common model, Avrami or the Tobin, the Malkin, the Urbanovici-Segal model (Supaphol, 2001).

The crystallization kinetic is traditionally studied thanks to crystallization exotherms from DSC analysis. So the relative degree of crystallinity, a function of time ($\theta(t)$), is obtained from the enthalpy of crystallization and can be expressed with the following equation: (Di Lorenzo, 1999; Supaphol, 2001).

$$\theta(t) = \frac{\int\limits_0^t (dH_c / dt) dt}{\int\limits_0^\infty (dH_c / dt) dt} \in [0,1] \qquad (1.7)$$

Where t is the elapsed time during the course of crystallization and ΔH_c the enthalpy of crystallization released during an infinitesimal time interval dt.

The Avrami model, the most widely used, makes it possible to describe the crystallization process from the relative crystallinity degree with the Equation 1.8:

$$\theta(t) = 1 - \exp\left[-(K_a t)^{n_a}\right] \qquad (1.8)$$

where K_a is the Avrami rate constant and n_a the Avrami exponent. K_a, expressed in time^{-na}, is dependent on the temperature and involves both nucleation and growth rate (Supaphol, 2001) whereas n_a, which should be an integer ranging from 1 to 4, is dependent on the type of nucleation (homogeneous or heterogeneous) and growth geometry (1D, 2D, 3D) (Di Lorenzo, 1999; Phuong, 2010), as shown in Table 1.5.

Table 1.5. Avrami exponents related to the crystal geometry, the nucleation type and the rate determination (the limiting mechanism).

Avrami Exponent n_a	Crystal Geometry	Nucleation Type	Rate determination
0.5	Rod	Athermal	Diffusion
1	Rod	Athermal	Nucleation
1	Disc	Athermal	Diffusion
1.5	Rod	Thermal	Diffusion
1.5	Sphere	Athermal	Diffusion
2	Rod	Thermal	Nucleation
2	Disc	Athermal	Nucleation
2	Disc	Thermal	Diffusion
2.5	Sphere	Thermal	Diffusion
3	Disc	Thermal	Nucleation
3	Sphere	Athermal	Nucleation
4	Sphere	Thermal	Nucleation

The half time of crystallization ($t_{1/2}$) is the time to achieve 50 % relative crystallinity. This time can be calculated by the Equation 1.9:

$$t_{1/2} = \left(\frac{\ln 2}{K_a} \right)^{1/n_a}$$

(1.9)

Aiming at improving Avrami, Tobin proposed a different equation which should describe the kinetics of phase transformation with an emphasis on growth site impingement:

$$\theta(t) = \frac{(K_t t)^{n_t}}{1 + (K_t t)^{n_t}} \in [0,1]$$

(1.10)

Where K_t and n_t are the Tobin rate constant and exponent. As for Avrami, n_t is dependent on the type of nucleation and the growth mechanism (Dangseeyun, 2004; Supaphol, 2001).

Considering the degree of crystallinity varies with the emergency of the primary nuclei and the rate of variation in the degree of crystallinity varies with the crystal growth rate, Malkin *et al.* (Malkin, 1984) postulated that the overall crystallization rate equals the summation of the rate. So it can be expressed as:

$$\theta(t) = 1 - \frac{C_0 + 1}{C_0 + \exp(C_1 t)} \in [0,1]$$

(1.11)

where C_0 and C_1 is the Malkin exponent and crystallization rate constant, respectively. C_0 represents the ratio of the crystal growth rate G to the primary nucleation rate I and C_1 is related to the overall crystallization crystallization rate.

So $C_0 \propto G/I$ and $C_1 = aG + bI$ where a and b are specific constants (Dangseeyun, 2004; Supaphol, 2001).

Urbanovici and Segal suggested a generalization of the Avrami model with the following equation:

$$\theta(t) = 1 - \left[1 + (r-1)(K_{us} t)^{n_{us}} \right]^{1/(1-r)} \in [0,1]$$

(1.12)

where K_{us} and n_{us} are the Urbanovici and Segal crystallization rate constant and exponent. The parameter r, above 0 but below 1, is the factor of deviation of this model from the Avrami model (Supaphol, 2001).

1.2.1.3.2. Nonisothermal crystallization kinetic

The crystallization in dynamic conditions, the nonisothermal crystallization, has also been the subject of numerous studies. It can take place from the melt with generally a constant cooling rate or from the cold state, after quenching below T_g, with a constant heating rate. Mostly the

non isothermal crystallization is performed under cooling conditions and is strongly dependent on the cooling rate. So at higher cooling rates, the crystallization peak occurs at lower temperatures whereas at lower cooling rates, it occurs at higher temperatures. As for the isothermal crystallization, the non isothermal one is described by several models: the modified Avrami and the Ozawa models and the Liu and Mo approach.

Considering the nonisothermal character of the process, the Avrami model has been modified. So Jeziorny used the same equation than Avrami (Equation 1.8) but the crystallization rate constant is recalculated to take into account the cooling rate (Chen, 2002; Chivrac, 2006; Phuong, 2010):

$$\ln K_c = \frac{\ln K_a}{\alpha} \tag{1.13}$$

where α is the cooling rate in °C.min^{-1}.

Ozawa proposed, in 1971, another modification of Avrami model by considering that the non-isothermal crystallization is the combination of many infinitesimal isothermal crystallization (Phuong, 2010). This approach takes into account the crystallization in function of the temperature (Chivrac, 2006; Ziaee, 2006):

$$\theta(T) = 1 - \exp\left[-\left(\frac{K_O}{\alpha}\right)^{n_O}\right] \tag{1.14}$$

Where K_O and n_O are the Ozawa crystallization rate constant and exponent, respectively and α the constant cooling or heating rate.

Then Liu and Mo developed a model which combines the Avrami and Ozawa models (Phuong, 2010):

$$\left(\frac{K_O}{K_a}\right)^{1/n_a} = \alpha \times t^m \tag{1.15}$$

Where m is the ratio of the Ozawa exponent and the Avrami exponent ($m = \frac{n_O}{n_a}$).

So the crystallinity degree is related to the cooling or heating rate and the crystallization time or temperature.

1.2.2. Semi-crystalline PLA structure

The PLA properties depend largely on the architecture of the polymer, that is to say the stereochemistry of the monomers which constitute the polymer. Indeed the D-lactic acid, in high proportion, induces some imperfections which prevent from polymer crystallization (Auras, 2004b). The crystalline phase proportion varies according to the L-lactic acid content. The higher this content is, the more the polymer chains can be organized and crystallize. So the PLLA crystallinity degree can reach 65 % (Di Lorenzo, 2006) whereas a PLA with a L-lactic acid content close to 93 % can crystallize up to 45 %.

1.2.2.1. Amorphous phase of PLA

The amorphous phase microstructure of PLA has been studied since few years in application of the three phase model, postulating that two fractions can be distinguished in the amorphous phase, a mobile fraction (MAF) and a rigid fraction (RAF) having a T_g shifted to higher temperature. As previously shown, the mobile amorphous fraction is calculated thanks to the Equation 1.6. In the case of PLA, the change in heat capacity of PLA at the glass transition (ΔC_p^0) varies according to the authors and therefore to the PLA grade. Arnoult *et al.* (Arnoult, 2007) measured 0.48 J.g^{-1}.K^{-1} for a PLLA with an estimated D-lactide content of 0.4 % whereas Pyda *et al.* (Pyda, 2004) measured 0.608 J.g^{-1}.K^{-1} for a PDLLA with 1.5 % of D-lactide. As for PET, the loss of segmental mobility of the amorphous phase PLA could be explained by the presence of a rigid amorphous phase. However contrary to PET, the RAF fraction is low up to obtain a crystallinity degree close to the maximum (between 30 and 40 % for PDLLA). Once this value is reached, a part of the MAF turns into RAF and so the RAF fraction increases. Arnoult *et al.* showed that this increase is limited at 25 % (Arnoult, 2007) of the sample whereas according to Del Rio *et al.* the RAF fraction increases with the annealing time to reach almost 50 % (Del Rio, 2010; Delpouve, 2009).

1.2.2.2. Crystalline structure of PLA

The crystalline phase of poly(lactic acid) has been mainly studied in the case of PLLA, while only few data is available on PDLLA or PDLA. Nevertheless the homopolymers present

probably a similar polymorphism but their handedness of molecular chains in the crystal lattice is opposite (Cartier, 2000). PLLA crystallizes under three main forms, dependent on the preparation conditions: α (α', α''), β and γ.

The **α-form** is the most common form of PLLA. It expands in normal crystallization conditions, such as crystallization from molten, glassy state or in solution (Kawai, 2007). The α-form is characterized by two antiparallel chains in a left-handed 10_3 helix conformation (Kawai, 2007; Zhang, 2005). As shown in Table 1.5, the chains are stacked in an orthorhombic or pseudo-orthorhombic crystalline unit cell. A notable structural feature of this α form is the distorsion of the helix conformation and the crystal structure change. According to the authors named in Table 1.6 the interactions between closest neighbour chains, that is to say the electrostatic dipole-dipole interactions, are the causes of these changing data.

Table 1.6. Previously reported data relative to the crystalline structure of the α-form of PLLA, adapted from (Pan, 2009).

Authors	Crystal System	a (nm)	b (nm)	c (nm)	Chain conformation
De Santis and Kovacs (De Santis, 1968)	Pseudo-orthorhombic	1.070	0.645	2.780	10_3 helix
Kalb and Pennings (Kalb, 1980)	Pseudo-orthorhombic	1.034	0.597		
Hoogsteen et al. (Hoogsteen, 1990)	Pseudo-orthorhombic	1.060	0.610	2.880	distorted 10_3 helix
Kobayashi et al. (Kobayashi, 1995)	Orthorhombic	1.050	0.610	2.880	10_3 helix
Brizzolara et al. (Brizzolara, 1996)	Orthorhombic	1.060	0.605	2.880	distorted 10_3 helix
Miyata et Masuko (Miyata, 1997)	Orthorhombic	1.078	0.604	2.870	
Iwata et Doi (Iwata, 1998; Sasaki, 2003)	Orthorhombic	1.070	0.615		
Sasaki et Asakura (Sasaki, 2003)	Orthorhombic	1.066	0.616	2.888	distorted 10_3 helix

a, b, c the lattice vectors.

The **α'-form** corresponds to a disordered α-form (Zhang, 2008). This crystal presents the same conformation than α-form but the stacking seems to differ. Indeed the cell unit dimensions are a = 1.074 nm, b = 0.620 nm and c = 2.880 nm. The ratio a/b corresponds to $3^{1/2}$, which is typical for a hexagonal crystal. The interlamellar space changes also with the crystalline form. It is higher in the case of α'-form than in the case of α-form (Delpouve,

2009; Kawai, 2007; Zhang, 2008). PLLA crystallizes in an α'-form at temperatures lower than 120 °C (Cho, 2006; Kawai, 2007; Pan, 2008a; Zhang, 2005). At temperatures lower than 100 °C the α'-form is predominant, while between 100 and 120 °C a mix of α and α'-form is observed (Zhang, 2008). The α'-form turns into a α–form upon an heating up to melting or upon an annealing at high temperature (120-160 °C), meaning the unit cell becomes more compact (Pan, 2008b; Yasuniwa, 2007; Zhang, 2008).

The **α"-form** has been discovered by Marubayashi *et al.* (Marubayashi, 2008). The α"-form is, like α'-form, a disordered α-form due to the exposition to high-pressure CO_2 below T_g. So below 40 °C, for a pressure between 3 and 15 MPa, only the α"-form is obtained. However, the increase in the temperature induces the formation of intermediate crystalline structure which is not formed from 50 °C and at a pressure above 3 MPa. This α"-form presents a poor chains packing and a lower crystal density, compared to α- and α'-form (Marubayashi, 2008).

The **β-Form** was detected the first time by Eling *et al.* in the beginning of 80's upon hot-drawing the melt-spun or solution spun PLLA fibres to a high draw ratio (Eling, 1982). Generally this form is obtained upon high temperature and high draw ratio stretching (Kawai, 2007).

Nevertheless, in these conditions, stretching leads to a mixture of α- and β-form with the α/β ratio depending on the draw ratio. Indeed, upon stretching at low temperature and/or low draw ratio, the obtained crystalline structure is an α-form. The β-form is characterized by a chain number varying according the author but whose the conformation is not modified, that is to say a 3_1 helical conformation. As shown in Table 1.7, the cell unit differs also: it is orthorhombic or trigonal (Puiggali, 2000; Zhang, 2005).

Table 1.7. Previously reported data relative to the crystalline structure of the β-form of PLLA, adapted from (Pan, 2009).

Authors	Crystal System	a (nm)	b (nm)	c (nm)	Chain conformation
Hoogsteen *et al.* (Hoogsteen, 1990)	Orthorhombic	1.031	1.821	0.900	6 chains, 3_1 helix
Kanamoto *et al.* (Sawai, 2002)	Orthorhombic	1.040	1.770	0.900	6 chains, 3_1 helix
Puiggali *et al.* (Puiggali, 2000)	Trigonal	1.052	1.052	0.880	3 chains, 3_1 helix

The **γ-crystalline form**, discovered in 2000 by Lotz *et al.* has been the subject of few studies. It is obtained by epitaxial crystallization (Cartier, 2000; Kawai, 2007; Zhang, 2005) on a hexamethylbenzene (HMB) substrate but the formation mechanism is still to be determined. The γ–form is characterized by two antiparallel helices with a 3_1 conformation packed in an orthorhombic cell unit whose dimensions are a = 0.995nm, b = 0.625nm and c = 0.880nm (Kawai, 2007).

1.2.2.3. Crystallization kinetics of PLA

The PLA crystallization kinetics has been widely investigated, where most studies have been carried out on PLLA. The PLA crystallization, isothermal or non isothermal, is related to the L-lactic acid content (Huang, 1998; Kolstad, 1996; Ling, 2006), the molecular weight of the polymer (Garlotta, 2001) and the cooling or heating rate and depends on the thermal history of the sample and the presence of nuclei in the matrix (Bouapao, 2009; Masirek, 2007) (Table 1.8). In the appropriate conditions (crystallization time and temperature) (Day, 2006; Di Lorenzo, 2006; Tsuji, 1995) the crystallinity degree of PLLA can reach 45 – 70 %. The crystallinity degree is calculated according to the Equation 1.16 in which ΔH_m is the measured enthalpy of melting, ΔH_c, the measured enthalpy of cold crystallization and $\Delta H_m^{100\%}$ the enthalpy of melting per mol of repeating unit of the perfect crystal of infinite size. This latter feature has been estimated by Fischer at 93 J.g^{-1} (Fischer, 1973) for PLLA. This value is the most often used but other values can be found in literature (146 J.g^{-1} (Jamshidi, 1988), 91 J.g^{-1} (Pyda, 2004)).

$$\chi_c = \frac{\Delta Hm - \Delta Hc}{\Delta H_m^{100\%}}$$

(1.16)

PLA crystallizes usually between 85 and 150 °C but its fastest rate of crystallization occurs between 95 and 115 °C (Di Lorenzo, 2005). The value of the crystallization half time ($t_{1/2}$) varies according to the authors. In the temperature range 95 to 115 °C the $t_{1/2}$ of PLLA for crystallization from the melt varies between 1.5 min to 5 min (Day, 2006; Di Lorenzo, 2006; Tsuji, 2006c). Nevertheless the optimum, 1.5 min, is obtained at around 110 °C for isothermal crystallization from melt (Figure 1.12) (Di Lorenzo, 2006).

Not only the ($t_{1/2}$) of PLA depends widely on the crystallization temperature but it is also linked to the crystallization type (isothermal or non isothermal, from cold or molten state). So, upon isothermal crystallization from the molten state, $t_{1/2}$ of PLLA, according to Di Lorenzo *et al.*, is below 2 min at 110 °C (Figure 1.12). Eventually upon non isothermal crystallization, $t_{1/2}$ lies also around 2 min (Huang, 2009; Tsuji, 2010; Wu, 2007). The more the isothermal crystallization temperature is far from this optimum, the more $t_{1/2}$ increases. For isothermal crystallization below 90 °C or above 130 °C, $t_{1/2}$ can be beyond 10 min (Di Lorenzo, 2006; Yasuniwa, 2007).
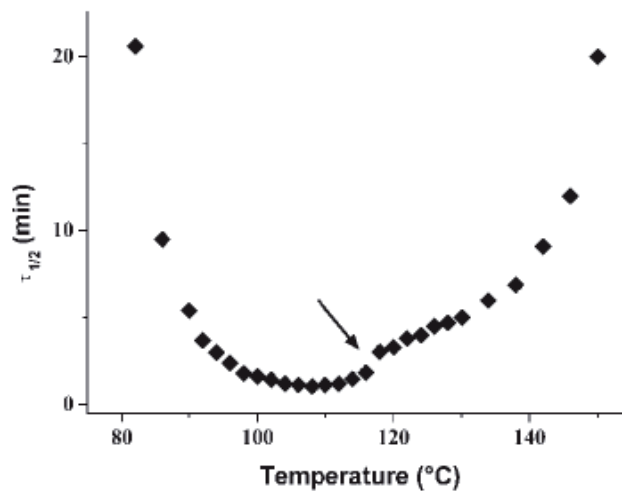
Figure 1.12. Half-time of crystallization ($t_{1/2}$) of PLLA as a function of isothermal crystallization temperature (Di Lorenzo, 2006).

Upon isothermal crystallization, the spherulites growth rate of PLA (96% L-lactide) is between 0.2 and 3 µm.min^{-1} according to the crystallization temperature and the authors (Kulinski, 2005; Li, 2010b; Masirek, 2007; Pantani, 2010; Xiao, 2009). with an optimum around 115 °C (Masirek, 2007). Moreover when the molecular weight is divided by a factor 5, the maximal growth rate increases from 3 to 7 µm.min^{-1} at 115 °C (Miyata, 1998). The spherulite growth rate is increased by the stereoregularity of PLA. Di Lorenzo *et al.* showed, in Figure 1.13, two optima, one at 117 °C where the rate reaches 10 µm.min^{-1} and another at 130 °C where the rate is 7 µm.min^{-1} (Di Lorenzo, 2006). Yuryev *et al.* noticed also these two optima but at different temperature. In their case, the first optimum is 5 µm.min^{-1} at 108 °C and the second one is at 4 µm.min^{-1} at 130 °C.
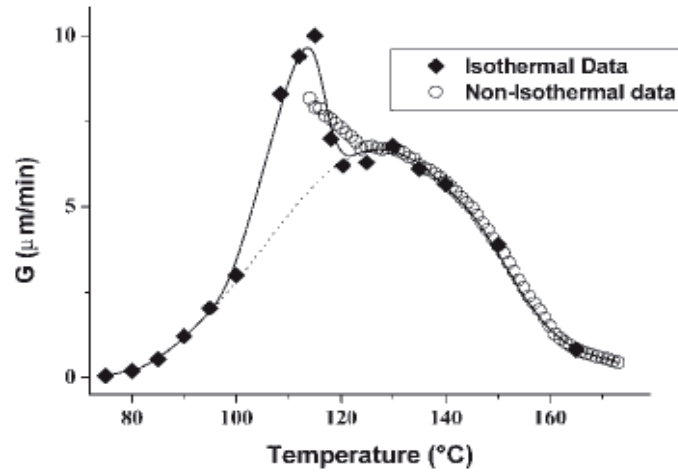
Figure 1.13. Spherulite growth rate of PLLA measured in isothermal and nonisothermal conditions (Di Lorenzo, 2006).

The isothermal crystallization kinetic is studied mainly with the Avrami equation (double logarithmic form in Equation 1.17), where n_a and K_a are the Avrami exponent and crystallization rate constant respectively.

$$\ln[-\ln(1-\theta(t))] = \ln K_a + n_a \ln t \tag{1.17}$$

The kinetic studies of the isothermal crystallization of neat PLA showed that n_a is around 1.8-2.6 between 80 and 135 °C (Ke, 2003; Pantani, 2010; Xiao, 2010). However, Lai *et al.* observed a n_a of 3.98 at 124 °C (Lai, 2004). In the same manner, the crystallization rate constant varies widely between 5.84×10^{-5} and 0.9 min^{-1} (Ke, 2003; Pantani, 2010; Tsuji, 2010).

Upon non isothermal crystallization the Avrami exponent took value between 2.1 and 4.82 whereas the Avrami crystallization rate were found between 0.0104 and 0.685.

Whatever the crystallization type, the kinetic study of the PLA crystallization, according Avrami, showed a two dimensional or three dimensional growth process, depending on the temperature, from predetermined nucleation with a combination of sporadic nucleation (Day, 2006; Tsai, 2010).

Table 1.8. Kinetics data of PLA from litterature: Cristallization mode from molten or cold state: isothermal (iso) or non isothermal (non iso), crystallization temperature (T_c), crystallization rate (CR), half time crystallization ($t_{1/2}$), Avrami modified crystallization rate (k_c), Avrami crystallisation rate (k_a) and exponent (n_a).

Authors	Provider (grade or L content)	M_n/M_w (g.mol^{-1})	-	iso or non iso	T_c (°C)	CR (µm.min^{-1})	$t_{1/2}$ (min)	k_c (min^{-n})	k_a (min^{-n})	n_a
Tsuji 2010	Polysciences Inc. PLLA	M_n = 570 000	cold	iso	107		1.02	0.634		4.82
				non iso			2.39	0.0104		
Ke & Sun 2003	Shimadzu Inc.	M_w = 120 000	molten	iso	102		14	-		
					80			-	5.84E-05	2.64
					90			-	2.04E-03	2.06
					95			-	2.25E-03	2.42
					100			-	5.16E-03	2.23
					105			-	5.58E-03	2.09
					110			-	3.10E-03	2.1
					115			-	2.47E-03	2.08
					120			-	1.08E-03	2.18
					125			-	2.63E-03	2.37
					130			-	1.04E-04	2.32
					135			-	1.84E-04	2.06
Day 2006	Unitika Ltd	-	cold	iso	85.4		10.2	-	9.90E-02	2.24
					90.4		5.92	-	1.87E-01	2.2
					95.5		3.2	-	1.57E-01	2.53
					100.6		2.15	-	1.76E-01	2.69
					105.6		1.95	-	3.72E-01	2.38
			molten		105.4		4.87	-	3.11E-01	2.07
					110.4		6.18	-	1.89E-01	2.18
					115.4		6.95	-	2.93E-01	1.97
					120.4		10.6	-	2.48E-01	1.9
					125.4		21.8	-	1.76E-01	1.82
					130.4		40.2	-	1.57E-01	1.71
Xiao 2010a,c	NatureWorks 4032D	M_w = 207 000	molten	iso	123	15		-		
					128	16		-		
					132	16.8		-		
					137	16.5		-		
					142	16.2		-		
					113		3.6	-	5.27E-04	2.4
					116		14.5	-	9.37E-05	1.8
					119		19.7	-	4.00E-05	1.9
					122		36.8	-	1.23E-05	1.9
					125		73.1	-	5.10E-06	1.8
					128		84	-	4.33E-07	2.3

Authors	Provider (grade or L content)	M_n/M_w (g/mol)	-	iso or non iso	Tc (°C)	CR ($\mu m.min^{-1}$)	t1/2	k_c (min^{-n})	k_a (min^{-n})	n_a
Lai 2004	Polysciences Inc. PLLA	$M_w =$ 200 000	molten	iso	124		11.5	-	2.91E-12	3.98
					105	3.4		-		
					110	3.9		-		
					115	4.3		-		
					120	4.3		-		
					125	3.6		-		
					130	2.1		-		
Tsuji 2006c	Unitika Ltd	-	molten	iso	125	2.31		-		
					130	2.2		-		
					135	1.96		-		
					140	1.6		-		
					150	0.7		-		
Su 2009	NatureWorks 4032D (98%L)	$M_n =$ 45 000	molten	iso	125	7.5		-		
				non iso	1			1.32E-03	-	2.2
					1.5			0.023	-	1.9
					2			0.0794	-	1.7
					3			0.244	-	1.7
Huang 2009	Wei Mon Industrial Co.	$M_n =$ 206 000	cold	non iso	2		5.15	-	0.1757	3.26
					3		4.1	-	0.2164	3.22
					4		3.52	-	0.253	3.33
					5		2.92	-	0.2658	3.19
Wu 2007	NatureWorks 4051D (96.7%L)		molten	non iso	1		7.49	3.52E-04	-	3.4
					2		4.19	7.61E-03	-	3.24
					5		3.1	4.28E-02	-	2.82
					10		1.42	6.85E-01	-	2.12
Liu 2010	Purac PLLA	$M_n =$ 140 000	molten	non iso	1			ca 0		5.4
					2			4.00E-03		4.9
					5			2.40E-01		4.5
					8			7.30E-01		2.8
					10			8.50E-01		2.6
	Purac PDLLA (98%L)	$M_n =$ 83 000	molten	non iso	1			1.00E-04		3.1
					2			3.00E-02		2.8
					3			1.50E-01		2.8
Li 2010a	NatureWorks PLA (98%L)	$M_n =$ 106 000	molten	non iso	1.25		8.53	1.00E-03		4.1
					2.5		5.56	3.00E-03		3.3
					5		3.72	1.30E-02		3
					10		1.42	0.317		2.1
Xiao 2010b	NatureWorks PLA 4032D	$M_w =$ 207 000	molten	non iso	1		22.9		0.00017	2.7
					2.5		6.3		0.00462	2.7
					5		3.5		0.02	2.8
					7.5		2.7		0.04808	2.7
					10		1.8		0.17175	2.6

Authors	Provider (grade or L content)	M_n/M_w (g/mol)	Initial state	iso or non iso	Tc (°C)	CR (µm.min^{-1})	t1/2	Kc (min^{-n})	Ka (min^{-n})	na
Li 2010b	2002D (95.7%L)	M_w = 100 000	molten	iso	105	0.75				
Masirek 2007	Cargill Dow (95.9%L)	M_w = 126 000	molten	iso	122	1.7				
					110	0.4				
DiLorenzo 2006	Boehringer (100%L)	M_w = 101 000	molten	iso	115	9				
				iso	130	7				
				iso	117	10				
				non iso	117	8				
				iso	108		<1.5			
				iso	120		3.5			
				iso	90		5			
				iso	140		7			
Bouapao 2009	Polysciences Inc. PLLA	M_w = 520 000	molten	iso	110	4.4				
					115	3.2				
					125	3.8				

1.3. Transport of small molecules through polymeric matrix

The need in gas barrier material is increasing in packaging field and particularly in the food, cosmetic, medical packaging and optoelectronic. Indeed due to recycling, marketing, and cost constraints, the glass and metal packaging were replaced by polymeric material whose barrier properties has to be understood to be improved.

In spite of the development of multilayer materials, plasma deposition, nanocomposites, active packaging (addition of scavengers in the polymer), the whole barrier food packaging does not exist for the moment. It is still difficult to choose the most suitable packaging to preserve the quality of a given foodstuff. Indeed the transfer is as well dependent on the polymer structure as on the permeant molecules and the environment.

1.3.1. Solution-diffusion mechanism

The mechanism of molecules transport is different according to the porosity of the packaging. This porosity is defined as the volume fraction of void space in a membrane. So below micropores dimension, diameter pore less than 2 nm (Dury-Brun, 2007), the membrane is considered as dense and the transfer in this material follows a solution-diffusion mechanism. This latter corresponds to the penetrant transport by penetration and crossing of the membrane by the molecules. The transport phenomena can be decomposed in three steps:

- Sorption of the molecules at the polymer surface.
- Diffusion inside the polymer matrix.
- Desorption on the other side of the polymer by evaporation in the case of water vapour or aroma compounds.

1.3.1.1. Solubility Coefficient

The general term of sorption includes the adsorption, absorption, clustering of aggregates or trapping in microvoids. The adsorption can be physical (van der Waals or electrostatic interactions) or chemical (chemical bonds between the polymer surface, the adsorbent, and the adsorbed compound). The absorption describes the dissolution of the penetrant in the rubber polymer. In the glassy state, the polymer behaves like adsorbent with specific

adsorption sites. This step is characterized by the solubility coefficient, a thermodynamic parameter which quantifies the solute molecules dispersed in the matrix at the equilibrium. Four classical modes of sorption make it possible to describe the sorption in the polymeric matrix and more particularly the nature of the dominant interactions (Table 1.9). The typical plots are represented in Figure 1.14. Two of these sorption models are a combination of the other models.

Table 1.9. Mode sorption and typical interactions associated.

Sorption mode	Main component interactions
Henry	polymer-polymer
Langmuir	polymer-polymer
Dual Mode	combination of Henry's and Langmuir modes
Flory-Huggins	penetrant-penetrant
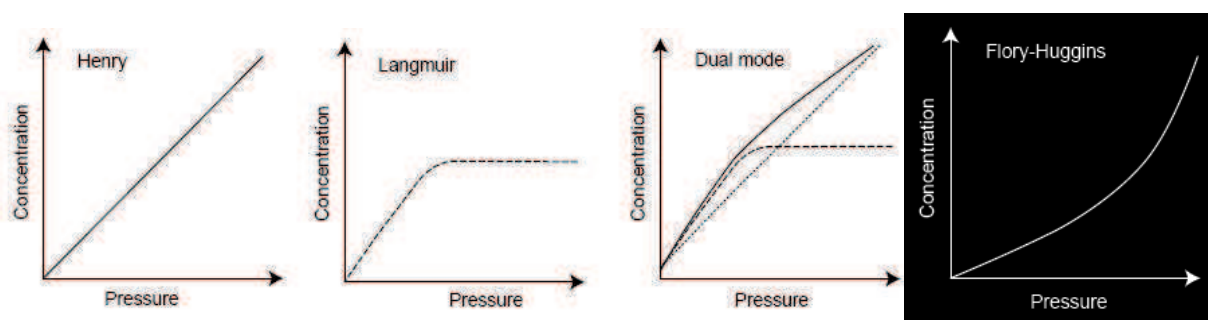
Figure 1.14. Typical isotherm plots of sorbed concentration versus vapour pressure.

1.3.1.1.1. Henry's law sorption

For low pressures, when the penetrant-penetrant and penetrant-polymer interactions are weak and the polymer-polymer interaction strong, the solubility of gas in rubber polymer is low and can be described by the Henry's law. For this ideal system, the solubility is independent of the concentration and so the sorption isotherm is linear which means that the penetrant concentration is proportional to its partial pressure:

$$C = k_D \times p \tag{1.18}$$

In that case, k_D is equals to the solubility coefficient of the penetrant in the polymer (Klopffer, 2001; Matteucci, 2006; Park, 2008).

Pino *et al.* (Pino, 2005) reported that this model is satisfactorily followed by oxygen, nitrogen and carbon dioxide solubility data in rubbery PE, at low pressure. Patzlaff *et al.* (Patzlaff,

2006) also showed that the concentration of propylene in polypropylene, in its rubber state, follows the Henry's law between 25 and 70 °C.

1.3.1.1.2. Langmuir-Mode sorption

In the case where the penetrant-polymer interaction is predominant, the sorption isotherm is highly non-linear, especially at high vapour pressures. It is due to the fact that the diffusing molecules occupy specific sites in the polymer and when all the sites are occupied a small quantity of diffusing molecules may solubilise in more densely packed regions within the polymer. The concentration of the penetrant is:

$$C_H = \frac{C_H' bp}{1+bp} \tag{1.19}$$

Where C_H' is the hole saturation constant and b is the hole affinity constant (Klopffer, 2001).

1.3.1.1.3. Dual-Mode sorption

This mode corresponds to the combination of the two previous modes: Henry's law and Langmuir. It postulates the existence of two populations of diffusing molecules in the case of sorption of low activity gases in glassy polymers. The concentration of gas molecules in the polymer can be expressed by:

$$C = k_D p + \frac{C_H' bp}{1+bp} \tag{1.20}$$

At high pressure, the slope is determined by the Henry's law solubility coefficient, k_D, whereas, at low to moderate pressure in glassy polymers, the Langmuir term controls the gas sorption (Matteucci, 2006).

In case of strong interactions (swelling or plasticization), this mode is not adapted.

This model described not only the methane solubility in rubbery HDPE at high pressure (above 100 bars) (Von Solms, 2004) but also the different gas solubility in polyimide silica composites (Joly, 1997). The solubility of methane in poly(n-butyl methacrylate) also exhibited a dual mode sorption behaviour (Nadakatti, 1995).

1.3.1.1.4. Flory-Huggins Mode

For more condensable gases, at high pressure, strong interactions occur between penetrants. So a non-linear sorption isotherm, which is convex to the pressure axis, is observed. This

curve form is characteristic of the dissolution of the penetrant vapour in the polymer above its T_g. It can be described by the Flory-Huggins equation:

$$\ln a = \ln \frac{p}{p^0} = \ln \phi_1 + (1 - \phi_1) + \chi (1 - \phi_1)^2 \qquad (1.21)$$

Where a represents the thermodynamic penetrant activity and is defined as the ratio of p and p^0, the pressure and the saturation vapour pressure, respectively. ϕ is the volume fraction of the penetrant dissolved in the polymer and χ the enthalpic interaction parameter between the polymer and the solute. When $\chi > 2$ the interactions between polymer and penetrant are small but when $\chi \leq 0.5$, the interaction are so strong that non-crosslinked polymer can dissolve in the penetrant (Matteucci, 2006; Mulder, 1996).

It appears that the calculation of the enthalpies interaction for five polymer-solvent binary systems show a dependence of χ to the temperature and especially for the pentane/polyisobutylene system at 318 K and for chlorobenzene/polyethylene at 413 K.

ENSIC Model

Due to the underestimation of the solvent clustering by the Flory-Huggins theory, a new model has been postulated, the ENSIC model (Favre, 1996) which is a compromise between Flory-Huggins model and multiparameter theories for binary systems. It considers the probability of insertion of one molecule of gas, vapour or solvent in a polymer/solvent matrix. Among these two species, one is present only in the condensed phase. Two main parameters are taken into account, the elementary affinity between the non polymeric compounds and either a polymer segment (k_p) or a sorbed solvent molecule (k_s). Solvent activity (a_s) and solvent volume fraction in the matrix ϕ_s are linked by the following equation which describes either concave or convex isotherms depending the values of k_p and k_s.

$$\phi_s = \frac{e^{(k_s - k_p)a_s} - 1}{(k_s - k_p)/k_p} \qquad (1.22)$$

The solvent clustering could be described by this model as soon as the solvent/solvent affinity is higher than the solvent/polymer affinity ($k_s > k_p$).

Favre *et al.* showed that this model described well the solubility of water in ethyl cellulose, cellulose acetate or poly(vinyl alcohol), but also the one of toluene in polydimethylsiloxane or polyethylene at different temperatures (Favre, 1996; Hirata, 2006).

62

1.3.1.2. Diffusion Coefficient

The molecular diffusion may be described by molecular transport as a result of the random motion of molecules. This kinetic parameter translates the dispersion of the molecules due to thermal agitation. The molecules diffuse through a dense membrane in the direction of decreasing chemical potentials until a thermodynamic equilibrium is reached.

The diffusion behaviour can be classified into three categories: (Masaro, 1999a; Modesti, 2004)

- The case I, fickian diffusion, in which the diffusion rate of the penetrant is much less than the relaxation rate of the polymer chain. In this case, the sorption equilibrium is rapidly established. Generally the considered polymers are in their rubbery state.
- The case II, the sorption controlled process, in which the diffusion rate is much more rapid than the relaxation rate of the polymer chains. This behaviour is observed for glassy polymers.
- The case III, the non fickian diffusion or anomalous diffusion which occurs when the diffusion and relaxation rates are similar.

Let us consider a monolayer membrane, whose thickness is l and the surface A, submitted to a penetrant and Q the total amount of penetrant which transfer through this membrane during a time t.

In the steady state, the quantity of penetrant, which crossed the membrane is J the flux density, given by:

$$J = \frac{Q}{A \times t}$$ (1.23)

The flux can be related to the average concentration, C, on both sides of the membrane thanks to k the total mass transfer coefficient across the membrane.

$$\frac{Q}{t} = k \times (C_1 - C_2)$$ (1.24)

where $C_1 > C_2$.

In 1855, Fick proposed to describe the flux of substance (J) with the following equation:

$$J = -D\vec{\nabla}C$$ (1.25)

63

Where D is the diffusion coefficient and $\vec{\nabla}C$, the concentration gradient between both sides of the membrane.

In a unidirectional case (direction x), when the thickness is much smaller than the other dimension, the equation is simplified in:

$$J_x = -D\frac{\partial C}{\partial x}$$ (1.26)

This first law of Fick is applicable when the following conditions are joined:

- The transfer is in the steady state, which means that the concentration does not vary with time and the flux is constant.
- The membrane is dense and homogeneous.
- The local equilibrium is reached instantaneously.
- The diffusion is unidirectional, perpendicularly to the considered surface.
- The initial concentration is uniform.
- The diffusion coefficient is constant and independent from time, space and concentration

In the transient state, the second law of Fick is applied. Derivated from the first law, the second law is used when the concentration varies with time and position. For a constant D and x between 0 and l, it can be written as (Mulder, 1996):

$$\frac{\partial C}{\partial t} = D\frac{\partial^2 C}{\partial x^2}$$ (1.27)

When steady state is reached, the penetrant diffuses in a constant manner in the material. If we suppose that the sorbed concentration of the penetrant is proportional to the concentration of the penetrant in contact with the surface of the film, the flux, J, can be expressed as

$$J = D\times\frac{(C_1 - C_2)}{l}$$ (1.28)

with D, the diffusion coefficient, l, the thickness and C_1 and C_2, the penetrant concentration on the both sides of the membrane ($C_1 > C_2$). According to the Henry's law,

$$C_1 - C_2 = S\times(p_1 - p_2)$$ (1.29)

Hence $J = \dfrac{D\times S\times(p_1 - p_2)}{l}$ (1.30)

The coefficient of permeability P is then the product of the coefficient of diffusion D ($m^2.s^{-1}$) and the coefficient of solubility S ($kg.m^{-3}.Pa^{-1}$)

1.3.1.3. Methods to study mass transfer

1.3.1.3.1. Methods to measure

Transfer of small molecules through membranes can be studied thanks to several measurements methods. However, three main methods exist to assess the transport coefficients: sorption-desorption, integral permeation and differential permeation (Flaconnèche, 2001).

The first method consists in recording the weight variation (uptake for sorption and loss for desorption) of the polymer sample with time. In a first place all the possible interfering molecules are removed from the chamber. Then the penetrant gas is introduced in this chamber up to a certain pressure and the measurement of the weight variation can begin. The measurement can be direct, by gravimetric methods, or indirect by pressure or volume measurements. The determination of the solubility coefficient, thanks to this method, is more accurate than by permeation. The apparent diffusion coefficient is calculated from the recorded data.

These data are obtained from gravimetric, volumetric or oscillation techniques, or from less used technique, such as inverse gas chromatography or freeze purge desorption.

The second method, the integral permeation, is performed in a closed chamber. The upstream pressure is maintained constant at a higher pressure than the downstream one to obtain a pressure difference and so to induce the transfer through the membrane. Consequently the gas crosses the membrane and is accumulated in a closed receiving chamber.

The permeation curve reaches asymptotically a maximum value for a long time and then the transport coefficient can be determined thanks to the time-lag method.

This method can be used from gravimetric, volumetric or manometric data, or from various analytical measurements by employing a gas different from that to analyse. Directly proportional to the gas amount which has passed through the membrane, some parameters can be assessed by analytical techniques (infrared spectroscopy, ultraviolet spectroscopy, mass spectroscopy, radio tracers or thermal conductivity).

The third method, the differential permeation, is on the same principle than the last one but the upstream chamber is opened and the pressure constant. It means that a gas stream sweeps the downstream chamber to pull the penetrant to a detector. Several detectors are added to this set up to measure the flux, such as mass spectrometer, gas analysers or thermal conductivity. This method has for advantage to make it possible the analysis of gas penetrant mixture. Indeed by using gas chromatography or mass spectrometry, each compound of the mixture can be detected and quantified to determine its transport coefficient.

1.3.1.3.2. Determination of transport coefficients

The determination of the permeability, diffusion and solubility coefficient is dependent on the measurement method: sorption-desorption or permeation methods.

<u>The permeation method</u>

This method makes it possible to measure the flux through a membrane, of thickness l and surface A, in function of the time. C_1, p_1 and C_2, p_2 are the concentrations and pressures in each side of this membrane. p_1 is much higher than p_2, close to 0. When the steady state is reached, the flux, J, is given by the Equation 1.28. From this flux, it is possible to determine the permeability coefficient, P, thanks to the following equation:

$$P = \frac{J \times l}{p_1} \tag{1.31}$$

As mentioned previously, before reaching the steady state, flux and concentration vary with time and can be expressed thanks to the Fick's second law:

$$\frac{Q(t)}{l \times C_1} = \frac{D \times t}{l^2} - \frac{1}{6} - \frac{2}{\pi^2} \sum_{1}^{\infty} \frac{(-1)^n}{n^2} \exp\left(\frac{-D \times n^2 \times \pi^2 \times t}{l^2}\right) \tag{1.32}$$

When t towards the very long time, the steady state is reached and the exponential term is negligible. So the last equation can be simplified as:

$$Q(t) = \frac{D \times C_1}{l}\left(t - \frac{l^2}{6D}\right) \tag{1.33}$$

The intercept on the x-axis called time lag (θ) is given by the following equation, which makes it possible to calculate the diffusion coefficient:

$$\theta = \frac{l^2}{6D} \tag{1.34}$$

Then thanks to the relationship between the transport coefficients, $P = D \times S$, the apparent solubility coefficient (S) can be obtained.

The sorption-desorption method

Various techniques are performed to measure the solubility coefficient of penetrant in a polymer sample. According to Crank, the variation of mass penetrant in the membrane can be expressed by:

$$\frac{m_t}{m_\infty} = 2\left(\frac{D \times t}{\left(l/2\right)^2}\right)^{1/2}\left(\pi^{-\frac{1}{2}} + 2\sum_{n=1}^{\infty}(-1)^n ierfc\left(\frac{n\left(l/2\right)}{\left(D \times t\right)^{1/2}}\right)\right) \tag{1.35}$$

Where l is the thickness of the membrane, m_t the mass uptake at time t and m_∞ the mass uptake at infinite time.

But this equation can be simplified, in case of a plane sheet symmetric and with a constant contact condition, in:

$$\frac{m_t}{m_\infty} = \left(\frac{16D}{\pi \times l^2}\right)^2\sqrt{t} \tag{1.36}$$

The recorded data make it possible to plot the relative weight variation in function of square root time to retrieve the slope and so the diffusion coefficient.

The solubility coefficient is also obtained at the equilibrium by:

$$S = \frac{m_\infty \times d}{m_0 \times p_i} \tag{1.37}$$

Where m_0 is the initial mass of the membrane, m_∞ is the mass gain at equilibrium, d is the density of the membrane and p_i the partial pressure of the penetrant in which the membrane was placed in the chamber.

So thanks to the diffusion and the solubility coefficients, the apparent permeability coefficient (P) can be retrieved.

1.3.2. Relation structure-barrier properties

The transport phenomena are highly dependent on the composition and the structure of the semi crystalline polymers. Several factors affect therefore directly the transfer such as the polymer chain unsaturation, the presence of lateral chains and the steric hindrance which restrain the chains mobility and packing. However the hydrogen bonding, the chain symmetry, the degree of crosslinking, the crystallinity degree and the orientation tend generally to decrease the transport in polymer matrix. Eventually the presence of polar group in the polymer may induce an enhancement of the barrier properties according to the penetrant (Pandey, 2001; Sangaj, 2004).

In a semi-crystalline polymer, two different phases can be distinguished: the crystalline and amorphous phase. The penetrant molecules cannot be sorbed or diffuse in the former phase. In the latter phase, the sorption and the diffusion of the penetrant molecules are linked to the free volume (statistical mechanical considerations) and to energetic or structural considerations. So at a molecular level, the transport mechanism is described by numerous models. However they differ according to the state of the polymer (glassy or rubbery) but also to its structure.

Nevertheless, the transport properties are also controlled by the diffusant properties (structure and concentration) and the temperature. Recently, Kwan *et al.* (Kwan, 2003) highlighted the fact that, without interference from polymer-penetrant, the transport behaviour of alkanes in polyamide is dependent on the shape of the penetrant and more specifically, is expected, in this case, to diffuse along their long axes.

1.3.2.1. Influence of the polymer structure

1.3.2.1.1. Glassy state

In the glassy state, at a temperature below T_g, the membrane is not in equilibrium due to the long process of relaxation. The mobility of the chain segments is limited and only few segments (side groups) have enough energy to rotate or twist locally. Consequently, diffusion process occurs at faster rate than relaxation process of the polymer matrix. This latter possesses more volume than it would at equilibrium (Figure 1.15) called excess hole free volume and in which the penetrant could be trapped. However, once the glassy polymer will be exposed to penetrant, the molecules dissolved in the matrix may change the polymer

structure. A decrease in T_g and an increase in the specific volume are then possible, it is the plasticization of the polymer.
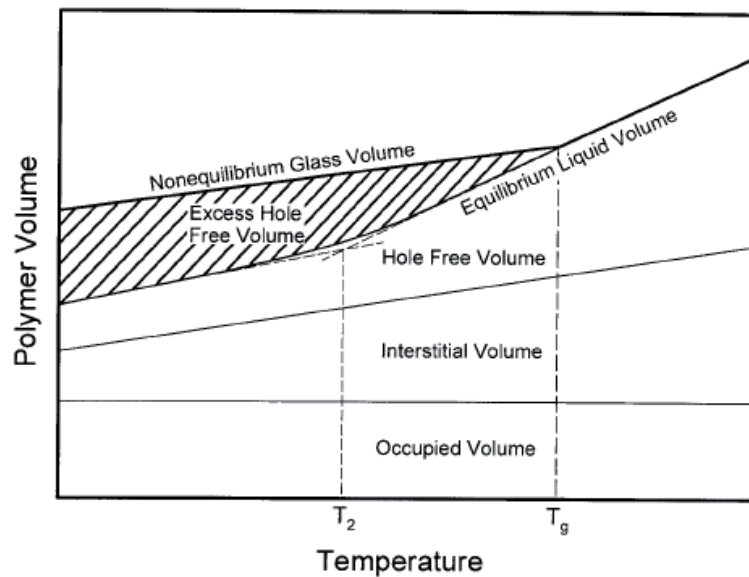
Figure 1.15. Schematic representation of the polymer specific volume versus the temperature (Kanehashi, 2005; Liu, 2002).

Hence, transport mechanisms are not well understood in the glassy polymer and most proposed models are phenomenological. So to describe the sorption and the diffusion of penetrant in a polymer below its T_g, two models are used: the dual-mode sorption model and the gas polymer matrix model.

As previously described, the dual-mode sorption model postulates two distinct populations (Figure 1.16):

- the first one whose molecules are dissolved in the solid polymer and obey to the Henry's law (Eq. 1.18)
- the second one whose molecules are trapped by adsorption on the walls of microvoids or holes and obey to the Langmuir type sorption (Eq. 1.19). These holes might be related to the excess free volume due to the slow relaxation occurring at T_g (Figure 1.15) or to the unrelaxed free volume frozen during T_g.

Guo and Barbari used this sorption model to explain the swelling of cellulose acetate in glassy state due to acetonitrile vapour (Guo, 2010). Serad *et al.* showed that the sorption of n-butane in PET is well described by this dual mode sorption model (Serad, 2001).
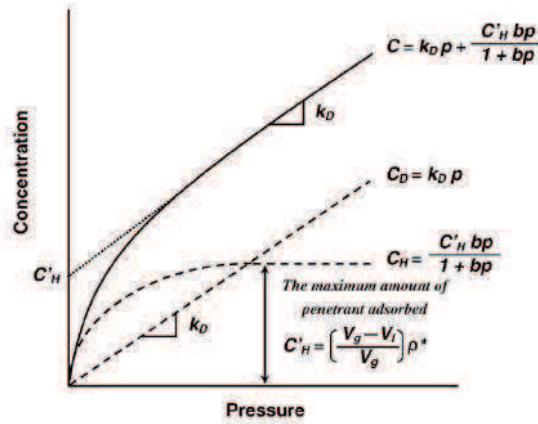
Figure 1.16. Schematic representation of the dual mode sorption isotherm (Kanehashi, 2005).

The gas-polymer matrix model, developed by Raucher and Sefcik (Raucher, 1983a, 1983b; Sefcik, 1983), expresses the dependence on the concentration of the sorption and gases transport phenomena due to the supposed interaction between one population of penetrant and the polymer matrix. The resulting structural properties and the dynamics of the polymer could be modified and thereby change the transport characteristics of the matrix. This model postulates that the penetrant jumps between chains is made easier by the interactions between already sorbed molecules and polymer matrix. Moreover the variation in the diffusion coefficient would be due to the enhancement of the chain mobility induced by the increase in the penetrant concentration.

Consequently a modification in the matrix structure (plasticization and antiplasticization) would influence the gas diffusion coefficient.

In the case where the decrease of T_g is proportional to the concentration, C, the interaction between penetrant and polymer would be expressed as follows:

$$S = S_0 \exp(-\alpha C) \tag{1.38}$$

$$D = D_0 \exp(\beta C) \tag{1.39}$$

Where α and β are constant and S_0 and D_0 are the transport coefficient in the limit of a zero concentration.

According to Brolly and al., it appears that the gas-polymer matrix model offers a satisfactory description of the experimental transport of CO_2 in PET and PEN. Indeed some interactions occur between CO_2 and these two glassy polyesters without giving evidence of two different populations (Brolly, 1996a, 1996b).

1.3.2.1.2. Rubbery state

In the rubbery state, the segmental motion of the polymeric chains is rapid and consequently in response to external changes, the structure can rearrange quickly. The transport is more rapid in rubbery polymer than glassy polymer, and dependent strongly of the glass transition temperature of the polymer. Indeed the increase in the chain flexibility and free volume furthers the diffusion of penetrant in the polymer matrix. Two mechanisms of diffusion are suggested in the rubbery polymer: free volume theory and the molecular model.

<u>The free volume theory</u>

The free volume theory was initially proposed by Cohen and Turnbull in 1959 (Cohen, 1959) to be suitable only for liquids. They envisioned these liquids as ensembles of uniform hard spheres and cavities formed by nearest neighbours. The free volume is thus defined as the volume not occupied by the matter.

In 1960 Fujita (Fujita, 1961) developed, in a promising way, the free volume theory model for mass transport in a ternary system (polymer, solvent and penetrant). Indeed molecular transport is assumed to be due to the continuous redistribution of free volume elements rather than the physically displacement of the neighbours which requires energy change. However this displacement is possible in the case where the volumes of nearest cavities are sufficiently large to receive the penetrant (Duda, 1996; Masaro, 1999a). The diffusion rate is therefore proportional to the probability of finding a hole volume $V*$, the minimum volume hole size, or larger adjacent to the hard sphere. Consequently the diffusion coefficient may be expressed by the following equation:

$$D = A \exp(-\gamma \frac{V*}{V^f}) \tag{1.40}$$

Where $V*$ is the minimum volume hole size into which a molecule can jump, V^f the free volume fraction of the system and γ a numerical factor between 0.5 and 1 which takes into account the possible overlap between free volumes. The free volume fraction is described as the ratio of the sum of the holes and the total volume, which gather the free volume and the occupied volume defined as the volume associated with the van der Waals radius of the molecules and their vibrational motions (Duda, 1996; Klopffer, 2001).

Also valid for a binary system, this model has been used by several authors to study gas diffusion in PE membranes (Kulkarni, 1983; Stern, 1986) or ketones and ester solvents in PMMA solutions (Zhu, 1992; Zhu, 1993). Eventually the Fujita's free volume model seems to

be adequate to describe the diffusion of small-sized diffusants in dilute and semi-dilute polymer solutions and gels (Masaro, 1999a).

However this model cannot be applied for a polymer-water system due to the numerous interactions.

In 1968 Yasuda *et al.* (Masaro, 1999b) assumes that the free volume in a binary system depends mostly on the volume fraction of the solvent because of:

- the higher mobility of the solvent compared to the polymer
- the large contribution of the solvent to the effective free volume
- the decreasing of the solvent diffusion with increasing the polymer concentration

This model is in agreement with experiments carried out with several polymers capable of swelling, and with water and strongly interacting molecules (Matsukawa, 1997) but it cannot be applied for the hydrogels chemically crosslinked.

Consequently in 1983, Peppas and Lusting (Peppas, 1987) developed a model for crosslinked polymer networks. Three different kinds of structure have been considered: non-porous hydrogels, micro-porous hydrogels (pore size > 0.1 µm) and macro-porous hydrogels (20 Å < pore size < 500 Å). These structures induce then different transport mechanism: convection, diffusion and coupled convection/diffusion.

This model is limited by the diffusant size and the ionic character of some diffusant which leads to numerous interactions.

Finally one of the most used models is the one of Vrentas and Duda (Vrentas, 1977a, 1977b; Vrentas, 1985a; Vrentas, 1985b) in which the contribution of the solvent and the polymer are taken into account for free volume. This model makes it possible to introduce several physical parameters such as temperature, activation energy, polymer concentration, solvent size and molecular weight of the penetrant. Nevertheless among the 14 parameters used in this model, 10 are necessary to apply it and predict the self diffusion coefficient although these parameters are not usually available in the literature. Despite this drawback, it seems that according to Zielinski *et al.* (Zielinski, 1996) there is a good agreement between this theory and the diffusion data of triisopropylbenzene in PS solution even in presence of toluene. In the same manner Hong *et al.* (Hong, 1997) showed a correlation between the Vrentas and Duda theory and the diffusion of toluene and chloroform in polyethylene-polystyrene networks.

To summarize all these free volume theory models are based on the jump from one free volume to another and to the relaxation dynamic of polymer to explain the diffusion. Thus the rearrangement of free volume creates holes through which diffusing particle pass.

The molecular model

Contrary to the free volume theory model, the molecular model is based on energy considerations. In this approach the diffusing molecule jump from one position to another when the activation energy for the system is sufficient. In this case, the system is defined as the solute and the surrounding polymer chains.

The first molecular models were simple and required some adjustments. Nevertheless the important idea was that the diffusion process was partially due to the cooperative segmental motions of the polymer. So Brandt (Brandt, 1959) suggests that the required activation energy is the sum of the intramolecular energy, used to bend the neighbouring chains and the intermolecular energy needed to overcome the attractive forces between chains and to create a cavity in the polymer structure. These energies are linked to the penetrant and polymer characteristics.

Some years later, DiBenedetto and Paul (DiBenedetto, 1964) developed one approach where the activation energy of diffusion equals the difference of potential energy between the normal state, dissolved state, and the activated state, in which the penetrant moves because of a cylindrical cavity.

In 1979, Pace and Datyner (Pace, 1979) suggested a theory based on the two last models: the penetrant diffuses along the chain direction (from Brandt) and jump perpendicularly to the main chain direction (from DiBenedetto and Paul).

1.3.2.1.3. Semi-crystalline polymers

As mentioned previously, the semi-crystalline polymer is composed of an amorphous phase and a crystalline phase. The solubility and diffusion of penetrant occurs exclusively in the amorphous phase whereas the crystalline phase acts as barrier for the penetrant transport. Moreover this excluded zone modifies the path of the penetrant molecules due to the increase of the tortuosity of the polymeric matrix. The size of the crystallites and the trapping of chains segment in the neighbouring crystalline lamellae can highly increase the tortuosity of the matrix.

Several polymers have been studied to assess the effect of the crystallinity on the penetrant transport in semi-crystalline polymers. It appears that the increase in the crystallinity degree induces a non linear decrease in the diffusion coefficient. This phenomenon is observed as well for polyethylene (low and high density) (Vittoria, 1995) as for polypropylene (iso- and atactic) (D'Aniello, 2000). The comparison, done on different grades of polymer to obtain various crystallinity degrees, leads to also attribute this decrease in diffusion coefficient to the difference in the molecular mass and the density of the polymers. The influence of crystallinity degree has also been studied for poly(ethylene terephthalate). So Sammon (Sammon, 2000) showed that the increase in crystallinity degree induces the decrease in the water and methanol diffusion coefficient in annealed and trans-esterified PET.

The density, resulting from crystallization, modifies also the transport coefficient. The increase in PE density induces a dramatic drop in oxygen permeability coefficient (Sangaj, 2004). Limm *et al.* (Limm, 2006) showed that the diffusion coefficient of limonene decreases proportionally to the density of different PE type. So the diffusion coefficient drops from 2 scale orders for densities between 0.87 and 0.97.

1.3.2.1.4. Oriented polymers

The orientation, by drawing or stretching, of the semi-crystalline polymers induces modification in the polymer structure and so in the transport. The orientation can be uniaxial or biaxial (simultaneous or sequential) and leads to diverse spatial distribution of the amorphous phase according to the orientation mode and rate. The orientation induces generally a closer chain packing and so restricts the chain mobility. Nevertheless the sequential stretching process can break the structure created by the uniaxial stretching and transform it into a new structure. Some experiments have been carried out on polyester films with various gases. Brolly *et al.* (Brolly, 1996a) showed that the diffusion coefficient increases with the orientation of PET. So the diffusion coefficient of CO_2 is doubled from a draw ratio of 1 to 4. This evolution is contradicted by McGonigle *et al.* who presented a decrease of CO_2, N_2 and Ar diffusion coefficient with the increase in the draw ratio of PET (McGonigle, 2001). A blend of PP/PVA highlighted this behaviour with a non condensable gas. Indeed a decrease of the diffusion coefficient of O_2 with the draw ratio up to 6×8 have been observed but an increase in the water vapour diffusion coefficient is also noticed and attributed to the high moisture permeability of PVA (Jang, 2004). However as the orientation process generally modifies the crystallinity degree in the same way, it is therefore difficult to solely impute the decrease in the diffusion coefficient to the orientation.

1.3.2.2. Influence of the structure of the diffusing molecule

The structure of the diffusing molecule influences strongly its mobility in the polymer matrix. More generally the increase in molecular weight induces a decrease in the diffusion coefficient in PP, LDPE and HDPE (Vitrac, 2006) due to the increasing steric hindrance. A lot of diffusion data are available for compounds of molecular weight from 100 to 1000. It is shown that increasing the chain length of alkane decreases the diffusion in polypropylene or polyethylene according to the exponent law, $D \propto M^{-\alpha}$. This α value corresponds to different diffusion mechanism. So for $\alpha \leq 1$, the diffusion mechanism is the one of the free volume theory. When $\alpha = 2$, the diffusion is controlled by the confinement of the molecule, without big groups or ramification (e.g. alkane), in the polymer matrix. For $\alpha > 2$, the molecular model is used to explain the diffusion of molecules with aromatic rings or ramification.

Nevertheless the effect of molecular weight is less important that the introduction of lateral methyl group (Reynier, 2001a). Indeed it was shown that the presence of aromatic groups or chain branching tends to modify the geometric shape of the molecules which induces a decrease in the diffusion coefficient (Brouillet, 2009). Reynier *et al.* displayed that for similar molecular weight, linear alkanes have higher diffusion coefficient than for the other molecules in PP and PE (Reynier, 2001b). In the same manner, Ducruet at al. showed that the increase in the size of the chain of fatty esters leads to a decrease in the diffusion coefficient whereas the solubility increases in PVC (Ducruet, 1996).

Generally permeant size and structure effects are much more marked for a polymer matrix in the glassy state than in the rubbery state (Dury-Brun, 2007; George, 2001). Indeed the increase in temperature (up to 40 °C, i.e. 38 °C below the T_g of PET) affects the absorption of flavour in glassy polymer (PET, PC and PEN) whereas the rubbery polymers (OPP and LLDPE) do not seem to be influenced (Van Willige, 2002). This effect on the glassy polymer is all the more than their T_g is close to the storage temperature.

The sorption in polymer matrix also depend on the penetrant polarity and hydrophobicity. In PP, Lebossé *et al.* showed that the sorption follows the inverse order of polarity. So ethyl 2-methylbutyrate is much less sorbed than limonene or decanal in PP (Lebosse, 1997). Van Willige *et al.* studied the absorption of flavour compounds in several polar and apolar polymer packaging films. It appears that the more apolar penetrant (limonene and myrcene) are more sorbed in apolar OPP than in polar PET. In the same way, the polar penetrant (hexyl acetate and nonanone) are more sorbed in polar PET and PEN than in apolar OPP and LLPE (Van Willige, 2002).

Moreover the transfer of penetrants in polymer matrix is dependent on their concentration in solution or their partial pressure. The sorption of benzaldehyde in PP and ethyl acetate and caproate in PE increases with their activity whatever the temperature is (Hirata, 2006; Qin, 2007). Some gases showed also an increase in the permeability coefficient with the pressure in polybutadiene. Nevertheless it is not the case for all the molecules whose diameter are less than 3,749 Å except krypton (Naito, 1996).

1.3.2.3. Temperature effect

The variation of the transfer coefficient with temperature is described by two models. The first one, called the William, Landel and Ferry's (WLF) model, is available for a small temperature interval (from T_g to T_g + 100 °C). The second and most often used model is the Arrhenius law. So the diffusion and solubility coefficients can be written as:

$$D = D_0 \times \exp\left(\frac{-E_D}{RT}\right) \tag{1.41}$$

$$S = S_0 \times \exp\left(\frac{-\Delta H_S}{RT}\right) \tag{1.42}$$

where D_0 and S_0 are the pre-exponential term which represent the limited values of this transfer coefficient for an infinite temperature.

E_D and ΔH_S are the activation energy of diffusion and the heat of solution of the penetrant in the polymer, respectively. R is the perfect gas constant.

For small non interactive molecules, such as helium, oxygen, nitrogen, the permeability in PE increases with the temperature (Mulder, 1996). For larger molecules such as organic molecules, similar behaviour is noticed for diffusion coefficient in PP with the increase in temperature (Reynier, 2001a).

Hirata *et al.* showed that the solubility coefficients of ethyl acetate and caproate in PE increase with the temperature between 20 and 35 °C (Hirata, 2006). In the same way, the oxygen transfer coefficients in PET are higher with the increase in experiment temperature (Auras, 2004a). The sorption of homologous series of alcohol in EVOH copolymers is also temperature dependent. More particularly, below T_g the sorption decreases with the increase in temperature whereas it is the contrary for temperatures above T_g. This phenomenon is due

to the apparent molar enthalpy of the penetrant ΔH_S which is expressed by the following relationship between the enthalpy of vaporization ΔH_{vap} and mixing ΔH_{mix} :

$$\Delta H_S = \Delta H_{vap} + \Delta H_{mix} \tag{1.43}$$

ΔH_{vap} is always negative and $\Delta H_{mix} \ll \Delta H_{vap}$. Hence ΔH_S is always negative.

So it is shown that, due to the condensability of the organic molecules, when the temperature increases, a decrease in their coefficient of solubility is noticed.

1.3.3. Barrier properties of PLA

The barrier properties of PLA have not been extensively studied. The first articles treating the permeability of PLA film have been published in 1997 (Shogren, 1997; Siparsky, 1997), when PLA started to be considered for packaging applications. PLA films with various L/D ratio, different crystallinity degree and blends with numerous additives and polymers have been tested these last years with gases, water vapour and organic compounds.

1.3.3.1. Gases

1.3.3.1.1. Oxygen

The oxygen permeability of amorphous PLA has been reported to be between 1.3 and 2.0 $\times 10^{-18}$ m^3.m.m^{-2}.s^{-1}.Pa^{-1} at 30 °C depending on the L/D ratio. Indeed, the increase in the L-lactide content, between 50 and 98.7 %, causes an increase in the solubility coefficient leading to the increase in the permeability (Bao, 2006; Komatsuka, 2008). However this modification of the permeability coefficient seems to be insignificant between 94 and 98% L-lactide content at 25 °C (Auras, 2003; Lehermeier, 2001). Figure 1.17 shows that whatever the L/D ratio, the oxygen barrier properties of PLA are intermediate between low oxygen barrier film (LDPE, PS) and good oxygen barrier films (unplasticized PVC and PET).

The oxygen transport coefficients of PLA, whatever the L/D ratio, are sensitive to the measurement temperature and water activity. Auras *et al.* (Auras, 2003) showed that the increase in the temperature leads to an increase in the oxygen permeability and solubility coefficients in dry conditions. However the increase in the water activity also induces an unexpected decrease of these two coefficients (Auras, 2003). On the contrary, the diffusion coefficient shows an increase with the water activity at each temperature (Auras, 2004a).

This behaviour is attributed to the plasticization effect on the amorphous phase by water molecules.
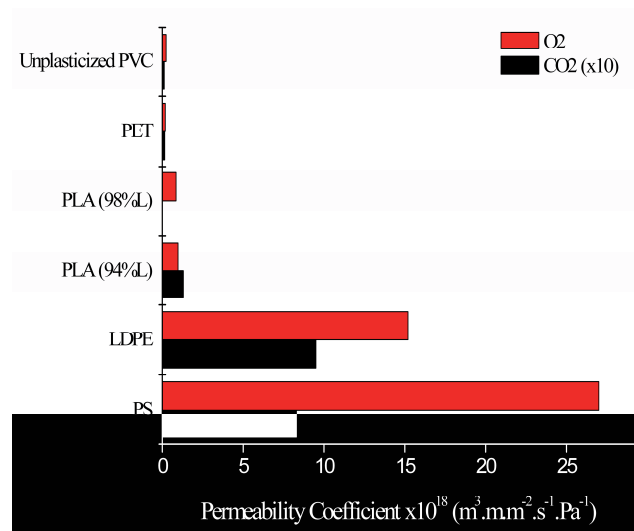
Figure 1.17. Oxygen and carbone dioxide barrier properties of unplasticized PVC, PET, LDPE, PS, and PLA at 25 °C. Data from (Auras, 2005; Colomines, 2010; Komatsuka, 2008; Pauly, 1999; Polyakova, 2001).

The effect of crystallinity has also been studied with PLA (Colomines, 2010) containing different L/D ratio (Colomines, 2010). The poly(98% L-lactide) with a higher crystallinity degree displays lower permeability coefficients than those of the poly(94% L-lactide). This effect has been confirmed by Drieskens *et al.* (Drieskens, 2009) who studied the effect of annealing on PLA transport coefficients. They showed that an increase in crystallinity induces a progressive decrease in permeability coefficient. The diffusion coefficient first sharply decreased (between 0 and 10 % of crystallinity) and then more gradually, while the solubility coefficient seemed to increase slowly with the crystallinity of PLA. Drieskens *et al.* (Drieskens, 2009) explained this behaviour, in the first phase of the crystallization, by an increase in the tortuosity, due to the presence of spherulites. In the second phase, improvement of the internal crystal structure may have induced the further decrease in the diffusion coefficient. The increasing crystallization may be accompanied, according to the authors, with a dedensification of the amorphous phase which may lead to the unexpected increase in the solubility coefficient of PLA (Drieskens, 2009). An overall decrease in the oxygen permeability with increasing crystallinity has also been observed by Sawada *et al.* (Sawada, 2010). Analysis of the experimental data showed the diffusion coefficient increased apparently for small crystallinity degrees and the solubility coefficient decreased over the whole range of tested crystallinity. Colomines *et al.* (Colomines, 2010), showed even a slight increase in oxygen permeability of PDLLA upon moderate crystallization. They suggested,

similarly to Drieskens *et al.* (Drieskens, 2009), dedensification was one of the causes of this unusual behaviour. Sawada *et al.* (Sawada, 2010) proposed a different hypothesis suggesting a continuous space at the interface between crystalline and amorphous domains, and this space, larger than gas molecules at low crystallinity degrees, could facilitate the gas diffusion in PLA.

The addition of plasticizer, used for improvement of mechanical properties, leads generally to an increase in the oxygen permeability coefficient due to the higher mobility of the polymer chain and higher free volume (Martino, 2009). On the contrary, the dispersion of nanoclays in PLA makes it possible to divide the permeability coefficient by 2 or 3 depending upon the type of the nanoclays (e.g. organomodified montmorillonite, cloisite 25A or 30B, organomodified synthetic fluorine mica) and exfoliation (Chang, 2003; Sinha Ray, 2003; Zenkiewicz, 2008).

1.3.3.1.2. Carbon Dioxide

The carbon dioxide permeability coefficient has been measured at 1.1×10^{-17} $m^3.m.m^{-2}.s^{-1}.Pa^{-1}$ at 25 °C (Auras, 2003) and, as previously observed in the case of oxygen, increases with the L-lactide content in PLA (Figure 1.17) and the temperature (Auras, 2003).

The crystallization of the PLA matrix induces a decrease in the carbone dioxide permeability coefficient (Bao, 2006; Oliveira, 2007). According Sawada *et al.* (Sawada, 2010) the effect of crystallinity on CO_2 permeability is similar to the one on oxygen, that is to say there is a slight increase in diffusion coefficient at low crystallinity followed by a decrease for 40 %, whereas solubility decreases slowly in relation with the crystallinity degree.

1.3.3.1.3. Nitrogen

The nitrogen transport coefficients of PLA are lower than those for oxygen (Bao, 2006). Moreover the reported value of nitrogen permeability, around 3.8×10^{-19} $m^3.m.m^{-2}.s^{-1}.Pa^{-1}$ (Komatsuka, 2008), is lower than the value for crystalline PS and LDPE (5.9 and 7.3×10^{-18} $m^3.m.m^{-2}.s^{-1}.Pa^{-1}$) (Komatsuka, 2008; Pauly, 1999) at 25 °C but higher than the one of unplasticized PVC (8.9×10^{-20} $m^3.m.m^{-2}.s^{-1}.Pa^{-1}$) (Komatsuka, 2008).

The L/D ratio might not affect the nitrogen permeability of PLA (Dorgan, 2001). The crystallinity effect has also been evaluated for this gas and it seems that the nitrogen permeability coefficient decreases with the increase in the crystallinity degree of PLA (Sawada, 2010).

1.3.3.1.4. Gas selectivity

The gas selectivity in PLA membrane depends on the chosen gas. Lehermeier *et al.* (Lehermeier, 2001) showed that the separation factor of CH_4 and CO_2, equal to 10, is not crystallinity and L/D ratio dependent. Only change in temperature makes it possible to increase this factor. Sawada *et al.* (Sawada, 2010) confirmed the inefficiency of the crystallinity on the permselectivity but also showed that the diffusivity and the solubility selectivity are not influenced by crystallinity. The gas permselectivity in PLA is larger than 120 for H_2/N_2, 6 for O_2/N_2, 23 for CO_2/N_2, 27 for CO_2/CH_4 and 1 for CH_4/N_2 (Sawada, 2010). The permselectivity of PLA is two times larger than those of LDPE and PVC for O_2/N_2 and CO_2/N_2 (Komatsuka, 2008).

1.3.3.2. Water vapour

The water vapour permeability of amorphous PLA varies from 1.8 to 2.3×10^{-14} $kg.m.m^{-2}.s^{-1}.Pa^{-1}$ at 25 °C (Rhim, 2009; Sanchez-Garcia, 2008; Tsuji, 2006b). As shown in Figure 1.18, the PLA data are lower than the one of PCL but higher than the one of PET, PS and PHBV.

Siparsky *et al.* (Siparsky, 1997) showed that the increase in the L-lactide content in PLA induced no significant modification of the water vapor permeability whatever the temperature and the relative humidity, except a decrease in the permeability coefficient at 90 % RH between 50 and 90 % of L-lactide content. This was not confirmed by Tsuji *et al.* and Auras *et al.* who showed a constant permeability, around $1.8\text{-}1.9 \times 10^{-14}$ $kg\ m\ m^{-2}\ s^{-1}\ Pa^{-1}$ at 20 °C and 40-90 % RH, despite an increase in the L-lactide content (Auras, 2003; Tsuji, 2006b).
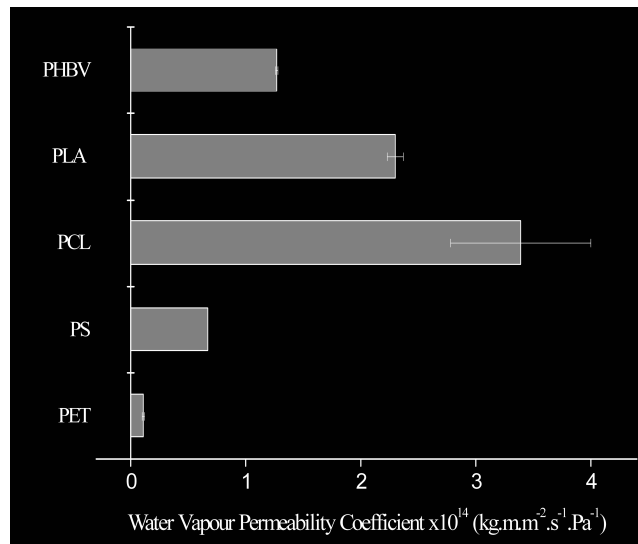
Figure 1.18. Water vapour permeability coefficient of PHB (Sanchez-Garcia, 2008), PLA (Sanchez-Garcia, 2008), PCL (Sanchez-Garcia, 2008), PS (Auras, 2004b) and PET (Auras, 2004b) at 25 °C.

The crystallinity degree does not reveal any change in the solubility coefficient whatever the temperature and the relative humidity are (Siparsky, 1997). Consequently the permeability coefficient seems to be controlled by the diffusion coefficients which increase with the crystallinity degree at certain temperature and relative humidity (Rhim, 2009). This is in contradiction with the decrease in permeability coefficients, reported by Tsuji *et al.* (Tsuji, 2006b) and Shogren (Shogren, 1997). Indeed, in their study, the diffusion and solubility coefficient decrease slightly with the crystallinity degree of PLLA (Yoon, 2000).

Furthermore, the effect of the temperature on measured water vapour permeability changes in function of the study. Auras *et al.* (Auras, 2003) showed a decrease of the permeability with the temperature, whereas Shogren (Shogren, 1997) highlighted an increase. Siparsky *et al.* (Siparsky, 1997) showed that the diffusion coefficients increase and the solubility coefficients decrease with the temperature at 90 % RH which is contradicted by Holm *et al.* (Holm, 2006) who showed higher values of moisture sorption at a higher temperature. The various and contradictory results show that the mechanism of water transport in PLA is not completely understood yet (Auras, 2004b). In particular the presence of water clusters in PLA matrix and their potential to diffuse in cluster form are still controversial (Yoon, 2000).

1.3.3.3. Organic compounds

The transport of organic compound in PLA has been the subject of only a few studies, but is of importance in food packaging applications. Ethylene, a compound accelerating fresh food ripening, plays an important part in the storage of fresh fruits. The ethylene permeability of amorphous PLA has been tested and evaluated at 6.8 $\times 10^{-18}$ m^3.m.m^{-2}.s^{-1}.Pa^{-1} (Lehermeier, 2001). This value is lower than the ethylene permeability of PET (3.0 $\times 10^{-20}$ m^3.m.m^{-2}.s^{-1}.Pa^{-1}) (Lehermeier, 2001) but higher than the value of LDPE (2.2 $\times 10^{-17}$ m^3.m.m^{-2}.s^{-1}.Pa^{-1}) (Pauly, 1999). Increasing the crystallinity in PLA induced, as for oxygen and carbon dioxide, a decrease in the ethylene permeability (Lehermeier, 2001; Sawada, 2010).

The transport coefficients of ethyl acetate, an aroma booster found in a large variety of aroma formulations, have been calculated from sorption of ethyl acetate in PLA experiments. The ethyl acetate permeability of PLA is 5.34 $\times 10^{-19}$ kg.m.m^{-2}.s^{-1}.Pa^{-1} at 30 °C and 0.3 activity. It is higher than the one of PET but lower than those of PP and LDPE. However, the ethyl acetate solubility coefficient in PLA, equal to 6.17 $\times 10^{-3}$ kg.m^{-3}.Pa^{-1} at 30 °C and 0.3 activity, is higher than the other polymers (Auras, 2006). This result is comparable to the value reported by Colomines *et al.* for an amorphous PLA with 99% L-lactide at 25 °C and 0.5 activity (Colomines, 2010). Moreover increasing the crystallinity of PDLLA provokes a decrease of the ethyl acetate solubility coefficient at 0.5 and 0.9 activity (Colomines, 2010).

The permeability of limonene through PLA, has been estimated by Auras *et al.* (Auras, 2006) at a maximal value of 9.96 $\times 10^{-21}$ kg.m.m^{-2}.s^{-1}.Pa^{-1} at 45 °C and with a limonene partial pressure of 258 Pa. The permeability value of this more hydrophobic molecule is lower than that of ethyl acetate in PLA and is lower than those measured for PET, PP and LDPE (Auras, 2006). Haugaard *et al.* confirmed the low limonene sorption in PLA by comparison with the one in HDPE (Haugaard, 2002).

The study of scalping aroma compounds by PLA during high pressure treatment highlighted the lower PLA uptake of organic molecules compared to the one in LDPE. Indeed ethyl hexanoate and limonene are more sorbed in the more apolar matrix, LDPE, than in PLA. On the contrary the more polar molecules, 2-hexanone and ethyl butanoate, are more sorbed by the more polar polymer matrix, PLA (Mauricio-Iglesias, 2011).

Consequently, it appears that the L/D ratio of PLA influences the gas permeability but no conclusion can be reached regarding the water vapour transport in this polymer. Moreover,

generally speaking, the crystallization of the PLA matrix makes it possible to decrease the gas permeability and the organic compound sorption in PLA. However, no agreement has been yet formed regarding the influence of crystallinity degree on the water vapour transport in PLA due to the variety of PLA composition (L-lactic acid content) and measurement systems.

The comparison with commonly used polymeric films, such as PS, PET or LDPE, highlights the fact that the barrier properties of neat PLA are better than those of polyolefins and PS, except for water vapour, but are still to be improved to reach the permeability coefficients of PET.

Chapitre 2

-

Matériels et méthodes

2.1. Matériels

2.1.1. Polymères

Le polylactide (P(D,L)LA CD92) étudié lors de cette thèse a été obtenu de notre collaboration avec le laboratoire ECPM et constitue un échantillon de recherche reconstitué à partir de différents grades. Fourni par Cargill Dow sous forme de granulés, la teneur en acide lactique de forme L de ce polymère est de 92 % environ. La masse molaire du polymère a été évaluée par chromatographie d'exclusion stérique (Tableau 2.1).

Quatre types de films de P(D,L),LA ont aussi été analysés lors de ce travail :

- un P(D,L)LA Biophan^{TM} 121 (Treofan, France) fourni sous forme de film de 20 µm d'épaisseur. Ce film est composé de trois couches, une couche centrale cristallisée et deux couches externes scellables.

- un P(D,L)LA Biomer L9000 (Biomer, Allemagne) sous forme de granulés. Le film a été réalisé, selon les préconisations de NatureWorks, par extrusion monovis à partir de granulés préalablement séchés dans une étuve sous vide (10^{-4} Pa) 80 °C pendant 8 h. L'extrudeuse de 30 mm de diamètre et 33 L/D est composée de 3 sections de vis sans élément de mélange tournant à 40 rpm, d'une filière de 100 mm de large. Le profil de température de l'extrudeuse pour les 6 zones est 180 °C - 185 °C - 190 °C - 195 °C - 205 °C et les éléments de mélange (4 Sulzer SMX®, Sulzer Chemtech) et la filière sont à 210 °C afin d'éviter la présence de granulés infondus et la dégradation du polymère. La température et la vitesse des rouleaux froids sont respectivement fixées à 25 °C et 10 m.min^{-1} afin d'obtenir un film de 80 mm de large et environ 120 µm d'épaisseur.

- Un P(D,L)LA de référence INGEO 2002D (NatureWorks), grade extrusion et thermoformage, et un autre de référence INGEO 4042D (NatureWorks), pour film biorienté. Une fois séchés à 90 °C pendant 8 h dans un sécheur à air sec, les granulés sont transformés par extrusion monovis dont le profil de température est 180 °C - 185 °C - 190 °C - 195 °C - 200 °C et les éléments de mélange et la filière sont à 200 °C. Une filière de 200 mm de large et des rouleaux froids, dont la température et la vitesse sont fixées à 20 °C et environ 1,7 m.min^{-1}, sont utilisés afin d'obtenir un film de 150 mm de large et environ 200 à 300 µm d'épaisseur.

Tableau 2.1. Principales caractéristiques des polylactides utilisés : teneur en L-lactide, masse molaire moyenne en nombre (M_n) et en poids (M_w).

Nom	Teneur en L-acide lactique	M_n (g.mol^{-1})	M_w (g.mol^{-1})
P(D,L)LA CD92	92 %[a]	90 500	248 900
P(D,L)LA Biophan	n.d.	90 000	172 000
P(D,L)LA Biomer L9000	92 – 99.5 %[b*]	91 000	174 000
P(D,L)LA 2002D	95,75 -96 %[c].	99 500	208 000
P(D,L)LA 4042D	92-95,7 %[d]	116 000	188 000

n.d. non déterminé. Les teneurs en L-lactide des produits n'ont pas été données par les producteurs.

[a] selon Martin et al., 2001, [b] selon Pillin *et al*, 2008 et Solarski *et al.*, 2008b, [c] selon Mihai *et al.*, 2002 et Carrasco *et al*, 2010, [d] selon Pillin *et al.*, 2006 et Stoclet *et al.*, 2011.
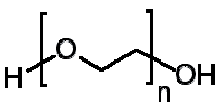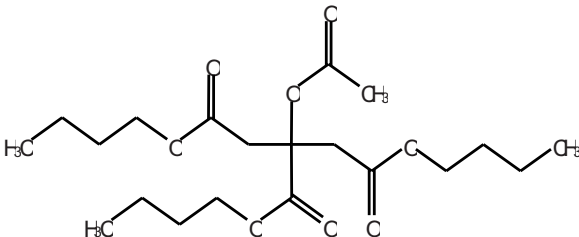
* Une forte incertitude demeure quant à la teneur en L-lactide de ce grade.

2.1.2. Additifs

Deux types de plastifiants, fournis par Sigma-Aldrich, ont été utilisés lors de ce travail : le poly(éthylène glycol) (PEG) et l'acétyl tributyl citrate (ATBC) qui ont été ajoutés au P(D,L)LA CD92 à des teneurs comprises entre 2,5 et 17 % en poids. Les caractéristiques de ces plastifiants sont rassemblées dans le Tableau 2.2.

Un agent nucléant, le talc Luzenac A7C (concentration ≥ 93 %, diamètre médian 6,5 µm), a été fourni par Rio Tinto Minerals (France). Il a été ajouté au P(D,L)LA à une teneur de 1 à 5 % en poids.
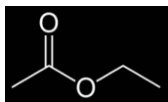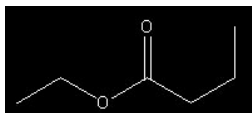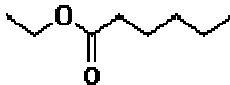
Tableau 2.2. Principales caractéristiques des plastifiants utilisés : formule développée, masse molaire, densité et températures de transition vitreuse (T_g) et de fusion (T_f).

Plastifiants	Formule développée plane	Masse molaire (g.mol^{-1})	Densité à 25 °C	T_g (°C)	T_f (°C)
Poly(éthylène glycol) (PEG)		Environ 300 [275-325]	1,125	- 76	[-8;-15]
Acétyl tributyl citrate (ATBC)		402,48	1,05	- 82,5	9

2.1.3. Gaz et composés d'arôme

L'hélium (He) et l'oxygène (O_2), fournis par Air Liquide (pureté 99,999 %), ont été utilisés afin de tester les propriétés barrières aux gaz du P(D,L)LA. La perméabilité aux composés d'arôme a été mesurée avec l'acétate d'éthyle, le butyrate d'éthyle et l'hexanoate d'éthyle (Tableau 2.3). Ces trois composés constituent une série homologue d'esters éthyliques au nombre de carbone croissant, induisant ainsi une polarité décroissante des composés de cette série.

Tableau 2.3. Principales caractéristiques des composés d'arôme étudiés.

Composés	Formule développée plane	Masse Molaire (g.mol^{-1})	Densité à 25 °C	Point d'ébullition (°C)	Pression de vapeur saturante (kPa)	Indices de Kovats	Log P*
Acétate d'éthyle		88,1	0,9245	77,1	10	872	0,73
Butyrate d'éthyle		116,6	0,879	121	1,510	1025	1,85
Hexanoate d'éthyle		144	0,869	168	1,71	1223	2,83

* P est défini comme le coefficient de partage octanol-eau.
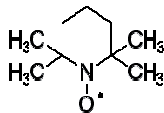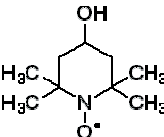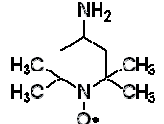
2.1.4. Sondes paramagnétiques nitroxides

Trois sondes ont été utilisées pour les expériences réalisées par Résonance Paramagnétique Electronique :

- 2,2,6,6 – tétraméthylpipéridine-1-oxyl (TEMPO) acheté chez Aldrich.
- 4-hydroxy – 2,2,6,6 – tétraméthylpipéridine-1-oxyl (TEMPOL) acheté chez Aldrich.
- 4-amino– 2,2,6,6 – tétraméthylpipéridine-1-oxyl (Amino-TEMPO) acheté chez Fluka.

Les caractéristiques de ces trois radicaux nitroxides sont rassemblées dans le Tableau 2.4.
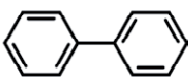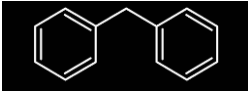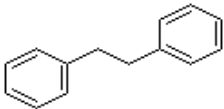
Tableau 2.4. Principales caractéristiques des sondes paramagnétiques utilisées.

Sondes	Formule développée plane	Masse molaire (g.mol^{-1})	Volume molaire (Å^3)
TEMPO		156,25	168
TEMPOL		172,25	174
AminoTEMPO		171,25	179

2.1.5. Sondes fluorescentes

Trois sondes fluorescentes, achetées chez Sigma-Aldrich, ont été mises en solution dans le dodécane afin de réaliser les expériences de microscopie à fluorescence. Ces sondes sont toutes composées de deux cycles aromatiques séparés par un nombre croissant de carbones comme montré dans le Tableau 2.5 :

Tableau 2.5 Principales caractéristiques des sondes fluorescentes.

	Biphényl	Diphénylméthane	Bibenzyl
Formule développée plane			
Masse molaire (g.mol^{-1})	154,2	182,3	168,2
Longueur d'onde d'émission et d'excitation	Ex: 270 nm, Em: 316 nm	Ex: 270 nm, Em: 290 nm	Ex: 270 nm, Em: 290 nm

2.1.6. Solvants

Deux solvants, fournis pas Sigma-Aldrich, ont été utilisés lors de ce travail :
- l'éthanol pour effectuer l'extraction des plastifiants et mettre en solution les sondes fluorescentes.
- l'hexadécane pour mettre en solution les composés d'arôme.

Les caractéristiques de ces solvants, de qualité HPLC, sont présentées dans le Tableau 2.6.

Tableau 2.6. Principales caractéristiques des solvants

Solvants	Formule	Masse molaire (g.mol^{-1})	Température d'ébullition (°C)
Ethanol	C_2H_5OH	46,1	78
Hexadécane	$C_{16}H_{34}$	226,4	287

2.2. Méthodes

2.2.1. Préparation des échantillons de P(D,L)LA CD92

2.2.1.1. Mélange à l'état fondu (Formulation, compoundage à l'état fondu)

Les granulés de P(D,L)LA CD92, les plastifiants et le talc (agent nucléant) sont séchés au préalable dans une étuve sous vide à 80 °C toute une nuit pour diminuer les risques d'hydrolyse du P(D,L)LA ultérieurement au cours du process thermique. Une fois séchés, les granulés de P(D,L)LA sont introduits avec le plastifiant, sous forme liquide, et le talc, sous forme de poudre, dans la chambre interne du Haake Rheocord 9000. Les granulés de P(D,L)LA et le talc sont introduits grâce à une coupelle en aluminium alors que le plastifiant est ajouté à l'aide d'une seringue. Le mélange des composés est effectué à 160 °C et 60 rpm pendant 15 min.

Un grand nombre de mélanges a été réalisé dans le cadre de ce travail afin de déterminer l'influence du plastifiant et de l'agent nucléant sur les propriétés du P(D,L)LA.

- P(D,L)LA pur : P(D,L)LA non additivé ayant subi les mêmes étapes de transformation (160 °C, 60 rpm, 15 min) afin de servir de témoin.
- P(D,L)LA + 1%, 2% ou 5% en poids de talc
- P(D,L)LA + x PEG (x = 2,5, 5, 9, 13 et 17 % en poids)
- P(D,L)LA + x ATBC (x = 2,5, 5, 9, 13 et 17 % en poids)
- P(D,L)LA + 1% talc + x PEG (x = 5, 9, 13 et 17 % en poids)
- P(D,L)LA + 1% talc + x ATBC (x = 5, 9, 13 et 17 % en poids)

Les P(D,L)LA formulés et le P(D,L)LA pur sont ensuite conservés dans un sachet en poly(éthylène).

2.2.1.2. Préparation des films

Le P(D,L)LA CD92 pur ou formulé est séché, avant thermo-compression, au moins 4 h à 90 °C dans une étuve sous vide (Bioblok Scientific Model 3518). Les mélanges sont thermo-compressés à 180 °C à l'aide d'une presse Télémécanique (15 tonnes):

Dans un premier temps, chaque mélange est fondu sans exercer de pression entre deux plaques de métal recouvertes d'une feuille de téflon lisse. Une fois fondu, le mélange est pressé en trois temps afin d'éliminer les bulles d'air : 30 s à 20 bars, 30 s à 50 bars et 1 min à 150 bars. Le film ainsi formé est alors trempé dans un bain d'eau à température ambiante puis conservé dans un dessiccateur rempli de pentoxyde de phosphore.

2.2.1.3. Incorporation des sondes paramagnétiques

Afin de réaliser des analyses de résonance paramagnétique électronique (RPE/ESR), des sondes paramagnétiques ont été incorporées aux mélanges de P(D,L)LA CD92 et de plastifiants selon deux modes, voie fondue ou phase vapeur.

<u>Voie fondue :</u> Chaque type de sonde, sous forme de poudre, est mélangé aux granulés de P(D,L)LA pur, dans une coupelle, avant d'être introduits dans le Haake. Le plastifiant est ensuite ajouté au mélange dans le Haake. La teneur en sonde dans le mélange P(D,L)LA est alors de 1500 ppm environ. Comme précédemment, le mélange est réalisé à 160 °C pendant 15 min à 60 rpm.

<u>Phase vapeur :</u> Des films de P(D,L)LA pur et formulé préparés par thermo-compression sont découpés en fins rectangles de 2 mm de largeur et introduits dans une enceinte fermée contenant un creuset percé contenant un type de sonde paramagnétique en quantité arbitraire. Cette enceinte est conservée à 70 °C pendant 19 jours dans une étuve.

2.2.1.4. Méthode de cristallisation en étuve

Les films de P(D,L)LA CD92 pur ou formulé avec 17 % d'ATBC et 1 % de talc sont cristallisés dans une étuve (Angeltoni Climatic System Massa Martana Type TY80 (PG Italy)) entre deux plaques de métal recouvertes de téflon lisse et surmontées d'un poids de 5 kg. Les échantillons sont placés dans l'étuve préalablement réglée à une température de 90 ou 120 °C pour le P(D,L)LA pur et 85 ou 100 °C pour le P(D,L)LA formulé. Les films sont soumis à cette température pour une durée fixe d'1h30 pour le P(D,L)LA pur et 10, 30 ou 60 min pour le P(D,L)LA formulé. Une fois ce temps écoulé, les échantillons sont retirés de l'étuve et laissés à refroidir à température ambiante.

2.2.1.5. Méthode de biétirage du P(D,L)LA

Les films de P(D,L)LA 2002D sont biétirés grâce à un prototype de marque Cellier développé par l'Université de Lille (Figure 2.1). Le cadre est composé de 4 pantographes (40 pinces) mis en mouvement par 2 vérins hydrauliques perpendiculaires, permettant un biétirage de manière simultanée (dans des directions orthogonales simultanément) ou séquentielle (dans une direction dans un premier temps puis dans la direction orthogonale dans un deuxième temps). Le biétirage est réalisé sur des échantillons de 105*105 mm ², chauffés au dessus de la T_g du P(D,L)LA (55 °C < T < 70 °C). La vitesse de sollicitation est fixée à 10 mm.min^{-1} soit 0,1 s^{-1}.
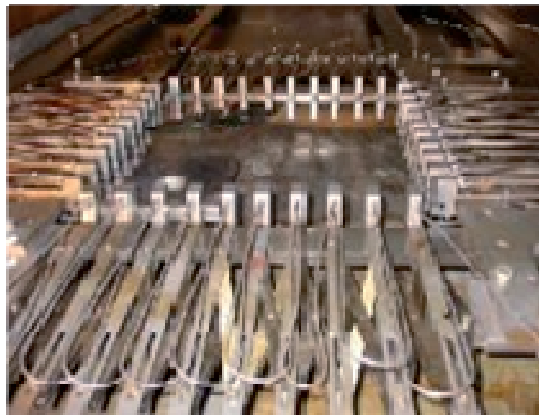
Figure 2.1. Photographie du prototype de cadre de biétirage (Cellier) de l'Université de Lille.

Les films de P(D,L)LA 4042D sont biétirés grâce à un appareil de l'Université de Belfast (Figure 2.2) dont le fonctionnement est similaire au précédent mais avec seulement 24 pinces. L'étirage est réalisé dans des directions orthogonales simultanément sur des échantillons de 75*75 mm² à une température de 100 °C à 1 s^{-1} ou 8 s^{-1}.

Pour chacun des grades de P(D,L)LA, plusieurs ratios d'étirage ont été testés, de 2×2 à 4×4. Quelques échantillons ont, après biétirage, subi une thermo-fixation afin d'obtenir des films thermiquement stables. Pour cela, l'échantillon est placé entre deux plaques de métal et placé dans une étuve à 130 °C pendant 30 min.
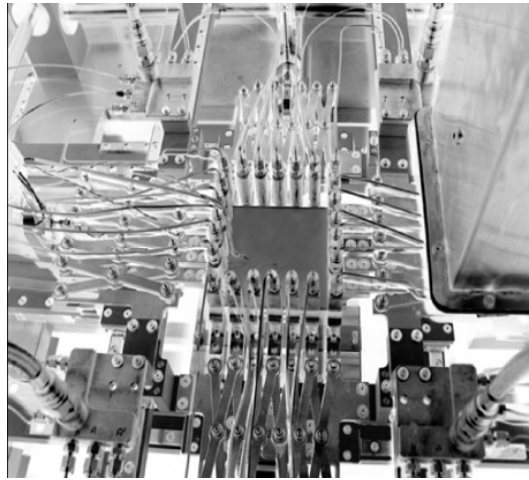
Figure 2.2. Photographie du cadre de biétirage de l'Université de Belfast.

2.2.2. Caractérisation des films de P(D,L)LA pur et formulés

Plusieurs méthodes de caractérisation ont été utilisées afin de déterminer les propriétés des films de P(D,L)LA.

Dans un premier temps, il a été nécessaire de s'assurer de la composition du mélange réalisé en déterminant notamment la teneur en plastifiant réellement présente dans le matériau et de mesurer la masse molaire du P(D,L)LA, après passage au mélangeur interne et fabrication des films par thermo-compression.

Dans un second temps, les propriétés thermiques, mécaniques et barrières du P(D,L)LA ont été analysées.

2.2.2.1. Mesure de l'épaisseur

La méthode de fabrication des films de P(D,L)LA conduit à la production de films hétérogènes en épaisseur. L'épaisseur est alors définie comme une moyenne de 9 mesures, 8 sur le contour et 1 au centre du film, réalisées avec un micromètre (Heidenhain).

2.2.2.2. Méthode d'extraction

Chaque film de P(D,L)LA pur (témoin d'extraction) et formulé est coupé en petits morceaux, pesé (exactement environ 3 g) puis placé dans un Soxhlet. Le Soxhlet est ensuite adapté sur un ballon contenant 150 mL d'éthanol et placé dans un chauffe-ballon. L'éthanol est ensuite porté à ébullition (90 °C pendant 7 h) afin d'extraire les plastifiants du film de P(D,L)LA

formulé. 3 à 4 cycles remplissage-siphonage sont ainsi effectués. Une fois l'extraction réalisée, les morceaux de film sont placés dans une étuve (3 jours à 60 °C) pour les sécher puis pesés afin de déterminer la perte de masse correspondant à celle du plastifiant présent dans le film. Les analyses ont été dupliquées.

2.2.2.3. Chromatographie d'exclusion stérique (CES/SEC)

La mesure de la masse molaire et de l'indice de polydispersité des échantillons de P(D,L)LA est réalisée par chromatographie d'exclusion stérique. 15 mg de chacun des échantillons de P(D,L)LA sont dissous dans 3 mL de chloroforme puis analysés à l'aide du système chromatographique.

Deux chaînes ont été utilisées lors de ce travail. Elles sont toutes les deux composées de deux colonnes PL-GEL Mixed-C (5 µm, 300 mm, Polymer Laboratories) précédées d'une précolonne PL-Gel 5 µm Guard (50 mm, Polymer Laboratories). Cependant la deuxième chaine est également constituée d'une colonne PLGel 100 Å (300 mm, Polymer Laboratories) suivant la précolonne.

La première chaîne est composée d'une pompe isocratique (GILSON 307), d'un four à colonne thermostaté à 30 °C (Waters Control Module II), d'un passeur automatique (Waters 717 plus autosampler), d'un réfractomètre Shimadzu RID-6A (range 16) et d'un détecteur UV SPD-M10A.

La deuxième chaîne chromatographique, de marque Shimadzu, est composée d'une pompe isocratique (LC-10AD), d'un dégazeur (DGU-14A), d'un four à colonne thermostaté à 25 °C (CTO-10A) et d'un passeur automatique (SIL-10AD), d'un réfractomètre Shimadzu RID-10A et d'un détecteur UV SPD-M10A.

Les analyses sont ainsi effectuées à 0,8 mL.min^{-1} dans le chloroforme (HPLC grade). Les masses molaires sont déterminées à partir d'une courbe de calibration réalisée à l'aide d'une gamme certifiée de standards polystyrène de masses comprises entre 580 et 1 650 000 g.mol^{-1} (Varian, réf: PL2010-0100).

Les données obtenues ont été retraitées par le logiciel Waters Empower 2.

2.2.2.4. Calorimétrie différentielle à balayage (DSC)

La DSC est une technique de mesure permettant de déterminer de manière qualitative et quantitative les transitions thermiques du P(D,L)LA et des mélanges P(D,L)LA

CD92/plastifiant/talc produits. L'appareil utilisé, DSC Q100 (TA Instruments), est équipé d'un système de refroidissement permettant de travailler entre -80 et 450 °C avec une précision de 0,1 °C. Le four de la DSC est balayé en permanence par de l'azote (50 mL.min^{-1}) afin d'assurer le transfert de chaleur à l'intérieur du four. Les échantillons, d'environ 10 mg, sont placés dans des creusets hermétiques en aluminium Tzéro.

Deux modes, standard et modulé, sont utilisées pour la caractérisation des échantillons de P(D,L)LA.

Le mode **standard** utilisé dans notre étude correspond à une rampe de température linéaire de 10 °C.min^{-1}. Il permet la détermination des températures de transition vitreuse, de cristallisation et de fusion et les enthalpies de cristallisation et de fusion. Le P(D,L)LA pur est analysé entre 0 et 190 °C tandis que la gamme de température pour le P(D,L)LA formulé est de -30 à 190 °C.

Le mode **modulé** correspond à une rampe de température linéaire de 1 °C.min^{-1} modulée par une sinusoïde d'amplitude de modulation de température sinusoïdale de ± 1.5 °C et de période 80 s. Ce mode permet de séparer les phénomènes apparaissant dans le signal reversing (transition vitreuse et fusion) des phénomènes apparaissant dans le signal non-reversing (relaxation enthalpique et cristallisation). La DSC modulée est donc utilisée afin d'évaluer plus précisément la température de transition vitreuse des échantillons de P(D,L)LA entre 0 et 80 °C dans le cas où nous souhaitons suivre l'évolution de la T_g en fonction de la formulation ou du traitement subi par les échantillons.

Cette technique est également utilisée afin d'étudier la cristallisation isotherme (températures et temps requis pour la cristallisation du P(D,L)LA pur et du mélange P(D,L)LA/17%ATBC/1%talc) et les cinétiques de cristallisation non isotherme du P(D,L)LA pur et formulé.

L'étude de la cristallisation isotherme est effectuée en mode standard grâce à la succession de 5 cycles (Figure 2.3):

- une montée en température jusqu'à 190 °C, puis conservation à cette température pendant 10 min afin d'éliminer l'histoire thermique du P(D,L)LA,

- une trempe à 20 °C afin d'éviter la cristallisation de l'échantillon (80 °C.min^{-1} maximum non contrôlé)

- une chauffe rapide (50 °C.min^{-1} en moyenne) jusqu'à la température de cristallisation prédéfinie (T$_c$). L'échantillon est ensuite conservé pendant une durée prédéfinie à T$_c$ (X min).
- une trempe à 0 °C pour le P(D,L)LA pur et -30 °C pour le P(D,L)LA formulé afin de conserver la structure formée pendant la cristallisation de l'échantillon.
- une chauffe à 10 °C.min^{-1} jusqu'à 190 °C.
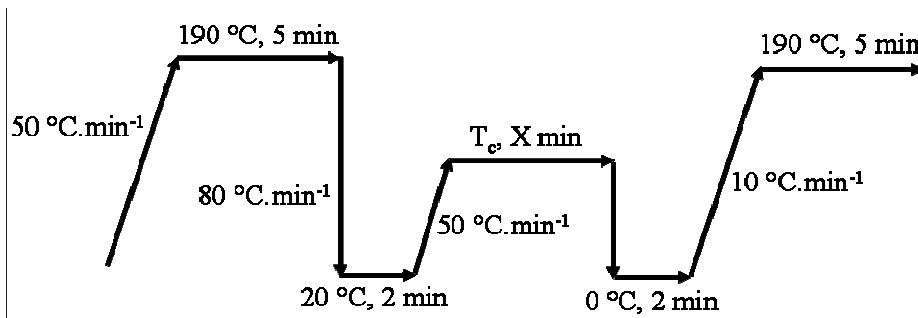
Figure 2.3. Schéma du programme de DSC pour l'étude de la cristallisation isotherme du P(D,L)LA CD92.

La détermination des températures de transition vitreuse, de cristallisation et de fusion et les enthalpies de cristallisation et de fusion est effectuée grâce au logiciel TA Universal Analysis.

L'étude de la cristallisation non-isotherme à partir de l'état fondu est effectuée en mode standard sur le P(D,L)LA CD92 formulé avec talc et ATBC ou PEG. Trois cycles successifs sont réalisés afin d'évaluer la cristallisation de toutes les formulations de P(D,L)LA réalisées :
- une montée en température jusqu'à 190 °C, puis conservation à cette température pendant 10 min afin d'éliminer l'histoire thermique du P(D,L)LA,
- un refroidissement à 10 °C.min^{-1} jusqu'à -30 °C, puis maintien à cette température pendant 5 min.
- une chauffe à 10 °C.min^{-1} jusqu'à 190 °C.

Une étude de l'effet de la vitesse de refroidissement a également été réalisée sur le P(D,L)LA pur, le P(D,L)LA avec 1 wt% de talc et le P(D,L)LA avec 1 wt% de talc et une teneur variable en ATBC (entre 4 et 17 wt%). Plusieurs vitesses de refroidissement ont été testées : 2, 5, 10, 15, 20 et 25 °C.min^{-1}. Deux cycles successifs ont été effectués sur chacun des échantillons :

-   une montée en température jusqu'à 190 °C, puis conservation à cette température pendant 10 min afin d'éliminer l'histoire thermique du P(D,L)LA,

-   un refroidissement à 2, 5, 10, 15, 20 et 25 °C.min^{-1} jusqu'à -30 °C.

2.2.2.5. Analyse mécanique dynamique (DMA)

L'analyse par DMA a été effectuée en mode de sollicitation traction-compression afin de caractériser les propriétés mécaniques et thermiques du P(D,L)LA pur et formulé.

Deux appareils ont été utilisés lors de ce travail, la DMA Tritec 2000 (Triton) et la DMTA V (TA Instruments).

L'emploi de la DMA Tritec 2000 s'est limité à la caractérisation des formulations de P(D,L)LA avec un taux de plastifiant inférieur ou égal à 9 % en poids et des échantillons de P(D,L)LA pur amorphes et recristallisés (publication n°4)

L'analyse a été réalisée sur des échantillons formulés de 10 mm de large et 5 mm de long alors que les dimensions des échantillons de P(D,L)LA pur étaient de 5 mm de large et 10 mm de long. La mesure a ainsi été effectuée avec une force et un déplacement dynamique de respectivement -0.5 N et 10 µm, entre 20 et 180 °C à 2 °C.min^{-1} et à la fréquence d'1 Hz.

La DMTA V a été employée afin de caractériser les échantillons de P(D,L)LA formulé avec une plus forte teneur en plastifiant (publication n° 2). Les mesures sont réalisées à une fréquence de 1 Hz et à une contrainte de 0,05 % sur des échantillons de forme rectangulaire (30 mm * 10 mm). Une rampe de température de 2 °C.min^{-1} a été appliquée entre -140 et 130 °C.

Le module de conservation (E'), représentant la rigidité et la composante élastique du matériau, le module de perte, représentant la composante visqueuse du matériau, et le facteur de perte (tan δ) sont enregistrés et analysés. Le maximum du pic du facteur de perte est associé à la température de transition vitreuse (relaxation α) du matériau analysé.

2.2.2.6. Test de traction

Les tests de traction ont été réalisés afin de caractériser l'influence de la formulation et du traitement thermique sur les propriétés mécaniques du P(D,L)LA. Des tests de traction uniaxiale ont été effectués à 5mm.min^{-1}, à température et humidité relative ambiante grâce à une machine de traction (Instron Model 4507) équipée de mors pneumatiques, afin de tenir

correctement les échantillons sous forme de film, et d'une cellule de force 100 N. Les échantillons d'épaisseur variant entre 100 et 300 μm ont été découpés sous forme d'haltère de type I BA.

L'essai se fait à partir d'éprouvette de 5 mm de largeur, une longueur de 58 mm et une partie utile Lo de 25 mm. L'épaisseur n'étant pas la même selon le film utilisé, elle est mesurée avant chaque essai.

Trois données caractéristiques sont mesurées grâce aux essais de traction : la contrainte au seuil ou à la rupture si l'échantillon ne présente pas de contrainte au seuil, l'élongation à la rupture et le module de Young. Chaque valeur donnée est le résultat de la moyenne de 5 ou 10 mesures.

2.2.2.7. Diffraction des rayons X (DRX / WAXD)

L'analyse par diffraction des rayons X permet de caractériser la structure cristalline des échantillons de P(D,L)LA CD92. L'appareil utilisé au Laboratoire National de métrologie et d'Essais de Trappes est un Diffractomètre Panalytical, X'Pert Pro MPD en configuration Bragg-Brentano utilisant une radiation CuKα monochromatisée au graphite. Cette géométrie permet une focalisation approchée du rayon incident. Les profils DRX sont réalisés pour un angle 2θ entre 5 et 35° avec un pas de 0.007° et 368.8 s. La cristallinité est mesurée comme le rapport de la somme des surfaces des pics cristallins, sur la surface totale du diffractogramme.

Des essais préliminaires ont été réalisés afin de définir le meilleur support à utiliser (spinner ou porte-film) ainsi que la forme de l'échantillon (films ou poudre obtenue par cryobroyage). La reproductibilité des analyses a également été testée sur un film de P(D,L)LA pur recristallisé en mesurant la cristallinité (Tableau 2.7) et en étudiant le déplacement des pics et leur intensité. Ainsi, dans un premier temps, un échantillon de P(D,L)LA pur recristallisé a été analysé sous forme de film dans deux supports différents : spinner, permettant de faire tourner l'échantillon sur lui-même et un support fixe MPSS (Multi-port sampling system).

Le spectre obtenu avec le spinner a été réalisé à 8 tr.min^{-1} tandis que le support MPSS ne tourne pas. Les spectres obtenus semblent similaires. Le taux de cristallinité mesuré n'est en rien modifié par le type de support. En revanche, une diminution de l'intensité des pics est observée lors de l'analyse sur le support Spinner (Figure 2.4).

La comparaison des spectres réalisés sur film et sur poudre met en évidence la similitude des valeurs de taux de cristallinité. De plus, il apparaît que les spectres sont semblables malgré un

changement dans l'intensité des pics. En effet, l'échantillon sous forme de poudre présente des pics de plus faible intensité (Figure 2.4).

Tableau 2.7. Mesure du taux de cristallinité en fonction des paramètres étudiés.

Support/forme	Taux de cristallinité (%)
MPSS/film	30
Spinner/film	30
Spinner/poudre	31
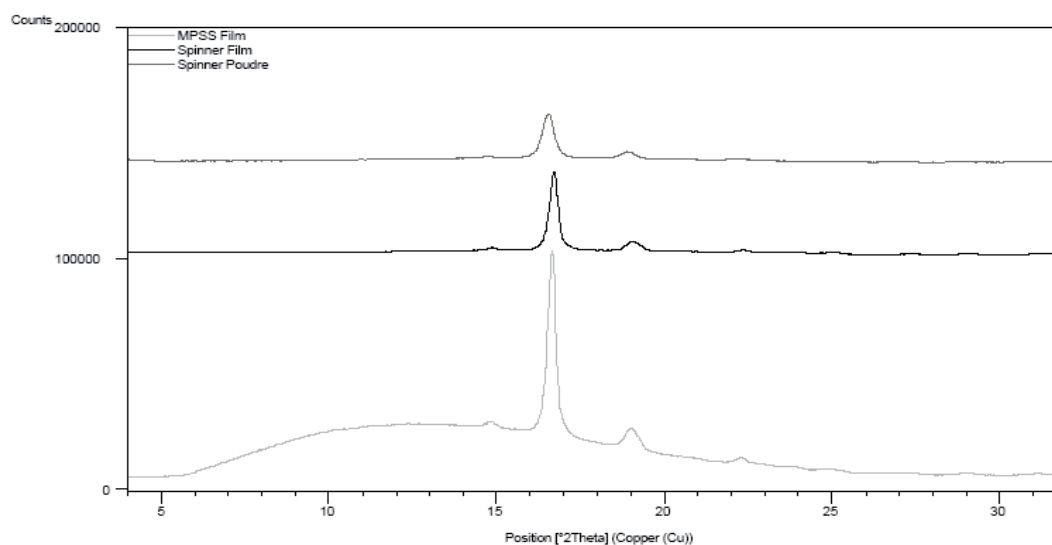
Figure 2.4. Superposition des spectres DRX de bas en haut, MPSS/Film, Spinner/Film et Spinner/Poudre.

La transformation du film en poudre n'apportant pas d'information supplémentaire et le spinner permettant de diminuer le halo amorphe, nous avons finalement choisi la configuration Spinner/film pour réaliser l'essai de répétabilité. Le même échantillon a donc été analysé 5 fois en changeant l'emplacement sur lequel les rayons X étaient focalisés. Le taux de cristallinité est en moyenne de 30 ± 1 %. La Figure 2.5 met en évidence une superposition de 4 des 5 essais avec une concordance des angles de déviation. Il semble donc que les analyses en DRX en configuration "support spinner/échantillon sous forme de film" soient parfaitement répétables.
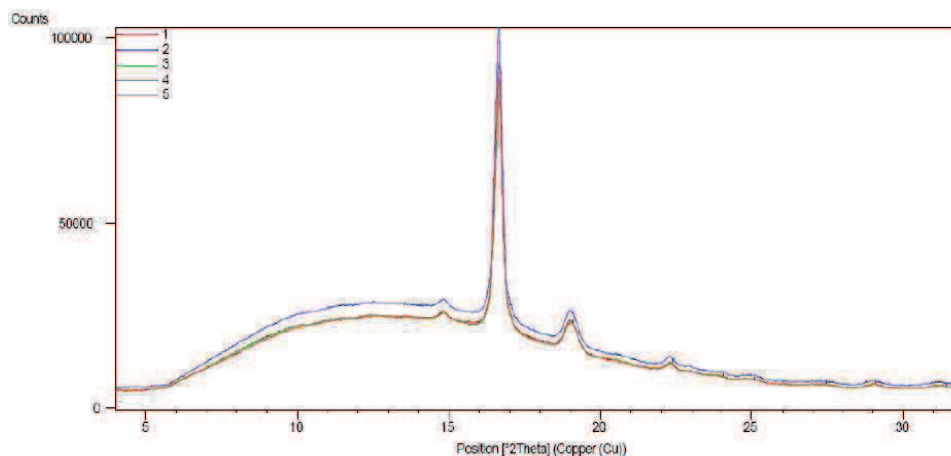
Figure 2.5. Superposition de 5 spectres DRX du P(D,L)LA pur cristallisé en configuration Spinner/film.

2.2.2.8. Perméabilité à l'hélium, l'oxygène, la vapeur d'eau et aux composés d'arôme

La perméabilité à divers composés, vapeur d'eau, gaz, composés organiques en phase vapeur a été testé pour le P(D,L)LA pur mais aussi pour le P(D,L)LA formulé.

2.2.2.8.1. Perméabilité à l'eau

Le coefficient de transmission de la vapeur d'eau (CTVE) des films de P(D,L)LA CD92 a été mesuré par gravimétrie suivant la norme NF H00-030 AFNOR à 25 °C et 50 % d'humidité relative (HR) et 38 °C et 90 %HR. Le CTVE est défini comme la masse de vapeur d'eau traversant en régime permanent l'unité de surface du film dans l'unité de temps dans les conditions de l'essai. La procédure consiste à mettre dans une capsule un déshydratant, chlorure de calcium anhydre sous forme de granules ($CaCl_2$), séché au préalable à 50 °C dans une étuve. Le film étudié, préalablement conditionné une nuit dans les conditions de mesure, est placé sur la capsule qui est ensuite scellée, grâce à de la cire d'abeille fondue, dans un bain marie à 100 °C (Figure 2.6). La surface d'échange ainsi obtenue est de 50,24 cm².

Chaque capsule est placée dans une enceinte thermostatée à humidité contrôlée (Bioblock Scientific VCN100). La vapeur d'eau traverse le film et est sorbée par le déshydratant, induisant ainsi une augmentation de la masse de la capsule. Un suivi de la prise de masse à 0,1 mg près est alors réalisé toutes les deux heures sur deux jours grâce à une balance (Kern 770, de précision 0,01 mg) afin d'obtenir le CTVE. Pour chaque capsule, la prise de masse (en gramme) en fonction du temps (en heure) est représentée graphiquement. La pente ainsi obtenue permet de retrouver le coefficient de transmission de la vapeur d'eau grâce à l'équation ci-dessous :

$$CTVE = \frac{pente \times 24}{S} = \frac{pente \times 24}{50,24.10^{-4}} ,$$ (2.1)

Chaque valeur de CTVE donnée est une moyenne de deux mesures réalisées en parallèle.
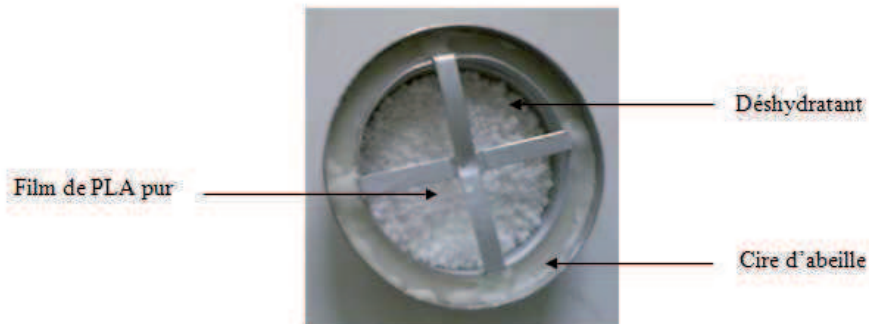
Figure 2.6. Photographie de la capsule permettant la mesure de la perméabilité à la vapeur d'eau.

2.2.2.8.2. Perméabilité à l'hélium

La vitesse de la transmission de l'hélium est mesurée à température et humidité relative ambiante. Le système utilisée a été développé par le Laboratoire P2AM (Propriétés-Architectures des Alliages et Mélanges), du CNAM et basé sur la norme ISO 15105-2 :2003. La mesure directe est réalisée grâce à un spectromètre de masse Alcatel ASM 142 utilisé comme détecteur jusqu'à l'obtention du régime stationnaire. Ce spectromètre de masse à déflexion magnétique est réglé sur la masse de l'hélium (m/e = 4) de manière à ne mesurer que le flux d'hélium. La mesure réalisée par le spectromètre de masse est en mode reniflage, c'est-à-dire à 1 bar.

Comme pour la mesure de perméabilité à l'oxygène, le système utilisé est composé de deux cellules (Figure 2.7): en amont, la cellule est balayée par un flux d'hélium qui traverse le film tandis qu'en aval, la cellule est balayée par un flux d'azote qui maintient une pression transmembranaire constante et induit ainsi un delta de pression nul. Des joints toriques assurent l'étanchéité du système. Les analyses ont été au minimum dupliquées.

La valeur de perméabilité est exprimée en fonction du débit volumique Q (mL.s^{-1}) donnée par le spectromètre de masse, de la différence de pression entre les compartiments amont (p_1) et aval (p_2), de l'épaisseur l (m) et de la surface de film (S = 23,75759.10^{-4} m²):

$$P = \frac{Q \times l}{S \times (p_2 - p_1)}$$ (2.2)

Le delta de pression étant de 1 bar, la valeur de perméabilité est calculée grâce à la relation ci-dessous:

$$P = \frac{Q \times 1.10^{-6} \times l}{23{,}75759.10^{-4} \times 1.10^{5}} \tag{2.3}$$

La valeur de perméabilité ainsi obtenue exprimée en $m^3.m.m^{-2}.s^{-1}.Pa^{-1}$.
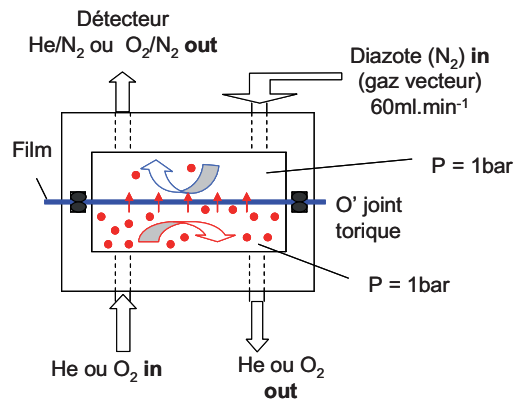
Figure 2.7. Schéma de la cellule de perméation pour l'oxygène et l'hélium.

2.2.2.8.3. Perméabilité à l'oxygène

La vitesse de la transmission de l'oxygène (ou OTR, oxygen transmission rate) est mesurée en mode dynamique à 23 °C et 0 %HR à l'aide d'un appareil Systech 8001. La mesure directe est réalisée selon la norme ASTMD 3985 grâce à un détecteur coulométrique. Le film est placé entre deux cellules (Figure 2.7): en amont, la cellule est balayée par un flux d'oxygène qui traverse le film tandis qu'en aval, la cellule est balayée par un flux d'azote qui maintient une pression transmembranaire constante. La mesure de la quantité d'oxygène traversant le film est réalisée jusqu'à l'obtention du régime stationnaire. La valeur de perméabilité est alors donnée par:

$$P = \frac{J \times l}{S \times (p_1 - p_2)} \tag{1.30}$$

avec J, la densité de flux ($m^3.m^{-2}.s^{-1}$), l (m), l'épaisseur de film, S (m²) la surface d'échange et p_1 et p_2 (Pa) la pression dans les compartiments amont et aval, respectivement.

J correspondant à la vitesse de transmission de l'oxygène ($cc.m^{-2}.j^{-1}$) et la différence de pression entre les deux compartiments étant de 1 bar lors des mesures, la perméabilité peut s'écrire :

$$P = \frac{OTR \times 1.10^{-6} \times l}{60 \times 60 \times 24 \times 1.10^{5}} \tag{2.4}$$

La valeur de perméabilité ainsi obtenue est en $m^3.m.m^{-2}.s^{-1}.Pa^{-1}$.

Les analyses ont été dupliquées.

2.2.2.8.4. Perméabilité aux composés d'arôme

La perméabilité du film industriel de P(D,L)LA Biophan® 121 (Treofan) à trois composés d'arôme (acétate d'éthyle, butyrate d'éthyle et hexanoate d'éthyle) a été mesurée à l'aide d'un dispositif composé d'une cellule de perméation couplée à un injecteur automatique PTI (Purge and Trap Injector, Chrompack CP 4010 PTI/TCT) et un chromatographe en phase gazeuse (GC 8000 Fisons instruments, Arcueil, France) avec détecteur FID (Figure 2.8).
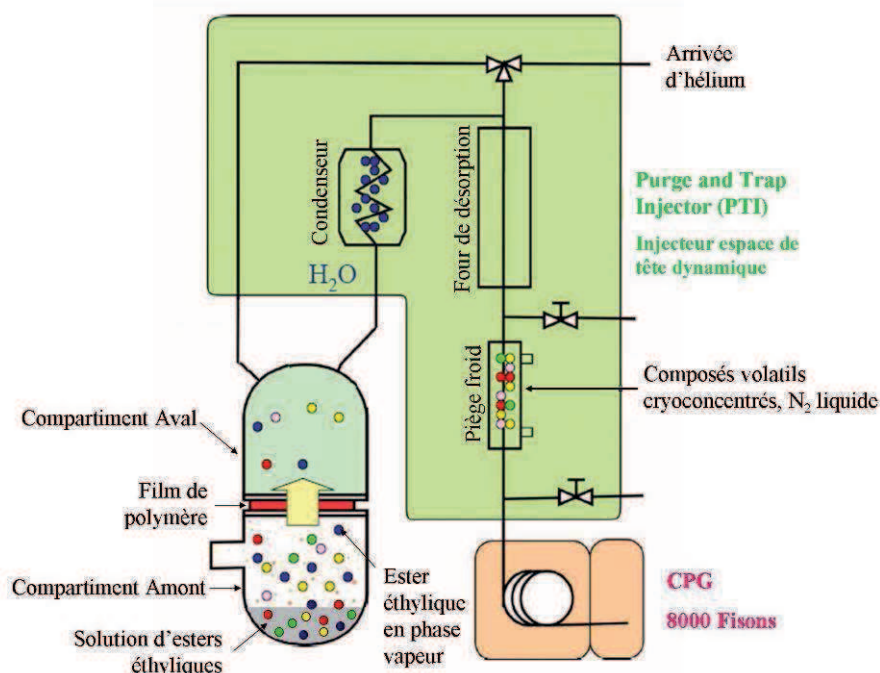
Figure. 2.8. Schéma du système de mesure des coefficients de perméabilité et diffusion aux composés organiques volatils.

Une étape d'optimisation des conditions opératoires de l'injecteur automatique a été réalisée sur des films de LDPE Goodfellow (Huntingten, Angleterre) d'une épaisseur de 125 μm, avant de pouvoir analyser le P(D,L)LA Biophan,.

Une solution mère des trois esters éthyliques est réalisée dans l'hexadécane puis diluée dans l'hexadécane de nouveau de manière à obtenir une solution de $1,305.10^{-3}$ mol.L^{-1} en acétate d'éthyle, $1,894.10^{-3}$ mol.L^{-1} en butyrate d'éthyle et de $1,211.10^{-2}$ mol.L^{-1} en hexanoate d'éthyle. Cette solution va servir à créer l'espace gazeux chargé en composés d'arôme qui sera en contact avec le film dans le compartiment amont de la cellule de perméation.

Le film étudié est coupé sous forme de cercle de 10 cm de diamètre et ensuite placé entre les deux compartiments de la cellule de perméation maintenus par une bride de serrage (Figure 2.9). Le compartiment aval présente une gorge arrondie de façon à placer un joint

torique qui assure l'étanchéité du système et une bride de serrage permet de maintenir les deux compartiments ensemble en évitant les fuites. 8 mL du mélange de trois esters éthyliques dans l'hexadécane sont introduits dans le compartiment amont de la cellule de 400 mL. Les mesures de perméabilité ont été réalisées à 25 °C ± 0.3 °C en plaçant la cellule dans une enceinte thermorégulée.

.
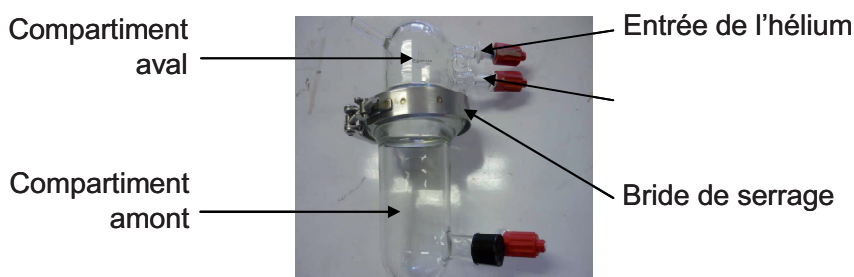
Figure 2.9. Photographie de la cellule de perméation

A intervalle de temps régulier (1 h), le compartiment aval de 140 mL est entièrement balayé pendant 10 min par le flux d'hélium (15 mL.min^{-1}), qui est aussi le gaz vecteur du CPG afin d'entraîner les composés ayant traversés le film. La concentration en composés d'arôme dans le compartiment est ainsi nulle après balayage et réaugmente une fois le balayage terminé (mode dynamique). Les composés d'arôme ayant perméé au travers du film sont entraînés par l'hélium jusqu'au piège cryogénique du PTI (tube capillaire CP sil 5 CB, 25 cm de longueur et 0,53 mm de diamètre, Chrompack) refroidi à -80 °C. Le tube précédant le piège est porté à 200 °C pendant la phase de 10 min de purge du compartiment aval afin d'éviter toute condensation dans cette partie.

Les composés d'arôme piégés sont ensuite rapidement désorbés en réchauffant le piège à 200 °C en 60 s et injectés dans un CPG équipé d'une colonne polaire (DBwax 0,32 × 30 m × 0,5 µm, Supelco, USA) et d'un détecteur DIF maintenu à 250 °C. Le programme de température du CPG est le suivant :

- 40 °C pendant 2 min

- chauffe à 6 °C.min^{-1} jusqu'à 130 °C

- 130 °C pendant 2 min.

L'acquisition et le traitement des données sont réalisés à l'aide du logiciel ChromCard (Fisons instruments 1.17). La mesure de la perméabilité est réalisée pendant 15 cycles d'une heure, ce qui permet d'atteindre un régime stationnaire pour chacun des composés étudiés.

Le coefficient de diffusion de chaque composé organique est calculé par la méthode du time lag (θ ou temps de retard). Celui-ci est mesuré en représentant la somme des aires des pics chromatographiques de chaque composé ayant perméé au cours du temps. Le point d'intersection de l'axe des abscisses et la courbe en phase de croissance linéaire est défini comme le time-lag (θ), c'est-à-dire le temps nécessaire à l'obtention du régime stationnaire.

$$D = \frac{l^2}{6 \times \theta}, \tag{1.32}$$

Où l est l'épaisseur du film en mètre, θ est le time lag en seconde et D est le coefficient de diffusion en m².s^{-1}.

Le coefficient de perméabilité est calculé grâce à la relation ci-dessous

$$P = \frac{J_{st}.l}{\Delta p} = \frac{dQ}{dt \times S} \times \frac{l}{\Delta p}, \tag{2.5}$$

avec J_{st} le flux stationnaire, Δp le gradient de pression entre le compartiment amont (p_1) et aval (p_2), Q la quantité de perméant ayant traversé le film (kg), S la surface d'échange (m²) et t le temps (s). La pression de vapeur dans le compartiment aval est négligeable devant la pression de vapeur dans le compartiment amont ($p_2 \ll p_1$) d'où

$$P = \frac{dQ}{dt \times S} \times \frac{l}{p_1}, \tag{2.6}$$

La pression de vapeur des esters éthyliques dans le compartiment amont est déterminée à l'aide du coefficient de partage massique, K, entre la solution de composé d'arôme et l'espace gazeux (Tableau 2.8). Ces valeurs de K ont été déterminées au préalable par Marta Bernasconi lors de son stage de master.

La détermination de la pression de vapeur des trois composés nécessite également de connaître la concentration en composé dans la solution d'hexadécane introduite dans le compartiment amont (8 mL). Cette concentration molaire (C) est alors rapportée à la masse (m_l) d'ester éthylique en phase liquide dans la cellule de perméation à l'aide de la masse molaire du composé (Tableau 2.3) :

$$m_l = \frac{C}{V} \times M, \tag{2.7}$$

La pression de vapeur en ester éthylique dans le compartiment amont de la cellule (p_1) peut alors être calculée à l'aide du coefficient de partage, K, et de la loi des gaz parfaits :

$$K = \frac{m_g}{m_l}, \tag{2.8}$$

avec m_g la masse d'ester en phase gazeuse dans la cellule.

$$p_1 = \frac{n \times R \times T}{V} = \frac{m_l \times K}{M} \times \frac{R \times T}{V}, \tag{2.9}$$

avec R, la constante des gaz parfaits (8,314 J.K^{-1}.mol^{-1}), T la température de mesure (298 K) et V le volume du compartiment amont de la cellule (400.10^{-6} m^3).

Tableau 2.8. Données caractéristiques des esters éthyliques lors de la mesure de perméabilité.

Composés	Coefficient de partage massique, K	Concentration molaire, C (mol.L^{-1})	Masse de composé (mg dans 8 mL)	Pression de vapeur (Pa)	Concentration dans l'espace gazeux (µg.L^{-1}/ ppm)
Acétate d'éthyle	0,12	1,305.10^{-3}	0,92	7,76	375 / 0,4
Butyrate d'éthyle	0,0174	1,894.10^{-3}	1,76	1,63	47 / 5.10^{-2}
Hexanoate d'éthyle	0,00198	1,211.10^{-2}	13,97	1,19	43 / 5.10^{-2}

2.2.2.9. Interaction du P(D,L)LA avec des composés d'arôme

2.2.2.9.1. Mesure de la solubilité de l'acétate d'éthyle par la méthode gravimétrique

Les cinétiques de sorption de l'acétate d'éthyle dans le P(D,L)LA ont été déterminées grâce à une microbalance de sorption (Intelligent Gravimetric Analyser 002, Hiden Isochema Ltd., Warrington, Royaume-Uni) de précision 0,2 µg et utilisé en mode statique. Conduites à 25 °C et 0 %RH, les mesures consistent à suivre l'évolution de la masse de l'échantillon en fonction du temps. Chaque échantillon de 30 à 60 mg est suspendu grâce à une spirale en acier inoxydable (Figure 2.10). Un manchon thermostaté permet de réguler la température à 25 °C. La microbalance est elle-même maintenue à 50 °C afin d'éviter toute condensation de composés et ainsi assurer la stabilité de la mesure.
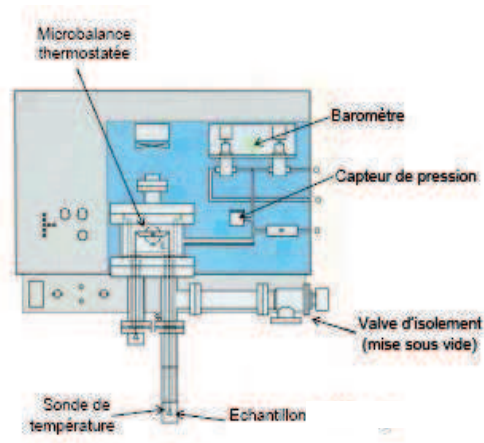
Figure 2.10. Schéma de la microbalance de sorption

Avant chaque mesure, le système est purgé jusqu'à 10^{-5} mbar pendant 24 h afin d'évacuer les éventuels composés volatils présents dans le film ou la chambre de mesure. La pression partielle en acétate d'éthyle est contrôlée à l'aide d'un capteur de pression (Baratron®, MKS Instruments, Wilmington, Massachusetts, USA) relié au réservoir d'acétate d'éthyle qui sert d'alimentation en composé volatil.

L'acquisition des données est réalisée par le logiciel fourni par Hiden jusqu'à ce que l'équilibre de sorption, défini par un changement de masse inférieur à 1 %, soit atteint ou que le temps défini au préalable soit écoulé. La solubilité de l'arôme dans le film a été calculée selon l'équation suivante :

$$S = M_\infty \times \frac{d}{p} \, , \tag{2.10}$$

Où S ($kg.m^{-3}.Pa^{-1}$) est le coefficient de solubilité de l'acétate d'éthyle, M_∞ ($kg.kg^{-1}$) la masse à l'équilibre, p (Pa) la pression partielle de vapeur de l'acétate d'éthyle et d ($kg.m^{-3}$) la masse volumique du film.

2.2.2.9.2. Influence des esters éthyliques sur la transition vitreuse du P(D,L)LA

Conditionnement

L'influence des composés d'arôme et de leur teneur sur la phase amorphe a été étudiée en conditionnant les films de P(D,L)LA dans une enceinte hermétique contenant des vapeurs d'esters éthyliques pendant 14 jours (Figure 2.11). Les films de P(D,L)LA ont été coupés en petits cercles de 5 mm de diamètre, en rectangle de 1 cm * 3 cm et en petits morceaux d'environ 5 cm². Ces échantillons sont disposés dans une cellule de 650 mL composée de 2

compartiments maintenus ensemble par une bride de serrage. A l'intérieur de cette cellule est également stockée une solution de composé d'arôme dans l'hexadécane dont la concentration varie en fonction de l'activité en composé d'arôme souhaitée dans l'espace gazeux de la cellule.
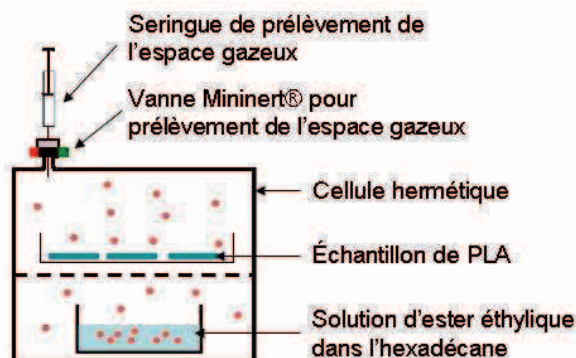
Figure 2.11. Schéma de la cellule de conditionnement des échantillons de polymère contenant une solution d'ester éthylique.

Trois composés d'arôme ont été testés, l'acétate d'éthyle, le butyrate d'éthyle et l'hexanoate d'éthyle, à 4 activités différentes, 0.1, 0.2, 0.5 et 0.9.

L'activité de chaque composé a été vérifiée en procédant à un prélèvement de l'espace gazeux de la cellule après équilibre. Ainsi, 0,5 mL de l'espace de tête de la cellule sont prélevés grâce à une seringue à gaz et une vanne Mininert® installée sur la cellule puis injectés dans un chromatographe en phase gazeuse Fisons GC 8000 (Fisons, France).

La concentration en composé d'arôme dans ces 0,5 mL a été déterminée à l'aide d'une courbe de calibration externe réalisée sur le même chromatographe en phase gazeuse (Annexe 1). Celle-ci a été établie à l'aide d'injection de 2 µL de solution de composé d'arôme dans le pentane de 0,216 à 0,866 mol.L^{-1}.

L'aire du pic (A en u.a.) obtenue en CPG est reliée à la masse (m en µg) de composé d'arôme dans 0,5 mL de l'espace gazeux par la pente de la courbe de calibration :

$$A = pente \times m$$

$$c = \frac{m \times 1.10^{-3}}{0,5.10^{-3}}, \tag{2.11}$$

La concentration, c, est ainsi exprimée en mg.L^{-1}.

L'utilisation de la loi des gaz parfaits a alors permis de relier la concentration en composé d'arôme à la pression partielle et enfin à l'activité dans la cellule.

$$p = \frac{n \times R \times T}{V} = \frac{c \times R \times T}{M}, \tag{2.12}$$

R est la constante des gaz parfaits égale à 8,314 J.K^{-1}.mol^{-1}, T, la température dans la cellule (25 °C soit 298 K) et M, la masse molaire du composé étudié (g.mol^{-1}, cf. Tableau 2.2).

L'activité, a, peut alors être calculée grâce à la pression de vapeur saturante, p_0 :

$$a = \frac{p}{p_0}, \tag{2.13}$$

Le CPG est équipé d'un injecteur split/splitless chauffé à 220 °C, d'une colonne capillaire (J&W Science, 30 m × 0.32 mm × 0.50 µm) et d'un détecteur FID à 250 °C. L'hydrogène est utilisé en tant que gaz vecteur à un débit de 37 cm.s^{-1}. La température du four est programmée de sorte à être maintenue à 30 °C pendant 5 min puis augmentée à 5 °C.min^{-1} jusqu'à 120 °C et maintenue à cette température pendant 5 min. L'échantillon gazeux est injecté en mode en mode splitless puis la vanne de purge est activée au bout de 1 min.

L'acquisition et le traitement des données sont réalisés grâce au logiciel Borwin Chromatography Software.

2.2.2.10. Résonance Paramagnétique Electronique, RPE

La RPE est une technique de spectroscopie hertzienne utilisé, dans le cadre de cette étude, pour évaluer la structure locale d'un matériau.

Cette technique nécessite, si aucun radical ni métal de transition n'est présent dans le matériau, d'incorporer des sondes paramagnétiques dans l'échantillon à analyser. Pour notre étude, trois sondes nitroxydes ont été incorporées selon le protocole présenté précédemment (cf. 2.1.1.3). L'intérêt des molécules nitroxydes comme marqueurs de spin est l'anisotropie de leur constante de couplage hyperfin (A_{zz}) en fonction de leur orientation dans un champ magnétique. Il en résulte que l'allure du spectre de RPE des nitroxydes est fortement liée au mouvement de la molécule et donc à sa mobilité.

Les échantillons enrichis en sonde sont introduits dans un tube puis celui-ci est placé dans la partie centrale du spectromètre RPE. Les échantillons, ainsi disposés à l'endroit où le champ magnétique est le plus important, sont ensuite soumis à une radiation électromagnétique de fréquence telle que la condition de résonance soit établie. Les spectres alors obtenus représentent l'énergie absorbée par la matière en fonction du champ.

Les spectres RPE ont été réalisés à l'aide d'un spectromètre Bruker ESP 300 (Wissembourg, France) fonctionnant avec un résonateur X-Band à une fréquence de 9,59 GHz. Cet appareil est équipé d'un Bruker ER 041 MR microwave bridge et d'une unité de température Bruker ER 4111 VT permettant de travailler entre -80 et 160 °C par saut de 5 à 10 °C. Chaque échantillon est maintenu 2 min à chaque température afin de s'assurer de l'équilibre thermique. Les spectres sont enregistrés entre 3335 et 3485G à une modulation et une amplitude de fréquence de 100 kHz et 1 G, respectivement. L'acquisition et le traitement des données sont réalisés avec le logiciel Bruker BioSpin WinEPR Acquisition Software for EMX.

Le couplage hyperfin ($2A_{zz}$), mesuré par la distance (en Gauss) entre les raies les plus extrêmes, permet de suivre l'évolution de la réorientation de la sonde dans un milieu. De plus, la valeur de ce couplage permet d'évaluer le temps de corrélation de réorientation du radical dans un milieu (τ_{corr}).
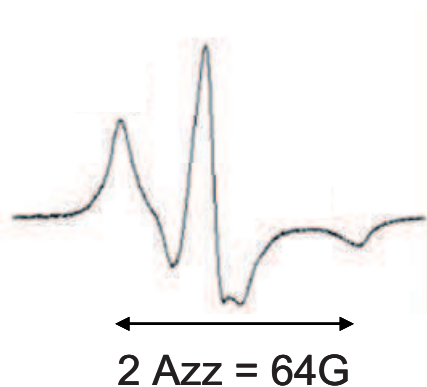
Figure 2.12. Spectre d'une sonde immobile. **Figure 2.13.** Spectre d'une sonde mobile
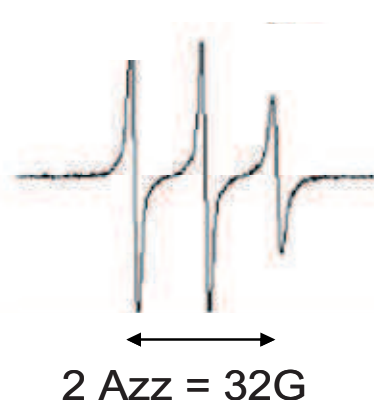
Le spectre de la Figure 2.12 est celui d'une molécule nitroxyde dans un milieu rigide (température $< T_g$), la molécule est donc immobilisée :

- Régime lent avec temps de corrélation de réorientation de cette molécule compris entre 10^{-7} s et 10^{-9} s.
- Distance séparant les deux extrémités du spectre ($2 A_{zz}$) de 64 Gauss.

Le spectre de la Figure 2.13 reflète par contre la liberté de mouvement de la molécule sonde dans un milieu fluide ou dans un matériau à une température supérieure à la T_g du matériau :

- Régime rapide avec temps de corrélation de réorientation de cette molécule compris entre 5.10^{-11} s et 10^{-9} s.
- Distance séparant les deux extrémités du spectre ($2 A_{zz}$) de 32 Gauss.

La mesure du T_{50G} d'une sonde dans un échantillon est, quant à elle, caractéristique du degré de mobilité de la sonde dans son environnement lors de montée en température. En effet, ce point expérimental correspond à la température à laquelle la sonde passe dans la matrice d'un état immobilisé (couplage hyperfin > 50 G) à un état libre (couplage hyperfin < 50 G).

2.2.2.11. Microscopie à fluorescence SOLEIL

L'objectif de cette méthode est d'estimer un coefficient de diffusion en se basant sur des observations en microscopie à fluorescence, réalisées sur le site de SOLEIL (Gif-sur-Yvette, France).

2.2.2.11.1. Préparation des échantillons

La préparation des échantillons a été réalisée en deux étapes, une première étape de formulation et une deuxième étape de mise en contact pour permettre la diffusion des molécules fluorescentes.

Cette technique nécessitant des échantillons fins et d'épaisseur bien homogène, deux films commerciaux ont été utilisés :

       - un film de P(D,L)LA, Biophan^{TM} 121 (Treofan), de 20 µm d'épaisseur,

       - un film de polypropylène (PP, AMCOR Research, UK) de 200 µm d'épaisseur a été réalisé par extrusion-soufflage après additivation avec un antioxydant fluorescent (Irganox 1076).

Les films ont été découpés sous forme de cercle de 2 cm de diamètre. L'étape de formulation a consisté à immerger les échantillons de PP dans des solutions de molécules fluorescentes. Ces solutions sont réalisées dans l'éthanol à une concentration de 0,005 mol.L^{-1}. Les solutions contenant les échantillons de PP sont conservées une semaine à 60 °C afin d'obtenir un matériau gorgé de molécules fluorescentes nommé fPP.

Un empilement de trois couches, P(D,L)LA vierge, PP formulé (fPP) et P(D,L)LA vierge, est ensuite réalisé selon le schéma ci-dessous (Figure 2.14), enveloppé dans une feuille d'aluminium et pressé entre deux couches de téflon et de bois avec un serre-joint afin d'avoir une pression homogène sur toute la surface des échantillons :
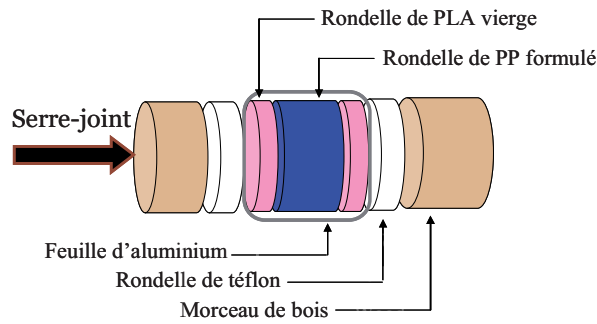
Figure 2.14. Schéma de l'empilement des trois couches P(D,L)LA/fPP/P(D,L)LA sur le principe de la méthode de Roe.(Lezervant, 2007; Roe, 1974)

Les empilements sont placés dans une étuve à 70 °C pendant 114 h. Une fois le temps de contact écoulé, les empilements sont placés dans l'azote liquide pour stopper la diffusion des molécules fluorescentes dans le P(D,L)LA.

Afin de pouvoir observer les profils de concentration au microscope à fluorescence, les empilements sont microtomés en fines bandes de 10 µm d'épaisseur et posés sur une lame de verre. Une fois recouverte d'une lamelle en quartz, les échantillons sont observés au microscope.

2.2.2.11.2. Le microscope à fluorescence

Le microscope POLYPHEME utilisé est construit autour d'un microscope inversé Olympus IX71 (Figure 2.15).
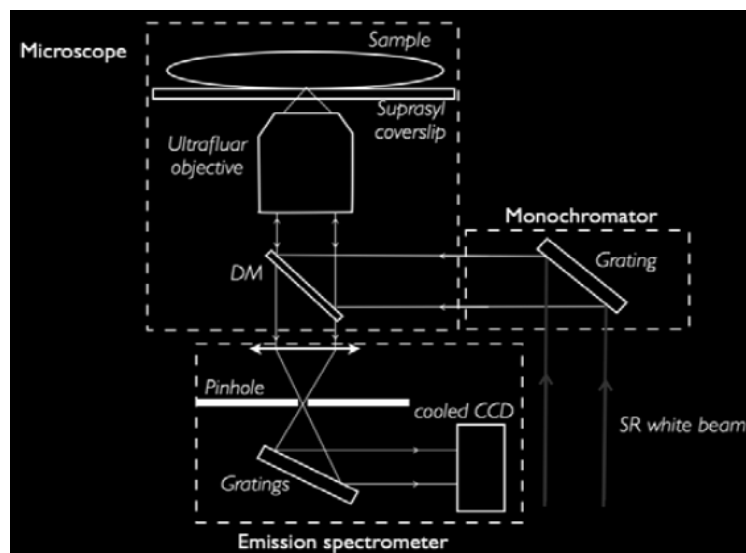
Figure 2.15. Schéma du microscope inversé POLYPHEME.

Le rayonnement Synchrotron, faisceau blanc, est monochromatisé puis réfléchi sur un miroir dichroïque orienté à 45° vers l'échantillon et l'objectif du microscope. Le faisceau excite les

fluorophores en un point précis de l'échantillon grâce à l'objectif. Le signal émis est ensuite renvoyé jusqu'à un diaphragme ajustable (pinhole) et récupé par un CCD.

L'acquisition des données est effectuée par le logiciel Labspec (Jobin-Yvon) et leur traitement par Matlab.

2.2.2.12. Traitement statistique des données

Une analyse de variance (ANOVA) a été réalisée, grâce au logiciel XLSTAT-Pro 7.0 (Addinsoft, Paris) sur les données de perméabilité et les résultats des tests de traction. En cas de différence significative entre moyennes ($p < 0,05$), un test de Duncan ou Fischer a été effectué afin de déterminer les différences entre paire de groupe.

Chapitre 3

-

Effet de la formulation sur les propriétés du P(D,L)LA

Le chapitre bibliographique a mis en évidence des propriétés mécaniques et barrière moyennes limitant les applications du PLA. Afin d'atteindre les performances des polymères pétro-sourcés en terme de propriétés mécaniques, la voie de la formulation a été choisie. Peu coûteuse et rapide, celle-ci permet de moduler facilement la structure du polymère en créant du volume libre et en facilitant la mobilité des chaînes polymère qui peuvent ainsi s'organiser en cristaux. L'étude de la littérature portant sur la formulation du P(D,L)LA a mis en évidence l'efficacité de deux plastifiants, le poly(éthylène glycol) (PEG) et l'acétyl tributyl citrate (ATBC). Ceux-ci ont, en plus de leur pouvoir plastifiant, l'avantage d'être aptes au contact alimentaire. L'agent nucléant choisi est le talc en raison de sa capacité à nucléer le P(D,L)LA à de faible teneur. En raison des faibles quantités disponibles pour chacune des formulations réalisées à l'état fondu dans un mélangeur interne, les films utilisés dans ce chapitre ont été réalisés par thermo-compression. Cette méthode a l'avantage de consommer peu de matière mais les films ainsi formés présentent une hétérogénéité d'épaisseur. Ceci a pu induire une certaine variabilité des mesures, en particulier pour les essais mécaniques et pour les mesures de perméation pour lesquels plusieurs mesures d'épaisseur ont été réalisées sur chaque échantillon et moyennées.

Dans un premier temps, une publication traitant de l'étude des caractéristiques des mélanges de P(D,L)LA CD92 avec les deux types de plastifiant est présentée (publication n°2). Il s'agit à la fois de vérifier la teneur en plastifiant dans les mélanges tout en mesurant l'influence des plastifiants sur la masse molaire, la température de transition vitreuse, les propriétés mécaniques et barrière du P(D,L)LA CD92. Dans un deuxième temps, une étude a été menée par DSC afin d'établir l'influence des plastifiants et/ou d'un agent nucléant sur la cinétique de cristallisation non-isotherme du P(D,L)LA CD92 (publication n°3).

3.1. Analysis of the structure-properties relationships of different multiphase systems based on plasticized poly(lactic acid) (Publication n°2)

Cécile Courgneau[1,2], Sandra Domenek [2], Alain Guinault[3], Luc Avérous[4], Violette Ducruet[1]

[1] INRA UMR 1145 Ingénierie Procédés Aliments, 1 avenue des Olympiades, F 91300 Massy, France.

[2] AgroParisTech UMR 1145 Ingénierie Procédés Aliments, 1 avenue des Olympiades, F 91300 Massy, France.

[3] CNAM, Laboratoire P2AM , 292 rue Saint-Martin, case courrier 322, 75141 Paris cedex 03, France.

[4] ECPM-LIPHT, EAc (CNRS) 4379, Université de Strasbourg, 25 rue Becquerel, 67087 Strasbourg Cedex 2, France.

3.1.1. Abstract

Poly(lactic acid) is one of the most promising biobased and biodegradable polymers for food packaging, an application which requires good mechanical and barrier properties. In order to improve the mechanical properties, in particular the flexibility, PLA plasticization is required. However plasticization induces generally a decrease in the barrier properties. Acetyl tributyl citrate (ATBC) and poly(ethylene glycol) 300 (PEG), highly recommended as plasticizers for PLA, were added up to 17 wt% in P(D,L)LA. In the case of PEG, a phase separation was observed for plasticizer contents higher than 5 wt%. Contrary to PEG, the T_g decrease due to ATBC addition, modelled with Fox's law, and the absence of phase separation, up to 17 wt% of plasticizer, confirm the miscibility of P(D,L)LA and ATBC. Contents equal or higher than 13 wt% of ATBC yielded a substantial improvement of the elongation at break, becoming higher than 300 %.

The effect of P(D,L)LA plasticization on the barrier properties was assessed by different molecules, with increasing interaction with the formulated material, such as helium, an inert gas, and oxygen and water vapour. In comparison to the neat sample, barrier properties against helium were maintained when P(D,L)LA was plasticized with up to 17 wt% of ATBC. The oxygen permeability coefficient and the water vapour transmission rate doubled for mixtures with 17 wt% ATBC in P(D,L)LA, but increased 5-fold in the PEG plasticized samples. This result is most likely caused by increased solubility of oxygen and water in the

PEG phase due to their mutual miscibility. To conclude, ATBC increases efficiently the elongation at break of P(D,L)LA while maintaining the permeability coefficient of helium and keeping the barrier properties against oxygen and water vapour in the same order of magnitude.

Keywords: poly(lactic acid); barrier properties; permeability; thermo-mechanical properties; plasticization.

3.1.2. Introduction

During the last decades, the consumption of petroleum based polymers have dramatically increased and particularly in the packaging field. Indeed, the plastic consumption of the world grew from 50 millions of tons in 1980 to 260 millions of tons in 2007 (Plastic Europe, 2009). However due to the negative ecological impact and the expected rise of the cost of fossil-based polymers, materials based on renewable resources are widely studied and appear on the market. Bio-based polymers covered approximately 0.2 % of the European plastic market in 2007, i.e. 75,000-100,000 tons (European-bioplastics, 2010). Polylactide (PLA) is one of the most promising commercial polymers for a large range of diverse application such as biomedical or packaging, having already important production volumes.

PLA is a good competitor for food packaging with a good clarity and a glass transition temperature higher than room temperature. However for this kind of application, PLA shows moderate mechanical and barrier properties (Bogaert, 2000; Weber, 2002), properties which are nonetheless crucial for preserving organoleptic and hygienic food quality during shelf-life (Siracusa, 2008). Besides, in this context the high brittleness of PLA limits its process ability and its applications. One way to modulate the material properties in the aim of improving the mechanical behaviour is the formulation approach by addition of plasticizers. Various plasticizers have been tested with PLA such as, e.g., glycerol and PLA oligomers (Martin, 2001), triacetine (Ljungberg, 2002), diethyl bishydroxymethyl malonate (Ljungberg, 2004), poly(1,2-butanediol), dibutyl sebacate acetyl glycerol monolaurate (Pillin, 2006), and polyadipates (Martino, 2006). However, only a few substances brought about substantial improvements of mechanical properties. Good candidates were, for example, poly(ethylene glycol) (PEG) and citrate derivates. Indeed, Baiardo *et al.* showed that the addition of PEG and acetyl tributyl citrate (ATBC) increased the elongation at break (Baiardo, 2003). This

effect has been confirmed by Labrecque *et al.* who demonstrated that among the four tested citrates, ATBC was the most efficient at a concentration of 20 wt% (Labrecque, 1997). PEG and citrate derivates induce a large decrease in the glass transition temperature (T_g) and the crystallization temperature (T_c). To give one example, a decrease of 20-25 °C of T_g and T_c has been shown by Ljungberg *et al.* for a PLLA plasticized with 15 wt% of citrate, although for contents higher than 20 wt% of plasticizer, a phase separation was observed (Ljungberg, 2005). Moreover PEG and ATBC are approved for food contact materials by the European legislation (EFSA, 2006). So these plasticizers appear to be good candidates for the formulation of PLA in the aim of an application as food packaging.

However, the use of plasticizers is generally linked to a loss in barrier properties, because of the increase in free volume in the materials and/or increased solubility of permeating molecules due to the presence of the plasticizer.

The gas barrier properties are a key point for food preservation, though. Of particular importance are oxygen and water vapour transmission. The presence of oxygen leads to the oxidization of lipids and to the creation of off-flavours, whereas water vapour could lead to the disequilibrium moisture content which causes the food rotting or drying. The oxygen barrier properties of the amorphous PLA are similar to the ones of high density poly(ethylene) (HDPE) and intermediate between poly(ethylene terephthalate) (PET) and poly(styrene) (PS) (Auras, 2005; Colomines, 2010). The water vapour permeability of P(D,L)LA is higher by one order of magnitude than the one of PS and PET and by 2 orders than the one of HDPE (Auras, 2005; Grulke, 1999). High water vapour permeability can be a positive feature for the conservation of fruits and vegetables, but the conservation of foodstuff with high water content is not possible in this case. Therefore, generally low water vapour permeability of the packaging material is targeted.

The present work is focused on the study of the effect of the plasticizers acetyl tributyl citrate (ATBC) and poly(ethylene glycol) (PEG) on the mechanical and barrier properties of amorphous P(D,L)LA. The plasticization was evaluated by analyzing the thermal and mechanical properties of amorphous P(D,L)LA. Although effects of those agents on mechanical properties are already described, no systematic study has been conducted taking into account the effect of the formulation on the mechanical and barrier properties of the resulting material. For that, three molecules have been studied in this work according to their possible interaction with P(D,L)LA and its plasticizers: (i) helium, a non condensable gas, (ii) oxygen, a non condensable gas with higher molecular volume and (iii) water vapour, water being a condensable molecule.

3.1.3. Experimental

3.1.3.1. Materials

The poly(lactic acid) pellets were provided by Cargill-Dow. The content of L-lactide was about 92 wt%. The average molecular weight was 9.0×10^4 g.mol^{-1} with a dispersity of 2.75. Acetyl tributyl citrate (ATBC) and Poly(ethylene glycol) (PEG), used as plasticizers, were purchased from Sigma Aldrich (France). The properties of these plasticizers are listed in Table 1. Calcium chloride was provided by Sigma Aldrich (France) and ethanol was supplied by Carlo Erba (France).

3.1.3.2. Sample Preparation

P(D,L)LA pellets and plasticizers were dried at 80 °C overnight in a vacuum oven. After that, the formulated P(D,L)LA samples were prepared by direct melt mixing of additives with P(D,L)LA in an internal mixer (Haake Rheocord 9000) at 160 °C and 60 rpm for 15 min. (Piorkowska, 2006; Pluta, 2004) Addition of PEG and ATBC were varied from 2.5 to 20 % of P(D,L)LA weight.

Once all the mixing materials were collected and dried during 4 h minimum at 80 °C, the different P(D,L)LA formulations were thermo-moulded by compression (Telemecanique, 15 tonnes) at 185 °C and 150 bars in a multistep process. The P(D,L)LA blends were melted between the hot plates without pressure for 3 min. Then they were pressed under 10 bar for 30s, 50 bar for 30 s and 150 bar for 1 min to remove air bubbles and obtain a film of approximately 100 µm thickness. At last the samples were quenched in water at ambient temperature.

3.1.3.3. Analysis Methods

3.1.3.3.1. Extraction of plasticizer from the formulated P(D,L)LA
Formulated P(D,L)LA films were cut in small pieces and placed in a Soxhlet apparatus with 150 mL of ethanol (7 h, 90 °C) to extract the plasticizer from P(D,L)LA. After that the film

pieces were placed in an oven (3 days, 60 °C) to dry them and then weighted to determine the loss of plasticizer. Analysis was done in duplicate.

3.1.3.3.2. Size Exclusion Chromatography (SEC)

The average molecular weight and the dispersity were measured by SEC using a Shimadzu apparatus equipped with an RID-10A refractive index detector and an SPD-M10A UV detector. The analyses were carried out at 30 °C and 0.8 mL.min^{-1} in chloroform on PL Gel Mixed-C and PLGel 100Å columns. The calibration was performed with PS standards from 580 to 1,650,000 g mol^{-1}.

3.1.3.3.3. Modulated Temperature Differential Scanning Calorimetry (MDSC)

The thermal analyses were performed with an MDSC Q100 (TA Instruments) under nitrogen atmosphere. The samples (about 10 mg) were put into hermetic aluminium pans (TZero, TA Instruments) to avoid the loss of plasticizer upon heating. The modulated mode was used to study the glass transition. The heating scans were performed under sinusoidal temperature modulation with a heating rate of 1 °C.min^{-1}, a period of 80 s and a modulation of ± 1.5 °C from 10 to 80 °C. The glass transition temperature (T_g) is taken at the midpoint of the specific heat increment from the reversing signal. All experiments were carried out in triplicate.

The standard mode was used to study the crystallinity degree of the samples (χ_c). The heating scans were performed with a heating rate of 10 °C.min^{-1} from -30 to 190 °C. The crystallinity degree is calculated with Equation 1:

$$\chi_c = \frac{\Delta H_m - \Delta H_c}{\Delta H_m^0},$$
(1)

Where ΔH_m is the enthalpy of melting, ΔH_c is the enthalpy of crystallization and ΔH_m^0 is the enthalpy of fusion per gram of repeating unit of the perfect crystal of infinite size, being 93 J.g^{-1} (Fischer, 1973). All experiments were carried out in triplicate.

3.1.3.3.4. Dynamic Mechanical Analysis (DMA)

Measurements were carried out with a DMTA V (TA Instruments) at a frequency of 1 Hz and 0.05 % strain. The samples were heated from -140 to 130 °C at 2 °C.min^{-1}. The relaxation temperature which can be associated with the glass transition was taken at the maximum of the peak of the damping factor (tan δ). Experiments were carried out in duplicate.

3.1.3.3.5. Tensile Test

The uniaxial tensile testing was carried out at room temperature, at a relative humidity (RH) varying between 40 and 60 % and at 5 mm.min^{-1} with an Instron tensile testing machine (Instron Model 4507) equipped with pneumatic jaws on type I BA dumbbell-shaped samples. The thickness of the samples varies from 100 to 150 µm. Each value is an average of 10 measurements.

3.1.3.3.6. Oxygen, helium and water vapour permeability

The direct measurement of the oxygen transmission rate (*OTR*) was monitored at 23 °C and 0 % RH with a Systech 8001 apparatus. The oxygen permeability tests have been performed at 0 % RH to avoid the plasticization effect of water on polymer sample. The helium transmission rate (*HeTR*) was measured at room temperature and at a relative humidity varying between 40 and 60 % RH, by a specific analyser developed by CNAM (Paris, France), based on the ISO norm 15105-2:2003. Oxygen and helium permeability were then obtained by dividing respectively *OTR* and *HeTR* by the film thickness. Experiments were carried out in duplicate. The oxygen diffusion coefficient was estimated with the time-lag method according to the following relationship:

$$\theta = \frac{l^2}{6D} \ ,$$
(2)

where l is the film thickness (m) and θ the time-lag (s). The time-lag is determined as the intercept of the time axis and the extrapolated linear steady state part of the curve for a representation of the amount of permeant passing through the film in time t versus time.

The water vapour transmission rate (*WVTR*) of the films was measured according to the norm NF H 00-030 at 25 °C and 50 % RH or 38 °C and 90 % RH. The procedure consists in putting in a cup calcium chloride ($CaCl_2$) which was previously dried at 50 °C in a drying oven. Then the film sample under investigation is placed on the cup and the borders are sealed with beeswax in order to obtain a specific exchange surface. After that, the cup is placed in a chamber at constant temperature and humidity. Water vapour has to pass through the film sample and to be sorbed on the desiccant $CaCl_2$. The weight uptake of $CaCl_2$ is measured regularly for two days to obtain the *WVTR* value. Given values are averages of two experiments.

The statistical analysis was realized with a one-way ANalysis Of VAriance (ANOVA). When the differences were significant (*p*<0.05), Duncan's test was used to check the differences between pairs of groups and was carried out using XLSTAT-Pro 7.0 software (Addinsoft, Paris, France).

3.1.4. Results and Discussion

The effects of plasticization on the thermal and mechanical properties of the P(D,L)LA samples were investigated. Two plasticizers PEG and ATBC, the properties of which are shown in Table 1, were added to P(D,L)LA. The miscibility of plasticizers and polymer can be estimated from the solubility parameters, which have been calculated thanks to the method of Hoy (Grulke, 1999). The values of solubility parameter of ATBC and PEG are close to the one of P(D,L)LA. Interaction parameters, shown in Table 1, have been calculated using the following equation (Grulke, 1999; Pillin, 2006):

$$\chi = \frac{V_1}{RT}(\delta_1 - \delta_2)^2 + B,$$ (3)

Where *R*, *T*, and *V₁* are the gas constant, the temperature and the molar volume of the component 1. δ_1 and δ_2 are the solubility parameter of the blends components. The term *B* is the entropic component of the interaction parameter. *B* often equals 0.34 for non polar systems. According to Pillin *et al.*, a blend can be considered as miscible if $\chi < 0.5$ (Murariu, 2008; Pillin, 2006). So it seems that P(D,L)LA and ATBC should be miscible whereas P(D,L)LA and PEG might be non miscible.

Table 1. Number average molecular mass (M_n), solubility parameters (δ), interaction parameter (χ) between P(D,L)LA and plasticizers and glass transition temperature (T_g) of P(D,L)LA pellets and plasticizers.

Substance	M_n (g.mol⁻¹)	δ (J.cm⁻³)¹ᐟ²	χ	T_g (°C)
P(D,L)LA pellets	90 500	20.4	-	56.0
PEG 300	300	23.1	1.1	-75.9
ATBC	402	19.9	0.38	-82.6

The melt mixing of P(D,L)LA with additives results often in a decrease of the molecular weight which can be due to the high sensitivity of P(D,L)LA to the thermo-mechanical input,

to the moisture or/and to transesterification reactions with additives (Lim, 2008). Therefore, the raw materials were extensively dried and the polymer molecular weights were followed by SEC. The SEC data are given in Table 2. A decrease in the molecular weight of neat P(D,L)LA is shown after melt-blending at 160 °C. According to Signori *et al.* (Signori, 2009) and Murariu *et al.* (Murariu, 2008), the average molecular weight of neat P(D,L)LA decreases slightly after mixing at 50-60 rpm and at high temperature (150-190 °C).

Table 2. Number and weight average molecular mass (M_n and M_w) and dispersity ($Đ$) of P(D,L)LA pellets and formulated P(D,L)LA.

	Plasticizer content per polymer weight (%)	Plasticizer content (wt%)	M_n (g mol^{-1})	M_w (g mol^{-1})	$Đ$
P(D,L)LA pellets	-	-	90 500	248 900	2.75
Neat P(D,L)LA	-	-	70 200	223 450	3.2
P(D,L)LA + PEG	2.5	2.5	74 400	174 000	2.3
	5	5	55 900	155 900	2.8
	10	9	41 150	90 500	2.2
	15	13	36 350	66 850	1.8
	20	17	27 500	49 925	1.8
P(D,L)LA + ATBC	2.5	2.5	92 300	212 950	2.3
	5	4	98 900	228 100	2.3
	10	9	76 650	182 500	2.4
	15	13	57 550	123 900	2.2
	20	17	55 050	133 950	2.4

Table 2 shows that the addition of PEG accentuates the decrease of the molecular weight, which may be due to the degradation of P(D,L)LA chains coupled to main chain scission and trans-esterification reactions between P(D,L)LA and PEG (Hyon, 1997). On the contrary, ATBC does not induce a decrease in M_n at low content in P(D,L)LA. Nevertheless, further addition of ATBC in P(D,L)LA results in a slight decrease in M_n. To summarize, the addition of plasticizer brings about a notable decrease in molecular weight in the case of PEG and shows only a slight drop in the case of ATBC. Therefore, given the nature of these results, it appears that ATBC seems to be preferable for the formulation of P(D,L)LA.

3.1.4.1. Efficiency of P(D,L)LA Plasticizing with PEG and ATBC

In order to measure the T_g, MDSC analysis was performed to separate the glass transition from the endothermic relaxation which is the result of cooperative rearranging movement occurring in the amorphous phase of the semi-crystalline polymers (Auras, 2004a; Solarski, 2005; Hutchinson, 2003). The analysis in MDSC makes it possible to determine more precisely the T_g of the systems, because the signal of the endothermic relaxation can be separated from the signal of the glass transition. The MDSC thermogrammes obtained at 1 °C.min^{-1} are shown in Figure 1.
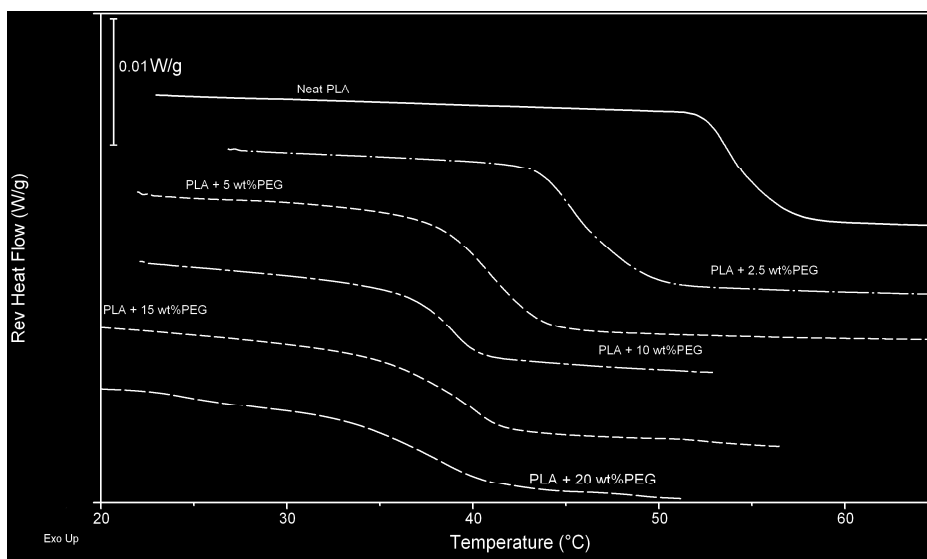
Figure 1a. MDSC thermograms for neat P(D,L)LA and formulated P(D,L)LA with PEG heated at 1 °C.min^{-1}. The curves were vertically shifted for legibility.
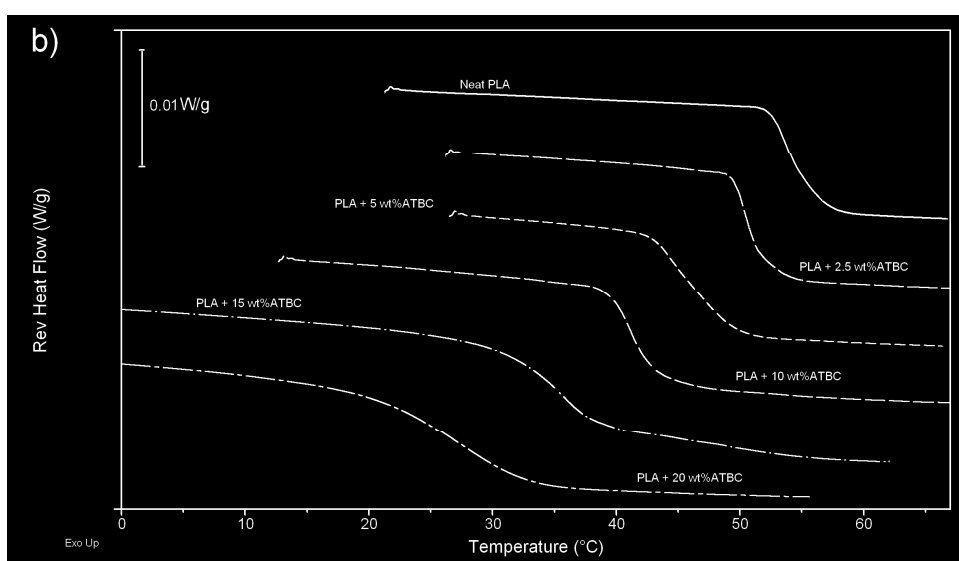
Figure 1b. MDSC thermograms for neat P(D,L)LA and formulated P(D,L)LA with ATBC heated at 1 °C .min^{-1}. The curves were vertically shifted for legibility.

Due to the lower temperature limit of the MDSC apparatus (-70 °C), it is not possible to detect the small variation in the heat capacity which should occur at the T_g of the plasticizer in case of phase separation. So a single T_g is detected for the plasticized P(D,L)LA in the studied temperature range. In accordance with the literature (Ljungberg, 2005; Pyda, 2005), the neat P(D,L)LA exhibits a T_g at 55 °C. A shift to lower temperature of the T_g is shown for the formulated P(D,L)LA (Figure 1 and Figure 2). With 17 wt% of PEG and ATBC, the T_g of P(D,L)LA blends decreases to 37 and 28 °C, respectively.
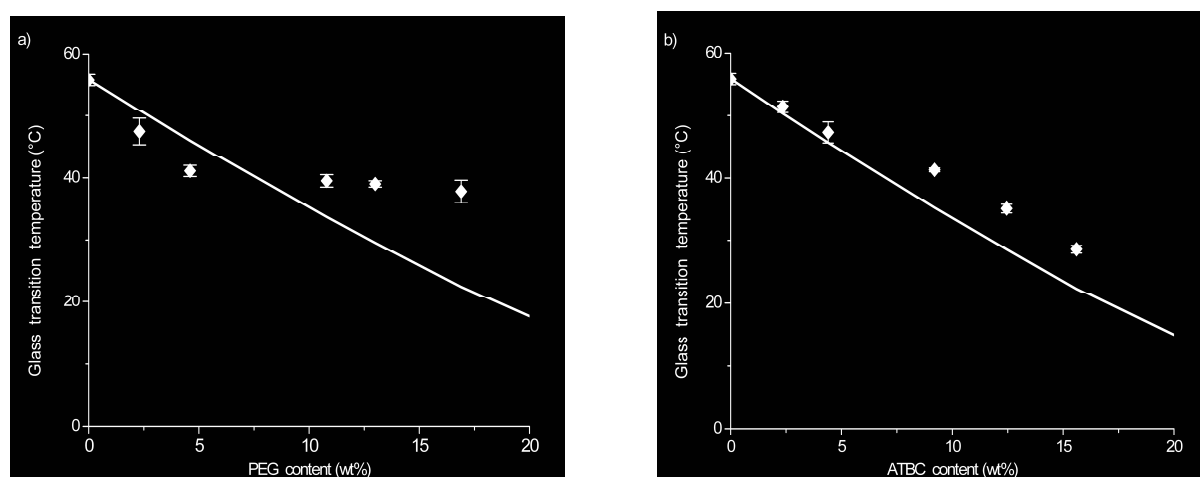
Figure 2. Glass transition temperature of P(D,L)LA/plasticizers: Experimental results (♦) and Fox equation (—). (a), PEG 300/P(D,L)LA; (b), ATBC/P(D,L)LA.

The action of a plasticizer is to increase the free volume and to decrease the polymer chain interactions which induce higher chain mobility at lower temperature. In the present case, the effect linked to plasticization is most probably superposed with a decrease of the glass transition temperature due to chain scission during the process (Table 2).

Among the equations used to predict the glass transition temperature for polymer blends as a function of the composition, the empirical Fox Equation is the most widely used:

$$\frac{1}{Tg} = \frac{w_1}{Tg_1} + \frac{w_2}{Tg_2}, \tag{4}$$

where T_g is the glass transition temperature of the blends, T_{g1} and T_{g2}, those of the components 1 and 2, and w_1 and w_2 the weight fraction of 1 and 2 determined after plasticizer extraction from formulated P(D,L)LA. The extractions of the plasticizer from the formulated film have shown that the melt-mixing in the internal mixer induced no significant loss of the plasticizer content in P(D,L)LA. The T_g values of the P(D,L)LA/PEG blends, plotted in Figure 2a, do not follow the empirical Fox equation. There is a levelling off of the T_g in the PEG case at about 38 °C despite the increase in plasticizer content. This behaviour was most

probably caused by the phase separation of PEG at concentrations higher than 9 wt%, which may be linked to the low interaction parameter shown in Table 1. Similar behaviour has been observed by several authors with PEG and other plasticizers (Kulinski, 2006; Pillin, 2006). Indeed Pillin *et al.* showed that for contents higher than 20 wt% of PEG 1000 (1,000 g.mol^{-1}) or other plasticizers in P(D,L)LA there was a levelling off of the T_g values (Pillin, 2006). Moreover a macroscopic separation phase has been observed for P(D,L)LA at 20 and 30 wt% of PEG 200 (200 g.mol^{-1}) and at 30 wt% of PEG 400 (400 g.mol^{-1}) by the same authors. Kulinski *et al.* observed also this behaviour for 12.5 wt% content of poly(propylene glycol) (Kulinski, 2006). According to Ljungberg *et al.*, the plasticizer migration to the film surface induces an increase in T_g and crystallization temperature and a material weakening (Ljungberg, 2003). The T_g values of P(D,L)LA/ATBC systems are plotted in Figure 2b and, unlike PEG, they are almost consistent with Fox equation. A slight exudation may be at the origin of this deviation. Indeed Fox equation predicts a T_g at 35.7 and 19.7 °C at 9 and 17 wt% of ATBC whereas the experimental value equals 41.3 ± 0.3 °C and 28.6 ± 0.6 °C respectively. There is plasticization up to 17 wt% content plasticizer. At 17 wt% of ATBC, the T_g of P(D,L)LA is in the range of ambient temperature.

To verify the hypothesis of phase separation which could explain the deviation from Fox's equation, the thermo-mechanical properties were analyzed in a temperature range from -140 to 130 °C by DMA. The response of the viscoelastic modulus is generally more sensitive than the small variation in heat capacity measured by MDSC. The results are plotted in Figures 3 and 4.

The decrease of the storage modulus (E') during the glass transition phase is often of several orders of magnitude. This signal is easier to be detected, even at small quantities of amorphous phase. In this work, the relaxation temperature associated with the T_g was taken at maximum of the peak of the damping factor related to the α-relaxation of the amorphous polymer and shown in Figures 3a and b.
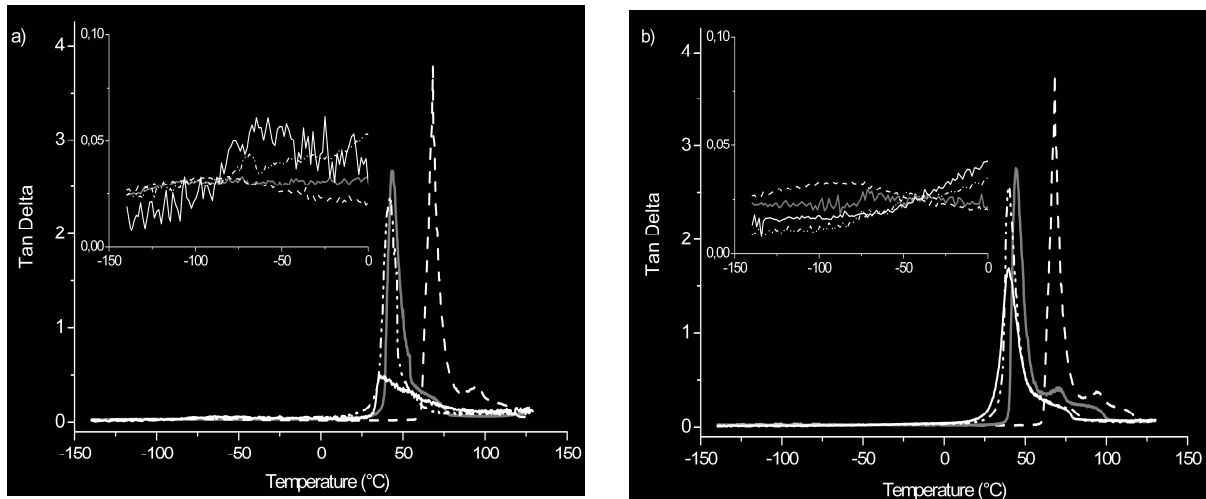
Figure 3. Evolution of the damping factor (tan delta) of neat P(D,L)LA and P(D,L)LA formulations with PEG (a) or ATBC (b). (– –) Neat P(D,L)LA, (—) P(D,L)LA + 9 wt% plasticizer, (–··) P(D,L)LA + 13 wt% plasticizer, (**—**) P(D,L)LA + 17 wt% plasticizer.

A broad peak in the damping factor is observed at lower temperature (-83 °C) for neat P(D,L)LA which may be attributed to a secondary relaxation, the β-relaxation of P(D,L)LA. The increase of the damping factor after the α-relaxation of P(D,L)LA, can be related to the cold crystallization of the samples, which also explains the increase of the storage modulus after 80 °C, as shown in Figures 4a and b.

The calculation of the crystallinity degree with the help of the first heating scan performed with the MDSC equipment shows that all the samples are totally amorphous ($\chi < 5$ %). Therefore upon heating the samples crystallize at temperature consistent with DMA measurements.

The superposition of the DMA curves shows that the maximum of tan δ decreases with the increase of plasticizer content in the P(D,L)LA. For example, at 17 wt% of PEG and ATBC, the glass transition of P(D,L)LA decreases from 67 °C to 49 °C and 41 °C respectively. These values are consistent with the MDSC data.

Looking into the glassy plateau at low temperatures, different behaviours are observed in function of the P(D,L)LA formulation. In the case of the samples formulated with PEG, a broad peak at -65 °C is detected in the damping factor with 13 wt% of plasticizer. At 17 wt% of PEG, the peak becomes higher at the same temperature with a significant loss in the storage modulus value. The temperature of this change in the glassy plateau was consistent with the value of the T_g of the plasticizer used, which was given in Table 1. This signal which can be attributed to a PEG phase in the sample, evidences a phase separation at PEG contents higher than 9 wt% (Deng, 2009; Ljungberg, 2003).

In the case of formulation with ATBC, for 9 wt% of plasticizer, a broad noisy peak in the damping factor is detected at -66 °C, which is not attributed. Indeed no signal in the storage modulus is detected at this temperature for the P(D,L)LA formulated with ATBC. An eventual phase separation, hinted by the deviation of the T_g from the predicted value of the Fox model could therefore not be confirmed by DMA data.
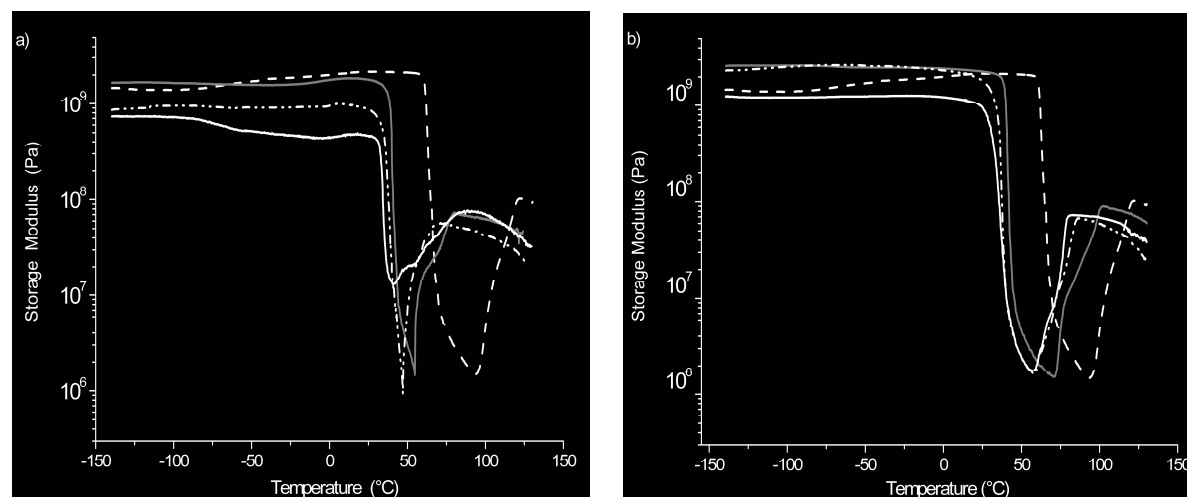
Figure 4. Evolution of the storage modulus (E') of neat P(D,L)LA and P(D,L)LA formulations with PEG (a) or ATBC (b). (– –) Neat P(D,L)LA, (–) P(D,L)LA + 9 wt% plasticizer, (–··) P(D,L)LA + 13 wt% plasticizer, (—) P(D,L)LA + 17 wt% plasticizer.

3.1.4.2. Mechanical properties of neat and formulated P(D,L)LA

P(D,L)LA displays a high Young modulus and brittleness, which in several cases constitutes an obstacle to successful application. So adding plasticizer goals to reduce brittleness and enhance the elongation. The results of the tensile test of the neat P(D,L)LA and plasticized P(D,L)LA with different plasticizer contents are summarized in Table 3. Young modulus calculated from DMA data are in general 2 times higher than the value obtained from uniaxial tensile tests.

Plasticized samples show an increase in the elongation at break of P(D,L)LA. This rise is associated with a drop of the Young modulus, the strength at yield and the storage modulus. At low plasticizer content in P(D,L)LA, that is to say below 9 wt%, the elongation at break stays constant whereas the strength at yield slowly decreases. Moreover in the case of PEG, the Young modulus decreases slowly already at small plasticizer contents whereas with ATBC it stays constant up to 9 wt%. As expected, at higher plasticizer level, a dramatic rise

in the elongation at break is observed, from 8 to about 140 and 500% with 17 wt% of PEG and ATBC, respectively.

Table 3. Mechanical properties of neat and formulated P(D,L)LA.

	Plasticizer content (wt%)	Storage Modulus DMA (MPa)	Young Modulus (MPa)	Elongation at break (%)	Strength at yield (MPa)
Neat P(D,L)LA	-	1730	1290 ± 60	8 ± 5	47 ± 7
P(D,L)LA + PEG	2.5	n.d.	1335 ± 145	5 ± 1	41 ± 9
	5	n.d.	1340 ± 85	5 ± 2	38 ± 7
	9	1670	910 ± 35	7 ± 2	30 ± 3
	13	924	545 ± 35	99 ± 43	18 ± 1
	17	731	320 ± 40	137 ± 34	16 ± 1
P(D,L)LA + ATBC	2.5	n.d.	1300 ± 70	4 ± 1	40 ± 8
	5	n.d.	1305 ± 65	8 ± 3	41 ± 9
	9	2530	1040 ± 55	16 ± 10	30 ± 5
	13	2490	615 ± 40	300 ± 179	22 ± 4
	17	1250	70 ± 20	503 ± 45	-

n.d., not determined

This difference in the behaviour of these two types of blends could be due to the decrease in the P(D,L)LA molecular weight plasticized with PEG (Table 2). It was shown in literature that a drop in molecular weight induces an increase in the brittleness and consequently a decrease in the elongation at break (Crank, 1975). The strength at yield and the Young modulus diminish dramatically with the plasticizers. Nevertheless the drop is less important with PEG compared to ATBC due to the PEG phase separation which decreases the P(D,L)LA plasticization effect. These data are mainly in agreement with literature which shows a decline in the Young modulus and the strength at yield while the elongation at break rises (Auras, 2004b; Labrecque, 1997; Ljungberg, 2003).

3.1.4.3. Gas barrier properties of neat and formulated P(D,L)LA

Table 4 and Figure 5 summarize the data of helium, oxygen and water vapour permeability in the steady state. The permeability coefficient (P) of these gases is linked to the diffusion coefficient, D, and the solubility coefficient, S, by the well-known relationship (Nielsen, 1994):

$$P = D \times S \tag{5}$$

D depends on the polymer structure and takes into account the free volume of the matrix and its tortuosity. S is dependent on the solubility of the gas molecules in material and consequently to the gas condensability.

The barrier properties of formulated and neat P(D,L)LA were compared with amorphous PET (aPET) and PS samples. Table 4 and Figure 5 show that helium and oxygen permeabilities of P(D,L)LA were intermediate between those of these two conventional packaging polymers which were generally and respectively classified as medium and poor barrier material. As shown in Figure 5 and taking into account the standard deviations, most of the P(D,L)LA formulations show equivalent helium permeabilities. The addition of plasticizers induces different effects according to the nature of the plasticizer. Formulation with ATBC, from 2.5 to 17 wt%, does not change the helium permeability whereas an increase of the helium permeability is noticed for P(D,L)LA up to 9 wt% of PEG.
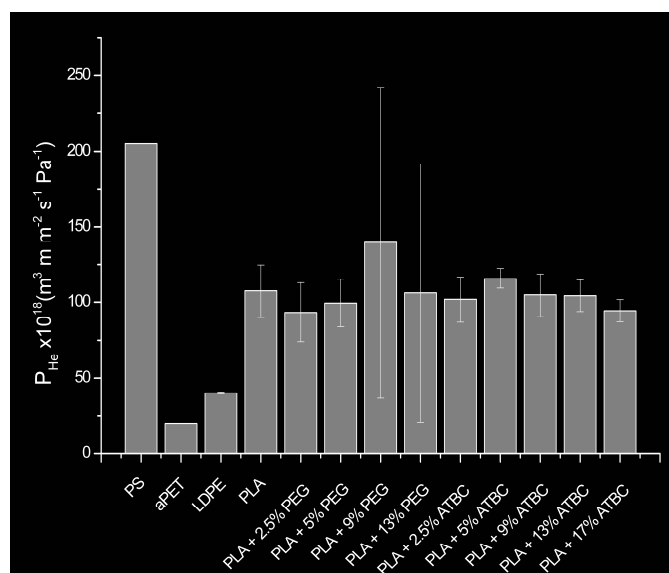
Figure 5. Helium permeability coefficient (P_{He}) of neat and formulated P(D,L)LA (PLA) with PEG and ATBC.

Moreover the standard deviations of the helium permeability values are largely higher for formulations with plasticizer contents higher than 9 wt% of PEG compared to ATBC. This behaviour could be explained by the brittleness of the samples after PEG phase separation, which causes microscopic cracks in the sample during measurement and consequently an increase in permeability. The stochastic occurrence of this problem increases the standard deviation of the repeat measurements.

Table 4. Oxygen and water vapour barrier properties of neat and formulated P(D,L)LA with PEG or ATBC.

	O_2 Permeability Coefficient $\times(10^{18}$ m^3 m m^{-2} s^{-1} Pa^{-1})	O_2 Diffusion Coefficient $\times 10^{12}$ (m² s^{-1})	*WVTR* 25 °C, 50 %RH (g m^{-2} day^{-1})	*WVTR* 38 °C, 90 %RH (g m^{-2} day^{-1})
PS	19	n.d.	n.d.	n.d.
aPET	0.4	n.d.	n.d.	n.d.
LDPE	n.d.	n.d.	2.2 ± 0.3	9.8 ± 2.4
P(D,L)LA	2.3 ± 0.1 [a]	1.6 ± 0.3 [a]	12.1 ± 5.7 [a]	61.9 ± 6.7 [a]
P(D,L)LA + 9% PEG	4.3 ± 0.5 [b]	5.2 ± 2.9 [b]	36.5 ± 2.6 [a]	191.9 ± 21.4 [b,c,d]
P(D,L)LA + 13% PEG	-	-	40.4 ± 12.5 [a,b]	202.1 ± 59.5 [c,d]
P(D,L)LA + 17% PEG	-	-	68.6 ± 17.2 [b]	300.5 ± 60.8 [d]
P(D,L)LA + 9% ATBC	2.6 ± 0.1 [a]	2.4 ± 0.1 [a,b]	16.0 ± 0.3 [a]	91.0 ± 5.1 [a,b]
P(D,L)LA + 13% ATBC	3.2 ± 0.4 [a]	2.8 ± 0.9 [a,b]	20.3 ± 0.3 [a]	129.9 ± 10.1 [a,b,c]
P(D,L)LA + 17% ATBC	5.0 ± 0.3 [c]	3.7 ± 0.7 [a,b]	21.7 ± 1.0 [a]	136.4 ± 7.8 [a,b,c]

WVTR, water vapour transmission rate.

n.d., not determined

[a,b,c,d] significant differences at $p < 0.05$ (Duncan)

Oxygen permeability was not determined at plasticizer contents lower than 9 wt%, because in this range no substantial change in mechanical properties was observed and the helium permeabilities were constant. Literature data give oxygen permeabilities of neat P(D,L)LA between 1.2 to 4.3×10^{-18} m^3.m.m^{-2}.s^{-1}.Pa^{-1} for different experimental set-ups (Auras, 2005; Bao, 2006; Sanchez-Garcia, 2007). As shown in Table 4, the oxygen permeability coefficient of neat P(D,L)LA is 2.5×10^{-18} m^3.m.m^{-2}.s^{-1}.Pa^{-1} which is in accordance with published data. The oxygen permeability data shows an increase with PEG content, which is shown by the value of 9 wt%. The samples with higher PEG content could not be measured, because they cracked in the measurement cell. Due to the phase separation of PEG, films are very fragile and they do not withstand the several hours of measurement in the apparatus. Contrary to helium permeability, oxygen permeability of P(D,L)LA formulated with ATBC increases with plasticizer content, in particularly at 17 wt% of ATBC, the value has been doubled. According to literature, the diffusion of the gas molecules is mainly due to the free volume in the polymer matrix (Ahn, 2008; Jang, 2004; McGonigle, 2001). The addition of plasticizer provokes an increase in the mobility of the polymer chains and by that in the free volume. Consequently an increase in the permeability coefficient is generally noticed (Martino, 2010). This rise in the free volume is accentuated by the decrease in the molecular weight observed in SEC (Table 2). Indeed the decrease in the size of the chain induces the formation of free volumes. Table 4 gives furthermore the diffusion coefficient of oxygen in the formulated samples calculated with the help of the time-lag method. The oxygen diffusion coefficient of

P(D,L)LA is intermediate between PET amounting to 3×10^{-13} $m^2.s^{-1}$ and PEHD being 1.7×10^{-11} $m^2.s^{-1}$ (DeLassus, 1994). As mentioned earlier, the diffusion coefficient is a kinetic parameter which responds to tortuosity and free volume. In the present case, all samples were amorphous. We suppose that the small increase in D with the increase of the plasticizer content is mainly due to the decrease in molecular weight in the sample, which has an action on the free volume. Permeability increases more than the diffusion coefficient, which points to increased solubility coefficient of oxygen in the plasticized sample. This hypothesis is supported by the observation that permeability of helium does not change with the increase of ATBC content; helium being a gas which is less interacting and supposedly less soluble in the polymer/plasticizer phase.

The analyses of water vapour permeability show that, at 25 °C and 50 % RH, the water vapour transmission rate ($WVTR$) of neat P(D,L)LA is 12.1 $g.m^{-2}.day^{-1}$ which is in accordance with Petersen *et al.* (Petersen, 2001). Contrary to ATBC which does not influence the $WVTR$, the addition of PEG at 9 wt% increases it threefold. This result is consistent with literature data which showed an increase in $WVTR$ with the plasticization of P(D,L)LA (Coltelli, 2008; Laohakunjit, 2004). However, we find an advantage for the ATBC formulated samples, where $WVTR$ at the highest plasticizer content is almost three times lower than in PEG formulations. As expected, at 38 °C and 90 % RH, the $WVTR$ of neat P(D,L)LA increases 5-fold compared to the $WVTR$ at 25 °C and 50 %RH. Moreover the increase in the $WVTR$ with the plasticizer amount is lower with ATBC than with PEG, up to three times higher and five times higher respectively. As $WVTR$ increases with the relative humidity and as water vapour is condensable, the evolution of the permeability is most probably due to the solubility of water vapour in the plasticizer.

3.1.5. Conclusions

Formulation of P(D,L)LA with plasticizers was investigated in this study as a strategy for improving the material properties. While PEG displays a limit of miscibility with P(D,L)LA and a phase separation, it clearly appears that ATBC is a more efficient plasticizer. The addition of ATBC in P(D,L)LA results in a decrease in T_g and a strong increase in the elongation at break at contents higher or equal to 13 wt%, which is associated to a drop of the Young modulus. However unlike to PEG-based systems, the materials with ATBC maintain their gas barrier properties up to 13 wt% of plasticizer. Beyond this content of ATBC, the

oxygen permeability coefficient and water vapour transmission rate rise. Nevertheless this rise is clearly less important than for PEG formulations which show a decrease in their barrier properties already at 9 wt% of PEG content. Taking into account these different results, ATBC is a more adapted plasticizer than PEG. Nevertheless a trade off has to be found between improvement of mechanical properties and loss of barrier properties, probably between 9 and 17 wt% of ATBC present in P(D,L)LA.

Furthermore the differences in gas and water vapour permeabilities could be attributed rather to their solubility in the plasticizer than to changes in diffusivity as all samples were amorphous. These findings lead us to pursue this work with the aim to modify the morphology of the plasticized material, in particular crystallization of P(D,L)LA with appropriated annealing treatments in order to improve the gas barrier properties by working on the tortuosity of polymer sample. So further work is currently in progress to investigate the relationship between microstructure of crystallized samples and the barrier properties of neat and formulated P(D,L)LA with ATBC.

3.1.6. Discussion et Commentaires

L'amélioration des propriétés du P(D,L)LA CD92 par la voie de la formulation, à l'aide de deux composés recommandés comme plastifiant du P(D,L)LA, le PEG et l'ATBC, a fait l'objet de cette publication. Ainsi les propriétés thermiques, mécaniques et barrière des systèmes multiphasiques P(D,L)LA/plastifiants ont été évaluées pour diverses teneurs en plastifiants.

L'étude des propriétés thermiques des mélanges a permis de mettre en évidence une exsudation d'un des deux plastifiants, confirmée, par la suite, à l'aide d'une analyse thermo-mécanique dynamique. Les propriétés mécaniques, quant à elles, ont été largement améliorées par la plastification avec une élongation à la rupture de plus de 300 %. Cependant, l'exsudation du PEG et la diminution de masse molaire du P(D,L)LA conduisent à une fragilisation des films de P(D,L)LA qui deviennent cassant.

Comme attendu, cette nette augmentation de la mobilité des segments de chaîne polymère induit une perte des propriétés barrière, à savoir dans le cas du PEG:

- une nette augmentation de la perméabilité et de la diffusion de l'oxygène.
- une augmentation de la vitesse de transmission de la vapeur d'eau quelles que soient les conditions de mesure.

Par contre, les propriétés barrière du P(D,L)LA ne sont modifiées qu'à partir d'une teneur de 13 % en poids d'ATBC. Au-delà, une hausse significative de la perméabilité et de la diffusion de l'oxygène et de la vitesse de transmission de l'eau à 38 °C est en effet observée.

La plastification du P(D,L)LA apparaît donc être une voie efficace pour améliorer les propriétés mécaniques du P(D,L)LA. Par contre, elle conduit à une baisse significative des propriétés barrière.

Une des voies les plus répandues pour l'amélioration des propriétés barrière est celle de la cristallisation qui permet de diminuer la solubilité et la diffusivité des molécules perméantes.

Désirant cristalliser les échantillons de P(D,L)LA afin d'évaluer l'impact de la cristallisation sur les propriétés barrière, il a été nécessaire d'étudier tout d'abord l'effet de la formulation sur la cinétique de cristallisation. La publication suivante présente donc l'influence de l'ajout de plastifiant, PEG ou ATBC, et d'agent nucléant, talc, sur la cinétique de cristallisation non-isotherme du P(D,L)LA CD92.

3.2. Non-isothermal crystallization kinetics of poly(L,D-lactide) - effect of plasticizers and nucleating agent (Publication n°3)

Cécile Courgneau[1,2], Violette Ducruet[1], Luc Avérous[3], Sandra Domenek[2]

[1]INRA UMR 1145 Ingénierie procédés Aliments, 1 avenue des Olympiades, F 91300 Massy, France.

[2]AgroParisTech UMR 1145 Ingénierie procédés Aliments, 1 avenue des Olympiades, F 91300 Massy, France.

[3]ECPM-LIPHT, EAc (CNRS) 4379, Université de Strasbourg, 25 rue Becquerel, 67087 Strasbourg Cedex 2, France.

3.2.1. Abstract

The non-isothermal crystallization kinetics of neat and formulated poly(L,D-lactide) (P(D,L)LA) with talc (nucleating agent) and/or plasticizers such as poly(ethylene glycol) (PEG) or acetyl tributyl citrate (ATBC) were investigated by using differential scanning calorimetry. A significant increase in the enthalpy of the crystallization peak was obtained upon addition of 5 wt% talc or 9 wt% PEG in P(D,L)LA. The sole addition of ATBC did not result in important crystallization. Talc and both plasticizers had, however, a synergistic effect because high crystallization degrees could be obtained for samples containing 1 wt % talc and more than 5 wt% of each plasticizer. In any case, PEG seemed to be more efficient than ATBC. A complex crystallization process was highlighted in presence of talc and/or plasticizer evidenced the appearance of three distinct regimes in the kinetic analysis according to modified Avrami model. The addition of PEG or ATBC in P(D,L)LA induced a decrease in the crystallization half-time while decreasing slightly the crystallization rate. The simultaneous presence of talc and plasticizer in P(D,L)LA induced an increase in the Avrami exponent during primary crystallization up to 6, highlighting a multidimensional growth mechanism.

The analysis of the experimental data showed that the Liu - Mo model could describe the non-isothermal crystallization of neat and formulated P(D,L)LA at various cooling rate, although

correlations were not excellent. The activation energy of non-isothermal crystallization of P(D,L)LA formulations was found to be negative and to decrease with the addition of ATBC.

Keywords: polylactide, poly(lactic acid), crystallization kinetics, plasticizer, nucleating agent

3.2.2. Introduction

Face to the waste management problem with plastic, wild landfill, accumulation of plastic debris in marine habitats (Moore, 2008), different environmental sustainable development politics were introduced recently through the world. They have been materialized partly by a will to reduce persistent pollution due to the durability and increasing usage of plastics (Thompson, 2009). In this context considerable efforts have been devoted to develop bio-based substitutes to petroleum-based polymers. In addition to their properties comparable to conventional polymers, bio-based materials have the advantages to use renewable raw materials and some of them have an end-of-life waste management by composting or anaerobic digestion to reduce landfilling (Song, 2009). Some of these bio-based polymers are already commercialized. PLA, derived from biomass, is one of the latter. PLA is available in large volume for various applications, such as biomedical application, packaging, electronic housing, textile, automobile interiors, and insulation in building (Bogaert, 2000; Gupta, 2007; Ikada, 2000; Shen, 2009). The properties of PLA, such as thermal, mechanical and barrier, are strongly dependent on the crystallinity degree and crystalline morphology, themselves strongly related to the L/D ratio of the lactic acid units (Huang, 1998; Kolstad, 1996; Tsuji, 2006).

PLA is known for its slow crystallization rate. The crystallization of the homopolymer PLLA has been extensively studied. In appropriate conditions (crystallization time and temperature) (Tsuji, 1995) the crystallinity degree of PLLA can reach 45-60 % (Day, 2006; Ling, 2006). In isothermal conditions, PLLA crystallizes between 85 and 150 °C with a fastest rate of crystallization in the range of 95-115 °C (Di Lorenzo, 2005, 2006). In the case of the heteropolymer P(D,L)LA it has been shown that the crystallinity degree (Liu, 2010) and the crystallization rate (Li, 2007) decrease with the increase in D-lactic acid content in P(D,L)LA (Huang, 1998). In non-isothermal processes, such as injection-moulding, the characteristics of P(D,L)LA show a significant drawback to produce samples at high processing rate. One way to improve the crystallization rate of PLA is by formulation, e.g. by adding a nucleating agent

which decreases the nucleation activation energy or a plasticizer which increases the mobility of polymer chains.

Diverse types of nucleating agent have been used for PLA such as clay, organic or inorganic compounds, talc or D-lactic acid to form stereocomplexes in order to improve the isothermal crystallization of PLA. The stereocomplexes of PLLA/PDLA are very efficient nucleating agent, since they can induce a decrease of the half time of crystallization ($t_{1/2}$) from 44.7 min for neat PLA to less than 2 min upon addition of 4 % of PDLA (Anderson, 2006; Schmidt, 2001). Organic compounds, such as N,N-ethylen-bis-12-hydroxystereamide or molecules having hydrazide end groups, can increase the nucleating density and crystallization rate of P(D,L)LA (Harris, 2008; Nam, 2006). Clays, which is used for reinforcement and improvement of the barrier properties, have been evaluated as nucleating agent. Nam *et al.* showed an increase in the spherulites diameter and the overall crystallization rate (Nam, 2003) whereas reduced crystallization ability is noticed by Pluta (Pluta, 2004) with organically modified montmorillonites. Talc, a very conventional filler, is good candidate although it showed a $t_{1/2}$ of 19 min with 6 % of talc in PLLA (Schmidt, 2001). Nevertheless the ability of talc to further the crystallization of P(D,L)LA has been highlighted by Harris and Lee (Harris, 2008) who gave at 115 °C a $t_{1/2}$ of 38.2 min and 0.6 min without and with 2 % of talc respectively. As previously mentioned, the addition of plasticizer may increase the mobility of segment polymers and thus increasing the crystallization rate of PLA. Various plasticizers were tested with PLA in order to diminish its brittleness, such as glycerol and oligomeric lactic acid (Martin, 2001), triacetine (Ljungberg, 2002), triphenyl phosphate (Xiao, 2009), polyadipates (Martino, 2009; Martino, 2006), poly(prolylene glycol) (Kulinski, 2005; Kulinski, 2006), poly(ethylene glycol) (Baiardo, 2003; Courgneau, 2011; Hu, 2003; Jacobsen, 1999; Kulinski, 2005; Martin, 2001), and acetyl tributyl citrate (Baiardo, 2003; Coltelli, 2008; Courgneau, 2011; Labrecque, 1997; Ljungberg, 2002). However few of them have been added to modify the isothermal crystallization rate of P(D,L)LA. As shown by Piorkowska *et al.* (Piorkowska, 2006) and Kulinski *et al.* (Kulinski, 2005) the addition of PPG (425 and 1000 g.mol^{-1}) or PEG (600 g.mol^{-1}) induces a significant increase in the crystal growth rate and particularly with PEG whose the content of 12.5 wt% in P(D,L)LA leads to a multiplication of the growth rate by 24. Therefore spherulites of 10 µm radius were formed after 15 min at 90 °C. Li and Huneault (Li, 2007) tested the effects of PEG (3350 g.mol^{-1}) and acetyl triethyl citrate on P(D,L)LA at 20 °C.min^{-1}. It turned out to be that the addition of PEG induced, contrary to neat P(D,L)LA, crystallization upon cooling and a large shift of the crystallization temperature to lower temperature. Triphenyl phosphate (TPP) has also been

tested on P(D,L)LA with good results. Xiao *et al.* (Xiao, 2010a; Xiao, 2009) showed that, upon isothermal crystallization, the crystal growth rate optimum is tripled and shifted to lower temperature thanks to the introduction of 20 % of TPP in P(D,L)LA. However the crystallization rate constant and $t_{1/2}$ decreased with the increase in TPP content. The synergistic effect of nucleating agent and plasticizer has been rarely studied. Xiao *et al.* (Xiao, 2010c) noticed that the addition of talc to the plasticized P(D,L)LA increased the crystallization rate constant if it was compared to neat P(D,L)LA but decreased if compared to the rate constant of plasticized P(D,L)LA. On the contrary Li and Huneault (Li, 2007) showed that the addition of PEG to P(D,L)LA/talc decreased $t_{1/2}$ and increased the crystallization peak temperature at various cooling rates.

In conclusion, plasticizing of P(D,L)LA has already received large attention and most of the studies were focussed on the effect on thermal and mechanical properties. Studies investigating the crystallization kinetics of such systems are far less numerous and the investigation of non-isothermal crystallization kinetics of P(D,L)LA, although important for the injection molding process, has been subject only to a few publications.

The aim of this study is to investigate and provide data on the effect of nucleating agent and plasticizer on the non-isothermal crystallization kinetics of P(D,L)LA. The nucleating ability of talc and the effect of PEG and ATBC, two efficient plasticizers of P(D,L)LA for improving mechanical properties, have been evaluated at various cooling rates. Two models, *i.e.* the Avrami – Jeziorny, and Liu – Mo model, were used to assess the influence of the plasticizer and the nucleating agent on the P(D,L)LA crystallization. The activation energies of neat and formulated P(D,L)LA were also estimated by the Kissinger method.

3.2.3. Experimental

3.2.3.1. Materials

The poly(lactic acid) pellets were provided by Cargill-Dow. The content of L-lactide was about 92 wt%. The average molecular weight was 9.0×10^4 g mol^{-1} with a dispersity of 2.75. Acetyl tributyl citrate (ATBC) and Poly(ethylene glycol), used as plasticizers, were purchased from Sigma Aldrich (France). The molecular weight of ATBC and PEG are 402 g.mol^{-1} and

around 300 g.mol^{-1}, respectively. Talc, with a median diameter of 13.5 µm, is used as a nucleating agent (RioTinto, Luzenac, France).

3.2.3.2. Sample Preparation

P(D,L)LA pellets, plasticizer and nucleating agent were dried at 80 °C overnight in a vacuum oven. P(D,L)LA and additives were introduced in the feeding zone of an internal mixer (Counter rotating mixer Rheocord 9000, Haake, USA) at 160 °C to melt P(D,L)LA pellets and mix at 60 rpm for 15 min. The ATBC or PEG content was varied between 4.5 and 17 wt% of P(D,L)LA. Talc was added at 1 wt% of P(D,L)LA.

After collecting and drying all the mixing materials during 4 h minimum at 80 °C, the different P(D,L)LA formulations were thermo-compressed at 185 °C and 150 bar. The films of approximately 150 µm thickness were then quenched at ambient temperature. Amorphous films were stored at ambient temperature in a desiccator over P_2O_5.

3.2.3.3. Thermal Analysis

The thermal characterization and the crystallization studied were performed with a differential scanning calorimeter (DSC Q100, TA Instruments) under nitrogen atmosphere (flow rate 50 mL.min^{-1}. The apparatus, equipped of a refrigerated cooling system (TA Instruments), is calibrated with indium as standard. The samples (about 10 mg) were put into hermetic aluminium pans (TZero, TA Instruments). The non-isothermal crystallization kinetic experiments were carried in two steps. The samples were heated to 190 °C at 10 °C.min^{-1} and maintained at this temperature 5 min to erase any thermal history. Then all the formulated P(D,L)LA were cooled down to -30 °C to study the non-isothermal crystallization from the melt. The different cooling rates are: 2, 5, 10, 15, 20 or 25 °C.min^{-1}. From the curves, the peak temperature of the crystallization (T_p) the peak enthalpy (ΔH_c), and the span of the peak ($T_{0.99}$ - $T_{0.01}$) were obtained. The temperatures $T_{0.01}$ and $T_{0.99}$ are the temperatures at which the relative degree of crystallinity amounts to 1 and 99 % respectively.

3.2.4. Results and Discussion

3.2.4.1. Non-isothermal crystallization behaviour

The crystallization exotherms from the melt of typical formulations of P(D,L)LA are plotted in Figure 1 and the corresponding enthalpies of crystallization (ΔHc) are given in Table 1.
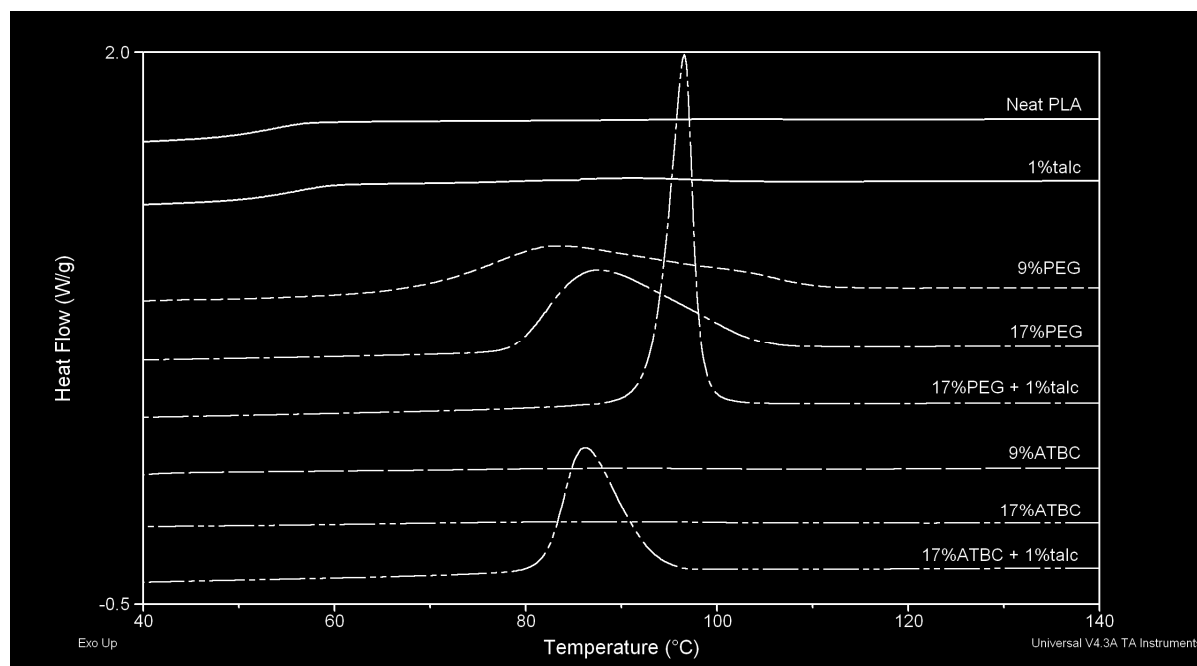
Figure 1. DSC thermograms for neat P(D,L)LA (PLA) and formulated P(D,L)LA cooled at 10 °C.min^{-1}.

The neat P(D,L)LA showed a broad very small peak of crystallization, spreading over more than 30 °C (Table 1), which yields high uncertainty in the description of its properties. The slow crystallization kinetics of P(D,L)LA are a well known issue. Some additives such as nucleating agents and plasticizers have been tested to overcome this drawback. The addition of talc, a widely used nucleating agent of P(D,L)LA, leads to a slight increase in the crystallization enthalpy but the peak is still hardly visible on Figure 1. Significant crystallization is obtained at 5 wt% talc, suggesting the need for a certain quantity of nuclei before efficient promotion of the crystallinity. In comparison, Xiao *et al.* (Xiao, 2010b), obtained a crystallization enthalpy of 29.6 J.g^{-1} upon addition of 1.2 % talc in neat P(D,L)LA and Li *et al.* (Li, 2010b) obtained 29.04 J.g^{-1} with 1 % of talc. One of the reasons might be the different D-lactic acid content in the samples. P(D,L)LA with higher D-lactic acid content crystallizes more slowly (Huang, 1998). The samples of Xiao *et al.* (Xiao, 2010b) and Li *et al.*

(Li, 2010a) contained approximately 2 % D-lactic acid, compared to approximately 8% D-lactic acid for our samples.

Furthermore, increasing the talc content increases the crystallization peak temperature and decreases the span of the peak (Table 1). It clearly shows that talc can promote the crystallization, with enlarging the crystallization window in the higher temperature range due to efficient nucleation. To facilitate the mobility of P(D,L)LA chains and further promote crystallization, the plasticizers acety tributyl citrate (ATBC) and polyethylene glycol (PEG) were used. The plasticization of P(D,L)LA by PEG induces an increase in the crystallization enthalpy, and decreases the width of the peak. At PEG contents higher than 5 wt% a maximum crystallinity degree seems to be reached (Table 1). Therefore this plasticizer furthers the crystallization of P(D,L)LA upon cooling by enhancing the polymer more noticeably in the lower temperature window, which also causes the peak temperature to shift down. ATBC, in contrary, showed much less efficiency in promoting crystallization. Even at 17 wt% of ATBC only small and broad peaks were obtained (Figure 1, Table 1).

The combination of both additives, plasticizer and nucleating agent, had the expected synergistic effect. In the case of PEG/talc, high crystallinity degrees were obtained. The peaks were comparatively thinner and shifted to higher temperatures. In the case of ATBC/talc, significant crystallization could be obtained for each formulation. For ATBC contents higher than 5 wt%, a maximum crystallinity degree was reached. The difference between both systems shows clearly that PEG is a more efficient plasticizer for P(D,L)LA than ATBC. Those results are qualitatively on agreement with the results of Li et $al.$ (Li, 2010a), based on PEG with a molecular weight of 6,000.

The relative crystallinity degree (X), as a function of temperature (T), is calculated from the energy released over the non-isothermal crystallization process. It can be defined by the Equation 1 where T_0 and T represent the onset and end of crystallization temperature, respectively and dH_c is the measured enthalpy of crystallization for an infinitesimal temperature range dT:

$$X(T) = \frac{\int_{T_0}^{T} (dH_c / dT) dT}{\int_{T_0}^{T_\infty} (dH_c / dT) dT},$$
(1)

Table 1. T_p, $T_{0.01}$-$T_{0.99}$, $t_{1/2}$, crystallization enthalpy (ΔH_c) and Avrami exponent (n_a) and crystallization rate (k_a and k_c) of neat P(D,L)LA, P(D,L)LA with various talc content and formulated P(D,L)LA with plasticizer and talc.

Samples	Plasticizer content (wt%)	T_p (°C)	$T_{0.01}$ -$T_{0.99}$ (°C)	$t_{1/2}$ (min)	ΔH_c (J.g^{-1})	Primary crystallization (5 < X (t) < 97%)			Secondary crystallization (97 < X (t) < 99.9%)		
						n_{a1}	$k_{a1} \times 10^3$ (min^{-n})	$k_{c1} \times 10^3$ (min^{-n})	n_{a2}	$k_{a2} \times 10^3$ (min^{-n})	$k_{c2} \times 10^3$ (min^{-n})
Neat P(D,L)LA	-	98.8 ± 4.4	28.4 ± 6.7	2.2 ± 0.6	0.4 ± 0.3	2.7 ± 0.2	115 ± 5	806 ± 4	4.0 ± 1.2	23 ± 8	684 ± 24
P(D,L)LA / 1 wt% talc	-	90.8 ± 2.6	29.6 ± 4.0	2.1 ± 0.3	4.9 ± 2.5	3.2 ± 0.1	65 ± 11	760 ± 12	3.5 ± 0.4	40 ± 21	718 ± 39
P(D,L)LA / 2 wt% talc	-	89.5 ± 0.1	34.5 ± 0.5	2.0 ± 0.2	8.2 ± 0.1	3.3 ± 0.5	67 ± 38	757 ± 45	2.8 ± 0.3	93 ± 23	788 ± 19
P(D,L)LA / 5 wt% talc	-	95.6 ± 0.1	24.5 ± 1.8	1.7 ± 0.4	29.4 ± 0.6	4.4 ± 0.9	22 ± 6	743 ± 106	2.8 ± 0.1	202 ± 57	850 ± 23
P(D,L)LA / PEG	5	79.9± 0.8	39.5 ± 4.3	2.2 ± 0.2	5.1 ± 3.5	2.8 ± 0.2	71 ± 26	764 ± 30	3.8 ± 0.5	19 ± 8	667 ± 30
	9	84.5 ± 2.0	44.7 ± 3.5	2.9 ± 0.3	33.5 ± 2.8	3.6 ± 0.4	15 ± 5	654 ± 23	3.1 ± 0.2	26 ± 9	693 ± 24
	13	82.2 ± 0.2	29.9 ± 0.6	2.7 ± 0.1	34.8 ± 0.6	3.4 ± 0.2	26 ± 7	694 ± 19	2.6 ± 0.3	135 ± 59	877 ± 110
	17	83.8 ± 6.8	28.5 ± 4.1	2.3 ± 0.1	32.1 ± 3.9	3.7 ± 0.3	35 ± 5	715 ± 9	2.8 ± 0.2	131 ± 62	858 ± 100
P(D,L)LA / talc / PEG	5	93.6 ± 0.5	17.0 ± 1.0	1.3 ± 0.1	32.2 ± 0.4	4.3 ± 0.3	233 ± 66	862 ± 26	1.9 ± 0.5	1101 ± 271	1008 ± 25
	9	100.3 ± 1.3	10.8 ± 0.4	1.0 ± 0.1	34.5 ±1.4	7.2 ± 1.0	661 ± 313	953 ± 44	1.9 ± 0.4	1874 ± 397	1064 ± 22
	13	98.3 ± 0.1	17.9 ± 4.0	1.7 ± 0.4	35.3 ± 0.6	9.9 ± 1.3	234 ± 38	592 ± 162	2.0 ± 0.4	848 ± 134	983 ± 15
	17	95.8 ± 5.3	13.0 ± 3.0	1.1 ± 0.1	31.5 ± 3.5	7.8 ± 1.0	291 ± 206	871 ± 58	1.6 ± 0.4	1666 ± 373	1051 ± 22
P(D,L)LA / ATBC	4	87.6 ± 7.4	38.3 ± 2.4	2.4 ± 0.1	0.2 ± 0.1	2.1 ± 0.2	133 ± 19	817 ± 11	5.9 ± 2.9	0.2 ± 0.2	611 ± 339
	9	85.9 ± 1.8	44.7 ± 1.0	2.3 ± 0.2	1.5 ± 0.2	2.3 ± 0.2	107 ± 35	797 ± 29	4.4 ± 0.5	6 ± 4	586 ± 57
	13	89.5 ± 6.5	52.2 ± 3.0	2.7 ± 0.2	3.3 ± 0.6	2.4 ± 0.1	68 ± 18	762 ± 22	3.5 ± 0.2	11 ± 5	633 ± 28
	17	78.9 ± 1.7	53.4 ± 2.2	2.8 ± 0.2	3.2 ± 2.0	2.5 ± 0.2	53 ± 23	740 ± 34	3.5 ± 0.3	11 ± 8	627 ± 42
P(D,L)LA / talc / ATBC	4	85.6 ± 0.1	35.3 ± 0.4	1.8 ± 0.1	11.7 ± 3.7	3.6 ± 0.2	35 ± 12	713 ± 22	2.4 ± 0.1	119 ± 8	808 ± 5
	9	91.2 ± 0.4	17.1 ± 0.9	1.5 ± 0.1	29.4 ± 0.3	7.7 ± 0.8	14 ± 7	647 ± 35	2.1 ± 0.2	840 ± 146	979 ± 24
	13	91.8 ± 1.8	14.8 ± 1.8	1.3 ± 0.2	27.8 ± 1.5	6.9 ± 0.9	47 ± 10	736 ± 156	2.3 ± 0.3	575 ± 265	966 ± 21
	17	87.6 ± 2.4	14.8 ± 1.6	1.3 ± 0.2	25.1 ± 1.7	8.1 ± 0.2	77 ± 13	774 ± 13	1.8 ± 0.4	1456 ± 318	1037 ± 24

If we consider that the difference temperature between the sample and the DSC furnace is negligible, the relative crystallinity degree as a function of time can be obtained from Equation 2, where α is the cooling rate (°C.min^{-1}) and t represents time (min).

$$t = \frac{T_0 - T}{\alpha} \ ,$$

(2)

The relative crystallinity is represented as a function of time for all the formulation of P(D,L)LA in Figure 2. All the curves present a sigmoidal profile with a linear trend between 0.2 and 0.8 of relative crystallinity. As it has been mentioned above, the addition of 1 wt% of talc in P(D,L)LA did not change notably the crystallization kinetic of P(D,L)LA. Nevertheless the slope of the linear part of the curve is higher for the P(D,L)LA/talc system than for neat P(D,L)LA. The addition of a plasticizer, PEG or ATBC, induces a shift of the curves to longer time. One important parameter to take from this plot is the half time ($t_{1/2}$) of crystallization, which is defined by the time from the onset to the time at which $\chi(t)$ equals 50 %. The $t_{1/2}$ is given in Table 1. One observes that the $t_{1/2}$ of the plasticized samples is always higher than the one of the neat sample, disregarding the plasticizer used.
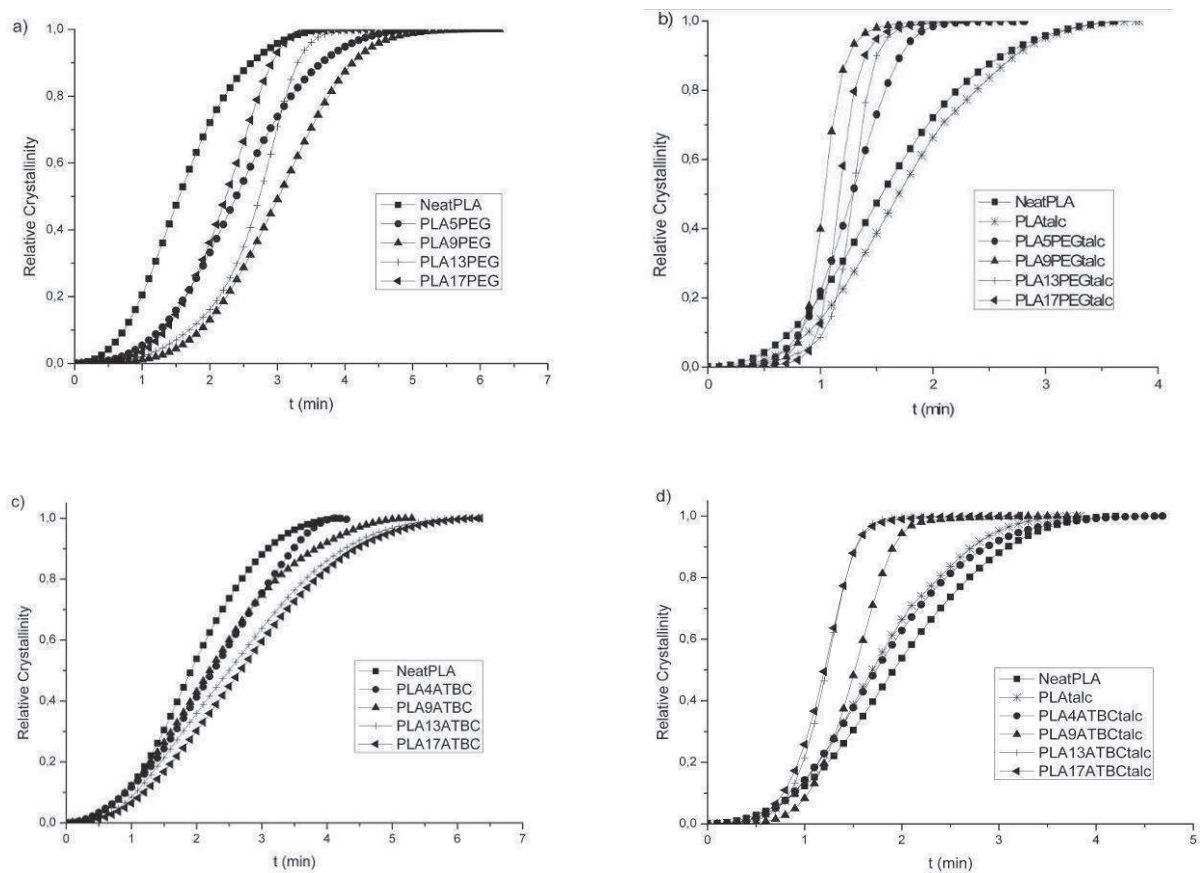
Figure 2. Variation of relative crystallinity versus crystallization time for (a) P(D,L)LA / PEG, (b) P(D,L)LA / talc / PEG, (c) P(D,L)LA / ATBC and (d) P(D,L)LA / talc / ATBC for non isothermal crystallization at 10 °C.min^{-1}.

Consequently one can conclude that the addition of only plasticizer hinders the crystallization of P(D,L)LA, on agreement with results previously observed for other systems (Li, 2010a). However the simultaneous presence of plasticizer and nucleating agent makes it possible to decrease the $t_{1/2,}$ where P(D,L)LA/ATBC/talc system crystallizes still more slowly than P(D,L)LA/PEG/talc.

Table 2. Number and weight average molecular weight (M_n and M_w) of neat and formulated P(D,L)LA.

Samples	Plasticizer content (wt%)	M_n (g.mol^{-1})	M_w (g.mol^{-1})
Neat P(D,L)LA*	-	66 700	158 000
P(D,L)LA / 1 wt% talc	-	50 850	137 750
P(D,L)LA / 2 wt% talc	-	88 100	226 450
P(D,L)LA / 5 wt% talc	-	54 450	122 400
P(D,L)LA / PEG*	5	55 850	155 850
	9	31 300	68 000
	13	36 350	66 850
	17	27 500	49 950
P(D,L)LA / talc / PEG	5	51 100	141 550
	9	26 500	50 700
	13	31 800	61 650
	17	27 200	49 600
P(D,L)LA / ATBC*	4	98 900	228 100
	9	59 100	143 650
	13	57 550	123 900
	17	55 050	133 950
P(D,L)LA / talc / ATBC	4	91 400	227 350
	9	59 900	149 250
	13	48 550	102 800
	17	51 350	117 450

*Data already published (Courgneau, 2011)

However, as shown in Table 2, the addition of PEG results in an important decrease in the molecular weight. The ability of PEG to degrade PLA has been already described for hydroxyl containing additives, one of the main mechanism could be polymer chain scission by transesterification (Hyon, 1997; Lim, 2008). On one hand, this degradation may increase the nucleation and so further the crystallization, but on the other hand this mechanism imparts the rheological and mechanical properties of the polymer and is generally unwanted. Furthermore, exudation of PEG occurs at plasticizer contents higher than 9 wt%, which was evidenced for PEG 300 by Courgneau *et al.* (Courgneau, 2011). The decrease of molecular weight is less important, when P(D,L)LA was plasticized with ATBC, which led us to

conclude, that even if PEG was more efficient than ATBC, this latter might be a better compromise for maintaining final product properties.

3.2.4.2. Avrami analysis of non-isothermal crystallization kinetics

To go further in the analysis of the crystallization kinetics, different approaches was carried out on the analysis of the DSC signal. The most common approach used to describe the overall isothermal crystallization is the Avrami equation (Avrami, 1939, 1940, 1941) given by Equation 3 where k_a and n_a are the Avrami crystallization rate and exponent, respectively.

$$X(t) = 1 - \exp(-k_a t^{n_a}) \in [0,1] , \tag{3}$$

The parameter n_a depends on the nucleation type (homogeneous or heterogeneous) and growth process parameters (rod, disc, sphere, sheaf) (Balamurugan, 2008).

Equation 3 can be transformed into Equation 4, by taking the double logarithmic form.

$$\log(-\ln(1 - X(t))) = \log k_a + n_a \log t , \tag{4}$$

Considering the non-isothermal character of the process, Jeziorny (Jeziorny, 1978) suggested to correct the value of k_a by taking into account the cooling rate of the experiment, as shown in Equation 5.

$$\log k_c = \frac{\log k_a}{\alpha} , \tag{5}$$

The n_a and k_a values have been determined upon cooling at 10 °C min^{-1} thanks to the plots of log(-ln(1-θ(t)) vs log t and then gathered in Table 1. Raw data are plotted in Figure 3.

Different shapes of the curves can be distinguished. For neat P(D,L)LA, a straight line is obtained and a deviation from this behaviour is found at a high relative crystallinity of 97 % (Figure 3a). When talc is included in the sample, the shape of the curve changes, showing now three different regimes: before 5 % of relative crystallinity (regime 1), between 5 and 97 % (regime 2) and after 97 % (regime 3). According to Xiao *et al.* (Xiao, 2010b) regime 1 and 2 correspond to the primary crystallization of P(D,L)LA while regime 3 is due to the secondary crystallization of P(D,L)LA. Parameters obtained in regime 2 and 3, corresponding to primary and secondary crystallization are given in Table 1.

Comparing the n_{a1} value of the neat sample with different authors, a consistent dimension was obtained. Xiao *et al.* (Xiao, 2010b) give 2.6, Li *et al.* (Li, 2010a) give 2.1, Wu *et al.* (Wu,

2007) show also 2.1 for a P(D,L)LA with 3.3 % of D-lactic acid, while Liu *et al.* (Liu, 2010) show 1.3 for a PLLA. This small value indicates that the primary crystallization may correspond to a two-dimensional, circular, and diffusion limited growth. Secondary crystallization had larger dimension, which is consistent with the results of Xiao *et al.* (Xiao, 2010b) The comparison of the k_{c1} values with the different authors gives a less coherent picture. Xiao *et al.* (Xiao, 2010b) announced 0.84, Li *et al.*(Li, 2010a) 0.317, Wu *et al.* (Wu, 2007) 0.685 and Liu *et al.* (Liu, 2010) 0.75 for the PLLA sample, which should display the fastest crystallization rate constant. Our hypothesis is that the exploiting of this value might be subject to experimental uncertainty, because of the very small peaks (here 0.4 J.g^{-1}) treated and an experimental difficulty to determine the baseline and therefore to define the induction time.

The evolution of the Avrami parameters with the increase in talc content shows that an increase in n_a and no modification in k_c (Table 1). The nucleating agent addition modifies the nature of the nucleation and the growth process parameters of the P(D,L)LA crystals to a higher dimension, which is still consistent with literature results (Li, 2010; Xiao, 2010b). Comparing the values of the neat sample and the P(D,L)LA/talc samples, a decrease k_{c1} is observed. A similar result was previously obtained by (Li, 2010; Xiao, 2010b), but not commented. The n_{a2} values of the P(D,L)LA/talc samples are smaller than the n_{a1} values for the higher talc concentrations. This is due to a restriction of the growth to lower dimension caused by restriction in space and lower temperature in the latter crystallization stage.

Figures 3b and 3c show the plots of log(-ln(1-X(t)) vs log t of the plasticized P(D,L)LA samples. Plasticizing results in the occurrence of 3 regimes during crystallization, although the change in the slope of the plot is stronger in the case of P(D,L)LA/PEG systems. The calculated Avrami parameters are shown in Table 1. Starting from 9 wt% of PEG, n_{a1} reached a value of 3.5 which does not vary with the plasticizer content. The n_a value suggests that plasticized P(D,L)LA with PEG crystallizes in higher dimension and is most probably less subject to diffusion limitation. Li *et al.* show in the case of PEG 6000 a still higher n_a of 4, which might point to even more efficiency of a PEG with higher molecular weight (Li, 2010). Table 1 shows furthermore that the n_{a2} value decreases slightly compared to n_{a1}, which might be interpreted as growth limitation in the latter crystallization stage.

In contrary, the n_{a1} of P(D,L)LA/ATBC is smaller with than the one of P(D,L)LA/PEG, whereas an increase is noticed for n_{a2}. Due to the low efficiency of ATBC as a plasticizer, the

growth mechanism might not be very different from the neat sample, also recalling that only very low final crystallinity degrees are reached in this case.
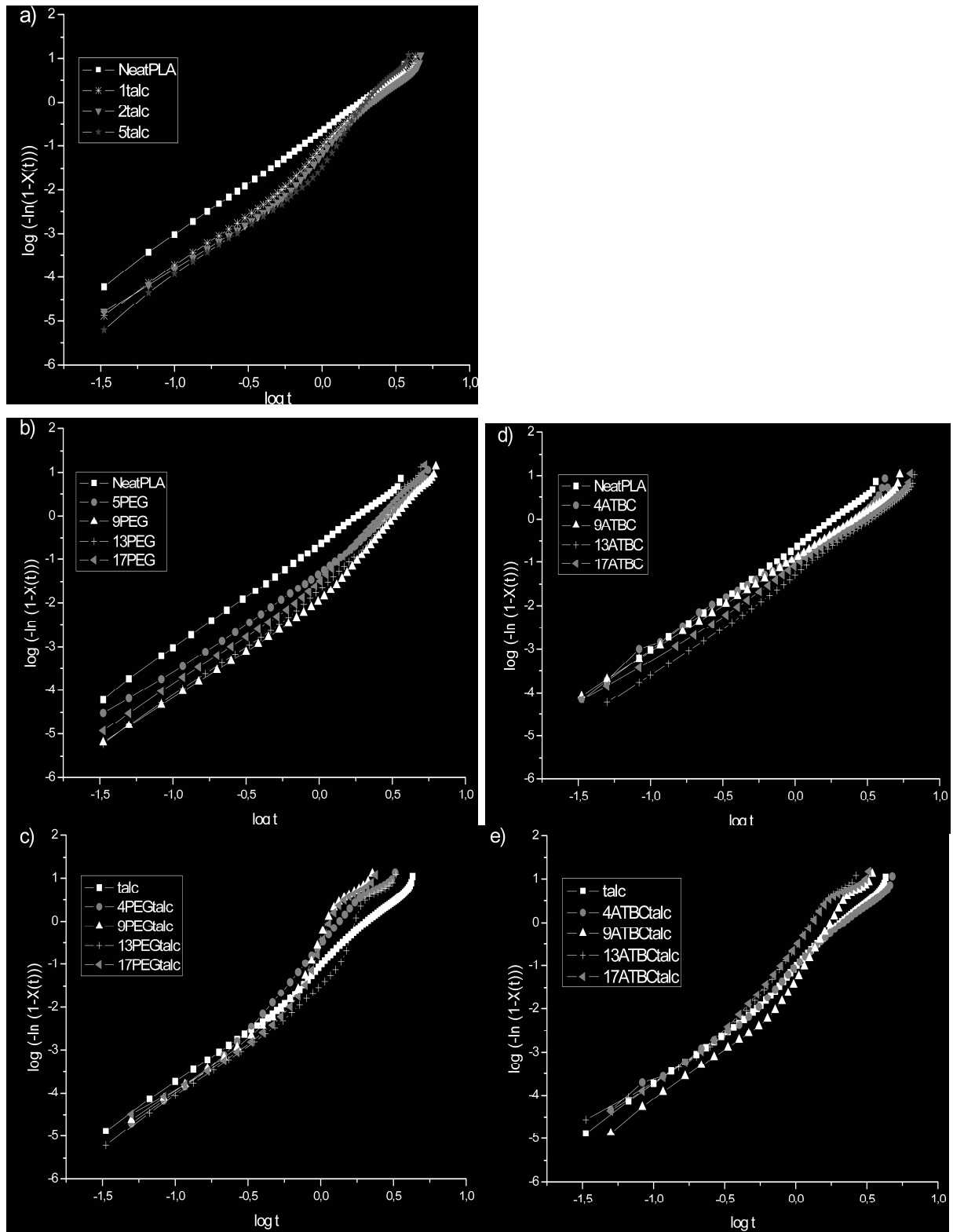
Figure 3. Plots of log (-ln(1-X(T))) versus log t for non isothermal crystallization at 10 °C.min^{-1} of (a) P(D,L)LA / talc, (b) P(D,L)LA / PEG, (c) P(D,L)LA / talc / PEG, (d) P(D,L)LA / ATBC and (e) P(D,L)LA / talc / ATBC.

So a disc-like growth seems to occur in regime 2. Xiao *et al.* (Xiao, 2010b) have notice a similar behaviour for the P(D,L)LA/triphenyl phosphate system.

The low dimension growth is followed by a spherulitic growth in regime 3 (Table 1). It can be due to the low crystallinity degree of the sample which makes it possible the growth in higher dimension in the last regime.

Observing the k_{c1} values of both formulations in Table 1, one sees that the rate constant rises in the case of increasing PEG plasticizing increasing n_{a1} values while it falls slightly with increasing n_{a1} in the ATBC case, which still points to the fact that ATBC seems to be less efficient than PEG in plasticizing P(D,L)LA. As mentioned previously, this difference of crystallization rate depending on the plasticizer may be due to the lower P(D,L)LA molecular weight of with PEG (Table 2).

The simultaneous presence of talc and PEG in P(D,L)LA leads in regime 2 to a large increase in the average n_a value up to 8 (Figures 3d and 3e, Table 1). Such n_a values were retrieved by Liu *et al.* (Liu, 1998) and Balamurugan and Maiti (Balamurugan, 2008) with polyamide 6. It suggests that the nucleation and growth geometry is complex, such as sheaf-like growth. As explained by Balamurugan and Maiti (Balamurugan, 2008), $n_a > 4$ may be due to an increasing rate of nucleation, implying simultaneous appearance of different growth mechanism, which is no longer constant throughout the crystallization process. This complex crystal growth leads to a disc-like growth in regime 3 with high crystallization rate, around 1370.10^{-3} min^{-n}. The constants retrieved for the PEG/talc system are based on significant experimental uncertainty. We suppose that this deviation is caused by the exudation of PEG from the P(D,L)LA/PEG films. This phenomenon has been previously described by Courgneau *et al.* for the same type of samples (Courgneau, 2011). The ATBC/talc system seems to be more stable, although primary crystallization is slower compared to the P(D,L)LA/PEG/talc sample. Compared to the results of Xiao *et al.* (Xiao, 2010b), it appears that the addition of ATBC and talc results in a faster crystallization kinetics of P(D,L)LA than with triphenyl phosphate and talc. Moreover, as shown by Xiao *et al.* (Xiao, 2010b) the simultaneous presence of nucleating agent and plasticizer induces a significant increase in n_a values in regime 2 while decreasing in regime 3. The n_{a2} value down to 2.4 suggests that the crystal growth of P(D,L)LA is restricted due to the crystal impingement and crowd and so they evolve in lower dimension.

Consequently whatever the plasticizer, the addition of talc and plasticizer to P(D,L)LA results in a complex crystallization, but accelerated growth kinetics.

3.2.4.3. Non-isothermal crystallization kinetics of P(D,L)LA/ATBC/talc at various cooling rates

Considering the plasticizer exudation at high content of PEG in P(D,L)LA and a large decrease in molecular weight of P(D,L)LA, the system of ATBC/talc seemed to be a better compromise for enhancing P(D,L)LA crystallization kinetics. To investigate the crystallization mechanism the non-isothermal crystallization of P(D,L)LA/ATBC/talc was studied at different cooling rates through different models.

Figure 4 shows the DSC thermograms of non-isothermal crystallization of neat and formulated P(D,L)LA at various cooling rate.
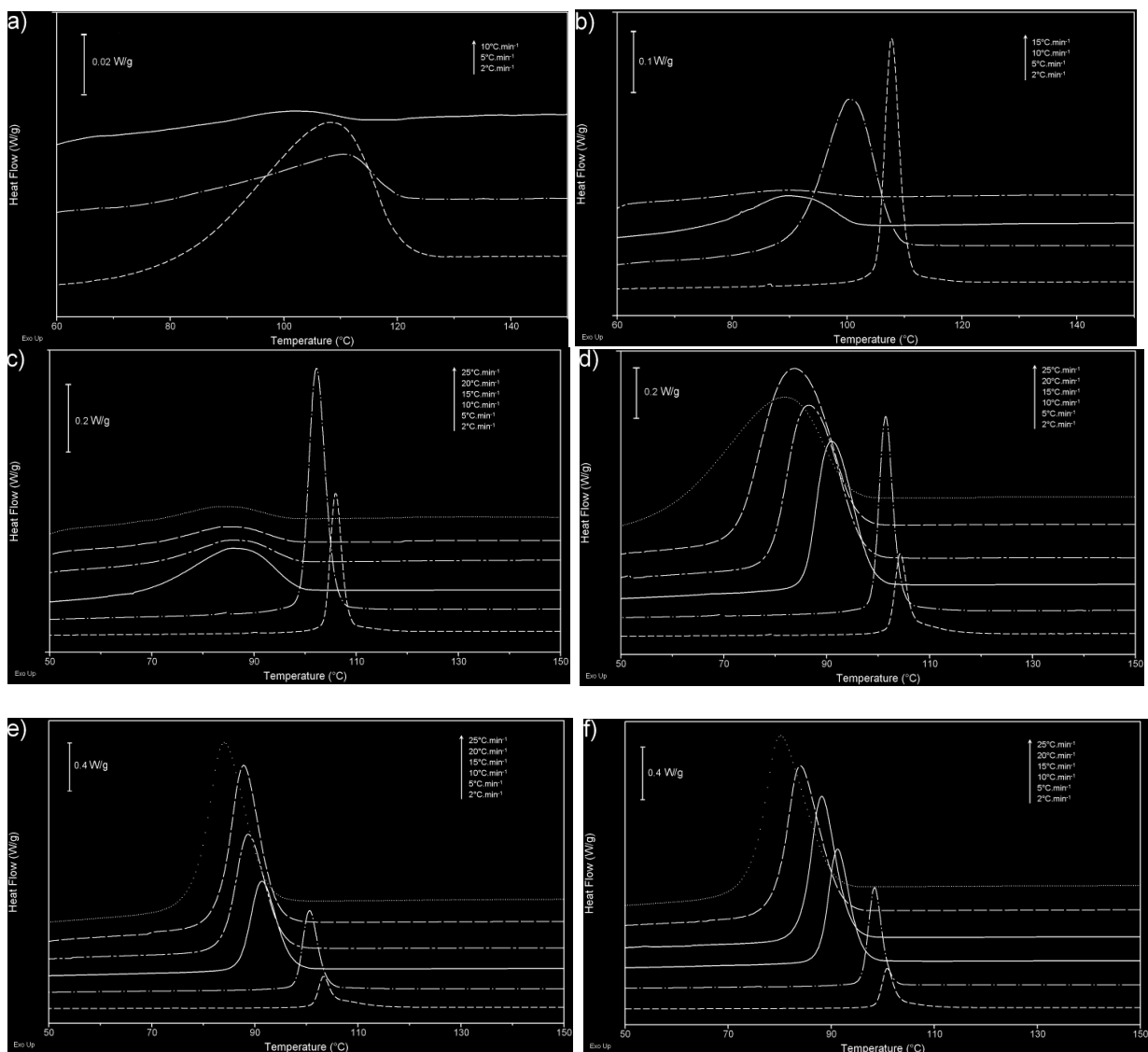
Figure 4. DSC thermograms for non isothermal crystallization at various cooling rate of (a) neat P(D,L)LA, (b) P(D,L)LA / talc, (c) P(D,L)LA / talc / 4 wt% ATBC, (d) P(D,L)LA / talc / 9 wt% ATBC, (e) P(D,L)LA / talc / 13 wt% ATBC and (f) P(D,L)LA / talc / 17 wt% ATBC.

Neat P(D,L)LA presents a small and broad peak at 10 °C.min^{-1} which shifts to higher temperature with the decrease in cooling rate. Similar shifts of the crystallization peak are observed in the case of the addition of talc and ATBC (Liu, 2010). An increase in the crystallization enthalpy is also noticed with the decrease in cooling rate for all the formulation of P(D,L)LA with talc and ATBC (Table 3). Moreover, a shoulder is shown at the right of the crystallization peak for P(D,L)LA formulated with talc and ATBC at the lower cooling rate (2 and 5 °C.min^{-1}).

3.2.4.4. Avrami analysis

Figure 5 presents the plots of log(-ln(1-θ(t))) versus log t from which n_a and k_a parameters are obtained. The corresponding values are given in Table 3. The average of n_{a1} of the neat sample is 2.9 and the average of n_{a2} is 3.5. Formulation of the neat P(D,L)LA increased the n_{a1} and diminished the n_{a2}. Among formulated P(D,L)LA/ATBC/talc samples the n_{a2} remained approximately constant, with an overall average value of ca. 2. As expected, both rate constants accelerated with increasing cooling ramp.

At the primary stage which corresponds to the fast crystal growth of P(D,L)LA, n_{a1} falls between 2.4 and 3.0 for neat P(D,L)LA and between 3.0 and 11 for all the formulated P(D,L)LA. The values of n, for the formulated P(D,L)LA, depend on the ATBC content and on the cooling rate. Thus n increases slightly with increasing the ATBC content in the blends and decreases with increasing the cooling rate.

So, for formulated P(D,L)LA at low cooling rate ($\alpha \leq 5$), n_{a1} is above 8.6 which is related to any physical crystallization mechanism. These high values might be due to the shoulder at high temperatures observed in the thermograms (Figure 4). At higher cooling rate, for P(D,L)LA/talc and P(D,L)LA/talc/4ATBC, n_{a1} value is around 3, which implies a spherulitic growth mechanism. However the higher plasticized P(D,L)LA show n_{a1} value above 3.6, which is, according to Avrami and Christian (Balamurugan, 2008), due to a sheaf-like growth or, more likely in our case of non isothermal crystallization, to an increasing nucleation rate throughout the crystallization process.

The crystallization rate constant shows an obvious dependency on the formulation and the cooling rate. For neat P(D,L)LA, k_a increases from 3.10^{-4} min^{-n} at 2 °C.min^{-1} to 0.11 min^{-n} at 10 °C.min^{-1}. The incorporation of talc, as ATBC, decreases the values of k and consequently of k_c. So the addition of talc and ATBC seems to hinder the crystallization of the polymer. At the secondary stage (from 0.95 relative crystallinity), which is attributed to the spherulites impingement or crystal perfection, the n_a values fall in the range 1.7-3.5. The n_a values of neat

P(D,L)LA are around 3-3.5 which could be interpreted as a spherulitic growth mechanism. The formulation of P(D,L)LA leads to a decrease in the range of n_{a2} values at 1.7-3.2.
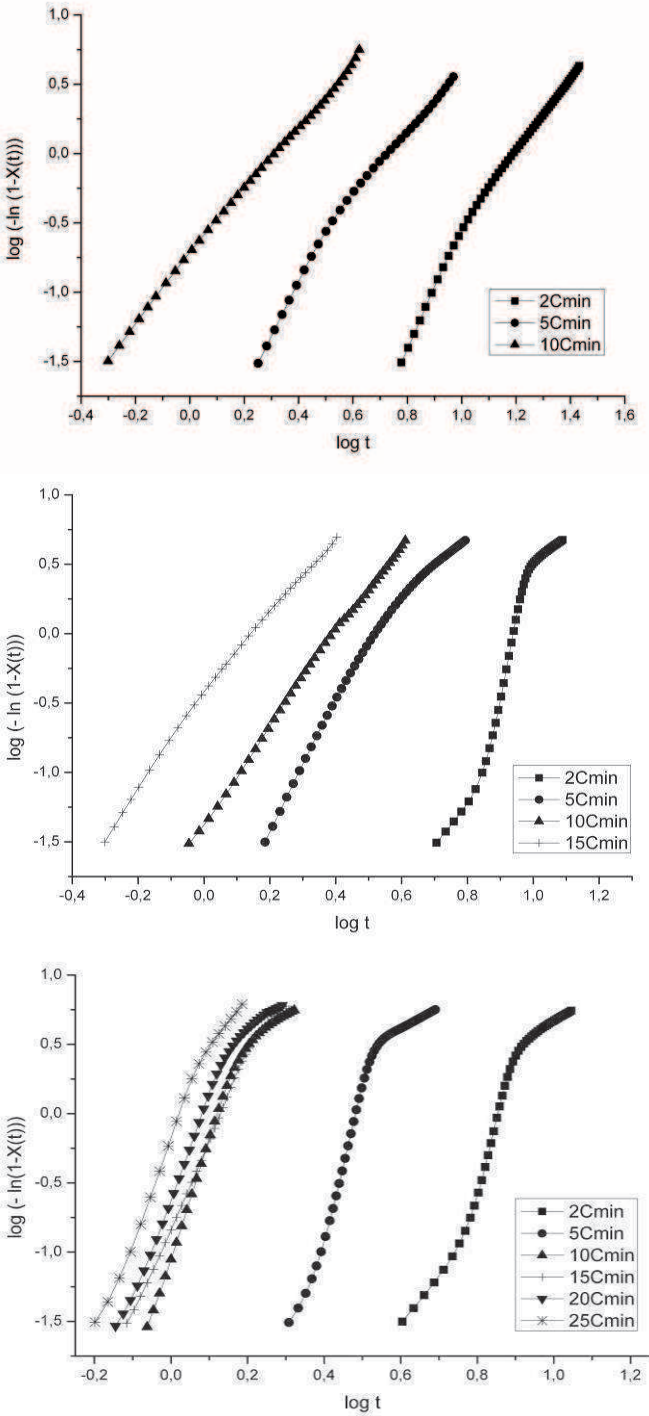
Figure 5. Plots of log (-ln(1-X(T))) versus log t for non isothermal crystallization of (a) neat P(D,L)LA, (b) P(D,L)LA / talc and (c) P(D,L)LA / talc / 17 wt% ATBC.

Table 3. Avrami parameters during non-isothermal crystallization of neat and formulated P(D,L)LA.

Samples	Cooling rate (°C.min⁻¹)	ΔHc (J.g⁻¹)	Primary crystallization ($5 < X(t) < 97\%$)			Secondary crystallization ($97 < X(t) < 99.9\%$)		
			n_{a1}	$k_{a1} \times 10^3$ (min⁻ⁿ)	$k_{c1} \times 10^3$ (min⁻ⁿ)	n_{a2}	$k_{a2} \times 10^3$ (min⁻ⁿ)	$k_{c2} \times 10^3$ (min⁻ⁿ)
Neat P(D,L)LA	2	33.4 ± 2.8	2.9 ± 0.2	0.4 ± 0.3	19.9 ± 6.6	3.0 ± 1.0	4.8 ± 3.1 × 10⁻²	6.7 ± 2.3
	5	3.3 ± 2.7	3.0 ± 0.2	8.6 ± 2.7	383.8 ± 26.4	3.4 ± 1.3	6.6 ± 5.5	324.6 ± 123.4
	10	0.4 ± 0.3	2.7 ± 0.2	115.1 ± 5.4	805.5 ± 3.8	4.0 ± 1.2	22.6 ± 7.8	683.6 ± 24.0
P(D,L)LA / talc	2	42.1 ± 0.7	9.2 ± 1.6	3.4 ± 2.7 × 10⁻⁷	1.8 ± 0.7 × 10⁻²	2.0 ± 0.5	45.6 ± 35.0	242.4 ± 66.6
	5	36.3 ± 2.8	5.8 ± 1.3	2.3 ± 2.6	270.8 ± 79.9	2.0 ± 0.3	204.8 ± 165.3	704.9 ± 109.7
	10	4.9 ± 2.5	3.2 ± 0.1	65.1 ± 10.9	760.3 ± 12.3	3.5 ± 0.4	39.9 ± 20.7	718.4 ± 38.9
	15	3.0 ± 1.6	3.1 ± 0.3	323.5 ± 65.1	926.7 ± 13.3	3.0 ± 0.4	320.4 ± 95.0	925.1 ± 19.7
P(D,L)LA / talc / 4 wt% ATBC	2	37.5 ± 1.9	11.6 ± 0.2	2.1 ± 1.6 × 10⁻⁸	4.3 ± 2.0 × 10⁻³	2.1 ± 0.2	32.3 ± 15.8	175.2 ± 48.5
	5	36.0 ± 0.9	8.6 ± 0.9	0.2 ± 0.1	178.8 ± 24.1	1.7 ± 0.2	371.2 ± 135.5	837.5 ± 58.8
	10	11.7 ± 3.7	3.6 ± 0.2	35.2 ± 11.8	713.4 ± 22.3	2.4 ± 0.1	118.7 ± 7.5	807.9 ± 5.2
	15	7.4 ± 4.4	3.1 ± 0.3	261.0 ± 79.6	912.3 ± 20.8	2.8 ± 0.2	290.3 ± 73.4	919.5 ± 16.8
	20	4.4 ± 2.9	3.1 ± 0.1	678.1 ± 67.7	980.6 ± 4.8	3.1 ± 0.2	532.1 ± 46.5	968.8 ± 4.2
	25	3.1 ± 1.5	3.2 ± 0.3	1177.3 ± 213.0	1006.1 ± 7.6	3.4 ± 0.4	948.2 ± 154.4	997.6 ± 6.3
P(D,L)LA / talc / 9 wt% ATBC	2	37.3 ± 0.6	10.0 ± 0.4	1.9 ± 2.5 × 10⁻⁷	1.2 ± 0.9 × 10⁻²	2.1 ± 0.3	25.5 ± 15.7	154.5 ± 48.9
	5	35.0 ± 0.5	9.2 ± 1.6	7.2 ± 1.3 × 10⁻³	93.5 ± 3.5	1.8 ± 0.2	307.6 ± 18.4	792.8 ± 10.9
	10	29.4 ± 0.3	7.7 ± 0.8	13.7 ± 7.1	646.9 ± 35.4	2.1 ± 0.2	840.1 ± 145.6	979.1 ± 24.1
	15	29.3 ± 0.6	5.2 ± 0.5	101.2 ± 59.9	852.8 ± 31.1	2.0 ± 0.4	1138.9 ± 626.5	1002.9 ± 34.3
	20	30.6 ± 0.3	5.5 ± 0.5	146.3 ± 124.5	897.8 ± 38.6	3.0 ± 2.2	852.5 ± 703.5	980.0 ± 44.6
	25	25.8 ± 2.1	3.6 ± 0.6	445.0 ± 322.6	962.2 ± 25.8	2.7 ± 0.1	561.7 ± 168.2	976.2± 11.0
P(D,L)LA / talc / 13 wt% ATBC	2	34.3 ± 0.3	9.6 ± 0.7	4.3 ± 4.3 × 10⁻⁷	1.9 ± 1.0 × 10⁻²	1.8 ± 0.1	44.2 ± 0.9	210.3 ± 2.1
	5	32.4 ± 1.3	10.7 ± 0.8	1.9 ± 2.6 × 10⁻³	64.1 ± 19.9	1.9 ± 0.3	222.0 ± 75.8	735.4 ± 50.5
	10	27.8 ± 1.5	6.9 ± 0.9	47.3 ± 10.1	736.3 ± 15.9	2.3 ± 0.3	574.8 ± 264.6	966.0 ± 20.6
	15	28.3 ± 2.0	6.3 ± 1.1	66.3 ± 31.2	831.5 ± 27.1	2.7 ± 0.4	820.9 ± 178.8	979.3 ± 13.5
	20	29.3 ± 2.3	6.3 ± 1.4	146.6 ± 4.0	908.5 ± 1.2	2.2 ± 0.6	1518.1 ± 643.6	1009.6 ± 31.5
	25	28.7 ± 3.1	5.4 ± 1.2	888.8 ± 645.2	983.1 ± 44.3	2.0 ± 0.5	1963.0 ± 1351.7	1016.2 ± 42.7
P(D,L)LA / talc / 17 wt% ATBC	2	34.7 ± 0.9	11.1 ± 1.6	4.7 ± 6.6 × 10⁻⁶	4.9 ± 7.0 × 10⁻²	1.8 ± 0.1	46.7 ± 13.1	231.4 ± 16.2
	5	32.7 ± 2.1	10.1 ± 1.1	4.1 ± 1.5 × 10⁻²	132.1 ± 10.0	2.0 ± 0.6	280.4 ± 118.2	760.8 ± 98.0
	10	25.1 ± 1.7	8.1 ± 0.2	77.3 ± 13.0	773.8 ± 12.6	1.8 ± 0.4	1456.0 ± 317.7	1036.7 ± 23.7
	15	25.2 ± 3.8	6.3 ± 0.3	208.5 ± 116.4	895.4 ± 31.6	3.2 ± 0.9	868.2 ± 418.7	984.1 ± 39.6
	20	28.2 ± 0.5	6.9 ± 1.4	685.7 ± 595.6	970.4 ± 49.1	1.8 ± 0.6	1995.0 ± 379.9	1030.0 ± 9.1
	25	29.1 ± 0.6	6.8 ± 0.4	618.2 ± 122.0	980.4 ± 8.2	3.6 ± 2.2	1410.1 ± 653.3	1011.0 ± 19.0

The crystallization rate constant is lower than in the primary stage for neat P(D,L)LA. However the formulated P(D,L)LA showed higher k_{c2} values in the secondary stage. So contrary to formulated P(D,L)LA, the crystallization rate of neat P(D,L)LA during secondary stage is lower than in the primary stage.

Considering the correlation coefficient, it appears that Avrami model with two stages describe well the crystallization kinetics of neat and formulated P(D,L)LA.

3.2.4.5. Liu and Mo analysis

Liu *et al.* (Liu, 1998; Liu, 1997) developed a model which combines the Avrami and Ozawa model, which was developed by Ozawa (Ozawa, 1971) from the Avrami equation. Ozawa (Ozawa, 1971) considered that the non-isothermal crystallization at constant cooling rate is the combination of many infinitesimal isothermal crystallization.:

$$X(T) = 1 - \exp\left[-\frac{k_O}{\alpha^{n_O}}\right], \tag{6}$$

Where k_O and n_O are the Ozawa crystallization rate constant and exponent, respectively and α the constant cooling rate. As for Avrami, the Ozawa exponent is dependent on the crystal growth and nucleation mechanism. In its double logarithmic form Equation 6 reads:

$$\log(-\ln(1 - X(T))) = \log k_O - m_O \log \alpha. \tag{7}$$

As explained by Long *et al.* (Long, 1995), the Ozawa approach predicts satisfactorily the crystallization for few polymers, such as poly(ethylene terephthalate), polypropylene, or high density polyethylene, but it is not fully adapted to P(D,L)LA (Liu, 2010). The poor linearity obtained in case of a large range of cooling rate which makes this model difficult to use. The deviation from linear Ozawa model, obtained for neat and formulated P(D,L)LA (Li, 2010a; Xiao, 2010b), may be explained by the secondary crystallization which is neglected by Ozawa model.

The Liu and Mo model (Liu, 1998; Liu, 1997) is described by the combination of the double logarithmic form of the Avrami and Ozawa models:

$$\log k_a + n_a \log t = \log k_O - n_O \log \alpha, \tag{8}$$

From this equation, Liu *et al.* wrote the following equation:

$$\log \alpha = \log F(T) - m \log t, \tag{9}$$

where $F(T) = \left(\dfrac{k_O}{k_a}\right)^{1/n_O}$ and m is the ratio of the Ozawa exponent and the Avrami exponent

($m = \dfrac{n_O}{n_a}$). Moreover $F(T)$ is related to the value of cooling rate chosen at a unit crystallization time at which the system has reached a certain value of relative crystallinity.

Figure 6 shows the plots, log α versus log t, for neat P(D,L)LA, P(D,L)LA/talc and P(D,L)LA / talc / 17 wt% ATBC at various relative crystallinities (0.2, 0.4, 0.5, 0.6, 0.8 and 0.9). A good linear relationship between log α and log t is noticed for neat P(D,L)LA. The values of F(T), m, calculated from the intercept and the slope of the plots, respectively, and the correlation coefficient (r^2) are gathered in Table 4.

The slopes of the curves increase slightly with the relative crystallinity. This value close to 1 suggests that the predictions of Avrami and Ozawa about nucleation and growth mechanism are not really different.

Table 4. Liu parameters for neat P(D,L)LA and P(D,L)LA with 1 wt% of talc at various relative crystallinities.

Sample	X (t) (%)	m	F(T)	r^2
Neat P(D,L)LA	20	0.85	12.8	0.999
	40	0.88	17.1	0.997
	60	0.90	21.7	0.998
	80	0.96	30.8	0.997
P(D,L)LA / talc	20	0.99	13.7	0.983
	40	1.07	17.6	0.979
	60	1.16	22.2	0.975
	80	1.25	29.1	0.967
P(D,L)LA / talc / 4 wt% ATBC	20	0.86	14.9	0.988
	40	0.89	18.5	0.989
	60	0.90	22.0	0.992
	80	0.91	26.5	0.994
P(D,L)LA / talc / 9 wt% ATBC	20	1.93	16.4	0.868
	40	2.51	24.6	0.910
	60	3.02	37.5	0.763
	80	3.61	48.9	0.979
P(D,L)LA / talc / 13 wt% ATBC	20	1.45	19.4	0.989
	40	1.54	24.0	0.987
	60	1.61	28.4	0.977
	80	1.70	34.5	0.962
P(D,L)LA / talc / 17 wt% ATBC	20	3.29	16.9	0.935
	40	3.52	24.9	0.925
	60	3.63	33.1	0.920
	80	3.64	43.4	0.900

The addition of talc induces a slight deviation from the Liu's model with a slight increase in the slopes compared with those for neat P(D,L)LA. As shown in Table 4, F(T) and m values seem similar for neat P(D,L)LA and P(D,L)LA with 1 wt% of talc, suggesting that the crystallization mechanism are similar for both samples. Moreover the value of the kinetic parameter, F(T), increases with the relative crystallinity for neat P(D,L)LA and P(D,L)LA with talc. Therefore at a unit crystallization time, the higher the relative crystallinity is, the higher is the needed cooling rate.

In addition to talc, the presence of ATBC leads to a larger deviation which increases with the ATBC content, highlighted by the drop of the correlation coefficient (Figure 6). The slow cooling rate at 2 °C.min^{-1} was not taken into account for the determination of F(T) and m values due to the shoulder observed on the thermograms in the case of P(D,L)LA/ATBC/talc. As neat P(D,L)LA and P(D,L)LA with talc, m and F(T) increase with the relative crystallinity. Moreover their values are higher than those of neat P(D,L)LA.
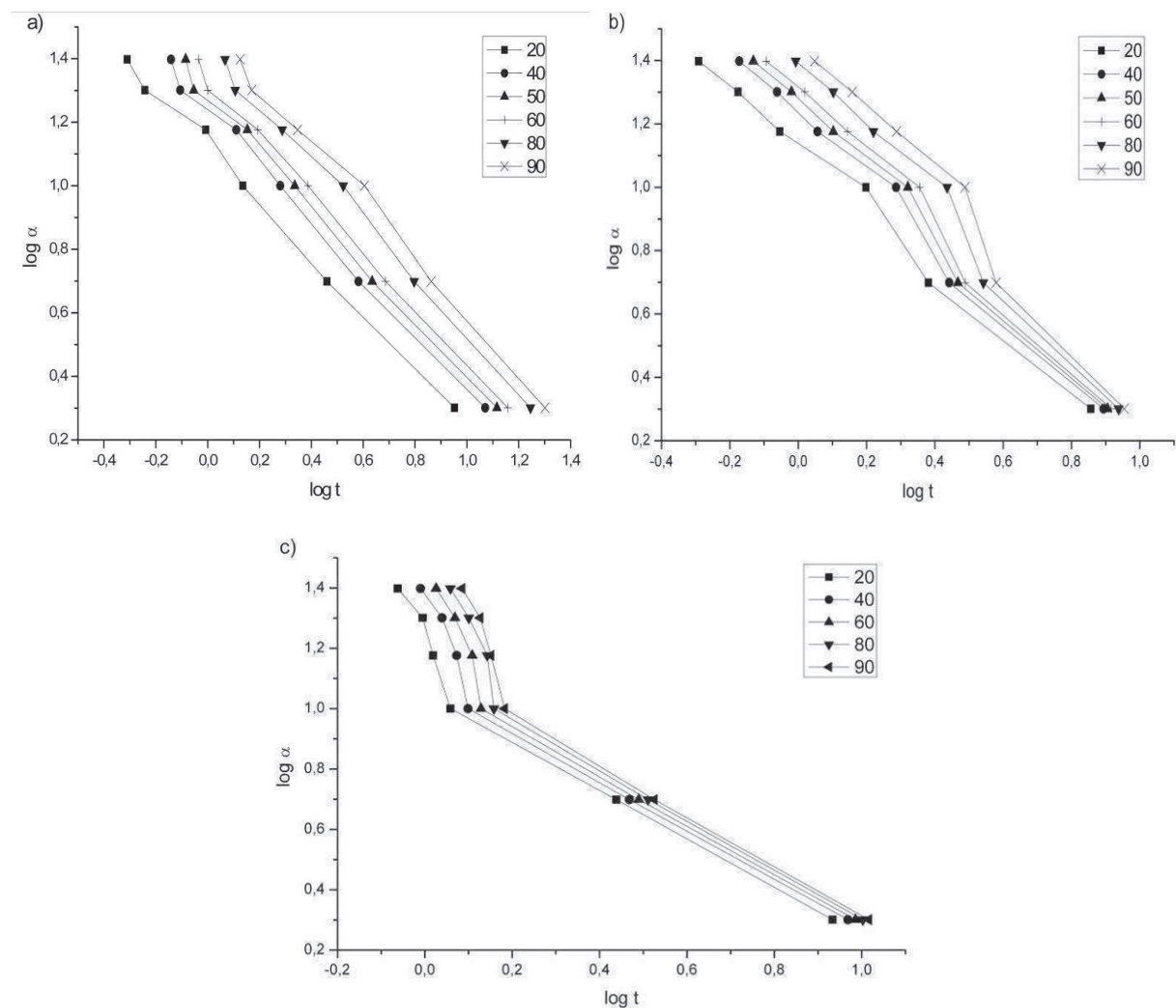
Figure 6. Plots of log α versus log t for non isothermal crystallization of (a) neat P(D,L)LA, (b) P(D,L)LA / talc and (c) P(D,L)LA / talc / 17 wt% ATBC (Liu – Mo model).

Nevertheless the meaning of these results is questionable due to the low correlation coefficient. Therefore it seems that the blend of P(D,L)LA with talc and ATBC only confirm that the prediction of Avrami and Ozawa model are different. As mentioned by Xiao *et al.* the higher value of F(T) obtained with the addition of talc and ATBC mean that the crystallization rate is slower for the formulated P(D,L)LA than for the neat one. Hence ATBC and talc seem to hinder the crystallization of P(D,L)LA.

3.2.4.6. Activation energy for non-isothermal crystallization

The values of the activation energy, being the energy barrier to crystallization can be calculated using Kissinger's method (Kissinger, 1956). The Kissinger method considers the variation of the peak temperature of the crystallization exotherm and the cooling rate according the Equation 10 where R is the universal gas constant (8.314 $J.mol^{-1}.K^{-1}$).

$$\frac{d\left(\ln\left(\alpha/T_p^{\,2}\right)\right)}{d\left(1/T_p\right)} = -\frac{E_a}{R}, \tag{10}$$

The activation energy, E_a, can be estimated from the slope of the plots ln (α/Tp^2) versus $1/Tp$. The E_a of these samples are negative for crystallization during cooling, which means that the reaction is deactivated by the temperature. As shown in Table 5, neat P(D,L)LA and P(D,L)LA with 1 wt% of talc have similar activation energy, while E_a decreases significantly for P(D,L)LA/talc/17wt% ATBC.

Table 5. Activation energy values for neat and formulated PDLLA calculated with Kissinger's method.

Sample	Activation Energy (kJ.mol⁻¹)	r^2
Neat PDLLA	-101.2	0.990
PDLLA / talc	-101.6	0.953
PDLLA / talc / 4 wt% ATBC	-118.9	0.992
PDLLA / talc / 9 wt% ATBC	-124.2	0.992
PDLLA / talc / 13 wt% ATBC	-129.9	0.986
PDLLA / talc / 17 wt% ATBC	-146.7	0.955

This study showed that the addition of talc does not affect the non-isothermal crystallization of P(D,L)LA whereas the addition of ATBC furthers the mobility of polymer in the crystallization site, and yields a reduction in activation energy but an increase in thermo sensitivity of the mechanism. Wu *et al.* published 75.32 $kJ.mol^{-1}$ for P(D,L)LA (3.3%D) (Liu, 2010; Wu, 2007) and Liu *et al.* 126 $kJ.mol^{-1}$. Both authors dropped the negative sign of the

cooling rate, which yields then positive activation energy. Nevertheless the dropping of the negative sign of the cooling rate is still debating (Vyazovkin, 2002).

Exploitation of the energy barrier, by the differential isoconversional method of Friedman (Friedman, 1969), was carried out by Xiao *et al.* (Xiao, 2010b) and Li *et al.* (Li, 2010a). Both authors showed negative activation energies. They reported that the addition of talc in P(D,L)LA yields higher activation energies. However, triphenyl phosphate (Xiao, 2010b) increased the energy barrier, while PEG (Li, 2010) decreased the energy barrier at contents higher than 5%, which shows in consistency with the other findings the higher efficiency of the PEG plasticizer

3.2.5. Conclusions

Non-isothermal crystallization kinetics studies of neat and formulated P(D,L)LA with nucleating agent and plasticizers have been studied using DSC. The temperature at which the crystallization process is completed decreases with the addition of plasticizer and even more with the nucleating agent. So the simultaneous presence of the both additives seems to further the crystallization of P(D,L)LA.

Avrami modified Jeziorny model has been used to study the non-isothermal crystallization of neat P(D,L)LA and P(D,L)LA formulated with talc and ATBC or PEG. Avrami analysis reveals that the non-isothermal crystallization can be divided into two distinct stages: primary and secondary crystallization. The values of n suggest that the nucleation and the crystal growth of both stages are very different. Moreover morphology studies by microscopy would be required to understand the complex crystallization mechanism occurring for formulated P(D,L)LA in the primary stage. The Avrami crystallization rate constants were found to increase with the cooling rate which means that the crystallization proceeds faster as cooling rate increased.

The Liu-Mo model describes the non-isothermal crystallization process of neat and formulated P(D,L)LA with talc and ATBC, although with poor correlation. However it provided a satisfactory description of the neat P(D,L)LA and P(D,L)LA/talc crystallization. The value of F(T) increased with increasing the relative crystallinity which indicates a higher cooling rate should be used to obtain a higher degree of crystallinity. The evolution of the activation energy with formulation, calculated thanks to the Kissinger method, suggests that the incorporation of ATBC and talc promotes crystallization of P(D,L)LA.

3.2.6. Discussion et commentaires

La cinétique de cristallisation non-isotherme du P(D,L)LA CD92 (environ 8% de D-lactide) pur et formulé a été étudié par calorimétrie différentielle à balayage (DSC) afin d'évaluer l'impact de l'ajout de plastifiants et de l'agent nucléant ainsi que leur effet synergique sur la cristallisation du P(D,L)LA.

Il a été montré qu'à 10 °C.min^{-1}, le P(D,L)LA pur ne présente qu'une très faible enthalpie de cristallisation avec une croissance cristalline sous forme de sphérolites. Il est nécessaire de diminuer fortement la vitesse de refroidissement à 2 °C.min^{-1} pour permettre une cristallisation importante du P(D,L)LA (33,4 J.g^{-1}). Néanmoins, cette diminution de la vitesse ne semble pas influer sur la forme des cristallites formés. De plus, un mécanisme de cristallisation en 2 régimes a été mis en évidence dont la limite est établie à 5 % de cristallinité relative.

L'ajout d'agent nucléant ou de plastifiant a induit la modification du mécanisme de cristallisation avec l'apparition d'un troisième régime. Ainsi la cristallisation est séparée en une cristallisation primaire constituée de deux régimes (régime 1 et 2), et une cristallisation secondaire constituée du régime 3:
- régime 1 avant 5% de cristallinité relative
- régime 2 entre 5 et 97% de cristallinité relative
- régime 3 après 97% de cristallinité relative

Le talc, l'agent nucléant, ne semble promouvoir la cristallisation du polymère qu'à partir de 5 % en poids, teneur à laquelle l'enthalpie de cristallisation est supérieure à 10 J.g^{-1}. Néanmoins cet ajout conduit à la formation de cristallites en une dimension supérieure (de la 2D à la 3D par exemple) sans modifier la vitesse de cristallisation.

Il a, par la suite, été montré que le PEG affecte nettement plus la cristallisation du P(D,L)LA que ne le fait l'ATBC. En effet, un changement du dimensionnement des cristallites est noté avec l'ajout de PEG aussi bien dans le régime 2 que 3.

Par contre l'ajout simultané du plastifiant et du talc induit une large diminution de la largeur du pic de cristallisation en augmentant notablement l'enthalpie de cristallisation. Cette modification s'accompagne d'une forte augmentation de la valeur de l'exposant d'Avrami (n_a) laissant supposer un mécanisme complexe de cristallisation, dû à une augmentation de la

vitesse de nucléation induisant l'apparition simultanée de différent mécanisme de croissance, aussi bien à 2 qu'à 25 °C.min^{-1}.

Les énergies d'activation calculées confirment que la seule addition de talc au P(D,L)LA ne suffit pas pour promouvoir sa cristallisation et qu'il est nécessaire de lui ajouter de l'ATBC pour permettre une cristallisation rapide et importante du P(D,L)LA.

3.3. Conclusions du Chapitre 3

En conclusion, il apparaît, au travers de ces deux publications, que la formulation est une approche efficace pour modifier à la fois les propriétés mécaniques et la cinétique de cristallisation du P(D,L)LA. Il a été montré, au travers des analyses des propriétés thermiques, mécaniques et barrière, que l'ATBC était un plastifiant plus efficace que le PEG, plastifiants mélangés au P(D,L)LA CD92 à l'état fondu.

En effet, des élongations à la rupture de près de 500 % et 137 % ont été obtenues avec l'addition de 17 % en poids d'ATBC et de PEG, respectivement. Cet écart peut s'expliquer par la diminution de la masse molaire du P(D,L)LA en présence de PEG induite par des réactions de transestérification et d'hydrolyse des chaînes polymères.

Néanmoins l'ajout seul d'ATBC, quelle que soit sa teneur, n'a pas permis de promouvoir la cristallisation lente du P(D,L)LA CD92, contrairement au PEG. Un agent nucléant, le talc, a donc été ajouté au plastifiant afin d'accélérer la cristallisation du P(D,L)LA. L'effet synergique de ces deux additifs a été alors mis en lumière par la diminution de l'énergie d'activation et par la cristallisation des échantillons même lors d'un refroidissement à 25 °C.min^{-1}. Une augmentation notable de l'enthalpie et de la vitesse de cristallisation a été remarquée dans le cas de l'ATBC tandis que l'effet du talc sur le P(D,L)LA plastifié avec le PEG s'est restreint à une faible augmentation de la vitesse de cristallisation.

L'étude de la plastification sur les propriétés barrière a montré, comme on pouvait s'y attendre une augmentation de la perméabilité à l'oxygène aussi bien avec l'ATBC qu'avec le PEG. Cependant, dans le cas de la vapeur d'eau, le caractère hydrophile du PEG a induit une perte des propriétés barrière des mélanges P(D,L)LA/PEG. Au contraire l'ATBC, à de fortes teneurs, n'a conduit qu'à un doublement de la valeur de transmission de la vapeur d'eau comparé au P(D,L)LA pur.

La comparaison des propriétés barrière du P(D,L)LA pur et formulé à celles des matériaux conventionnels met en évidence la nécessité de diminuer la perméabilité aux gaz, en particulier l'oxygène pour pouvoir utiliser le PLA en tant qu'emballage (cf. Figure 1.17). Pour cela, l'approche de la cristallisation a été envisagée. Son effet sur les propriétés barrière du P(D,L)LA pur et formulé fait l'objet du chapitre suivant.

Chapitre 4

-

Effet de la cristallisation sur les propriétés barrière du P(D,L)LA

Dans le chapitre précédent, nous avons mis en évidence l'effet de la formulation sur les propriétés du P(D,L)LA CD92 aussi bien ses propriétés thermiques, que mécaniques ou barrière. Il a été montré que l'ATBC est un plastifiant plus efficace pour le P(D,L)LA que le PEG en raison de sa faible exsudation. Comme attendu, une diminution des propriétés barrière aux gaz et à la vapeur d'eau a été mesurée sur le P(D,L)LA amorphe une fois formulé. Celle-ci est moins importante dans le cas de la plastification par l'ATBC que par le PEG.

L'étude cinétique de cristallisation, présentée dans la seconde publication, a montré que la formulation avait pour effet de promouvoir la cristallisation du P(D,L)LA mais ceci en changeant le dimensionnement des cristaux formés.

Par conséquent, nous nous sommes attachés dans ce chapitre à étudier les effets de la cristallisation du P(D,L)LA CD92 pur et formulé sur ses propriétés. Ainsi dans un premier temps pour chacune des publications, les conditions de cristallisation des échantillons ont été mises au point. Dans un deuxième temps, l'effet de la cristallisation sur les propriétés mécaniques et barrière a été évalué. Deux gaz, l'hélium et l'oxygène, et un composé organique volatil, l'acétate d'éthyle, ont été utilisés comme sondes afin de déterminer l'effet de la structure sur les propriétés de transport du P(D,L)LA.

La publication n°4 présentée dans ce chapitre compare des P(D,L)LA Biomer L9000 préalablement extrudés amorphes et cristallisés par thermo-compression et un P(D,L)LA commercial (P(D,L)LA Biophan®) afin d'évaluer l'effet du taux de cristallinité sur la perméabilité à l'oxygène et sur la sorption de l'acétate d'éthyle.

La publication n°5 complète les conclusions de l'article précédent en identifiant les formes cristallines formées selon les conditions de recristallisation du P(D,L)LA CD92. De plus, l'effet de la formulation sur la cristallisation et les propriétés barrière a été mis en évidence par la détermination des coefficients de transport.

L'effet du biétirage est présenté dans un proceeding qui a pour objet la comparaison de deux procédés sur deux grades de P(D,L)LA : P(D,L)LA 2002D et P(D,L)LA 4042D. Les cristallinités induites par le procédé sont comparées et mis en relation avec les mesures de perméabilité à l'hélium et à l'oxygène subséquemment réalisées.

L'influence de trois composés organiques volatils sur la structure du P(D,L)LA CD92 a enfin été évaluée en réalisant des mesures par DSC, DMTA et gravimétrie.

4.1. Barrier properties of poly(lactic acid) and its morphological changes induced by aroma compound sorption (Publication n°4)

Gael Colomines[a], Violette Ducruet[b], Cécile Courgneau[b,c], Alain Guinault[a], Sandra Domenek[c]

[a]Cnam, Laboratoire des Matériaux industriels polymères, 292 rue Saint-Martin, case courrier 322, 75141 Paris cedex 03, France

[b] INRA, UMR 1145 Ingénierie Procédés Aliments, 1 avenue des Olympiades, F-91300 Massy, France

[c] AgroParisTech, UMR 1145 Ingénierie Procédés Aliments, 1 avenue des Olympiades, F-91300 Massy, France

4.1.1. Abstract

The barrier properties of poly(lactic acid) (PLA) play a key role in food packaging applications. For their optimization, the influence of crystallinity on the barrier properties of P(D,L)LA and the interaction of P(D,L)LA with the aroma compound ethyl acetate were investigated. P(D,L)LA film samples with various crystallinities were fabricated by flat die extrusion and thermo-compression and compared to P(D,L)LA Biophan®. The degree of crystallinity had no effect on the oxygen permeability. However, an increase of crystallinity caused a decrease in ethyl acetate sorption. The sorption isotherm of ethyl acetate obtained using microgravimetry showed a steep increase with increasing aroma activity, a form which is consistent with a plasticization effect. This behaviour was verified using differential scanning calorimetry and dynamic mechanical analysis. Sorption caused a marked decrease in the glass transition temperature well below room temperature to approximately 0 °C. Furthermore, P(D,L)LA underwent a solvent-induced crystallization when equilibrated in ethyl acetate atmosphere at an activity of 0.5. The results obtained show the importance of considering possible interactions between polymer and foodstuff during the optimization step of polymeric materials for food packaging applications.

Keywords: poly(lactic acid), barrier properties, thermo-mechanical properties.

4.1.2. Introduction

The past few years, marked by the paradigm of sustainable development, have brought about a renewed interest in biodegradable polymers originating from renewable resources. The most important market for those novel polymers will be the packaging sector, within which food packaging represents approximately 65% by volume. Among bio-source-based polymers emerging on the food market, the semi-crystalline polyester poly(lactic acid) (PLA) is one of the most applied because of its relatively low cost and ease of processing.

Initially used in biomedical applications (Peniston, 2007) such as self-degrading suture materials, PLA has promising properties and it is approved for food contact (Conn, 1995). It is well adapted for the packaging of fresh products with short shelf-life. In order to increase the use of PLA packaging volume it is also important to offer functional packaging for products with longer shelf-life. Important functionalities of packaging are not only to ensure food safety, but also to guarantee the organoleptic quality of the packed product during its shelflife. Therefore, the barrier properties of the packaging polymer against the transfer of small molecules, such as O_2, CO_2 or H_2O, are important. In particular, oxygen is an excellent oxidizing agent of lipids (Sajilata, 2007) which can cause deterioration of product quality. Moreover, barrier properties against larger volatile molecules, such as aroma compounds, need to be assessed since the transfer of these compounds into the polymer could cause a modification of the aroma formulation of the packaged food leading to a deterioration of its quality (Berlinet, 2005; Ducruet, 2007; Dury-Brun, 2007; Saint-Eve, 2008).

Barrier properties of semi-crystalline polymers are affected by the crystallinity of the polymer, since crystalline zones are excluded volumes where molecules cannot sorb or diffuse (Michaels, 1961). Furthermore in the amorphous regions, the diffusion mechanism is different according to whether the polymer is in a rubbery or a glassy state at the temperature of use. For example, highly augmented mass and gaseous transfers can occur during the hot-conditioning of food.

The crystallinity of PLA has been widely studied with respect to the morphology of the crystalline structure (de Oca, 2007; Ling, 2006a; Ling, 2006b) and to the influence of nucleating agents (Pluta, 2007) and plasticizers (Martino, 2006). The gaseous transfer of O_2, CO_2 and H_2O through P(D,L)LA films has already been investigated by several authors (Auras, 2004a; Auras, 2005a; Auras, 2003; Holm, 2006; Oliveira, 2006; Petersen, 2001; Rhim, 2006). The CO_2 permeability coefficient of P(D,L)LA is lower than that of polystyrene

(PS), but higher than that of poly(ethylene terephthalate) (PET) (Auras, 2003). Similar performance of P(D,L)LA was described for O_2 (Auras, 2005a; Holm, 2006). The barrier properties of P(D,L)LA against water vapour, however, are not as good as those of PET and PS, although a decrease in the water permeability coefficient of P(D,L)LA can be achieved by varying the film fabrication conditions. For example, an increase of temperature for biaxial oriented films results in a decrease of the water vapour permeability (Auras, 2005a).

The barrier properties of P(D,L)LA against aroma compounds have been the subject of only a few studies to date (Auras, 2004a; Auras, 2003). Auras and co-workers (Auras, 2004a) showed that P(D,L)LA has an excellent performance against limonene, a hydrophobic aroma compound found in orange juice. However, more hydrophilic molecules, such as ethyl acetate, a booster and enhancer for fruit aroma often present in high quantity, can be sorbed to an approximately two-fold greater extent in the hydrophilic polyester PLA in comparison to PET, polypropylene (PP) and low-density polyethylene (LDPE). Since aroma compounds are mainly hydrophobic molecules, PLA seems to be a promising material with efficient aroma barrier properties comparable to PET.

However, to date, the link between barrier properties and crystallinity has been the subject of only a few studies. No data have been published on the influence of the sorption of volatile organic molecules, such as aroma compounds, in PLA on its morphological and thermo-mechanical properties, particularly the influence on the glass transition. From an application point of view, this knowledge will be helpful in the design of PLA with efficient barrier properties not only in food packaging applications. Therefore, in the study reported here, P(D,L)LA samples with various crystallinities were prepared and studied. An industrial sample of P(D,L)LA film (Biophan®) was used as reference. For sample fabrication, the extrusion–thermocompression technique was preferred to the casting technique often used as a model process, in order to avoid a plasticizing effect due to the residual solvent which can affect the gas barrier properties (Rhim, 2006). Ethyl acetate was used as a model volatile molecule, because it is used in high concentrations in many fruity aroma formulations where it plays an important role in the top note. It is the most hydrophilic molecule in the homologous series of ethyl esters used in aroma formulations. Oxygen barrier properties and ethyl acetate sorption were investigated as functions of the crystallinity of the P(D,L)LA film. The thermo-mechanical consequences of ethyl acetate sorption were characterized using DSC and dynamic mechanical analysis (DMA).

4.1.3. Experimental

4.1.3.1. Materials

P(D,L)LA Biophan 121 film (Treofan, France) was provided as a film of 30 μm in thickness being composed of three layers: a core layer of white P(D,L)LA and two external layers of sealable P(D,L)LA. It contained lactide monomers in D- and L-conformation, although the exact proportion was not specified in the manufacturer's datasheet. Its oxygen transmission rate was equal to 675 $cm^3.m^{-2}.day^{-1}.bar^{-1}$ at 23 °C and 50 % relative humidity (RH) according to the Treofan data sheet (oxygen permeability P_{O2} = 2.344 × 10^{-18} $m^3.m.m^{-2}.s^{-1}.Pa^{-1}$). P(D,L)LA Biomer L9000 (Biomer, Germany), being mainly in the L-conformation and containing approximately 1% D-lactic acid, was purchased as pellets. An analysis of the molecular weight by size exclusion chromatography (SEC) resulted in the following characteristics: number-average molecular weight (M_n) of 90,000 and weight-average molecular weight (M_w) of 170,000. The pellets were dried at 80 °C under vacuum for 8 h before use. Ethyl acetate and hexadecane (p.a. quality) were purchased from Sigma Aldrich (France).

4.1.3.2. Extrusion and thermo-compression of P(D,L)LA films

The extruded P(D,L)LA film was prepared from dried Biomer pellets (vacuum pressure of 10^{-4} Pa, 8 h at 80 °C) using a single-screw extruder of 30 mm diameter with a barrel of length-to-diameter ratio of 33 and a three-section screw without mixing elements and turning at 40 rpm. The temperature profile of the six zones of the screw was 180 – 185 – 190 – 195 – 205 – 205 °C. The temperature profile of the mixer device (4 Sulzer SMX®) and the die was defined at 210 °C, in order to avoid non-melted particles and degradation. A flat die of 100 mm in width and chill roll equipment were used to manufacture a film of 80 mm in width and approximately 190 μm in thickness. The roll temperature and roll speed were fixed, respectively, at 25 °C and 10 $m.min^{-1}$.

In order to obtain a P(D,L)LA film sample with defined crystallinity and without residual stress, the extruded film was subsequently reheated and moulded using a thermal press (Specac Press, UK). Extruded films were sandwiched between a Teflon film and a stainless steel plate. The sandwich was held at 200 °C for 1 min without pressure to ensure temperature

equilibrium and complete melting of P(D,L)LA. Then, a pressure of 3.4 bar (340 kPa) was applied for 4 min. The film was subsequently quenched in water at room temperature (23 °C) yielding amorphous, quenched P(D,L)LA. In the following this sample will be referred to as quenched P(D,L)LA. The quenched samples where reheated at various temperatures and durations under compression (0.5 bar (50 kPa)) to obtain P(D,L)LA samples with various degrees of crystallinity. The recrystallized samples were quenched in water at room temperature. These samples will be referred to as recrystallized P(D,L)LA. Sample thickness was measured with a handheld micrometer to be 190 ± 30 µm.

4.1.3.3. Conditioning of PLA films in ethyl acetate atmosphere

The P(D,L)LA samples were equilibrated in an ethyl acetate atmosphere at an activity of 0.5 for 3 days in a hermetic cell at 25 °C. The activity was calculated as p/p_0, with p being the partial pressure and p_0 the vapour pressure of ethyl acetate at saturation. The duration of 3 days was a minimum time span to ensure the equilibration of the ethyl acetate concentration gradient within the samples. The activity of ethyl acetate in the atmosphere of the equilibration cell was generated with a solution in hexadecane containing 3.3×10^{-2} mol.L^{-1} ethyl acetate. An amount of 10 mL of this solution was put into a hermetic cell (volume of 0.8 L) equipped with a Mininert® valve. The concentration of ethyl acetate in the atmosphere was measured after equilibration for 6 h at 25 °C. For that, 0.5 mL of the atmosphere was withdrawn using a gas syringe through the Mininert valve and analysed using a Fisons GC 8000 gas chromatograph (Fisons, France) equipped with a DB-Wax capillary column (J&W Science; 30 m length × 0.32 mm inner diameter × 0.50 µm film thickness). The temperature of the splitless/split injector was 220 °C with a purge time of 1.5 min. The temperature of the flame ionization detector was 250 °C. The carrier gas was hydrogen with a linear velocity of 37 cm.s^{-1}. The oven temperature was programmed to increase from 40 to 130 °C at 5 °C.min^{-1}.

The concentration of ethyl acetate was calculated by external calibration. The calibration curve of ethyl acetate was set up by injection of 2 µL of the calibration solutions which were ethyl acetate in pentane (Sigma, France, p.a. quality; 0.216, 0.433, 0.649 and 0.866 mol.L^{-1}). Ethyl acetate activity was determined using the perfect gas law.

4.1.3.4. Analysis methods

4.1.3.4.1. Size exclusion chromatography

The molecular weight of the polymer samples was determined using SEC with a Shimadzu liquid chromatograph equipped with an LC-10AD isocratic pump, a DGU-14A degasser, an SIL-10AD automated injector and a CTO-10A thermostat oven. The fractionation was performed on a series of two PL-Gel mixed C (5μm, 300 mm) columns and a PL-100A (300 mm) column (Polymer Laboratories) preceded by a pre-column PL-Gel 5 μm Guard (50 mm, Polymer Laboratories) using chloroform (Merck, HPLC grade) as elution solvent. The flow rate was 0.8 mL.min^{-1}, temperature was 25 °C and injection volume was 100 μL. The fractions were detected using a Shimadzu RID-10A refractive index detector. Sample concentration was 4–5 mg.mL^{-1}. The system was calibrated with a polystyrene calibration kit of low dispersity (580–1,650,000).

4.1.3.4.2. Differential scanning calorimetry

The crystallinity of the P(D,L)LA samples was measured using a Pyris 1 (Perkin Elmer, France) DSC instrument. Tests were performed at 10 °C.min^{-1} from 0 to 200 °C in hermetic aluminium pans. The degree of crystallinity (χ_c) of the PLA samples was calculated using the following equation:

$$\chi_c = \frac{\Delta H_m - \Delta H_c}{\Delta H_m^0} \; , \tag{1}$$

where ΔH_m is the enthalpy of melting considering the small exothermal event at the beginning of the melting peak, ΔH_c is the enthalpy of crystallization and ΔH_m^0 is the enthalpy of fusion per gram of perfect crystal of infinite size (totally crystalline polymer), being 93 J.g^{-1} (Fischer, 1973; Oliveira, 2006). The glass transition temperature was measured using temperature-modulated DSC (TMDSC) with a QSC 100 instrument (TA Instruments, France).

The heating scan was performed under sinusoidal temperature modulation with a heating rate of 1 °C.min^{-1}, a period of 80 s and a modulation of ± 1.5 °C between −30 and 90 °C. Hermetic aluminium pans (Tzero, TA Instruments) were used, which are able to withstand an internal pressure of 3 bar (300 kPa). The absence of weight loss was verified for each experiment by weighing. All measurements were made in triplicate. Each apparatus was

equipped with an intracooler in order to reach low temperatures. All tests were performed under nitrogen atmosphere.

4.1.3.4.3. Dynamic mechanical analysis

Tension measurements were carried out with a Tritec 2000 DMA instrument (Triton Technology, France) at a frequency of 1 Hz and 0.1 % strain. Polymer samples (10.25 mm long, 5 mm wide and ca 0.2 mm thick) were heated from −50 to 200 °C at 2 °C.min^{-1}. The temperature of the glass transition was taken at the peak of the damping factor (tan δ). Measurements were done in triplicate.

4.1.3.4.4. Oxygen permeability

The oxygen transmission rate was measured at 23 °C and 0 %RH using a Systech 8001 (France) apparatus. Measurements were done in duplicate.

4.1.3.4.5. Sorption isotherm

The sorption isotherm of ethyl acetate was measured at 25 °C and 0 %RH with a static method, using an electronic microbalance (Intelligent Gravimetric Analyzer 002, Hiden Isochema Ltd, Warrington, UK) with a sensitivity of 0.2 µg. Film samples (30 – 40 mg) were suspended from the microbalance by a stainless steel spiral which was contained in a thermo-regulated cell at 25 °C. The microbalance itself was maintained at 50 °C to ensure stability during the weight measurement by prevention of solvent condensation. Before measurements, the samples were purged for 24 h at 10^{-5} mbar (10^{-3} Pa) to remove all volatile compounds sorbed in the film and present in the chamber. Then, in order to set the aroma activity, the ethyl acetate partial pressure was set using a pressure transducer (Baratron®, MKS Instruments, Wilmington, MA, USA) linked to a tank with a vapour phase saturated in ethyl acetate. The mass uptake of samples was recorded automatically with the time. The sorption equilibrium was defined as less than 1% change in the film mass or after 20 h, even if the macroscopic equilibrium was not reached. The apparent ethyl acetate solubility S (kg.m^{-3}.Pa^{-1}) was calculated according to

$$S = M_{\infty} \times \frac{d}{p},\tag{2}$$

where M_{∞} is the equilibrium sorption obtained theoretically after infinite time (kg.kg^{-1}), d is the film density (kg.m^{-3}) and p is the compound vapour partial pressure (Pa). Each measurement was done in triplicate.

The microbalance was calibrated regularly during maintenance periods for pressure, mass and temperature by the following methods.

• The microbalance weight measurement was calibrated using three Class F1 calibrated weights of 20, 50 and 100 mg. Nine measurements were made with different combinations of the three weights to check the balance linearity as well as the microbalance measurement span by use of a least squares fit.

• The loading of a single F1 calibrated weight of 100 mg, with tolerance of 50 µg, was used to check the balance conformance. Typically the determined weight was within $\pm$ 20 µg of the nominal value.

• The 100 mbar Baratron capacitance manometer was factory calibrated, with a specified accuracy of 0.15 % of reading.

• The sample temperature is measured using a platinum resistance thermometer (PT100 1/10 Class B) adjacent to the sample position. The measurement electronics span and offset were determined using high-precision resistances, individually calibrated using a traceable ohmmeter. The platinum resistance thermometer sensor conformance was verified to within 0.2 °C by immersion in a distilled water/ice mix and by comparison with a calibrated glass thermometer at ambient temperature.

• The drift of the microbalance was estimated using a blank experiment to be 0.07 mbar.min^{-1}.

4.1.3.4.6. Statistical analysis

Statistical analysis was done with a one-way analysis of variance (ANOVA). When the differences were significant ($p < 0.05$), Duncan's test was used to check the differences between pairs of groups and was carried out using XLSTAT-Pro 7.0 software (Addinsoft, Paris, France).

4.1.4. Results and discussion

4.1.4.1. Sample preparation

In order to test the influence of the crystallinity of PLA samples on barrier properties, P(D,L)LA films with various crystallinities were fabricated by thermo-compression of extruded films. Because P(D,L)LA exhibits low crystallization kinetics, it is easy to prepare

film samples with various degrees of crystallinity. The high glass transition temperature at approximately 60 °C allows the quenching of the P(D,L)LA samples from the melt at room temperature. Samples were subsequently annealed at various temperatures and times. The operation conditions used in this work are given in Table 1.

The annealing temperatures were low in order to obtain small spherulites giving generally better mechanical properties. The annealing time was limited in order to limit sample degradation. Table 1 shows the molecular weight characteristics of the different samples. The extrusion and thermo-compression treatment results in a decrease of molecular weight.

Figure 1 shows heating scans of three samples: extruded P(D,L)LA (curve a), quenched P(D,L)LA (curve b) and P(D,L)LA crystallized in the heating press (curve c). The heating scan of the extruded P(D,L)LA shows an endothermic relaxation event that is superposed on the glass transition temperature (T_g), preventing the determination of the T_g value. Annealing the samples at temperatures higher than T_g nearly eliminated the endothermic relaxation (curves b and c), which is a result of cooperative rearranging movements (Hutchinson, 2003). The extruded and quenched P(D,L)LA (curves a and b) show a cold crystallization at ca 100 °C and a double melting endotherm at ca 170 °C. The double melting peak of P(D,L)LA has been studied using modulated DSC (Ling, 2006a; Shieh, 2007).
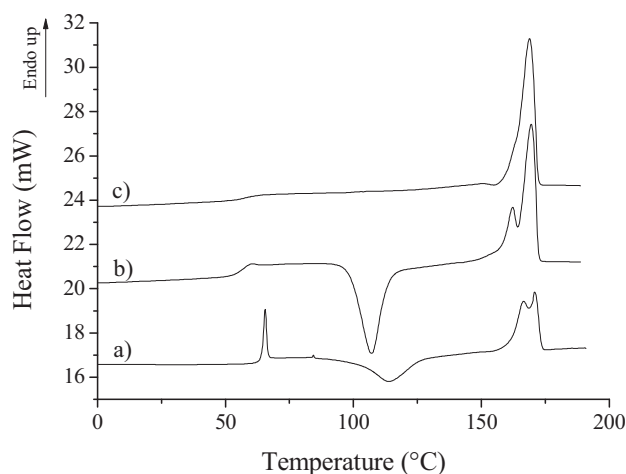
Figure 1. Heat flow curves of P(D,L)LA samples in the first heating cycle: a) extruded P(D,L)LA, b) quenched P(D,L)LA, c) recrystallized P(D,L)LA (92 °C/25 min).

The current interpretation is a melting–recrystallization phenomenon where the lower endotherm corresponds to the melting of initially present crystals. The partially molten material is thought to be able to recrystallize forming more perfect crystals melting at higher temperature in the second endotherm (Ling, 2006a; Ling, 2006b; Peniston, 2007;

Table 1. Influence of the recrystallization conditions on the thermal properties of P(D,L)LA films and the oxygen permeability.

	T_c (°C)	ΔH_c (J.g^{-1})	T_m (°C)	ΔH_m (J.g^{-1})	χ_c (%)	M_n (g.mol^{-1})	M_w (g.mol^{-1})	P_{O2}x10^{18} m^3.m.m^{-2}.s^{-1}Pa^{-1}
Extruded film	100.5 (±0.2)	33.4 (±0.4)	164.3 (±2.8)	35.5 (±0.2)	2 (±1)	97,000	170,000	1.94 (±0.03)[c]
Quenched P(D,L)LA	97.9 (±0.6)	31.9 (±0.7)	166.5 (±0.4)	37.7 (±0.8)	6% (±2)	92,000	175,000	2.50 (±0.18)[b]
80 °C 15min recrystallized P(D,L)LA	91.6 (±0.8)	30.0 (±1.3)	166.9 (±1.7)	37.2 (±0.5)	8% (±3)	n.d	n.d	n.d
85 °C 15min recrystallized P(D,L)LA	82.3 (±0.6)	8.6 (±2.5)	168.3 (±0.5)	36.0 (±0.1)	29% (±4)	n.d	n.d	n.d
90 °C 15min recrystallized P(D,L)LA	/	0	165.7 (±1.4)	36.0 (±0.2)	39% (±1)	n.d	n.d	n.d
92 °C 25min recrystallized P(D,L)LA	/	0	167.9 (±0.3)	36.7 (±0.6)	39% (±1)	80,000	167,000	2.86 (±0.08)[a]
P(D,L)LA Biophan™	/	0	138.9 (±0.7)	17.9 (±0.1)	19% (±1)	90,000	172,000	2.11 (±0.08)[c]

T_c crystallization temperature, ΔH_c crystallization enthalpy, T_m melting temperature, ΔH_m melting enthalpy, χ_c crystallinity degree, P_{O2} oxygen permeability, n.d. not determined, [a,b,c]significant differences at $p < 0.05$ (Duncan).

Sarasua, 1998). Melting of all P(D,L)LA samples is accompanied by a small exothermal event. This exothermal signal overlapping is well observed in TMDSC and has been previously reported by Zuza *et al.* (Zuza, 2008) and Ohtani *et al.* (Ohtani, 2003) It has been suggested that the cause is the recrystallization of already existing α crystals into an α polymorph of higher perfection (Ohtani, 2003).

The thermal properties of our P(D,L)LA samples are given in Table 1. The degree of crystallinity is calculated according to Equation 1. We notice that the crystallization temperature (T_c) and melting temperature (T_m) do not change with annealing temperature. Values of ΔH_m are similar for all P(D,L)LA Biomer samples which illustrates the absence of degradation of polymer during sample preparation because there is no change in the ability of P(D,L)LA to crystallize. Similar conclusions have been drawn for the polyester PET (Kint, 2003). Values of ΔH_c decrease with the heating temperature which permits one to follow the crystallization process and to calculate the increase of the degree of crystallinity. On the one hand, as expected, ΔH_c decreases with the annealing temperature which permits one to follow the crystallization process with an increase of the degree of crystallinity. On the other hand, ΔH_m values are similar which illustrates the absence of degradation for all samples based on P(D,L)LA Biomer during sample preparation. These results show that there is no change in the ability of P(D,L)LA to crystallize which is in accordance with previous work on PET (Kint, 2003). The maximum degree of crystallinity realizable with our experimental set-up is approximately 40 % which is in accordance with the results of Ling and Spruiell (Ling, 2006b) and MacDonald *et al.* (MacDonald, 1996). No difference between the sample annealed at 90 °C for 15 min and that annealed at 92 °C for 25 min is observed in the DSC analysis.

The impact of crystallization on the viscoelastic properties of the P(D,L)LA samples was further investigated using thermo-mechanical analysis. Figure 2 plots curves of uniaxial tensile storage modulus (E') as a function of temperature. The sample recrystallized at 92 °C shows the highest E' in the glassy plateau. The loss of E' during the glass transition at approximately 60 °C depends on the quantity of amorphous phase in the sample. We see that it is largest for the quenched P(D,L)LA film. Incompletely recrystallized samples show an increase in E' after T_g, which has been shown to be caused by the cold crystallization phenomenon (Urayama, 2001). The recrystallization induces a stiffening of the macromolecular chains being responsible for the increase in the storage modulus. The final decrease of the storage modulus at high temperature corresponds to crystal melting in the

film. DMA being a more sensitive technique than DSC to observe physical transition phenomena in polymers allows us to distinguish between the samples recrystallized at higher temperature. The sample compressed for 15 min at 90 °C is still able to recrystallize as we can see from the peak of the storage modulus in the rubbery plateau, a phenomenon not observed in the curve of the sample treated at 92 °C.
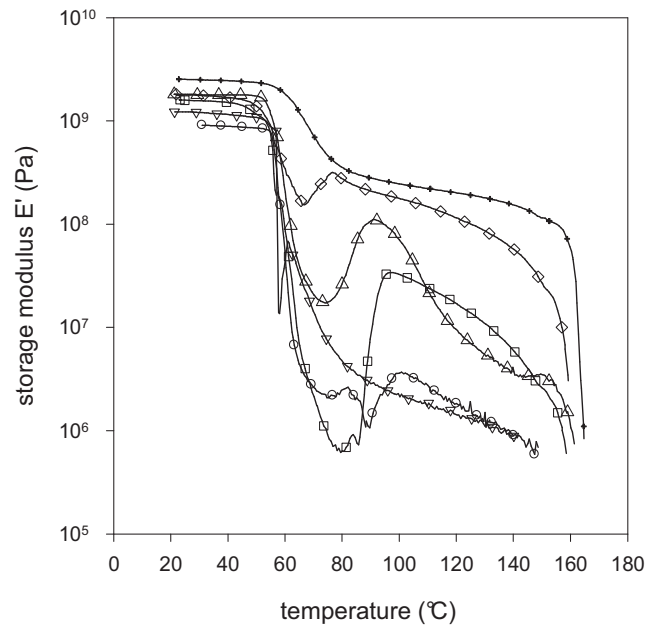
Figure 2. Evolution of the storage modulus with temperature of P(D,L)LA samples having different crystallinity. Symbols: extruded P(D,L)LA (o), quenched P(D,L)LA (□), annealed P(D,L)LA 15 min 80 °C (△), 15 min 85 °C (▽), 15 min 90 °C (◇), and 25 min 92 °C (+).

To investigate of the effect of crystallinity on the barrier properties of the P(D,L)LA films we worked on the extruded blank, the quenched sample and the film thermo-compressed for 25 min at 92 °C. The latter will be referred to as recrystallized film.

4.1.4.2. Gas barrier properties

The oxygen permeability of the various samples is given in Table 1. Literature data give oxygen permeabilities between 2.3×10^{-18} and 4.6×10^{-18} $m^3.m.m^{-2}.s^{-1}.Pa^{-1}$ for various experimental set-ups (Auras, 2006; Auras, 2005a; Sanchez-Garcia, 2007). Our results are consistent with those data. The oxygen permeability of the P(D,L)LA Biophan film is in accordance with the values given by the manufacturer. Compared to conventional packaging polymers, P(D,L)LA shows behaviour intermediate between that of PET and PS, being, respectively, good oxygen barrier packaging with an oxygen permeability of ca 0.4×10^{-18} $m^3.m.m^{-2}.s^{-1}.Pa^{-1}$ and a low oxygen barrier material with oxygen permeability of

19×10^{-18} m³.mm⁻².s⁻¹.Pa⁻¹ (Pauly, 1999). The statistical analysis of the data, given in Table 1, shows that the films behave significantly different. The recrystallized sample has the highest oxygen permeability, which is not the expected result. For example, crystallization, in particular cold crystallization from the glassy state, is a common way to improve gas barrier properties of PET (Natu, 2005). Furthermore, a decrease of the water vapour transfer rate with increasing crystallinity has already been shown for P(D,L)LA (Tsuji, 2006). The decrease of the gas permeability with crystallinity is generally explained in terms of two factors. First, the inclusion of impermeable crystallites decreases the amount of the amorphous phase through which gas molecules can permeate. Second, impermeable crystals increase the tortuosity of the transport path. The former effect affects the total solubility of the permeant in the material, the later affects the diffusion coefficient. However, in many cases the decrease of solubility with crystallinity is smaller than expected from the increase of crystallinity. This behaviour is explained by the decrease of the average amorphous phase density or de-densification with increasing crystallinity resulting from conformational restrictions imposed by the crystallinity on the polymer chain in the amorphous phase. The less dense amorphous phase includes higher free volume and shows therefore higher gas solubility (Sekelik, 1999).

In our case, an increase of oxygen permeability is observed. Although significant after three measurements, the increase is very small, because, from a technological point of view, a relevant effect includes the change of an order of magnitude in permeability. We propose two hypotheses for our findings. First, although the DSC and DMA results clearly show the crystallinity of the recrystallized P(D,L)LA, no apparent spherulites are observed with a microscope under cross-polarized light, which is in contrast to the observations of Solarski *et al.* (Solarski, 2005) or Tsuji and Ikada (Tsuji, 1995). The morphology can be explained by the low recrystallization temperature used in this work to obtain small spherulites. Therefore, we suggest that the spherulites in our film samples might be too small to create a more tortuous path for the oxygen molecules and thus to decrease the gas permeability. It has been described for PET that an increase in the size of the superstructure in the crystalline phase decreases the gas permeability due to an increase of the tortuosity (Natu, 2005).

A second hypothesis might be the de-densification of the amorphous phase which counteracts the decrease of the quantity of permeable amorphous phase due to crystallization. De-densification of the amorphous phase in PET has been shown by Liu *et al.* (Liu, 2004) to be responsible for the higher oxygen permeability of bottle walls processed under conditions of higher thermal exposure, although the treatment led to an increase in the volume fraction of impermeable crystals. A decrease in the permeable amorphous phase density causing an

increase of gas permeability through heat-set PET was also shown by Qureshi *et al.* (Qureshi, 2000). It has been shown for poly(L-lactic acid) (PLLA), in comparison to PET, that there is an important decoupling between crystalline and surrounding amorphous phase (Arnoult, 2007; Mano, 2005; Zuza, 2008). This behaviour is attributed to the high flexibility of the macromolecular chain, which is able to fold easily on the crystal surface. The result would be less tied molecules between amorphous and crystalline phase (Mano, 2005), a factor limiting the possibility of de-densification of the amorphous phase. Further research and careful measuring of the phase densities of P(D,L)LA should be carried out in order to get more insight into the transport mechanisms.

4.1.4.3. Aroma compound sorption

The mass uptake of ethyl acetate in the P(D,L)LA samples is plotted in Figure 3. The plots show an upwards trend and are convex in relation to the ethyl acetate activity axis. In the case of semi-crystalline polymers in their glassy state, the sorption isotherm at low partial pressures of penetrant is concave to the pressure axis and convex only at high activities (Serad, 2001). This behaviour is generally described by the dual-mode sorption model (combination of Henry's and Langmuir's sorption modes). At high penetrant activities, the convex form is usually described for semi-crystalline polymers in their rubbery state, such as hydrophobic polymers in contact with organic compounds. Examples for this type of sorption isotherm are the sorption of ethyl acetate and ethyl hexanoate into LDPE (Hirata, 2006) or benzaldehyde into PP (Qin, 2007). The behaviour is generally described with the Flory–Huggins or the engaged species induced clustering (ENSIC) model (Favre, 1996).

Figure 3 shows that the comparative data obtained after 20 h of sorption seem to be consistent with an ENSIC or Flory–Huggins sorption isotherm. Nevertheless the given mass uptakes are under-estimated due to the fact that the equilibrium is not always reached after 20h of sorption experiment. At an activity of 0.5, the recrystallized P(D,L)LA film shows an ethyl acetate mass uptake significantly lower than that of the other P(D,L)LA films. The mass uptake of the recrystallized sample remains small compared to the other samples up to an activity of 0.7. Between activities of 0.7 and 0.9 the sorption of ethyl acetate increases strongly. We suggest that this is caused by a change in the sorption mechanism due to the formation of ethyl acetate clusters in the polymer, which is consistent with the ENSIC model. At an activity of 0.9, there is a difference between the sorption of all samples, with the recrystallized film sorbing the smallest and the P(D,L)LA Biophan film the highest quantity.

The reason why the Biophan film sorbs more than the amorphous samples could not be determined. Various hypotheses can be suggested. The exact formulation of the Biophan film is not known; technical adjuvant contained in the polymer may enhance ethyl acetate sorption. Furthermore, the film has two sealable faces which are amorphous, probably accounting for a major part of the sorption. A second hypothesis is the comparatively small thickness of the sample. The thermo-compressed P(D,L)LA Biomer samples are fivefold thicker, which may induce an error in the apparent solubility coefficient because the macroscopic equilibrium value is not reached.
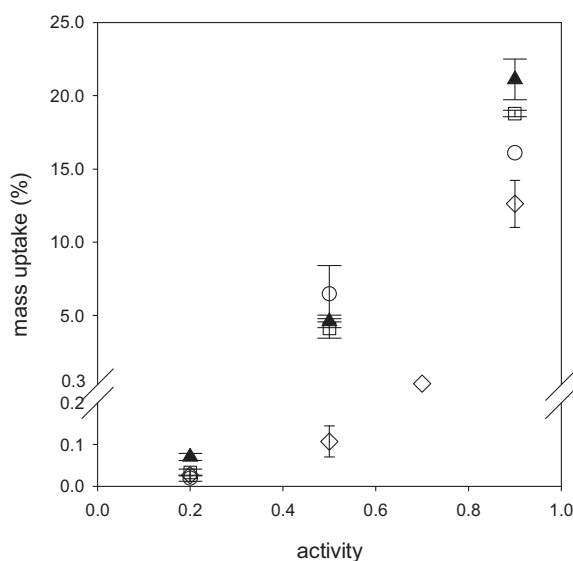
Figure 3. Apparent sorption isotherm of ethyl acetate in the different P(D,L)LA samples with various crystallinity. In order to display the differences of the small values, the ordinate was cut between 0.2 and 0.3 % mass uptake (kg ethyl acetate/ kg polymer). Symbols: (o) extruded P(D,L)LA, (□) quenched P(D,L)LA, (◇) recrystallized P(D,L)LA, (▲) P(D,L)LA Biophan™.

The kinetics of the sorption allow us to calculate the apparent solubility coefficients (S) of ethyl acetate in the P(D,L)LA samples at various activities (p/p_0) according to Equation 2. However, the P(D,L)LA samples reach the stationary state of the sorption curve only at an activity of 0.2. In order to compare the behaviour of the P(D,L)LA samples, the apparent solubility coefficients were calculated from the near-equilibrium value of the mass uptake after 20 h of contact. The results are shown in Figure 4. The recrystallized sample sorbs the smallest quantity of ethyl acetate whatever the activity, because the sorption occurs only in the amorphous phase of the polymer. The results at an activity of 0.5 are of the same order of magnitude as the results of Auras *et al.* (Auras, 2004a) who measured, using a different

experimental set-up, a solubility coefficient of 6.17×10^{-3} kg.m^{-3}.Pa^{-1} at 30 °C and an activity of 0.3 for P(D,L)LA 98 % L-isomers.
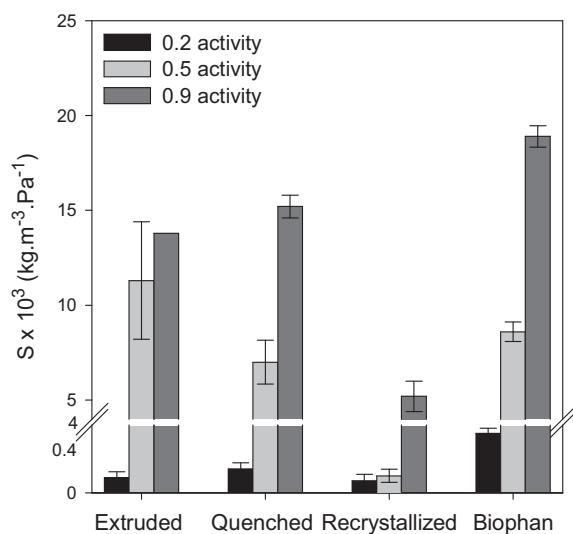
Figure 4. Apparent solubility coefficient (*S*) of ethyl acetate in P(D,L)LA samples with varying crystallinity at different activities (*p/p$_0$*) at 25 °C. In order to display the small values, the ordinate was cut between 0.4 and 4.10^{-3} kg.m^{-3}.Pa^{-1}.

In comparison, the solubility coefficients of ethyl acetate in the P(D,L)LA samples are higher than those obtained in LDPE and PP. The solubility coefficient of the rather hydrophilic molecule ethyl acetate in those hydrophobic polymers ranges from 1.52×10^{-3} kg.m^{-3}.Pa^{-1} at an activity of 0.5 to 1.92×10^{-3} kg.m^{-3}.Pa^{-1} at an activity of 0.9 (Hirata, 2006). Nielsen and Giacin (Nielsen, 1994) measured the solubility coefficient of ethyl acetate in PP using a gravimetric procedure at an activity of 0.5 and 22 °C as equal to 3.2×10^{-3} kg.m^{-3}.Pa^{-1}. These comparisons show that the ethyl acetate solubility is roughly two times higher in P(D,L)LA compared to the polyolefins PP and PE. The reason is most probably the more hydrophilic character of the P(D,L)LA chains which facilitates the sorption of the comparatively hydrophilic molecule ethyl acetate. Actually, ethyl acetate is the most hydrophilic aroma compound in the homologous series of ethyl esters, and it was chosen here in order to test the performance of P(D,L)LA in a rather unfavourable case. Since aroma compounds are in the main more hydrophobic than ethyl acetate, good performance of the barrier properties of P(D,L)LA can be expected. Auras *et al.* (Auras, 2004a) showed, for example, that the sorption of hydrophobic limonene in P(D,L)LA was apparently smaller than that in LDPE and PP.

4.1.4.4. Influence of aroma compound sorption on the thermal properties of P(D,L)LA

The form of the sorption isotherm consistent with the ENSIC model suggests the plasticizing of the polymer matrix. In order to test the effect of sorption on the thermo mechanical properties of the P(D,L)LA samples, they were analysed after 3 days equilibration in ethyl acetate atmosphere at an activity of 0.5. The results are given in Table 2.

The glass transition temperature was measured using TMDSC which allows the determination in the first heating scan although the enthalpic relaxation peak is superposed on the T_g signal as shown in Figure 1. Figure 5 shows the heat flow curve of the various samples before (Figure 5a) and after (Figure 5b) equilibration in ethyl acetate atmosphere. One observes the broadening of the glass transition region to more than 20 °C. This flat transition is easier to determine in the modulated heating scan. We note an increase of T_g with increasing crystallinity for the PLA Biomer samples before conditioning in ethyl acetate atmosphere. This increase is consistent with the results of Delpouve *et al.* (Delpouve, 2008). Those authors showed that there was a complex polymer relaxation phenomenon indicating two distinct glass transition dynamics. The low- temperature process is assigned to segmental motions in the interspherulitic amorphous phase and the high temperature process can be assigned to the presence of an intraspherulitic amorphous phase being more constrained. Zuza *et al.* (Zuza, 2008) found a similar increase of T_g for semi-crystalline P(D,L)LA.

Table 2. Glass transition temperature (T_g) and degree of crystallinity (χ_c) of P(D,L)LA films determined by DSC and by DMA before and after sorption of ethyl acetate (EA) during the conditioning in EA atmosphere at 0.5 activity and 25 °C for 3 days.

Material	χ_c (%)		MDSC		DMA	
	before EA sorption	after EA sorption	T_g (°C) before EA sorption	T_g (°C) after EA sorption	T_g (°C) before EA sorption	T_g (°C) after EA sorption
extruded P(D,L)LA	2 (±1)	46 (±5) [a]	56.7 (±0.6)	-0.3 (±8.8) [a]	62.3 (±0.2)	52.1 (±1.1) [b]
quenched P(D,L)LA	6 (±2)	46 (±2) [a]	56.8 (±1.3)	1.9 (±5.9) [a,b]	62.8 (±0.3)	49.8 (±0.4) [c]
recrystallized P(D,L)LA	39 (±1)	52 (±3) [a]	63.3 (±1.2)	-5.7 (±0.3) [a]	71.2 (±2.2)	52.0 (±0.1) [b,c]
P(D,L)LA Biophan™	19 (±1)	22(±4) [b]	50.9 (±0.1)	16.9 (±1.9) [b]	67.9 (±0.1)	55.2 (±0.1) [a]

[a,b,c] significant differences at p < 0.05 (Duncan)

They showed furthermore a shift of 15 °C to higher temperatures of T_g of semi-crystalline PLLA compared to amorphous poly(D,L-lactic acid), which may explain the observed difference between the recrystallized sample and P(D,L)LA Biophan. If we turn our attention now to the T_g results after conditioning of the P(D,L)LA samples in ethyl acetate atmosphere, no significant difference in T_g as a function of crystallinity is observed, except PLA Biophan, as is evident from the statistical analysis in Table 2. However, the broadening of the glass transition leads to a higher uncertainty of the value of T_g taken at the midpoint of the transition. What is important here, especially for packaging applications of PLA, is the large shift of the value of T_g far below room temperature. Even if the shift of T_g of PLA Biophan is smaller, the value is still below room temperature. A very negative effect of the sorption of aroma compounds such as ethyl acetate on the barrier properties of packaging materials during the storage of food products can be expected. Actually, the transfer phenomena are known to accelerate at temperatures higher than T_g. Table 2 also gives the T_g values recorded using DMA and obtained at the peak of the damping factor. The decrease of T_g after conditioning of the samples in ethyl acetate atmosphere is still important, but recorded values are much higher than those from DSC. A significant difference between P(D,L)LA Biophan and the other samples is observed. Furthermore, there seems to be a difference between the quenched sample and the extruded and recrystallized ones.
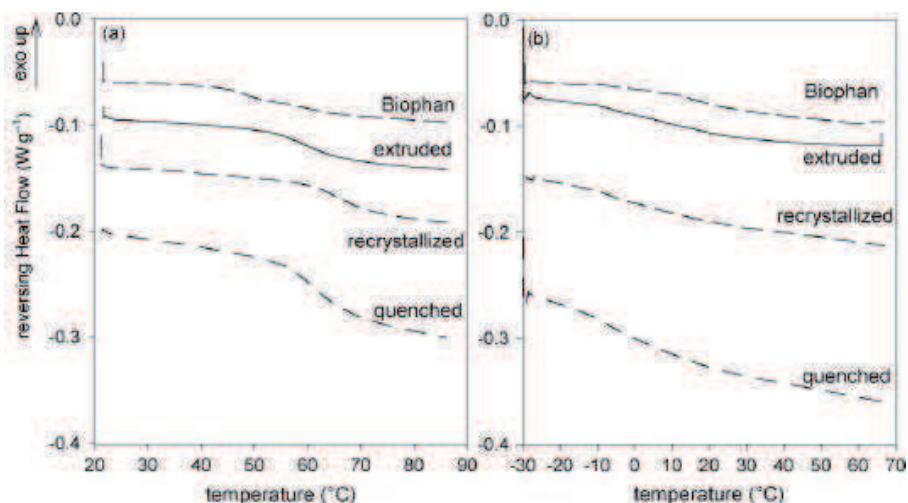
Figure 5. Heat flow curves of P(D,L)LA samples before (Figure 5a) and after (Figure5b) equilibration in ethyl acetate atmosphere at 0.5 activity and 25 °C for 3 days.

However, this difference is not confirmed by the DSC values, where problems of ethyl acetate evaporation are avoided. On the one hand, the results of the mechanical testing are generally higher than those from DSC; on the other hand, we suppose that samples dry during the DMA

measurements. One reason is the large surface of the samples exposed to the surrounding air; a second is the smaller heating rate used and thus the longer time of exposure. Moreover, hermetic capsules were used for DSC analysis to avoid aroma evaporation, which is confirmed by the unchanged sample weight after the measurements.

Figure 6 plots the evolution of *E'* with temperature. We observe a broadening of the glass transition, a result also seen in the DSC analysis. The conditioning in ethyl acetate atmosphere has no impact on the value of *E'* in the glassy plateau, except for the recrystallized sample. *E'* after conditioning is even higher than the initial one for the extruded sample. What is interesting is the evolution of *E'* in the rubbery plateau. As already explained in the discussion of Figure 2, we observe a peak in the modulus curve due to the cold crystallization of the sample before conditioning. Comparing to the equilibrated films, we find an increase in *E'* in the case of the quenched and the extruded samples and no cold crystallization peak. On the contrary, the moduli of the P(D,L)LA Biophan and the recrystallized samples are lower after conditioning, which is expected due to the plasticizing of the polymer.

Our interpretation is that ethyl acetate induces crystallization of the P(D,L)LA samples, which can explain the increase of the storage modulus in the rubbery plateau and the absence of the cold crystallization peak. Another result pointing to solvent-induced crystallization during the conditioning in ethyl acetate atmosphere is the whitening of the film samples.
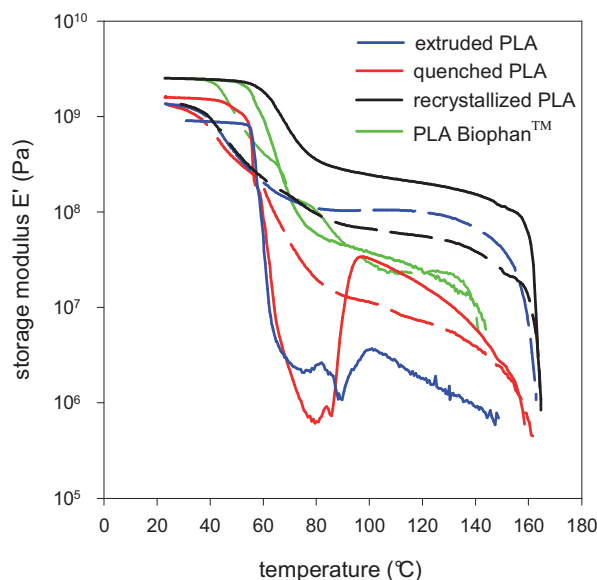
Figure 6. Thermo-mechanical properties of P(D,L)LA films before (solid line) and after conditioning (dashed line) in ethyl acetate atmosphere at an activity of 0.5 and 25 °C for 3 days.

The degree of crystallinity of the P(D,L)LA samples before and after conditioning in ethyl acetate atmosphere calculated using Equation 1 is given in Table 2. A clear increase of the degree of crystallinity up to the value of the recrystallized film is observed, and all P(D,L)LA samples, except P(D,L)LA Biophan, are classified in the same statistical group. PLA Biophan shows no induced crystallization. We suggest that this behaviour might be caused by the different chirality of the Biophan sample, because the crystallization kinetics are strongly dependent on the D- and L-content of the copolymer (Auras, 2006). Solvent-induced crystallization has already been described for the semi-crystalline polyester PET (Durning, 1985; Ouyang, 2004; Ouyang, 2002; Serad, 2001), in particular by Serad *et al.* (Serad, 2001) and by Ouyang *et al.* (Ouyang, 2002) who showed the crystallization of PET in contact with acetaldehyde and acetone, respectively. Ouyang and Shore (Ouyang, 1999a, 1999b) showed for the solvent-induced phenomenon that the sample dimensions increased after the sorption of the solvent due to swelling of the polymer. This caused the release of internal stress bringing about more mobility of the polymer chain and enabling crystallization at low temperature. In our case, in the same manner, the transport of ethyl acetate in amorphous P(D,L)LA seems to be accompanied by the induced crystallization of the polymer.

4.1.5. Conclusions

P(D,L)LA film samples (1% D-lactide) with various crystallinities were prepared by flat die extrusion and thermo-compression and compared to P(D,L)LA Biophan having unknown D,L-conformation. Crystallinity does not seem to be the key factor for the improvement of the barrier properties of P(D,L)LA against oxygen. The oxygen transfer rate of P(D,L)LA Biophan was significantly different from that of the P(D,L)LA Biomer. However, the sorption of the aroma compound ethyl acetate decreased with increasing crystallinity. In this case, P(D,L)LA Biophan behaved like the amorphous P(D,L)LA Biomer samples. There are differences in the sorption mechanism of gaseous molecules, such as oxygen, and volatile organic compounds, because in the latter case the solubility coefficient has a dominating effect on the permeability. The sorption isotherm was compatible with the ENSIC model, which predicts the plasticizing of the polymer matrix. This was confirmed by DSC and DMA measurements, which showed moreover a solvent-induced crystallization of P(D,L)LA Biomer, evidencing a strong plasticizing effect. For the application of polyesters and more

specifically P(D,L)LA in food packaging, good barrier properties are required. Consequently the extent of the change of the thermo mechanical properties of polymer matrix when brought into contact with organic compounds, such as aroma compounds, is an important finding. The important decrease of the glass transition of P(D,L)LA upon the sorption of an aroma compounds well below ambient temperature has an impact on its barrier properties and thus the stability of food products at room temperature. This clearly shows the need to carefully optimize packaging material by taking into account the interaction of polymer matrix and packed foodstuff over the whole of the shelf-life.

4.1.6. Discussion et commentaires

Les propriétés barrière du P(D,L)LA Biomer L9000 à l'oxygène ainsi que l'effet de la sorption d'une molécule organique volatile sur les propriétés du P(D,L)LA ont été évalués. Le but de cette étude était de déterminer l'effet de la cristallisation et plus particulièrement du taux de cristallinité sur les propriétés de transport du P(D,L)LA mais aussi de connaître l'influence de la sorption de l'acétate d'éthyle sur la structure des films de P(D,L)LA.

Ainsi dans un premier temps, la cristallisation par thermo-compression de P(D,L)LA extrudé amorphe a permis de montrer que l'augmentation du taux de cristallinité ne permettait pas de diminuer la perméabilité à l'oxygène du P(D,L)LA. Ce résultat pourrait être expliqué par deux hypothèses :

- la petite taille des sphérolites formés lors de la cristallisation qui ne permet pas d'augmenter le coefficient de diffusion (Figure 4.1). Ces micrographies mettent en évidence le fait qu'aucune distinction de taille de sphérolites n'est possible en fonction de la température de cristallisation froide.
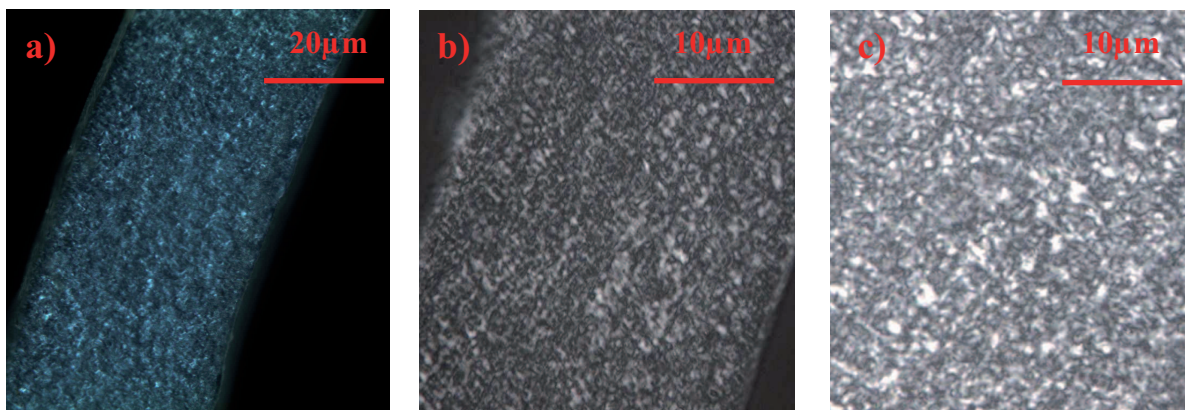
Figure 4.1. Micrographie de P(D,L)LA Biomer L9000 pur après cristallisation froide pendant 2 h à 120 °C a) (grossissement 20), b) (grossissement 40) et pendant 2 h à 90 °C c) (grossissement 40).

- la dé-densification probable de la phase amorphe créée par la cristallisation du polymère qui forme des passages préférentiels pour les molécules diffusantes.

Dans un second temps, l'analyse de la cristallinité et de la température de transition vitreuse du P(D,L)LA après contact avec l'acétate d'éthyle en phase vapeur a mis en évidence la plastification et la cristallisation induite des échantillons. Il apparaît que quelle que soit la cristallinité du P(D,L)LA Biomer L9000 avant contact, la sorption de cette molécule

organique induit une forte cristallisation des échantillons. De plus, la plastification induite résulte en une forte diminution de la T_g jusqu'en dessous de la température ambiante.

Après nous être intéressés au P(D,L)LA pur, des essais similaires ont été réalisés sur un P(D,L)LA CD92 formulé avec du talc et de l'ATBC afin d'évaluer l'impact de la formulation sur la structure cristalline formée par traitement thermique et par contact avec un composé organique volatil. La relation entre la structure et les propriétés barrière a alors été étudiée par l'utilisation de trois molécules sondes plus ou moins inter-agissantes avec la matrice : l'hélium, l'oxygène et l'acétate d'éthyle. Ce travail est présenté dans la publication suivante.

4.2. Effect of crystallization on barrier properties of formulated polylactide (Publication n°5)

Cécile Courgneau[1,2], Sandra Domenek[2], Régis Lebossé[3], Alain Guinault[4], Luc Avérous[5], Violette Ducruet[1*]

[1] INRA UMR 1145 Ingénierie Procédés Aliments, 1 avenue des Olympiades, F 91300 Massy, France.

[2] AgroParisTech UMR 1145 Ingénierie Procédés Aliments, 1 avenue des Olympiades, F 91300 Massy, France.

[3] LNE, Laboratoire National de métrologie et d'Essais, 29 avenue Roger Hennequin - 78197 Trappes cedex, France

[4] CNAM, Laboratoire P2AM , 292 rue Saint-Martin, case courrier 322, 75141 Paris cedex 03, France.

[5] ECPM-LIPHT, EAc (CNRS) 4379, Université de Strasbourg, 25 rue Becquerel, 67087 Strasbourg Cedex 2, France.

4.2.1. Abstract

Polylactide (PLA), a biodegradable polymer obtained from biomass, was formulated with a nucleating agent, talc, and a plasticizer, acetyl tributyl citrate (ATBC) and cold crystallized in α- and α'-form. The barrier properties of crystallized PLA were investigated in function of the formulation and the crystalline form, thanks to three molecules with increasing polymer interactions, i.e. helium, oxygen and ethyl acetate (EA). Contrary to the expectations, the oxygen diffusion coefficient in neat and formulated PLA did not decrease with crystallization. An increase of the diffusion coefficient was even noticed for the most interacting probe, EA, in formulated PLA.

Conditioning of neat and formulated PLA in an atmosphere containing EA vapour caused a modification of the material structure by plasticization and induced crystallization even at small EA activities. The plasticizing effect caused a T_g shift to below ambient temperature. In

the case of neat PLA induced crystallization in solely α-form was obtained, and in the case of formulated PLA a blend of α and α' forms was observed.

4.2.2. Introduction

Due to their environmental merits, biomass-based polymers have been widely studied and particularly polylactide. Subject of an increasing number of publications, PLA presents great interest for industrial and commodity application (Bogaert, 2000; Gupta, 2007; Ikada, 2000). Worldwide production capacity is dramatically increasing from 74 kTons p.a. in 2003 to 229 kTons p.a. in 2009 and should amount 833 kTons p.a. in 2020 (Shen, 2009).

Ease of processing, mechanical properties, high glass transition temperature, and high transparency, make PLA a promising material as packaging or container. However its high brittleness and poor barrier properties restrict its application domain. Such a latter property is required e.g., for packaging to preserve organoleptic food quality during shelf life by preventing alteration of food due to excessive oxygen or water vapour transfers or loss of aroma compounds (Berlinet, 2008; Dury-Brun, 2007).

The gas barrier properties of neat P(D,L)LA have been already studied, but mainly for amorphous films (Auras, 2004a; Komatsuka, 2008; Petersen, 2001). The oxygen barrier properties of amorphous P(D,L)LA are similar to the one of high density poly(ethylene) (HDPE) and intermediate between poly(ethylene terephthalate) (PET) and polystyrene (PS) (Auras, 2005b; Cava, 2006; Colomines, 2010; Sanchez-Garcia, 2007). Unlike gases, the organic molecule barrier properties of P(D,L)LA have been less extensively studied (Auras, 2006; Colomines, 2010; Haugaard, 2002; Mauricio-Iglesias, 2011). Auras *et al.* (Auras, 2006) showed that the solubility coefficient of limonene in P(D,L)LA is lower than the one in PET, PS, polypropylene (PP), HDPE and low density poly(ethylene) (LDPE) (Haugaard, 2002). Ethyl acetate (EA), a solvent largely used in inks and adhesives, showed on the contrary a comparatively higher solubility coefficient in P(D,L)LA. To give an example, the solubility coefficient of EA can be 2 fold higher in P(D,L)LA than in PET, PP and LDPE.

One way to improve the barrier properties of semi-crystalline polymers is to increase their crystallinity. Crystalline zones are presumed excluded volumes through which molecules

cannot diffuse and in which they cannot sorb (Michaels, 1961) in contrary to amorphous zones where diffusion is possible. However, according to the study of Kanehashi *et al.* (Kanehashi, 2010) on 300 crystalline or liquid crystalline polymers, the permeability and diffusion coefficients of gas are not significantly affected by the crystallinity at low crystallinity degree. The influence of crystallinity on the barrier properties has been rarely studied for PLA and has led to contradictory results due to the lack of knowledge about the crystalline structure of the materials studied, in particular in the case of P(D,L)LA.

The crystalline morphology of PLA depends on the stereochemistry (Sarasua, 1998), the crystallization kinetics (Di Lorenzo, 2006; Miyata, 1998), temperature (T_c), and the thermal history (cold or melt crystallization) (Ling, 2006a; Ling, 2006b; Pluta, 2002).

Furthermore, PLA is known for its low crystallization rate. Nevertheless similarly to other semi-crystalline polymers, decreasing the nucleation activation energy and increasing the mobility of the chain segments are keys elements to increase the PLA crystallization rate (Lai, 2004; Li, 2010; Xiao, 2009). An efficient way to decrease the nucleation activation is to add nucleating agent whereas the mobility of the chain segment can rise due to the addition of plasticizer.

Several nucleating agent have been tested on PLA. An example is the stereocomplex of P(L)LA and P(D)LA (Anderson, 2006; Schmidt, 2001), which induces a decrease of the crystallization half time of P(L)LA at an incorporation content less than 10 %. Some researches have shown that organic compounds can be successful in playing the role of a nucleating agent. N,N-ethylen-bis-12-hydroxystereamide leads to an increase of the nucleation density (multiplied by 10) and crystallization rate (from 5 to 20 times) (Harris, 2008; Nam, 2006). Kawamoto and al. have shown that other organic compounds based on hydrazide groups can increase the crystallization temperature upon cooling (Kawamoto, 2007). Other nucleating agents, such as sodium salts, calcium lactate, $CaCO_3$, TiO_2 and $BaSO_4$, have demonstrated a lower efficiency (Li, 2007; Liao, 2007). Data show that these substances are less efficient than talc, which is widely used as nucleating agent since the crystallization rate is 65 fold higher than the P(D,L)LA alone (Harris, 2008; Ke, 2003; Li, 2007).

Various types of plasticizers were used to modify the PLA properties, such as oligomeric lactic acid (Martin, 2001), triacetine (Ljungberg, 2002), diethyl bishydroxymethyl malonate (Ljungberg, 2005), poly(1,2-butanediol), dibutyl sebacate acetyl glycerol monolaurate (Pillin, 2006), triphenyl phosphate (Xiao, 2009), polyadipates (Martino, 2009; Martino, 2006), poly(propylene glycol) (Kulinski, 2005; Kulinski, 2006), poly(ethylene glycol) (Baiardo,

2003; Hu, 2003; Jacobsen, 1999; Kulinski, 2005; Martin, 2001), and acetyl tributyl citrate (Baiardo, 2003; Coltelli, 2008; Labrecque, 1997; Ljungberg, 2002). The major part of these plasticizers is approved for food contact ("2002/72/EC Commission Directive of 6 August 2002 relating to plastic materials and articles intended to come into contact with foodstuffs. " 2002; EFSA, 2006). According to literature, acetyl tributyl citrate seems to be the most efficient plasticizer because, in addition to be FDA approved, it efficiently decreases the glass transition temperatures and improves significantly the mechanical properties of P(D,L)LA (Baiardo, 2003; Coltelli, 2008; Courgneau, 2011; Labrecque, 1997).

Consequently, the formulation of P(D,L)LA with both talc and ATBC appears as a good way to increase the crystallization rate of P(D,L)LA and should induce an improvement of the barrier properties. The purpose of this paper is to assess the relationships between the crystallization and the gas (helium and oxygen) and ethyl acetate barrier properties, of neat and formulated P(D,L)LA. The mechanical properties were also tested on neat and formulated P(D,L)LA, before and after annealing. The crystalline structure of the neat and formulated recrystallized P(D,L)LA was determined by Differential Scanning Calorimetry (DSC) and with Wide Angle X-Ray Diffraction (WAXD).

4.2.3. Experimental

4.2.3.1. Materials

The polylactide pellets were provided by NatureWorks. The content of L-lactide was about 92 wt%. The average molecular weight was 9.0×10^4 g.mol^{-1} with a dispersity (Đ) of 2.75. Acetyl tributyl citrate (ATBC), used as a plasticizer, was purchased from Sigma Aldrich (France). Talc, used as a nucleating agent, was provided by RioTinto (Luzenac, France). Ethyl acetate and hexadecane were supplied by Sigma Aldrich (France).

4.2.3.2. Sample Preparation

P(D,L)LA pellets, plasticizer and nucleating agent were dried at 80 °C overnight in a vacuum oven. After that, the formulated P(D,L)LA samples were prepared by direct melt mixing of additives with P(D,L)LA in an internal mixer (Haake Rheocord 9000) at 160 °C and 60 rpm

for 15 min. Concentrations of ATBC and talc were 17 wt% and 1 wt% in the blend respectively.

To decrease the water content, the materials were dried during 4 h minimum at 80 °C before processing. P(D,L)LA samples were transformed by thermo-compression (Telemecanique, 15 Tons) at 185 °C and 150 bars to obtain a film of approximately 300 µm thickness. After compression, the films were quenched to ambient temperature. Non-annealed films were stored at ambient temperature in a desiccator with P_2O_5.

The films were annealed in a air-circulating oven (Angeltoni Climatic System Massa Martana Type TY80) at the recrystallization temperature (90 or 120 °C for neat PLA and 85 or 100 °C for the formulated one, respectively) during different durations (90 min for neat PLA and 10, 30 or 60 min for the formulated one, respectively).

4.2.3.3. Conditioning of PLA film in ethyl acetate atmosphere

The annealed P(D,L)LA film samples were equilibrated in an ethyl acetate atmosphere at 0.2 and 0.5 activity for two weeks in a hermetic vessel at 25 °C with the help of the method published by Colomines *et al.* (Colomines, 2010). The 0.2 and 0.5 activities were generated by 0.8 and 2.2 mol.L^{-1} ethyl acetate solutions in hexadecane, respectively, and controlled by gas chromatography. The activity is the ratio p/p_0 with p the partial pressure and p_0 the vapour pressure of ethyl acetate at saturation.

4.2.3.4. Analysis methods

4.2.3.4.1. Differential Scanning Calorimetry (DSC).

The thermal analyses were performed with an MDSC Q100 (TA Instruments) under nitrogen atmosphere. The samples (about 10 mg) were put into hermetic aluminium pans (TZero, TA Instruments). The standard mode was used to perform isotherm from cold state and to study the crystallization.

To investigate the kinetics of isothermal crystallization, neat and formulated P(D,L)LA were heated at 190 °C for 10 min to erase thermal history of the sample and then cooled to 20 °C and reheated to the crystallization temperature at 50 °C.min^{-1}. Hence the isothermal crystallization begins from 15 min.

The half-time of crystallization, $t_{1/2}$, is defined as the time at which half of the final crystallinity is developed. After 3h of crystallization, the sample is cooled down to room

temperature. Finally the sample is heated at 10 °C.min^{-1} to 190 °C to get the melt temperature. The equilibrium melting temperatures of neat and formulated P(D,L)LA is the intersection of the resulting straight line (T$_m$ = f (T$_{cc}$)) with the line T$_m$=T$_{cc}$.

A baseline was carried out with a sapphire at each temperature with the same thermal program than for P(D,L)LA samples.

For analyzing the crystallinity degree of samples (χ_c), heating scans were performed with a heating rate of 10 °C min^{-1} from -30 to 190 °C. The χ_c of neat P(D,L)LA was calculated with equation 1, where ΔH_m is the enthalpy of melting, ΔH_{cc} is the enthalpy of cold crystallization and ΔH_m^0 is enthalpy of fusion per gram of the perfect crystal of infinite size, being 93 J.g^{-1} (Fischer, 1973).

$$\chi_c = \frac{\Delta H_m - \Delta H_{cc}}{\Delta H_m^0}, \tag{1}$$

The equivalent crystallinity degree (χ_{ce}) of formulated P(D,L)LA was calculated with the Equation 2 where x_{PLA} is the mass fraction of P(D,L)LA in the formulated P(D,L)LA.

$$\chi_{ce} = x_{PLA} \times \frac{\Delta H_m - \Delta H_{cc}}{\Delta H_m^0}, \tag{2}$$

All experiments were carried out in triplicate.

4.2.3.4.2. Size Exclusion Chromatography (SEC)

The average molecular weights were measured by SEC using a Shimadzu apparatus equipped with an RID-10A refractive index detector and an SPD-M10A UV detector. The analyses were carried out at 30 °C and 0.8 mL.min^{-1} in chloroform on a PLgel 5µm Guard column and two PL Gel 5µm Mixed-C columns. The calibration was performed with PS standards from 580 to 1,650,000 g.mol^{-1}.

4.2.3.4.3. Wide Angle X-Ray Diffraction (WAXD)

The wide angle X-ray diffraction experiments were conducted at 50 kV, 35 mA, using CuKα radiation monochromatized with a graphite monochromator (Panalytical, X'Pert Pro MPD). The diffractograms were recorded for 2θ angles between 5 and 35° with a step size and time of 0.007° and 368.8 s, respectively.

4.2.3.4.4. Tensile test

The uniaxial tensile testing was carried out at room temperature and at 5 mm.min^{-1} with an Instron tensile testing machine (Instron Model 4507) equipped with pneumatic jaws on type I BA dumbbell shaped samples. The thickness of the samples varies from 200 to 300 µm. Each value is an average of 5 measurements.

4.2.3.4.5. Oxygen, helium and water vapour permeability

The direct measurement of the oxygen transmission rate (OTR) was monitored at 23 °C and 0 % RH with a Systech 8001 apparatus. The helium transmission rate (HeTR) was measured at room temperature and at a relative humidity varying between 40 and 60 % RH, by a specific analyser developed by CNAM (Paris, France), based on the ISO norm 15105-2:2003. Oxygen and helium permeability were then obtained by dividing respectively OTR and HeTR by the film thickness. Experiments were carried out in duplicate. The diffusion coefficients (*D* en m².s^{-1}) were estimated with the time-lag method according to the Equation 3, where *l* is the film thickness (m) and *θ* the time-lag (s). The time-lag is determined as the intercept of the time axis and the extrapolated linear steady state part of the curve for a representation of the amount of permeant passing through the film in time t versus time.

$$D = \frac{l^2}{6\theta} \ ,$$ (3)

In the helium case, the time lag accounted only for a few seconds causing poor repeatability in its determination. Consequently, the helium diffusion coefficients presented in this work is an approximate value to tentatively compare its order of magnitude with the diffusion coefficient of the other probes.

The solubility coefficients (*S*) were calculated by the general Equation 4, with *P* being the gas permeability

$$P = D \times S \ ,$$ (4)

4.2.3.4.6. Ethyl acetate sorption kinetics

The sorption isotherm of ethyl acetate (EA) was measured at 25 °C and 0 % RH with a static method, using an electronic microbalance (Intelligent Gravimetric Analyzer 002, Hiden Isochema Ltd.,Warrington, UK) with a sensitivity of 0.2 µg. The film samples (30-60 mg) were suspended from the microbalance by a stainless steel spiral which was contained in a thermoregulated cell, at 25 °C. The microbalance was maintained at 50 °C to ensure stability during the weight measurement by the prevention of the solvent condensation. Before the

measurement, the samples were purged for 24 hours at 10^{-5} mbar to remove all volatile compounds sorbed in the film and present in the chamber. Then the ethyl acetate partial pressure was set using a pressure transducer (Baratron®, MKS Instruments, Wilmington, Massachusetts, USA) linked to a tank with a vapour phase saturated in ethyl acetate. The mass uptake of the sample was recorded automatically with the time at 0.2 activity.

The apparent ethyl acetate solubility S (kg.m^{-3}.Pa^{-1}) was calculated according to the Equation 5, where m_{∞} is the equilibrium sorption obtained theoretically after infinite time (kg.kg^{-1}), d is the film density (kg.m^{-3}) and p the compound vapor partial pressure (Pa). Each sample was measured in duplicate.

$$S = m_{\infty} \times \frac{d}{p} ,$$ (5)

The microbalance is calibrated regularly during the maintenance periods for pressure, mass and temperature. The used methods were previously published by Colomines *et al.* (Colomines, 2010).

4.2.3.4.7. Estimation of EA diffusion coefficient

In case of formulated P(D,L)LA, the diffusion coefficient was calculated from the Equation 6, where m_{∞} is the equilibrium sorption obtained theoretically after infinite time (kg.kg^{-1}), m_t, the mass at time t (s), l, the thickness of the film (m) and D, the diffusion coefficient (m².s^{-1}).

$$\frac{m_t}{m_{\infty}} = \left(\frac{16 \times D}{\pi \times l^2} \right)^{1/2} \sqrt{t} ,$$ (6)

In case of neat non-annealed and recrystallized P(D,L)LA, the equilibrium was not reached. Consequently the diffusion coefficients have been estimated with the Equation 6 from equilibrium state experiments carried out at higher temperature.

4.2.3.4.8. Statistical analysis

The statistical analysis was done with a one-way ANalysis Of VAriance (ANOVA). When the differences were significant ($p < 0.05$), Fischer's test was used to check the differences between pairs of groups and was carried out using XLSTAT-Pro 7.0 software (Addinsoft, Paris, France). Statistical analysis has been carried out separately for neat P(D,L)LA and formulated P(D,L)LA.

4.2.4. Results and discussion

4.2.4.1. Optimization of crystallization conditions

The melting temperatures versus the cold crystallization temperatures for neat and formulated PLA are plotted in Figure 1. The equilibrium melting temperature was calculated at 173.5 °C for neat P(D,L)LA. This temperature decreases with the addition of ATBC and talc to 163.5 °C. The melting point depression is noticeably higher than the one marked by Xiao *et al.* with 15 wt% of triphenyl phosphate in P(D,L)LA (Xiao, 2010b).
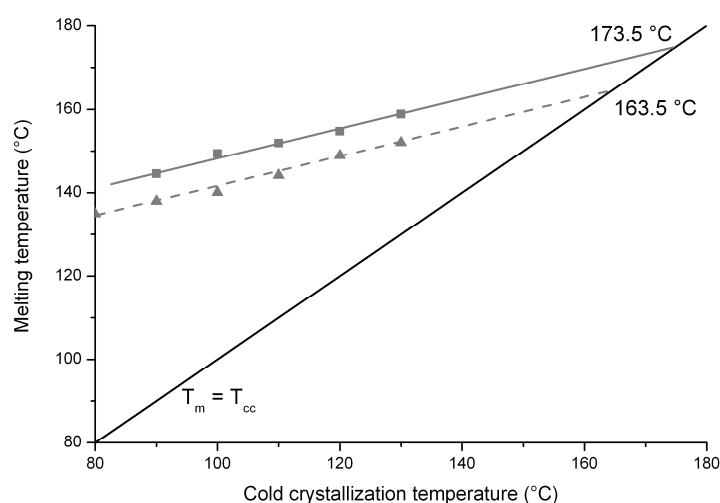
Figure 1. Hoffman-Weeks plots for neat (■) and formulated (▲) PLA.

According the literature (Kawai, 2007; Pan, 2009; Pan, 2007; Zhang, 2008), PLA may crystallize during thermal treatment under 2 forms, the α and α' form. A high crystallization temperature (Tc > 130 °C) induces the formation of α-form whereas a low Tc (80 °C < Tc < 110 °C) leads to the formation of an α'-form (disordered α-form). In the range of 110 to 130 °C, the forms α and α' coexist (Kawai, 2007; Pan, 2009; Zhang, 2008). To evaluate the influence of the polymorphism with a constant crystallinity degree on the mechanical and barrier properties, two cold crystallization temperatures were chosen for neat P(D,L)LA: 90 °C to obtain an α-form and 120 °C to assure the formation of the ordered and disordered α-form. The degree of undercooling of neat P(D,L)LA is evaluated at 54 and 35 °C for 90 and 120 °C, respectively.

As the optimum melting temperature decreases with the formulation, lower cold crystallization temperatures, 85 and 100 °C, were selected to crystallize the formulated

samples in the oven. The degree of undercooling of formulated P(D,L)LA is then evaluated at 52 and 40 °C for, 85 and 100 °C, respectively.
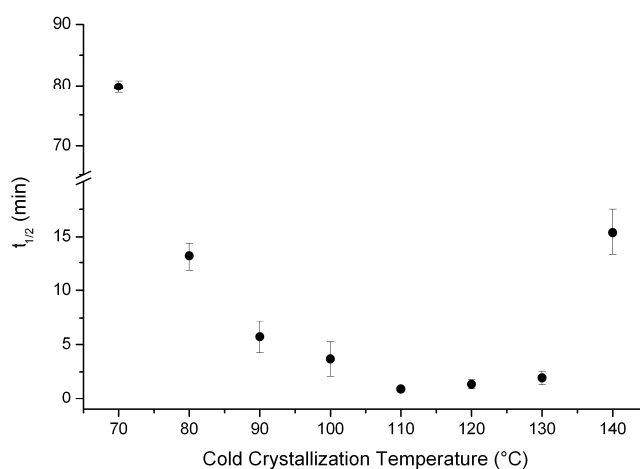
Figure 2. Half-time of crystallization of neat P(D,L)LA as a function of isothermal cold crystallization temperature.

The half-time of crystallization ($t_{1/2}$) of neat P(D,L)LA measured in isothermal conditions after cooling from the melt is plotted in Figure 2 as a function of the cold crystallization temperature. The optimum $t_{1/2}$, 1.5 min, is measured at 110 °C.

Crystallization isotherms were performed by DSC to determine the crystallization duration to obtain fully crystallized samples. As shown in Figure 3, the crystallization peak time of neat P(D,L)LA was observed at 5.9 and 0.5 min, at 90 and 120 °C, respectively. Moreover, as shown in Figure 2, the half-time of crystallization, at 90 and 120 °C, is below 5 min. Hence, to assure the full crystallization of the sample in the oven, the annealing time is chosen to be more than 20 times the neat P(D,L)LA $t_{1/2}$, i.e. for 90 min at both temperatures.

As expected, the formulation increases the crystallization rate. The isotherms of the formulated P(D,L)LA show a sharp peak at 0.1 min at 85 °C (Figure 3). In the case of crystallization at 100 °C, the crystallization peak was completed after 1.5 min, a time which was completely inside the phase of temperature stabilization of our DSC apparatus. To assess the influence of crystallization duration and crystal perfection, the formulated samples were crystallized for 10 and 30 min at 85 °C and 10, 30 and 60 min at 100 °C, which is much larger that the presumed half-time of crystallization of formulated P(D,L)LA.
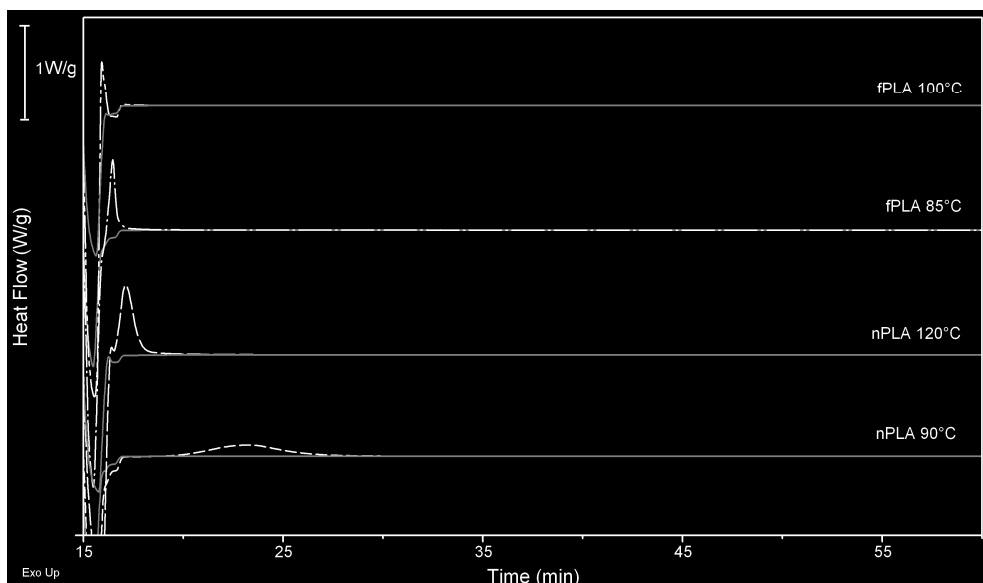
Figure 3. DSC thermograms for neat and formulated P(D,L)LA (black lines) during isothermal cold crystallization at 90 and 120 °C for neat P(D,L)LA and 85 and 100 °C for formulated P(D,L)LA. Baseline, obtained with sapphire at each crystallization temperature, are grey solid lines. The curves were vertically shifted for legibility.

4.2.4.2. Characterization of the crystal structure and mechanical properties.

Results obtained on the crystallinity degrees of the non-annealed and annealed neat and formulated P(D,L)LA samples are listed in Table 1. The DSC data show an increase in the crystallinity degree with the recrystallization temperature for the neat PLA. Film samples annealed in the oven show smaller crystallinity degrees, most probably due to a less well controlled temperature. In the case of DSC annealing the crystallinity degree reached 52 %, whereas in the oven maximum was recorded at 43 %. The crystallization conditions did not lead to a change in the crystallinity degree of the formulated P(D,L)LA. The crystallinity degree reached around 31 %, whatever the crystallization temperature and duration, which was lower than the one observed in the case of the neat sample.

A decrease in the crystallinity degree with plasticization was also observed by Xiao *et al.* (Xiao, 2010a) for P(D,L)LA-based blends with triphenyl phosphate. The formulated samples annealed at 85 °C for 10 min showed discrepancy between the DSC experiment and samples annealed in the oven, which could be attributed to a temperature gradient in the oven. PLA is highly sensitive to thermal treatments which may induce a decrease in the molecular weight (Harris, 2010; Lim, 2008) mainly due to hydrolysis. Therefore, the polymer molecular weights were analysed and are given in Table 1.

Table 1. Crystallinity degree of neat and formulated P(D,L)LA samples after recrystallization in the DSC oven and in the ventilated oven. Number and weight average molecular mass (M_n and M_w) of P(D,L)LA pellets, amorphous and recrystallized neat and formulated P(D,L)LA. Mechanical properties of the neat and formulated PLA samples, before and after recrystallization.

	Recrystallization conditions	Notation of the samples	Crystallinity degree (%)		M_n (g mol^{-1})	M_w (g mol^{-1})	Stress (MPa)	Elongation at break (%)	Young Modulus (MPa)
			in the DSC apparatus	in the oven					
P(D,L)LA pellets	-	-	-	-	90 500	248 900	-	-	-
Neat P(D,L)LA	-	(a)	-	-	55 350	103 100	40.9 ± 3.5 [a]	5 ± 2 [a]	1398 ± 23 [a]
	90 °C, 1 h 30	(b)	46	36 ± 2	56 850	109 900	46.4 ± 8.3 [a]	5 ± 2 [a]	1216 ± 106 [b]
	120 °C, 1 h 30	(c)	52	43 ± 1	66 250	122 050	53.0 ± 1.0 [b]	5 ± 1 [a]	1287 ± 22 [b]
Formulated P(D,L)LA	-	(d)	-	-	44 000	82 800	15.8 ± 0.8 [a]	477 ± 20 [a]	38 ± 16 [a]
	85 °C, 10 min	(e)	37	3 ± 3	55 350	106 050	19.4 ± 4.4 [b]	523 ± 103 [a]	84 ± 24 [b]
	85 °C, 30 min	(f)	38	32 ± 1	54 450	93 500	20.0 ± 2.6 [b]	59 ± 24 [b]	347 ± 21 [d]
	100 °C, 10 min	(g)	38	31 ± 1	43 100	74 850	18.9 ± 0.4 [b]	86 ± 22 [b]	304 ± 13 [c]
	100 °C, 30 min	(h)	n.d.	31 ± 2	41 000	93 950	19.7 ± 1.8 [b]	59 ± 30 [b]	379 ± 53 [e]
	100 °C, 1 h	(i)	39	30 ± 1	48 500	107 550	18.9 ± 1.1 [b]	66 ± 32 [b]	349 ± 32 [d,e]

n.d.: not determined

[a,b,c,d,e] : significant differences at $p < 0.05$ (Fischer); Statistical analysis has been carried out separately for neat PLA and formulated PLA.

The molecular weights of neat and formulated PLA film are 103,000 and 83,000 g.mol^{-1} respectively, indicating a degradation phenomenon during the blending step. No significant decrease in the molecular weight is noticed during the annealing in the oven for the different systems.

Figure 4 shows the thermograms of neat and formulated P(D,L)LA after recrystallization. The melting behaviour depends on the crystallization temperature and consequently on the crystal form. As shown in Figure 4a, the non-annealed neat P(D,L)LA shows cold crystallization during heating. The exotherm is followed by two endotherms spanning from 140 to 160 °C. The sample recrystallized at 90 °C displays small exotherm prior to the single melting endotherm whereas the sample recrystallized at 120 °C shows a double melting peak. According to Pan and Inoue (Pan, 2009), the exotherm prior to the melting peak is due to the transformation of the α'-form crystal into α-form upon heating. The explanation is different for the usual double endotherm. According to Shieh and Liu (Shieh, 2007), the occurrence of the double melting peak may be explained by a melting-recrystallization mechanism. They suggest that the first melting peak is due to the melting of crystals formed during heating or during the recrystallization step at a temperature between 110 and 130 °C while the second peak corresponds to the melting of the more perfect crystals which were formed in the partially molten material.

Figure 4b shows the thermograms of the non-annealed and recrystallized formulated P(D,L)LA. As expected, the formulation of non-annealed and amorphous P(D,L)LA induces a decrease in the temperature of the thermal transitions compared to non-annealed and amorphous neat P(D,L)LA (Figure 4). The plasticizer addition leads to an increase in the free volume and a decrease in the polymer chain interactions which yields higher chain mobility at lower temperature. Then, the glass transition temperature of the non-annealed samples drops from 58.1 to 28.6 °C with the formulation (Table 2) whereas the cold crystallization temperature decreases from 110 to 80 °C.

The formulated recrystallized P(D,L)LA samples display no cold crystallization peak, except for 85 °C/10 min. The crystallization peak, pointing between 70 and 80 °C, is followed by the melting peaks, a small one around 130 °C and the dominant one at 150 °C. This double endotherm is also visible for the sample recrystallized 10 min at 100 °C.

Apparently, short recrystallization durations do not allow for crystal perfection and show therefore a melting-recrystallization phenomenon, whereas at longer duration perfect α-forms are obtained.
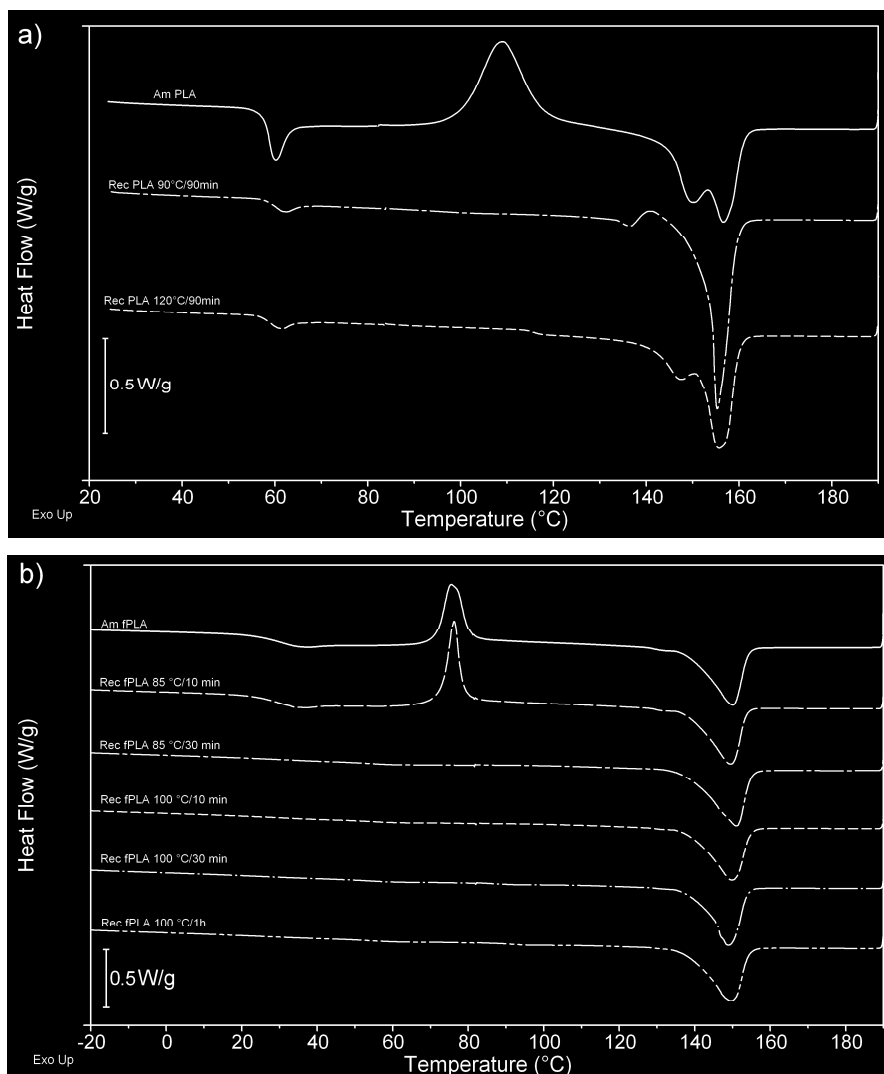
Figure 4. DSC thermograms for neat P(D,L)LA (a) and formulated P(D,L)LA (b) heated at 10 °C.min⁻¹ after isothermal cold crystallization. The curves were vertically shifted for legibility.

Table 2. Glass transition temperature and crystallinity degree of neat and formulated P(D,L)LA by DSC and WAXD before and after contact with ethyl acetate (EA) for two weeks at 0.2 and 0.5 activity and 25 °C.

Samples	Recrystallization conditions	Glass transition temperature (°C)			Crystallinity degree (%) by DSC			Crystallinity degree (%) by WAXS		Crystalline form	
		Before EA contact	After EA contact 0.2 activity	After EA contact 0.5 activity	Before EA contact	After EA contact 0.2 activity	After EA contact 0.5 activity	Before EA contact	After EA contact 0.5 activity	Before EA contact	After EA contact 0.5 activity
Neat P(D,L)LA	-	58.1 ± 1.2	27.1 ± 0.8	19.5 ± 2.3	3 ± 1	26 ± 1	37 ± 4	0.5	33	amorphous	α
	90 °C, 1h30	58.7 ± 0.7	n.d.	20.3 ± 1.1	36 ± 2	n.d.	30 ± 1	31	35	α'	α'
	120 °C, 1h30	58.4 ± 0.7	59.3 ± 0.3	19.6 ± 0.7	43 ± 1	44 ± 1	39 ± 2	40	43	α	α
Formulated P(D,L)LA	-	28.6 ± 0.6	8.3 ± 0.2	4.4 ± 0.1	2 ± 1	31 ± 3	34 ± 1	2	21	amorphous	α ,α'
	85 °C, 30 min	25.1 ± 3.2	16.4 ± 0.1	9.8 ± 0.1	32 ± 1	34 ± 1	31 ± 1	34	34	α ,α'	α ,α'
	100 °C, 1h	24.6 ± 3.0	16.4 ± 0.2	11.3 ± 0.7	30 ± 1	33 ± 1	29 ± 1	38	41	α ,α'	α ,α'

n.d.: not determined

206

The WAXD patterns of neat and formulated recrystallized samples are depicted in Figure 5. Distinct diffractions peaks were observed for the neat recrystallized samples according to the annealing temperature. As given in literature (Cho, 2003; Kawai, 2007; Pan, 2009; Zhang, 2008), the samples recrystallized at 90 °C exhibit an α'-form crystal structure characterized by intense peaks at 16.5° and 18.9°, due to the diffraction from (200) and/or (110) planes and to the arising from (203) plane, respectively. Weak reflections are also observed at 12.3, 14.7 and 22.2° due to the diffraction from the (103), (010) and (015) planes. A weak peak is also seen at 24.7° which is also characteristic of the α'-form (Pan, 2007). The sample recrystallized at 120 °C presents a shift of the most two intense peaks to 16.7 and 19.1°. Moreover these samples show an increase of the intensity of the peaks at 12.3 and 22.2 ° and the appearance of peaks at 20.8, 23.0, 24.0 and 25.1° which are fully characteristic of the α-form. These data confirmed the formation of the α'-form at low crystallization temperature (below 100 °C) and of the α-form at higher crystallization temperature (above 120 °C) (Kawai, 2007; Pan, 2009; Zhang, 2008).
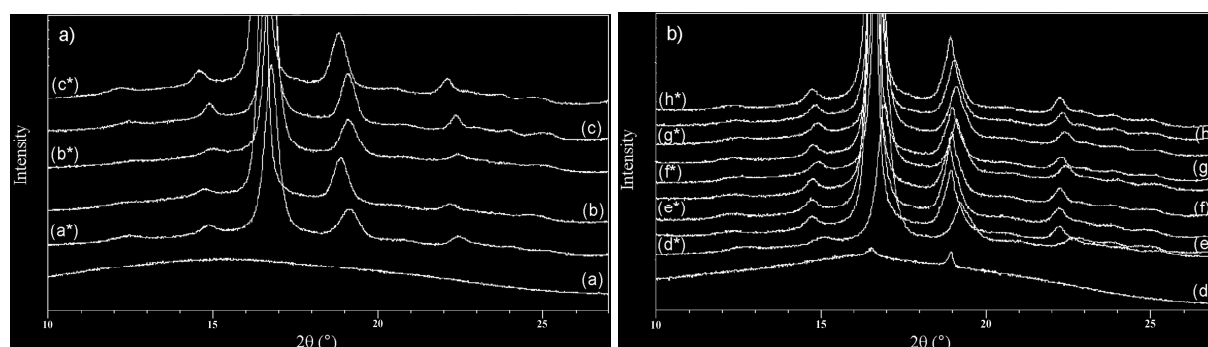
Figure 5. WAXD patterns for a) neat PLA and b) formulated PLA before and after contact with ethyl acetate. The correspondence of letter notation is done in Table 1. The samples after contact are noted with (*).

The formulated crystallized P(D,L)LA presented similar WAXD pattern to the one of neat P(D,L)LA and the peaks at 9.7 and 28.6° (not shown) characteristic of the talc. Whatever the crystallization temperature and time, the formulated samples showed similar 2θ values and intensities. As shown in Figure 5, the profile seems similar than the one of the neat P(D,L)LA recrystallized at 90 °C but a slight shift of the peak from 18.9 to 19.0° and the appearance of a peak at 23.8° are noticed. To conclude, WAXD pattern seem to be a combination of α and α'-forms whatever the crystallization temperature and time used for the formulated samples.

Therefore, contrary to the neat P(D,L)LA which presents distinct crystal structure according to the crystallization temperature, the formulated P(D,L)LA seems to not be affected by the

annealing conditions at 85 and 100 °C by crystallizing under a combination of α and α'-forms. This absence of modification induced by the formulation and the different annealing conditions, is confirmed by Xiao *et al.* (Xiao, 2010b) in the case of triphenyl phosphate and by Piorkowska *et al.* (Piorkowska, 2006) with PEG and poly(propylene glycol).

Non-annealed amorphous P(D,L)LA displays a moderate Young's Modulus and maximum stress and a low elongation at break (Figure 6) (Auras, 2004b; Coltelli, 2008; Jia, 2009; Murariu, 2008).
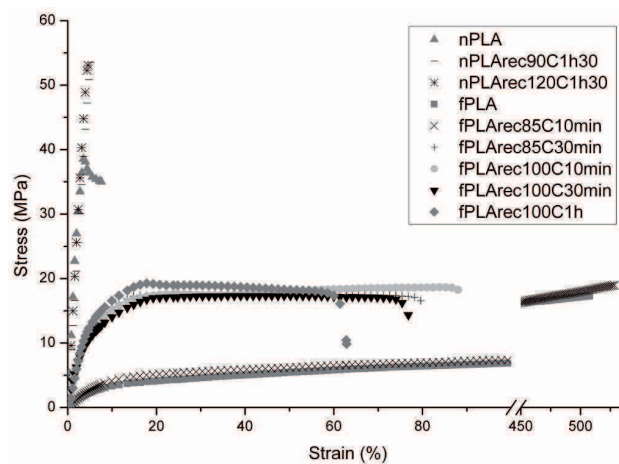
Figure 6. Stress-elongation curves of neat (nPLA) and formulated PLA (fPLA).

As shown in Table 1, the recrystallization of neat P(D,L)LA induces no significant modification of the mechanical properties. The recrystallized neat P(D,L)LA shows brittle fracture. The elongations at break are below 5 % and the maximum stresses are around 50 MPa whatever the recrystallization temperature. As expected, the formulation with 17 wt% of ATBC and 1 wt% of talc leads to a dramatic rise in the elongation at break and a decrease in the maximum stress which reach 477 % and 15.8 MPa respectively (Figure 6) (Baiardo, 2003; Coltelli, 2008; Labrecque, 1997; Yu, 2008). The result is due to the addition of plasticizer which facilitates polymer chain slippage during the tensile tests (Kulinski, 2005).

Contrary to neat P(D,L)LA, formulated P(D,L)LAs show modification in the mechanical properties upon increase of the crystallinity degree. At around 30 % of crystallinity, the annealed formulated samples show an elongation at break divided by 8 compared to the non-annealed formulated P(D,L)LA. Moreover the maximum stresses remain steady whereas the Young moduli increase with the recrystallization conditions.

According to Kulinski and Piorkowska (Kulinski, 2005), the diverse lamellae orientations induce different local stresses and strains which may lead to localized fractures. These

fractures weaken the plasticized material which provokes a decrease in the elongation at break. Moreover it has been observed that the crystallization of the plasticized P(D,L)LA exudes the plasticizer into the amorphous phase at the interspherulitic boundaries and at the spherulite peripheries (Piorkowska, 2006). This significant local concentration of plasticizer may weaken the links between lamellae or among neighbouring spherulites thus causing fissures in case of stress.

4.2.4.3. Effect of crystallization on the barrier properties

The helium and oxygen transport coefficients and the ethyl acetate diffusion and apparent solubility coefficients are listed in Table 3. The well-known Equation 3 makes it possible to link the permeability coefficient P of helium or oxygen to a kinetic parameter, the diffusion coefficient D, and to a thermodynamic parameter, the solubility coefficient S. D is related to the polymer structure and takes into account the free volume of the matrix and the tortuosity. S is dependent on the solubility of the gas molecules or aroma compounds in the material. Helium is considered as an inert gas contrary to oxygen which may interact with polymer and additives. Ethyl acetate is an organic vapour, and miscible with PLA and ATBC.

As shown in Table 3, the helium permeability coefficients of non-annealed neat P(D,L)LA are not significantly modified by the addition of plasticizer and nucleating agent. It is probably due to the low interaction of helium with the matrix and the plasticizer. The crystallization of neat P(D,L)LA samples induces a significant decrease of the helium permeability coefficient although they keep the same order of magnitude. This trend is not retrieved in the case of the crystallized formulated P(D,L)LA. The decrease in the gas permeability coefficients is often explained in literature (Drieskens, 2009) by the inclusion of spherulites in the polymer matrix. These impermeable spherulites diminish the amorphous fraction through which the gas molecules can permeate and then affect the gas solubility. Moreover the crystals rise the tortuosity of the gas molecules routes and consequently modify their diffusion coefficients.

Contrary to the expectations, the apparent helium diffusion coefficient has an approximate value of 3.10^{-11} m².s^{-1} in neat P(D,L)LA and seemed to increase with the crystallization up to 1×10^{-10} m².s^{-1}. However, in accordance to expectation, the increase in crystallinity degree of samples likely affected the apparent solubility coefficient which slightly decreased from 7 to 0.7×10^{-6} m^3.m^{-3}.Pa^{-1} upon crystallization.

Table 3. Helium (He) and oxygen (O_2) permeability and oxygen and ethyl acetate (EA) diffusion and solubility coefficients in neat and formulated P(D,L)LA before and after recrystallization. The helium and oxygen data of P(D,L)LA with 2 wt% of talc and P(D,L)LA with 17 wt% of ATBC are given as references.

Samples	Recristallization conditions	χ (%)	crystalline form	$P_{He} \times 10^{18}$ ($m^3.m.m^{-2}.s^{-1};Pa^{-1}$)	$P_{O2} \times 10^{18}$ ($m^3.m.m^{-2}.s^{-1}.Pa^{-1}$)	$D_{O2} \times 10^{12}$ ($m^2.s^{-1}$)	$S_{O2} \times 10^6$ ($m^3.m^{-3}.Pa^{-1}$)	$D_{EA} \times 10^{17}$ ($m^2.s^{-1}$)	$S_{EA} \times 10^6$ ($m^3.m^{-3}.Pa^{-1}$)
Neat P(D,L)LA	-	3 ± 1	amorphous	100.9 ± 6.4 [a]	2.30 ± 0.09 [a]	1.37 ± 0.29 [a]	1.7 ± 0.3 [a]	2.4	1.3×10^{-1}
	90 °C, 1h30	36 ± 2	α'	88.2 ± 6.9 [b]	1.96 ± 0.08 [b]	2.21 ± 0.01 [a]	0.9 ± 0.1 [b]	n.d.	1.2×10^{-1}
	120 °C, 1h30	43 ± 1	α	70.7 ± 1.4 [c]	1.32 ± 0.16 [b]	2.05 ± 0.60 [a]	0.7 ± 0.1 [b]	1.6	n.d.
P(D,L)LA / 2 wt% talc	-	6 ± 1	amorphous	110.2 ± 8.9	2.17 ± 0.02	2.02 ± 0.68	1.1 ± 0.1	n.d.	n.d.
P(D,L)LA / 17 wt% ATBC	-	2 ± 1	amorphous	98.0 ± 6.7	5.01 ± 0.29	3.71 ± 0.67	1.4 ± 0.2	n.d.	n.d.
Formulated P(D,L)LA (PLA/1wt%talc /17wt%ATBC)	-	2 ± 1	amorphous	106.6 ± 11.2 [a]	4.49 ± 0.95 [a]	6.03 ± 1.38 [a]	0.8 ± 0.2 [a]	1×10^4	14.5
	85 °C, 30 min	32 ± 1	α ,α'	97.6 ± 14.7 [a]	7.10 ± 0.12 [b]	7.49 ± 0.12 [a]	1.0 ± 0.1 [a]	5×10^4	15.2
	100 °C, 30 min	31 ± 2	α ,α'	99.0 ± 6.5 [a]	6.84 ± 0.92 [b]	8.10 ± 0.98 [a]	0.8 ± 0.1 [a]	n.d.	n.d.
	100 °C, 1h	30 ± 1	α ,α'	100.9 ± 7.8 [a]	7.62 [b]	9.65 [a]	0.8 [a]	7×10^4	9.4

[a,b,c,d,e] significant differences at $p < 0.05$ (Fischer). Statistical analysis has been carried out separately for neat PLA and formulated PLA.

n.d. non determined.

The value of the oxygen permeability of neat non-annealed P(D,L)LA (Table 3) is in agreement with the literature (Auras, 2004a; Bao, 2006; Petersen, 2001; Sanchez-Garcia, 2007). The corresponding diffusion coefficient, is close to those obtained by Sawada *et al.* (Komatsuka, 2008; Sawada, 2010) at 35 °C but lesser than those given by Bao *et al.* (Bao, 2006) for an amorphous sample at 30 °C. Contrary to helium, the oxygen transport coefficients vary with the formulation. The oxygen permeability and diffusion coefficient doubled and even quadrupled respectively for formulated P(D,L)LA compared to neat P(D,L)LA. The oxygen transport properties are affected by the test temperature, which is close to the T_g for the formulated P(D,L)LA. This may induce an increase of the transport coefficients. Moreover, according to literature, the diffusion of the gas molecules is closely linked to the free volume of the amorphous phase. Consequently, the rise in the free volume linked to the formulation might induce an increase in the diffusion coefficient and consequently in the permeability coefficient of oxygen for the non-annealed PLA (Ahn, 2008; Coltelli, 2008; Jang, 2004; McGonigle, 2001).

As expected and noticed for helium, the crystallization of neat P(D,L)LA samples induces a decrease in oxygen permeability coefficient although they keep the same order of magnitude. This evolution is not directly linked to the crystalline form since, despite different crystalline structure, both neat recrystallized P(D,L)LAs present similar diffusion coefficients.

Contrary to neat PLA, the oxygen permeability coefficient of formulated P(D,L)LA increases slightly with the crystallization. Crystallization in formulated P(D,L)LA may induce plasticizer segregation towards the amorphous phase leading to an increase of approximately 30 % of the plasticizer content in the remaining amorphous phase. Courgneau *et al.* (Courgneau, 2011) showed that the oxygen permeability in amorphous P(D,L)LA evolves with the plasticizer content. Consequently the enhanced oxygen permeability confirms the plasticizer enrichment of the amorphous phase with the crystallization of the formulated P(D,L)LA. Moreover according to Kulinski and Piorkowska (Kulinski, 2005), the presence of high content of plasticizer could induce accumulation of plasticizer outside the growing spherulites causing weakness of interspherulitic boundaries. Therefore, different local stresses and strains may lead to localized crazing cracks creating routes for transport of the gaseous molecules. This increase in the oxygen permeability may confirm the weakness of the crystallized formulated P(D,L)LA observed previously by tensile tests. No significant modification of the oxygen diffusion coefficient was noticed with the crystallization for neat or formulated P(D,L)LAs, though. This surprising result might be caused by a dedensification of the amorphous phase or by the appearance of a rigid amorphous fraction created by the

P(D,L)LA crystallization. The dedensification phenomenon has been shown by several authors for PET (Hu, 2005; Lin, 2002; Qureshi, 2000) and PEN (Hu, 2002) and suggested for P(D,L)LA (Colomines, 2010). For instance, Hu *et al.* (Hu, 2002) showed that the decrease in amorphous phase density of PEN, resulting from the crystallization, caused a significant rise in oxygen diffusion and solubility coefficients of the amorphous phase thus hindering the improvement of the gas barrier properties of the material. The concept of three phases with a mobile amorphous fraction (MAF), a rigid amorphous fraction (RAF) and a crystalline phase has also been suggested to explain the evolution of the oxygen diffusion coefficient. In the heterogeneous stack model, the RAF is located between adjacent lamellae within spherulites and hence the MAF is at the interspherulitic boundaries (del Rio, 2010). Drieskens *et al.* (Drieskens, 2009) suggested that the RAF was less dense than MAF which could create preferential ways for oxygen molecules through the P(D,L)LA samples. According to Sawada *et al.* (Sawada, 2010), the increase in the crystallinity degree, i.e. the arrangement of the polymer chains in lamellas, induces the formation of continuous pathway. In the case of a gas molecule which volume is smaller than the interlamellar space, diffusion would be facilitated. They showed an increase of permeation for H_2, O_2, N_2 and CH_4 in P(D,L)LA up to 20 % of crystallinity, and a slow down starting around 40 %. They explained the behaviour by the junction of crystal lamellae (Sawada, 2010). In our case a decrease of the diffusion coefficient with higher degree of crystallinity was not observed in the case of the neat samples.

We showed furthermore that the oxygen solubility coefficients of neat P(D,L)LA decrease with the increase in the crystallinity degree but *without* being affected by the crystalline type (α vs. α'-form). The decrease of the solubility coefficient is an expected result, considering that the creation of crystalline structure lowers the amount of amorphous phase available for gas sorption. Such behaviour has also been experimentally observed in the case of PET (Natu, 2005; Sekelik, 1999).

These effects of the crystallization on the diffusion and solubility coefficient contradict the previous results of Driesken *et al.* (Drieskens, 2009), who reported an oxygen diffusion coefficient divided by 5 and an oxygen solubility coefficient multiplied by 3 with the increase of crystallinity degree, from 0 to around 40 %. However the results of gas solubility are in accordance with Sawada *et al.* (Sawada, 2010) who showed a slight decrease of oxygen solubility with the crystallization.

Experiments were then carried out with a far more interacting molecule, ethyl acetate. Already sorption experiments showed a large influence of formulation on the sorption coefficient, which increased two orders of magnitude compared to neat samples probably due

to miscibility of EA with ATBC. However the crystallization of neat and formulated P(D,L)LA did *not* modify the apparent EA solubility coefficient. The constancy of the apparent solubility coefficient despite the annealing of neat and formulated P(D,L)LA is not consistent with the Henry sorption model. This suggests that at 0.2 activity of EA the structure of the samples is modified during the experiment by the contact with the organic compound. As reported by Colomines *et al.* (Colomines, 2010) and Naga *et al.* (Naga, 2011), the contact with organic vapours, such as EA, leads to plasticization and the solvent induced on the crystallization of the samples.

As in the case of oxygen, the EA diffusion coefficient in neat P(D,L)LA was not modified by crystallization. The annealing of the formulated samples showed even a slight increase in the EA diffusion coefficient, although values stay in the same order of magnitude. In the EA case, the dedensification hypothesis seemed to be unlikely due to the size of the molecule. Therefore the effect of EA on the P(D,L)LA structure was investigated more thoroughly by conditioning the different samples in EA atmosphere at 0.2 activity.

Data on the glass transition and crystallinity degree are given in Table 2. The glass transition temperature was measured during the first heating scan although the enthalpic relaxation peak was superposed on the T_g signal. As already observed by Colomines *et al.* (Colomines, 2010) EA acts as a plasticizer of P(D,L)LA, which causes the T_g to shift near or even below the measuring temperature of the sorption experiment being 23 °C. The sorption measurement is in this case done in the glass transition region which most likely explains the observed increase of the diffusion coefficient. Moreover, as shown by Colomines *et al.* (Colomines, 2010), the thermal recrystallization did not induce any difference in the decrease of T_g of the neat P(D,L)LA, whereas a gap of 5 °C is seen between the non-annealed and the annealed formulated P(D,L)LA.

The assessment of the crystallinity degree shows, for the non-annealed samples a strong increase in crystallinity degree. In order to further study the EA induced crystallization, samples were conditioned in EA atmosphere at higher activity (0.5) and crystallinity was analyzed by DSC and WAXD. The results are summarized in Table 2 and Figure 5. The non-annealed neat sample showed a single melting peak in DSC which may be attributed to the formation of α-form by EA contact. This behaviour was confirmed by WAXD which show the appearance of peaks, characteristic of the α-form.

On the contrary, no modification of the crystallinity degree was observed for the annealed neat P(D,L)LA, as well by DSC than by WAXD. Moreover, these samples exhibit, after EA contact, thermograms and WAXD patterns similar to those before contact, which mean that

no modification of the crystal structure is induced by EA contact for the annealed neat P(D,L)LA.

The non-annealed formulated P(D,L)LA crystallized up to 21 % whereas the annealed formulated P(D,L)LA did not show any increase in the crystallinity degree. The WAXD pattern of non-annealed formulated P(D,L)LA showed intense peaks after EA vapour contact in agreement with the induced crystallization having both, α and α'-form crystals. No significant modification was observed on the annealed and formulated P(D,L)LA pattern which means that the EA contact did not modify the structure of the formulated P(D,L)LA previously crystallized.

4.2.5. Conclusions

Crystallization of neat and formulated P(D,L)LA was investigated regarding its impact on barrier properties. Different types of behaviour are noticed according to the probe molecule. In particular, helium is sensitive to the density variation between amorphous and crystalline phase of the polymer matrix, oxygen to free volume of amorphous phase and ethyl acetate presents high chemical interaction with the polymer.

Hence helium permeability coefficient decreased with the crystallization and was found independent on the polymer formulation. Two different behaviours were observed for oxygen transport coefficients: (i) in the case of neat P(D,L)LA, the permeability coefficient slightly decreases whereas the diffusion coefficient increases with the crystallinity degree. This behaviour may be explained by the dedensification of the interspherulitic amorphous phase which creates pathways for the oxygen molecules. (ii) in the case of formulated P(D,L)LA, the permeability coefficient increases upon crystallization due to the plasticizer enrichment of the amorphous phase, resulting in an increase in oxygen diffusion coefficient. No impact of P(D,L)LA polymorphism (α- and α'-form) on gas barrier properties was observed in this work for both probe molecules. The behaviour of P(D,L)LA with EA is much more complex because of its interaction with the matrix. The vapour contact with this organic molecule induces the plasticization and the crystallization of amorphous neat P(D,L)LA in α-form and in a combination of α- and α'-form in the case of non-annealed formulated P(D,L)LA. Consequently, in comparison with annealing, the contact with EA vapour appears as an easy and innovative way to crystallize P(D,L)LA into α-form.

The relationship barrier properties/PLA microstructure is complex and dependent on the probe used. To date to reach a consensus between authors and a clear conclusion, works still need to be pursued in order to understand the effect of PLA microstructure on gas barrier properties. Moreover our work highlights the importance of considering chemical interaction of organic vapours with PLA structure in the development of PLA commodity applications.

4.2.6. Discussion et commentaires

Cette étude a porté sur l'effet de la structure cristalline sur les propriétés barrière de P(D,L)LA CD92 pur et formulé avec un agent nucléant et un plastifiant. De plus, une comparaison des formes cristallines du P(D,L)LA pur et formulé, cristallisé par traitement thermique à différentes températures et par contact avec une molécule organique, a été effectuée par analyse DRX.

Cette étude a mis en évidence une dépendance à la température de cristallisation de la forme cristalline formée pour le P(D,L)LA pur alors que le P(D,L)LA formulé ne cristallise que sous un mélange de forme α et α'. L'analyse subséquente des propriétés barrière des échantillons cristallisés a montré que la forme cristalline ne semblait pas influer sur les propriétés barrière. Néanmoins une diminution de la perméabilité à l'hélium et à l'oxygène est notée avec l'augmentation de la cristallinité du P(D,L)LA pur alors que le coefficient de diffusion ne varie pas, ce qui est contraire à ce qui est généralement montré dans la littérature.

L'étude de l'influence du contact avec l'acétate d'éthyle en phase vapeur, réalisée dans la publication 4 avec des P(D,L)LA Biomer L9000 purs de cristallinité variable, a été poursuivie dans la publication 5 sur des échantillons de P(D,L)LA CD92 pur et formulé. Il a été ainsi mis en évidence que le contact avec l'acétate d'éthyle, à une activité de 0,5, conduit à une plastification et une cristallisation des échantillons aussi bien pur que formulé. De plus, l'analyse de la structure cristalline résultant du contact avec l'acétate d'éthyle montre que le P(D,L)LA pur cristallise sous une forme α alors que le P(D,L)LA formulé cristallise sous la forme d'un mélange α et α'. Il apparaît donc que les deux modes de cristallisation, traitement thermique et contact avec un composé organique, conduisent à la formation des mêmes structures cristallines, pour chacun des P(D,L)LA.

4.3. Interaction d'esters éthyliques avec le P(D,L)LA extrudé amorphe

Les résultats des publications 4 et 5 mettent en évidence un phénomène de plastification et de cristallisation induite par l'acétate d'éthyle, composé organique utilisé comme solvant ou comme molécule d'arôme, à une activité de 0,5. Nous avons cherché à savoir si ce phénomène dépendait de la nature du composé organique, et ainsi si ce comportement pouvait être mis en évidence pour deux esters de la même série homologue avec le P(D,L)LA et(ou) de l'activité de l'acétate d'éthyle. En parallèle, une détermination de la prise de masse des échantillons de P(D,L)LA Biomer L9000 en contact avec des vapeurs de composés organiques a été réalisée. En premier lieu, l'activité de chaque composé d'arôme dans la cellule a été déterminée à l'aide d'une analyse par chromatographie en phase gazeuse avec calibration externe. Ensuite des films de P(D,L)LA amorphe ont été mis en contact avec des vapeurs de composés organiques dans des cellules qui ont été ensuite hermétiquement closes. Une évaluation de la prise de masse a été réalisée sur certains échantillons afin de déterminer la teneur en composés organiques dans le matériau après contact en phase gazeuse pendant 15 jours. Les échantillons de P(D,L)LA Biomer L9000 ont été caractérisés par DSC et DMA afin d'étudier les modifications de structure liée au contact en phase gazeuse avec les molécules organiques.

4.3.1. Matériels et méthodes

4.3.1.1. Matériels

Les échantillons de P(D,L)LA étudiés proviennent d'un film de P(D,L)LA Biomer L9000 (Biomer, Allemagne). Ce film a été fabriqué au Laboratoire P2AM (Propriétés-Architectures des Alliages et Mélanges) du Cnam par extrusion monovis à l'aide d'une extrudeuse de 30 mm de diamètre et 33 L/D, composée de 3 sections de vis sans élément de mélange tournant à 40 rpm et d'une filière de 100 mm de large. Le profil de température de l'extrudeuse pour les 6 zones est 180 °C – 185 °C - 190 °C – 195 °C - 205 °C et les éléments de mélange (4 Sulzer SMX®, Sulzer Chemtech) et la filière sont à 210 °C. La température et la vitesse des rouleaux froids sont respectivement fixées à 25 °C et 10 m.min^{-1} afin d'obtenir un film de 80 mm de large et environ 120 µm d'épaisseur.

4.3.1.2. Mise en contact

Le film de P(D,L)LA a été préalablement découpé aux dimensions adaptées pour les pesées et les mesures en DSC et DMA puis placé dans une cellule en verre, équipée d'une vanne Mininert® (Figure 2.9) et fermée à l'aide d'une bride de serrage.

Les échantillons de P(D,L)LA sont laissés en contact en phase vapeur avec les molécules organiques pendant 15 jours à 25 °C dans une enceinte thermostatée (Aqualytic) et à différentes activités, 0,1, 0,2, 0,5 et 0,9. L'activité correspond au rapport p/p_0, avec p la pression partielle en ester éthylique et p_0, la pression de vapeur saturante de chacun des esters éthyliques. L'activité est générée grâce à une solution d'ester éthylique, dans l'hexadécane, dont la concentration varie selon l'activité souhaitée (Tableau 4.1). L'activité est contrôlée par prélèvement de l'espace gazeux à l'aide d'une seringue à gaz et analyse par chromatographie en phase gazeuse. La quantité d'ester dans l'espace gazeux est exprimée en concentration (mg.L^{-1}/ ppm).

Tableau 4.1. Concentration dans la solution et dans l'espace gazeux des trois esters éthyliques pour chaque activité.

Activité	Concentration (mol.L^{-1}) dans la solution			Concentration (mg.L^{-1}/ ppm) dans l'espace gazeux		
	AE	BE	HE	AE	BE	HE
0,1	0,42	0,11	-	54,0 / 58,4	7,9 / 9,0	-
0,2	0,84	0,27	-	108 / 117	16,2 / 18,0	-
0,5	2,3	0,66	0,81	266 / 288	36,8 / 41,9	9,0 / 10,4
0,9	5,22	1,19	1,6	379 / 410	71,7 / 81,6	14,9 / 17,1

4.3.1.3. Calorimétrie différentielle à balayage (DSC)

La mesure des températures caractéristiques du P(D,L)LA et du taux de cristallinité a été réalisée grâce à une DSC Q100 (TA Instruments), équipée d'un système de refroidissement. Le four de la DSC est balayé en permanence par de l'azote (50 mL.min^{-1}). Les échantillons, d'environ 10 mg, sont placés dans des creusets hermétiques en aluminium Tzéro afin d'éviter l'évaporation des composés organiques lors de la chauffe.

Deux modes, standard et modulé, sont utilisées pour la caractérisation des échantillons de P(D,L)LA.

- Le mode **standard,** rampe de température linéaire de 10 °C.min^{-1} entre -30 à 190 °C, permet la détermination des enthalpies de cristallisation et de fusion. Le taux de cristallinité est calculé grâce à l'équation suivante :

$$\chi_c = \frac{\Delta H_m - \Delta H_c}{\Delta H_m^0}$$ où ΔH_m et ΔH_c sont les enthalpies de fusion et cristallisation du PLA, respectivement et ΔH_m^0, de valeur 93 J.g^{-1} (Fischer, 1973), l'enthalpie de fusion par gramme de cristal de taille infinie.

- Le mode **modulé** est utilisé pour la mesure de la T_g entre -30 et 80 °C. Il consiste en une rampe de température linéaire de 1 °C.min^{-1} modulée par une sinusoïde d'amplitude de modulation de température sinusoïdale de ± 1.5 °C et de période 80 s.

4.3.1.4. Analyse mécanique dynamique (DMA)

La DMTA V (TA Instruments) a été utilisée afin de caractériser les propriétés mécaniques et thermiques du P(D,L)LA avant et après contact avec les esters éthyliques. Les mesures de tension-compression sont réalisées à une fréquence de 1 Hz et à une déformation de 0,05 % sur des échantillons de forme rectangulaire (30 mm * 10 mm). Une rampe de température de 2 °C.min^{-1} a été appliquée entre -140 et 130 °C. Le maximum du pic du facteur de perte (*tan δ*) est associé à la T_g du matériau analysé.

4.3.2. Résultats et discussion

La caractérisation des échantillons de P(D,L)LA a été réalisée avant et après contact avec trois esters éthyliques, l'acétate d'éthyle (AE), le butyrate d'éthyle (BE) et l'hexanoate d'éthyle (HE). L'analyse en DSC des échantillons après contact nous permet d'évaluer l'effet plastifiant du composé organique sorbé dans la matrice P(D,L)LA. Comme montré dans la Figure 4.2, le PLA avant contact est amorphe. Il présente une T_g à 60 °C et un pic de cristallisation étendu entre 90 et 130 °C suivi d'un pic de fusion à 170 °C. La mise en contact avec l'acétate d'éthyle induit une diminution de toutes les températures de transition thermiques. Une diminution de près de 30 °C est visible après 15 jours de contact avec l'AE à une activité de 0,2. La mise en contact à de plus fortes activités induit une plastification plus importante qui conduit à un aplatissement de la transition vitreuse qui n'est ainsi plus visible

sur le thermogramme présenté (Figure 4.2). Un déplacement du pic de fusion vers les plus basses températures est également noté. Ainsi la température de fusion diminue avec l'augmentation de l'activité en AE, passant de 170 °C à 154 °C à 0 et 0,9 d'activité en AE, respectivement. Par conséquent, l'efficacité de la plastification dépend de l'activité en composé organique auquel le PLA est soumis et donc de la quantité sorbée.
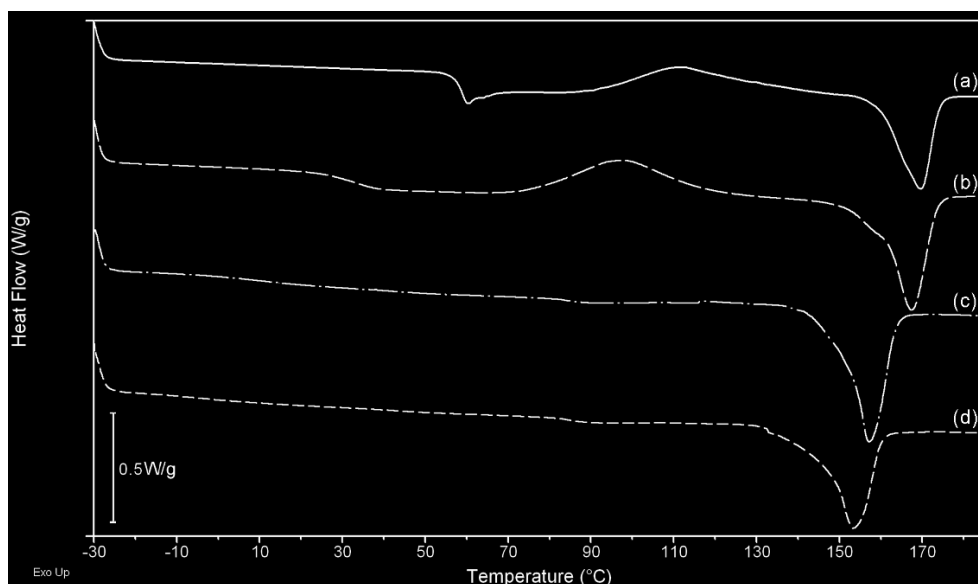
Figure 4.2. Thermogrammes du P(D,L)LA Biomer L9000 avant (a) et après contact avec l'acétate d'éthyle à une activité de 0,2 (b), 0,5 (c) et 0,9 (d).

Le P(D,L)LA a également été mis en contact avec deux autres composés organiques. La Figure 4.3 montre le P(D,L)LA avant et après contact avec l'AE, le BE et l'HE à une même activité de 0,5. Il apparaît que le P(D,L)LA est moins sensible au BE et à l'HE qu'à l'AE. En effet, le PLA présente un déplacement des transitions thermiques vers les plus basses températures mais celui-ci est minime comparé au déplacement après contact avec l'AE. En effet, la température de transition vitreuse diminue de 3 et 1 °C après contact avec le BE et l'HE, respectivement. Le contact avec BE induit une diminution de 3 °C des températures de cristallisation et de fusion tandis qu'avec HE, aucune modification de ces températures n'est notée. Il est également notable que le pic de cristallisation après contact avec le BE et l'HE vers 110 °C est bien apparent, contrairement à celui de l'échantillon après contact avec l'AE, mais plus aplatie que pour le PLA avant contact. Il semble donc que le contact avec ces trois composés conduise à une cristallisation complète du PLA après contact avec l'AE et seulement partielle après contact avec le BE et l'HE.
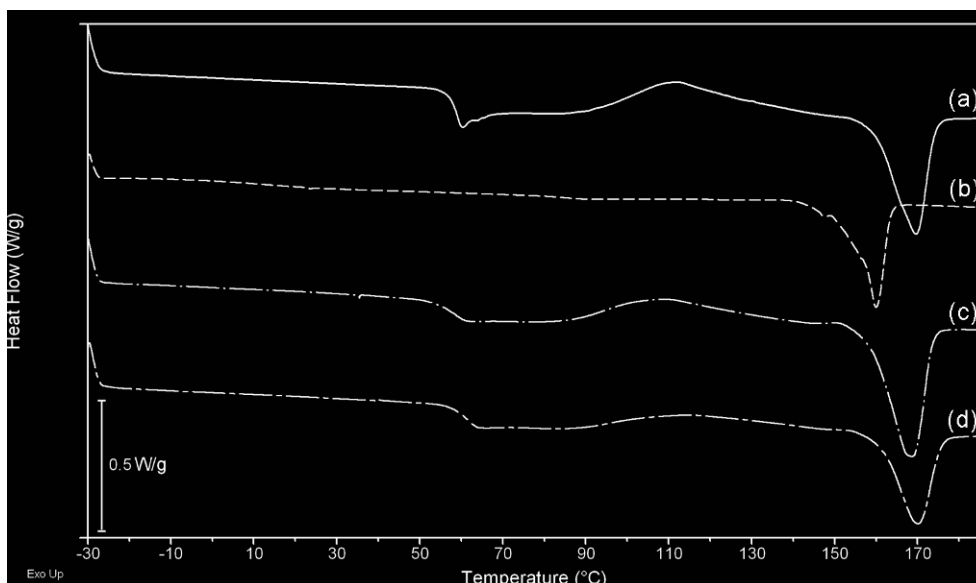
Figure 4.3. Thermogrammes du P(D,L)LA Biomer L9000 avant (a) et après contact avec l'acétate d'éthyle (b), le butyrate d'éthyle (c) et l'hexanoate d'éthyle (d) à une activité de 0,5.

La Figure 4.4 présente l'évolution de la température de transition vitreuse T_g du PLA en fonction de l'activité pour les trois esters éthyliques. Une nette diminution de T_g est observée après contact ave l'AE dès 0,1 d'activité. Cette baisse est continue jusqu'à 0,9 d'activité pour laquelle la température de transition vitreuse est proche de 0 °C.
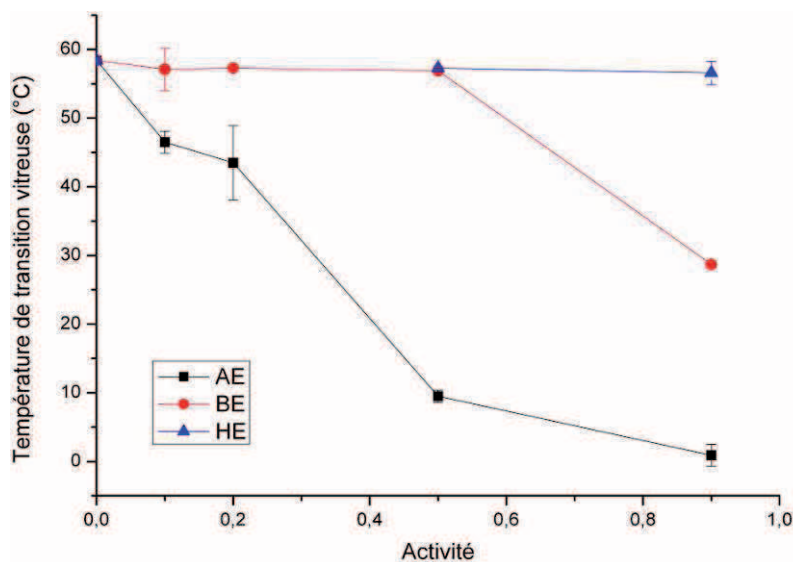
Figure 4.4. Température de transition vitreuse du P(D,L)LA Biomer L9000, mesurée par DSC, avant et après contact vapeur pendant 15 jours avec les trois esters éthyliques (AE,BE,HE) à différentes activités.

Cette évolution est bien différente de celle observée pour le contact avec le BE et l'HE. En effet, pour BE, la diminution de la T_g n'est observée qu'au delà de 0,5 d'activité alors qu'une très légère baisse de T_g est mise en évidence pour l'HE.
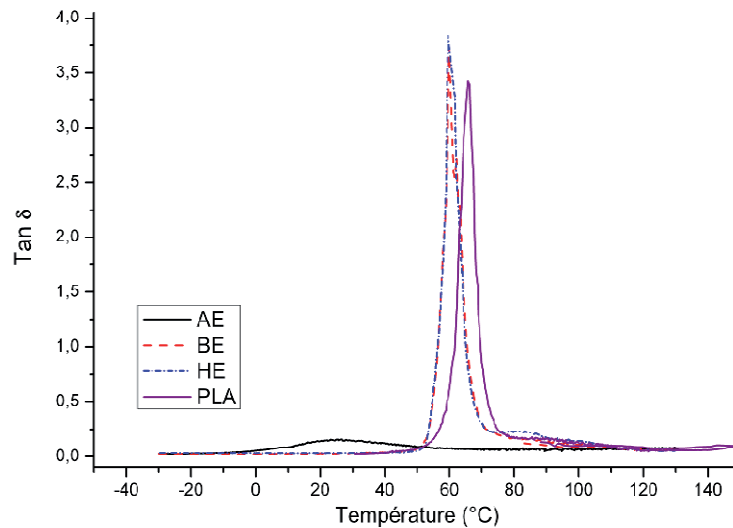
Figure 4.5. Evolution du facteur de perte (*tan δ*) du P(D,L)LA Biomer L9000, mesurée par DMA, avant contact (PLA) et après contact avec l'acétate d'éthyle (AE), le butyrate d'éthyle (BE) et l'hexanoate d'éthyle (HE) à une activité de 0,5 pendant 15.

Les valeurs de T_g déterminées par DMA grâce au sommet du pic *tan δ* mettent en évidence des valeurs de T_g qui évoluent selon l'ester éthylique avec lequel le P(D,L)LA a été mis en contact gazeux. La Figure 4.5 met en évidence une faible diminution de la T_g après contact avec le BE et l'HE alors qu'avec AE une chute de 40 °C de la T_g est observée.

Tableau 4.2. Température de transition vitreuse et module de conservation à température ambiante du P(D,L)LA Biomer L9000 mesurés par DMA avant et après contact pendant 15 jours avec les trois esters éthyliques à différentes activités.

Activité	Température de transition vitreuse (°C)			Module de conservation E' (GPa)		
	Acétate d'éthyle	Butyrate d'éthyle	Hexanoate d'éthyle	Acétate d'éthyle	Butyrate d'éthyle	Hexanoate d'éthyle
0	67,4 ± 1,3	67,4 ± 1,3	67,4 ± 1,3	2,69 ± 0,55	2,69 ± 0,55	2,69 ± 0,55
0,1	61,6 ± 3,4	60,7 ± 1,7	n.d.	2,93 ± 0,52	3,21 ± 0,28	n.d.
0,2	61,6 ± 2,9 30,2 ± 4,4	61,5 ± 4,5	n.d.	3,55 ± 0,26	4,12 ± 0,70	n.d.
0,5	24,2 ± 0,4	59,9 ± 1,0	60,4 ± 1,2	3,53 ± 0,64	3,63 ± 0,85	3,02 ± 0,21
0,9	15,6 ± 5,9	58,2 ± 2,2	60,1 ± 2,7	6,45 ± 0,81	3,39 ± 0,33	3,27 ± 0,23

Les valeurs affichées dans le Tableau 4.2 montrent que la plastification du P(D,L)LA est visible dès 0,1 d'activité avec l'acétate et le butyrate d'éthyle. Le contact du P(D,L)LA avec l'AE à une activité de 0,2 résulte en une double T_g à 61,6 et 30,2 °C. L'augmentation de l'activité a pour effet de supprimer cette double T_g pour n'en retrouver qu'une seule à de plus

basses températures (en dessous de 25 °C). Il semble donc que le P(D,L)LA soit plastifié en deux étapes, en surface dans un premier temps et puis à cœur dans un second temps.

Les deux autres composés organiques ne montrent pas un tel effet plastifiant. En effet une très faible diminution de la T_g (6 à 9 °C) est observée malgré une forte activité en contact. La valeur de T_g, mesurée par DMA après contact avec le BE à une activité de 0,9, est ainsi en contradiction avec celle obtenue par DSC. Cette différence peut s'expliquer par une évaporation de BE pendant l'analyse en DMA (système ouvert) alors qu'en DSC, l'échantillon étant contenu dans une capsule hermétique, le composé organique reste en contact avec le P(D,L)LA. Ce comportement n'est pas retrouvé dans le cas de l'AE en raison de la plus forte interaction de ce composé avec le P(D,L)LA (Figures 4.3 et 4.4).
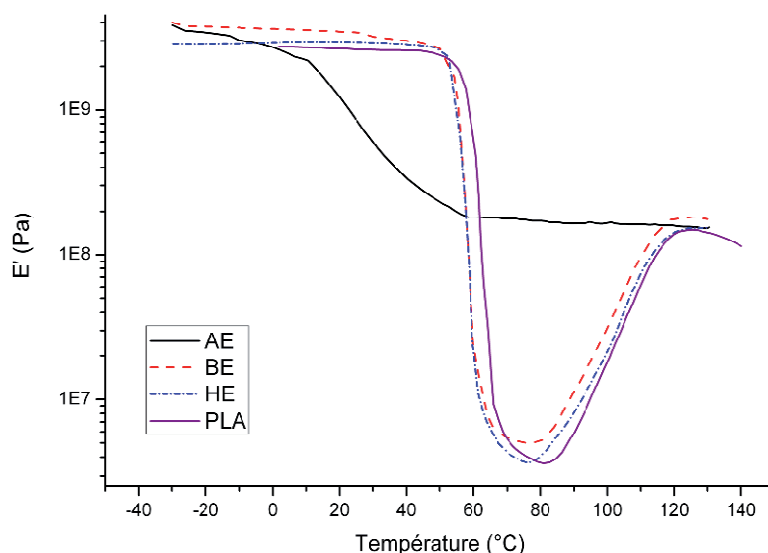
Figure 4.6. Evolution du module de conservation (*E'*), mesuré par DMA, avec la température, du P(D,L)LA Biomer L9000, avant contact (PLA) et après contact avec l'acétate d'éthyle (AE), le butyrate d'éthyle (BE) et l'hexanoate d'éthyle (HE) à une activité de 0,5 pendant 15 jours.

L'évolution des propriétés mécaniques du P(D,L)LA en fonction de la température, avant et après contact à 0,5 d'activité en AE, BE et HE, est montrée par la Figure 4.6. Il apparaît que le P(D,L)LA avant contact présente un module de conservation (*E'*) à 2,69 GPa. Ce module diminue à 60 °C, au moment de la transition vitreuse, pour atteindre 4 MPa à 80 °C puis augmente jusqu'à 100 MPa lorsque le P(D,L)LA cristallise. Le P(D,L)LA mis en contact avec le BE et l'HE, à une activité de 0,5, ne montre aucune modification des propriétés mécaniques. Comme pour le P(D,L)LA avant contact, une diminution drastique de trois ordres de grandeur du module *E'* est observée à 60 °C suivie d'une augmentation significative

à partir de 80 °C. En revanche, le contact avec l'AE induit une diminution progressive du module à partir de -10 °C jusqu'à 60 °C, température à laquelle il atteint un plateau.

Il apparaît donc que les échantillons de P(D,L)LA, mis en contact avec l'AE à une activité de 0,5, ne cristallisent pas pendant la montée en température. Ce comportement s'explique par le fait que les échantillons sont cristallisés avant l'analyse en DMA, c'est à dire lors de la mise en contact avec l'AE. Ces résultats corroborent parfaitement les résultats obtenus par DSC présentés dans la Figure 4.3. Des propriétés mécaniques différentes sont donc mises en évidence en fonction du composé organique pour une même activité.

Les valeurs du module de conservation à faible température ont été regroupées dans le Tableau 4.2. Le contact avec les esters éthyliques, quelle que soit l'activité, ne semble pas induire de modification du module, excepté l'AE à 0,9 d'activité. En effet, après contact à cette activité le module du P(D,L)LA est doublé par rapport à celui du PLA avant contact.

Comme montré par DMA (Figure 4.6) et DSC (Figure 4.3), les échantillons, après contact avec les composés organiques à une activité de 0,5, ne cristallisent pas dans le cas de l'AE, ou peu dans le cas du BE et de l'HE, pendant la rampe de température. Les taux de cristallinité des échantillons avant et après contact ont été regroupés dans le Tableau 4.3.

Il s'avère que, dès 0,1 d'activité, la mise en contact avec l'AE et le BE pendant 15 jours conduit à une cristallisation du P(D,L)LA. Ce taux de cristallinité augmente progressivement avec l'activité en AE pour finalement atteindre 35 % pour une activité de 0,9. Le même taux de cristallinité est mesuré pour le BE à 0,9 d'activité. En revanche, la mise en contact avec l'HE à 0,9 d'activité ne permet de cristalliser le P(D,L)LA que jusqu'à 12 %.

Tableau 4.3. Taux de cristallinité du P(D,L)LA Biomer L9000 avant et après contact vapeur pendant 15 jours avec les trois esters éthyliques à différentes activités.

Activité	Taux de cristallinité (%)		
	Acétate d'éthyle	Butyrate d'éthyle	Hexanoate d'éthyle
0	2 ± 1	2 ± 1	2 ± 1
0,1	20 ± 2	14 ± 3	n.d.
0,2	27 ± 14	12 ± 1	n.d.
0,5	31 ± 9	16 ± 2	10 ± 1
0,9	35 ± 1	34 ± 1	12 ± 3

n.d. non déterminé

La mesure gravimétrique de la prise de masse présentée dans la Figure 4.7 montre que plus l'activité augmente, plus la prise de masse augmente. Ainsi une prise de masse de 0.7 % est mesurée après contact avec l'AE à 0,1 d'activité alors que celle de BE n'atteint que 0,2 %. A une activité de 0.9, la prise de masse atteint environ 18 % avec l'AE, 0,7 % avec le BE et 0,6 % pour l'HE. Ceci peut s'expliquer, en partie, par la plus faible concentration en HE qu'en AE dans la solution d'ester éthylique déposée dans la cellule.

La comparaison du Tableau 4.3 et de la Figure 4.7 montre que pour une prise de masse équivalente (environ 0,6 %), le taux de cristallinité résultant varie entre 12 et 34 % selon l'ester éthylique. L'HE est moins interagissant avec le P(D,L)LA que ne l'est le BE ou l'AE, du fait probablement de son hydrophobicité plus grande que les deux autres esters éthyliques.
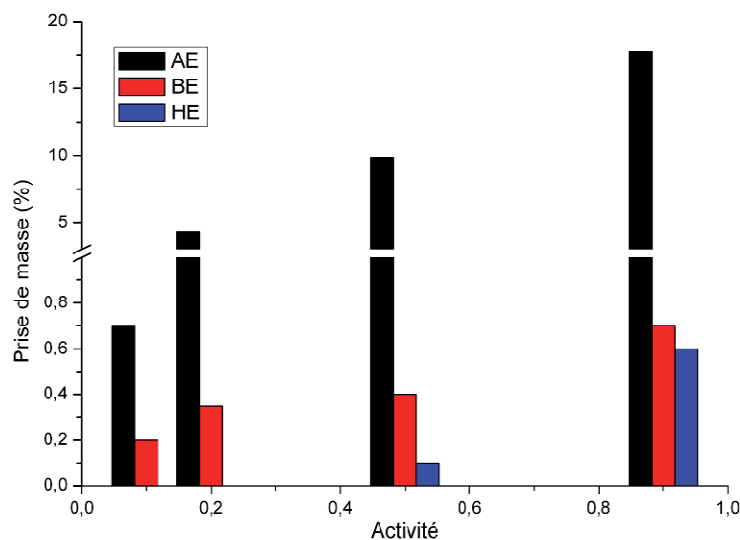
Figure 4.7. Evolution de la prise de masse en % du P(D,L)LA Biomer L9000 après 15 jours de contact en phase vapeur en fonction de l'activité de chaque ester éthylique.

De plus, à prise de masse équivalente, aux environs de 1 %, le BE a un effet plastifiant plus grand que l'AE (Figure 4.8). En effet, à cette concentration, la T_g chute vers 30 °C pour le BE alors que pour l'AE la teneur dans le matériau doit être plus forte, aux environs de 6-8 %, pour faire baisser la T_g vers 30 °C.
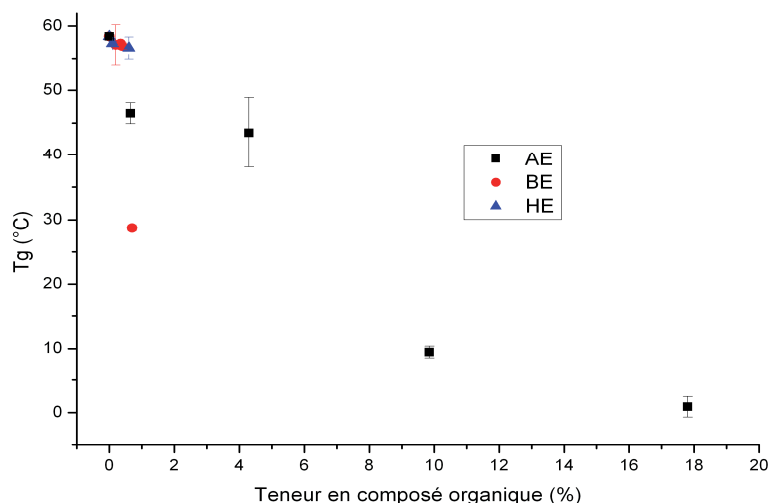
Figure 4.8. Evolution de la température de transition vitreuse (T_g) en fonction de la teneur en composé organique dans le P(D,L)LA Biomer L9000 après 15 jours de contact en phase vapeur.

Ces résultats de prise de masse obtenus par gravimétrie sont proches de ceux mesurés par microbalance de sorption (Figure 3 de la publication n°4) pour de fortes activités (≥ 0,5, Figure 4.9). Cependant, il est à noter que les mesures gravimétriques après sortie de cellule sont peut-être réalisées hors équilibre. Cela peut donc signifier que la prise de masse est sous estimée par cette mesure.
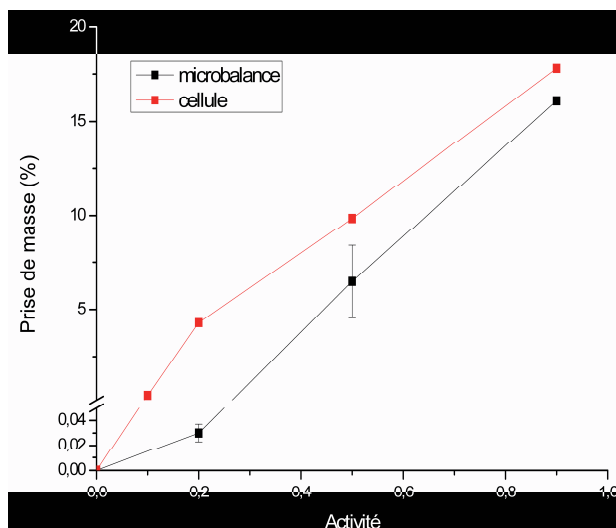
Figure 4.9 Comparaison de la prise de masse par mise en contact à l'état gazeux de l'acétate d'éthyle en cellule et dans la microbalance.

Il a été montré, dans la publication n°4, que pour les faibles activités (≤ 0.2), la prise de masse d'AE dans le P(D,L)LA est décrite par la loi d'Henry. Par contre, au-delà que ce soit en gravimétrie et en microbalance, une forte augmentation de la prise de masse est observée qui s'accompagne d'un phénomène de plastification. Celui-ci est confirmé par les résultats de

DSC qui ont montré une baisse de la transition vitreuse de près de 50 °C à 0,5 d'activité pour AE. L'évolution des prises de masse du P(D,L)LA pour les contact avec le BE et HE est différente de celle obtenue pour l'AE (Figure 4.8), montrant une faible voire une absence de plastification, qui est confirmée par les analyses en DSC et DMA.

Afin de pouvoir conclure quant au pouvoir plastifiant de chacun des composés et à leur influence sur la cristallisation du P(D,L)LA, il serait judicieux de répéter l'expérience en isoconcentration dans l'espace gazeux à diverses concentrations.

4.3.3. Discussion et commentaires

La mise en contact d'échantillons de P(D,L)LA Biomer L9000 avec des vapeurs d'esters éthyliques en cellule hermétique nous permet bien d'observer une modification des propriétés thermiques et mécaniques du PLA. Il apparaît que le choix de l'activité en ester éthylique à laquelle le P(D,L)LA est soumis est crucial pour l'évolution des propriétés du polymère. En effet, la T_g et la cristallinité du P(D,L)LA varient en fonction de la teneur en composé organique dans le matériau.

Ce résultat peut être perçu aussi bien de manière positive que de manière négative selon le but recherché :

- positif : le P(D,L)LA semble peu sensible au contact avec des concentrations faibles en BE et HE (environ 70 ppm de BE et 12 ppm de HE à 0.9 d'activité dans l'espace gazeux), habituellement rencontrées dans les formulations aromatiques, ce qui rend ce matériau intéressant pour l'emballage alimentaire. En effet, ces composés sont largement présents dans les produits alimentaires, tels que le vin ou les viennoiseries à des teneurs allant jusqu'à 125 µg.L^{-1} et 73 µg.L^{-1} pour respectivement, BE et HE, dans le vin (Duarte, 2010) et jusqu'à 3 et 2 g.L^{-1}, respectivement, dans l'arôme "viennoiserie " (Dury-Brun, 2006).

- négatif : le BE ou l'HE ne semble pas parvenir à induire une cristallisation complète du PLA à des concentrations inférieures à 70 ppm de BE et 12 ppm de HE dans l'espace gazeux. Il apparaît donc nécessaire, dans le but d'utiliser le pouvoir de cristallisation de ces composés organiques, d'utiliser de fortes concentrations, allant jusqu'à l'immersion du P(D,L)LA dans le composé organique. Cette démarche entreprise par Naga (Naga, 2010) semble présenter de bons résultats mais une quantité plus importante de composé organique est alors nécessaire engendrant un procédé plus coûteux et plus difficile à mettre en place au niveau industriel.

Par contre, il a été mis en évidence qu'une activité de 0,1 en AE suffit pour voir une modification significative de la T_g et de la cristallinité du P(D,L)LA. Cela s'explique par la sorption des composés dans le P(D,L)LA. Alors que la prise de masse à une activité de 0,9 est inférieure à 1 % pour le BE et l'HE, celle-ci atteint près de 18 % avec l'AE. L'affinité du P(D,L)LA pour les esters éthyliques diminue donc avec l'augmentation de leur

hydrophobicité. Le contraire est observé dans le cas des polyoléfines en raison de leur hydrophobicité (Dury-Brun, 2007). Les composés d'arôme utilisés dans le domaine alimentaire étant majoritairement hydrophobes, il apparaît que le PLA est un bon candidat pour l'emballage alimentaire et la préservation des arômes du produit au contact.

Après avoir testé la cristallisation par traitement thermique et induite par le contact avec les composés organiques, nous nous sommes intéressés, cette fois-ci, à la cristallisation induite par un procédé industriel. Plusieurs techniques de mise en forme sont utilisées dans le domaine de l'emballage et notamment le biétirage. L'effet de ce procédé sur les propriétés barrière du P(D,L)LA 2002D et du P(D,L)LA 4042D a donc été étudié dans le sous-chapitre suivant.

4.4. Influence du biétirage sur la structure cristalline du PLA et des propriétés barrière aux gaz

Etant parvenu à former une structure cristalline par traitement thermique et contact avec un composé organique (publications 4 et 5), un nouveau procédé conduisant à une cristallisation partielle des polymères a été testé sur le P(D,L)LA : le biétirage. Pour cela, deux systèmes ont été employés :

- le premier est un prototype développé par l'Université de Lille qui permet de réaliser un biétirage simultané ou séquentiel à 10 mm.min^{-1} entre 55 et 70 °C. (Collaboration avec Valérie Miri, maître de conférences, Université de Lille, UMET UMR 8207)

- le second est un appareil de l'Université de Belfast avec lequel l'étirage a été effectué à une vitesse d'élongation de 1 et 8 s^{-1} à 100 °C. (Collaboration avec Gary Menary, Queen's University of Belfast, School of Mechanical & Aerospace Engineering)

L'effet du biétirage a ainsi été évalué en termes de cristallinité et propriété barrière à l'hélium et à l'oxygène pour le P(D,L)LA 2002D et le P(D,L)LA 4042D dans le proceeding présenté ci-dessous.

The effect of the stretching of PLA extruded films on their crystallinity and gas barrier properties

A. Guinault[a], G.H. Menary[b], C.Courgneau[c], D. Griffith[b], V. Ducruet[c], V.Miri[d], C. Sollogoub[a]

[a] CNAM – Industrial Polymer Materials Laboratory P2AM – 292 rue Saint-Martin, 75141 Paris cedex 03- France

[b] School of Mechanical & Aerospace Engineering, Queen's University Belfast, BT9 5AH, UK

[c] INRA UMR 1145 Food process engineering-1 avenue des Olympiades, 91744 Massy cedex- France

[d] UMET UMR 8207, Université de Lille, Villeneuve d'Ascq, France

4.4.1. Abstract

Driven by environmental concerns, new polymers based on renewable resources are arriving on the market to replace conventional polymers, obtained from petroleum, for different applications like food packaging. One of the most prominent polymers among these materials is polylactide (PLA), a biodegradable, thermoplastic, aliphatic polyester derived from renewable resources, such as corn starch (in the U.S.A.) or sugarcanes (in the rest of the world). However this polymer presents different disadvantages and especially low gas barrier properties (Auras, 2003). Thermal crystallization can be used to increase its gas barrier properties but long times are necessary (Guinault, 2010) and are not compatible with an industrial process. Another way to increase the gas barrier properties consists in stretching the film in order to increase its crystallinity and so its diffusion coefficient. We have prepared stretched P(D,L)LA films with different stretch ratio and we have studied the effect of the stretching parameters on the gas barrier properties of P(D,L)LA films. Finally we compared this process with the isothermal crystallization process by taking into account the crystallinity degree and the crystalline morphology.

Keywords: PLA, polylactide, gas barrier properties, crystallization, stretching.

4.4.2. Introduction

Driven by environmental concerns, new polymers based on renewable resources are arriving on the market to replace conventional polymers, obtained from petroleum, on different applications like food packaging. One of the most prominent polymers among these materials is polylactide (PLA), a biodegradable, thermoplastic, aliphatic polyester derived from renewable resources, such as corn starch (in the U.S.A.) or sugarcanes (in the rest of the world). Two forms are available, the PLLA that is the homopolymer and the P(D,L)LA that contains D-lactic acid and is cheaper than PLLA. However, these polymers present different disadvantages like low barrier properties and low mechanical properties (Auras, 2003).

In order to increase the gas barrier properties of polymeric materials, different solutions can be used like increasing crystallinity, or by association with higher barrier polymer by multilayer coextrusion and film coating, even plasma deposition. Previous works (Guinault, 2010) showed that crystallization required around 30 to 90 minutes to occur and then to improve the gas barrier properties, but this time was not consistent with process requirements. Another industrial solution used to increase the gas barrier properties consists in drawing the films in order to generate macromolecule orientation and crystalline lamellae, as for poly(ethylene terephthalate) (PET) (Lu, 2001). P(D,L)LA was studied in term of biaxial stretching but results was only reported on the effect on its mechanical properties and on the crystalline morphology formed by drawing. Ou and Cakmak (Ou, 2008) reported the effect of biaxial stretching on the crystalline structure of P(D,L)LA films while Grijpma *et al.* (Grijpma, 2002) and Stoclet *et al.* (Stoclet, 2007) showed the improvement of the mechanical properties of the P(D,L)LA by orientation. About gas permeability, different results have been published by Auras (Auras, 2005a) for example, but except from Delpouve *et al.* (Delpouve, 2009), who worked on water vapour, no work correlated the stretching parameters (stretch ratio, rate and mode) to the gas barrier properties.

The present work deals with the effect of the macromolecule orientation and the strain-induced crystallization on the gas barrier properties, especially oxygen and helium for its little size and its non-interaction with P(D,L)LA contrary to oxygen. Different processes were used for biaxial stretching like simultaneous biaxial stretching and sequential biaxial stretching and different stretch ratios and rates were tested. As biaxial stretching is usually followed by an annealing to induce thermal stability, drawing and post annealing were examined separately in order to determine the role of each step on the improvement of helium or oxygen barrier

properties and the relationships between the structure and the helium barrier properties were tried to be highlighted. The effect of the stretching on the gas barrier properties was finally compared to the effect of a single cold crystallization.

4.4.3. Experimental

4.4.3.1. Materials and Film Extrusion

Two NatureWorks P(D,L)LA were tested, a P(D,L)LA reference INGEO 2002D done for extrusion and thermoforming and a P(D,L)LA reference INGEO 4042D made for biaxially oriented films. After drying the pellets at 80 °C during 4 hours minimum in a vacuum oven, the P(D,L)LA 2002D was firstly thermo-moulded by compression (Telemecanique) at 185 °C and 150 bar in a multistep process ended by quenching in water. Films of approximately 100 μm thickness were obtained. Concerning P(D,L)LA 4042D, the pellets were dried during 8 hours at 90 °C in a drying air system and processed by single screw extrusion at 200 °C (following the processing guide of NatureWorks (NatureWorks, 2011)) to obtain films of 150 mm width and around 250 to 300 μm thickness with a flat die and a chill roll. Cooling temperature was fixed at 20 °C in order to avoid crystallization of the P(D,L)LA films, as it was shown in our previous work (Colomines, 2010).

4.4.3.2. Film Drawing

Biaxial drawing experiments were performed on two devices. The first one is a prototype Cellier tenter of the University of Lille. This system consists of four pantographs, each equipped with ten pneumatic grips. Stretching is realized by two of the pantographs linked to hydraulic jacks moving at right angles, and operated in a temperature-regulated oven (Stoclet, 2007). Simultaneous and sequential biaxial stretching can be performed on this device. Square specimens of gauge length 105 mm were biaxially drawn in the temperature range between 55 and 70 °C, using a constant jack speed of 10 mm.min^{-1} which corresponds to an initial strain rate of 0.1 s^{-1}. This device was used for P(D,L)LA 2002D.

The second one is an apparatus of the University of Belfast (Martin, 2005). The sample dimensions are 75 mm square. As for the first apparatus, the test temperature and the

stretching ratio can be modified. The tests were performed at a strain rate of 1 s^{-1} and 8 s^{-1} at 100 °C. This device was used for P(D,L)LA 4042D.

The major difference between the two devices stayed in the heating: the first one permitted to keep the heating on the initial surface during the stretching while, for the second one, the film is heated and then stretched without heating.

4.4.3.3. Biaxially Oriented Films Annealing

Annealing, named classically heat set (NatureWorks, 2011), must be performed after the drawing in order to obtain a thermally stable film. The processing guide of NatureWorks (NatureWorks, 2011) proposed to carry out the films at a temperature comprised between 125 and 140 °C. The films were then placed between two iron plates and placed in an oven at the desired temperature during the desired time.

4.4.3.4. Analysis methods

4.4.3.4.1. Thermal Analysis

A Pyris 1 (Perkin Elmer) DSC was used to determine the crystallinity degree of the samples using the melting enthalpy of a 100 % crystalline PLA = 93 $J.g^{-1}$ (Fischer, 1973). The crystallinity degrees were determined during the first heating of the films by subtracting the heat of cold crystallization to the melting enthalpy. Tests were performed at 10 $°C.min^{-1}$ from 0 to 200 °C under nitrogen atmosphere in hermetic aluminium pans. Measurements were duplicated. The apparatus was equipped with an intracooler. To have enough mass for an accurate measurement by DSC, which was difficult to obtain when the film were more and more stretched, film samples were superposed in the pans.

4.4.3.4.2. Helium and Oxygen Permeability

The helium transmission rate was measured at room temperature and 0 % RH, by a specific analyser developed by Cnam, based also on the ISO 15105-2:2003. The helium permeability was determined from the transmission rate by taking into account the thickness of the films. Measurements were duplicated.

The oxygen permeability was measured with a Systech analyser 8001 at 23 °C and 0 % RH. The thickness of the drawn films was defined as the average value of 9 measurements.

4.4.4. Results and discussion

4.4.4.1. Effect of Temperature and Mode on Biaxial Stretching Behavior

Previous works (Delpouve, 2009) have shown that the mode used in biaxial stretching of P(D,L)LA led to different results of permeability. So P(D,L)LA 2002D films were firstly simultaneous biaxially oriented at 55, 65 and 70 °C on the collier prototype, following the indications of NatureWorks processing guide (NatureWorks, 2011).

At 55 °C and even at 65 °C, despite the fact that the polymer was above its glass transition temperature, the temperature was not enough to obtain interesting draw ratio. Only 2.5×2.5 draw ratio has been achieved. At 70 °C, it was possible to reach a maximum draw ratio of 3.25×3.25. By contrast, only a 2.5×2.5 draw ratio had been successfully obtained using the sequential mode.

As it happened for P(D,L)LA 2002D, the biaxial stretching of P(D,L)LA 4042D is limited to a low stretch ratio of 4×4, despite the fact that the temperature has been largely increased to succeed this ratio (100 °C versus 70 °C for P(D,L)LA 2002D). This increase of temperature was needed for P(D,L)LA 4042D because the film was not maintained in temperature during stretching, contrary to the process used for the P(D,L)LA 2002D. The maximum stretch ratio obtained in this study is therefore in agreement with the processing guide of NatureWorks (NatureWorks, 2011) and perhaps it was due to the increase of the stretch temperature. As it was not possible to work with the same low stretch rate of 0.1 s^{-1} used previously, the stretching speed was fixed at 1 s^{-1} and 8 s^{-1}, in order to study the film cooling effect during the stretching but no different behaviour was highlighted. The same maximum stretching ratio of 4×4 was obtained whatever the strain rate.

4.4.4.2. Effect of Biaxial Stretching on Helium and oxygen Permeability

The helium permeabilities of the stretched P(D,L)LA 2002D films were in the same order of magnitude as those of extruded films (Table 1). Considering the measurements error due mainly to the thickness measurements, both simultaneous and sequential modes brought equivalent helium permeability results.

These results were surprising because it is well known for PET that biaxial stretching led to a significant decrease of the permeability, usually the barrier improvement factor is around 2 to

3 for oxygen permeability. The oxygen permeability measurements confirmed the results obtained with helium. But it was certainly due to the too little stretching ratio imposed on the P(D,L)LA 2002D films.

Table 1. Helium and oxygen permeability and crystallinity degree of extruded and drawn P(D,L)LA 2002D films.

	Extruded film	Simultaneous stretched P(D,L)LA 3.25×3.25	Sequential stretched P(D,L)LA 2.5×2.5
Helium permeability (10^{-18} m^3.m.m^{-2}.s^{-1}.Pa^{-1})	97.7 – 89.5	85.1	87.1
Oxygen permeability (10^{-18} m^3.m.m^{-2}.s^{-1}.Pa^{-1})	2.2 – 2.5	61.7*	2.2
Crystallinity degree (%)	2	23.6 – 25.9	20.7 – 23.8

* : the value was certainly overestimated because of the low thickness of the films that made them brittle

Figure 1 clearly showed that drawing led to a slight decrease of the helium permeability of P(D,L)LA 4042D, but only for 4×4 stretching ratio. This effect was not affected by the stretch rate, considering the measurement errors. For 3×3 draw ratio, the helium permeability was not modified by the stretching whilst it increased slightly for the 2×2 stretch ratio. This effect could be explained by a de-densification during heating (Liu, 2004) of the amorphous phase that has lost its slight macromolecule orientation obtained during the extrusion process.
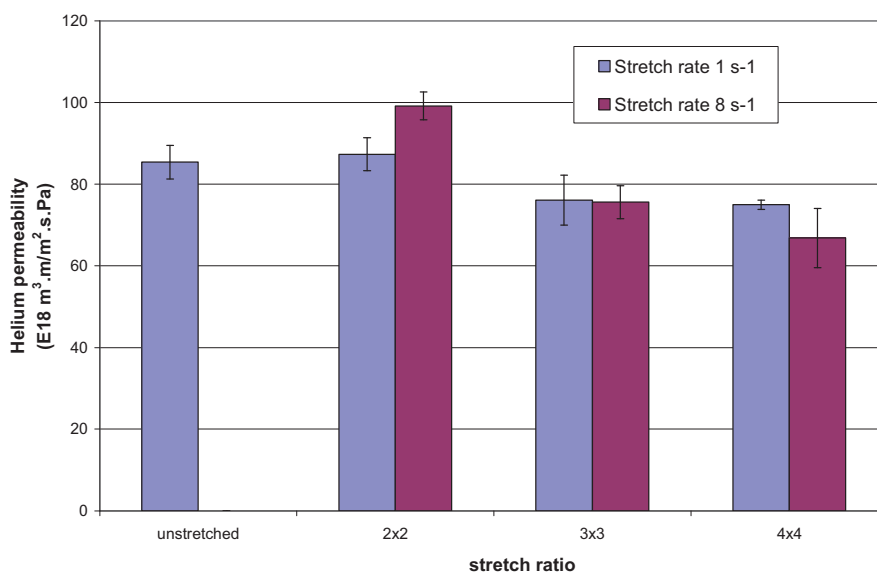
Figure 1. Evolution of helium permeability of P(D,L)LA 4042D drawn films as a function of the stretch ratio at two stretch rates, 1 s^{-1} and 8 s^{-1}.

4.4.4.3. Effect of Biaxial Stretching on Thermal Properties

The DSC measurements showed that the biaxial stretching of P(D,L)LA 2002D led to a significant increase of the crystallinity degree of the extruded films (Table 1). Surprisingly, this increase of crystallinity did not induce a decrease of the helium and oxygen permeability as we demonstrated with an isothermal crystallization (Guinault, 2010).

Concerning the P(D,L)LA 4042D film, Table 2 clearly showed that the crystallinity degree was significantly increased by drawing, only for the 4×4 stretching ratio. The crystallinity was about 20 %, which was lower than crystallinity degrees obtained by annealing extruded films at 130 °C during 90 minutes. In these last conditions, crystallinity was around 35 % and one of our previous works (Guinault, 2010) clearly showed that this crystallinity level induced a decrease of the helium permeability by a factor around 2.

Table 2. Crystallinity degrees and cold crystallization temperature of extruded P(D,L)LA 4042D films, annealed extruded films and drawn extruded films.

	Extruded film	Annealed extruded film	2×2 drawn extruded film (1/s)	3×3 drawn extruded film (1/s)	4×4 drawn extruded film (1/s)
Crystallinity degree (%)	3.7 – 0.6	36.3 – 34.4	0.6 – 7.0	0 – 15	18 – 30.8
Cold crystallization temperature (°C)	130 – 128	-	126 – 117	86 – 100	85 – 87
Helium permeability (10^{-18} m^3.m.m^{-2}.s^{-1}.Pa^{-1})	91.2 – 79.5	52.7 – 65.8	81.6 – 93.1	67.4 – 84.8	73.4 – 76.6

However, as expected, an advantage of the drawing was to decrease the cold crystallization temperature as it is shown in Table 2 and Figure 2. The cold crystallization temperature of the 2×2 drawn films was less affected by the drawing than those of the 3×3 and 4×4 drawn films. Thus the decrease was more important as the stretch ratio was higher.
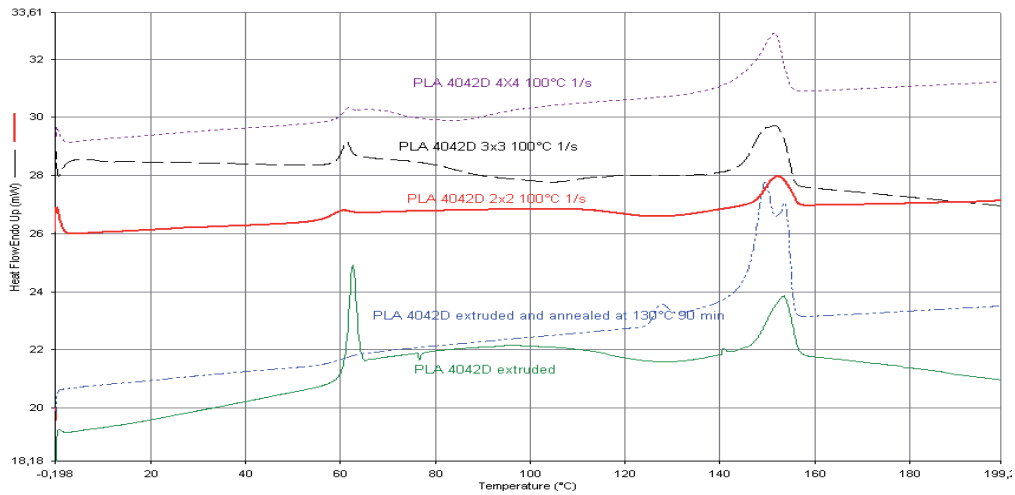
Figure 2. Thermograms of the first heating of extruded, extruded and annealed, 2×2, 3×3 and 4×4 drawn extruded P(D,L)LA 4042D.

4.4.4.4. Effect of Annealing on Thermal Properties and Helium Permeability of drawn films

DSC tests performed on the annealed 2×2, 3×3 and 4×4 drawn films confirmed that the performed annealing was sufficient to obtain a total crystallization of each drawn film, which was shown by the disappearance of the cold crystallization peak (Figure 3), while our previous work (Guinault, 2010) had shown that unstretched films needed an annealing at 130 °C during 90 minutes.
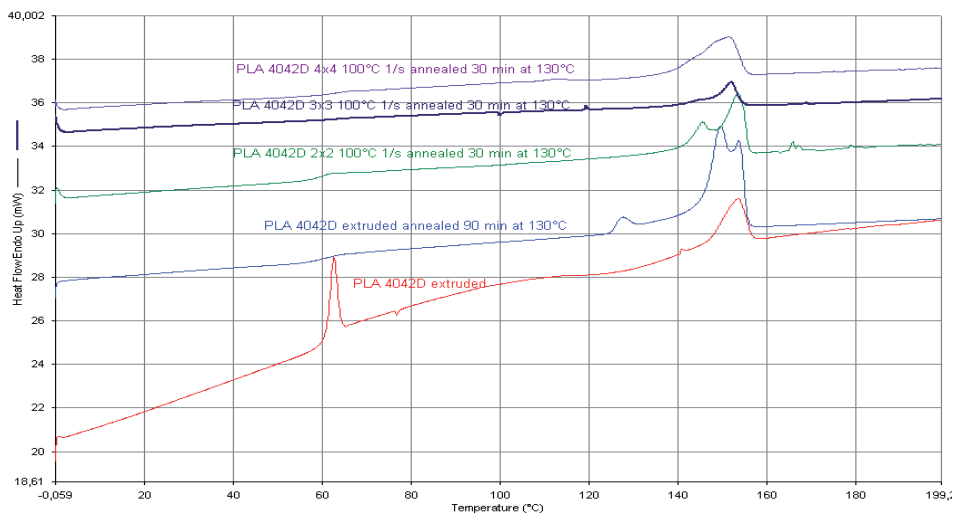
Figure 3: Thermograms of the first heating of the annealed extruded, 2×2, 3×3 and 4×4 drawn extruded P(D,L)LA 4042D.

Table 4 presented both the measurements of the crystallinity degree and the helium permeability of the unannealed and of the annealed drawn films. The crystallinity degrees were increased by the annealing step, whatever the draw ratio and reached nearly the level obtained with single cold recrystallization process. Nevertheless this crystallinity increase did not improve the helium barrier property of the annealed drawn films as expected. It seemed that permeability of the stretched films was more affected by the macromolecule orientation than by the crystalline morphology, considering the certainly lower size of the crystallites formed by stretching than those formed by direct cold crystallization.

Table 4. Crystallinity degrees and helium permeability of drawn and annealed P(D,L)LA 4042D films.

	2×2 drawn extruded film (1/s)		3×3 drawn extruded film (1/s)		4×4 drawn extruded film (1/s)	
	unannealed	annealed	unannealed	annealed	unannealed	annealed
Crystallinity degree (%)	0.6 – 7.0	29.6 – 28.8	0 - 15	27.4 – 28.4	18 – 30.8	30.6 – 34.5
Helium permeability (10^{-18} m^3.m.m^{-2}.s^{-1}.Pa^{-1})	81.6 – 93.1	87.5*	67.4 -84.8	84.7*	73.4 – 76.6	122.9**

*: measurements not duplicated because of the difficulty to prepare the samples
**: the value was certainly surestimated because of the low thickness of the films that made them brittle

4.4.5. Conclusions

This study showed that it is possible to biaxially draw P(D,L)LA films and to obtain maximum stretch ratio around 4×4, which was in agreement with the processing guide of NatureWorks (NatureWorks, 2011). Nevertherless they were obtained by performing the tests at relative high stretch temperature. The effect of the biaxial drawing on the gas permeability was very slight, whatever the drawing ratio, which could be explained by the low drawing ratios achieved for P(D,L)LA films and also perhaps by the high temperature used that could modify crystallization. Despite an increase of the crystallinity degree with an annealing step (heat set), the helium permeability was not improved as it can be done by a single annealing. However, the drawing step led to a significant decrease of the cold crystallization temperature.

Discussion et commentaires

Des films de P(D,L)LA ont été biétirés, de manière simultanée et séquentielle à différentes vitesses, afin de modifier la morphologie du polymère. Le but de cette étude était de corréler les paramètres d'étirage du film de P(D,L)LA préalablement extrudé à ses propriétés barrière. Une évaluation de l'effet du recuit après étirage (thermo-fixation) sur les propriétés du P(D,L)LA a également été réalisée.

Les résultats de ce travail ont mis en évidence la nécessité de travailler à haute température pour atteindre des taux de biétirage important pour le PLA (4×4). Ces taux restent cependant inférieurs à ceux obtenus habituellement pour le PET, avec une extension plane de 21.

La comparaison des procédés de cristallisation a montré que :

- le biétirage simultané ou séquentiel du P(D,L)LA 2002D (environ 96 % de L-lactide), jusqu'à 3,25 ×3,25, conduisait à des taux de cristallinité aux alentours de 23%, taux inférieurs à ceux obtenus par thermo-compression (environ 35%) qui n'induisaient aucune modification de la perméabilité à l'hélium et à l'oxygène.

- l'augmentation du ratio d'étirement du P(D,L)LA 4042D (environ 92-96 % de L-lactide), à 4×4, a permis d'augmenter la cristallinité et par la même de diminuer faiblement la perméabilité à l'hélium. La cristallisation induite par le biétirage a semblé moins efficace que la cristallisation induite par le traitement thermique pour diminuer la perméabilité aux gaz du P(D,L)LA.

- la thermo-fixation effectuée sur les échantillons biétirés de P(D,L)LA 4042D a permis d'augmenter de manière significative les taux de cristallinité mais en n'induisant aucune amélioration des propriétés barrière à l'hélium.

Il semble donc que le biétirage à des ratios d'étirage inférieurs à 4 ne soit pas une solution efficace pour l'amélioration des propriétés barrière du P(D,L)LA. En effet, malgré une cristallisation induite par l'orientation des chaînes de polymère relativement importante, allant jusqu'à 30%, le biétirage n'induit qu'une faible diminution de la perméabilité à l'hélium. Cette orientation s'accompagne en général d'une augmentation de la densité de la phase amorphe. Or dans le cas du PLA, la différence de densité entre phase amorphe et phase cristalline est déjà faible. Par conséquent une étude de l'évolution de la densité sur les propriétés barrière semble être intéressante à développer. De plus, il apparaît que la thermo-fixation annihile les améliorations résultantes du biétirage en raison du relâchement des

contraintes au niveau de la phase amorphe (Delpouve, 2009). L'ensemble de ces procédés, biétirage simultané ou séquentiel à divers ratio et thermofixation, a probablement un effet sur la morphologie cristalline. Une étude systématique de ces structures nous permettrait de faire un lien entre procédé, structure et propriétés.

De plus, des essais seraient à réaliser sur des PLAs aux teneurs en L-lactide plus importantes afin d'évaluer l'influence de la stéréochimie du polymère sur sa structure après biétirage et ses propriétés barrière résultantes.

4.5. Conclusions du Chapitre 4

Les publications n°4 et 5 et le proceeding ESAFORM 2011 mettent en évidence la possibilité de modifier la structure amorphe de divers P(D,L)LA en une structure semi-cristalline selon trois procédés différents, le traitement thermique, le contact avec un solvant et le biétirage.

Le procédé a alors été mis en relation avec la structure résultante et les propriétés de différents grades de P(D,L)LA. L'analyse des propriétés thermiques, mécaniques et barrière de ces polyesters recristallisés a ainsi montré une faible dépendance à la cristallinité aussi bien pour le P(D,L)LA pur que pour le P(D,L)LA formulé.

En effet, la cristallisation de P(D,L)LA Biomer L9000 pur extrudé (environ 1% de D-lactide) n'a induit aucune diminution de la perméabilité à l'oxygène mettant en évidence :

- la possible formation de petits sphérolites ne conduisant pas à une augmentation du trajet des molécules diffusantes.
- un phénomène de dé-densification de la phase amorphe suite à la cristallisation du polymère.
- la présence d'une fraction amorphe mobile et une fraction amorphe rigide moins dense créant des passages préférentiels pour les molécules diffusantes.

En revanche, la cristallisation du P(D,L)LA CD92 pur thermo-compressé (8% de D-lactide), utilisé dans la publication n°5, induit une faible diminution de la perméabilité à l'oxygène.

Ces résultats contradictoires sont représentatifs des données de la littérature qui ont montré pour un P(D,L)LA dont la teneur en L-lactide est de 96 % (ce serait le cas du 2002D) :

- une diminution progressive de la perméabilité à l'oxygène avec la cristallinité (Drieskens, 2009).
- aucune influence de la cristallinité à 25 % (Komatsuka, 2008).
- une diminution de la perméabilité au-delà de 20 % de cristallinité (Sawada, 2010).

Le paradigme selon lequel, la cristallisation du polymère induit l'amélioration de ses propriétés barrières est toujours sujet à controverse pour de nombreux polymères, comme l'a montré Kanehashi *et al.* (Figure 4.10) contrairement au PE. Il semble qu'une étude plus fine de la microstructure permettrait de comprendre la variabilité observée pour plusieurs grades de P(D,L)LA.
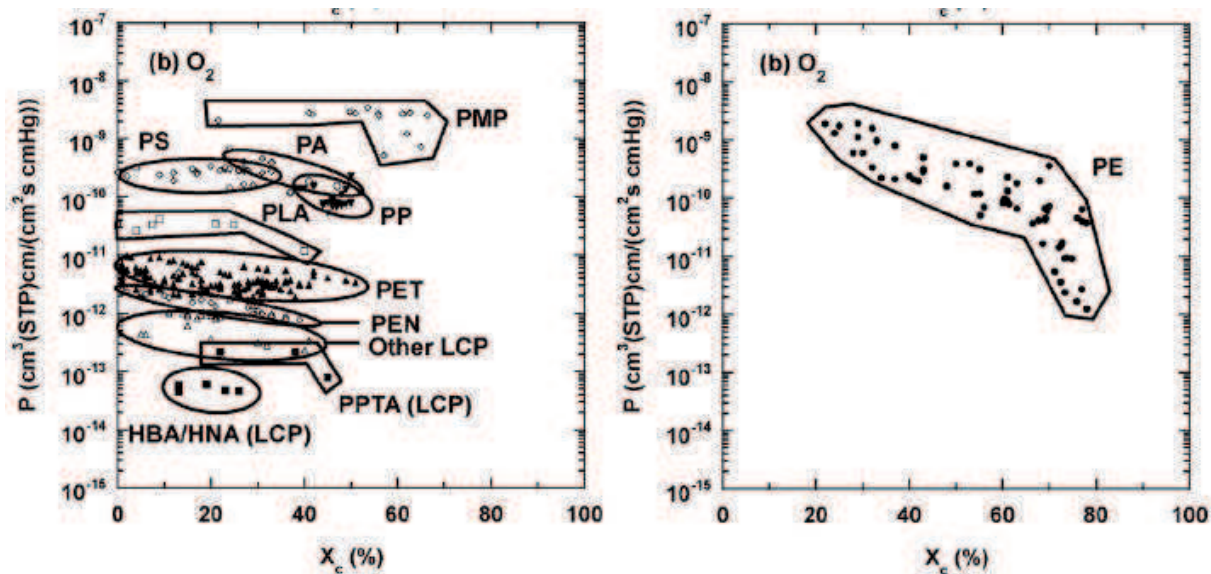
Figure 4.10. Perméabilité de l'oxygène dans des polymères semi-cristallins en fonction de leur taux de cristallinité.

Le contact d'esters éthyliques avec le P(D,L)LA a également mis en évidence une modification de la structure dont l'intensité varie avec le composé et sa concentration. L'étude de la structure ainsi formée a révélé la formation d'une forme cristalline α pour le P(D,L)LA pur et un mélange de forme α et α' pour le P(D,L)LA formulé. Le contact avec un solvant approprié semble donc être un moyen efficace pour cristalliser le P(D,L)LA.

Une détermination indépendante des coefficients de transport de gaz et de solutés de plus forte masse molaire apparaît être, dans un premier temps, un moyen efficace pour tenter de mieux comprendre les mécanismes de transfert de molécules à travers le PLA. De cette manière, la dépendance de la perméabilité à la diffusion ou à la solubilité pourrait être mise en évidence. Pour cela, différentes méthodes doivent être employées afin de mesurer les coefficients de diffusion dans le P(D,L)LA pur et formulé.

Deux approches exploratoires sont présentées dans le chapitre suivant. Elles sont suivies d'une étude de la microstructure afin d'évaluer l'hétérogénéité des échantillons étudiés.

Chapitre 5

-

Approches exploratoires

pour l'évaluation des propriétés de transport et de

l'hétérogénéité des échantillons

Comme il a été montré précédemment dans la partie bibliographique, la détermination des propriétés barrière d'un polymère est indispensable pour de nombreuses applications, telles que les films barrière pour l'emballage alimentaire ou protection de contenu en général et même pour les membranes pour dépollution ou les piles à combustible.

Trois principales méthodes permettent de mesurer les coefficients de transport : la sorption-désorption, la perméation intégrale et la perméation différentielle. La première méthode permet de déterminer directement le coefficient de solubilité du composé diffusant. A partir des données enregistrées, il est possible de calculer le coefficient de diffusion apparent. Une fois ces deux coefficients obtenus, il est alors possible d'en déduire le coefficient de perméabilité grâce à la relation $P = D \times S$. Les seconde et troisième méthodes, quant à elles, permettent de déterminer directement le coefficient de perméabilité. Le coefficient de diffusion est calculé après traitement des données brutes alors que le coefficient de solubilité est déduit des mesures des deux autres coefficients par la relation donnée précédemment.

Dans les chapitres 3 et 4, des systèmes de perméation aux gaz ont été utilisés afin de déterminer les coefficients de perméabilité, P, de l'hélium et de l'oxygène dans le P(D,L)LA. A partir de l'évolution des flux de gaz, il a été possible de mesurer le temps de retard et ainsi de calculer le coefficient de diffusion D. Le coefficient de solubilité a ensuite été calculé à partir des coefficients P et D obtenus.

Dans le chapitre 4, une microbalance de sorption nous a permis de mesurer le coefficient de solubilité de l'acétate d'éthyle dans divers types de P(D,L)LA. Le coefficient de diffusion de cette molécule organique dans le P(D,L)LA a, par la suite, été déterminé à l'aide de l'évolution de la prise de masse au cours du temps. Dury-Brun *et al.* ont mis en évidence la variabilité des coefficients de transport (P, D et S) de l'hexanoate d'éthyle dans divers matériaux d'emballage en faisant une comparaison de deux approches méthodologiques (sorption-désorption ou perméation) (Dury-Brun, 2008). Ces auteurs montrent que la détermination des coefficients de diffusion est dépendante de la méthodologie utilisée et par conséquent les valeurs données dans la littérature présentent de grande variabilité pour un même type de matériau.

Habituellement il est ainsi intéressant d'utiliser des méthodologies variées pour déterminer les paramètres D, S et P de manière indépendante par approche de perméation et sorption. Mais des approches plus originales voire locales ont aussi été développées ayant pour but de proposer et d'optimiser d'autres outils de mesure de coefficient de transport de composés organiques dans des polymères vitreux ou caoutchoutiques.

De nombreuses méthodologies permettent de mesurer le coefficient de diffusion de molécules, de faible et moyenne masse molaire, mais le système de détection associé est dépendant du type de

diffusant étudié : visible en IR (Gillet; Moisan, 1980; Riquet, 1998), UV/visible (Ferrara, 2001), ou en fluorescence (Lezervant, 2007), et de faible masse pour être analysé en chromatographie gazeuse (Karaiskakis, 2004). Ainsi deux types d'approche ont été envisagés: les études cinétiques et les études basées sur des profils de concentration. Les études cinétiques comprennent les cinétiques de sorption, déjà utilisées pour l'acétate d'éthyle, et les cinétiques de perméation utilisées précédemment pour les gaz permanents, oxygène et hélium. Les études basées sur les profils de concentration sont réalisées dans la masse ou par contact solide/solide au sein d'un empilement de films, ce sont ici des mesures directes de la diffusion.

Dans ce chapitre, nous développons les méthodologies qui ont permis de déterminer les coefficients de transport, plus particulièrement le coefficient de diffusion à différentes échelles d'observation. La première méthode abordée dans ce chapitre vise à déterminer le coefficient de diffusion de composés organiques (esters éthyliques) dans le P(D,L)LA par une méthode macroscopique appelée méthode du lag-time à l'aide d'un système de perméation utilisé en mode semi-dynamique. La seconde méthode est une méthode macroscopique mais locale qui consiste à mesurer in-situ le coefficient de diffusion de molécules fluorescentes dans le P(D,L)LA en utilisant la microscopie à fluorescence en configuration épi.

La troisième méthode développée permet d'évaluer, de manière qualitative, la diffusivité ou mobilité moléculaire de radicaux stables dans le P(D,L)LA par Résonance Paramagnétique Electronique (RPE) afin de sonder l'hétérogénéité des échantillons étudiés (publication n°6). Cette caractéristique est ensuite reliée à la dynamique des segments de chaîne polymère de P(D,L)LA pur et plastifié.

5.1. Détermination des coefficients de diffusion de composés organiques volatils

Le système que nous avons utilisé pour la mesure du coefficient de perméabilité et de diffusion a été mis en place par Yuichi Hirata lors de son séjour post-doctoral au laboratoire (Hirata, 2006). Le système de mesure est constitué d'une cellule de perméation placée dans une enceinte thermostatée à 25 °C et reliée à injecteur PTI lui-même connecté à un chromatographe en phase gazeuse.

Toutefois avant de pouvoir effectuer l'étude sur le P(D,L)LA, un travail d'optimisation a, dans un premier temps, dû être effectué afin de s'assurer de la répétabilité des mesures.

5.1.1. Matériels et méthodes

5.1.1.1. Matériels

Deux types de film commercial ont été étudiés lors de ce travail :
- Polyéthylène basse densité (LDPE) Goodfellow (Huntingten, Angleterre) d'épaisseur 125 μm..
- P(D,L)LA Biophan® 121 (Treofan) d'épaisseur 20 μm. Ce film est composé de trois couches, deux couches externes scellables et une couche centrale cristallisée.

5.1.1.2. Préparation de la solution d'esters éthyliques

Une solution des trois esters éthyliques est réalisée dans l'hexadécane avec une concentration en acétate d'éthyle de $1,305.10^{-3}$ mol.L^{-1}, en butyrate d'éthyle de $1,894.10^{-3}$ mol.L^{-1} et en hexanoate d'éthyle de $1,211.10^{-2}$ mol.L^{-1}. Cette solution (8 mL introduit) va servir à créer l'espace gazeux chargé en composés d'arôme qui sera en contact avec le film dans le compartiment amont de la cellule de perméation.

5.1.1.3. Méthode d'analyse de la perméabilité des composés organiques dans des films polymères

La perméabilité des films aux trois esters éthyliques a été mesurée à l'aide d'un dispositif composé d'une cellule de perméation couplée à un injecteur automatique PTI (Purge and Trap Injector, Chrompack CP 4010 PTI/TCT) et un chromatographe en phase gazeuse (GC 8000 Fisons instruments, Arcueil, France) équipé d'une colonne polaire (DBwax 0,32 × 30 m × 0,5 µm, Supelco, USA) et d'un détecteur DIF. Le film à étudier est placé entre les deux compartiments de la cellule de perméation maintenus par une bride de serrage (schéma du système, cf. Figure 2.6 du Matériels et Méthodes).

A intervalle de temps régulier (40 min pour le LDPE et 1 h pour le P(D,L)LA), le compartiment aval est entièrement balayé par le flux d'hélium afin d'entraîner les composés ayant traversés le film jusqu'au PTI. Les composés d'arôme piégés sont ensuite rapidement désorbés et injectés dans le CPG. La mesure du flux est enregistrée pendant 15 cycles, ce qui permet d'atteindre un régime stationnaire ou flux stationnaire pour chacun des composés étudiés.

Deux paramètres avaient été identifiés comme étant susceptibles d'affecter la reproductibilité : la pression du système et l'étape de backflush. Une fois les composés injectés dans la colonne, le backflush est une étape de nettoyage du système par un flux d'hélium en sens inverse de la purge permettant d'enlever tout résidu rémanent éventuel et limitant ainsi l'effet mémoire du système.

Deux pressions de travail du système, 20 et 40 kPa, et l'ajout de l'étape de backflush, ont été testés afin d'estimer leur influence sur les valeurs de coefficient de diffusion calculées. Pour cela, un film commercial de polyethylène basse densité (LDPE) a été choisi.

5.1.2. Résultats et Discussion

5.1.2.1. Détermination du coefficient de diffusion

Les composés organiques collectés et par la suite injectés dans le système chromatographique sont détectés et enregistrés sous la forme d'un chromatogramme (Figure 5.1).
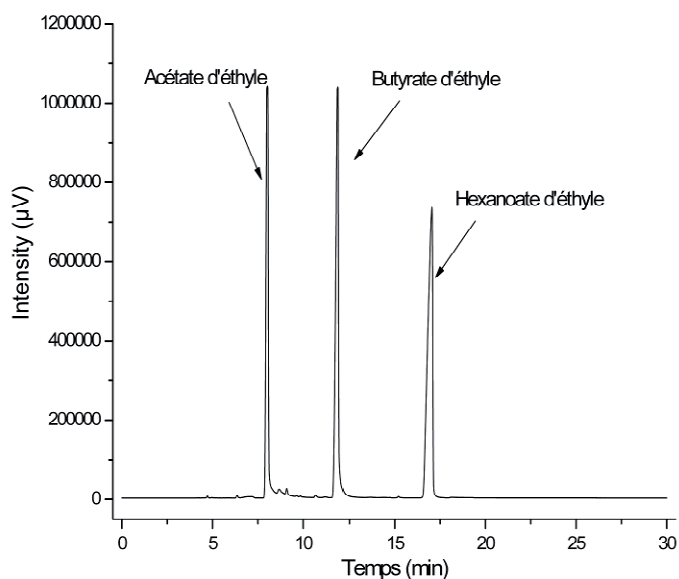
Figure 5.1. Exemple de chromatogramme des trois esters éthyliques ayant perméé à travers un film de LDPE au cours d'un cycle.

Le programme de température choisi permet de séparer correctement les trois esters éthyliques dans l'ordre suivant : acétate d'éthyle, butyrate d'éthyle et hexanoate d'éthyle.

L'aire de chaque pic, proportionnelle à la quantité de chacun des composés accumulés dans le compartiment aval pendant un cycle, est collectée pour chacun des cycles de l'expérience puis sommée de façon à tracer la somme des aires en fonction du temps (Figure 5.2).
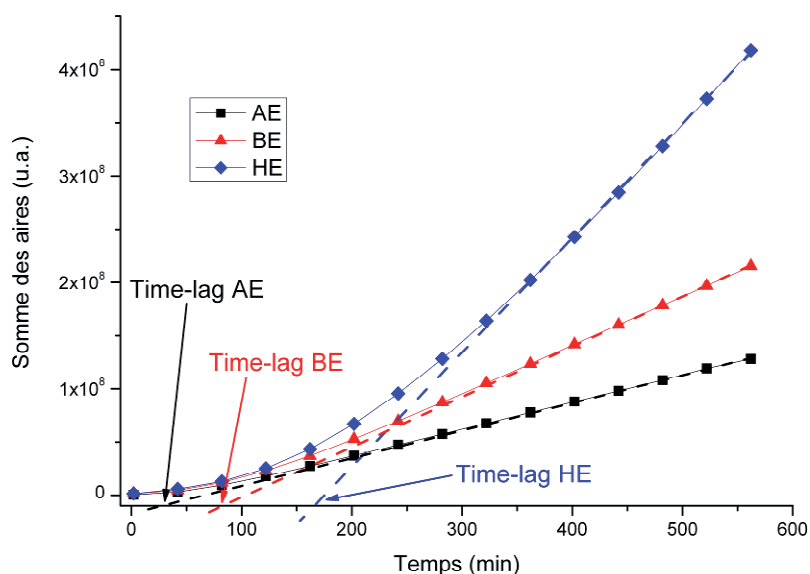
Figure 5.2. Evolution de la somme des aires des pics chromatographiques caractéristiques des esters éthyliques ayant perméé à travers un film de LDPE en fonction du temps.

Les time-lag (temps de retard, θ) sont alors mesurés grâce à la représentation de la somme des aires en fonction du temps. L'intersection de l'axe des abscisses et de la droite correspondant à la

croissance linéaire de la somme des aires en fonction du temps permet de retrouver la valeur de time-lag pour chacun des composés étudiés.

Le coefficient de diffusion est ensuite calculé à l'aide de l'Equation (1.34) où l (m) est l'épaisseur du film polymère considéré :

$$\theta = \frac{l^2}{6D}$$ (1.34)

Le coefficient de perméabilité P est égal à

$$P = \frac{J_{st}.l}{\Delta p} = \frac{dQ}{dt \times A} \times \frac{l}{\Delta p}$$ (5.1)

Avec J_{st} le flux stationnaire, Δp le gradient de pression entre le compartiment amont et aval, Q la quantité de perméant ayant traversé le film (kg), A la surface d'échange (m²) et t le temps (s).

5.1.2.2. Optimisation

Les coefficients de diffusion et leur coefficient de variation associé, avec et sans l'étape de backflush, pour chacun des composés organiques étudiés dans le LDPE ont été regroupés dans le Tableau 5.1.

Tableau 5.1. Comparaison des time-lag, coefficients de diffusion et de leur coefficient de variation associé en fonction de l'ester éthylique étudié avec ou sans étape de backflush pour le LDPE, à 40 kPa et 20 kPa.

Esters éthyliques	Avec backflush			Sans backflush					
	40 kPa			40 kPa			20 kPa		
	Time-lag (min)	$D \times 10^{12}$ (m².s⁻¹)	CV (%)	Time-lag (min)	$D \times 10^{12}$ (m².s⁻¹)	CV (%)	Time-lag (min)	$D \times 10^{12}$ (m².s⁻¹)	CV (%)
Acétate d'éthyle	$14{,}7 \pm 2{,}4$	$2{,}9 \pm 0{,}5$	16	$52{,}1 \pm 13{,}4$	$0{,}85 \pm 0{,}20$	24	$47{,}6 \pm 8{,}7$	$0{,}90 \pm 0{,}16$	18
Butyrate d'éthyle	$31{,}1 \pm 0{,}9$	$1{,}4 \pm 0{,}1$	3	$110{,}6 \pm 37{,}3$	$0{,}42 \pm 0{,}15$	36	$96{,}9 \pm 9{,}8$	$0{,}44 \pm 0{,}04$	10
Hexanoate d'éthyle	$48{,}1 \pm 46{,}9$	$1{,}7 \pm 1{,}6$	98	$183{,}9 \pm 26{,}6$	$0{,}23 \pm 0{,}03$	14	$179{,}7 \pm 17{,}0$	$0{,}24 \pm 0{,}02$	9

Les valeurs de time-lag obtenues sans backflush sont 3 à 4 fois plus élevées qu'avec backflush.

Les valeurs mesurées du coefficient de diffusion montrent que celui-ci diminue avec la taille de la molécule aussi bien avec que sans backflush.

De Lassus (DeLassus, 1994) a montré que la valeur de coefficients de diffusion de l'hexanoate d'éthyle est de $0{,}52 \times 10^{-12}$ m².s⁻¹ dans un film de LDPE. La valeur de D de l'HE, sans l'étape de backflush, est donc plus proche de la valeur trouvée dans la littérature. De plus, contrairement au

cas avec backflush, une diminution des valeurs de D est observée avec l'augmentation de la masse molaire de la molécule diffusante. Ce comportement s'explique par le caractère cinétique du coefficient de diffusion qui décrit la vitesse à laquelle les molécules perméantes traversent le film. Ce coefficient est lié à la taille du volume libre de la matrice polymère par rapport à la taille des molécules diffusantes.

Les coefficients de variation calculés mettent en évidence une plus grande répétabilité des mesures dans le cas de l'expérience sans backflush qu'avec backflush.

Au regard des ces résultats, il semble donc plus adéquat de réaliser les mesures de coefficient de diffusion sans l'étape de backflush. Les expériences suivantes ont donc été réalisées sans backflush.

L'effet de la pression du système a également été étudié en comparant les mesures de coefficient de diffusion des composés organiques dans le LDPE, obtenus à 20 et 40 kPa (Tableaux 5.1).

La pression du système semble peu influencer la détermination du time-lag et du coefficient de perméabilité puisque ceux-ci présentent des valeurs similaires à 20 et 40 kPa. Toutefois la répétabilité des mesures est bien supérieure à 20 kPa qu'à 40 kPa pour chacun des composés mais reste peu satisfaisante et bien au delà de celle évaluée par Hirata *et al.* en 2006 (Hirata, 2006) en utilisant une solution aqueuse d'esters éthyliques comme source de vapeur en composés d'arôme. Les coefficients de variation pour D sont tous inférieurs à 20 % pour une pression du système égale à 20 kPa. Il semble donc qu'une plus forte pression induit une variabilité des mesures de coefficient de diffusion et de perméabilité dans les films de LDPE.

Comme précédemment à 40 kPa, les time-lag mesurés à 20 kPa augmentent et donc les coefficients de diffusion diminuent avec l'augmentation de la taille de la molécule diffusante.

La comparaison des coefficients de diffusion met en évidence des résultats cohérents et similaires quelques soient le composé organique et la pression de travail. En effet, le coefficient de diffusion de l'acétate d'éthyle dans le LDPE est égal à environ $0,9 \times 10^{-12}$ m².s^{-1}.

Les analyses sur le P(D,L)LA Biophan® ont ensuite été réalisées sans backflush et à 20 kPa afin d'obtenir une plus grande répétabilité des mesures.

5.1.2.3. Mesure du coefficient de diffusion des esters éthyliques dans le P(D,L)LA Biophan®.

Pour ce travail, un P(D,L)LA commercial, le P(D,L)LA Biophan® a été utilisé en raison de sa faible épaisseur, ce qui diminue le temps de mesure nécessaire pour l'obtention du flux

stationnaire. Les déterminations des valeurs de time-lag et du coefficient de diffusion sont réalisées de la même manière que précédemment pour le LDPE.

Tableau 5.2. Time-lag, coefficient de diffusion de l'AE, du BE et de l'HE dans le P(D,L)LA Biophan® à 20 kPa, sans backflush, n= 4.

Esters éthyliques	Time-lag (min)	$D \times 10^{15}$ (m².s^{-1})	CV (%)
Acétate d'éthyle	166,6[a] ± 73,7	7,39 ± 3,27	44
Butyrate d'éthyle	188,3[a] ± 49,9	6,15 ± 1,88	31
Hexanoate d'éthyle	183,2[a] ± 14,9	6,18 ± 0,46	7

[a] différences significatives à $p < 0,05$ (Duncan)

La mesure des time-lag pour chacun des composés organiques étudiés ne montre aucune différence significative. En effet, un time-lag moyen de 180 min est obtenu pour les trois esters éthyliques. Par conséquent, les coefficients de diffusion mesurés pour ces trois esters éthyliques dans le P(D,L)LA Biophan® ne mettent en évidence aucune différence significative en fonction du composé étudié (Tableau 5.3). Le coefficient de variation étant de 44 % pour l'acétate d'éthyle, il semble impossible de distinguer une évolution des coefficients de diffusion en fonction des esters éthyliques. Alors que nous nous attendions à voir, comme pour le LDPE, une diminution de D avec l'augmentation de la masse molaire du diffusant, les résultats ci-dessus ne semblent pas suivre cette évolution. De plus, il apparaît que la valeur de D pour l'acétate d'éthyle est largement supérieure à celle mesurée par microbalance, soit $2,4 \times 10^{-17}$ m².s^{-1}. Ainsi la différence significative, entre la valeur de D de l'acétate d'éthyle dans le P(D,L)LA déterminée par sorption-désorption et celle obtenue par perméation, confirme bien les conclusions de Dury-Brun *et al*. avec l'hexanoate d'éthyle pour un papier imprégné et recouvert d'une substance hydrophobe (Dury-Brun, 2008).

Des mesures complémentaires semblent nécessaires afin de mesurer les coefficients de perméabilité de ces esters éthyliques dans le P(D,L)LA.

De plus, au regard du faible écart entre les coefficients de diffusion des trois molécules, aussi bien dans le cas du LDPE et du P(D,L)LA, nous pouvons conclure (i) que la variabilité entre les manipulations est trop forte pour pouvoir mettre en lumière l'effet de la masse molaire du perméant sur les coefficients de transport ou/et (ii) que la plastification et la recristallisation induites par le contact vapeur avec les composés organiques sont plus ou moins importantes d'une molécule à une autre (cf. chapitre 4.3) et donc qu'elles perturbent plus ou moins fortement la diffusion des molécules dans la matrice.

Ainsi au vu de la plastification et cristallisation obtenues avec d'autres grades de P(D,L)LA (publication 4 et 5), une analyse DSC a été effectuée sur les films de P(D,L)LA Biophan® et P(D,L)LA CD92 après mesure de la perméation.
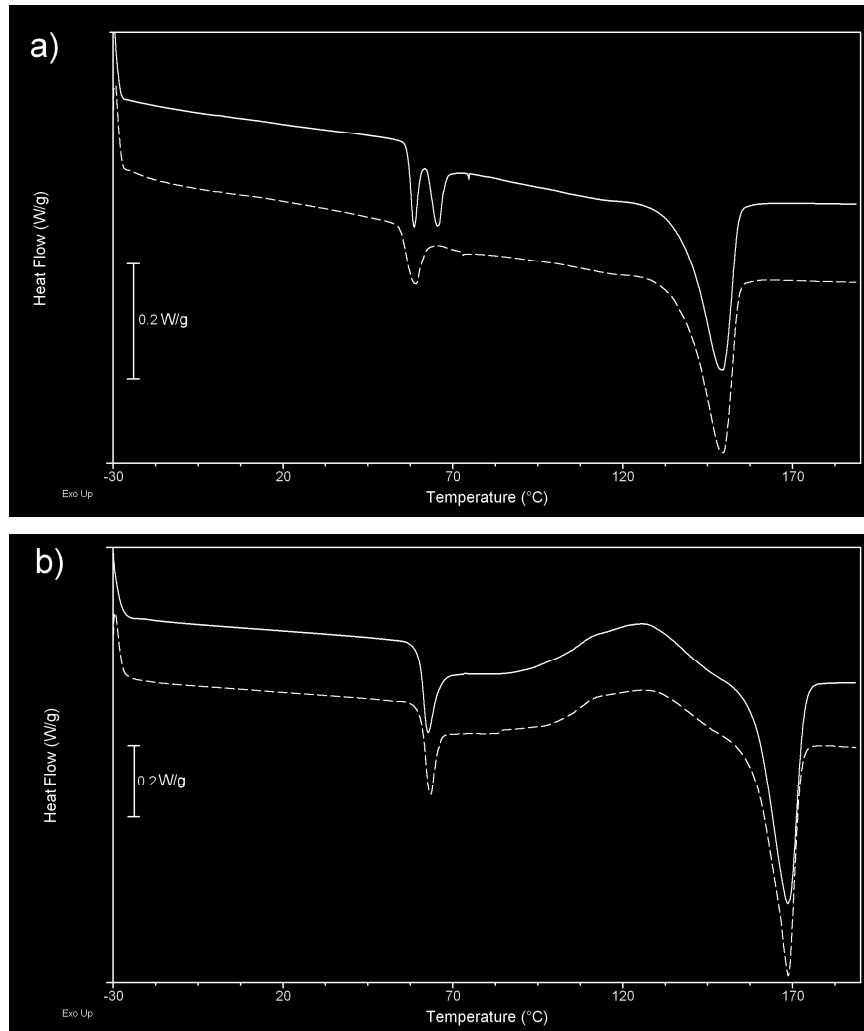
Figure 5.3 Thermogrammes du a) P(D,L)LA Biophan® et du b) P(D,L)LA CD92 avant (ligne pleine) et après (ligne pointillée) mesure de perméation aux esters éthyliques.

Une modification du signal du P(D,L)LA Biophan® (entre 55 et 65 °C), et donc de la structure, est visible mais sans diminution notable de la température de transition vitreuse (Figure 5.3a). Quant au P(D,L)LA CD92, aucune modification de signal après contact avec les esters éthyliques n'est mesurée (Figure 5.3b). De plus, aucune modification de la cristallinité n'est visible sur ces deux grades de P(D,L)LA après contact . Il semble donc que les concentrations en composés organiques dans l'espace gazeux soient trop faibles pour induire une modification de la structure du P(D,L)LA après 20 h de contact en perméation.

Cette modification de structure observée pour le P(D,L)LA Biophan® pourrait être à l'origine de l'absence d'écart entre les time-lags des différentes molécules organiques. En effet, ceux-ci seraient fortement sensibles aux phénomènes transitoires non-diffusifs (plastification, cristallisation, gonflement…) et donc varieraient peu en fonction de la molécule mais plutôt en fonction des modifications de l'état de la matrice.

5.2. Détermination du coefficient de diffusion par mesures in-situ.

Cette méthode a été développée dans le contexte de la thèse de Manuel Durand (Durand, 2010) traitant de la simulation des dynamiques moléculaires de la diffusion d'oligomères dans des polymères fondus. Cette simulation est indispensable afin de déterminer la relation existant entre la structure chimique de solutés de masse intermédiaire (monomère, additif) et leur coefficient de diffusion dans les polymères. En effet, la diffusion de molécules revêt une importance considérable puisqu'elle contrôle en partie la durée de vie et la contamination éventuelle de substance mis en contact avec le matériau. Ainsi la contamination de produits alimentaires par les constituants d'emballage, le vieillissement de polymère ou la réactivité dans les solides pourraient être prédits.

Comme il a été montré précédemment dans la partie bibliographique, une dépendance très forte existe entre les coefficients de diffusion et la masse molaire des solutés de masse intermédiaire : $D \propto M^{-\alpha}$ (Kwan, 2003; Reynier, 2001a; Reynier, 2001b). Cependant il apparaît que cette dépendance à la masse molaire est bien supérieure dans les structures semi-cristallines que dans les polymères fondus. Des valeurs de α entre 0,6 et 3 sont retrouvées pour la diffusion de molécules, de structure diverse et de masse variant entre 16 et 1177 g.mol^{-1}, dans un polyéthylène basse densité à 23 °C.(Vitrac, 2006b) Néanmoins, pour définir une loi d'échelle, des molécules homologues doivent être étudiées. Ainsi Kwan *et al.* ont déterminé une loi d'échelle avec α entre 2 et 4,7 selon la température (23 à 85 °C) pour la diffusion d'une série de n-alcanes (de C_6 à C_{17}) dans un polyamide amorphe.

La mesure à l'échelle macroscopique du coefficient de diffusion dans des matrices denses repose sur une étude de profils de concentration grâce à une méthode d'empilement de couches à travers lesquelles la molécule étudiée va diffuser. Le nombre de Fourier, F_0, représentant le temps de diffusion adimensionné permet de prendre en compte le temps de contact et de la géométrie des échantillons. Ainsi F_0 relie le coefficient de diffusion (D en m².s^{-1}) au temps de contact ($t_{contact}$ en s) et à l'épaisseur des échantillons (l en m) selon l'Equation suivante :

$$F_0 = \frac{D \times t_{contact}}{l^2} \tag{5.2}$$

La comparaison des profils de concentration expérimentaux, obtenus par empilement, et ceux obtenus par simulation, en prenant en compte le temps et la géométrie fournis des valeurs de F_0, permet alors de calculer une valeur de coefficient de diffusion.

Deux types d'empilement sont couramment utilisés, l'empilement selon Moisan et l'empilement selon. Roe :

- La méthode de Moisan nécessite une source en sonde moléculaire de grande épaisseur et de concentration élevée de manière à l'estimer comme constante au cours de l'expérimentation. L'empilement consiste ensuite à superposer des couches de film vierge sur la source épaisse. Une simulation numérique de la désorption de la source et la diffusion dans les couches superposées est réalisée (Figure 5.9). Celle-ci met en évidence un appauvrissement de la source et une surestimation de la valeur de D en particulier pour les faibles valeurs de F_0.

- La méthode de Roe consiste à introduire un film source (formulé) au milieu d'un empilement de films vierges. Cette méthode a pour désavantage d'induire un effet de dilution important dépendant du nombre de films empilés. Les faibles concentrations des diffusants peuvent alors être difficilement quantifiables.

L'objectif de ce travail est de mettre au point une technique de référence pour la mesure du coefficient de diffusion (D) supérieur à 10^{-17} m².s^{-1} en utilisant les profils de concentration. Pour cela, la méthode de Roe a été adaptée au cas du PLA en réalisant un empilement de seulement trois couches afin d'éviter le problème de dilution (Figure 5.4). La détermination de D, à partir de ces profils de concentration, pour des molécules de masse molaire moyenne dans un polymère, a été réalisée grâce à une méthode locale et non destructive basée sur la fluorescence des molécules étudiées.
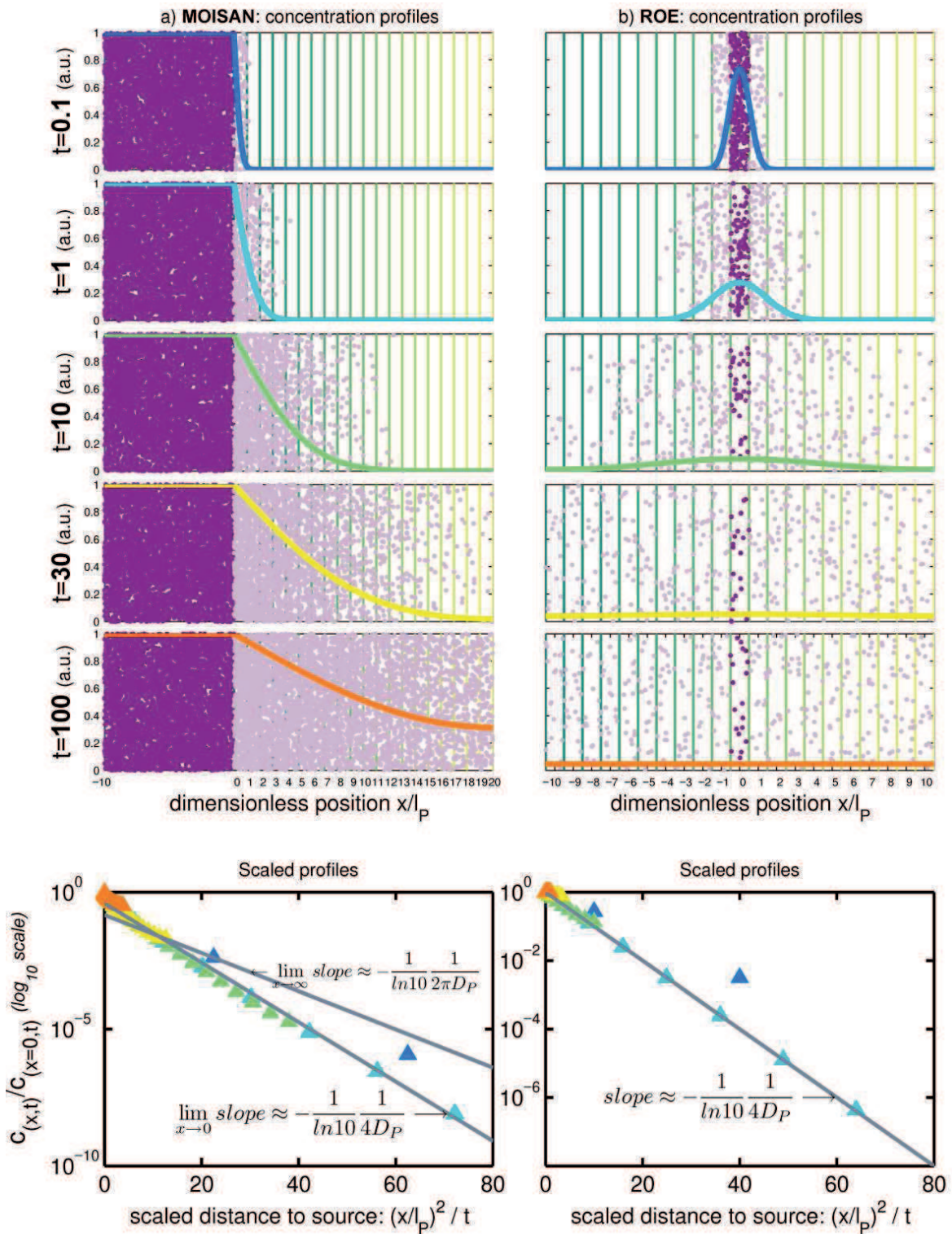
Figure 5.4. Principes de détermination des coefficients de diffusion par contact solide/solide selon les méthodes de Moisan et Roe. a) en utilisant une cire comme source non-limitante entre -10 et 0, b) en utilisant une couche centrale formulée en position 0. Chaque cas est constitué de vingt couches réceptrices. La concentration locale est représentée soit par un profil continu normalisé soit comme des particules aléatoirement réparties dans chaque couche. L'échelle de temps est choisie de manière à coïncider avec une valeur de coefficient de diffusion D_P de 1. Notons que $ln10$ apparaît, dans la pente, en tant que logarithme décimal au lieu du logarithme naturel.

5.2.1. Matériels et méthodes

5.2.1.1. Matériels

Deus films commerciaux ont été utilisés pour ce travail :
- Le film de P(D,L)LA Biophan®, de 20 µm d'épaisseur, est composé de trois couches, deux couches scellables de chaque côté d'une couche de PLA cristallisé.
- Le polypropylène (PP), de 200 µm d'épaisseur, a été réalisé par extrusion-soufflage (AMCOR Research, UK) et contient un antioxydant fluorescent (Irganox 1076).

Les trois sondes fluorescentes (Sigma-Aldrich) utilisés pour les expériences de microscopie à fluorescence ont été mises en solution dans l'éthanol. Ces sondes sont toutes composées de deux cycles aromatiques séparés par un nombre croissant de carbones comme montré dans le Tableau 2.4.

5.2.1.2. Préparation des échantillons

L'étape de formulation du PP a consisté à immerger les échantillons de PP dans des solutions de molécules fluorescentes dans l'éthanol à une concentration de 0,005 mol.L^{-1} pendant une semaine à 60 °C afin d'obtenir un matériau gorgé de molécules fluorescentes nommé fPP. Ce matériau constitue le film source pour les mesures. Un empilement de trois couches, P(D,L)LA vierge, PP formulé (fPP) et P(D,L)LA vierge, est ensuite réalisé selon la Figure 2.14. Les empilements sont ensuite placés dans une étuve à 70 °C pendant 114 h puis placés dans l'azote liquide pour stopper la diffusion des molécules fluorescentes dans le PLA.

Afin de pouvoir observer les profils de concentration au microscope à fluorescence, les empilements sont microtomés transversalement en fines bandes de 10µm d'épaisseur et posés sur une lame de verre. Une fois recouverte d'une lamelle en quartz, les échantillons sont observés au microscope avec un objectif à immersion.

5.2.1.3. Microscopie en épifluorescence

Le microscope POLYPHEME utilisé est construit autour d'un microscope inversé Olympus IX71. Le rayonnement Synchrotron, faisceau blanc, excite les fluorophores en un point précis de l'échantillon grâce à l'objectif. Le signal émis est ensuite renvoyé jusqu'à un diaphragme ajustable (pinhole) et récupéré par un CCD.

Un spectre d'émission de fluorescence est réalisé tous les 0,5 µm sur les 20 µm d'épaisseur du P(D,L)LA. L'acquisition des données est effectuée par le logiciel Labspec (Jobin-Yvon) et leur traitement par Matlab.

5.2.2. Résultats et discussion

Un travail préliminaire de détermination des longueurs d'onde de travail a été réalisé dans un premier temps, à l'aide des spectres d'émission (Figure 5.5) après excitation des molécules fluorescentes à 275 nm.
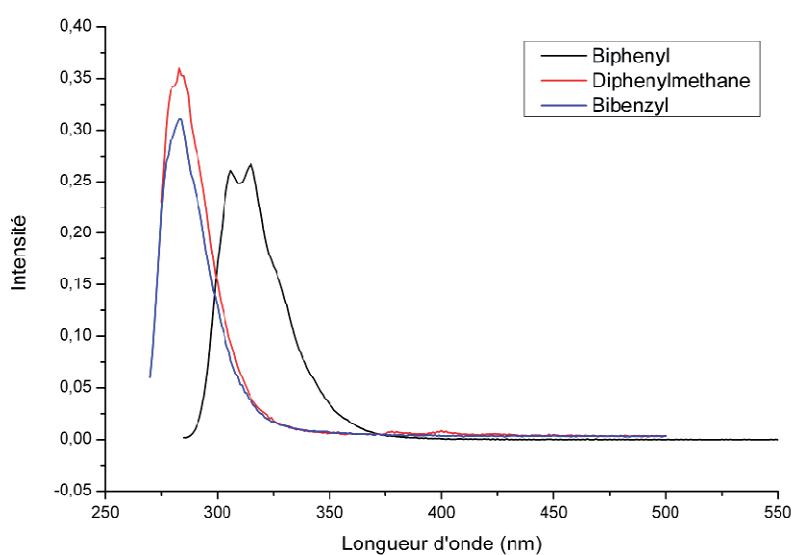
Figure 5.5. Spectre d'émission des trois molécules fluorescentes utilisées, excitées à 275 nm.
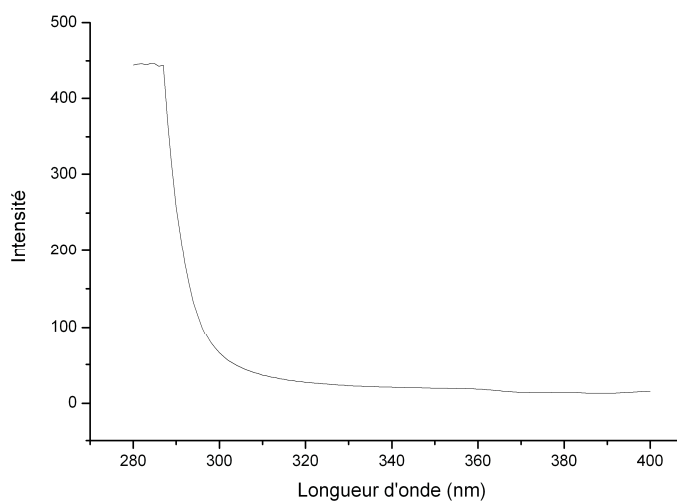
Figure **5.6.** Spectre d'émission du P(D,L)LA Biophan®, excité à 280 nm.

Ainsi, il apparaît que les longueurs d'onde à considérer sont 315 nm pour le biphényl et 285 nm pour le diphenylméthane et le bibenzyl. Le P(D,L)LA ne s'avère avoir aucune bande d'absorption à ces longueurs d'onde (Figure 5.6).

Dans un second temps, les trois couches de matériaux après mise en contact pendant 114 h et microtomées, ont été observées par microscopie à fluorescence en configuration épi (Figure 5.7).
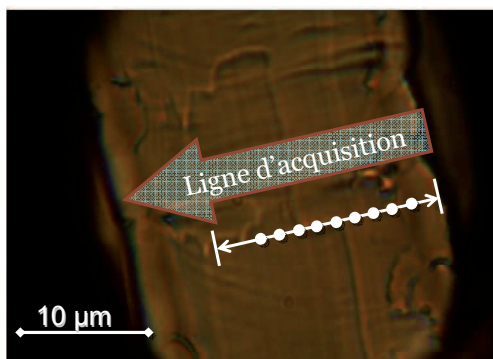
Figure 5.7. Micrographie d'une coupe microtomée de P(D,L)LA Biophan® le long de son épaisseur.

Un exemple de spectres ainsi obtenus est montré dans la Figure 5.8 pour chacun des points de mesure le long de l'épaisseur de l'échantillon. Une évolution de l'intensité des pics est ainsi observée grâce à la modification de couleur du pic à 315 nm : plus le pic est bleu clair, plus l'intensité est importante. L'intensité est donc plus importante entre 5 et 25 µm qu'aux extrémités (avant 5 µm et après 25 µm). Cela s'explique par le fait que les mesures ont été démarrées en dehors de l'échantillon. En effet, les coupes microtomées n'étant pas planes, la micrographie manque de netteté au niveau de la surface des échantillons (Figure 5.7), ce qui explique la difficulté à déterminer la surface des coupes. Ainsi pour s'affranchir de la variation due à la détermination de la surface, toutes les mesures ont démarrées en dehors de l'échantillon étudié.
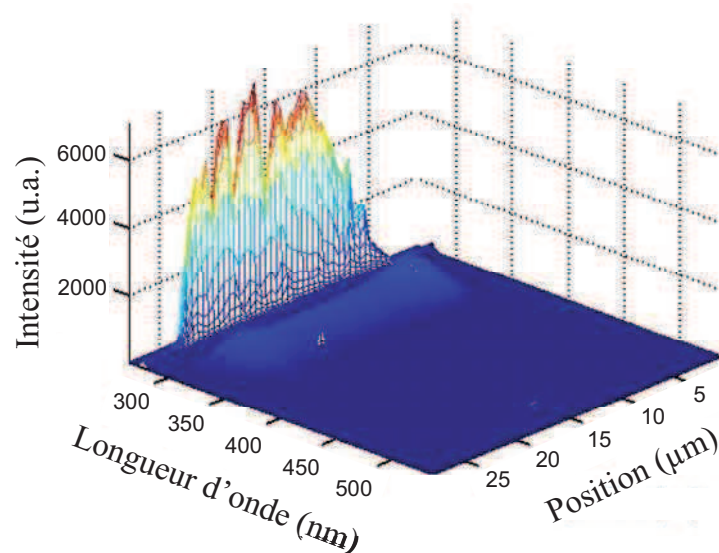
Figure 5.8. Profils spectraux de fluorescence du biphényl en 2D sur les coupes transversales de PP (longueur d'onde × position).

Chaque spectre ainsi obtenu a ensuite été soumis à un traitement permettant de soustraire la ligne de base et intégrer les pics d'émission spécifiques de manière à obtenir un graphe de l'intensité en fonction de la position (Figure 5.9).
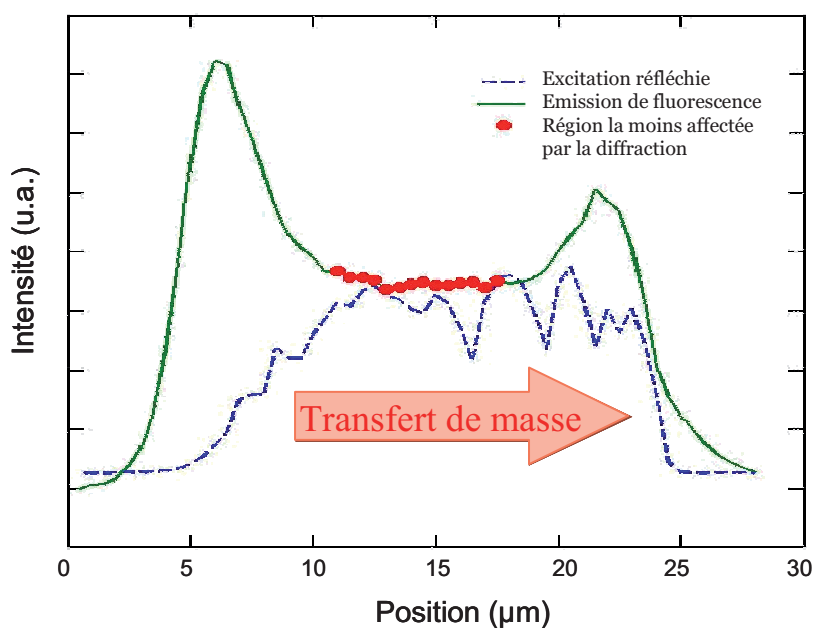
Figure 5.9. Profil de l'intensité en fonction de la position dans l'échantillon de P(D,L)LA Biophan® mis en contact avec le PP formulé.

Au regard du profil normalisé obtenu, il a été nécessaire de prendre en compte la diffraction lumineuse liée à la défocalisation (échantillon non plan et coupe approximative liée à l'absence

de rigidité des matériaux). Cette diffraction lumineuse prend la forme de pic à environ 6 µm et 22 µm sur les profils d'intensité.

Une modélisation numérique des données théoriques portant sur le transport diffusionnel a été réalisée en parallèle en tenant compte de la géométrie des échantillons, du temps et de la température de contact mais également du coefficient de partage entre le PP et le P(D,L)LA. Cette modélisation a pour but de comparer théorie et expérimentation afin de déterminer le nombre de Fourier associé. Cette modélisation permet de générer les profils d'intensité présentés en Figure 5.10 en fonction d'un nombre de Fourier variant entre 0,0001 et 10.
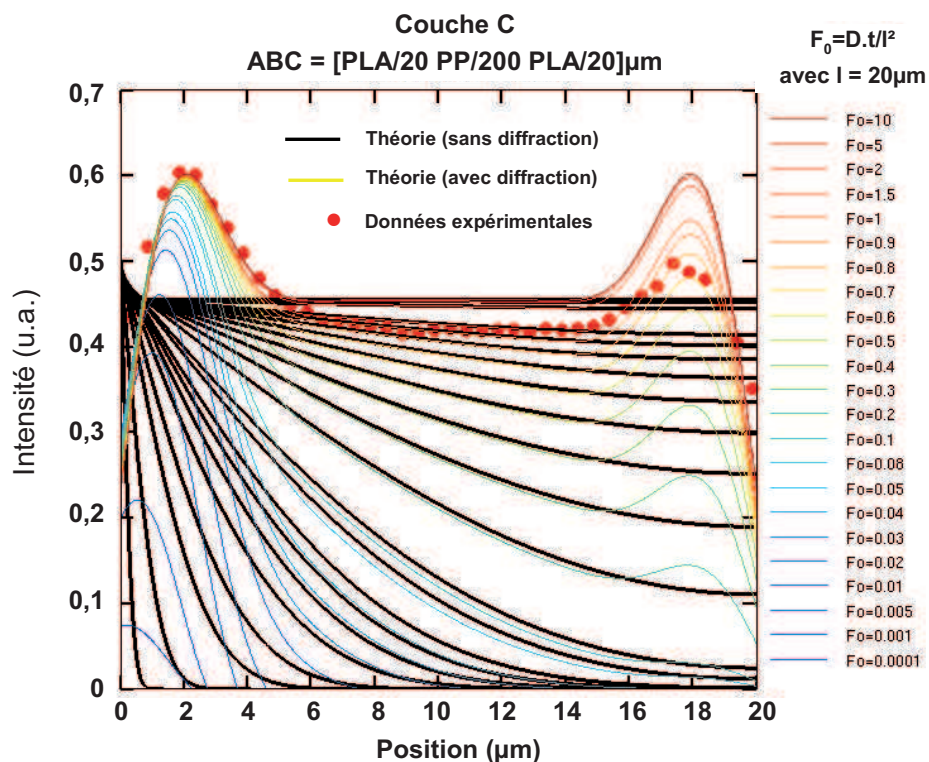
Figure 5.10. Profil d'intensité théorique simulé pour le P(D,L)LA Biophan®d'épaisseur 20 µm.

Ainsi il apparaît, lorsque les résultats expérimentaux sont comparés aux données théoriques simulées (Figure 5.10) que le nombre de Fourier pour le biphényl dans le P(D,L)LA est proche de 1,5. Cette méthode de comparaison des profils théoriques et expérimentaux a ainsi permis de déterminer un coefficient de diffusion pour le biphényl dans le P(D,L)LA Biophan® de l'ordre de $1,5.10^{-15}$ m².s^{-1} à 70 °C.
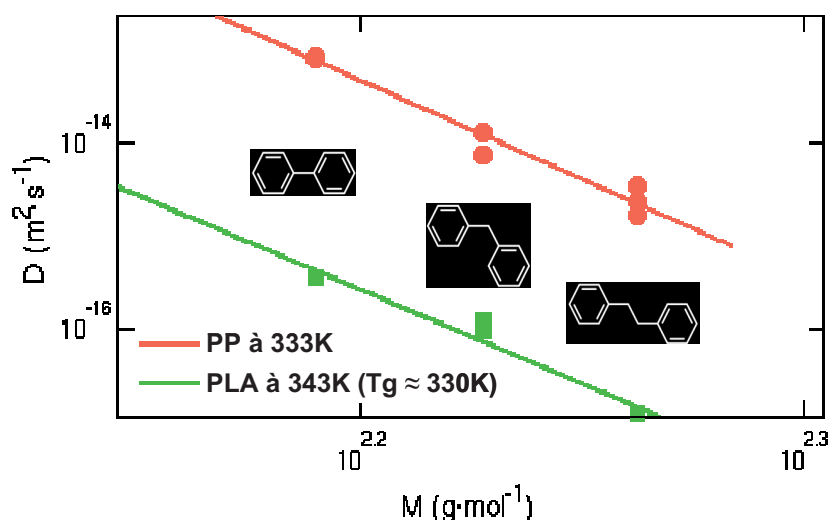
Figure 5.11. Evolution des coefficients de diffusion en fonction de la masse molaire de la molécule fluorescente dans le P(D,L)LA Biophan® et le PP AMCOR.

La série homologue de traceurs fluorescents utilisés lors de ce travail met en évidence une diminution du coefficient de diffusion avec l'augmentation du nombre de carbone séparant les deux noyaux aromatiques (Figure 5.11). Plus exactement, il semble que l'ajout d'un carbone entre les deux phényls conduit à une diminution des valeurs de D d'un facteur 3. Cette évolution est comparable à celle observée avec les esters éthyliques (ajout d'un carbone à la chaine aliphatique) dans le LDPE par mesure de perméation semi-dynamique mais bien différente de celle constatée, pour les mêmes molécules et dans les mêmes conditions, pour le P(D,L)LA Biophan®.

De plus, il apparaît que la dépendance du coefficient de diffusion à la masse molaire des molécules fluorescentes est confirmée puisque le logarithme de D semble proportionnel à la masse molaire. La valeur de α est ainsi estimée à 20.

Une telle valeur de α, est largement supérieure aux données déjà existantes dans la littérature pour les polyoléfines et reste à être confirmée par de nouvelles analyses. En effet, Vitrac *et al.* (Vitrac, 2007) et Kwan *et al.* (Kwan, 2003) ont mis en évidence des valeurs de α comprise entre 2 et 6 pour des alcanes (C_{12} à C_{28}) respectivement dans le LDPE, à une température supérieure à sa T_g, et le polyamide (PA), à des températures de part et d'autre de sa T_g.

Les expériences menées sur le PP, en parallèle pour servir de référence, avec les mêmes molécules fluorescentes ont mis en évidence une même valeur de α, soit 20 (Figure 5.11). Par conséquent, quel que soit le polymère considéré, il semble que la diffusion, dans un polymère semi-cristallin, de molécules possédant des noyaux aromatiques est régie par une loi d'échelle bien différente de celle observée pour les molécules linéaires (type alcane) dans LDPE (Vitrac, 2007) ou le PA (Kwan, 2003).

5.3. Evaluation des dynamiques moléculaires de sondes nitroxydes dans le PLA pur et plastifié.

Le projet de publication suivant présente une méthode destinée à sonder l'hétérogénéité d'échantillons à l'aide de molécules paramagnétiques dans le P(D,L)LA pur et plastifié en utilisant un appareil à résonance paramagnétique électronique (RPE/ESR). Deux modes d'incorporation des sondes dans le P(D,L)LA CD92 ont été testés, l'incorporation en phase vapeur et l'incorporation par voie fondue. Des spectres RPE ont ensuite été réalisés au cours du temps afin de sonder la diffusion des molécules paramagnétiques dans l'épaisseur du film. Des spectres ont également été obtenus lors de montée en température afin de mesurer les temps de relaxation des sondes permettant d'évaluer la dynamique des chaînes de polymère et les énergies d'activation de chacun des mélanges.

Probing molecular dynamics along the thickness of neat and plasticized polylactides by ESR methods (Publication n°6)

Cécile Courgneau[1,2], Olivier Vitrac[1], Anne-Marie Riquet[1]

[1]INRA, UMR 1145 Food Process Engineering, 1 avenue des Olympiades, F 91300 Massy, France.

[2]AgroParisTech, UMR 1145 Food Process Engineering, 1 avenue des Olympiades, F 91300 Massy, France.

5.3.1. Abstract

Improving the barrier properties to gas and organic compounds of biosourced polyesters, such as polylactides (PLA), by increasing their crystallinity has been suggested by several authors. This paper investigates the risk of microphase separation for a technological approach that would involve a plasticization of PLA with common plasticizers: Acetyl tributyl citrate (ATBC) and Poly(ethylene glycol) (PEG). Overplasticization effects following microphase separation were monitored along the film thickness by exposing dynamically thermo-compressed films to nitroxides spin-probes. The method enabled a scan of the local polymer mobility for different concentration profiles in spin-probes, with in particular a maximum moving continuously in time towards the geometric centre. The results were interpreted as excess local temperatures that would give similar ESR spectra relaxation in the bulk. It was shown that measured excess temperatures could be related to local shifts in the glass transition temperature along the film thickness.

Keywords: polylactide, microphase separation, spin-probe ESR, diffusion, polymer relaxation

5.3.2. Introduction

The use of renewable resources for food packaging material producing is interesting for environmental reasons. The amount of waste increases whereas landfill capacities are limited. Moreover persistent pollution and limited fossil fuel resources are major concerns in our current

society (Shen, 2009). Bio-based polymers may offer solution to lessen our dependence to petroleum stocks while lightening solid waste disposal issues (Lim, 2008). Aliphatic polyesters such as polylactides (PLA) offer an attractive alternative to synthetic polymers with similar mechanical properties (Auras, 2005; Petersen, 2001; Walker, 2007; Wang, 2003). Barrier properties to gas (Bao, 2006; Komatsuka, 2008), water vapor (Tsuji, 2006) and organic compounds (Auras, 2006; Colomines, 2010) have been studied extensively over the past decade. PLA is ranked between polystyrene and poly(ethylene terephthalate) (PET) for its barrier properties to oxygen with permeability values close to high density polyethylene ones. Permeability to gas or small solutes in thermoplastics tends to increase exponentially with the fractional free volume to cohesive energy density ratio (Duda, 1996). In the case of PLA, few correlations have been proposed to correlate its structure with its transport properties. Available studies targeted the effect of crystallinity (Drieskens, 2009; Hu, 2005; Hu, 2002; Kanehashi, 2010; Natu, 2005; Sawada, 2010; Sekelik, 1999) on the sorption and diffusion of oxygen. It was shown that the permeability decrease with crystallinity, well-established on a polyester such as PET (down to 50 % without orientation) (Hu, 2005; Sekelik, 1999), could not be easily reproduced at lab scale with PLA. Some groups showed an enhancement (Drieskens, 2009; Sawada, 2010) and others non-significant effects (Colomines, 2010). The complication arises from the slow crystallization rate of unplasticized poly(L-lactide) with typical half time crystallization of 2 min at 110 °C (Di Lorenzo, 2006).

To get reproducible results at industrial scale, a possible strategy could be to plasticize PLA to accelerate cold crystallization. Previous results (Courgneau, 2011) showed however that the incorporation of linear plasticizers such as poly(ethylene glycol) (PEG) led to significant exudation. The current work aims at assessing possible micro-phase separation and heterogeneities in P(D,L)LA blended with different plasticizers and concentrations: PEG and acetyl tributyl citrate (ATBC), which do not yield detectable exudation in differential scanning calorimetry (DSC). Our motivation was to get an imaging of the molecular dynamics of small probes along the film thickness (half thickness: 75 µm) in well equilibrated P(D,L)LA-plasticizer blends. Such profiles were obtained by studying non-equilibrium sorption and desorption kinetics of stable nitroxide radicals by electron spin resonance (ESR). Resonance spectra obtained for different probe concentration profiles were compared with similar profiles obtained at equilibrium to separate relaxation dynamics close to the surface and in depth.

The paper is organized as follows. Section two describes the methodology of preparation of blends and our ESR technique. Preliminary results showed that only nitroxide probes strictly larger than TEMPO (2,2,6,6-Tetramethylpiperidin-1-oxyl, molecular mass 156 g.mol^{-1}) led to a

temperature transition between fast and slow rotational motions close to room temperature. Hence, two spin-probes were used to increase the detectability of change in molecular dynamics for a same measurement temperature. Section three presents firstly the changes in relaxation spectra with time when a same processed film is exposed to decreasing probe vapour partial pressures. Exposure conditions were chosen to maintain during the whole experiment a strong disequilibrium between the surface and the ambience. The maximum concentration in the film was thus moving from the surface towards the material centre. The concept of excess temperature was demonstrated by showing that localized 2D ESR spectra and bulk 2D spectra were almost invariant by temperature translation. An attempt of validation as a deviation of the local glass transition temperature (T_g) is proposed. Diffusional mechanisms of probes in neat and plasticized P(D,L)LA are finally discussed in Section 4.

5.3.3. Experimental

5.3.3.1. Materials

Polylactide pellets were supplied by ECPM-LIPHT (France). The content in L-lactide was about 92 wt% (P(D,L)LA CD92). The average molecular weight was of $9.0\text{-}10^4$ g.mol^{-1} with a polydispersity index of 2.75.

Plasticizers, Acetyl tributyl citrate (ATBC) and Poly(ethylene glycol) (PEG), were purchased from Sigma Aldrich (France). Spin-probes, 4-hydroxy – 2,2,6,6 – tetramethylpiperidine-1-oxyl (TEMPOL) and 4-amino– 2,2,6,6 – tetramethylpiperidine-1-oxyl (AminoTEMPO) were supplied by Aldrich (France) and Fluka (France) respectively. Table 1 lists the typical properties of plasticizers and spin-probes.

5.3.3.2. Methods

5.3.3.2.1. Film preparation

Before use, P(D,L)LA pellets and plasticizers were dried at 80 °C overnight in a vacuum oven. Films were possibly formulated with plasticizers and spin-probes in molten state within an internal mixer (Haake Rheocord 9000) at 160 °C and 60 rpm for 15 min. Two different levels of plasticizers, either PEG or ATBC, were considered: 9 and 17 wt%. When directly incorporated to

formulation, a concentration of 0.15 wt% was used for both spin-probes. Final blends were dried during a minimum of 4 h at 80 °C.

Neat and plasticized P(D,L)LA films were processed by thermo-compression (press model: 15 tonnes, Telemecanique, France) at 185 °C and 150 bars in a multistep process. P(D,L)LA blends were first molten between both hot plates without pressure for 3 min. They were subsequently successively pressed under 10 bars for 30 s, 50 bars for 30 s and finally 150 bars for 1min to remove air bubbles. The final film thickness was approximately of 0.15 mm for surface area of ca. 100 cm^2. All films were quenched in water at ambient temperature.

Table 1. Physical properties of the neat P(D,L)LA, the plasticizers and the probes: molecular weight (M), molecular volume (V), glass transition temperature (T_g) and Melting temperature (T_m).

Substances	M (g.mol^{-1})	V (Å^3)	T_g (K)	Tm (K)	Molecular structure
P(D,L)LA	60 000	-	332	428	
PEG	300	-	208	262	
ATBC	402	-	190	282	
TEMPOL (Tol)	172.25	174	-	342-344	
AminoTEMPO (AT)	171.25	179	-	273	

Experimental

Variable concentration profiles in spin-probes with a maximum moving towards the centre of films were obtained out by exposing the films to probe vapors within a sorption vessel at 343 K (above the melting point of probes and above the glass transition temperature of the tested P(D,L)LA). The sorption experiment was carried in a finite volume (ca. 1200 cm^3) in equilibrium with a finite amount of liquid probes (ca. 20 mg) and subjected to a periodic renewal (14 renewals, initially every day and subsequently every three days) of the whole gas phase by fresh air at 343 K. The design ensured that a complete consumption of the liquid probe amount (by either sorption or due to air renewal) was achieved after 8 days of contact. As a result, the profiles during the first 8 days corresponded to a sorption situation with a maximum at the immediate surface whereas profiles after 8 days obeyed to a desorption situation with a maximum translating progressively towards the centre. Samples consisted in small 20 × 2 × 0.15 mm^3 strips. All neat and plasticized samples were exposed to the same enriched probe vapor ambience in the same flask to get comparable results with exposure time.

Renewal times were used to acquire the ESR spectrum of each sample at 298 K. All acquisitions were performed in less than 20 min with an initial cooling time of 5 min. Last acquisition occurred after 29 days of residence time in the sorption vessel at 343 K.

Such conditions ensured that the maximum intensity of the paramagnetic signal for different exposure times was related to probes located at different depths. As the diffusion coefficients of the probe within P(D,L)LA varied plasticization level, ESR measurements for a same exposure time corresponded however to different positions between samples except for small contact times.

Interpretation

The principles of mass diffusion of a spin-probe into the sample under dynamic exposure were interpreted with the help of a simple diffusion model. At time $t = 0$, a probe-enriched atmosphere with partial pressure equal to $p_\infty(t = 0)$ is put in contact with a sample of thickness $2l$. The atmosphere is subjected to kinetic losses due to either transfer to the sample or to some leakages with an atmosphere with a probe partial pressure $p_0 = 0$. By assuming that mass flux at the sample-air interface ($x = 0$) is controlled by a mass transfer coefficient, h, and a Henry constant, k, the transport and mass balance equations become in one dimension:

$$\begin{cases} \dfrac{\partial C(x,t)}{\partial t} = \dfrac{\partial}{\partial x}\left(D(x)\dfrac{\partial}{\partial x}C(x,t) \right) \ for\ 0 \leq x \leq l \\[3mm] \dfrac{\partial C(x=0,t)}{\partial x} = \dfrac{h}{RT}\left(kC(x=0,t) - p_\infty(t) \right) \\[3mm] \dfrac{\partial C(x=l,t)}{\partial x} = 0 \\[3mm] \dfrac{dp_\infty(t)}{dt} = \dfrac{A}{V_\infty}\left[\alpha\left(p_0 - p_\infty(t)\right) + h\left(kC(x=0,t) - p_\infty(t)\right) \right] \end{cases} \qquad (1)$$

where α is a constant controlling the dilution rate of the probe-enriched atmosphere. R and T are the gas constant and the absolute temperature respectively. A and V_∞ are the surface contact area and the volume of the atmosphere in contact respectively.

Figure 1 presents the simulated probe concentration profile along the film half-thickness $C(x,t)$ for typical chemical affinities of the probe (i.e. k values) for the film while keeping constant all other parameters. Without changing the conclusions, a uniform diffusion coefficient in the film, $D(x)$, and large mass Biot number $Bi = hl/D > 100$ were assumed. System of Equations 1 was discretized in space according to a finite volume discretization method (strictly verifying the mass balance) and integrated in time via a second order backward difference scheme. Scaling parameters A/V_∞ and α were chosen to fit the discontinuous experimental dilution profile with a theoretical continuous one (Figure 1a). Depletion time, $t_{depletion}$, was defined as the time to reach a maximum bulk concentration in the film (Figure 1c) and used as time scale to plot simulated results. Corresponding concentrations profiles are plotted in Figure 1b for times shorter and longer than depletion time. Important features such as the position of maximum of concentration in the film and the position of 99th percentile (first position x_{99} such that

$\int_0^{x_{99}} C(x,t)dx = 0.99\int_0^1 C(x,t)dx$) are depicted in Figure 1d. For times shorter than depletion time,

probes were located within a region positioned at the interface and thickening linearly with the square root of time. By contrast, depletion time triggered a situation where the maximum of concentration started to move in the material linearly with the square root of time. It is worth to notice that the displacements of the position of the maximum and of the 99th percentile were almost independent of the chemical affinity of the probe and were only controlled by the value of the probe diffusion coefficient in the tested material. As diffusion coefficients were unknown in materials comparison, relative estimations of probe penetration depths were achievable from measured bulk concentration kinetics by assuming similar k values. For a same k value, the ratio of diffusion coefficients between two materials was indeed given by the square ratio of initial slopes plotted in Figure 1c.
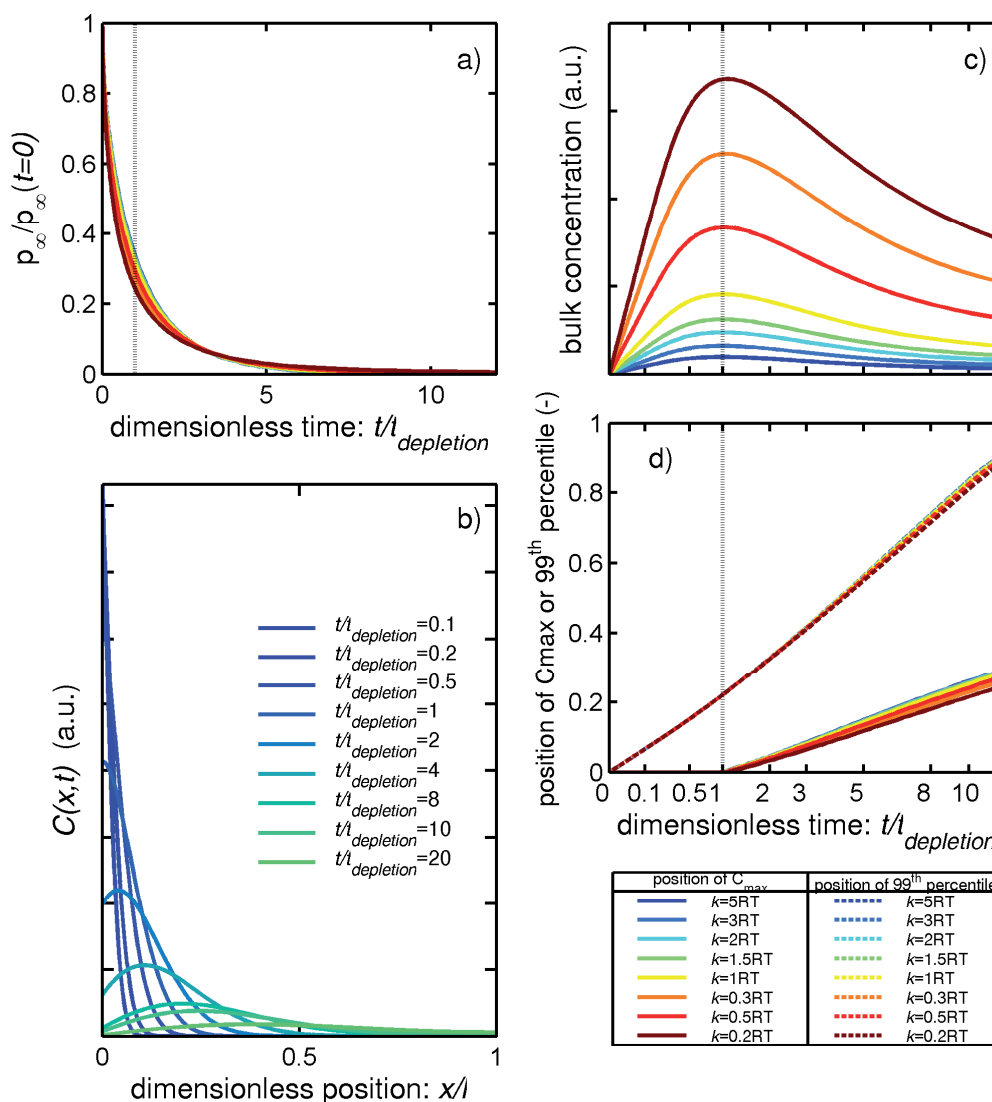
Figure 1. Simulation of the (a) temporal evolution of the normalized spin-probe vapor pressure in the whole gas phase of the flask, (b) concentration profile in the normalized film thickness depending on exposure time, (c) time dependent bulk concentration according to the chemical affinity and (d) the time-dependent maximum concentration position in the film according to the chemical affinity.

5.3.3.2.3. Thermal analyses

The thermal analyses were performed with a modulated differential scanning calorimeter (model: MDSC Q100, TA Instruments, USA) under nitrogen atmosphere. The samples (ca. 10 mg) were put into hermetic aluminium pans (TZero, TA Instruments) to avoid any loss of plasticizer and spin-probe upon heating. The glass transition temperature was determined under a sinusoidal temperature modulation of $\pm$ 1.5 K (period 80 s) applied to a temperature ramp from 283 K up to 353 K with a heating rate of 1 K.min^{-1}. The glass transition temperature (T_g) was defined from the reversing signal as the midpoint of specific heat increments on both sides of T_g. All experiments were carried out in triplicate.

5.3.3.2.4. Electron Spin Resonance (ESR) measurements and interpretation

Samples containing spin-probes incorporated either during processing (so called "melt") or by vapor sorption (so called "vapor") were inserted vertically in ESR tubes as $20 \times 2 \times 0.15$ mm^3 strips. Tubes were sealed before measurement to avoid probe losses during temperature scan measurements. Temperature scans lasting 2-3 hours were only applied to samples with uniform concentration in spin-probes (i.e. with probes incorporated during processing).

ESR measurements were carried out with a Brucker ESP 300 Spectrometer (Wissembourg, France) operating with a X-Band resonator at a microwave frequency of 9.59 GHz and equipped with a Bruker ER 041 MR microwave bridge and a Bruker ER 4111 VT variable-temperature unit. For all measurements, a 150 G scan range was used with a modulation in frequency and amplitude of 100 kHz and 1 G respectively. For temperature scans, ESR spectra were recorded from 175 to 430 K with steps from 5 to 10 K and a holding time of 2 min. All acquisitions were carried with BioSpin WinEPR Acquisition Software for EMX (Brucker, Germany) and subsequently chained to Matlab (Matlab, USA) with importation features provided by EasySpin toolbox version 3.1.6 (Stefan Stoll, 2003). Interpretation and detailed analysis of 789 collected spectra were carried out with a proprietary toolbox so-called "spinosaurus".

The interpretation of spectra follows the method described by Kovarski (Kovarski, 1997) for both liquid and polymers. Similar analyses were also performed on polymers by Veksli *et al.* (Veksli, 2000), Švajdlenková and Bartoš (Švajdlenková, 2009) and Wolińska-Grabczyk *et al.* (Wolinska-Grabczyk, 2005) Important quantities derived from ESR spectra are sketched in Figure 2. Outer hyperfine extrema ($2A_{zz}$) were assessed by the distance separating outer peaks. T_{50G} was defined from a set of scans in temperature as the temperature for which $2A_{zz}$ equals 50 G. This temperature reflects the fluctuations of the microenvironment around the spin-probe that are able to hinder its relaxation mechanism from free motions (when $2A_{zz} < 50$ G) to motions in confined space (when $2A_{zz} > 50$ G). By assuming an isotropic radical rotation, rotational mechanisms of spin-probes were revealed by the shift of extremum positions of outer triplet components as temperature increases:

$$R = \Delta H_- / \Delta H_+ \qquad (2)$$

where $\Delta H_{\pm} = \left| \Delta H(\tau) - \Delta H(\tau \to \infty) \right|$ are the shifts of extrema positions of outer components in relation to dispositions of the same extrema at the lowest temperature, T_0, when the relaxation time diverges. Rotational model was determined by the $R(\Delta H_+)$ dependence. Values ranging

from 1.5 to 3 are characteristic of continuous Brownian rotational diffusion, while values lower than 1.5 reveals a jump-tumbling rotation.
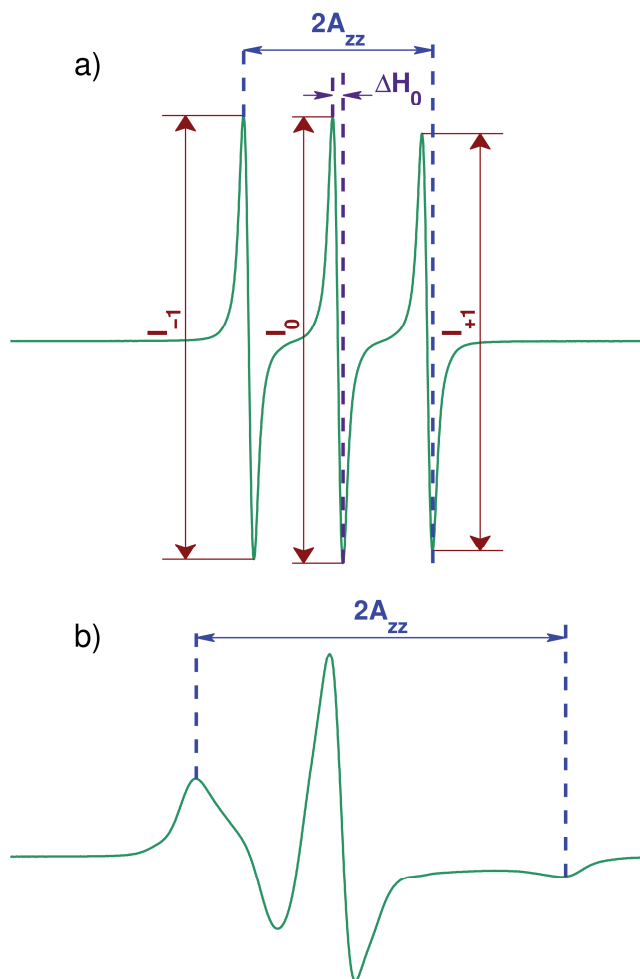
Figure 2. Typical ESR-spectra of nitroxide radicals with: (a) slow relaxation rate and (b) fast relaxation rate. Main characteristic spectral parameters are also indicated.

Correlation times, τ_{corr}, were performed for both slow and fast rotational regimes by using two different models. In the fast relaxation regime, τ_{corr} was estimated by from the Kivelson's theory (Wolinska-Grabczyk, 2005) as:

$$\tau_{corr}(T) = 0.65 \cdot 10^{-9} \Delta H_0 \left(\sqrt{\frac{I_0}{I_{+1}}} + \sqrt{\frac{I_0}{I_{-1}}} - 2 \right) \tag{3}$$

where ΔH_0 is the line width (in G) of the central line (assessed from peak to peak). I_{+1}, I_0, and I_{-1} are the intensities of the lines (assessed from peak to peak) in weak, intermediate and strong fields respectively.

In the slow relaxation regime, τ_{corr} was extrapolated from the external spectrum at a reference temperature (T_0) with extremely high correlation times (Goldman, 1972; Veksli, 2000) as a power law:

$$\tau_{corr}(T) = a\left(1 - \frac{A_{zz}(T)}{A_{zz}(T_0)}\right)^b$$ (4)

where a and b are constants depending on the mode of diffusion. For Brownian isotropic rotational diffusion mode, $a = 5.4 \times 10^{-10}$ and $b = -1.36$, while for a jump tumbling diffusion, $a = 1.1 \times 10^{-10}$ and $b = -1.01$ (Kovarski, 1997; Riquet, 2003).

In experiments with dynamic exposure to spin-probe vapors, the amount of absorbed was estimated by the number of unpaired spins contributing to the measured resonance. This quantity, M, is proportional to the area under the curve of microwave absorption, P, against applied magnetic field. As ESR spectra are recorded as the first derivative of the power curve (i.e. as $dP/dH\,(H)$), M was calculated with a double integration according to:

$$M \propto \int_{Ha}^{Hb}\left(\int_{Ha}^{H}\frac{dP}{dH}\bigg|(h)dh\right)dH$$ (5)

subjected to the following boundary conditions:

$P(Ha) = P(Hb) = dP/dH\,|(Ha) = dP/dH\,|(Hb) = 0$. Such conditions were fulfilled by removing the residual baseline, when it existed, between extreme field values.

5.3.4. Results and discussion

5.3.4.1. Molecular dynamics of spin probes along the film thickness

Dynamic exposure to spin-probe vapors was used to assess the molecular dynamics of probes along the film thickness (half-thickness: $l/2 = 75$ µm) with a goal of detecting possible local heterogeneities. Exposure to vapors were carried out at relatively high temperature (70 °C), above the glass transition temperature of all samples (5 different samples), to induce significant penetration depths during tractable diffusion times (lower than one month). All samples were previously subjected to significant annealing to avoid undesirable evolution of the polymer itself during the experiment. The variation of the DSC endotherm with time showed that annealing times lower than 2 days at 70 °C were enough to reach a constant crystallinity.

All samples were exposed to the same atmosphere during the same experiment, so that the typical depletion time of the atmosphere was the same for all samples close to 8 days. It is worth

to notice that each sample might "feel" the depletion differently according to the chemical affinity of the spin-probe for the considered sample (see Equation 1 and Figure 1). ESR spectra of all samples were acquired on a regular basis (from 1 to 3 days intervals) at a constant temperature chosen lower than the glass transition temperature (300 K) to minimize the perturbations on the spin-probe concentration profiles. Cooling prior measurement and ESR acquisitions all samples were performed within 20 min. Bidimensional Temperature × Field profiles (minimum 20 scans) were acquired only for $t = 18$ days (i.e. far from the depletion time) and corresponded to an additional perturbation of 2 hours for all samples.

Typical TEMPOL ESR spectra at 300 K for different exposure times are compared in Figure 3 to the spectrum obtained when the probe is uniformly dispersed in the melt (reference).

All spectra were normalized to present the same spectral energy density. Similar results including a narrow triplet were obtained with the spin-probe AminoTEMPO. It was verified that similar ESR spectra were obtained when the spin-probe was uniformly distributed before and after annealing. Annealing was however avoided for the reference as it induced a significant loss in spin-probes and consequently an uncontrolled change in the concentration profile. Figure 3a shows that ESR spectra did not vary with exposure time in unplasticized samples (neat P(D,L)LA). By contrast, a significant evolution was observed in plasticized samples but with different trends according to the plasticizer. With ATBC used as plasticizer at the highest concentration 17 wt% (Figure 3b), the ESR spectrum tends to converge to the spectrum obtained with a uniform concentration profile (so-called "melt"). As the convergence appears after the depletion period (8 days), the theoretical separation between the two observed behaviors from "fast" to "slower" relaxation appears far from the surface. Samples formulated with PEG at 17 wt% led to an opposite behavior with a high self-similarity with the "melt" response at the very beginning of the exposure. For exposure times longer than depletion period (i.e. deeper in the material), much slower relaxations were observed.
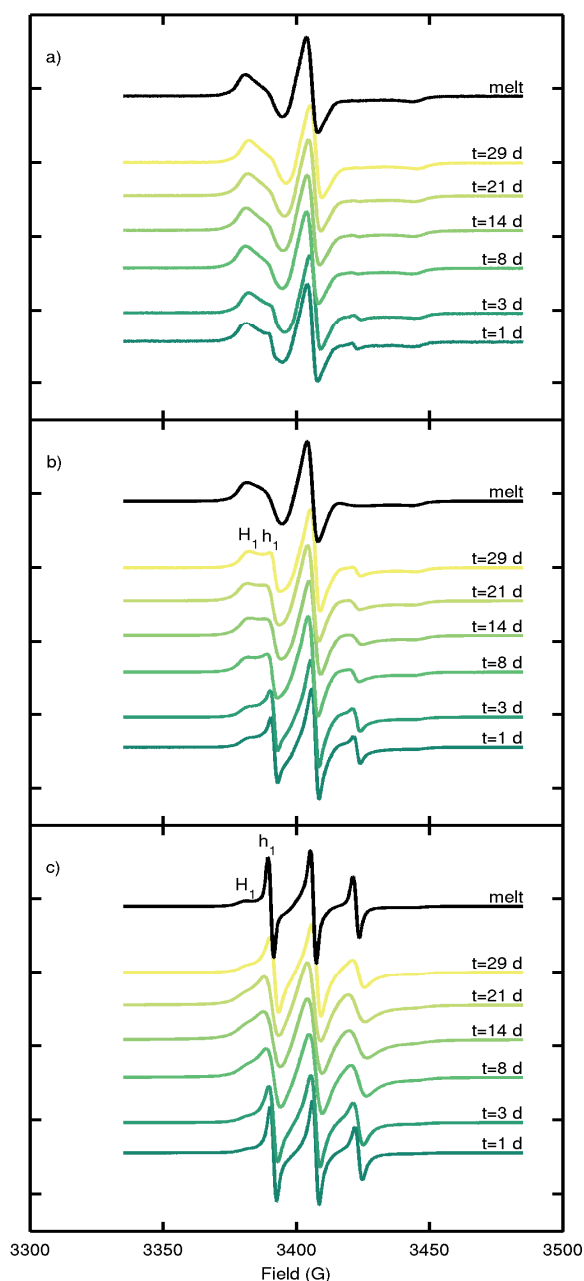
Figure 3. Time-dependent ESR spectra (TEMPOL spin probe) during dynamic exposure to TEMPOL vapors in formulated films: (a) neat P(D,L)LA, (b) P(D,L)LA with 17 wt% of ATBC and (c) P(D,L)LA with 17 wt% of PEG. The reference spectrum when the probe is incorporated in melt is also plotted.

A crude analysis of ESR spectra acquired for different exposure times demonstrated that an heterogeneous plasticization of P(D,L)LA samples was achieved with all plasticizers when they were used at the highest concentration (17 wt%). As a whole, spin-probes have much faster reorientation dynamics close to the interface than in the bulk. In the case of PEG, an initiated phase separation between P(D,L)LA and the plasticizer was detected both by a greasy/sticky contact and by an increasing deviation of ESR spectra with "melt" when exposure time

increased. It is argued that there is a partitioning of the probe in favor of the PEG exsudate rather than in favor of the plasticized polymer. Hence the concentration profile when the spin-probe is incorporated in melt would not be uniform at least close to the surface.

Further insights were gained by integrating the microwave power curve (see Equation 5) and by analyzing fluctuations of the low field line in response to heterogeneous microenvironments Low field components H_1 and h_1 depicted in Figure 3 were related to the spin-probe fractions with slow and fast relaxations respectively. The amount of unpaired spins and ratios H_1/h_1 results are represented in Figure 4 and compared to similar values when the spin-probe is dispersed uniformly in melt. Indeed, highly sensitive and specific ESR measurements at 300 K enabled without calibration the detection and the measurement of the relaxation of small amounts of spin-probes even after the initial depletion period. The amount of unpaired spins plotted in Figure 4a matched accordingly theoretical spin-probe concentration kinetics depicted in Figure 1c. In particular, the initial linearization as the square root of time supported the initial assumption of a diffusive transport of spin-probes with an apparent diffusion coefficient that was constant during the exposure experiment.

Larger amounts were absorbed in plasticized samples with almost symmetric peaks in samples plasticized with PEG. This condition confirmed the apparent highest chemical affinity of the spin-probe for PEG-plasticized films and consequently for PEG (see similar effects in Figure 1c). As depletion effects were delayed in ATBC-plasticized and in neat P(D,L)LA, it was inferred that slower diffusion coefficients and possibly higher Henry constants occurred in these samples. As a result, the spatial information retrieved from dynamic exposure to spin-probes was related to smaller length scales for these films. In neat P(D,L)LA, another practical consequence was that the amount of absorbed spin-probes was up to 80 times lower than in PEG-plasticized films. Figure 4b illustrates how fast the mobility of the probe measured in time converged to the behavior assessed in the bulk when the spin-probe spread in the film. For exposure times longer than the time required to observe depletion effects (in Figure 4a), time scales expressed on square root scale could directly related to the depth of the maximum of the concentration in the sample, as illustrated on the theoretical example depicted in Figure 1d. When the concentration gradient is only controlled by the random walk of spin-probes, the constant of proportionality is given by the square root of the spin-probe diffusion coefficient. This last quantity ($\sqrt{D}$) was a priori unknown but it was known to be proportional to slope of the initial mass uptake versus the square root of time (see Figure 1c). For a same depletion time, the spin-probe penetration depth was

therefore higher in highly plasticized samples with depth ratios varying as the initial slopes of absorbed amounts plotted in Figure 4a. It is worth to notice that the apparition of depletion effects might be delayed for unplasticized sampled by possible spin-probe cross exchange between samples, as they were all exposed to the same head-space composition during both sorption and desorption stages.
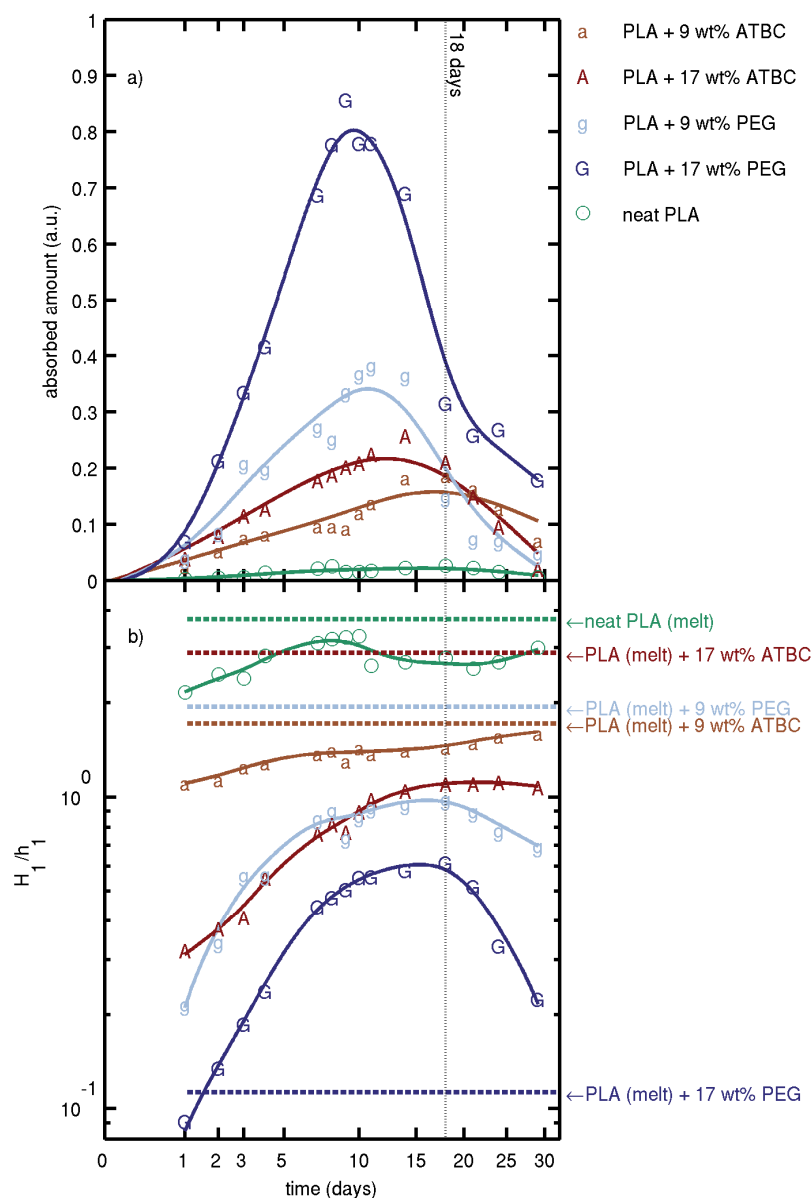
Figure 4. Evolutions as the square root of time of: (a) the absorbed amount of TEMPOL at 70 °C in neat and plasticized P(D,L)LA and (b) of the intensity ratio H_1/h_1 for neat and plasticized P(D,L)LA. Reference $H1/h1$ ratios when the probe was incorporated in melt are plotted in horizontal dashed lines in (b). All ESR measurements were performed at 300 K.

For short exposure times, ESR measurements were related to a concentration-averaged mobility starting from the immediate surface down to a front moving towards the geometric centre (i.e. almost no spin-probe at the centre). As described by Vitrac and Hayert (Vitrac, 2006a), spin-

probes concentration profiles decrease almost linearly with position (see Figure 1b) in a material with smooth variations of activity and diffusion coefficients. In this perspective, measurements in "melt" samples would correspond to the response of the spin-probe at thermodynamical equilibrium, when the concentration profile is uniform. The distance between the measured ratio H_1/h_1 and the theoretical ratio at equilibrium plotted as a horizontal line in Figure 4b assessed the difference in mobility with "melt" when the spin-probe diffusion front progressed in the material. After the depletion period, the spin-probe relaxation far from the surface was mainly sampled. This ideal description applied well to all studied cases except for P(D,L)LA films plasticized with PEG at high concentrations, for which the ratio H_1/h_1 overpassed its maximum theoretical value for a uniform concentration profile. This outstanding behavior was associated to a spin-probe sorption into a strongly heterogeneous material subjected to partial exsudation of the plasticizer. The highest chemical affinity of spin-probe for the exsudate would explain the observed decrease in the ratio H_1/h_1 (faster relaxation) after the depletion period. Such a trend occurred for all concentrations in PEG and could occur in a much lesser extent in P(D,L)LA samples plasticized with ATBC at the highest concentration as no further increase in the ratio H_1/h_1 was detected during the desorption stage. Neat P(D,L)LA and low plasticized films with ATBC matched theoretical behaviors with a detectable gradient of mobility close to the surface. When related to penetration depths, the H_1/h_1 gradient was extremely high in neat P(D,L)LA (higher mobility appear only near the immediate surface), high close to the surface in P(D,L)LA plasticized at high concentration with ATBC and at all concentrations in PEG and lower elsewhere (partial phase separation), low in P(D,L)LA plasticized at low concentration with ATBC with a rapid convergence to the bulk mobility (almost uniform plasticization).

5.3.4.2. Variation of polymer chain dynamics along the film thickness

Variation in polymer chain dynamics along the thickness was assessed by comparing the spin-probe MD obtained in similar materials when the spin-probe is uniformly distributed in the material and when it is concentrated in a specific region.

Figure 5. Comparisons of 2D Field×Temperature TEMPOL spectra in melt and after 18 days of exposure to probe vapors at 70 °C. The left column compares typical spectra with measurement temperature shifts that maximize their resemblance. The right column plots on a Van't Hoff diagram the correlation times for all measured spectra. Depicted conditions are: (a) neat P(D,L)LA, (b) P(D,L)LA with 9 wt% of PEG, (c) P(D,L)LA with 17 wt% of PEG, (d) P(D,L)LA with 9 wt% of ATBC, (e) P(D,L)LA with 17 wt% of ATBC. The results corresponding to the reference temperature T = 300 K appears either as thick lines or dashed lines.

Polymer chain dynamics was interpreted as equivalent temperatures giving similar spin-probe MD. The equivalent temperature was defined as the temperature that minimizes the mean square distance between ESR spectra obtained in the "melt" and when the sample was exposed to spin-probe vapors. It was *a priori* assumed that the corresponding temperature shift was independent of the temperature used for ESR measurements and types of relaxation, fast or slow. This assumption enabled a crude comparison without the help of any theory or any assumption regarding the true mechanism of reorientation of the considered spin-probe. Subsequent comparisons relied on relaxation times and therefore on inherent theories that support their calculations.

Bi-dimensional Temperature×Field relaxation spectra of TEMPOL spin-probe at equivalent temperatures are compared in Figure 5 for an exposure time of 18 days. This exposure time ensured that the concentration profile in spin-probes was maximal close to the surface but not at the immediate surface. Measurement temperatures in "melt" were chosen as reference and the equivalent measurement temperatures in "vapor" samples were inferred from the constant temperature shift ΔT that minimizes the global root mean square distance (RMS) plotted in Figure 7a. Almost continuous 2D relaxation spectra were obtained by interpolating spectra along Temperature direction with cubic Hermite polynomials. Prior interpolation, 1D Field spectra were rescaled and translated to yield spectra respectively with similar energy norm and with a same position for the central line (its position at 300 K was chosen as reference). Accurate comparisons with almost vanishing residues were obtained for neat P(D,L)LA and a low level of ATBC. In this case, the temperature shift was minimal and confirmed that properties below the surface were similar to bulk ones without detectable inhomogeneity. In samples plasticized with PEG and high levels of ATBC, the temperature shift was significantly positive, from 40 °C down to 10 °C. Due to disparate H_1/h_1 ratios, the goodness of the fit was lower and only an overall fit matching in particular the span of each spectrum was achievable.
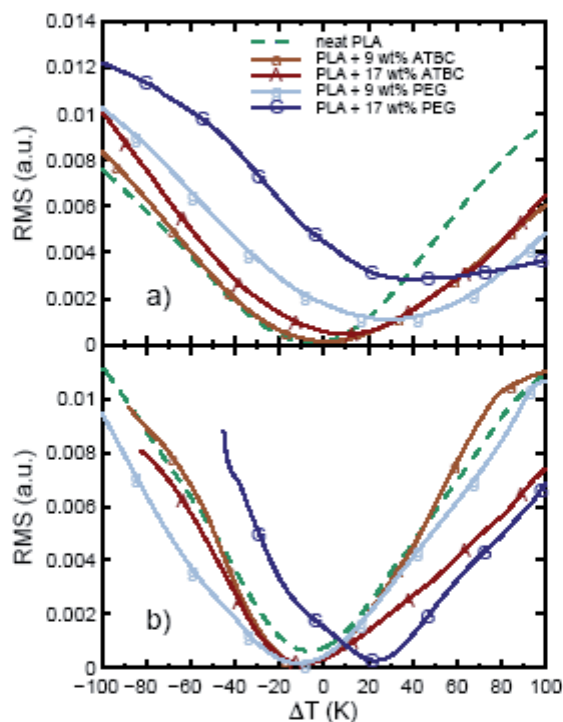
Figure 7. Root-mean-square distances (RMS) between 2D Field×Temperature spectra obtained in melt and after 18 days of exposure to probe vapors at 70 °C. Distances are plotted against different temperature shifts ΔT of vapor spectra for: (a) TEMPOL and (b) AminoTEMPO spin probes. Corresponding spectra with minimal residues are plotted respectively in Figures 4 and 5.

Further details were gained by comparing the correlation times between "melt" and "vapor" samples as plotted in the right column of Figure 5 as Van't Hoff plots. As detailed in Equations 3 and 4, this parameter derived from the Kivelson's theory takes into account the relative heights of peaks and the span of the central line in the fast relaxation mode (i.e. at high temperature) and only the span of the spectrum in the slow relaxation mode (i.e. at low temperatures). As a whole, similar conclusions were drawn for temperatures close to ambient or above. Such conditions led to almost overlapping curves with positive temperature shifts. The temperature shift was particularly significant, up to 100 K, for samples plasticized with high levels of PEG (Figure 5e). At low temperature, the temperature shift appeared positive and stronger at low levels in plasticizers (Figures 5b and 5d) due to a large discrepancy in activation energies between "melt" and "vapor" samples with activation energies near 13 kJ.mol^{-1} and 50 kJ.mol^{-1} respectively. At low temperature and high level in plasticizers (Figures 5c and 5e), the temperature shift assessed on correlation time was assessed opposite with close activation energies in both "melt" and "vapor" samples with values ranged between 34 and 88 kJ.mol^{-1}. Small differences observed in neat P(D,L)LA were not considered significant as they were related mainly on slow relaxations spectra (Figure 5a).
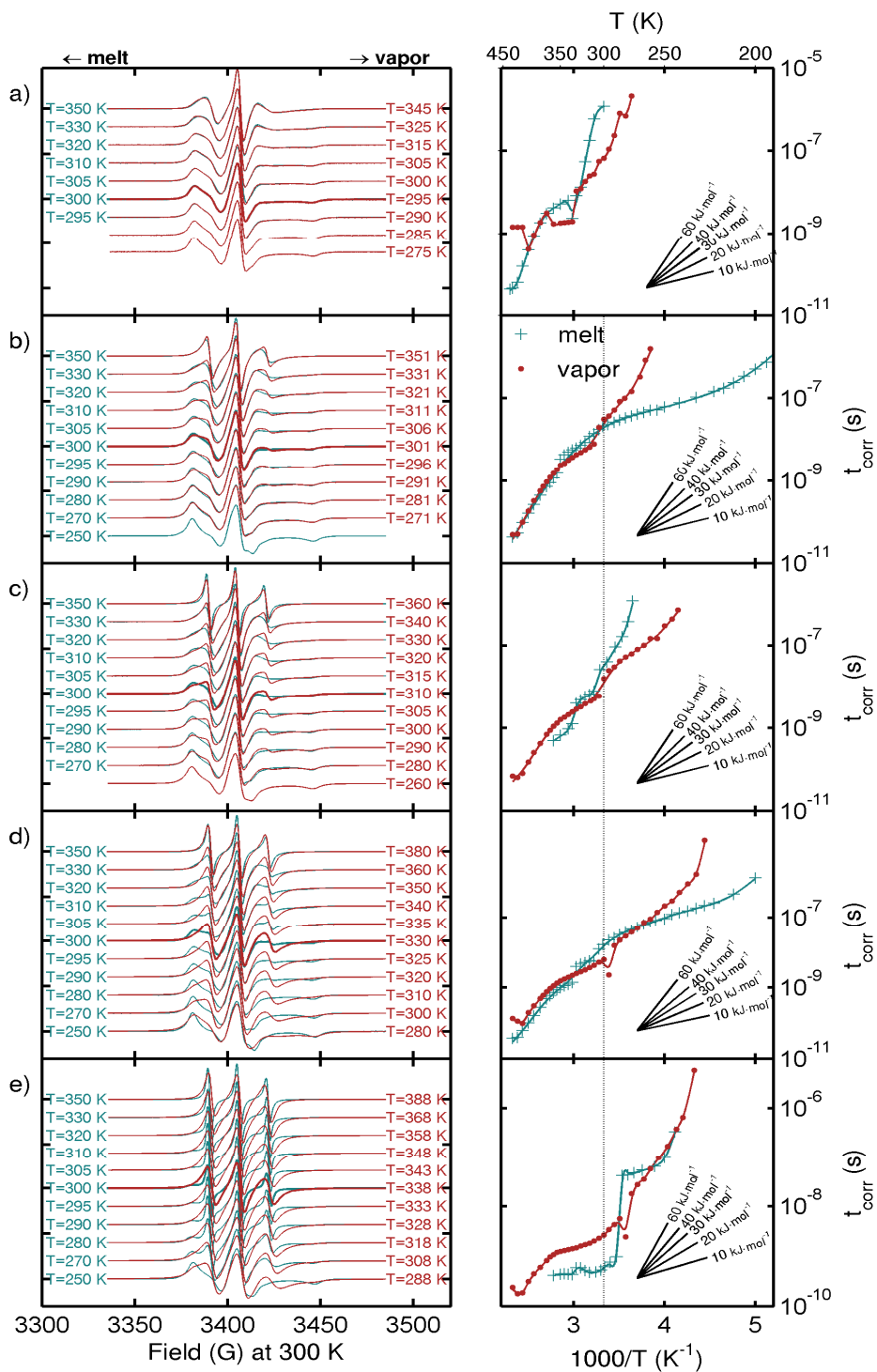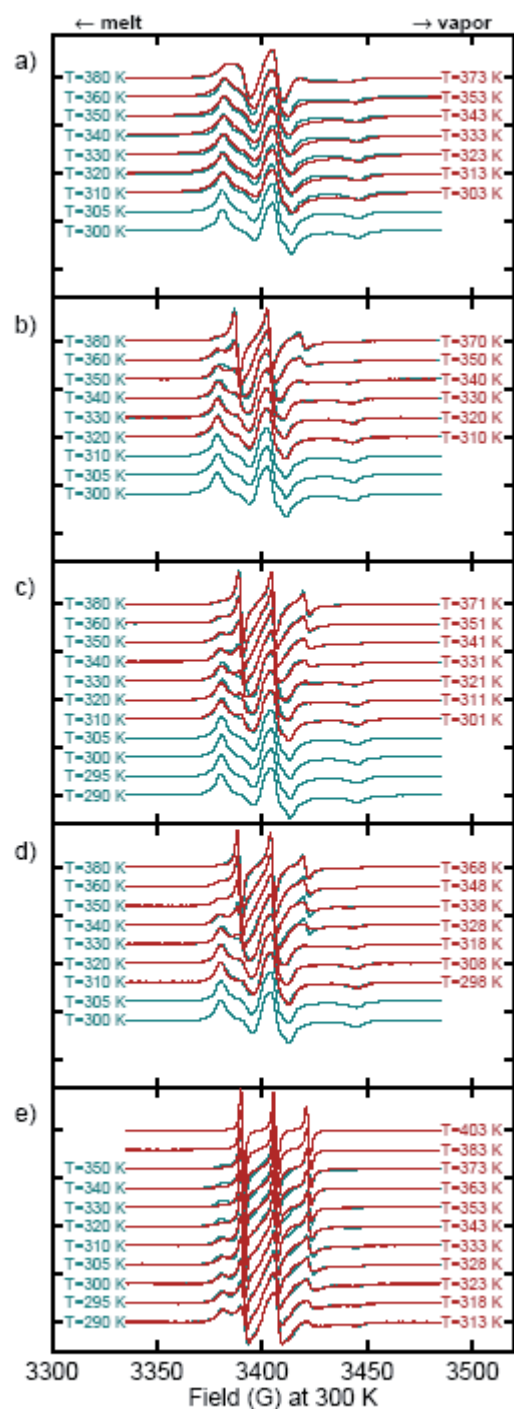
Figure 6. Comparisons of 2D Field×Temperature AminoTEMPO spectra in melt and after 18 days of exposure to probe vapors at 70 °C. Vapor spectra were temperature shifted to maximize their resemblance with melt spectra. Depicted conditions are: (a) neat P(D,L)LA, (b) P(D,L)LA with 9 wt% of PEG, (c) P(D,L)LA with 17 wt% of PEG, (d) P(D,L)LA with 9 wt% of ATBC, (e) P(D,L)LA with 17 wt% of ATBC. The results corresponding to the reference temperature T = 300 K appears either as thick lines.

Replacing TEMPOL spin-probe by AminoTEMPO did not change previous conclusions. As AminoTEMPO relaxed more slowly than TEMPOL (i.e. as shown in Table 1 the vector NH_2-$NO^\bullet$ is longer than the vector HO-$NO^\bullet$), the comparisons for a same range of temperatures were

however mainly supported by slow relaxation spectra and the sensitivity of the method to detect a significant temperature shift was lower. The results of the crude comparison of AminoTEMPO spectra are plotted in Figures 6 and 7b. Neat P(D,L)LA and low plasticized P(D,L)LA samples were fitted similarly with a slightly negative temperature shifts (Figure 7b). At high levels in plasticizers, RMS curves were asymmetric with ATBC towards positive temperature shifts and a temperature shift of 20 °C was estimated with PEG.

Variation of chain dynamics along the film thickness comparatively to bulk was reconstructed from the relaxation times of spectra acquired during the exposure of samples to TEMPOL vapors (see Figure 3). An equivalent temperature for spectra of vapor samples measured at 300 K was inferred by looking for the temperature in the right column of Figure 5 that gives a similar relaxation time in "melt" samples.
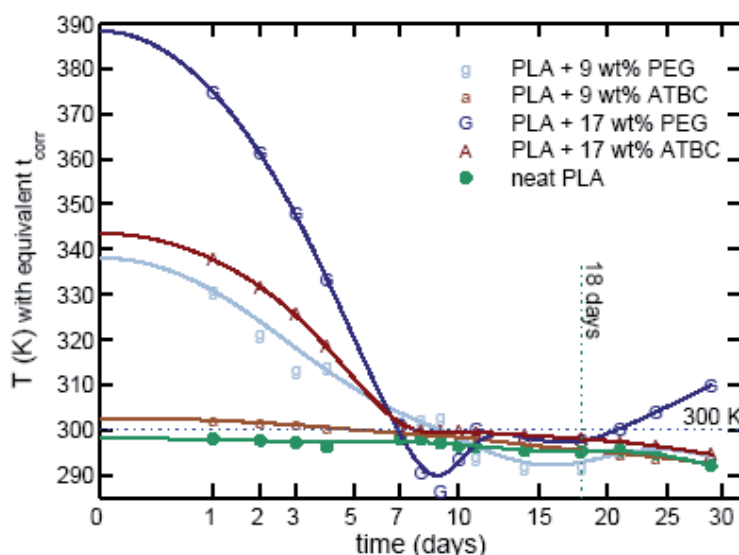
Figure 8. Temporal evolution (square root of time) of the temperature "felt" by the TEMPOL spin probe when the films are exposed to probe vapors at 70 °C. This equivalent temperature is obtained by comparing the correlation times measured dynamically at 300 K with the measured correlation time at different temperatures in a homogenous sample (melt) as depicted in Figure 4 (right column).

When plotted versus the square root of time as shown in Figure 8, such an approach gives the equivalent temperature profile along the film thickness. The profile showed an equivalent temperature up to 390 K significantly in excess of the measurement temperature (300 K) near the surface for all samples plasticized with PEG and with the highest level in ATBC. For all other samples, there was no significant excess temperature comparatively to bulk and confirmed a homogeneous polymer relaxation in the bulk. Homogeneous chain dynamics was recovered in highly plasticized samples only after the depletion period when the maximum of spin-probe

concentration penetrated deeper in the sample. Due to the ratio of diffusion coefficients, the thickness of the inhomogeneous region with excess mobility was 1.8 times larger in samples plasticized with PEG than in the samples plasticized with ATBC.

5.3.4.3. Quantitative correlations between spin-probe MD and chain dynamics

Previous interpretations were mainly qualitative and did not allow *a priori* a direct conversion of excess temperatures into shifts of local glass transition temperatures (T_g). This subsection proposes a first interpretation of temperature as local changes in T_g. In this perspective, the existence of invariants by temperature translation between samples with localized and uniform spin-probe concentrations is discussed according to the span of spectra ($2A_{zz}$), the mechanism or reorientation of the spin-probe and finally according to calibration curves between T_{50G} and T_g measured in the bulk. As a guiding principle, it was indeed thought that local excess temperatures estimated from correlation times at a constant ESR measurement temperature (300 K) and T_{50G} shifts interpolated from 2D Temperature×Field measurements were closely related to local T_g variations and almost independent of the considered spin-probe.

Figure 9 compares outer hyperfine splitting values ($2A_{zz}$) versus the ESR measurement temperature for both local (vapor) and bulk spectra. Corresponding Temperature×Field spectra are plotted in Figures 5 and 6 for TEMPOL and AminoTEMPO spin-probes respectively. Local and bulk curves were nearly self-similar with sigmoidal shape and almost overlapping for neat PLA and films plasticized with ATBC. By contrast, significant shifts towards lower temperatures occurred for local spectra acquired in films plasticized with PEG. When expressed on a same temperature reference scale, the detected temperature shifts had similar magnitudes with opposite signs than local excess temperatures (few K at 18 days) assessed from correlation times (see Figures 5, 6 and 8). It is emphasized that the splitting of the low field line into two peaks, denoted H_1 and h_1 in Figure 1, in samples subjected to a microphase separation might generate sharp variations in A_{zz} values each time the ratio H_1/h_1 crossed the unitary value. This effect was particularly significant for the 2D spectra of AminoTEMPO dispersed films plasticized with 17 wt% PEG (Figure 9d). By reducing the measured spectra to the temperature that yields theoretically $2A_{zz} = 50$ G, denoted T_{50G}, shifts in T_{50G} were similar for both spin-probes, with values ranging from 279 K to 382 K. It is worth to notice that this property was not available in dynamic experiments involving exposure to vapors as most of ESR measurements were

performed at single temperature of 300 K (see Figures 4 and 8), except after 18 days for which a temperature scan was performed.
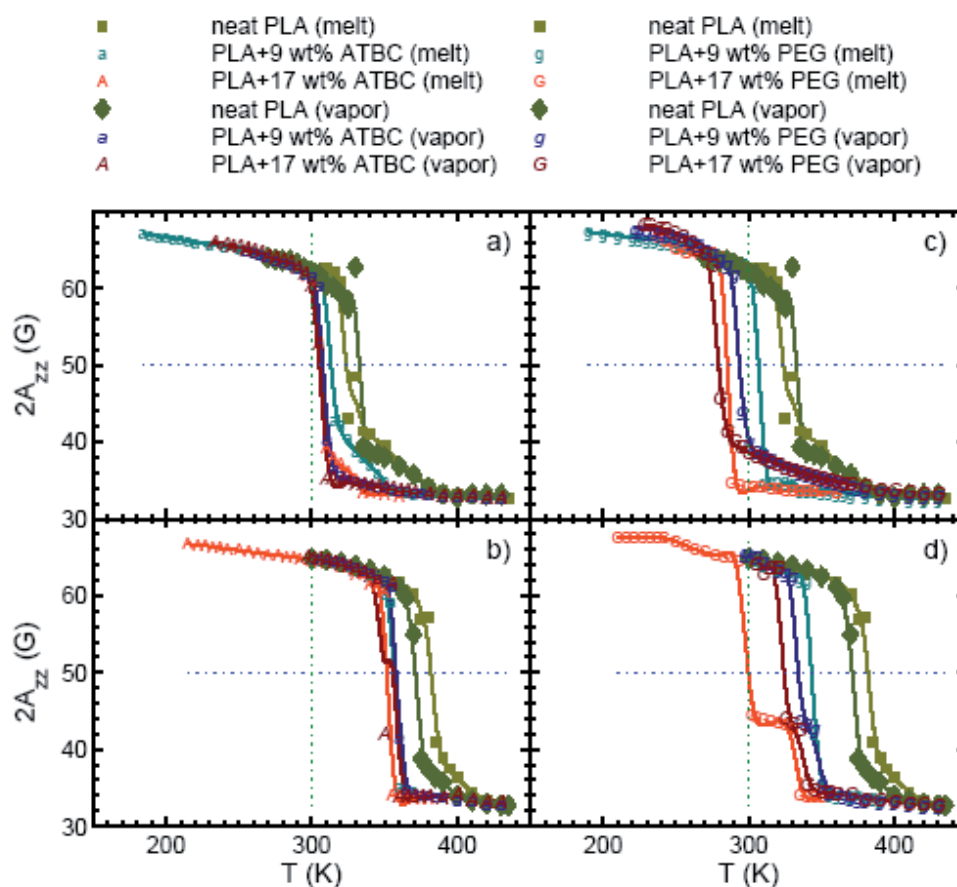
Figure 9. Outer extrema separation (*2Azz*) against measured temperatures for P(D,L)LA films plasticized with (a-b) ATBC and (c-d) PEG as probed with (a,c) TEMPOL and (b,d) AminoTEMPO.

Previous analyses showed that the position of the central line was shifted with temperature. This effect was accounted in particular in 2D translated spectra plotted in Figures 5 and 6. It was related to asymmetric displacements of low and high field lines as shown in Figure 10 for slow relaxation spectra. In this relaxation regime, ESR spectra were not averaged on all motions accessible to spin-probes and were integrated over particular spin-probe orientations. Spectral broadening and inward shift were hence used to diagnose the molecular rotational diffusion model for different temperature measurements, samples and spin-probes. Displacements of the high field line larger than for the low field one ($R \gg 1$) highlighted Brownian rotational diffusion whereas uniform broadening ($R \rightarrow 1$) revealed an orientation process controlled by Poissonian dynamics (*i.e.* discontinuous jump process separated by long dwelling times). In our experiments, the interpretation was complicated by inhomogeneities in the film that contributed

to superpose the response of spin-probe in differently plasticized environments in the bulk and in a less extent after 18 days of exposure to spin-probe vapors. Globally, a discontinuous jump process tended to dominate with non-monotonous variations with temperature. Besides, TEMPOL characteristic curves (Figures 10a and 10c) corresponding to "melt" and "vapor" samples looked similar but translated along both the Field and R directions: similar mechanisms occurring but for different conditions. Such results enforced the original assumption that exposing films to spin-probe vapors would help to separate the contribution of probes closer to the surface and therefore with excess mobility (i.e. with higher R value). It was not however possible to conclude similarly with AminoTEMPO spin-probe due to the strong dissimilarities between characteristic curves between "melt" and "vapor" plasticized films (Figures 10b and 10d). Good agreement was however found between "melt" and "vapor" neat P(D,L)LA.
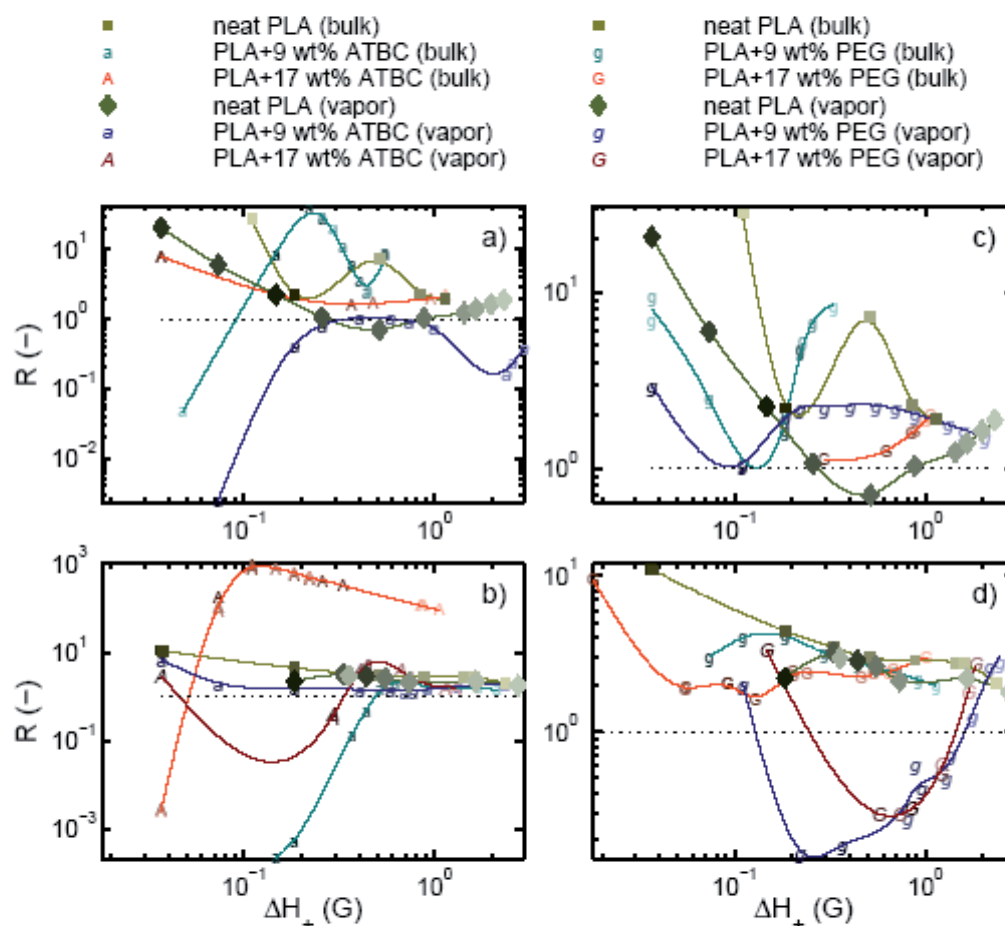
Figure 10. Dependence of R on $\Delta H+$ (corresponding to Fig. 8) for P(D,L)LA films plasticized with (a-b) ATBC and (c-d) PEG as probed with (a,c) TEMPOL and (b,d) AminoTEMPO.

Spectra acquired during dynamic exposure to spin-probes were interpreted as local temperature shifts above the temperature of measurement (300 K) (see Figures 4, 5 and 8) but did not allow a

direct comparison with T_g. Further insights were drawn by comparing T_{50G} to T_g values measured on bulk films in DSC. In absence of phase separation, as in neat P(D,L)LA, measured T_g values matched local ones but only apparent T_g values were achievable for the others. Figure 11 plots T_{50G} values estimated in "melt" and "vapor" (after 18 days of exposure to spin-probe vapors) films versus apparent T_g. T_{50G} values given by TEMPOL spin-probes were in good agreement with T_g of neat P(D,L)LA close to 332 K (Figure 11a). By contrast, T_{50G} determinations from AminoTEMPO relaxation spectra overestimated significantly the T_g of neat PLA with values up to 380 K (Figure 11b). Both spin-probes detected a significant decrease in T_{50G} when the plasticizing level increased. Besides, both spin-probes yielded accordingly similar T_{50G} values in "melt" and "vapor" films when P(D,L)LA films were plasticized with ATBC.
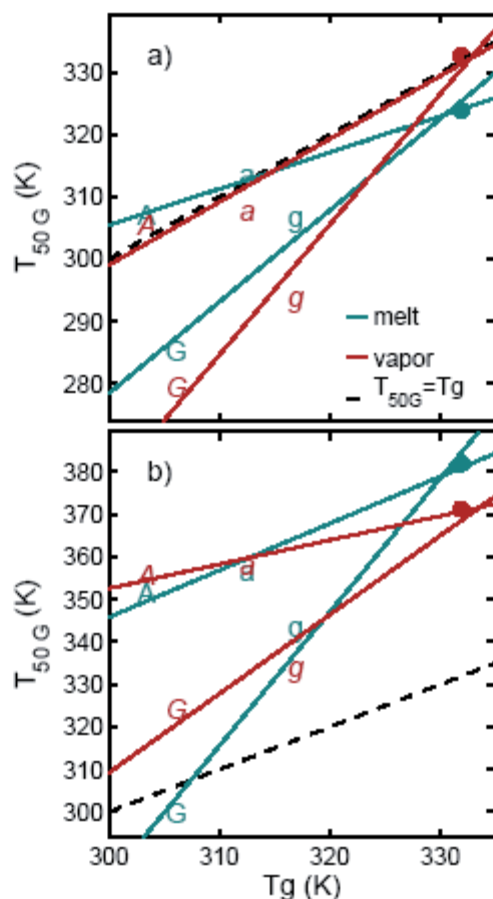
Figure 11. Comparison between T_g values measured by DSC analysis and estimated by T_{50G} values from results depicted in Figure 8 for (a) TEMPOL and (b) AminoTEMPO spin probes. Films tested are represented by: (●) neat P(D,L)LA, (g) P(D,L)LA with 9 wt% of PEG, (G) P(D,L)LA with 17 wt% of PEG, (a) P(D,L)LA with 9 wt% of ATBC, (A) P(D,L)LA with 17 wt% of ATBC.

This result was expected as both spin-probes were known to monitor bulk properties and not superficial properties after 18 days of exposure to vapors (see Figure 4). In addition, TEMPOL

generated T_{50G} values very close to real T_g ones for all plasticizing levels in ATBC (Figure 11a). When PEG was used as plasticizer, T_{50G} derived from TEMPOL spectra were much lower than measured T_g values with deviations down to 20 K and 25 K at 17 wt% in PEG respectively in "melt" and "vapor" films. Such description was consistent with a higher chemical affinity of TEMPOL for the exsudate and consequently to an oversampling of the mobility near the surface.

5.3.5. Conclusions

The general goal of the present study was to assess the risk of micro-phase separation in polylactide (PLA) films processed in presence of plasticizers. Plasticizing is indeed commonly proposed to accelerate the crystallization kinetic during cooling. The work contributed to two kinds of complementary results: i) methodological developments for the non-intrusive determination of microphase separation along the thickness in thin thermoplastic films and ii) an application of this method to P(D,L)LA thermo-compressed films formulated with conventional plasticizers, Acetyl tributyl citrate (ATBC) and Poly(ethylene glycol) (PEG).

Variations in polymer chain relaxation along the film thickness induced by a partial polylactide-plasticizer demixion were assessed by analyzing the relaxation spectra of two nitroxide spin-probes with different spatial distributions. To achieve accurate detections of small variations in the microenvironment of spin-probes, 1D (Field) and 2D (Temperature×Field) spectra obtained for different localizations of the spin-probe in the material were compared with the same spectra when their distributions were equilibrated in the same plasticized film (i.e. uniform distribution for an homogeneous film). Two modes of sampling along the thickness were investigated by controlling the exposure of samples to spin-probe vapors: i) by thickening the distribution of spin probes starting from the outer surface (sorption mode) and ii) by moving the maximum of concentration towards the geometric centre of the film (desorption mode after initial depletion). Due to many inherent unknowns in possibly heterogeneous films, it was not possible to control the absolute position of spin-probes but, as all samples were subjected dynamically to the same ambience, it was possible: i) to reconstruct bulk and extreme surface properties and ii) to reach relative comparison between samples. Two quantities extracted from the increasing amount of unpaired spins were particularly useful to interpret kinetics as spatial variations: i) its initial slope versus square root of time giving the relative length scale factor, ii) its maximum giving the end of the depletion period. Heterogeneous local dynamics of spin-probes were revealed by a split of the low field line in ESR spectra and its significant deviation with its theoretical value in a

similar plasticized film with an equilibrated distribution in spin-probes. As the response of the spin-probe depended on the considered nitroxide, TEMPOL or AminoTEMPO, the relaxation of spin-probe could not be directly related to any property of the polymer. It was however showed that ESR spectra were almost invariant by temperature translation and could be used to reconstruct a local excess temperature comparatively to the same response for an equilibrated distribution in spin-probes. The result was the reconstruction of temperature profile along the thickness that reproduced the theoretical temperature that would give the same spin-probe relaxation. In over-plasticized regions, the reconstructed temperature appeared higher than the temperature at which ESR measurement was performed, typically 300 K in our ESR measurements. To check whether the temperature in excess could be interpreted as local shift in polymer glass transition temperature (T_g), T_{50G} extracted from Temperature×Field spectra and T_g were crudely compared. Without any fitting, T_{50G} determined with TEMPOL as spin-probe predicted remarkably T_g of P(D,L)LA for all levels in ATBC. In films plasticized with PEG, a calibration procedure was required.

Macroscopically, films plasticized with PEG appeared subject to phase separation for the whole concentration range 9 - 17 wt% with a significant exsudation at 17 wt%. A similar behavior but with twice less over-plasticizing effect occurred also with 17% of ATBC. Excess polymer mobility decrease sharply from the interface towards the geometric center with surface excess temperatures of 90 K, 45 K and 40 K for 17 wt% PEG, 17 wt% ATBC and 9 wt% PEG respectively. At 9 wt% ATBC, a uniform plasticization was achieved with a T_g shift of 20 K comparatively to neat P(D,L)LA. Although it was not to possible to relate the effect to any excess polymer mobility, variations of spin-probe relaxation near the film surface suggested that additional heterogeneities at microscopic scale might exist in neat P(D,L)LA films (on a length scales lower than 1 µm) and in P(D,L)LA films plasticized with 9 wt% ATBC (on few micrometers). Such effects could be related either to an excess of chain ends close to the surface (e.g. due to hydrolysis) or small changes in the morphology of crystallites.

Further works aim at extending the method to detect dynamically interactions between the polymer and the polymer in contact such as local plasticization or swelling.

5.3.6. Discussion et commentaires

Cette étude a été réalisée dans le but de sonder l'hétérogénéité des échantillons utilisés pour la détermination des coefficients de transport dans le P(D,L)LA. Il a été mis en évidence que la microstructure du P(D,L)LA semble affecter ses propriétés barrières. Par conséquent il est nécessaire de développer des méthodes permettant d'évaluer la présence de microphases dans le P(D,L)LA CD92 pur et plastifié.

Dans un premier temps, des sondes nitroxides ont été incorporées dans le matériau par phase vapeur et dans le polymère à l'état fondu lors de la formulation. Ce dernier mode d'incorporation a permis l'obtention d'un matériau à l'équilibre servant de référence (distribution uniforme des sondes dans un matériau homogène). Une comparaison des spectres des matériaux de référence et de ceux obtenus à intervalle régulier durant l'incorporation en phase vapeur a permis de détecter de manière précise les variations de micro-environnement des sondes nitroxides.

Pour cela, il a été nécessaire d'effectuer une corrélation entre la variation des spectres dans le temps et dans l'espace. Celle-ci a été réalisée grâce à l'épaississement de la distribution des sondes dans le matériau (par sorption des sondes) et le déplacement du maximum de concentration de sondes vers le centre de l'échantillon (désorption des sondes après épuisement de leur source).

Dans un deuxième temps, la mobilité des sondes a été reliée à la mobilité des segments de chaîne polymère. Pour cela, des balayages en température ont été réalisés pour tous les échantillons, aussi bien après incorporation en phase vapeur (à 18 jours) qu'après incorporation directement dans la masse (à l'état fondu). La comparaison des spectres obtenus pour les deux modes d'incorporation a montré qu'une simple translation en température permettait de les faire pratiquement se superposer. Cette valeur de translation en température a alors été reliée au déplacement de température locale de transition vitreuse du matériau étudié et par la même à la mobilité de ses segments de chaîne. Ceci seulement pour les échantillons plastifiés par ATBC car une bonne corrélation entre les valeurs de T_g, reliée au polymère, et les valeurs de T_{50G}, reliée aux sondes nitroxides avait préalablement été constatée.

Par cette approche, nous avons confirmé que le P(D,L)LA CD92 plastifié avec le PEG présente une forte exsudation du plastifiant en particulier à une teneur de 17 % en poids. Une faible exsudation de l'ATBC lors de la plastification à 17 % en poids a également été constatée du fait de la forte mobilité des chaînes polymère, ressentie par les sondes nitroxides, à la surface de

l'échantillon. Enfin, le P(D,L)LA pur et le P(D,L)LA plastifié avec 9 % d'ATBC en poids ont montré qu'une hétérogénéité à l'échelle microscopique pouvait exister. Un tel résultat pourrait être relié à un excès de bout de chaînes polymère à la surface des films (en raison de l'hydrolyse du PLA) ou à des petites variations dans la morphologie des cristallites entre la surface et le centre des films.

5.4. Conclusions du chapitre 5

Dans les chapitres précédents, des systèmes de perméation aux gaz et de sorption d'esters éthyliques par mesure microgravimétrique avaient été employés. Ce dernier chapitre a permis de développer deux différentes approches exploratoires de détermination des coefficients de transport. Ainsi les coefficients de diffusion, de sorption et de perméabilité de composés organiques ont pu être mesurés de manière indépendante afin de connaître l'impact de chacun des coefficients sur les propriétés barrière du P(D,L)LA.

Une première approche de mesure de coefficient de diffusion de composés organiques volatils par perméation a été mise en place pour le P(D,L)LA. L'étude réalisée a permis de montrer l'effet de deux paramètres, la pression du système et l'étape de backflush, sur la répétabilité des mesures dans le cas du LDPE et d'un P(D,L)LA de faible épaisseur. Il semble donc que les mesures soient plus répétables sans l'étape de backflush et à une pression de travail de 20 kPa. Les coefficients de diffusion des esters éthyliques testés dans le P(D,L)LA Biophan® sont de l'ordre de 6.10^{-15} m².s^{-1}. Toutefois ce dispositif reste à optimiser pour la mesure du coefficient de perméabilité. Comme montré par Dury-Brun *et al.* pour le transport de l'hexanoate d'éthyle dans le papier et le polypropylène biorienté (Dury-Brun, 2008), la différence entre les valeurs de coefficient de diffusion de l'acétate d'éthyle mesurés par microbalance ou par perméation met en évidence le fait que ces méthodologies ne peuvent être utilisées que comme des moyens de comparaison entre polymères et ne doivent en aucun cas être comparées l'une à l'autre. La mesure par sorption du coefficient de solubilité de l'acétate d'éthyle a mis en évidence une plastification des échantillons durant la mesure pour une activité supérieure à 0,2. Celle-ci a été confirmée par la mise en contact d'échantillons de P(D,L)LA Biomer L9000 avec des composés organiques en cellule hermétique à des activités comprises entre 0,1 et 0,9. Cette méthode a également montré que le P(D,L)LA cristallise par contact vapeur avec ces composés. Il semble donc que les concentrations dans l'espace gazeux d'AE, 0,4 ppm (375 µg.L^{-1}), de BE, 5.10^{-2} ppm (47 µg.L^{-1}) et d'HE, 5.10^{-2} ppm (43 µg.L^{-1}) (Tableau 2.8), utilisées pour les mesures de perméation, ne soient pas suffisantes pour modifier la structure du PLA. En effet, dans le chapitre 4, nous avions montré que la cristallisation induite par l'AE et le BE n'est seulement détectée qu'à partir d'une concentration de 58,4 ppm d'EA et de 10,4 ppm pour l'HE.

Deux approches ont donc été utilisées, la sorption-désorption et la perméation, pour lesquelles les activités en diffusant étudié pouvaient induire des modifications du matériau au cours de la manipulation. Afin de pouvoir comparer ses deux approches, il aurait été souhaitable de travailler

en iso-activité. Cependant ceci reste difficile à réaliser du fait de la limite de détection de chacune des méthodes. De plus, les activités étant « méthodologie dépendantes », il serait nécessaire, dans l'idéal, d'utiliser une méthodologie à dilution infinie où l'on se situe dans le cas de faibles interactions avec le polymère c'est-à-dire sans modification de la structure au cours du transfert. Ce cas idéal est difficilement dimensionnable pour toutes les approches méthodologiques traditionnelles, sorption, perméation dans la mesure où on est limité par la détection physique des molécules (flux, masse sorbée). Ces conditions (activités inférieures à 0.1) ont tout de même été remplies lors des mesures par perméation et microbalance. En revanche, la gravimétrie nécessite des activités importantes afin de pouvoir mesurer la prise de masse et a pour conséquence une plastification et une cristallisation des échantillons. Néanmoins, pour les faibles activités, le recours à l'extraction et analyse par multiple headspace extraction (MHE) du matériau est possible et permettrait de quantifier les faibles prises de masse effectuées dans ces conditions.

La seconde approche, la mesure de coefficient de diffusion in-situ a été mise au point dans le cadre de temps de faisceau accordé au Synchrotron Soleil. Cette mesure utilise le principe des profils de concentration dans le temps et l'espace pour mesurer les coefficients de diffusion (Moisan, 1980; Roe, 1974). Dans le cas présent, la mesure est réalisée par microscopie de fluorescence, ce qui a nécessité l'utilisation de molécules fluorescentes, de masse molaire et d'encombrement plus important que ceux des molécules organiques précédemment utilisées. De plus, cette méthode requière une préparation longue mais sans équipement particulier et une simulation des profils de concentration afin de retrouver par simple comparaison le nombre de Fourier associé au coefficient de diffusion de chacune des molécules.

Une diminution du coefficient de diffusion a été mise en évidence avec l'augmentation du nombre de carbone séparant les deux noyaux aromatiques. Cette évolution est similaire à celle observée dans le cas d'une polyoléfine, le polypropylène.

La troisième approche consiste à sonder les dynamiques moléculaires locales de long de l'épaisseur de films de P(D,L)LA CD92 pur et plastifié. Elle permet ainsi de mettre en évidence des séparations de phase à l'échelle microscopique le long de l'épaisseur des échantillons. Il a ainsi été montré, comme précédemment par DSC et DMTA (publication n°1), une forte exsudation du PEG quelle que soit la teneur en plastifiant dans le P(D,L)LA. Par contre, une exsudation de l'ATBC pour une teneur de 17% en poids a également été constatée alors que l'analyse en DSC et DMTA ne permettait pas une telle conclusion. Il semble donc que la RPE soit une méthode efficace pour sonder l'hétérogénéité des échantillons à l'échelle microscopique. Il reste maintenant à tester son efficacité dans la détection dynamique des interactions

polymère/composé organique qui peuvent conduire à une plastification, un gonflement ou à la cristallisation du polymère.

Conclusions Générales

Le transport des petites molécules dans des matrices polymères denses revêt une portée significative dans un certain nombre d'applications des matériaux plastiques, telles les applications d'emballage et de conservation des contenus fragiles, les applications dans le domaine des membranes, mais également dans le vieillissement des thermoplastiques. Afin de maîtriser les propriétés barrière d'une structure polymère et pouvoir ainsi concevoir des structures adaptées à une application donnée, la compréhension de la relation structure/fonction est indispensable.

Les travaux de ce mémoire ont été focalisés plus précisément sur l'étude de la relation structure-propriétés barrière du P(D,L)LA. L'objectif était ainsi de mieux comprendre les mécanismes rentrant en jeu dans le transfert de molécules gazeuses et de composés organiques dans le PLA. Un des moyens envisagés pour l'amélioration de cette compréhension a donc été de moduler la structure du polymère afin d'évaluer son impact sur ses propriétés de transport. Nous nous sommes ainsi basés sur les résultats de Michaels et Parker (Michaels, 1959) qui ont montré que la cristallisation du polyéthylène conduit à une diminution des coefficients de transport, puisque les phénomènes de transport ont lieu dans la phase amorphe du polymère semi-cristallin. Cette modification des propriétés barrière avec la structure cristalline a aussi été montrée dans le cas de l'oxygène pour un polyester pétro-chimique, le PET (Hu, 2005; Sekelik, 1999).

Dans le cadre de la présente étude, plusieurs morphologies du P(D,L)LA ont été conçues en variant la fraction de volume libre de la phase amorphe au sein du matériau, grâce à l'addition de plastifiant, et/ou en variant la quantité de phase amorphe par la création de cristaux à l'aide de divers procédés.

Notre démarche expérimentale a donc consisté à :
- formuler le PDLLA avec un plastifiant et un agent nucléant
- cristalliser le PDLLA pur et formulé par un procédé classique de traitement thermique ou par simple chauffe en étuve
- cristalliser le PDLLA pur et formulé par biétirage
- optimiser et développer des méthodes de détermination de coefficient de diffusion

Effet de la plastification/formulation

Deux types de plastifiants ont été testés lors de cette étude dans le but, d'une part, d'améliorer les propriétés mécaniques du P(D,L)LA CD92 en le rendant plus ductile et, d'autre part, de favoriser la cristallisation. Pour cela, un agent nucléant a également été ajouté au P(D,L)LA

afin d'étudier l'effet synergique avec le plastifiant sur la cristallisation du P(D,L)LA. Les résultats obtenus ont mis en évidence un pouvoir plastifiant du PEG dans le P(D,L)LA important, constaté par une forte diminution de la T_g et une forte cristallisation du P(D,L)LA lors de refroidissement à 10 °C.min^{-1}. Moins efficace en tant que plastifiant que le PEG, l'ajout d'ATBC dans le P(D,L)LA présente néanmoins l'avantage d'engendrer moins de scission de chaines lors du processus de mélange, de largement augmenter l'élongation à la rupture tout en maintenant des propriétés barrière aux gaz proches de celle du P(D,L)LA pur, malgré une baisse de T_g proche de l'ambiante. L'utilisation de l'ATBC serait donc plus adaptée à la plastification du P(D,L)LA, malgré son pouvoir plastifiant moyen.

L'ajout de talc au P(D,L)LA a permis de favoriser la cristallisation du P(D,L)LA pur et plastifié avec l'ATBC rendant ainsi possible la cristallisation à partir du fondu à 25 °C.min^{-1}..

Effet de la cristallisation

Le traitement thermique ou recuit à partir du vitreux, première voie de cristallisation, a été testé sur le P(D,L)LA pur dans le but d'améliorer ses propriétés barrière. Néanmoins, il est vite apparu que l'augmentation de la cristallinité par voie thermique ne conduisait pas forcément à une diminution des coefficients de transport des molécules gazeuses. Ainsi l'hypothèse de départ selon laquelle les propriétés barrière sont dépendantes de la cristallinité (Michaels, 1959) n'a pas encore été prouvée dans le cas du P(D,L)LA et cette hypothèse a été discutée récemment pour d'autres polymères semi-cristallins (Kanehashi, 2010) Les résultats contradictoires obtenus avec des P(D,L)LA de stéréochimie différente, dans le chapitre 4, sont confirmés par la littérature pour des P(D,L)LA de même teneur en L-lactide, balayant ainsi l'hypothèse selon laquelle, les différences observées de coefficients de transport pourraient être attribué à la stéréochimie du polymère. Néanmoins d'autres hypothèses sont avancées pour expliquer la variabilité des résultats obtenus par des cristallisations du P(D,L)LA effectuées à partir du vitreux :

- la présence de sphérolites de P(D,L)LA de petite taille qui ne constitueraient pas un obstacle assez important au transfert de gaz.

- la dédensification de la phase amorphe, déjà observé pour le PET (Lin, 2002; Qureshi, 2000).

- la présence d'une fraction amorphe mobile (MAF) et d'une fraction amorphe rigide (RAF), mise en évidence dans le P(D,L)LA (Del Rio, 2010; Delpouve, 2009; Zuza, 2008). En augmentant les temps de recuit, le pourcentage de RAF augmente et la

RAF, moins dense que la MAF, créerait des chemins préférentiels pour le transfert des molécules de gaz au travers de la matrice P(D,L)LA.

La deuxième voie empruntée pour cristalliser le P(D,L)LA est celle du biétirage. Les résultats obtenus à des ratios d'étirage relativement faibles, 4×4, montrent que le biétirage permet bien de cristalliser le P(D,L)LA à des taux de 15 à 30 %. Une diminution de la perméabilité à l'hélium n'est obtenue qu'en réalisant des films avec un ratio de 4×4. En deçà de cette valeur, aucun effet n'est mis en évidence. La comparaison, à un taux de cristallinité similaire, d'un échantillon biétiré et d'un échantillon cristallisé par voie thermique révèle que le traitement thermique affecte nettement plus la perméabilité que ne le fait le biétirage. Indépendamment du taux de cristallinité, le biétirage est utilisé pour permettre une organisation/orientation de la phase amorphe conduisant généralement à un empilement serré (dense) des chaînes polymères. Cette restriction de la mobilité, et par conséquent, de la diffusion au sein des chaînes polymères, mériterait d'être évaluée et mise en relation avec la structuration des phases cristalline et amorphe résultante du biétirage à l'aide d'un jeu de molécules perméantes plus large.

Une voie de cristallisation induite par contact vapeur, à température ambiante, avec l'acétate d'éthyle (AE) a enfin été explorée. La forte interaction de l'AE avec le P(D,L)LA a conduit, non seulement à une forte plastification du P(D,L)LA, mais aussi à la formation de cristallites de forme α avec le P(D,L)LA pur. L'effet de la formulation du P(D,L)LA CD92 sur les coefficients de transport de l'AE a été négligeable et une forme cristalline spécifique a même été produite.

Une des problématiques évoquées dans la discussion autour des propriétés barrière est la détermination des coefficients de transport de composés organiques. Deux types d'approches méthodologiques existent, la sorption-désorption et la perméation qui permettent une détermination des coefficients de solubilité, S, et de diffusion, D. Ces approches conduisent généralement à des mesures de ces coefficients très variables et peu comparables (Dury-Brun 2007), du fait soit de déterminations non indépendantes ou de mesures dépendantes des pressions partielles ou concentrations en composés organiques.

Dans le cadre du mémoire, le développement de méthodes pour la détermination des coefficients de transport a été effectué sur des molécules de masse molaire plus grande que les gaz précédemment évoqués, tels que les esters éthyliques et les molécules fluorescentes.

La première méthode consiste à mesurer les coefficients de diffusion de molécules organiques dans le P(D,L)LA Biophan® par une méthode de perméation semi-dynamique en utilisant une pression partielle faible en composés organiques (inférieure à 7,5 Pa). L'optimisation du dispositif, sur des films de LDPE, a mis en évidence une faible diminution des coefficients de diffusion avec l'augmentation de la taille des molécules organiques. Néanmoins au vu de la forte variabilité des mesures, la différence observée entre les coefficients de diffusion de chacune des molécules étudiées n'a pas permis de déterminer une loi d'échelle ($D = \propto M^{\alpha}$) pour les esters éthyliques dans le LDPE. Il est probable que les conditions opératoires menées avec un réservoir amont contenant les composés volatils en solution ne permet pas de générer une pression partielle constante pour chacun des composés et ainsi de mesurer convenablement les perméabilités sur des films. Un dispositif annexe de génération de vapeur en mode dynamique serait à développer sur ce dispositif pour alimenter en continu le compartiment amont de la cellule de perméation. L'utilisation de cette méthode pour la détermination des coefficients de transport dans le P(D,L)LA Biophan® n'a pas permis de déterminer des coefficients pour chacun des composés organiques étudiés.

La seconde méthode, employée avec des molécules fluorescentes, a permis une mesure in-situ des coefficients de diffusion dans le P(D,L)LA Biophan® par une technique ne requérant pas d'outils bien spécifiques. Basée sur la détermination de profil de concentration en molécules fluorescentes dans le P(D,L)LA, elle ne nécessite qu'une simulation préalable des profils afin de retrouver le coefficient de diffusion par simple comparaison. La très forte dépendance du coefficient de diffusion à la masse ainsi obtenue ($\alpha = 20$) pour le P(D,L)LA Biophan® reste à être confirmée par des mesures sur des séries homologues différentes.

Enfin, une dernière méthode a été développée lors de ce travail dans le but de sonder, à l'échelle microscopique, les hétérogénéités du matériau dues à l'exsudation de plastifiant. Pour cela, la résonance paramagnétique électronique a été utilisée en incorporant selon deux procédés deux types de sondes nitroxides. Une exsudation de l'ATBC, ainsi que celle du PEG, a été ainsi constatée, confirmant l'efficacité d'une telle méthode. Au vu de sa sensibilité, il semble possible de pouvoir sonder de manière dynamique les interactions constatées entre polymère et composé organique qui s'accompagnent de plastification, de cristallisation ou même gonflement de la matrice.

Le PLA est un matériau depuis longtemps utilisé dans le domaine biomédical et potentiellement utilisable pour une large gamme d'applications notamment dans les usages de commodité. Son caractère biosourcé ainsi que sa dégradabilité ont fait de lui un matériau intéressant dans le cadre du développement durable et de réduction des déchets. Toutefois le PLA pur présente des verrous technologiques importants tels qu'une forte fragilité et une tenue à la température limitée, avec une T_g proche de 60 °C et des propriétés barrière moyennes rendant son utilisation restreinte dans le domaine de l'emballage et nécessitant des améliorations. Dans cette étude nous montrons qu'une simple étape de plastification a permis d'augmenter très largement son élongation à la rupture. Par contre en augmentant la cristallinité du polymère, il est apparu que cette modification de la structure ne permettait pas d'améliorer de façon significative les propriétés barrière du P(D,L)LA. D'autres approches telles que l'ajout de nanocharges sont menées par de nombreuses autres équipes de recherche pour l'amélioration des propriétés barrière aux gaz du P(D,L)LA. Néanmoins, ces travaux n'ont pas mis en évidence des résultats, en terme de coefficient de transport, beaucoup plus prometteurs que ceux obtenus par cristallisation, soit en général un coefficient de diffusion divisé par 2 (Martino, 2010).

De nos travaux, il apparait qu'une compréhension plus intégrée des mécanismes macroscopiques de transport en relation avec la structure du P(D,L)LA ne pourra se faire que par évaluation de la microstructure et des phénomènes diffusionnels à une échelle plus microscopique et locale

Perspectives

Les perspectives de ce travail sont nombreuses en raison des hypothèses et pistes de travail qu'il a permises d'ouvrir. En effet, l'influence de la cristallisation sur les propriétés barrière du PLA est toujours en débat du fait des résultats contradictoires présentés dans la littérature (Drieskens, 2009; Sawada, 2010) et dans ce travail (publication n° 3 et 4). Ainsi après avoir travaillé à l'échelle macroscopique en étudiant l'effet du taux de cristallinité sur les coefficients de transport, il semble nécessaire d'approfondir ce travail par une étude de la microstructure. Plusieurs techniques peuvent, dans un premier temps, permettre de moduler cette microstructure :

i) la voie du biétirage semble être un procédé à développer pour le PLA dans la mesure où le biétirage permet d'imposer une structure aussi bien à la phase cristalline qu'à la phase amorphe. Le biétirage peut ainsi induire un changement de forme cristalline dont la présence

pourra éventuellement affecter les propriétés barrière. Plusieurs techniques permettent d'étudier en détail cette structure :

- le WAXS et le SAXS afin de qualifier les morphologies cristallines.

- le PALS pour évaluer le volume libre présent dans le matériau après biétirage.

- la DSC pour quantifier la fraction amorphe rigide et la fraction amorphe mobile.

ii) la voie de la cristallisation induite par les solvants à température ambiante. Sa structure cristalline a pour le moment été qualifiée par WAXS. Néanmoins, aucune mesure n'a été réalisée pour étudier la phase amorphe résultante. Il serait également intéressant d'analyser la cristallisation par microcopie en tant réel pour savoir si la cristallisation est homogène sur toute la surface en contact et à quelle vitesse les composés diffusent à l'intérieur du matériau.

iii) afin d'améliorer sa dépendance à la température, de nombreux travaux portant sur la synthèse du PLA ont été réalisés et ont finalement permis d'étendre sa gamme d'utilisation.
Il s'agit notamment des stéréocomplexes de PLA. Ce matériau, constitué de chaînes de PLLA et de PDLA, présente des propriétés thermiques et mécaniques améliorées, comparé au PDLLA. Cette démarche pourrait s'appliquer à l'amélioration des propriétés barrière. Dirigée *a priori* pour obtenir des structures à façon, la voie de la synthèse chimique ou enzymatique, associée ou non au procédé, permettrait d'obtenir les propriétés barrières attendues du PLA.

Annexes

Annexe I : Thermogrammes du P(D,L)LA CD92 obtenus par DSC en mode classique et modulé
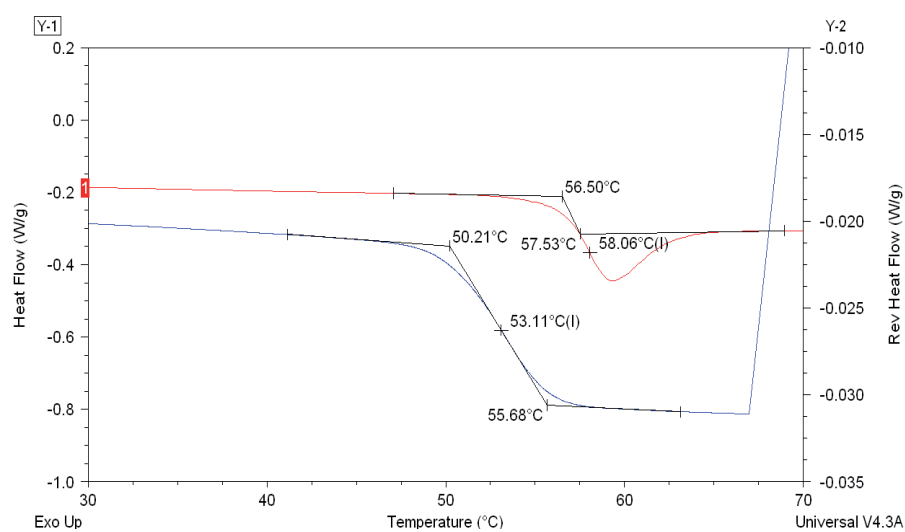
Figure iii. Thermogrammes du P(D,L)LA CD92 obtenus par DSC classique à 10 °C.min^{-1} (rouge) et DSC modulée à 1 °C.min^{-1} (bleu).

Annexe II : Courbes de calibration des esters éthyliques par CPG
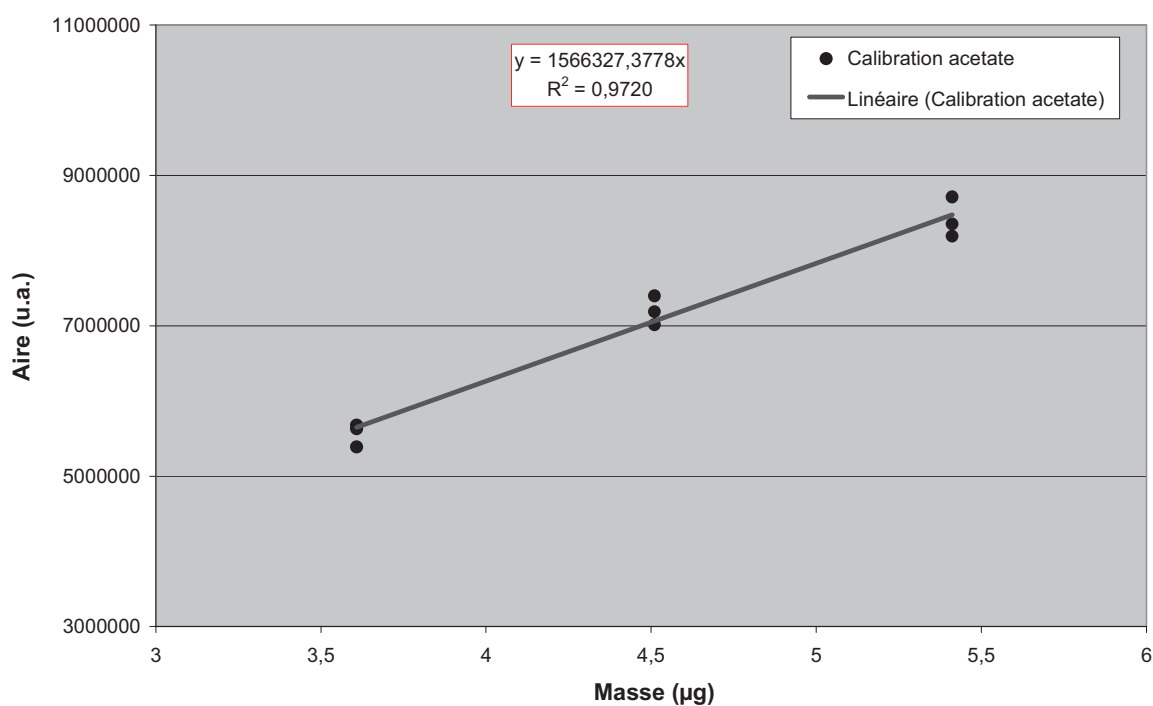
Figure iv. Courbe de calibration de l'acétate d'éthyle par CPG dans les conditions d'analyse de la perméation de composés d'arôme.
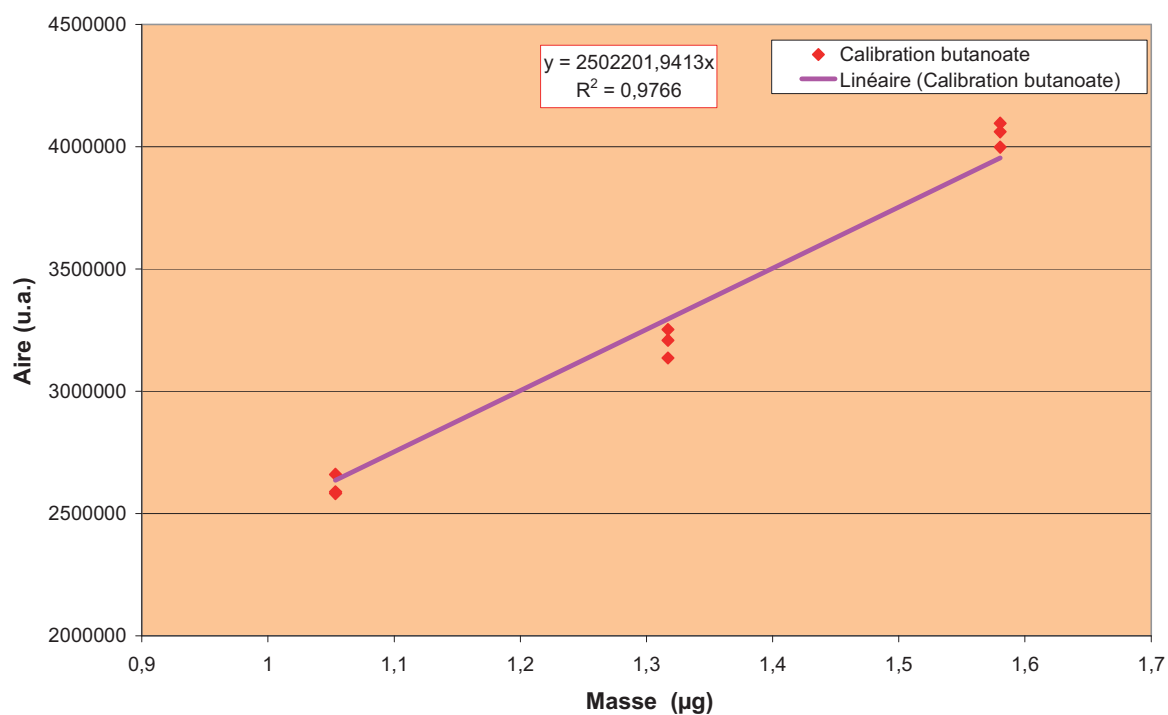
Figure v. Courbe de calibration du butyrate d'éthyle par CPG dans les conditions d'analyse de la perméation de composés d'arôme.
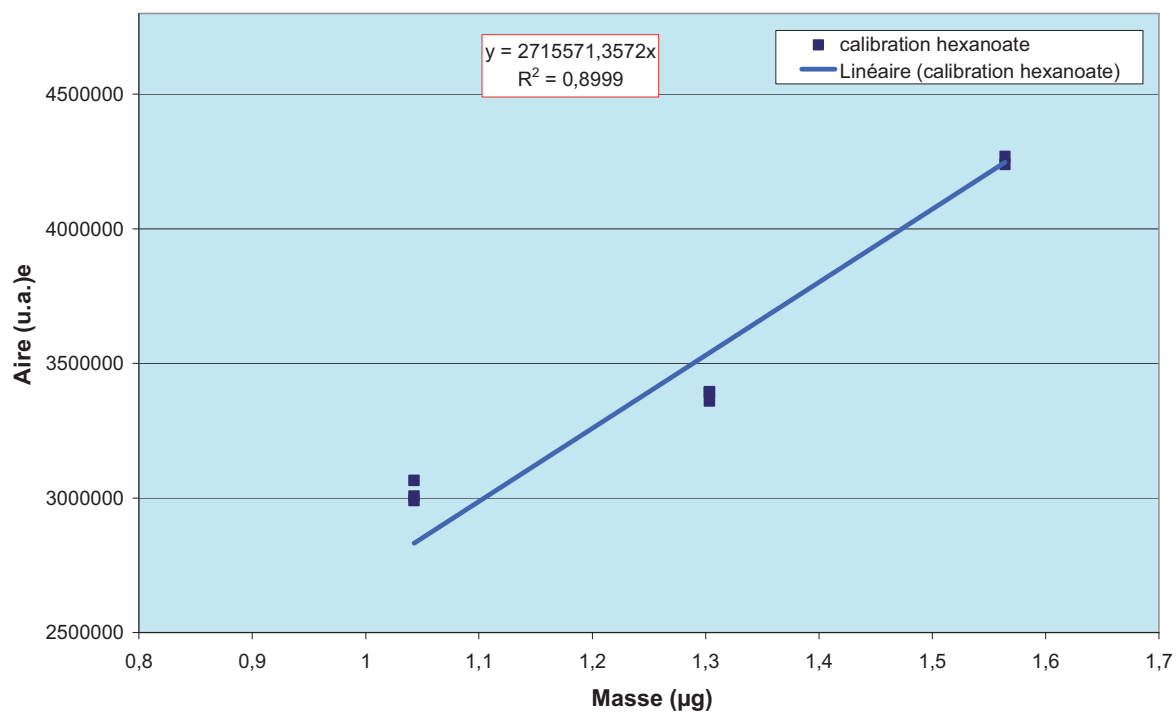
Figure vi. Courbe de calibration de l'hexanoate d'éthyle par CPG dans les conditions d'analyse de la perméation de composés d'arôme.

Annexe III : Cinétique de perméation des esters éthyliques dans le LDPE et le P(D,L)LA Biophan®
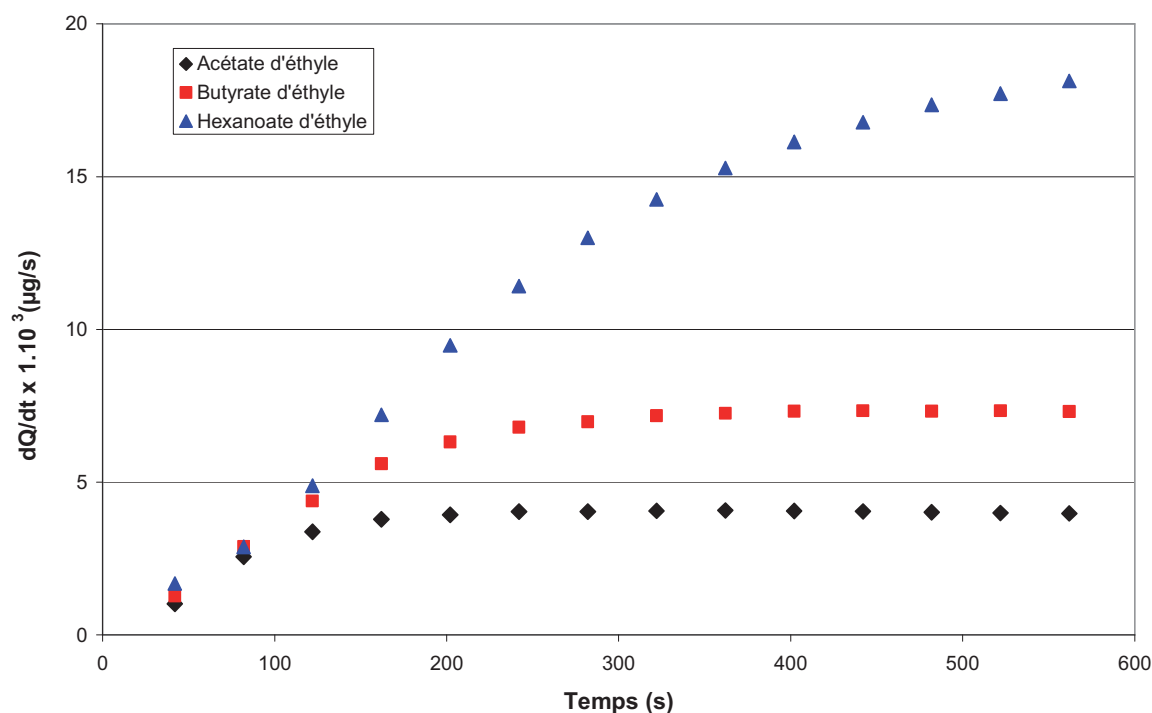
Figure vii. Evolution du Flux de composé organique à travers le LDPE en fonction du temps, sans backflush et à 20 kPa.
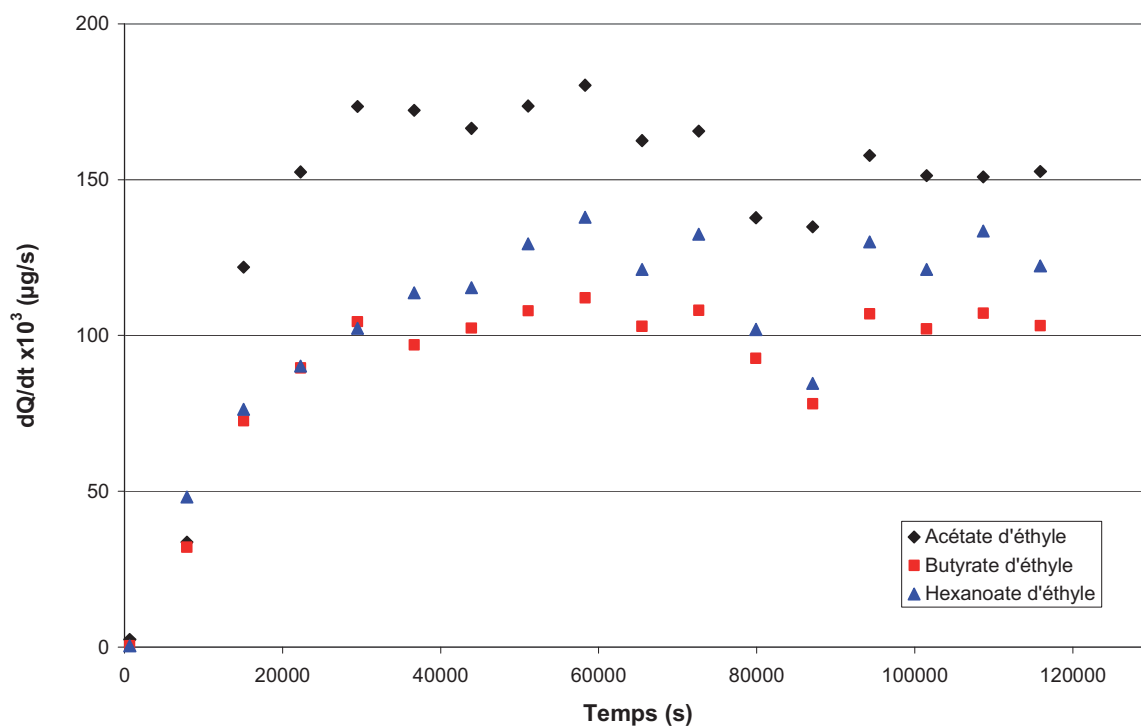
Figure viii. Evolution du Flux de composé organique à travers le P(D,L)LA Biophan® en fonction du temps, sans backflush et à 20 kPa.

Annexe IV : Etude des propriétés thermo-mécaniques du P(D,L)LA CD92 pur et formulé

Une étude par analyses thermo-mécanique dynamique a été réalisée sur les films de P(D,L)LA CD92 pur et formulé dans le but de déterminer la température de transition vitreuse de chacun des mélanges. L'utilisation de cette technique très sensible a pour but de détecter les faibles modifications de la T_g et de pouvoir ainsi comparer l'effet de la teneur en plastifiant et de la présence d'agent nucléant sur les propriétés thermo-mécaniques du P(D,L)LA. Compte tenu de la forte chute de module (de l'ordre de 2 à 3 décades) observée au niveau de la transition vitreuse pour un autre polyester, le PET (Dong, 2002), il semble nécessaire de réaliser un travail d'optimisation des paramètres d'analyse. Cette optimisation a été réalisée à 2 °C.min^{-1} avec la DMA Tritec 2000 (Triton) en mode compression-traction sur une gamme de température restreinte (25-160 °C) dans laquelle se situe la T_g du P(D,L)LA. Plusieurs paramètres sont à optimiser afin de déterminer à la fois le module de conservation au plateau haut, à température inférieure à la T_g, et au plateau bas, à température supérieure à la T_g:

- la force statique appliquée
- le déplacement dynamique
- les dimensions de l'échantillon

Deux forces statiques, -0.5 et -0.25 N ont été appliquées sur le ressort à un échantillon de P(D,L)LA de dimension 10 mm de longueur, 5 mm de largeur et 0,2 mm d'épaisseur. La procédure a alors consisté à faire un balayage en déformation dynamique aux températures de 25 et 80 °C, en imposant systématiquement les deux forces statiques –0,25 et –0,5 N sur le ressort de la DMA.

Comme montré dans la Figure vix, le module de conservation varie peu en fonction de la force appliquée et du déplacement à la température de 25 °C (état vitreux). Par contre, une différence significative du module est observée à 80 °C (état caoutchoutique) en fonction de la force appliquée. Ces faibles valeurs de module peuvent s'expliquer par le fait que la force statique appliquée, -0,25 N, soit à la limite de force de l'appareil. Il apparaît donc que seule la force statique de -0,5 N permet d'obtenir des modules de conservation nettement plus importants et donc plus proches des valeurs qui auraient pu être mesurées par traction classique.
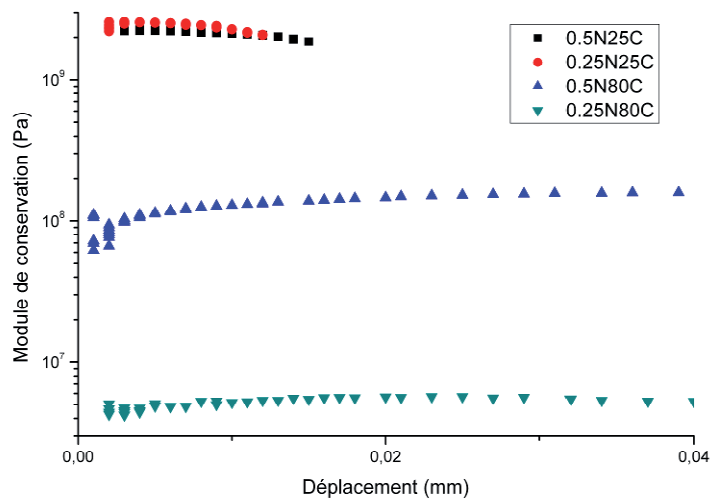
Figure ix. Test de balayage en déplacement dynamique en fonction de la force statique appliquée au P(D,L)LA CD92 pur, à 25 et 80 °C.

Au regard des résultats présentés, il apparaît que la force statique la plus adaptée pour le P(D,L)LA est -0,5 N. Avec une telle valeur, le balayage en déplacement dynamique appliqué au P(D,L)LA montre que le module n'évolue pas à 25 °C pour des déplacements dynamiques inférieurs à 10 µm (< 0,1% d'élongation), correspondant à une force inférieure à 1,5 N (zone d'élasticité linéaire), alors qu'il atteint son maximum, à 80 °C, pour des déplacements dynamiques supérieurs à 15 µm (> 0,15 %), correspondant à une force supérieure à 0,1 N.

Le choix du déplacement dynamique est donc crucial et est optimisé par le biais de tests de balayage en température (Figure x). Plusieurs valeurs de déplacement dynamiques ont été testées: 5, 10, 15, 25 et 50 µm.

Deux déplacements dynamiques, 25 et 50 µm mettent en évidence une faible valeur du module de conservation avant la T_g. Cela confirme les résultats obtenus précédemment (Figure ix) qui montraient un déplacement dynamique optimal aux alentours de 10 µm. Les déplacements dynamiques de 5, 10 et 15 µm semblent conduire à des valeurs du même ordre de grandeur avant la T_g. De plus, il apparaît que le déplacement dynamique de 5 µm induit une réponse bruitée du module de conservation. L'augmentation du déplacement diminue le bruit observé à partir de 85 °C. Comme montré dans la Figure x, à 25 °C et -0,5 N, la valeur du module de conservation semble moins importante autour de 10 qu'autour de 15 µm. Le choix du déplacement appliqué au P(D,L)LA sera donc de 10 µm.
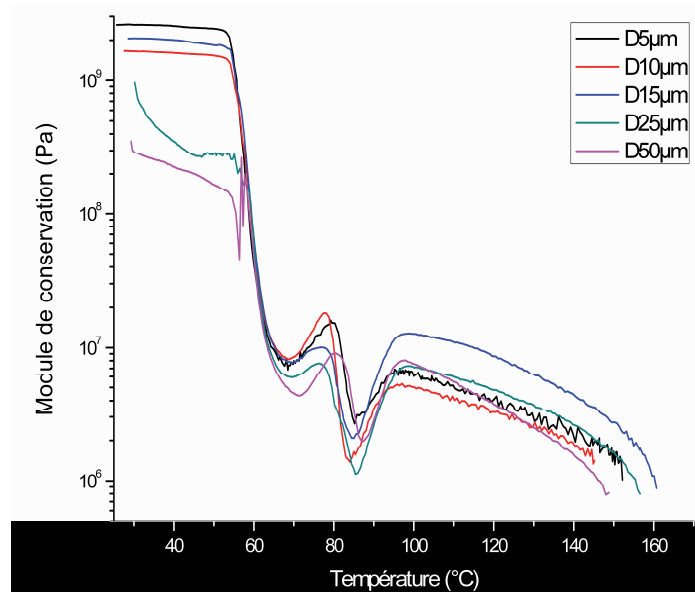
Figure x. Balayage en température en fonction du déplacement dynamique appliqué à un échantillon de P(D,L)LA CD92 pur.

Les dimensions de l'échantillon ont ensuite fait l'objet de travaux en vue de minimiser le bruit à 85 °C. Trois dimensions ont été testées pour un film de P(D,L)LA de même épaisseur de 0.2 mm. Deux différentes largeurs (L) et longueurs (l) ont été testées (Figure xi).
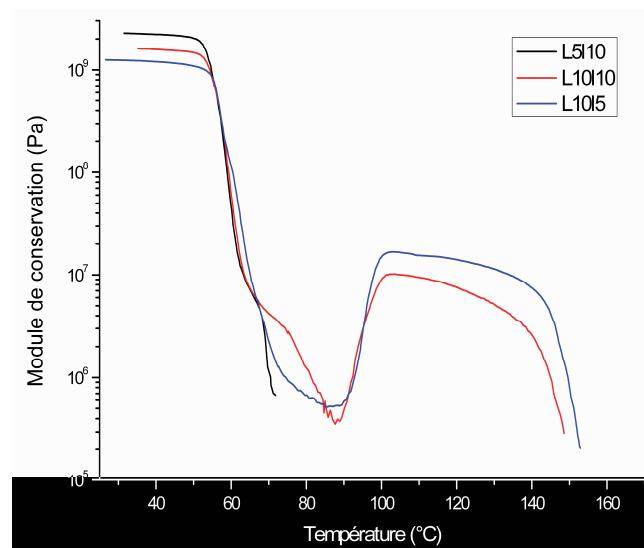
Figure xi. Balayage en température en fonction des dimensions de l'échantillon de P(D,L)LA CD92 pur.

Le test effectué sur l'échantillon de 5 mm de large et 10 mm de long s'est arrêté avant la fin du programme en raison de la limite inférieure du module de conservation imposée par l'appareil dans ces conditions. L'échantillon de 10 mm de long et de large met en évidence

une variation de la mesure (bruit) pour les faibles valeurs de module. Par contre, avec un échantillon de 10 mm de large et 5 mm de long, le module de conservation est mesuré jusqu'à la fin de la montée en température sans être bruité pour les faibles valeurs du module.

Par conséquent, la mesure en DMA est réalisée sur des échantillons de 10mm de large et 5mm de long avec une force et un déplacement dynamique de respectivement –0,5 N et 10 µm, entre 20 et 180 °C à 2 °C.min⁻¹.

L'optimisation effectuée, une analyse des échantillons de P(D,L)LA pur et formulé avec une teneur en plastifiant inférieure à 9 % en poids a été réalisée.

La Figure xii présente l'évolution du module de conservation avec la température des P(D,L)LA en fonction de leur teneur en PEG et de la présence de talc. Comme attendu, avant T_g, le module du P(D,L)LA pur est supérieur aux modules après plastification de la matrice P(D,L)LA. Une baisse du module de 2.4 GPa à 0.8 GPa est observée entre le P(D,L)LA pur et le P(D,L)LA avec 9 % en poids de PEG. De plus, il apparaît que l'addition de 1 wt% de talc dans chacun des mélanges ne modifie pas significativement les modules, ni au plateau haut (avant T_g) ni au plateau bas (après T_g).
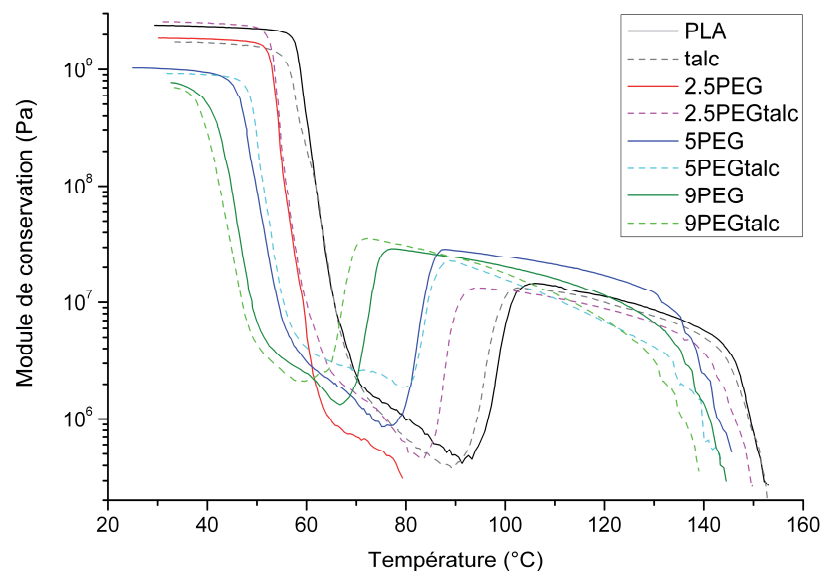
Figure xii. Evolution du module de conservation (E') avec la température en fonction de la teneur en PEG dans le P(D,L)LA CD92 sans (ligne continue) ou avec 1% en poids de talc (ligne en pointillée)

317

La chute du module de 2 à 3 décades, correspondant à la T_g du mélange, se déplace vers les plus faibles températures, de 58 à 25 °C, avec l'augmentation de la teneur en PEG, confirmant ainsi l'effet plastifiant du PEG. L'étude de l'évolution du facteur de perte, tan δ, en température met en évidence une diminution progressive de la T_g avec la teneur en PEG avec ou sans talc (Figure xiii).
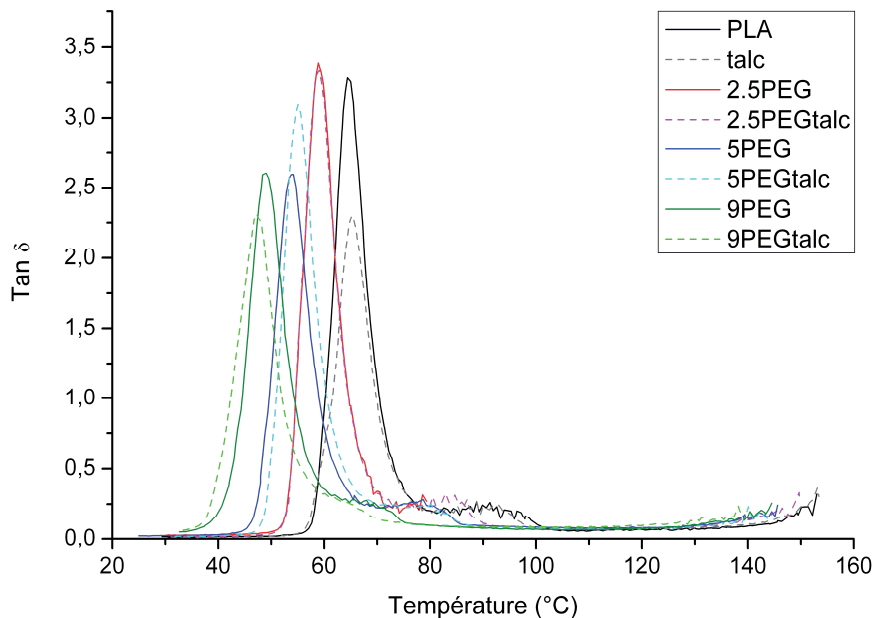
Figure xiii. Evolution du facteur de perte, tan δ, avec la température en fonction de la teneur en PEG dans le P(D,L)LA CD92 sans (ligne continue) ou avec 1% en poids de talc (ligne en pointillée).

La chute du module est, par la suite, suivie d'une ré-augmentation due à la recristallisation du mélange. Comme la T_g, la température de cristallisation, température à laquelle le module ré-augmente, se déplace vers les plus faibles températures. Enfin, une deuxième baisse du module est observée, 40 à 50°C après la cristallisation des échantillons, qui est attribuée au début de la fusion de chacun des mélanges.

La Figure xiv présente l'évolution du module de conservation avec la température des P(D,L)LA en fonction de leur teneur en ATBC et de la présence de talc. Contrairement au PEG, l'ajout d'ATBC jusqu'à 9 wt% n'induit aucune diminution du module au plateau haut. Celui-ci se situe autour de 2.4 GPa malgré une teneur de 9 % en poids d'ATBC.

.
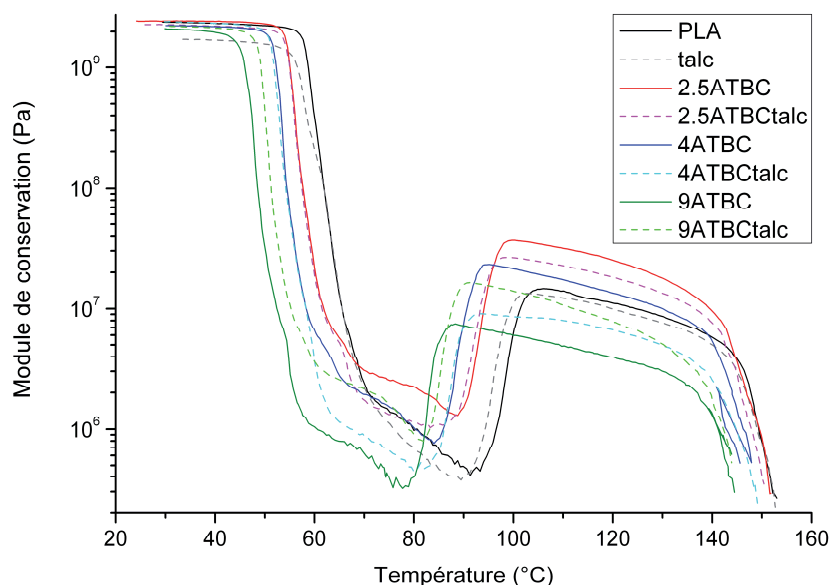
Figure xiv Evolution du module de conservation (*E'*) avec la température en fonction de la teneur en ATBC dans le P(D,L)LA CD92 sans (ligne continue) ou avec 1% en poids de talc (ligne en pointillée).

Comme précédemment pour le PEG, une chute du module, se déplaçant vers les plus faibles températures avec la teneur en ATBC, est ensuite observée lors de la rampe de température. Cependant cette chute ne commence qu'à partir de 40 °C avec 9 % en poids d'ATBC alors qu'elle était constatée à 25 °C pour une même teneur en PEG. L'évolution du pic de facteur de perte met en évidence une diminution de moins de 15 °C avec la teneur en ATBC (Figure xv).
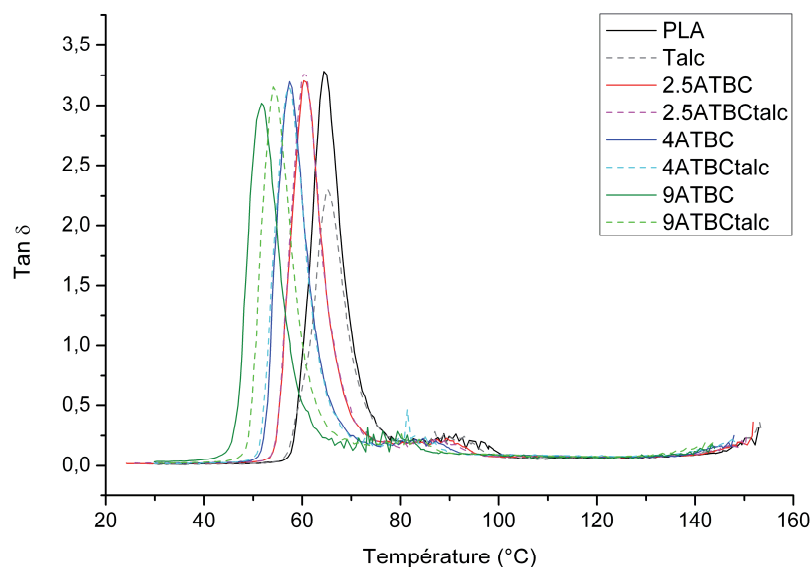
Figure xv. Evolution du facteur de perte, tan δ, avec la température en fonction de la teneur en ATBC dans le P(D,L)LA CD92 sans (ligne continue) ou avec 1% en poids de talc (ligne en pointillée).
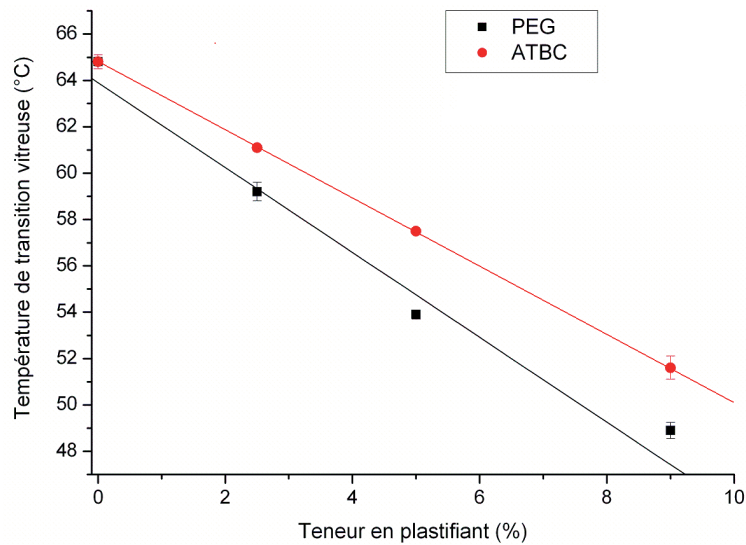
Figure xvi. Evolution de la température de transition vitreuse du P(D,L)LA formulé, mesurée par DMA, en fonction de la teneur en plastifiant dans le P(D,L)LA.

L'étude des matériaux de P(D,L)LA formulés met en évidence une plastification plus importante avec le PEG qu'avec l'ATBC, observée par une diminution du module de conservation au plateau haut et une baisse de la température de transition vitreuse (Figure xvi). Néanmoins, la plastification semble plus linéaire avec l'ATBC qu'avec le PEG. Ceci pourrait s'expliquer par l'exsudation du PEG à 9 wt%, induisant ainsi l'apparition de la T_g à plus forte température. Il apparaît également que l'ajout de talc ne modifie pas les propriétés thermomécaniques du P(D,L)LA. Par conséquent la publication n°2 n'a porté que sur des échantillons de P(D,L)LA CD92 formulé sans talc.

Annexe V : Courbes de traction du P(D,L)LA CD92
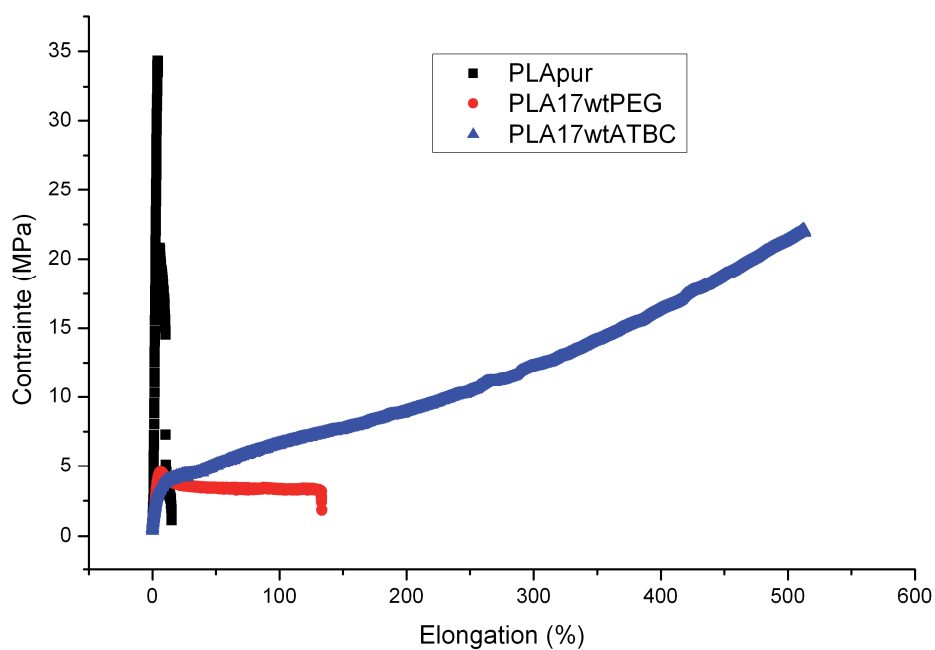
Figure xvii. Courbes contrainte vs élongation de films de P(D,L)LA CD92 pur, P(D,L)LA CD92 avec 17 wt% de PEG et 17 wt% d'ATBC amorphe à température ambiante.

Références bibliographiques

2002/72/EC Commission Directive of 6 August 2002 relating to plastic materials and articles intended to come into contact with foodstuffs. . (2002). In T. E. Commission (Ed.): Official Journal.

Agarwal, M., Koelling, K. W., Chalmers, J. J. (1998). Characterization of the degradation of polylactic acid polymer in a solid substrate environment. *Biotechnology Progress, 14*(3), 517-526.

Ahn, J., Chung, W.-J., Pinnau, I., Guiver, M. D. (2008). Polysulfone/silica nanoparticle mixed-matrix membranes for gas separation. *Journal of Membrane Science, 314*(1-2), 123-133.

Albertsson, A. C., Srivastava, R. K. (2008). Recent developments in enzyme-catalyzed ring-opening polymerization. *Advanced Drug Delivery Reviews, 60*(9), 1077-1093.

Alcimed. (2011). *Usage des résines biosourcées: Quels développements en France, dans l'Union Européenne et dans le monde ?* : ADEME, France.

Anderson, K. S., Hillmyer, M. A. (2006). Melt preparation and nucleation efficiency of polylactide stereocomplex crystallites. *Polymer, 47*(6), 2030-2035.

Androsch, R., Wunderlich, B. (2005). The link between rigid amorphous fraction and crystal perfection in cold-crystallized poly(ethylene terephthalate). *Polymer, 46*(26), 12556-12566.

Arnoult, M., Dargent, E., Mano, J. F. (2007). Mobile amorphous phase fragility in semi-crystalline polymers: Comparison of PET and PLLA. *Polymer, 48*(4), 1012-1019.

Auras, R. A., Harte, B., Selke, S., Hernandez, R. (2003). Mechanical, Physical, and Barrier Properties of Poly(Lactide) Films. *Journal of Plastic Film and Sheeting, 19*(2), 123-135.

Auras, R., Harte, B., Selke, S. (2004a). Effect of water on the oxygen barrier properties of poly(ethylene terephtalate) and polylactide films. *Journal of Applied Polymer Science, 92*, 1790-1803.

Auras, R., Harte, B., Selke, S. (2004b). An Overview of Polylactides as Packaging Materials. *Macromolecular Bioscience, 4*(9), 835-864.

Auras, R., Singh, S. P., Singh, J. J. (2005). Evaluation of oriented poly(lactide) polymers vs. existing PET and oriented PS for fresh food service containers. *Packaging Technology ans Science, 18*, 207-216.

Auras, R., Harte, B., Selke, S. (2006). Sorption of Ethyl Acetate and d-limonene in Poly(lactide) Polymers. *Journal of the Science of Food and Agriculture, 86*, 648-656.

Averous, L., Boquillon, N. (2004). Biocomposites based on plasticized starch: thermal and mechanical behaviours. *Carbohydrate Polymers, 56*, 111-122.

Avérous, L. (2008). Polylactic acid: synthesis, properties and applications. In B. N. a. G. A. (Ed.), *Monomers, Polymers and Composites from Renewable Resources* (Vol. Chap. 21, pp. 433-450): Elsevier Limited Publication.

Avérous, L. (2009). Polylactic acid: synthesis, properties and applications. In N. Belgacem & A. Gandini (Eds.), (Vol. 21, pp. 433-450): Elsevier Limited Publication.

Avinc, O., Khoddami, A. (2009). Overview of Poly(lactic acid) (PLA) Fibre. *Fibre Chemistry, 41*(6), 391-401.

Avinc, O., Khoddami, A. (2010). Overview of Poly(lactic acid) (PLA) Fibre Part II: Wet Processing; Pretreatment, Dyeing, Clearing, Finishing, and Washing Properties of Poly(lactic acid) Fibres. *Fibre Chemistry, 42*(1), 68-78.

Avrami, M. (1939). Kinetics of Phase Change. I. General Theory. *Journal of Chemical Physics, 7*(12), 1103-1112.

Avrami, M. (1940). Kinetics of Phase Change. II. Transformation-Time Relations for Random Distribution of Nuclei. *Journal of Chemical Physics, 8*(2), 212-224.

Avrami, M. (1941). Kinetics of Phase Change. III. Granulation, Phase Change, and Microstructure. *Journal of Chemical Physics, 9*(2), 177-184.

Baiardo, M., Frisoni, G., Scandola, M., Rimelen, M., Lips, D., Ruffieux, K., et al. (2003). Thermal and Mechanical Properties of Plasticized Poly(L-lactic acid). *Journal of Applied Polymer Science, 90*, 1731-1738.

Balamurugan, G. P., Maiti, S. N. (2008). Nonisothermal crystallization kinetics of polyamide 6 and ethylene-co-butyl acrylate blends. *Journal of Applied Polymer Science, 107*(4), 2414-2435.

Baltieri, R. C., Mei, L. H. I., Bartoli, J. (2003). Study of the Influence of Plasticizers on the Thermal and Mechanical Properties of Poly(3-hydroxybutyrate) Compounds. *Macromolecular Symposia, 197*, 33-44.

Bao, L., Dorgan, J. R., Knauss, D., Hait, S., Oliveira, N. S., Maruccho, I. M. (2006). Gas permeation properties of poly(lactic acid) revisited. *Journal of membrane Science, 285*, 166-172.

Barber, F. A., Elrod, B. F., McGuire, D. A., Paulos, L. E. (2000). Bioscrew fixation of patellar tendon autografts. *Biomaterials, 21*(24), 2623-2629.

Berlinet, C., Ducruet, V., Brillouet, J., Reynes, M., Brat, P. (2005). Evaluation of aroma compounds from orange juice stored in polyethylene terephthalate (PET). *Food Additives and Contaminants, 22*(2), 185-195.

Berlinet, C., Brat, P., Ducruet, V. (2008). Quality of orange juice in barrier packaging material. *Packaging Technology ans Science, 21*, 279-286.

Bodmeier, R., Oh, K. H., Chen, H. (1989). The effect of the addition of low-molecular weight poly (D,L Lactide) drug delivery systems. *International Journal of Pharmaceutics, 51*, 1-8.

Bogaert, J.-C., Coszach, P. (2000). Poly(lactic acids): A potentiel solution to plastic waste dilemna. *Macromolecular Symposia, 153*, 287-303.

Bordes, P., Pollet, E., Avérous, L. (2009). Nano-biocomposites: Biodegradable polyester/nanoclay systems. *Progress in Polymer Science, 34*, 125-155.

Bouapao, L., Tsuji, H., Tashiro, K., Zhang, J., Hanesaka, M. (2009). Crystallization, spherulite growth, and structure of blends of crystalline and amorphous poly(lactide)s. *Polymer, 50*(16), 4007-4017.

Bourbigot, S., Fontaine, G. (2010). Flame retardancy of polylactide: an overview. *Polymer Chemistry, 1*(9), 1413-1422.

Brandt, W. W. (1959). Model Calculation of the Temperature Dependence of Small Molecule Diffusion in High Polymers. *The Journal of Physical Chemistry, 63*(7), 1080-1085.

Brizzolara, D., Cantow, H.-J., Diederichs, K., Keller, E., Domb, A. J. (1996). Mechanism of the Stereocomplex Formation between Enantiomeric Poly(lactide)s. *Macromolecules, 29*(1), 191-197.

Brolly, J. B., Bower, D. I., Ward, I. M. (1996a). Diffusion and sorption of CO2 in poly(ethylene terephthalate) and poly(ethylene naphthalate). *Journal of Polymer Science Part B: Polymer Physics, 34*(4), 769-780.

Brolly, J. B., Bower, D. I., Ward, I. M. (1996b). Finite difference modeling of the gas transport process in glassy polymers. *Journal of Polymer Science Part B: Polymer Physics, 34*(4), 761-768.

Brouillet, S., Fugit, J.-L. (2009). Solutions to reduce release behavior of plasticizers out of PVC-made equipments: binary blends of plasticizers and thermal treatment. *Polymer Bulletin, 62*(6), 843-854.

Byun, Y., Kim, Y. T., Whiteside, S. (2011). Characterization of an antioxidant polylactic acid (PLA) film prepared with alpha-tocopherol, BHT and polyethylene glycol using film cast extruder. *Journal of Food Engineering, 100*(2), 239-244.

Cabedo, L., Feijoo, J. L., Villanueva, M. P., Lagaron, J. M., Gimenez, E. (2006). Optimization of biodegradable nanocomposites based on aPLA/PCL blends for food packaging applications. *Macromolecular Symposia, 233*, 191-197.

Carothers, W., Dorough, G., van Natta, F. (1932). Studies of polymerization and ring formation. X. The reversible polymerization of six membered cyclic esters. *Journal of the American Chemical Society, 54*, 761-772.

Carrasco, F., Pages, P., Gamez-Perez, J., Santana, O. O., Maspoch, M. L. (2010). Processing of poly(lactic acid): Characterization of chemical structure, thermal stability and mechanical properties. *Polymer Degradation and Stability, 95*(2), 116-125.

Cartier, L., Okihara, T., Ikada, Y., Tsuji, H., Puiggali, J., Lotz, B. (2000). Epitaxial crystallization and crystalline polymorphism of polylactides. *Polymer, 41*(25), 8909-8919.

Cava, D., Giménez, E., Gavara, R., Lagaron, J. M. (2006). Comparative Performance and Barrier Properties of Biodegradable Thermoplastics and Nanobiocomposites versus PET for Food Packaging Applications. *Journal of plastic film & sheeting, 22*, 265-274.

Chanfreau, S., Mena, M., Porras-Dominguez, J. R., Ramirez-Gilly, M., Gimeno, M., Roquero, P., et al. (2010). Enzymatic synthesis of poly-l-lactide and poly-l-lactide-co-glycolide in an ionic liquid. *Bioprocess and Biosystems Engineering, 33*(5), 629-638.

Chang, Y. N., Mueller, R. E., Iannotti, E. L. (1996). Use of low MW polylactic acid and lactide to stimulate growth and yield of soybeans. *Plant Growth Regulation, 19*(3), 223-232.

Chang, J.-H., An, Y. U., Sur, G. S. (2003). Poly(lactic acid) nanocomposites with various organoclays. I. Thermomechanical properties, morphology, and gas permeability. *Journal of Polymer Science Part B: Polymer Physics, 41*(1), 94-103.

Chen, C., Fei, N., Peng, S., Zhuang, Y., Dong, L., Feng, Z. (2002). Nonisothermal crystallization and melting behavior of poly(3-hydroxybutyrate) and maleated poly(3-hydroxybutyrate). *European Polymer Journal, 38*(8), 1663-1670.

Chen, H., Cebe, P. (2008). Vitrification and Devitrification of Rigid Amorphous Fraction of PET during Quasi-Isothermal Cooling and Heating. *Macromolecules, 42*(1), 288-292.

Chivrac, F., Pollet, E., Avérous, L. (2006). Nonisothermal Crystallization Behavior of Poly(butylene adipate-co-terephthalate)/Clay Nano-biocomposites. *Journal of Polymer Science : Part B : Polymer Physics, 45*, 1503-1510.

Cho, J., Baratian, S., Kim, J., Yeh, F., Hsiao, B. S., Runt, J. (2003). Crystallization and structure formation of poly(l-lactide-co-meso-lactide) random copolymers: a time-resolved wide- and small-angle X-ray scattering study. *Polymer, 44*(3), 711-717.

Cho, T.-Y., Strobl, G. (2006). Temperature dependent variations in the lamellar structure of poly(l-lactide). *Polymer, 47*(4), 1036-1043.

Cohen, M. H., Turnbull, D. (1959). Molecular Transport in Liquids and Glasses. *The Journal of Chemical Physics, 31*(5), 1164-1169.

Colomines, G., Ducruet, V., Courgneau, C., Guinault, A., Domenek, S. (2010). Barrier properties of poly(lactic acid) and its morphological changes induced by aroma compound sorption. *Polymer International, 59*(6), 818-826.

Coltelli, M.-B., Maggiore, I. D., Bertoldo, M., Signori, F., Bronco, S., Ciardelli, D. (2008). Poly(lactic acid) Properties as a Consequence of Poly(butylene adipate-co-terephthalate) Blending and Acetyl Tributyl Citrate Plasticization. *Journal of Applied Polymer Science, 110*, 1250-1262.

Conn, R. E., Kolstad, J. J., Borzelleca, J. F., Dixler, D. S., Filer Jr, L. J., Ladu Jr, B. N., et al. (1995). Safety assessment of polylactide (PLA) for use as a food-contact polymer. *Food and Chemical Toxicology, 33*(4), 273-283.

Courgneau, C., Domenek, S., Guinault, A., Avérous, L., Ducruet, V. (2011). Analysis of the structure-properties relationships of different multiphase systems based on plasticized poly(lactic acid). *Journal of polymers and the environment,* 19 (2), 362-371.

Crank, J. (1975). *The mathematics of diffusion*. Oxford: Clarendon Press.

D'Aniello, C., Guadagno, L., Gorrasi, G., Vittoria, V. (2000). Influence of the crystallinity on the transport properties of isotactic polypropylene. *Polymer, 41*(7), 2515-2519.

Dangseeyun, N., Srimoaon, P., Supaphol, P., Nithitanakul, M. (2004). Isothermal melt crystallization and melting behavior for three linear aromatic polyesters. *Thermochimica Acta, 409*, 63-77.

Datta, R., Tsai, S. P., Bonsignore, P., Moon, S. H., Frank, J. R. (1995). Technological and Economic-Potential of Poly(Lactic Acid) and Lactic-Acid Derivatives. *Fems Microbiology Reviews, 16*(2-3), 221-231.

Day, M., Nawaby, A., Liao, X. (2006). A DSC study of the crystallization behaviour of polylactic acid and its nanocomposites, *Journal of Thermal Analysis and Calorimetry* (Vol. 86, pp. 623-629): Akadémiai Kiadó, co-published with Springer Science+Business Media B.V., Formerly Kluwer Academic Publishers B.V.

De Jong, S. J., Arias, E. R., Rijkers, D. T. S., van Nostrum, C. F., Kettenes-van den Bosch, J. J., Hennink, W. E. (2001). New insights into the hydrolytic degradation of poly(lactic acid): participation of the alcohol terminus. *Polymer, 42*(7), 2795-2802.

De Oca, H. M., Ward, I. M. (2007). Structure and mechanical properties of poly(L-lactic acid) crystals and fibers. *Journal of Polymer Science Part B: Polymer Physics, 45*(8), 892-902.

De Santis, P., Kovacs, A. (1968). Molecular conformation of poly(S-lactic acid). *Biopolymers, 6*, 299-306.

Degee, P., Dubois, P., Jacobsen, S., Fritz, H. G., Jerome, R. (1999). Beneficial effect of triphenylphosphine on the bulk polymerization of L,L-Lactide promoted by 2-ethylhexanoic acid tin (II) salt. *Journal of Polymer Science Part a-Polymer Chemistry, 37*(14), 2413-2420.

Del Nobile, M. A., Conte, A., Buonocore, G. G., Incoronato, A. L., Massaro, A., Panza, O. (2009). Active packaging by extrusion processing of recyclable and biodegradable polymers. *Journal of Food Engineering, 93*(1), 1-6.

Del Rio, J., Etxeberria, A., Lopez-Rodriguez, N., Lizundia, E., Sarasua, J. R. (2010). A PALS contribution to the supramolecular structure of poly(L-lactide). *Macromolecules, 43*, 4698-4707.

DeLassus, P. T. (1994). Sorption and diffusion of flavors in plastic packaging. In R. J. M. Gorrin & J. V. Leland (Eds.), *Flavor-food interactions* (pp. 152-161). Washington DC: ACS Symposium Series.

Delpouve, N., Saiter, A., Mano, J. F., Dargent, E. (2008). Cooperative rearranging region size in semi-crystalline poly(l-lactic acid). *Polymer, 49*(13-14), 3130-3135.

Delpouve, N. (2009). *Etude de la microstructure et des phénomènes de relaxation dans un polyester biodégradable: le poly(acide lactique) (PLA).* Thèse, Université de Rouen, Rouen.

Deng, K., Felorzabihi, N., Winnik, M. A., Jiang, Z., Yin, Z., Yaneff, P. V., et al. (2009). Investigation of morphology and miscibility of isotactic polypropylene, ethylene-butene copolymer and chlorinated polyolefin blends via LSCFM, SEM, WAXD, and DMA. *Polymers for Advanced Technologies, 20*(3), 235-245.

Di Lorenzo, M. L., Silvestre, C. (1999). Non-isothermal crystallization of polymers. *Progress in Polymer Science, 24*(6), 917-950.

Di Lorenzo, M. L. (2005). Crystallization behavior of poly(L-lactic acid). *European Polymer Journal, 41*, 569-575.

Di Lorenzo, M. L. (2006). The Crystallization and Melting Processes of Poly(L-lactic acid). *Macromolecular Symposia, 234*(1), 176-183.

DiBenedetto, A. T., Paul, D. R. (1964). An interpretation of gaseous diffusion through polymers using fluctuation theory. *Journal of Polymer Science Part A: General Papers, 2*(2), 1001-1015.

Dlubek, G., Sen Gupta, A., Pionteck, J., Häßler, R., Krause-Rehberg, R., Kaspar, H., et al. (2005). Glass transition and free volume in the mobile (MAF) and rigid (RAF) amorphous fractions of semicrystalline PTFE: a positron lifetime and PVT study. *Polymer, 46*(16), 6075-6089.

Dong, W., Zhao, J., Li, C., Guo, M., Zhao, D., Fan, Q. (2002). Study of the amorphous phase in semicrystalline poly(ethy1ene terephthalate) via dynamic mechanical thermal analysis. *Polymer Bulletin, 49*(2), 197-203.

Dorgan, J. R., Lehermeier, H. J., Palade, L.-I., Cicero, J. (2001). Polylactides: Properties and Prospects of an Environmentally Benign Plastic from Renewable Resources. *Macromolecular Symposia, 175*, 55-66.

Drieskens, M., Peeters, R., Mullens, J., Franco, D., Lemstra, P. J., Hristova-Bogaerds, D. G. (2009). Structure versus properties relationship of poly(lactic acid). I. Effect of

crystallinity on barrier properties. *Journal of Polymer Science Part B: Polymer Physics, 47*(22), 2247-2258.

Drumright, R. E., Gruber, P. R., Henton, D. E. (2000). Polylactic acid technology. *Advanced Materials, 12*(23), 1841-1846.

Duarte, W. F., Dias, D. R., Oliveira, J. M., Teixeira, J. A., de Almeida e Silva, J. B., Schwan, R. F. (2010). Characterization of different fruit wines made from cacao, cupuassu, gabiroba, jaboticaba and umbu. *LWT - Food Science and Technology, 43*(10), 1564-1572.

Dubois, P., Ropson, N., Jerome, R., Teyssie, P. (1996). Macromolecular Engineering of Polylactones and Polylactides. 19. Kinetics of Ring-Opening Polymerization of Îμ-Caprolactone Initiated with Functional Aluminum Alkoxides. *Macromolecules, 29*(6), 1965-1975.

Ducruet, V. J., Rasse, A., Feigenbaum, A. E. (1996). Food and packaging interactions: Use of methyl red as a probe for PVC swelling by fatty acid esters. *Journal of Applied Polymer Science, 62*(10), 1745-1752.

Ducruet, V., Vitrac, O., Saillard, P., Guichard, E., Feigenbaum, A., Fournier, N. (2007). Sorption of aroma compounds in PET and PVC during the storage of a strawberry syrup. *Food Additives and Contaminants, 24*, 1306-1317.

Duda, J. L., Zielinski, J. M. (1996). Free volume theory. In P. Neogi (Ed.), *Diffusion in polymers* (Vol. 32, pp. 143-171). New York: Marcel Dekker, Inc.

Durand, M. (2010). *Molecular dynamics simulations of oligomer diffusion in polymer melts.* Thèse, Université de Strasbourg, Strasbourg.

Durning, C. J., Russel, W. B. (1985). A mathematical model for diffusion with induced crystallization: 2. *Polymer, 26*(1), 131-140.

Dury-Brun, C. (2006). *Transferts de molécules volatiles entre une matrice solide alimentaire et un emballage souple.* Thèse, Université de Bourgogne, Dijon.

Dury-Brun, C., Chalier, P., Desobry, S., Voilley, A. (2007). Multiple Mass Transfers of Small Volatile Molecules Through Flexible Food Packaging. *Food Reviews International, 23*, 199-255.

Dury-Brun, C., Hirata, Y., Guillard, V., Ducruet, V., Chalier, P., Voilley, A. (2008). Ethyl hexanoate transfer in paper and plastic food packaging by sorption and permeation experiments. *Journal of Food Engineering, 89*(2), 217-226.

EFSA. (2006). Opinion of the Scientific Panel on food additives, flavourings, processing aids and materials in contact with food (AFC) on a request related to a 10th list of substances for food contact materials. *The EFSA Journal, 273*, 1-26.

El-Taweel, S. H., Höhne, G. W. H., Mansour, A. A., Stoll, B., Seliger, H. (2004). Glass transition and the rigid amorphous phase in semicrystalline blends of bacterial

polyhydroxybutyrate PHB with low molecular mass atactic R, S-PHB-diol. *Polymer, 45*(3), 983-992.

Eling, B., Gogolewski, S., Pennings, A. J. (1982). Biodegradable materials of poly(l-lactic acid): 1. Melt-spun and solution-spun fibres. *Polymer, 23*(11), 1587-1593.

Enomoto, K., Ajioka, M., Yamagouchi, A. (1994). Polyhydroxycarboxylic acid and preparation process thereof Mitsui Toatsu Chemicals, Incorporated (Tokyo, JP).

European-bioplastics. (2010). from http://www.european-bioplastics.org/

Favre, E., Nguyen, Q. T., Clément, R., Néel, J. (1996). The engaged species induced clustering (ENSIC) model: a unified mechanistic approach of sorption phenomena in polymers. *Journal of Membrane Science, 117*(1-2), 227-236.

Ferrara, G., Bertoldo, M., Scoponi, M., Ciardelli, F. (2001). Diffusion coefficient and activation energy of Irganox 1010 in poly(propylene-co-ethylene) copolymers. *Polymer Degradation and Stability, 73*(3), 411-416.

Fischer, E. W., Sterzel, H. J., Wegner, G. (1973). Investigations of the structure of solution grown crystals of lactide copolymers by means of chemical reactions. *Kolloid-Z. u. Z. Polymere*, *251*, 980-990.

Flaconnèche, B., Martin, J., Klopffer, M. H. (2001). Transport Properties of Gases in Polymers: Experimental Methods. *Oil and Gas Science and Technology-Review IFP, 56*(3), 245-259.

Fortunati, E., Armentano, I., Iannoni, A., Kenny, J. M. (2010) Development and thermal behaviour of ternary PLA matrix composites. *Polymer Degradation and Stability, 95*(11), 2200-2206.

Friedman, H. L. (1969). New methods for evaluating kinetic parameters from thermal analysis data. *Journal of Polymer Science Part B: Polymer Letters, 7*(1), 41-46.

Fujita, H. (1961). Diffusion in polymer-diluent systems. *Advances in Polymer Science, 3*, 1-47.

Fukushima, K., Murariu, M., Camino, G., Dubois, P. (2010). Effect of expanded graphite/layered-silicate clay on thermal, mechanical and fire retardant properties of poly(lactic acid). *Polymer Degradation and Stability, 95*(6), 1063-1076.

Furukawa, T., Sato, H., Murakami, R., Zhang, J., Duan, Y.-X., Noda, I., et al. (2005). Structure, Dispersibility, and Cristallinity of Poly(hydroxybutyrate)/Poly(L-Lactic acid) Blends Studied by FT-IR Microspectroscopy and Differential Scanning Calorimetry. *Macromolecules, 38*, 6445-6454.

Garlotta, D. (2001). A literature review of poly(lactic acid). *Journal of Polymers and the Environment, 9*(2), 63-84.

George, S. C., Thomas, S. (2001). Transport phenomena through polymeric systems. *Progress in Polymer Science, 26*(6), 985-1017.

Ghorpade, V. M., Gennadios, A., Hanna, M. A. (2001). Laboratory composting of extruded poly(lactic acid) sheets. *Bioresource Technology, 76*(1), 57-61.

Gillet, G., Vitrac, O., Desobry, S. (2011) A fast method to assess the composition of a polyolefin: An application to compliance testing of food contact materials. *Journal of Applied Polymer Science, 119*(3), 1492-1515.

Goldman, S. A., Bruno, G. V., Freed, J. H. (1972). Estimating slow-motional rotational correlation times for nitroxides by electron spin resonance. *The Journal of Physical Chemistry, 76*(13), 1858-1860.

Goncalves, C. M. B., Tome, L. C., Coutinho, J. A. P., Marrucho, I. M. (2011) Addition of alpha-Tocopherol on Poly(lactic acid): Thermal, Mechanical, and Sorption Properties. *Journal of Applied Polymer Science, 119*(4), 2468-2475.

Grijpma, D. W., Altpeter, H., Bevis, M. J., Feijen, J. (2002). Improvement of the mechanical properties of poly(D,L-lactide) by orientation. *Polymer International, 51*(10), 845-851.

Gruber, P., Hall, E., Kolstad, J., Iwen, M., Benson, R., Borchardt, R. (1992). Continuous process for manufacture of lactide polymers with controlled optical purity Cargill, Incorporated (Minnetonka, MN).

Gruber, P., Hall, E., Kolstad, J., Jeffrey, J., Iwen, M., Mattew, L., et al. (1994). Continuous process for manufacture of lactide polymers with purification by distillation Cargill, Incorporated (Minnetonka, MN).

Grulke, E. A. (1999). Solubility Parameter Values. In J. Brandrup, E. H. Immergut & E. A. Grulke (Eds.), *Polymer Handbook* (Vol. 2, pp. 675-714). New York: John Wiley & Sons, Inc.

Gu, J. H., Huang, Y. J., Beekman, A., Goldenberg, M. (2010). Simplified preparation of low polydispersity, low molecular weight poly(D,L-lactic acid) by liquid/liquid phase separation for drug delivery systems with discussion of molecular weight characterization. *Polymer International, 59*(12), 1571-1577.

Guinault, A., Sollogoub, C., Domenek, S., Grandmontagne, A., Ducruet, V. (2010). Influence of crystallinity on gas barrier and mechanical properties of pla food packaging films. *International Journal of Material Forming, 3*(0), 603-606.

Guo, J., Barbari, T. A. (2010). A dual mode interpretation of the kinetics of penetrant-induced swelling and deswelling in a glassy polymer. *Polymer, 51*(22), 5145-5150.

Gupta, M. C., Deshmukh, V. G. (1982a). Thermal Oxidative-Degradation of Poly-Lactic Acid .1. Activation-Energy of Thermal-Degradation in Air. *Colloid and Polymer Science, 260*(3), 308-311.

Gupta, M. C., Deshmukh, V. G. (1982b). Thermal Oxidative-Degradation of Poly-Lactic Acid .2. Molecular-Weight and Electronic-Spectra During Isothermal Heating. *Colloid and Polymer Science, 260*(5), 514-517.

Gupta, A. P., Kumar, V. (2007). New emerging trends in synthetic biodegradable polymers - Polylactide: A critique. *European Polymer Journal, 43*(10), 4053-4074.

Hakkarainen, M., Albertsson, A. C., Karlsson, S. (1996). Weight losses and molecular weight changes correlated with the evolution of hydroxyacids in simulated in vivo degradation of homo- and copolymers of PLA and PGA. *Polymer Degradation and Stability, 52*(3), 283-291.

Hans, M., Keul, H., Moeller, M. (2009). Ring-Opening Polymerization of DD-Lactide Catalyzed by Novozyme 435. *Macromolecular Bioscience, 9*(3), 239-247.

Harris, A. M., Lee, E. C. (2008). Improving Mechanical Performance of Injection Molded PLA by Controlling Cristallinity. *Journal of Applied Polymer Science, 107*, 2246-2255.

Harris, A. M., Lee, E. C. (2010). Heat and humidity performance of injection molded PLA for durable applications. *Journal of Applied Polymer Science, 115*(3), 1380-1389.

Hartmann, M. (1998). Biopolymers from renewable resources. In D. Kaplan (Ed.), (pp. 367-411). Berlin, Germany: Springer-Verlag.

Haugaard, V., Weber, C., Danielsen, B., Bertelsen, G. (2002). Quality changes in orange juice packed in materials based on polylactate. *European Food Research and Technology, 214*(5), 423-428.

Haugaard, V. K., Danielsen, B., Bertelsen, G. (2003). Impact of polylactate and poly(hydroxybutyrate) on food quality. *European Food Research and Technology, 216*, 233-240.

Hiltunen, K., Harkonen, M., Seppala, J. V., Vaananen, T. (1996). Synthesis and Characterization of Lactic Acid Based Telechelic Prepolymers. *Macromolecules, 29*(27), 8677-8682.

Hiltunen, K., Seppala, J. V., Harkonen, M. (1997). Effect of Catalyst and Polymerization Conditions on the Preparation of Low Molecular Weight Lactic Acid Polymers. *Macromolecules, 30*(3), 373-379.

Hirata, Y., Ducruet, V. (2006a). Effect of temperature on the solubility of aroma compounds in polyethylene film. *Polymer testing, 25*, 690-696.

Hirata, Y., Massey, M., Relkin, P., Numes, P., Ducruet, V. (2006b). Influence of proteins on the release of aroma compounds into polymer film. In W. B. a. M. Petersen (Ed.), *Flavour Science Recent advances and trends. Proc. of the 11th Weurman Flavour Research Symposium* (pp. 473-476). Roskilde, Danemark: Elsevier.

Hiroi, R., Ray, S. S., Okamoto, M., Shiroi, T. (2004). Organically modified layered titanate: A new nanofiller to improve the performance of biodegradable polylactide. *Macromolecular Rapid Communications, 25*(15), 1359-1364.

Holm, V. K., Ndoni, S., Risbo, J. (2006). The stability of Poly(lactic acid) Packaging Films as Influenced by Humidity and Temperature. *Journal of Food Science, 71*, E40-E44.

Holten, C., Müller, A., Rehbinder, D. (1971). *Lactic acid: properties and chemistry of lactic acid and derivatives*. Weinheim, Germany: Verlag Chemie.

Hong, S.-U., Duda, J. L. (1997). Penetrant transport in polyethylene-polystyrene semi-interpenetrating polymer networks. *Journal of Applied Polymer Science, 65*(1), 51-57.

Hoogsteen, W., Postema, A. R., Pennings, A. J., Ten Brinke, G., Zugenmaier, P. (1990). Crystal structure, conformation and morphology of solution-spun poly(L-lactide) fibers. *Macromolecules, 23*(2), 634-642.

Hu, Y. S., Liu, R. Y. F., Zhang, L. Q., Rogunova, M., Schiraldi, D. A., Nazarenko, S., et al. (2002). Oxygen Transport and Free Volume in Cold-Crystallized and Melt-Crystallized Poly(ethylene naphthalate). *Macromolecules, 35*(19), 7326-7337.

Hu, Y., Hu, Y. S., Topolkaraev, V., Hiltner, A., Baer, E. (2003a). Aging poly(lactide)/poly(ethylene glycol) blends. Part2. Poly(lactide) with high stereoregularity. *Polymer, 44*, 5711-5720.

Hu, Y., Hu, Y. S., Topolkaraev, V., Hiltner, A., Baer, E. (2003b). Crystallization and phase separation in blends of high stereoregular poly(lactide) with poly(ethylene glycol). *Polymer, 44*, 5681-5689.

Hu, Y. S., Hiltner, A., Baer, E. (2005). Improving oxygen barrier properties of poly(ethylene terephthalate) by incorporating isophthalate. II. Effect of crystallization. *Journal of Applied Polymer Science, 98*(4), 1629-1642.

Huang, J., Lisowski, M. S., Runt, J., Hall, E. S., Kean, R. T., Buehler, N., et al. (1998). Crystallization and Microstructure of Poly(l-lactide-co-meso-lactide) Copolymers. *Macromolecules, 31*(8), 2593-2599.

Huang, J.-W., Hung, Y. C., Wen, Y.-L., Kang, C.-C., Yeh, M.-Y. (2009). Polylactide/Nano- and Micro-Scale Silica Composite Films. II. Melting Behavior and Cold Crystallization. *Journal of Applied Polymer Science, 112*, 3149-3156.

Hutchinson, J.M. (2003). Studying the glass transition by DSC and TMDSC. *Journal of thermal analysis and calorimetry*, *72*(2), 619-629.

Hutchinson, J.M. (2009). Determination of the glass transition temperature. Methods correlation and structural heterogeneity. *Journal of thermal analysis and calorimetry*, 98(3), 579-589.

Hyon, S.-H., Jamshidi, K., Ikada, Y. (1997). Synthesis of polylactides with different molecular weights. *Biomaterials, 18*(22), 1503-1508.

Hyon, S. H., Jamshidi, K., Ikada, Y. (1998). Effects of residual monomer on the degradation of DL-lactide polymer. *Polymer International, 46*(3), 196-202.

Ikada, Y., Tsuji, H. (2000). Biodegradable polyesters for medical and ecological applications. *Macromolecular Rapid Communications, 21*(3), 117-132.

Iwata, T., Doi, Y. (1998). Morphology and Enzymatic Degradation of Poly(l-lactic acid) Single Crystals. *Macromolecules, 31*(8), 2461-2467.

Jacobsen, S., Fritz, H. G. (1999). Plasticizing Polylactide-The Effect of Different Plasticizers on the Mechanical Properties. *Polymer Engineering and Science, 39*(7), 1303-1310.

Jacobsen, S., Fritz, H. G., Degée, P., Dubois, P., Jérôme, R. (2000). Single-step reactive extrusion of PLLA in a corotating twin-screw extruder promoted by 2-ethylhexanoic acid tin(II) salt and triphenylphosphine. *Polymer, 41*(9), 3395-3403.

Jamshidi, K., Hyon, S. H., Ikada, Y. (1988). Thermal Characterization of Polylactides. *Polymer, 29*(12), 2229-2234.

Jamshidian, M., Tehrany, E. A., Imran, M., Jacquot, M., Desobry, S. (2010) Poly-Lactic Acid: Production, Applications, Nanocomposites, and Release Studies. *Comprehensive Reviews in Food Science and Food Safety, 9*(5), 552-571.

Jang, J., Lee, D. K. (2004). Oxygen barrier properties of biaxially oriented polypropylene/polyvinyl alcohol blend films. *Polymer, 45*(5), 1599-1607.

Jeziorny, A. (1978). Parameters characterizing the kinetics of the non-isothermal crystallization of poly(ethylene terephthalate) determined by d.s.c. *Polymer, 19*(10), 1142-1144.

Jia, Z., Tan, J., Han, C., Yang, Y., Dong, L. (2009). Poly(ethylene glycol-co-propylene glycol) as a Macromolecular Plasticizing Agent for Polylactide: Thermomechanical Properties and Aging. *Journal of Applied Polymer Science, 114*, 1105-1117.

Joly, C., Goizet, S., Schrotter, J. C., Sanchez, J., Escoubes, M. (1997). Sol-gel polyimide-silica composite membrane: gas transport properties. *Journal of Membrane Science, 130*(1-2), 63-74.

Kalb, B., Pennings, A. J. (1980). General crystallization behaviour of poly(l-lactic acid). *Polymer, 21*(6), 607-612.

Kale, G., Auras, R., Singh, S. P., Narayan, R. (2007a). Biodegradability of polylactide bottles in real and simulated composting conditions. *Polymer Testing, 26*(8), 1049-1061.

Kale, G., Kijchavengkul, T., Auras, R., Rubino, M., Selke, S. E., Singh, S. P. (2007b). Compostability of bioplastic packaging materials: An overview. *Macromolecular Bioscience, 7*(3), 255-277.

Kanehashi, S., Nagai, K. (2005). Analysis of dual-mode model parameters for gas sorption in glassy polymers. *Journal of Membrane Science, 253*(1-2), 117-138.

Kanehashi, S., Kusakabe, A., Sato, S., Nagai, K. (2010). Analysis of permeability; solubility and diffusivity of carbon dioxide; oxygen; and nitrogen in crystalline and liquid crystalline polymers. *Journal of Membrane Science, 365*(1-2), 40-51.

Karaiskakis, G., Gavril, D. (2004). Determination of diffusion coefficients by gas chromatography. *Journal of Chromatography A, 1037*(1-2), 147-189.

Kashima, T., Kameoka, T., Higouchi, C., Ajioka, M., Yamagouchi, A. (1995). Aliphatic polyester and preparation process thereof Mitsui Toatsu Chemicals, Inc. (Tokyo, JP).

Kattan, M., Dargent, E., Grenet, J. (2002). Three phase model in drawn thermoplastic polyesters: comparison of differential scanning calorimetry and thermally stimulated depolarisation current experiments. *Polymer, 43*(4), 1399-1405.

Kawai, T., Rahman, N., Matsuba, G., Nishida, K., Kanaya, T., Nakano, M., et al. (2007). Crystallization and Melting Behavior of Poly (l-lactic Acid). *Macromolecules, 40*(26), 9463-9469.

Kawamoto, N., Sakai, A., Horikoshi, T., Urushihara, T., Tobita, E. (2007). Nucleating agent for poly(L-lactic acid) - An optimization of chemical structure of hydrazide compound for advanced nucleation ability. *Journal of Applied Polymer Science, 103*(1), 198-203.

Ke, T., Sun, X. (2003). Melting Behavior and Crystallization Kinetics of Starch and Poly(lactic acid) composites. *Journal of Applied Polymer Science, 89*, 1203-1210.

Kint, D. P. R., Martínez de Ilarduya, A., Sansalvadó, A., Ferrer, J., Muñoz-Guerra, S. (2003). Microstructure and crystallization of melt-mixed poly(ethylene terephthalate)/poly(ethylene isophthalate) blends. *Journal of Applied Polymer Science, 90*(11), 3076-3086.

Kissinger, H. E. (1956). Variation of Peak Temperature with Heating Rate in Differential Thermal Analysis. *Journal of research of the National Bureau of Standards, 57*(4), 217-221.

Klopffer, M. H., Flaconnèche, B. (2001). Transport properties of gases in polymers: Bibliographic review. *Oil and Gas Science and Technology-Review IFP, 56*(3), 223-244.

Kobayashi, J., Asahi, T., Ichiki, M., Oikawa, A., Suzuki, H., Watanabe, T., et al. (1995). Structural and optical properties of poly-lactic acids. *Journal of applied physics, 77*, 2957-2973.

Kobayashi, S., Makino, A. (2009). Enzymatic Polymer Synthesis: An Opportunity for Green Polymer Chemistry. *Chemical Reviews, 109*(11), 5288-5353.

Kolstad, J. J. (1996). Crystallization kinetics of poly(L-lactide-co-meso-lactide). *Journal of Applied Polymer Science, 62*, 1079-1091.

Komatsuka, T., Kusakabe, A., Nagai, K. (2008). Characterization and gas transport properties of poly(lactic acid) blend membranes. *Desalination: Part 2, The Fourth Conference of Aseanian Membrane Society, 234*(1-3), 212-220.

Kopinke, F. D., Remmler, M., Mackenzie, K., Moder, M., Wachsen, O. (1996). Thermal decomposition of biodegradable polyesters .2. Poly(lactic acid). *Polymer Degradation and Stability, 53*(3), 329-342.

Kovarski, A. L. (1997). Molecular Dynamics of Aditives in Polymers. In A. L. Kovarski (Ed.), *New concepts in polymer science* (1st ed., Vol. 1, pp. 53-83). Utrecht, The Netherlands: VSP

Kowalski, A., Duda, A., Penczek, S. (2000). Kinetics and Mechanism of Cyclic Esters Polymerization Initiated with Tin(II) Octoate. 3. Polymerization of l,l-Dilactide. *Macromolecules, 33*(20), 7359-7370.

Kricheldorf, H. R., Kreiser-Saunders, I., Boettcher, C. (1995). Polylactones: 31. Sn(II)octoate-initiated polymerization of L-lactide: a mechanistic study. *Polymer, 36*(6), 1253-1259.

Kulinski, Z., Piorkowska, E. (2005). Crystallization, structure and properties of plasticized poly(L-lactide). *Polymer, 46*, 10290-10300.

Kulinski, Z., Piorkowska, E., Gadzinowska, K., Stasiak, M. (2006). Plasticization of Poly(l-lactide) with Poly(propylene glycol). *Biomacromolecules, 7*(7), 2128-2135.

Kulkarni, S. S., Stern, S. A. (1983). The diffusion of CO2, CH4, C2H4, and C3H8 in polyethylene at elevated pressures. *Journal of Polymer Science: Polymer Physics Edition, 21*(3), 441-465.

Kumari, A., Yadav, S. K., Yadav, S. C. (2010) Biodegradable polymeric nanoparticles based drug delivery systems. *Colloids and Surfaces B-Biointerfaces, 75*(1), 1-18.

Kwan, K. S., Subramaniam, C. N. P., Ward, T. C. (2003a). Effect of penetrant size and shape on its transport through a thermoset adhesive: I. n-alkanes. *Polymer, 44*(10), 3061-3069.

Kwan, K. S., Subramaniam, C. N. P., Ward, T. C. (2003b). Effect of penetrant size, shape, and chemical nature on its transport through a thermoset adhesive. II. Esters. *Polymer, 44*(10), 3071-3083.

Labrecque, L. V., R.A.Kumar, V.Davé, Gross, R. A., McCarthy, S. P. (1997). Citrate Esters as Plasticizers for Poly(lactic acid). *Journal of Applied Polymer Science, 66*, 1507-1513.

Lai, W.-C., Liau, W.-B., Lin, T.-T. (2004). The effect of end groups of PEG on the crystallization behaviors of binary crystalline polymer blends PEG/PLLA. *Polymer, 45*, 3073-3080.

Laohakunjit, N., Noomhorm, A. (2004). Effect of plasticizers on mechanical and barrier properties of rice starch film. *Starch/Stärke, 56*, 348-356.

Lebosse, R., Ducruet, V., Feigenbaum, A. (1997). Interactions between Reactive Aroma Compounds from Model Citrus Juice with Polypropylene Packaging Film. *Journal of Agricultural and Food Chemistry, 45*(8), 2836-2842.

Lehermeier, H. J., Dorgan, J. R., Way, J. D. (2001). Gas permeation properties of poly(lactic acid). *Journal of Membrane Science, 190*, 243-251.

Lezervant, J. (2007). *Activation des phénomènes de migration dans les emballages: Application à la sécurité alimentaire des aliments emballés.* Université de Reims Champagne-Ardennes, Reims.

Li, S. M., Garreau, H., Vert, M. (1990). Structure-Property Relationships in the Case of the Degradation of Massive Poly(Alpha-Hydroxy Acids) in Aqueous-Media .3. Influence of the Morphology of Poly(L-Lactic Acid). *Journal of Materials Science-Materials in Medicine, 1*(4), 198-206.

Li, H., Huneault, M. A. (2007). Effect of nucleation and plasticization on the crystallization of poly(lactic acid). *Polymer, 48*, 6855-6866.

Li, M., Hu, D., Wang, Y., Shen, C. (2010a). Nonisothermal crystallization kinetics of poly(lactic acid) formulations comprising talc with poly(ethylene glycol). *Polymer Engineering & Science, 50*(12), 2298-2305.

Li, Y., Wu, H., Wang, Y., Liu, L., Han, L., Wu, J., et al. (2010b). Synergistic effects of PEG and MWCNTs on crystallization behavior of PLLA. *Journal of Polymer Science Part B: Polymer Physics, 48*(5), 520-528.

Liao, R., Yang, B., Yu, W., Zhou, C. (2007). Isothermal Cold Crystallization Kinetics of Polylactide/Nucleating Agents. *Journal of Applied Polymer Science, 104*, 310-317.

Lim, L. T., Auras, R., Rubino, M. (2008). Processing technologies for poly(lactic acid). *Progress in Polymer Science, 33*(8), 820-852.

Limm, W., Begley, T. H., Lickly, T., Hentges, S. G. (2006). Diffusion of limonene in polyethylene. *Food Additives and Contaminants: Part A, 23*(7), 738-746.

Lin, J., Shenogin, S., Nazarenko, S. (2002). Oxygen solubility and specific volume of rigid amorphous fraction in semicrystalline poly(ethylene terephthalate). *Polymer, 43*(17), 4733-4743.

Ling, X., Spruiell, J. E. (2006a). Analysis of the complex thermal behavior of poly(L-lactid acid) film.II. Samples crystallized from the melt. *Journal of Polymer Science : Part B : Polymer Physics, 44*, 3378-3391.

Ling, X. Y., Spruiell, J. E. (2006b). Analysis of the complex thermal behavior of poly(L-lactic acid) film. I. Samples crystallized from the glassy state. *Journal of Polymer Science Part B-Polymer Physics, 44*(22), 3200-3214.

Liu, T., Mo, Z., Wang, S., Zhang, H. (1997). Nonisothermal melt and cold crystallization kinetics of poly(aryl ether ether ketone ketone). *Polymer Engineering & Science, 37*(3), 568-575.

Liu, S., Yu, Y., Cui, Y., Zhang, H., Mo, Z. (1998). Isothermal and nonisothermal crystallization kinetics of nylon-11. *Journal of Applied Polymer Science, 70*(12), 2371-2380.

Liu, R. Y. F., Schiraldi, D. A., Hiltner, A., Baer, E. (2002). Oxygen-barrier properties of cold-drawn polyesters. *Journal of polymer science: Part B: Polymer Physics, 40*, 862-877.

Liu, R. Y. F., Hu, Y. S., Schiraldi, D. A., Hiltner, A., Baer, E. (2004). Crystallinity and oxygen transport properties of PET bottle walls. *Journal of Applied Polymer Science, 94*(2), 671-677.

Liu, L. S., Finkenstadt, V. L., Liu, C. K., Jin, T., Fishman, M. L., Hicks, K. B. (2007). Preparation of poly(lactic acid) and pectin composite films intended for applications in antimicrobial packaging. *Journal of Applied Polymer Science, 106*(2), 801-810.

Liu, Y., Wang, L., He, Y., Fan, Z., Li, S. (2010). Non-isothermal crystallization kinetics of poly(L-lactide). *Polymer International, 59*(12), 1616-1621.

Ljungberg, N., Wesslén, B. (2002). The effects of plasticizers on the dynamic mechanical and thermal properties of poly(lactic acid). *Journal of Applied Polymer Science, 86*(5), 1227-1234.

Ljungberg, N., Andersson, T., Wesslén, B. (2003a). Film extrusion and film weldability of poly(lactic acid) plasticized with triacetine and tributyl citrate. *Journal of Applied Polymer Science, 88*, 3239-3247.

Ljungberg, N., Wesslen, B. (2003b). Tributyl citrate oligomers as plasticizers for poly(lactic acid) : thermo-mechanical film properties and aging. *Polymer, 44*, 7679-7688.

Ljungberg, N., Wesslen, B. (2004). Thermomechanical Film Properties and Aging of Blends of Poly(lactic acid) and Malonate Oligomers. *Journal of Applied Polymer Science, 94*, 2140-2149.

Ljungberg, N., Wesslen, B. (2005). Preparation and properties of plasticized poly(lactic acid) films. *Biomacromolecules, 6*, 1789-1796.

Long, Y., Shanks, R. A., Stachurski, Z. H. (1995). Kinetics of polymer crystallisation. *Progress in Polymer Science, 20*(4), 651-701.

Lopez Rubio, A., Hernandez Munoz, P., Catala, R., Gavara, R., Lagaron, J. (2005). Improving packaged food quality and safety. Part 1: Synchrotron X-ray analysis. *Food Additives and Contaminants, 22*(10), 988–993.

Lowe, C. (1954). In U. Patent (Ed.): DuPont.

Lu, X. F., Hay, J. N. (2001). Crystallization orientation and relaxation in uniaxially drawn poly(ethylene terephthalate). *Polymer, 42*(19), 8055-8067.

Lunt, J. (1998). Large-scale production, properties and commercial applications of polylactic acid polymers. *Polymer Degradation and Stability, 59*, 145-152.

Lyu, S. P., Schley, J., Loy, B., Lind, D., Hobot, C., Sparer, R., et al. (2007). Kinetics and time-temperature equivalence of polymer degradation. *Biomacromolecules, 8*(7), 2301-2310.

MacDonald, R. T., McCarthy, S. P., Gross, R. A. (1996). Enzymatic Degradability of Poly(lactide): Effects of Chain Stereochemistry and Material Crystallinity. *Macromolecules, 29*(23), 7356-7361.

Malkin, A. Y., Beghishev, V. P., Keapin, I. A., Bolgov, S. A. (1984). General treatment of polymer crystallization kinetics—Part 1. A new macrokinetic equation and its experimental verification. *Polymer Engineering & Science, 24*(18), 1396-1401.

Mano, J. F., Gómez Ribelles, J. L., Alves, N. M., Salmerón Sanchez, M. (2005). Glass transition dynamics and structural relaxation of PLLA studied by DSC: Influence of crystallinity. *Polymer, 46*(19), 8258-8265.

Martin, O., Averous, L. (2001). Poly(lactic acid): plasticization and properties of biodegradable multiphase systems. *Polymer, 42*(14), 6209-6219.

Martin, P. J., Tan, C. W., Tshai, K. Y., McCool, R., Menary, G. H., Armstrong, C. G., et al. (2005). Biaxial characterisation of materials for thermoforming and blow moulding. *Plastics, Rubber and Composites, 34*(5-6), 276-282.

Martino, V. P., Ruseckaite, R. A., Jiménez, A. (2006). Thermal and Mechanical Characterization of Plasticized poly(L-lactide-co-D,L-lactide) Films for Food Packaging. *Journal of Thermal Analysis and Calorimetry, 86*(3), 707-712.

Martino, V. P., Jiménez, A., Ruseckaite, R. A. (2009). Processing and Characterization of poly(lactic acid) Films Plasticized with Commercial Adipates. *Journal of Applied Polymer Science, 112*, 2010-2018.

Martino, V. P., Ruseckaite, R. A., Jiménez, A., Averous, L. (2010). Correlation between Composition, Structure and Properties of Poly(lactic acid)/Polyadipate-Based Nano-Biocomposites. *Macromolecular Materials and Engineering, 295*(6), 551-558.

Marubayashi, H., Akaishi, S., Akasaka, S., Asai, S., Sumita, M. (2008). Crystalline structure and morphology of poly(L-lactide) formed under high-pressure CO. *Macromolecules, 41*(23), 9192-9203.

Masaro, L., Zhu, X. X. (1999a). Physical models of diffusion for polymer solutions, gels and solids. *Progress in Polymer Science, 24*(5), 731-775.

Masaro, L., Zhu, X. X. (1999b). Self-Diffusion of End-Capped Oligo(ethylene glycol)s in Poly(vinyl alcohol) Aqueous Solutions and Gels. *Macromolecules, 32*(16), 5383-5390.

Mascheroni, E., Guillard, V., Nalin, F., Mora, L., Piergiovanni, L. (2010). Diffusivity of propolis compounds in Polylactic acid polymer for the development of anti-microbial packaging films. *Journal of Food Engineering, 98*(3), 294-301.

Masirek, R., Piorkowska, E., Galeski, A., Mucha, M. (2007). Influence of Thermal History on the Nonisothermal Crystallization of Poly(L-lactide). *Journal of Applied Polymer Science, 105*, 282-290.

Mathew, A. P., Oksman, K., Sain, M. (2006). The effect of morphology and chemical characteristics of cellulose reinforcements on the crystallinity of polylactic acid. *Journal of Applied Polymer Science, 101*(1), 300-310.

Matsukawa, S., Ando, I. (1997). Study of Self-Diffusion of Molecules in a Polymer Gel by Pulsed-Gradient Spin-Echo 1H NMR. 2. Intermolecular Hydrogen-Bond Interaction between the Probe Polymer and Network Polymer in N,N-Dimethylacrylamideâˆ'Acrylic Acid Copolymer Gel Systems. *Macromolecules, 30*(26), 8310-8313.

Matsumura, S., Mabuchi, K., Toshima, K. (1997). Lipase-catalyzed ring-opening polymerization of lactide. *Macromolecular Rapid Communications, 18*(6), 477-482.

Matteucci, S., Yampolskii, Y., Freeman, B. D., Pinnau, I. (2006). Membranes for gas and vapor separation. In Y. Yampolskii, I. Pinnau & B. D. Freeman (Eds.), *Materials science of membranes for gas and vapor separation* (pp. 1-47). Chichester: John Wiley and Sons Ltd, The Atrium.

Mauricio-Iglesias, M., Peyron, S., Chalier, P., Gontard, N. (2011). Scalping of four aroma compounds by one common (LDPE) and one biosourced (PLA) packaging materials during high pressure treatments. *Journal of Food Engineering, 10*, 9-15.

McGonigle, E.-A., Liggat, J. J., Pethrick, R. A., Jenkins, S. D., Daly, J. H., Hayward, D. (2001). Permeability of N2, Ar, He, O2 and CO2 through biaxially oriented polyester films -- dependence on free volume. *Polymer, 42*(6), 2413-2426.

McNeill, I. C., Leiper, H. A. (1985). Degradation Studies of Some Polyesters and Polycarbonates .2. Polylactide - Degradation under Isothermal Conditions, Thermal-Degradation Mechanism and Photolysis of the Polymer. *Polymer Degradation and Stability, 11*(4), 309-326.

Mensitieri, G., Di Maio, E., Buonocore, G., Nedi, I., Oliviero, M., Sansone, L., et al. (2010). Processing and shelf life issues of selected food packaging materials and structures from renewable resources. *Trends in Food Science & Technology*.

Michaels, A. S., Parker, R. B. (1959). Sorption and flow of gases in polyethylene. *Journal of Polymer Science, 41*(138), 53-71.

Michaels, A. S., Bixler, H. J. (1961). *Journal of Polymer Science, 50*, 393-412.

Mihai, M., HuneaultM.A., Favis B. D., Li H. (2007). Extrusion foaming of semi-crystalline PLA and PLA/Thermoplastic starch blends. *Macromolecular Bioscience*, *7*(7), 907-920.

Miyata, T., Masuko, T. (1997). Morphology of poly(-lactide) solution-grown crystals. *Polymer, 38*(16), 4003-4009.

Miyata, T., Masuko, T. (1998). Crystallization behaviour of poly(L-lactide). *Polymer, 39*(22), 5515-5521.

Modesti, M., Dall'Acqua, C., Lorenzetti, A., Florian, E. (2004). Mathematical model and experimental validation of water cluster influence upon vapour permeation through hydrophilic dense membrane. *Journal of Membrane Science, 229*(1-2), 211-223.

Moisan, J. Y. (1980). Diffusion des additifs du polyethylene--I: Influence de la nature du diffusant. *European Polymer Journal, 16*(10), 979-987.

Moore, C. J. (2008). Synthetic polymers in the marine environment: A rapidly increasing, long-term threat. *Environmental Research, 108*(2), 131-139.

Mulder, M. (1996). Transport in membranes. In *Basic principles of membrane technology* (2nd ed., pp. 210-279). Dordrecht: Kluwer Academic publishers.

Mullin, J. W. (2001). Nucleation. In b. Heinemann (Ed.), *Crystallization* (Fourth ed., pp. 181-215). Oxford: Reed Educational and Professional Publishing Ltd.

Murariu, M., Ferreira, A. D. S., Alexandre, M., Dubois, P. (2008). Polylactide (PLA) designed with desired end-use properties: 1.PLA compositions with low molecular weight ester-like plasticizers and related performances. *Polymers for Advanced Technology, 19*, 636-646.

Nadakatti, S. M., Kim, J. H., Stern, S. A. (1995). Solubility of light gases in poly(n-butyl methacrylate) at elevated pressures. *Journal of Membrane Science, 108*(3), 279-291.

Naga, N., Yoshida, Y., Inui, M., Noguchi, K., Murase, S. (2011). Crystallization of amorphous poly(lactic acid) induced by organic solvents. *Journal of Applied Polymer Science, 119*(4), 2058-2064.

Naito, Y., Kamiya, Y., Terada, K., Mizoguchi, K., Wang, J.-S. (1996). Pressure dependence of gas permeability in a rubbery polymer. *Journal of Applied Polymer Science, 61*(6), 945-950.

Nam, J. Y., Sinha Ray, S., Okamoto, M. (2003). Crystallization Behavior and Morphology of Biodegradable Polylactide/Layered Silicate Nanocomposite. *Macromolecules, 36*(19), 7126-7131.

Nam, J. Y., Okamoto, M., Okamoto, H., Nakano, M., Usuki, A., Matsuda, M. (2006). Morphology and crystallization kinetics in a mixture of low-molecular weight aliphatic amide and polylactide. *Polymer, 47*, 1340-1347.

Nampoothiri, K. M., Nair, N. R., John, R. P. (2010). An overview of the recent developments in polylactide (PLA) research. *Bioresource Technology, 101*(22), 8493-8501.

Natu, A., Lofgren, E., Jabarin, S. (2005). Effect of morphology on barrier properties of poly(ethylene terephthalate). *Polymer Engineering & Science, 45*(3), 400-409.

NatureWorks. (2011). NatureWorks® PLA Processing Guide for Biaxially Oriented Film. Retrieved 15/01/2011, 2011

Nielsen, L. E., Landel, R. F. (1994a). Stress strain behavior and strength. In F. LL (Ed.), *Mechanical properties of polymers and compositesa* (pp. 265-267). New York: Marcel Decker Inc.

Nielsen, T. J., Giacin, J. R. (1994b). The sorption of limonene/ethyl acetate binary vapour mixtures by a biaxially oriented polypropylene film. *Packaging Technology and Science, 7*(5), 247-258.

Noda, I., Satkowski, M. M., Dowrey, A. E., Marcott, C. (2004). Polymer alloys of Nodax copolymers and poly(lactic acid). *Macromolecular Bioscience, 4*(3), 269-275.

Ohkita, T., Lee, S. H. (2006). Thermal degradation and biodegradability of poly (lactic acid)/corn starch biocomposites. *Journal of Applied Polymer Science, 100*(4), 3009-3017.

Ohtani, Y., Okumura, K., Kawaguchi, A. (2003). Crystallization Behavior of Amorphous Poly(L-Lactide). *Journal of Macromolecular Science, Part B: Physics, 42*(3), 875 - 888.

Okano, K., Tanaka, T., Ogino, C., Fukuda, H., Kondo, A. (2010). Biotechnological production of enantiomeric pure lactic acid from renewable resources: recent achievements, perspectives, and limits. *Applied Microbiology and Biotechnology, 85*(3), 413-423.

Oksman, K., Skrifvars, M., Selin, J. F. (2003). Natural fibres as reinforcement in polylactic acid (PLA) composites. *Composites Science and Technology, 63*(9), 1317-1324.

Oliveira, N. S., Gonçalves, C. M., Coutinho, J. A. P., Ferreira, A., Dorgan, J., Marrucho, I. M. (2006). Carbon dioxide, ethylene and water vapor sorption in poly(lactic acid). *Fluid Phase Equilibria, 250*(1-2), 116-124.

Oliveira, N. S., Dorgan, J., Coutinho, J. A. P., Ferreira, A., Daridon, J. L., Marrucho, I. M. (2007). Gas solubility of carbon dioxide in poly(lactic acid) at high pressures: Thermal treatment effect. *Journal of Polymer Science Part B: Polymer Physics, 45*(5), 616-625.

Omnexus. (2010). Retrieved december 2010, 2010, from http://www.omnexus.com/tc/biopolymers/article_survey_195.aspx

Ou, X., Cakmak, M. (2008). Influence of biaxial stretching mode on the crystalline texture in polylatic acid films. *Polymer, 49*, 5344-5352.

Ouyang, H., Shore, S.-H. (1999a). Ethyl-Acetate transport in poly(ethylene terephthalate). *Journal of Applied Physics, 85*(2), 1148-1152.

Ouyang, H., Shore, S.-H. (1999b). The mass transport in poly(ethylene terephthalate) and related induced-crystallization. *Polymer, 40*(19), 5401-5406.

Ouyang, H., Lee, W.-H., Shih, M.-C. (2002). Three Stages of Crystallization in Poly(ethylene terephthalate) during Mass Transport. *Macromolecules, 35*(22), 8428-8432.

Ouyang, H., Lee, W.-H., Ouyang, W., Shiue, S.-T., Wu, T.-M. (2004). Solvent-Induced Crystallization in Poly(ethylene terephthalate) during Mass Transport:â€‰ Mechanism and Boundary Condition. *Macromolecules, 37*(20), 7719-7723.

Ozawa, T. (1971). Kinetics of non-isothermal crystallization. *Polymer, 12*(3), 150-158.

Pace, R. J., Datyner, A. (1979). Statistical mechanical model for diffusion of simple penetrants in polymers. I. Theory. *Journal of Polymer Science: Polymer Physics Edition, 17*(3), 437-451.

Pal, P., Sikder, J., Roy, S., Giorno, L. (2009). Process intensification in lactic acid production: A review of membrane based processes. *Chemical Engineering and Processing, 48*(11-12), 1549-1559.

Pan, P., Kai, W., Zhu, B., Dong, T., Inoue, Y. (2007). Polymorphous Crystallization and Multiple Melting Behavior of Poly(l-lactide):â€‰ Molecular Weight Dependence. *Macromolecules, 40*(19), 6898-6905.

Pan, P., Zhu, B., Kai, W., Dong, T., Inoue, Y. (2008a). Effect of crystallization temperature on crystal modifications and crystallization kinetics of poly(L-lactide). *Journal of Applied Polymer Science, 107*(1), 54-62.

Pan, P., Zhu, B., Kai, W., Dong, T., Inoue, Y. (2008b). Polymorphic Transition in Disordered Poly(L-lactide) Crystals Induced by Annealing at Elevated Temperatures. *Macromolecules, 41*(12), 4296-4304.

Pan, P., Inoue, Y. (2009). Polymorphism and isomorphism in biodegradable polyesters. *Progress in Polymer Science, 34*(7), 605-640.

Pandey, P., Chauhan, R. S. (2001). Membranes for gas separation. *Progress in Polymer Science, 26*(6), 853-893.

Pandey, J. K., Ahn, S. H., Lee, C. S., Mohanty, A. K., Misra, M. (2010) Recent Advances in the Application of Natural Fiber Based Composites. *Macromolecular Materials and Engineering, 295*(11), 975-989.

Pantani, R., De Santis, F., Sorrentino, A., De Maio, F., Titomanlio, G. (2010). Crystallization kinetics of virgin and processed poly(lactic acid). *Polymer Degradation and Stability, 95*(7), 1148-1159.

Park, H. B., Lee, Y. M. (2008). Polymeric membrane materials and potential use in gas separation. In N. N. Li, A. G. Fane, W. S. W. Ho & T. Matsuura (Eds.), *Advanced*

Membrane Technology and Applications (pp. 633-670). New Jersey: John Wiley and Sons, Inc. Hoboken.

Patzlaff, M., Wittebrock, A., Reichert, K. H. (2006). Sorption studies of propylene in polypropylene. Diffusivity in polymer particles formed by different polymerization processes. *Journal of Applied Polymer Science, 100*(4), 2642-2648.

Pauly, S. (1999). Permeability and diffusion data. In J. Brandrup, E. H. Immergut & E. A. Grulke (Eds.), *Polymer Handbook* (Vol. 2, pp. 543-569). New York: John Wiley & Sons, Inc.

Penczek, S., Duda, A., Szymanski, R., Biela, T. (2000). What we have learned in general from cyclic esters polymerization. *Macromolecular Symposia, 153*(1), 1-15.

Peniston, S. J., Choi, S. J. (2007). Effect of sterilization on the physicochemical properties of molded poly(L-lactic acid). *Journal of Biomedical Materials Research Part B: Applied Biomaterials, 80B*(1), 67-77.

Peppas, N. A., Lustig, S. R. (1987). *Hydrogels in medicine and pharmacy* (CRC Press ed. Vol. 1): Boca Raton.

Perego, G., Cella, G. D., Bastioli, C. (1996). Effect of Molecular Weight and Crystallinity on Poly(lactic acid) Mechanical Properties. *Journal of Applied Polymer Science, 59*(37-43).

Persin, Z., Stana-Kleinschek, K., Foster, T., van Dam, J. E. G., Boeriu, C. G., Navard P. (2011). Challenges and opportunities in polysaccharides research and technology: The EPNOE views for the next decade in the areas of Materials-; Food- and Health Care. *Carbohydrate polymers*.

Petersen, K., Vaeggemose Nielsen, P., Bertelsen, G., Lawther, M., Olsen, M., Nilsson, N., et al. (1999). Potential of biobased materials for food packaging. *Trends in Food Science & Technology, 10*, 52-68.

Petersen, K., Nielsen, P. V., Olsen, M. B. (2001). Physical and mechanical properties of biobased materials - Starch, Polylactate and polyhydroxybutyrate. *Starch/Stärke, 53*, 356-361.

Phuong, N. T., Villoutreix, G. (2010). Non-isothermal crystallization kinetics of short bamboo fibers reinforced recycled polypropylene composites. *Journal of reinforced plastics and composites, 19*(17), 2576-2591.

Pillin, I., Montrelay, N., Grohens, Y. (2006). Thermo-mechanical characterization of plasticized PLA : Is the miscibility the only significant factor ? *Polymer, 47*(13), 4676-4682.

Pillin, I., Montrelay, N., Bourmaud, A., Grohens, Y., (2008) Effect of thermo-mechanical cycles on the physico-chemical properties of poly(lactic acid). *Polymer Degradation and Stability*, *93*(2), 321-328.

Pino, M., Duckett, R. A., Ward, I. M. (2005). Single and mixed gas diffusion through polyethylene films. *Polymer, 46*(13), 4882-4890.

Piorkowska, E., Kulinski, Z., Galeski, A., Masirek, R. (2006). Plasticization of semi-cristalline poly(L-lactide) with poly(propylene glycol). *Polymer, 47*, 7178-7188.

Pitt, C. G., Gratzl, M. M., Kimmel, G. L., Surles, J., Schindler, A. (1981). Aliphatic Polyesters .2. the Degradation of Poly(Dl-Lactide), Poly(Epsilon-Caprolactone), and Their Copolymers Invivo. *Biomaterials, 2*(4), 215-220.

Plastic Europe. (2009). *The Compelling Facts about Plastics - An analysis of European plastics production, demand and recovery for 2008*. Brussels: (Association of Plastics Manufacturers).

Pluta, M., Galeski, A. (2002). Crystalline and Supermolecular Structure of Polylactide in Relation to the Crystallization Method. *Journal of Applied Polymer Science, 86*, 1386-1395.

Pluta, M. (2004). Morphology and properties of polylactide modified by thermal treatment, filling with layered silicates and plasticization. *Polymer, 45*, 8239-8251.

Pluta, M., Jeszka, J. K., Boiteux, G. (2007). Polylactide/montmorillonite nanocomposites: Structure, dielectric, viscoelastic and thermal properties. *European Polymer Journal, 43*(7), 2819-2835.

Polyakova, A., Liu, R. Y. F., Schiraldi, D. A., Hiltner, A., Baer, E. (2001). Oxygen-barrier properties of copolymers based on ethylene terephthalate. *Journal of Polymer Science Part B: Polymer Physics, 39*(16), 1889-1899.

Pradhan, R., Misra, M., Erickson, L., Mohanty, A. (2010). Compostability and biodegradation study of PLA-wheat straw and PLA-soy straw based green composites in simulated composting bioreactor. *Bioresource Technology, 101*(21), 8489-8491.

Puiggali, J., Ikada, Y., Tsuji, H., Cartier, L., Okihara, T., Lotz, B. (2000). The frustrated structure of poly(-lactide). *Polymer, 41*(25), 8921-8930.

Puppi, D., Chiellini, F., Piras, A. M., Chiellini, E. (2010). Polymeric materials for bone and cartilage repair. *Progress in Polymer Science, 35*(4), 403-440.

Purac. (2010). december 2010, from http://www.purac.com

Pyda, M., Bopp, R. C., Wunderlich, B. (2004a). Heat capacity of poly(lactic acid). *The Journal of Chemical Thermodynamics, 36*(9), 731-742.

Pyda, M., Bopp, R. C., Wunderlich, B. (2004b). Heat capacity of poly(lactic acid). *Journal of Chemical Thermodynamics, 36*(9), 731-742.

Pyda, M., Wunderlich, B. (2005). Reversing and Nonreversing Heat Capacity of Poly(lactic acid) in the Glass Transition Region by TMDSC. *Macromolecules, 38*(25), 10472-10479.

Qin, Y., Rubino, M., Auras, R., Lim, L. T. (2007). Use of a magnetic suspension microbalance to measure organic vapor sorption for evaluating the impact of polymer converting process. *Polymer Testing, 26*(8), 1082-1089.

Qureshi, N., Stepanov, E. V., Schiraldi, D., Hiltner, A., Baer, E. (2000). Oxygen-barrier properties of oriented and heat-set poly(ethylene terephthalate). *Journal of Polymer Science Part B: Polymer Physics, 38*(13), 1679-1686.

Raquez, J. M., Narayan, R., Dubois, P. (2008). Recent advances in reactive extrusion processing of biodegradable polymer-based compositions. *Macromolecular Materials and Engineering, 293*(6), 447-470.

Raucher, D., Sefcik Michael, D. (1983a). Gas Transport and Cooperative Main-Chain Motions in Glassy Polymers. In *Industrial Gas Separations* (Vol. 223, pp. 89-110): AMERICAN CHEMICAL SOCIETY.

Raucher, D., Sefcik Michael, D. (1983b). Sorption and Transport in Glassy Polymers. In *Industrial Gas Separations* (Vol. 223, pp. 111-124): AMERICAN CHEMICAL SOCIETY.

Ray, S. S., Okamoto, M. (2003a). Biodegradable polylactide and its nanocomposites: Opening a new dimension for plastics and composites. *Macromolecular Rapid Communications, 24*(14), 815-840.

Ray, S. S., Yamada, K., Okamoto, M., Ogami, A., Ueda, K. (2003b). New polylactide/layered silicate nanocomposites. 3. High-performance biodegradable materials. *Chemistry of Materials, 15*(7), 1456-1465.

Ray, S. S., Yamada, K., Okamoto, M., Ueda, K. (2003c). New polylactide-layered silicate nanocomposites. 2. Concurrent improvements of material properties, biodegradability and melt rheology. *Polymer, 44*(3), 857-866.

Reynier, A., Dole, P., Feigenbaum, A. (2001a). Additive diffusion coefficients in polyolefins. II. Effect of swelling and temperature on the D = f(M) correlation. *Journal of Applied Polymer Science, 82*(10), 2434-2443.

Reynier, A., Dole, P., Humbel, S., Feigenbaum, A. (2001b). Diffusion coefficients of additives in polymers. I. Correlation with geometric parameters. *Journal of Applied Polymer Science, 82*(10), 2422-2433.

Rhim, J.-W., Mohanty, A. K., Singh, S. P., Ng, P. K. W. (2006a). Effect of the processing methods on the performance of polylactide films: thermocompression versus solvent casting. *Journal of Applied Polymer Science, 101*, 3736-3742.

Rhim, J.-W., Mohanty, K. A., Singh, S. P., Ng, P. K. W. (2006b). Preparation and Properties of Biodegradable Multilayer Films Based on Soy Protein Isolate and Poly(lactide). *Industrial & Engineering Chemistry Research, 45*(9), 3059-3066.

Rhim, J.-W., Hong, S.-I., Ha, C.-S. (2009). Tensile, water vapor barrier and antimicrobial properties of PLA/nanoclay composite films. *LWT - Food Science and Technology, 42*(2), 612-617.

Righetti, M. C., Tombari, E., Lorenzo, M. L. D. (2008). Crystalline, mobile amorphous and rigid amorphous fractions in isotactic polystyrene. *European Polymer Journal, 44*(8), 2659-2667.

Riquet, A. M., Wolff, N., Laoubi, S., Vergnaud, J. M., Feigenbaum, A. (1998). Food and packaging interactions: Determination of the kinetic parameters of olive oil diffusion in polypropylene using concentration profiles. *Food Additives and Contaminants, 15*(6), 690 - 700.

Riquet, A.-M., Feigenbaum, A., Colonna, P., Lourdin, D. (2003). Molecular mobility in starchy materials studied by electron spin resonance. *Journal of Applied Polymer Science, 88*(4), 990-997.

Roe, R.-J., Bair, H. E., Gieniewski, C. (1974). Solubility and diffusion coefficient of antioxidants in polyethylene. *Journal of Applied Polymer Science, 18*(3), 843-856.

Saint-Eve, A., Levy, C., Moigne, M. L., Ducruet, V., Souchon, I. (2008). Quality changes in yogurt during storage in different packaging materials. *Food Chemistry, 110*, 285-293.

Sajilata, M. G., Savitha, K., Singhal, R. S., Kanetkar, V. R. (2007). Scalping of Flavors in Packaged Foods. *Comprehensive Reviews in Food Science and Food Safety, 6*(1), 17-35.

Salame, M. (1986). The use of barrier polymer in food and beverage packaging. *Journal of Plastic Film Sheeting, 2*, 321-334.

Sammon, C., Yarwood, J., Everall, N. (2000). A FTIR-ATR study of liquid diffusion processes in PET films: comparison of water with simple alcohols. *Polymer, 41*(7), 2521-2534.

Sanchez-Garcia, M. D., Gimenez, E., J.M.Lagaron. (2007). Novel PET Nanocomposites of Intesrest in Food Packaging Applications and Comparative Barrier Performance with Biopolyester Nanocomposites. *Journal of plastic film & sheeting, 23*, 133-148.

Sanchez-Garcia, M. D., Gimenez, E., Lagaron, J. M. (2008). Morphology and barrier properties of solvent cast composites of thermoplastic biopolymers and purified cellulose fibers. *Carbohydrate Polymers, 71*, 235-244.

Sangaj, N. S., Malshe, V. C. (2004). Permeability of polymers in protective organic coatings. *Progress in Organic Coatings, 50*(1), 28-39.

Sangwan, P., Wu, D. Y. (2008). New insights into polylactide biodegradation from molecular ecological techniques. *Macromolecular Bioscience, 8*(4), 304-315.

Sarasua, J.-R., Prud'homme, R. E., Wisniewski, M., Borgne, A. L., Spassky, N. (1998). Crystallization and melting Behavior of Polylactides. *Macromolecules, 31*, 3895-3905.

Sasaki, S., Asakura, T. (2003). Helix Distortion and Crystal Structure of the α-Form of Poly(l-lactide). *Macromolecules, 36*(22), 8385-8390.

Sawada, H., Takahashi, Y., Miyata, S., Kanehashi, S., Sato, S., Nagai, K. (2010). Gas transport properties and crystalline structures of poly(lactic acid) membranes. *Transactions of the Materials Research Society of Japan, 35*(2), 241-246.

Sawai, D., Takahashi, K., Imamura, T., Nakamura, K., Kanamoto, T., Hyon, S.-H. (2002). Preparation of Oriented beta-Form Poly(L-lactic acid) by Solid-State Extrusion. *Journal Polymer Science Part B: Polym Physic, 40*, 95-104.

Schick, C., Wurm, A., Mohammed, A. (2003). Formation and disappearance of the rigid amorphous fraction in semicrystalline polymers revealed from frequency dependent heat capacity. *Thermochimica Acta, 396*(1-2), 119-132.

Schmidt, S. C., Hillmyer, M. A. (2001). Polylactide stereocomplex crystallites as nucleating agents for isotactic polylactide. *Journal of Polymer Science Part B: Polymer Physics, 39*(3), 300-313.

Schwach, G., Coudane, J., Engel, R., Vert, M. (1996). Zn lactate as initiator of DL-lactide ring opening polymerization and comparison with Sn octoate. *Polymer Bulletin, 37*(6), 771-776.

Sefcik, M. D., Schaefer, J., May, F. L., Raucher, D., Dub, S. M. (1983). Diffusivity of gases and main-chain cooperative motions in plasticized poly(vinyl chloride). *Journal of Polymer Science: Polymer Physics Edition, 21*(7), 1041-1054.

Sekelik, D. J., Stepanov, E. V., Nazarenko, S., Schiraldi, D., Hiltner, A., Baer, E. (1999). Oxygen barrier properties of crystallized and talc-filled poly(ethylene terephthalate). *Journal of Polymer Science Part B: Polymer Physics, 37*(8), 847-857.

Serad, G. E., Freeman, B. D., Stewart, M. E., Hill, A. J. (2001). Gas and vapor sorption and diffusion in poly(ethylene terephthalate). *Polymer, 42*(16), 6929-6943.

Shen, L., Haufe, J., Patel, M. K. (2009). *PROBIP 2009, Product overview and market projection of emerging bio-based plastics. Report commissioned by EPNOE and European Bioplastics*: Group Science, Technology and Society (STS), Copernicus Institute for Sustainable Develpment and Innovation Utrecht University.

Shen, L., Worrell, E., Patel, M. (2010). Present and future development in plastics from biomass. *Biofuels Bioproducts & Biorefining-Biofpr, 4*(1), 25-40.

Sheth, M., Kumar, R. A., Davé, V., Gross, R. A., McCarthy, S. P. (1997). Biodegradable polymer blends of poly(lactic acid) and poly(ethylene glycol). *Journal of Applied Polymer Science, 66*, 1495-1505.

Shieh, Y.-T., Liu, G.-L. (2007). Temperature-Modulated Differential Scanning Calorimetry Studies on the Origin of Double Melting Peaks in Isothermally Melt-Crystallized

Poly(L-lactic acid). *Journal of Polymer Science : Part B : Polymer Physics, 45*, 466-474.

Shogren, R. (1997). Water vapor permeability of biodegradable polymers. *Journal of Polymers and the Environment, 5*(2), 91-95.

Signori, F., Coltelli, M.-B., Bronco, S. (2009). Thermal degradation of poly(lactic acid) (PLA) and poly(butylene adipate-co-terephthalate) (PBAT) and their blends upon melt processing. *Polymer Degradation and Stability, 94*(1), 74-82.

Sinha Ray, S., Yamada, K., Okamoto, M., Ogami, A., Ueda, K. (2003). New Polylactide/Layered Silicate Nanocomposites. 3. High-Performance Biodegradable Materials. *Chemistry of Materials, 15*(7), 1456-1465.

Siparsky, G., Voorhees, K., Dorgan, J., Schilling, K. (1997). Water transport in polylactic acid (PLA), PLA/ polycaprolactone copolymers, and PLA/polyethylene glycol blends. *Journal of Polymers and the Environment, 5*(3), 125-136.

Siracusa, V., Rocculi, P., Romani, S., Rosa, M. D. (2008). Biodegradable polymers for food packaging: a review. *Trends in Food Science & Technology, 19*(12), 634-643.

Sodergard, A., Nasman, J. H. (1994). Stabilization of Poly(L-Lactide) in the Melt. *Polymer Degradation and Stability, 46*(1), 25-30.

Södergård, A., Stolt, M. (2002). Properties of lactic acid based polymers and their correlation with composition. *Progress in Polymer Science, 27*(6), 1123-1163.

Solarski, S., Ferreira, M., Devaux, E. (2005). Characterization of the thermal properties of PLA fibers by modulated differential scanning calorimetry. *Polymer, 46*, 11187-11192.

Solarski, S., Ferreira, M., Devaux, E., Fontaine, G., Bachelet, P., Bourbigot, S., et al. (2008a). Designing polylactide/clay nanocomposites for textile applications: Effect of processing conditions, spinning, and characterization. *Journal of Applied Polymer Science, 109*(2), 841-851.

Solarski, S., Ferreira, M., Devaux, E. (2008b). Ageing of polylactide and polylactide nanocomposite filaments. *Polymer Degradation and Stability*, *93*(3), 707-713.

Song, J. H., Murphy, R. J., Narayan, R., Davies, G. B. H. (2009). Biodegradable and compostable alternatives to conventional plastics (Vol. 364, pp. 2127-2139).

Stefan Stoll, U. o. C. (2003). EasySpin Retrieved 15/09/2010, 2010, from http://www.easyspin.org/

Stern, S. A., Sampat, S. R., Kulkarni, S. S. (1986). Tests of a "free-volume" model of gas permeation through polymer membranes. II. Pure Ar, SF6, CF4, and C2H2F2 in polyethylene. *Journal of Polymer Science Part B: Polymer Physics, 24*(10), 2149-2166.

Stoclet, G., Elkoun, S., Miri, V., Seguela, R., Lefebvre, J. M. (2007). Crystallization and mechanical properties of poly(D, L)lactide-based blown films. *International Polymer Processing, 22*(5), 385-388.

Stoclet, G., Seguela, R., Lefebvre, J. M., Elkoun, S., Vanmansart, C. (2010) Strain-Induced Molecular Ordering in Polylactide upon Uniaxial Stretching. *Macromolecules, 43*(3), 1488-1498.

Stoclet, G., Seguela, R., Lefebvre, J.-M., (2011) Morphology, thermal behavior and mechanical properties of binary blends of compatible biosourced polymers; Polylactide/polyamide 11. *Polymer*, *52*(6), 1417-1425.

Stolt, M., Sodergard, A. (1999). Use of Monocarboxylic Iron Derivatives in the Ring-Opening Polymerization of l-Lactide. *Macromolecules, 32*(20), 6412-6417.

Storks, K. H. (1938). An Electron Diffraction Examination of Some Linear High Polymers. *Journal of the American Chemical Society, 60*(8), 1753-1761.

Stridsberg, K., Ryner, M., Albertsson, A.-C. (2000). Dihydroxy-Terminated Poly(l-lactide) Obtained by Controlled Ring-Opening Polymerization: Investigation of the Polymerization Mechanism. *Macromolecules, 33*(8), 2862-2869.

Supaphol, P. (2001). Application of the Avrami, Tobin, Malkin, and Urbanovici-Segal macrokinetic models to isothermal crystallization of syndiotactic polypropylene. *Thermochimica Acta, 370*(1-2), 37-48.

Su, Z., Guo, W., Liu, Y., Li, Q., Wu, C. (2009). Non-isothermal crystallization kinetics of poly(lactic acid)/modified carbon black composite. *Polymer Bulletin, 62*, 629-642.

Suyama, T., Tokiwa, Y., Ouichanpagdee, P., Kanagawa, T., Kamagata, Y. (1998). Phylogenetic affiliation of soil bacteria that degrade aliphatic polyesters available commercially as biodegradable plastics. *Applied and Environmental Microbiology, 64*(12), 5008-5011.

Švajdlenková, H., Bartoš, J. (2009). Spin probe mobility in relation to free volume and relaxation dynamics of glass-formers: A series of spin probes in poly(isobutylene). *Journal of Polymer Science Part B: Polymer Physics, 47*(11), 1058-1068.

Takagi, Y., Yasuda, R., Yamaoka, M., Yamane, T. (2004). Morphologies and mechanical properties of polylactide blends with medium chain length poly(3-hydroxyalkanoate) and chemically modified poly(3-hydroxyalkanoate). *Journal of Applied Polymer Science, 93*(5), 2363-2369.

Taubner, V., Shishoo, R. (2001). Influence of processing parameters on the degradation of poly(L-lactide) during extrusion. *Journal of Applied Polymer Science, 79*(12), 2128-2135.

Thompson, R. C., Swan, S. H., Moore, C. J., vom Saal, F. S. (2009). Our plastic age (Vol. 364, pp. 1973-1976).

Tokiwa, Y., Calabia, B. P. (2006). Biodegradability and biodegradation of poly(lactide). *Applied Microbiology and Biotechnology, 72*(2), 244-251.

Tsai, C.-C., Wu, R.-J., Cheng, H.-Y., Li, S.-C., Siao, Y.-Y., Kong, D.-C., et al. (2010). Crystallinity and dimensional stability of biaxial oriented poly(lactic acid) films. *Polymer Degradation and Stability, 95*(8), 1292-1298.

Tsuji, H., Ikada, Y., Hyon, S. H., Kimura, Y., Kitao, T. (1994). Stereocomplex Formation between Enantiomeric Poly(Lactic Acid) .8. Complex Fibers Spun from Mixed-Solution of Poly(D-Lactic Acid) and Poly(L-Lactic Acid). *Journal of Applied Polymer Science, 51*(2), 337-344.

Tsuji, H., Ikada, Y. (1995). Properties and morphologies of poly(-lactide): 1. Annealing condition effects on properties and morphologies of poly(-lactide). *Polymer, 36*(14), 2709-2716.

Tsuji, H., Ikada, Y. (1996). Crystallization from the melt of poly(lactide)s with different optical purities and their blends. *Macromolecular Chemistry and Physics, 197*(10), 3483-3499.

Tsuji, H., Ikada, Y. (1999). Stereocomplex formation between enantiomeric poly(lactic acid)s. XI. Mechanical properties and morphology of solution-cast films. *Polymer, 40*(24), 6699-6708.

Tsuji, H., Suzuyoshi, K. (2002a). Environmental degradation of biodegradable polyesters 1. Poly(epsilon-caprolactone), poly[(R)-3-hydroxybutyrate], and poly(L-lactide) films in controlled static seawater. *Polymer Degradation and Stability, 75*(2), 347-355.

Tsuji, H., Suzuyoshi, K. (2002b). Environmental degradation of biodegradable polyesters 2. Poly(epsilon-caprolactone), poly [(R)-3-hydroxybutyrate], and poly(L-lactide) films in natural dynamic seawater. *Polymer Degradation and Stability, 75*(2), 357-365.

Tsuji, H., Fukui, I. (2003). Enhanced thermal stability of poly(lactide)s in the melt by enantiomeric polymer blending. *Polymer, 44*(10), 2891-2896.

Tsuji, H., Tezuka, Y. (2004). Stereocomplex Formation between Enantiomeric Poly(lactic acid)s. 12. Spherulite Growth of Low-Molecular-Weight Poly(lactic acid)s from the Melt. *Biomacromolecules, 5*(4), 1181-1186.

Tsuji, H. (2005). Poly(lactide) stereocomplexes: Formation, structure, properties, degradation, and applications. *Macromolecular Bioscience, 5*(7), 569-597.

Tsuji, H., Ogiwara, M., Saha, S. K., Sakaki, T. (2006a). Enzymatic, alkaline, and autocatalytic degradation of poly(L-lactic acid): Effects of biaxial orientation. *Biomacromolecules, 7*(1), 380-387.

Tsuji, H., Okino, R., Daimon, H., Fujie, K. (2006b). Water Vapor Permeability of Poly(lactide)s : Effects of Molecular Characteristics and Cristallinity. *Journal of Applied Polymer Science, 99*, 2245-2252.

Tsuji, H., Takai, H., Saha, S. K. (2006c). Isothermal and non-isothermal crystallization behavior of poly(L-lactic acid) : Effects of stereocomplex as nucleating agent. *Polymer, 47*, 3826-3837.

Tsuji, H., Sawada, M. (2010). Accelerated crystallization of poly(L-lactide) by physical aging. *Journal of Applied Polymer Science, 116*, 1190-1196.

Tweed, E., Stephens, H., Riegert, T. (2009). Polylactic acid blown film and method of manufacturing same: Plastic Suppliers, Inc. (Columbus, OH)

Urayama, H., Kanamori, T., Kimura, Y. (2001). Microstructure and Thermomechanical Properties of Glassy Polylactides with Different Optical Purity of the Lactate Units. *Macromolecular Materials and Engineering, 286*(11), 705-713.

Urayama, H., Kanamori, T., Kimura, Y. (2002). Properties and biodegradability of polymer blends of POly(L-lactide)s with different optical purity of the lactate units. *Macromolecular Materials and Engineering, 287*(2), 116-121.

van Aardt, M., Duncan, S. E., Marcy, J. E., Long, T. E., O'Keefe, S. F., Sims, S. R. (2007). Release of antioxidants from poly(lactide-co-glycolide) films into dry milk products and food simulating liquids. *International Journal of Food Science and Technology, 42*(11), 1327-1337.

Van Willige, R., Schoolmeester, D., Van Ooij, A., Linssen, J., Voragen, A. (2002). Influence of Storage Time and Temperature on Absorption of Flavor Compounds from Solutions by Plastic Packaging Materials. *Journal of Food Science, 67*(6), 2023-2031.

Veksli, Z., Andreis, M., Rakvin, B. (2000). ESR spectroscopy for the study of polymer heterogeneity. *Progress in Polymer Science, 25*(7), 949-986.

Vermeiren, L., Devlieghere, F., van Beest, M., de Kruijf, N., Debevere, J. (1999). Developments in the active packaging of foods. *Trends in Food Science & Technology, 10*(3), 77-86.

Vert, M., Li, S. M., Spenlehauer, G., Guerin, P. (1992). Bioresorbability and Biocompatibility of Aliphatic Polyesters. *Journal of Materials Science-Materials in Medicine, 3*(6), 432-446.

Vitrac, O., Hayert, M. (2006a). Identification of Diffusion Transport Properties from Desorption/Sorption Kinetics: An Analysis Based on a New Approximation of Fick Equation during Solid-Liquid Contact. *Industrial & Engineering Chemistry Research, 45*(23), 7941-7956.

Vitrac, O., Lézervant, J., Feigenbaum, A. (2006b). Decision trees as applied to the robust estimation of diffusion coefficients in polyolefins. *Journal of Applied Polymer Science, 101*(4), 2167-2186.

Vitrac, O., Mougharbel, A., Feigenbaum, A. (2007). Interfacial mass transport properties which control the migration of packaging constituents into foodstuffs. *Journal of Food Engineering, 79*(3), 1048-1064.

Vittoria, V. (1995). Influence of the crystallinity on the transport properties of polyethylene. *Journal of Materials Science, 30*(15), 3954-3958.

von Oepen, R., Michaeli, W. (1992). Injection moulding of biodegradable implants. *Clin Mater, 10*(1-2), 21-28.

Von Solms, N., Nielsen, J. K., Hassager, O., Rubin, A., Dandekar, A. Y., Andersen, S. I., et al. (2004). Direct measurement of gas solubilities in polymers with a high-pressure microbalance. *Journal of Applied Polymer Science, 91*(3), 1476-1488.

Vrentas, J. S., Duda, J. L. (1977a). Diffusion in polymer–solvent systems. II. A predictive theory for the dependence of diffusion coefficients on temperature, concentration, and molecular weight. *Journal of Polymer Science: Polymer Physics Edition, 15*(3), 417-439.

Vrentas, J. S., Duda, J. L. (1977b). Diffusion in polymer—solvent systems. I. Reexamination of the free-volume theory. *Journal of Polymer Science: Polymer Physics Edition, 15*(3), 403-416.

Vrentas, J. S., Duda, J. L., Ling, H. C. (1985a). Free-volume theories for self-diffusion in polymer–solvent systems. I. Conceptual differences in theories. *Journal of Polymer Science: Polymer Physics Edition, 23*(2), 275-288.

Vrentas, J. S., Duda, J. L., Ling, H. C., Hou, A. C. (1985b). Free-volume theories for self-diffusion in polymer–solvent systems. II. Predictive capabilities. *Journal of Polymer Science: Polymer Physics Edition, 23*(2), 289-304.

Vyazovkin, S. (2002). Is the Kissinger Equation Applicable to the Processes that Occur on Cooling? *Macromolecular Rapid Communications, 23*(13), 771-775.

Walker, A. M., Tao, Y., Torkelson, J. M. (2007). Polyethylene/starch blends with enhanced oxygen barrier and mechanical properties: Effect of granule morphology damage by solid-state shear pulverization. *Polymer, 48*(4), 1066-1074.

Wang, Y., Xiao, Y., Zhang, Q., Gao, X.-L., Fu, Q. (2003). The morphology and mechanical properties of dynamic packing injection molded PP/PS blends. *Polymer, 44*(5), 1469-1480.

Wang, Y. M., Steinhoff, B., Brinkmann, C., Alig, I. (2008). In-line monitoring of the thermal degradation of poly(L-lactic acid) during melt extrusion by UV-vis spectroscopy. *Polymer, 49*(5), 1257-1265.

Wang, R. Y., Wang, S. F., Zhang, Y., Wan, C. Y., Ma, P. M. (2009). Toughening Modification of PLLA/PBS Blends via In Situ Compatibilization. *Polymer Engineering and Science, 49*(1), 26-33.

Weber, C. J., Haugaard, V., Festersen, R., Bertelsan, G. (2002). Production and applications of biobased pacakging materials for the food industry. *Food Additives and Contaminants, 19*(supplement), 172-177.

Weir, N. A., Buchanan, F. J., Orr, J. F., Dickson, G. R. (2004a). Degradation of poly-L-lactide: Part 1: in vitro and in vivo physiological temperature degradation. *Proceedings of the Institution of Mechanical Engineers Part H-Journal of Engineering in Medicine, 218*(H5), 307-319.

Weir, N. A., Buchanan, F. J., Orr, J. F., Farrar, D. F., Dickson, G. R. (2004b). Degradation of poly-L-lactide: Part 2: increased temperature accelerated degradation. *Proceedings of the Institution of Mechanical Engineers Part H-Journal of Engineering in Medicine, 218*(H5), 321-330.

Wolinska-Grabczyk, A., Bednarski, W., Jankowski, A., Waplak, S. (2005). Temperature dependence of molecular motions in the polyurethane-based membranes studied with paramagnetic spin probe. *Polymer, 46*(8), 2461-2471.

Wu, D., Wu, L., Wu, L., Xu, B., Zhang, Y., Zhang, M. (2007). Nonisothermal Cold Crystallization Behavior and Kinetics of Polylactide/Clay Nanocomposites. *Journal of Polymer Science: Part B: Polymer Physics, 45*, 1100-1113.

Wunderlich, B. (2003). Reversible crystallization and the rigid-amorphous phase in semicrystalline macromolecules. *Progress in Polymer Science, 28*(3), 383-450.

Xiao, H., Lu, W., Yeh, J.-T. (2009). Effect of plasticizer on the crystallization behavior of poly(lactic acid). *Journal of Applied Polymer Science, 113*(1), 112-121.

Xiao, h., Liu, F., Jiang, T., Yeh, J.-T. (2010a). Kinetics and crystal structure of isothermal crystallization of poly(lactic acid) plasticized with triphenyl phosphate. *Journal of Applied Polymer Science, 117*(5), 2980-2992.

Xiao, H., Yang, L., Ren, X., Jiang, T., Yeh, J.-T. (2010b). Kinetics and crystal structure of poly(lactic acid) crystallized nonisothermally: Effect of plasticizer and nucleating agent. *Polymer Composites, 31*(12), 2057-2068.

Xiao, H. W., Li, P., Ren, X., Jiang, T., Yeh, J.-T. (2010c). Isothermal crystallization kinetics and crystal structure of poly(lactic acid): Effect of triphenyl phosphate and talc. *Journal of Applied Polymer Science, 118*(6), 3558-3569.

Yasuniwa, M., Iura, K., Dan, Y. (2007). Melting behavior of poly(l-lactic acid): Effects of crystallization temperature and time. *Polymer, 48*(18), 5398-5407.

Yokohara, T., Okamoto, K., Yamaguchi, M. (2010). Effect of the Shape of Dispersed Particles on the Thermal and Mechanical Properties of Biomass Polymer Blends Composed of Poly(L-lactide) and Poly(butylene succinate). *Journal of Applied Polymer Science, 117*(4), 2226-2232.

Yoon, J.-S., Jung, H.-W., Kim, M.-N., Park, E.-S. (2000). Diffusion coefficient and equilibrium solubility of water molecules in biodegradable polymers. *Journal of Applied Polymer Science, 77*(8), 1716-1722.

Yu, J., Wang, N., Ma, X. (2008). Fabrication and Characterization of Poly(lactic acid)/Acetyl Tributyl Citrate/Carbon Black as Conductive Polymer Composites. *Biomacromolecules, 9*(3), 1050-1057.

Zenkiewicz, M., Richert, J. (2008). Permeability of polylactide nanocomposite films for water vapour, oxygen and carbon dioxide. *Polymer Testing, 27*(7), 835-840.

Zhang, X. C., Wyss, U. P., Pichora, D., Goosen, M. F. A. (1992). An Investigation of the Synthesis and Thermal-Stability of Poly(Dl-Lactide). *Polymer Bulletin, 27*(6), 623-629.

Zhang, L. L., Xiong, C. D., Deng, X. M. (1996). Miscibility, crystallization and morphology of poly(beta-hydroxybutyrate)/poly(d,l-lactide) blends. *Polymer, 37*(2), 235-241.

Zhang, J., Duan, Y., Sato, H., Tsuji, H., Noda, I., Yan, S., et al. (2005). Crystal Modifications and Thermal Behavior of Poly(l-lactic acid) Revealed by Infrared Spectroscopy. *Macromolecules, 38*(19), 8012-8021.

Zhang, J., Tashiro, K., Tsuji, H., Domb, A. J. (2008). Disorder-to-Order Phase Transition and Multiple Melting Behavior of Poly(l-lactide) Investigated by Simultaneous Measurements of WAXD and DSC. *Macromolecules, 41*(4), 1352-1357.

Zhao, J., Wilkins, R. M. (2005). Low molecular weight polylactic acid as a matrix for the delayed release of pesticides. *Journal of Agricultural and Food Chemistry, 53*(10), 4076-4082.

Zhu, X. X., Macdonald, P. M. (1992). Pulsed-gradient spin-echo NMR measurements of the diffusion coefficients of ketones in poly(methyl methacrylate). *Macromolecules, 25*(17), 4345-4351.

Zhu, X. X., Wang, F., Nivaggioli, T., Winnik, M. A., Macdonald, P. M. (1993). Poly(methyl methacrylate) film dissolution and solvent diffusion coefficients: correlations determined using laser interferometry-fluorescence quenching and pulsed-gradient spin-echo NMR spectroscopy. *Macromolecules, 26*(24), 6397-6402.

Ziaee, Z., Supaphol, P. (2006). Non-isothermal melt- and cold-crystallization kinetics of poly(3-hydroxybutyrate). *Polymer testing, 25*, 807-818.

Zielinski, J. M., Sillescu, H., Romdhane, I. H. (1996). 1,3,5-triisopropylbenzene diffusion in polystyrene solutions. *Journal of Polymer Science Part B: Polymer Physics, 34*(1), 121-130.

Zuza, E., Ugartemendia, J. M., Lopez, A., Meaurio, E., Lejardi, A., Sarasua, J.-R. (2008). Glass transition behavior and dynamic fragility in polylactides containing mobile and rigid amorphous fractions. *Polymer, 49*(20), 4427-4432.

Résumé

La compréhension de la relation structure-propriété est un élément indispensable pour la conception et l'amélioration des matériaux, notamment ceux utilisés dans le domaine de l'emballage alimentaire. Afin de contribuer à la compréhension des phénomènes de transport dans le polylactide (PLA), les travaux de ce mémoire se sont portés sur la modulation de la microstructure du PLA en lien avec ses propriétés barrière aux gaz (oxygène, hélium) et aux composés organiques (esters éthyliques, sondes fluorescentes). La microstructure a été modulée i) par l'ajout de plastifiant (ATBC, PEG), ii) par la cristallisation selon trois procédés, le traitement thermique, la cristallisation induite par des composés organiques et le biétirage. Ces approches ont permis, respectivement, de faire varier le pourcentage de phase amorphe par rapport à la phase cristalline, la fraction de volume libre au sein de la phase amorphe, et la structure cristalline. L'augmentation de la cristallinité par recuit à partir du vitreux n'a pas conduit à une diminution systématique et importante des coefficients de transport des molécules de gaz (oxygène, hélium). Deux hypothèses principales ont ainsi été formulées pour expliquer ce comportement : la dédensification de la phase amorphe et la présence d'une phase amorphe mobile et d'une phase rigide. L'influence du biétirage sur les propriétés barrière aux gaz a été très limitée même au plus fort ratio d'étirage (4×4). Néanmoins cette technique a l'avantage de permettre la réalisation de morphologies différentes.

L'étude des coefficients de transport par plusieurs méthodes (sorption, perméation, diffusion par contact solide/solide) a permis de mettre en évidence la loi d'échelle ($D \propto M^{\alpha}$) dans le cas des molécules fluorescentes et a permis une première estimation du coefficient alpha. Une approche par Résonance Paramagnétique Electronique a permis de mettre en évidence des séparations de phase des systèmes plastifiés par ATBC et PEG. Cette méthode pourrait constituer un des moyens de sonder les hétérogénéités locales et les changements microstructuraux liés à l'interaction de molécules perméantes et de la matrice polymère, lors du transport.

Mots-clés : Polylactide, propriétés barrière, perméabilité, formulation

Summary

The understanding of the relationship between structure and properties is fundamental for materials conception and improvement, in particular for those used in food packaging industry. To contribute to the understanding of the transport phenomena in polylactide (PLA), this study was focused on the PLA microstructure modulation related to its gas (oxygen, helium) and organic compounds (ethyl esters, fluorescent molecules) barrier properties. The microstructure was modulated i) by adding plasticizers (ATBC, PEG), ii) by crystallizing according to 3 processes, thermal treatment, organic compounds induced crystallization and biaxially orientation. These approaches respectively enabled to vary, the ratio of amorphous phase and crystalline phase, free volume fraction into amorphous phase and the crystalline structure. The increase in crystallinity degree, by annealing from cold state, did not result in a systematic and significant decrease of the gas molecules transport coefficient (oxygen, helium). Two main hypotheses were formulated to explain this behaviour: de-densification of amorphous phase and presence of a mobile and a rigid amorphous phase. The influence of biaxially orientation on gas barrier properties was strongly limited even at the highest stretching ratio (4×4). Nevertheless several morphologies can be formed thanks to this technique.

The transport coefficient study by several methods (sorption, permeation and diffusion by solid/solid contact) highlighted a scale law ($D \propto M^{\alpha}$) with fluorescent molecules and allowed to a first estimation of α coefficient. Thanks to Electronic Spin Resonance approach, phase separation of plasticized systems by ATBC and PEG were highlighted. This method could be one of the means to probe the local heterogeneities and the micro-structural changes related to the interaction of permeating molecules and polymer matrix during transport.

Keywords: Polylactide, barrier properties, permeability, formulation